



HAL
open science

Drug Sensitivity and Clonal Evolution Under Targeted Treatment of High-Risk Neuroblastoma

Irène Jiménez

► **To cite this version:**

Irène Jiménez. Drug Sensitivity and Clonal Evolution Under Targeted Treatment of High-Risk Neuroblastoma. Cancer. Université Paris-Saclay, 2021. English. NNT : 2021UPASL046 . tel-03712009

HAL Id: tel-03712009

<https://theses.hal.science/tel-03712009>

Submitted on 2 Jul 2022

HAL is a multi-disciplinary open access archive for the deposit and dissemination of scientific research documents, whether they are published or not. The documents may come from teaching and research institutions in France or abroad, or from public or private research centers.

L'archive ouverte pluridisciplinaire **HAL**, est destinée au dépôt et à la diffusion de documents scientifiques de niveau recherche, publiés ou non, émanant des établissements d'enseignement et de recherche français ou étrangers, des laboratoires publics ou privés.

Drug sensitivity and clonal evolution
under targeted treatment
of high-risk neuroblastoma

*Etude de la sensibilité aux drogues et de
l'évolution clonale sous thérapies ciblées du
neuroblastome de haut risque*

Thèse de doctorat de l'université Paris-Saclay

École doctorale n°582 : Cancérologie : biologie-médecine-santé (CBMS)

Spécialité de doctorat : Aspects moléculaires et cellulaires de la biologie

Unité de recherche : INSERM U830, Equipe labellisée LNCC, SIREDO Oncology Center,
Institut Curie, 75005 Paris, France

Référent : Faculté de Médecine

Thèse présentée et soutenue à Paris, le 6 juillet 2021, par

Irene JIMÉNEZ

Composition du Jury

Gilles VASSAL

Professeur, université Paris-Saclay
Gustave Roussy, Villejuif (France)

Président

Nicolas ANDRE

Professeur, Hôpital de la Timone, Marseille (France)

Rapporteur & Examineur

Marie CASTETS

Docteure, Centre de Recherche en Cancérologie de Lyon (France)

Rapporteur & Examinatrice

Sally GEORGE

Docteure, Institute of Cancer Research, London (United Kingdom)

Examinatrice

Birgit GEOERGER

Docteure, Gustave Roussy, Villejuif (France)

Examinatrice

Gudrun SCHLEIERMACHER

Docteure, Institut Curie, Paris (France)

Directrice de thèse

Université Paris-Saclay

Espace Technologique / Immeuble Discovery

Route de l'Orme aux Merisiers RD 128 / 91190 Saint-Aubin, France

Table of contents

Acknowledgements	7
List of abbreviations	9
Synthèse.....	11
I - Introduction	13
1. Neuroblastoma.....	13
1.1 Epidemiology, staging, standard treatment and outcome.....	13
1.2 Molecular characteristics of neuroblastoma.....	15
1.3 Cell plasticity and role of epigenetics in neuroblastoma	19
2. Intratumor heterogeneity and clonal evolution.....	20
2.1 Intratumor heterogeneity.....	21
2.1.1 Spatial genetic heterogeneity	21
2.1.2 Temporal heterogeneity.....	22
2.2 Origins of intratumoral heterogeneity	23
2.2.1 Genomic instability.....	23
2.2.2 Clonal evolution	24
2.3 Evidences of clonal evolution in neuroblastoma	25
3. Molecular therapeutic targets.....	27
3.1 Precision medicine programs in Pediatric Oncology.....	27
3.2 Targeted therapies for Neuroblastoma	31
3.2.1 Genetic targets.....	32
3.2.2 Targeting epigenetics.....	38
3.2.3 Exploring synthetic lethal approaches	40
4. Drug sensitivity screening of anticancer compounds.....	43
II - Thesis objectives	45
III - Results.....	47
1. Study of the <i>in vitro</i> drug sensitivity of high-risk neuroblastoma	47
1.1 High-throughput drug screening in experimental neuroblastoma models.....	47
1.1.1 Scientific context.....	47
1.1.2 Overall hypothesis and objectives.....	48
1.1.3 Analysis of drug cytotoxicity.....	48
1.1.4 High-throughput drug screening using cell lines	49
1.1.5 High-throughput drug screening using PDTC models.....	52
1.1.5.1 High-risk neuroblastoma PDX models	52
1.1.5.2 Obtaining PDTCs	54
1.1.5.3 Experimental pipeline.....	54
1.1.5.4 Screening of PDTC models with the COMPASS core drug library	56
1.1.5.5 Screening of PDTC models using an in-house drug library.....	58
1.1.5.6 Common drugs to the in-house and COMPASS libraries.....	61

1.1.5.7 Concluding remarks	62
1.1.6 Use of PDTCs to test chemo-drug combinations	63
1.1.6.1 Experimental pipeline	63
1.1.6.2 Analysis of the chemotherapy-targeted drug combinations in PDTC	65
1.1.6.3 Concluding remarks	67
1.2 G-quadruplex structures as potential targets in high risk neuroblastoma.....	69
1.2.1 Scientific context.....	69
1.2.2 Hypotheses and objectives	71
1.2.3 Phenotype of high-risk neuroblastoma cell lines and PDX models.	72
1.2.4 Experimental workflow	74
1.2.5 Growth study and population doubling time estimation in 384-wp	75
1.2.6 Evaluation of chemoresistance in 5 high-risk neuroblastoma cell lines	76
1.2.7 Studies of cytotoxicity of G4-L compounds alone	78
1.2.8 Next steps.....	81
1.2.9 Concluding remarks.....	82
2. Clonal evolution of high-risk NB under targeted therapies	85
2.1 Scientific context	85
2.2 In vivo experiments for the study of clonal evolution under treatment	88
2.2.1 Experimental pipeline.....	88
2.2.2 Ethical considerations of <i>in vivo</i> experimentation	89
2.2.3 Treatment schedules	89
2.2.4 <i>In vivo</i> treatment efficacy	90
2.2.4.1 Determination of the treatment efficacy	90
2.2.4.2 Analysis of treatment efficacy	91
2.2.5 Prediction of the <i>in vivo</i> response.....	92
2.2.6 Tumor DNA sampling, processing and sequencing	93
2.2.7 Bioinformatics pipeline	93
2.3 Analysis of the clonal evolution of NB under treatment by WES	96
2.3.1 Study of the variability	96
2.3.2 How clones evolve under treatment	98
2.3.3 Modelization of clonal evolution	102
2.3.3.1 Bioinformatics analysis.....	103
2.3.3.2 Insights in clonal architecture and evolution after treatment.....	103
2.4 Perspectives: cfDNA as a surrogate of tumor DNA in PDX models	106
2.4.1 Blood sampling and processing.....	106
2.4.2 cfDNA extraction, qualification and sequencing.....	107
2.4.3 Feasibility study in one cfDNA sample	108
2.4 Concluding remarks	110
3. <i>Combinatorial therapeutics for ALK-aberrant neuroblastoma</i>	111
3.1 Scientific context	111
3.2 Paper manuscript	113
3.3 Next steps	135
IV - Discussion and perspectives	137
In vitro drug sensitivities in neuroblastoma	137
In vivo studies of clonal evolution in neuroblastoma.....	139
ALK preclinical studies in neuroblastoma	141
Publication strategies.....	142

V - Conclusion	143
References.....	145
Appendix.....	175
Appendix 1: Supplementary table 1	175
Appendix 2: treatment efficacy charts.....	179
Model GR-NB4	179
Model GR-NB10.....	181
Model HSJD-NB-005.....	183
Model IC-pPDX-17.....	185
Model IC-pPDX-75.....	187
Model IC-pPDX-109	189
Appendix 3: whole-exome sequencing quality control	191
Model IC-pPDX-17.....	191
Model IC-pPDX-75.....	191
Model IC-pPDX-109	192
Model GR-NB4	192
Model GR-NB10.....	193
Appendix 4: papers published during the PhD.....	195
Circulating tumor DNA analysis enables molecular characterization of pediatric renal tumors at diagnosis.....	197
Bromodomain and extraterminal protein inhibitors in pediatrics: a review of the literature... 209	
Pediatric patient with renal cell carcinoma treated by successive anti-angiogenics drugs: a case report and review of the literature.....	219
Molecular diagnosis of retinoblastoma by circulating tumor DNA analysis.....	225
Frequency and prognostic impact of ALK amplifications and mutations in the European Neuroblastoma Study Group (SIOPEN) high-risk neuroblastoma trial (<i>abstract</i>).....	243
Phase 1 dose-escalation and pharmacokinetic study of regorafenib in pediatric patients with recurrent or refractory solid malignancies (<i>abstract</i>).....	245
Transition cells between noradrenergic and mesenchymal identities as a source of cell heterogeneity and plasticity in neuroblastoma (<i>abstract</i>).....	247

Acknowledgements

Un grand merci à Gudrun Schleiermacher pour son soutien constant, à tout moment. Pour m'avoir confié ce projet qui s'est élargi et pris forme au fur et à mesure. Et pour m'avoir appris des choses bien au-delà de la science, même si elle ne le sait peut-être pas.

A toute l'équipe RTOP, de qui je me sens vraiment part. J'espère vous avoir donné au moins un centième de ce que vous m'avez donné à moi. Merci à Jaydutt Bhalshankar et Elnaz Saberi-Ansari pour le temps passé dans l'analyse des données de séquençage.

Un grand merci à Elaine Del Nery, toujours prête à aider et toujours avec un sourire. Cela a été un vrai plaisir de collaborer avec toi. Merci à toute ton équipe, BioPhenics, qui a tellement mis ses forces dans mon projet : Juliette, Elodie, Fanny, Aurianne, Maxime.

Merci à Pierre Gestraud, pour tout le temps passé à analyser la montagne de data générés.

Merci à Didier Decaudin et Fariba Nemati, pour tout le travail que le LIP a fait pour ce projet, sans vous cela n'aurait pas été possible.

Merci à Pierre Verrelle pour nous avoir inspiré le beau projet G4-L et à Marie-Paule Teulade pour nous avoir confié ses précieuses molécules

A Didier Surdez et Sakina Zaidi, merci pour le travail monumental fait avec les PDX.

A Isabelle Janoueix, Cécile Pierre-Eugène et Cécile Thirant pour nos échanges toujours enrichissants.

Merci à Olivier Delattre pour les réunions scientifiques stimulantes.

A Sergio Román-Román pour ton accueil et ta bienveillance.

A Angel M. Carcaboso, siempre reactivo y dispuesto a ayudar.

A Birgit Geoerger, Jenny Da Costa et Tiphaine Adam-de-Baumais pour avoir facilité les échanges de matériel et de données qui ont permis de développer en partie ce projet.

Thanks to Sally George, Lizzie Tucker, Deborah Tweddle, Lou Chesler and Lindi Chen, for our monthly Wednesday morning meetings, always inspiring.

A Hélène Pacquement, quand je serai grande je voudrais être comme toi.

A Daniel Orbach, le meilleur collègue de bureau qui est devenu un grand chef maintenant.

A François Doz, pour avoir déposé en moi autant de confiance. Je n'ai toujours pas compris pourquoi.

A Jean Michon, sans qui je ne serais jamais venue à Curie. Merci de m'avoir donné cette opportunité immense, sans connaître de moi que mon goût particulier pour la musique ancienne et le *lied* allemand.

Et surtout merci aux personnes qui n'ont pas besoin que je leur dise merci. Vous savez qui vous êtes et ce que chacune représente pour moi.

List of abbreviations

384-wp	384-well plates
aCGH	Array comparative genomic hybridization
ALKi	ALK inhibitor
ALT	Alternative lengthening of telomeres
ChIP-seq	Chromatin Immunoprecipitation Sequencing
CNA	Copy-number alteration
CTG	CellTiter Glo
cfDNA	Cell-free DNA
ctDNA	Circulating-tumor DNA
DNMT	DNA methyltransferase
DSS	Drug sensitivity score
G4	G-quadruplex
G4-L	G4-ligand
HDACi	Histone deacetylase inhibitor
HR-NB	High-risk neuroblastoma
INRG	International Neuroblastoma Risk Group
INSS	International Neuroblastoma Staging System
ITH	Intra-tumor heterogeneity
LoF	Loss-of-function
NB	Neuroblastoma
NGS	Next-generation sequencing
PDX	Patient-derived xenograft
PDTC	PDX-derived tumor cells
RTV	Relative tumor volume
SL	Synthetic lethality
SNV	Single-nucleotide variation
TGI	Tumor growth inhibition
RNA-seq	RNA sequencing
RTK	Receptor tyrosine kinase
RTV	Relative tumor volume
scDNA	Single-cell DNA
scRNA	Single-cell RNA
VAF	Variant allele fraction
WES	Whole-exome sequencing
WGS	Whole-genome sequencing

Synthèse

Le neuroblastome (NB) est la tumeur solide extra crânienne la plus fréquente de l'enfance. Du point de vue clinique, elle se caractérise par une diversité clinique extrêmement importante, allant de cas de très bon pronostic à des formes dites de haut risque dont la survie à 5 ans ne va pas au-delà de 50% malgré des traitements très intensifs. Le comportement clinique de la maladie est profondément lié à la biologie de la tumeur. Peu d'anomalies génétiques ont été décrites de façon récurrente, les plus fréquentes affectant les gènes *MYCN*, *ALK*, *TERT* ou *ATRX*. Il s'agit d'une des tumeurs les plus hétérogènes du point de vue moléculaire, avec des clones caractérisés par des anomalies génétiques propres, dont le comportement détermine l'évolution de la maladie. Le NB de haut risque (NB-HR) reste un défi pour les cliniciens. Ainsi, il est crucial d'approfondir notre compréhension des principales difficultés auxquelles sont confrontés les cliniciens dans la prise en charge de ces patients : la rechute tumorale et la résistance aux traitements.

Pour y parvenir, il est d'abord impératif d'explorer de nouvelles stratégies de traitement, probablement en combinaison, pour surmonter la résistance au traitement, à la fois primaire et acquise. Sur la base des approches de médecine personnalisée émergentes en oncologie pédiatrique, l'utilisation *in vitro* de criblages de drogues à haut débit permet l'étude de thérapies ciblées basées sur le profil moléculaire de la tumeur ou la découverte de réponses thérapeutiques non prédites. Nous avons pu valider cette approche dans un groupe de 6 lignées cellulaires (dont 2 lignées de NB) portant des anomalies génétiques ciblables propres : chez toutes les lignées, au moins une classe thérapeutique de drogues prédite comme active a été confirmée. Nous avons exploré cette approche *ex vivo* dans 13 modèles de xénogreffes dérivées de patients (PDXs) de NB-HR en utilisant une librairie de drogues incluant différentes classes thérapeutiques. Cela nous a permis de montrer que l'ensemble des différents modèles criblés montrent une sensibilité particulière aux inhibiteurs de HDAC.

Deuxièmement, dans une perspective thérapeutique, il est indispensable de mieux comprendre les processus d'hétérogénéité intratumorale qui conduisent à l'évolution clonale afin d'isoler les clones qui seraient susceptibles de déterminer le comportement de la tumeur, notamment la résistance au traitement. En utilisant 6 différents modèles de PDX de NB-HR, l'étude de l'évolution clonale du NB-HR risque sous traitement ciblé nous a permis de montrer que des modifications surviennent dans les cellules tumorales sous traitement, avec évolution des sous-clones et apparition de nouvelles mutations.

Troisièmement, tout cela ouvre une porte aux traitements ciblés, non seulement de deuxième, mais spécialement de première ligne. Seuls quelques biomarqueurs puissants ont été décrits pour prédire la réponse aux traitements, dont les anomalies du gène *ALK*. Nous avons exploré l'efficacité *ex vivo* et *in vivo* des inhibiteurs de *ALK*, seuls et en combinaison, dans quatre modèles PDX de NB-HR comportant une anomalie de *ALK*. La combinaison spécifique de lorlatinib (inhibiteur de *ALK*) et idasanutline (inhibiteur de *MDM2*) a montré une synergie spectaculaire dans un modèle *ALK* amplifié.

En conclusion, ce travail représente une nouvelle approche à l'étude de la résistance ainsi que la sensibilité aux traitements du NB-HR, qui a pour but ultime d'améliorer les stratégies thérapeutiques des enfants atteints de cette maladie. Nous avons pu mettre en évidence *ex vivo* par criblage de drogues à haut débit la cytotoxicité particulière des HDAC inhibiteurs dans le NB-HR. De plus, nous avons pu déchiffrer des événements génétiques sous-jacents à l'évolution clonale du NB-HR après traitement ciblé. Finalement, la combinaison lorlatinib et idasanutline apporte de l'espoir pour l'approche thérapeutique des NB avec des anomalies de *ALK*.

I - Introduction

1. Neuroblastoma

1.1 Epidemiology, staging, standard treatment and outcome

Neuroblastoma is an embryonal tumor that arises in the developing sympathetic nervous system. Its cell of origin is thought to be an incompletely committed precursor cell derived from neural crest tissues (Hoehner et al., 1996; Matthay et al., 2016; Dong et al., 2020; Jansky et al., 2021), resulting in tumors located in the adrenal glands and/or all along the sympathetic chain ganglia. Thus, it can present in the neck, chest, abdomen or pelvis. Neuroblastoma is mainly sporadic with, in most times, any evidence of predisposition or hereditary events.

Neuroblastoma is the most common cancer diagnosed during the first year of life, and its incidence is around 10 cases per million (Stiller and Parkin, 1992). The median age at diagnosis of neuroblastoma is 18 months, with 40% of patients younger than 12 months (London et al., 2005). The incidence steadily decrease over the first 10 years, with very rare onset at adolescent and adult age, in which it tends to be much more indolent, but lethal (Mossé et al., 2014). Indeed, the prognostic contribution of age to outcome in this disease is a key: patients younger than 18 months have a much better overall survival compared to older children (Cohn et al., 2009). The clinical behavior of neuroblastoma is dramatically heterogeneous, from spontaneous and complete regression (Hero et al., 2008; Brodeur, 2018) to very aggressive tumors. Indeed, high-risk neuroblastoma accounts approximately 15% of all childhood cancer deaths (Park et al., 2010). This diverse clinical presentation and course depend highly on the tumor biology, which is intimately related to age at diagnosis.

Multiple efforts have been done in the last years to develop a risk-classification algorithm for patients with newly diagnosed neuroblastoma which allows the stratification and treatment adaptation according to the different risk groups. The most widely accepted system currently used is the International Neuroblastoma Risk Group (INRG) staging system, which divides patients into four broad categories (very low risk, low risk, intermediate risk and high risk) according to the 5-year event-free survival rates of >85%, >75 to ≤85%, ≥50 to ≤75%, and <50%, respectively (Monclair et al., 2009). These categories were proposed on the basis of the analysis of (1) age at diagnosis, (2) INRG tumor stage, defining disease stages as local (L1 and L2, without or with image-defined risk factors, respectively) or metastatic (M and MS), (3) histologic category, (4) grade of tumor differentiation, (5) DNA ploidy, (6) segmental chromosomal alterations and (7) copy-number status of *MYCN* oncogene (Table 1). High-risk neuroblastomas account for nearly 50% of all newly diagnosed neuroblastomas (Cohn et al., 2009; Pinto et al., 2015). With the current advances in molecular characterization based on high-throughput techniques such as next-generation DNA and RNA sequencing, these risk groups are being redefined based on new molecular biomarkers and mechanistic pro-

cesses, with the identification of very low-risk, very high-risk or even ultra-high-risk subgroups (Saarinen-Pihkala et al., 2013; Peifer et al., 2015; Ackermann et al., 2018; Depuydt et al., 2018; Duan and Zhao, 2018; Morgenstern et al., 2018).

Risk group	INRG stage	IDRFs in primary tumor	Distant metastases	Age (months)	Histological category	Grade of differentiation	MYCN status	Genomic profile	Ploidy
Very-low	L1	Absent	Absent	Any	GNB nodular, NB	Any	-	Any	Any
Very-low	L1 or L2	Any	Absent	Any	GN, GNB intermixed	Any	-	Any	Any
Low	L2	Present	Absent	<18	GNB nodular, NB	Any	-	Favorable	Any
Low	L2	Present	Absent	≥18	GNB nodular, NB	Differentiating	-	Favorable	Any
Low	MS	Any	Present	<12	Any	Any	-	Favorable	Any
Intermediate	L2	Present	Absent	<18	GNB nodular, NB	Any	-	Unfavorable	Any
Intermediate	L2	Present	Absent	≥18	GNB nodular, NB	Differentiating	-	Unfavorable	Any
Intermediate*	L2	Present	Absent	≥18	GNB nodular, NB	Poorly differentiated, undifferentiated	-	Any	Any
Intermediate	M	Any	Present	<18	Any	Any	-	Any	Hyper-diploid
Intermediate	M	Any	Present	<12	Any	Any	-	Unfavorable and/or diploid	
Intermediate	MS	Any	Present	12-18	Any	Any	-	Favorable	Any
Intermediate	MS	Any	Present	<12	Any	Any	-	Unfavorable	Any
High	L1	Absent	Absent	Any	GNB nodular, NB	Any	+	Any	Any
High	L2	Present	Absent	≥18	GNB nodular, NB	Poorly differentiated, undifferentiated	+	Any	Any
High	M	Any	Present	12-18	Any	Any	-	Unfavorable and/or diploid	
High	M	Any	Present	<18	Any	Any	+	Any	Any
High	M	Any	Present	≥18	Any	Any	Any	Any	Any
High	MS	Any	Present	12-18	Any	Any	-	Unfavorable	Any
High	MS	Any	Present	<18	Any	Any	+	Any	Any

Table 1 (Matthay et al., 2016): Modified International Neuroblastoma Risk Groups. These criteria have been modified from the original report (Cohn et al., 2009) to account for emergent genomic data and current treatment approaches (Schleiermacher et al., 2010; Park et al., 2016). Favourable corresponds to absence and unfavourable to the presence of segmental chromosome alterations. +, amplified; -, non-amplified; GN, ganglioneuroma; GNB, ganglioneuroblastoma; IDRF, image-defined risk factor; INRG, International Neuroblastoma Risk Groups; NB, neuroblastoma. 2. Some clinical trial groups consider that patients with stage L2 neuroblastoma with unfavourable pathology who are >18 months of age should be treated as high-risk, as excellent prognosis was achieved with intensive chemotherapy, often followed by radiation and autologous haematopoietic stem cell transplantation.

Outcome of patients with low and intermediate-risk neuroblastoma is excellent and current efforts are directed to decrease early and late therapy-related toxicities in this group of patients, while maintaining its very good outcome. This is being evaluated currently in the SIOPEN LINES trial (Low- and Intermediate-Risk Neuroblastoma European Study; ClinicalTrials.gov identifier NCT01728155). On the contrary, high-risk neuroblastoma patients still have a very poor prognosis despite the very intensive treatment, slightly improved over the last 30 years. Indeed, the 5-year overall survival has improved from 29% in the 90's to 50% in patients diagnosed between 2005 and 2010 (Figure 1, Pinto et al., 2015, Oberthuer et al., 2015).

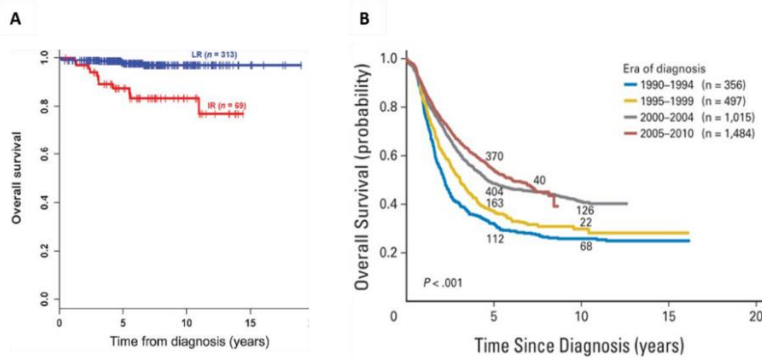


Figure 1: A (Oberthuer et al., 2015): Kaplan–Meier estimates for overall survival (OS) in a cohort of 382 non-high-risk neuroblastoma (HR-NB) patients. Five-year OS for patients of the low-risk (n=313) and intermediate-risk (n=69) cohorts was 0.98 ± 0.01 and 0.87 ± 0.04 respectively. B (Pinto et al., 2015): Probability of OS among 3,352 Children's Oncology Group (COG) patients with HR-NB diagnosed between 1990 and 2010 according to era. Five-year OS rates (+ SE) for patients diagnosed between 1990 and 1994, 1995 to 1999, 2000 to 2004, and 2005 to 2010 are $29\% \pm 0.02$, $34\% \pm 0.02$, $47\% \pm 0.02$, and $50\% \pm 0.02$, respectively.

This increase in overall survival is attributed, amongst others, to the progress in staging, introduction of myeloablative therapy and immunotherapy as well as improved local treatments. Currently, standard-of-care treatment strategy for high-risk neuroblastoma consists of three treatment blocks. First, induction, consisting on standard chemotherapy (to reduce tumor burden by shrinking the primary tumor and reducing metastases). Induction chemotherapy includes a rotary combination of several compounds (commonly carboplatin, cisplatin, etoposide, cyclophosphamide, doxorubicin, vincristine and topotecan). Second, consolidation treatment by high-dose –myeloablative– chemotherapy by busulfan and melphalan followed by autologous stem-cell rescue, and local control by surgical resection and external-beam radiotherapy of the primary tumor. This treatment phase is used to eliminate remaining disease. Finally, the postconsolidation phase includes anti-ganglioside 2 immunotherapy and cis-retinoic acid for the treatment of the minimal residual disease. The overall treatment takes approximately 1 year (Ladenstein et al., 2017, 2018; Morgenstern et al., 2018).

Whereas the majority of high-risk neuroblastoma patients primarily respond to this standard treatment, approximately 20% of patients progress early or are refractory to standard induction therapy. Furthermore, half of the patients who achieve remission undergo relapse of the disease, which is subsequently resistant to standard chemotherapy and frequently represents an incurable situation (Matthay et al., 1993, 1999; London et al., 2011). Indeed, patients who undergo relapse have a poorer median overall survival than patients with refractory disease (11 vs. 28 months respectively, Moreno et al., 2017).

1.2 Molecular characteristics of neuroblastoma

The clinical heterogeneity as well as the high metastatic rate and poor prognosis of high-risk neuroblastoma have led to intense research into its biology. This had two main objectives: on one hand, the identification of prognostic biomarkers to better stratify patients, and on the other hand, the identification of predictive biomarkers to find new molecular targets. Molecular biology has been used since the 1980s with the discovery that high-level amplifications of the *MYCN* oncogene were observed in approximately 20% of tumors. (Brodeur et al., 1984; Schwab et al., 1983; Seeger et al., 1985). *MYCN* amplifications have profound negative effects on the clinical outcome and are

associated with advanced tumor stage, tumor relapse and disease progression. Indeed, *MYCN* amplification is considered an independent high-risk factor, regardless of the stage of the disease or the age at diagnosis, and was the first biomarker to find its place in the algorithm of management of this disease in the INRG staging system. Since then, multiple efforts have been done to identify molecular biomarkers or therapeutic targets in order to improve the knowledge and, ultimately, the survival of the high-risk forms of the disease.

On the genomic level, other prognostic molecular biomarker considered in the INRG staging system are DNA copy-number alterations (CNAs). Tumor ploidy is one of the most significant prognostic markers for children less than 18 months old, and infants with hyperdiploid tumors have significantly increased survival (Look et al., 1991). With the arrival of array-based comparative genomic hybridization (aCGH), neuroblastoma CNAs have been segregated into two main global categories. On one hand, segmental chromosomal alterations (gains or losses of segments of chromosome arms) are higher risk and are associated with more clinically aggressive disease (Janoueix-Lerosey et al., 2009; Schleiermacher et al., 2010). Among segmental CNAs, frequent copy number losses occur at 1p, 3p, 4p, and 11q, while copy number gains occur recurrently on 1q, 2p, 7q, 11q13.3, 12q, and 17q. Interestingly, 1p loss and 17q gain are often associated to *MYCN* amplification, whereas 11q loss almost never co-occurs with *MYCN* amplification (Bown et al., 1999; Attiyeh et al., 2005). In addition, the acquisition of new segmental CNAs at relapse occur in both tumors that had or did not have a segmental genomic profile at diagnosis, giving strong evidences of the importance of segmental alterations in tumor progression (Schleiermacher et al., 2010). On the other hand, tumors presenting gains or losses of whole chromosomes are associated with excellent survival.

Overall, neuroblastoma has a low mutation burden, estimated at below 2 mutations per Mb of coding genome (Molenaar et al., 2012; Pugh et al., 2013; Gröbner et al., 2018; Hwang et al., 2019), and the number of somatic mutations at time of diagnosis is correlated with patient age (Fransson et al., 2020). Neuroblastoma is characterized by a heterogeneous mutation spectrum with few recurrently altered genes (Pugh et al., 2013; Brady et al., 2020). After *MYCN*, *TERT* is amongst the most frequent altered gene in neuroblastoma. Rearrangements affecting the upstream region of *TERT* transcription starting site are found in 10-17% of the cases and seem to appear exclusively in high-risk tumors (Peifer et al., 2015; Valentijn et al., 2015; Ackermann et al., 2018). *ATRX* loss-of-function (LoF) mutations account for approximately 10% of neuroblastomas and are characteristic of older patients. Actually, in adolescents 40% of neuroblastomas harbor *ATRX* LoF mutations whereas this aberration occurs in less than 20% of younger patients. This genetic feature is related to indolent course but poor outcome (Cheung et al., 2012). Both *MYCN* amplifications and *TERT* rearrangements lead to telomere maintenance by induction of telomerase, whereas *ATRX* LoF mutations induce telomere maintenance by activation of the alternative lengthening of telomeres (ALT) pathway. These three conditions identify three almost non-overlapping groups of high-risk neuroblastoma, each associated with very poor prognosis (Valentijn et al., 2015; Zeineldin et al., 2020) and has led to the proposition of a mechanistic classification of clinical phenotypes in neuroblastoma. Thus, patients whose tumors lack telomere maintenance mechanisms have an excellent prognosis, whereas the prognosis of patients whose tumors harbor telomere maintenance mechanisms (by telomerase

activation or ALT) is substantially worse. In addition, survival rates are lowest for neuroblastoma patients whose tumors harbored telomere maintenance mechanisms in combination with RAS and/or p53 pathway mutations (Figure 2, Ackermann et al., 2018). A recent study has shown that there is no difference in event-free or overall survival between patients with ALT-positive tumors stratified into high-risk and those predicted as low/intermediate risk, indicating that the current risk stratification is underestimating the poor prognosis of ALT-positive tumors (Hartlieb et al., 2021). Other reports have pointed out the importance of other chromatin remodeling and epigenetic modifier genes (such as *SMARCA4*, *MLL3* or *ARID1B*) in neuroblastoma oncogenesis, which would account for 8% of neuroblastomas (Bellini et al., 2019).

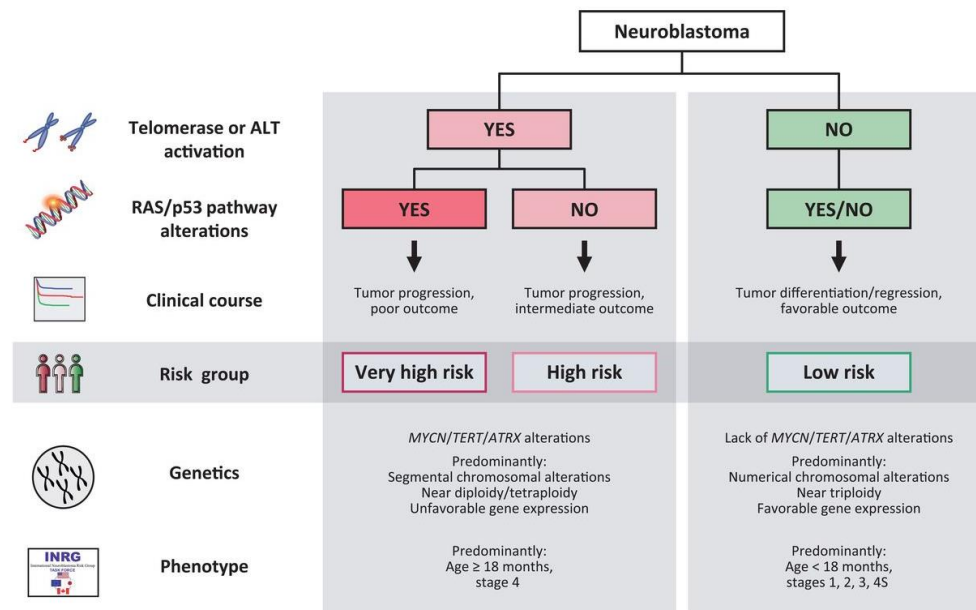


Figure 2 (Ackermann et al., 2018): Representation of the proposed mechanistic definition of clinical neuroblastoma subgroups. The classification is built on the presence or absence of telomere maintenance mechanisms and RAS or p53 pathway mutations. In addition, associations with other genetic features (*MYCN*, *TERT*, and *ATRX* alterations; segmental copy number alterations; tumor cell ploidy; gene expression-based classification) and clinical characteristics (age at diagnosis, stage of disease) are indicated.

Activating *ALK* mutations are found in approximately 8% of newly diagnosed neuroblastomas (George et al., 2008; Janoueix-Lerosey et al., 2008; Bellini et al., 2015a, 2015a). *ALK* is a tyrosine kinase receptor which plays an important role in the RAS/MAPK, PI3K/AKT and JAK/STAT pathways (Osajima-Hakomori et al., 2005). Three mutation hotspots in its kinase domain (F1174, R1275 and F1245) represent 85% of all forms of *ALK* mutations (Pugh et al., 2013; Bresler et al., 2014) and the presence of the F1174 *ALK* hotspot mutation is more often associated to *MYCN* amplification (Bellini et al., 2015a). *ALK* can also be activated by *genomic* amplification in 1-2% of neuroblastomas, almost exclusively associated with co-amplification of *MYCN*, conferring poorer prognosis (De Brouwer et al., 2010; Bellini et al., 2021, *in press*). The incidence of *ALK* mutations increases in relapsed neuroblastomas, accounting for about 20% of the relapsed cases. Indeed, relapsed neuroblastomas are enriched in targetable mutations, especially of the RAS-MAPK pathway (Schleiermacher et al., 2014; Eleveld et al., 2015; Padovan-Merhar et al., 2016). Furthermore, mutations in the RAS pathway appear in about 4% of the cases, including *PTPN11*, *NF1*, *NRAS*, *KRAS*, and *BRAF* genes (Brady et al., 2020).

Other recurrent altered genes in neuroblastoma, observed in about 10% of the cases, are *SHANK2* (frequently disrupted by structural variants, Lopez et al., 2020) and *PTPRD* (structural

variants and focal deletions). Finally, *TP53* and *FGFR1* mutations are observed in about 1% of neuroblastomas. Recurrent somatic alterations are summarized in Figure 3 (Brady et al., 2020).

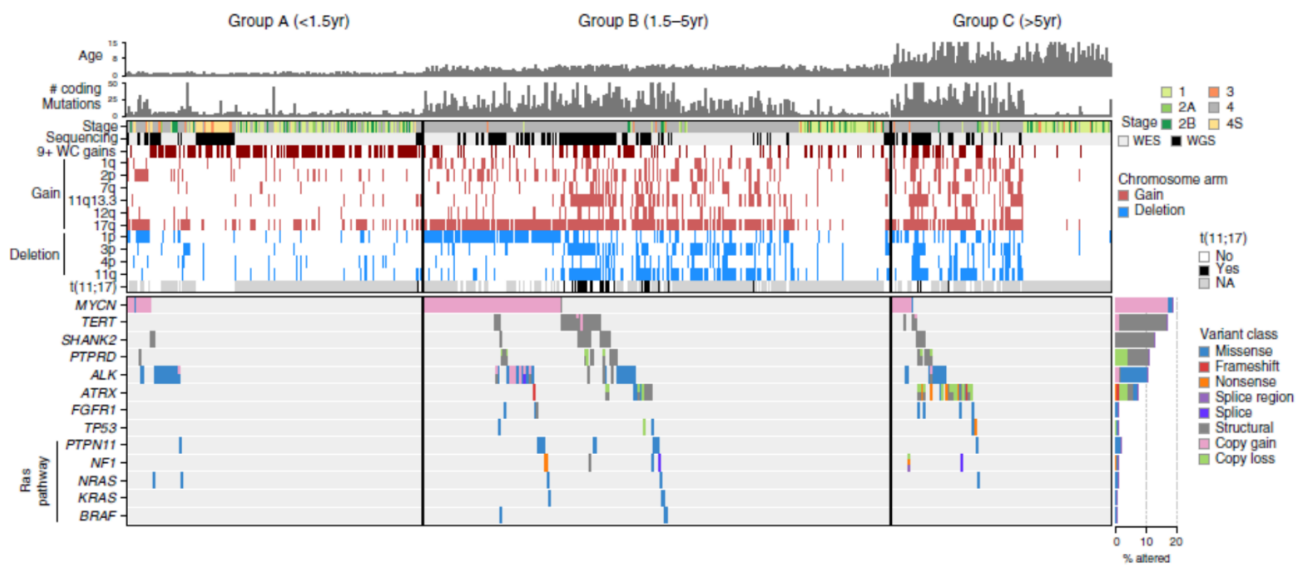


Figure 3 (Brady et al., 2020) : Recurrent somatic alterations by age group in neuroblastoma. Top, age at diagnosis and number of coding mutations in each of 685 neuroblastoma samples (662 diagnosis, 23 relapse) sequenced by WGS or WES, with samples categorized into <18 months of age at diagnosis (group A, n = 206), 18 months to 5 years (group B, n = 325), and 5 or more years (group C, n = 154). Middle, segmental chromosome copy changes and structural variants; blue indicates segmental copy loss, red indicates segmental copy gain, white indicates no change. 9+ WC gains samples (gain of nine or more whole chromosomes) are shown in dark red. Bottom, somatic variants in driver genes.

Beyond the genetic alterations reported in neuroblastoma, a large number of studies have focused on the analysis of differential expression patterns in neuroblastoma, in order to identify the ones that might enable to distinguish patients with different clinical courses and thus define different prognostic groups in high-risk disease. Several studies have identified gene expression signatures which reliably correlated to patient outcome (Asgharzadeh et al., 2006, 2012; Vermeulen et al., 2009; Fardin et al., 2010; Oberthuer et al., 2010; Garcia et al., 2012). However, there almost no overlap between the genes of the different signatures rendering cross-study comparisons unfeasible.

Finally, hereditary neuroblastoma is rare and occurs in approximately 1-2% of cases. It is usually inherited in an autosomal dominant manner, with incomplete penetrance, similarly to retinoblastoma, following the classic two-hit model (Knudson and Strong, 1972). Germline *ALK* gain-of-function or *PHOX2B* loss-of-function mutations (Trochet et al., 2004; Janoueix-Lerosey et al., 2008; Bourdeaut et al., 2012) predispose to the majority of inherited neuroblastoma cases. Furthermore, genome-wide association studies (GWASs) have identified that three polymorphisms (rs6939340A>G, rs4712653T>C, and rs9295536C>A) within the *CASC15* gene at 6p22 are significantly associated with neuroblastoma susceptibility (Maris et al., 2008). In addition, common variations in the *BARD1* gene at 2q35 are specifically associated with high-risk neuroblastoma, whereas polymorphisms within *DUSP12* at 1q23.3, *DDX4* and *IL31RA* at 5q11.2, and *HSD17B12* at 11p11.2 were associated with low-risk neuroblastoma (Nguyễn et al., 2011).

1.3 Cell plasticity and role of epigenetics in neuroblastoma

Cell plasticity, described as the ability of cells to adopt different identities along a phenotypic spectrum, has been described since decades in neuroblastoma to decipher the cell of origin of the disease (Cooper et al., 1992). Tumor cells are exposed to diverse environmental conditions (metabolic, signaling molecules, stromal elements, therapeutic agents), which can fuel changes in the cellular phenotype. Such changes may involve genetic alterations, but they more commonly involve transcriptional and especially epigenetic fluctuations. Thus, the occurrence of many cancers is the result of the accumulation of genetic and epigenetic changes. Unlike genetic alterations, epigenetic changes are reversible and can dynamically respond to diverse signals (Inomistova et al., 2019) without changes in the DNA sequence. The term “epigenetic” defines all changes in gene expression and chromatin structure that are not coded in the DNA sequence itself. Epigenetic modifications consist mainly of DNA methylation, histone modification, chromatin reorganization, and RNA-associated silencing. For example, DNA-methylation in neuroblastoma reveals that silencing of caspase-8 and RAS-association domain family 1 isoform A (*RASSF1A*) are important in the development and progression of the disease. Both genes are often found to be methylated in primary neuroblastoma samples and the methylation status of these genes is significantly associated with survival (Decock et al., 2011).

Furthermore, epigenetic modifications are well known as regulators of tissue-specific gene expression, cellular differentiation, genomic imprinting, and X-chromosome inactivation (Bollati and Baccarelli, 2010). Although loss of normal cell identity and function is intrinsic to the malignant process, cancer cells undergo further phenotypic changes during tumor progression and treatment. The resulting flexibility in cell state can facilitate multiple aspects of tumor progression, including tumor initiation and metastasis, immune evasion, and chemoresistance. Consequently, elucidating the mechanisms by which cancer cells exploit plasticity to manage with selective pressures may lead to novel therapeutic opportunities (Yuan et al., 2019). In this sense, super-enhancer-associated transcription factor (TF) networks have been shown to underlie lineage identity. Indeed, most neuroblastomas include two types of tumor cells with divergent gene expression profiles: undifferentiated mesenchymal cells (associated to *PHOX2B*, *HAND2* and *GATA3* TRs) and committed adrenergic cells (associated to *AP-1* TF), which can interconvert and resemble cells from different lineage differentiation stages. A third intermixed type has also been identified. These different cell states, identified by Chromatin Immunoprecipitation Sequencing (ChIP-seq) analysis, are linked to specific super-enhancer-associated TF network. These findings could have clinical impact, since mesenchymal cells seem more chemoresistant and are enriched in post-therapy and relapse tumors. This plasticity and the relative resistance of mesenchymal cells to therapeutic agents may facilitate escape from current therapies, and targeted therapy against this cell subtype could represent a method to impede relapse (Boeva et al., 2017; van Groningen et al., 2017). In conclusion, these findings show that intratumoral heterogeneity in neuroblastoma is not a random process but is brought about by consistent regulatory programs.

2. Intratumor heterogeneity and clonal evolution

Advances in molecular diagnostics and NGS technologies have been key for uncovering the genetic process of conversion from a nonmalignant to a malignant cell, which occurs through the sequential acquisition of alterations that lead to cellular proliferation, evasion of cell death signals, induction of angiogenesis and activation of tissue invasion and metastasis programmes (Hanahan and Weinberg, 2011). The often stochastic nature of cancer initiation reinforces the notion that the development and progression of cancer does not follow a fixed course, but should rather be viewed as an integrated destabilization of key cellular processes (Hanahan and Weinberg, 2011; Dagogo-Jack and Shaw, 2018). As tumor evolves, cancer cells generate a molecularly heterogeneous bulk of different cells with different molecular signatures which in turn will be associated with differential anticancer sensitivity or resistance. This heterogeneity can be the result of genetic, transcriptomic, epigenetic or phenotypic changes.

At the population level, tumor heterogeneity can be divided into intertumoral and intratumoral heterogeneity. Intertumoral heterogeneity refers to heterogeneity between patients with the same histological type, which results from patient-specific factors (germline variations, somatic mutations and environmental factors). Intratumoral heterogeneity refers to heterogeneity among the tumor cells of a single patient. At the same time, intratumoral heterogeneity can have spatial (irregular distribution of genetically different subpopulations) and temporal (dynamic genetic variations over time) characteristics. With the development of the personalized approaches, genetic alterations have been therapeutically exploited using molecularly targeted agents. Despite important initial responses, almost all pediatric cancers develop resistance to targeted therapies. This observation lends support to the current understanding of cancer as a dynamic, rather than molecularly stagnant, disease. Indeed, the findings of multiple studies across a diverse range of cancer types suggest that intratumoral heterogeneity drives the evolution of cancers and fosters drug resistance (Bhang et al., 2015).

Sequencing of spatially or temporally distinct tumor regions has begun to uncover the intricate extent of diversity within tumor (McGranahan and Swanton, 2017). These studies have revealed that the degree of ITH can be highly variable, with between 0 and over 8,000 thousand coding mutations found to be heterogeneous within primary tumors or between primary and metastatic or recurrence sites (Johnson et al., 2014). Despite the biases regarding differences in sampling procedures, tumor stage or sequencing depth, it is clear that certain tumors, such as melanoma and lung cancer, harbor a significantly larger homogeneous coding mutational burden (related to ultraviolet light and tobacco smoke, respectively) than other cancers, such as neuroblastoma, which harbors one of the highest ITH proportion ([Alexandrov et al., 2020](#); [Eleveld et al., 2015](#); [Figure 4, McGranahan & Swanton, 2017](#)).

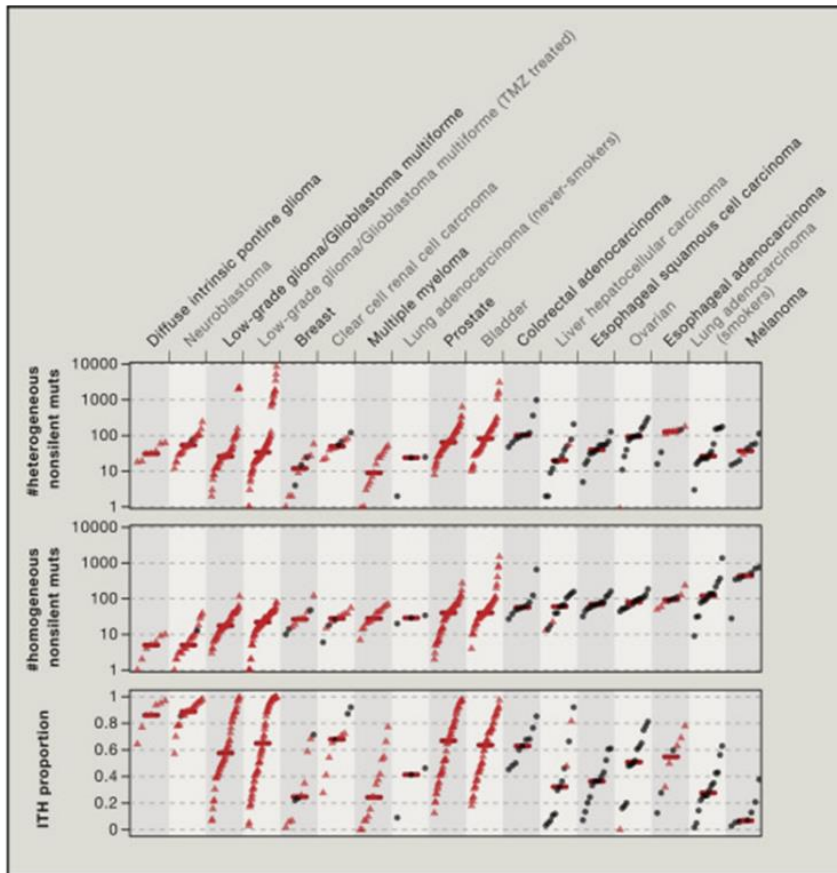


Figure 4 (McGranahan and Swanton, 2017): Heterogeneity of non-silent mutations from multiple-sample sequencing across a range of cancer types. For each tumor type, each point represents one tumor, with the proportion of heterogeneous mutations (ITH proportion), as well as the absolute numbers of heterogeneous and homogeneous non-silent mutations. Black circles represent treatment naive tumors, with red triangles indicating tumors that have received treatment. These data are restricted to non-silent mutations and does not include copy-number alterations.

2.1 Intratumor heterogeneity

2.1.1 Spatial genetic heterogeneity

The uneven distribution of genetically diverse subpopulations within a tumor (in a single anatomical location or across different sites) is known as spatial heterogeneity. This spatial heterogeneity can result in the presence of different key molecular alterations unequally distributed across different regions of the tumor (Gerlinger et al., 2014; Yates et al., 2015; Hao et al., 2016). An example is the coexistence of *MYCN*-amplified and non-*MYCN*-amplified tumor cell clones described in neuroblastoma, associated with worse prognosis (Berbegall et al., 2018; Campbell et al., 2020). Alternatively, spatial heterogeneity might also manifest as the ubiquitous presence of key molecular driver alterations across all tumor cells, with diverse unequally distributed additional molecular alterations (Harbst et al., 2016). These findings could have a prognostic value, since tumors with high levels of copy-number heterogeneity might predispose patients to inferior clinical outcomes (Jamal-Hanjani et al., 2017).

Our current understanding of the extent of intratumoral heterogeneity in cancers is largely derived from analysis of bulk tumor specimens; however, most bulk specimens consist of a mixture of nonmalignant cells and diverse subpopulations of cancer cells. Recognizing the limitations of this

type of analysis, several studies have used single-cell sequencing for the isolation and characterization of individual cells within a mixed population. The consequences of heterogeneity at the single-cell level are under study and several published studies suggest that a substantial level of genetic diversity exists between individual cancer cells (Malikic et al., 2019; Nam et al., 2021).

In addition, spatial heterogeneity is also a common finding when comparing spatially distinct disease sites. The degree of genetic discordance between the primary tumor and metastatic sites might reflect whether the metastases occurred as late events or arose through dissemination early in the course of tumor development (Birkbak and McGranahan, 2020). In addition, even when cancer cells at primary and metastatic sites share a common ancestor, site-specific factors could promote genetic divergence after initial colonization of metastatic sites (Hu and Curtis, 2020; Thole et al., 2020).

2.1.2 Temporal heterogeneity

Data from studies employing serial biopsy sampling to characterize the evolution of tumors have demonstrated that treatment can alter the molecular composition of tumors over time by creating shifts in the mutational spectrum. Both targeted therapies and chemotherapies influence the path of cancer evolution. For example, the treatment of glioblastoma with temozolomide can enrich for transition mutations in mismatch repair genes, leading to the development of hypermutated phenotype (Daniel et al., 2019). Even in the context of a clonal driver, resistance to targeted therapies is frequent in the advanced disease setting and may be driven by the selection of resistance cancer cells present at low frequencies prior to therapy or may evolve through *de novo* mutations that are acquired during therapy.

Furthermore, taking in account that cancer is dependent on the activity of specific pathways, genetic resistance mechanisms to targeted therapy show how genomic instability enables tumors to create the appropriate subclone, which contains the (re)activated pathway (Misale et al., 2014). Combination therapy approaches that act through distinct pathways may help circumvent these different problems, taking in account that the feasibility of these approaches may be complicated by the toxicity of combination therapy, as well as the occurrence of mutations that confer resistance to multiple drugs.

Since the genomic complexity of a tumor generally increases with exposure to sequential systemic therapies, if the subclonal diversity within the tumor is viewed as a snapshot, rather than longitudinally, it will provide little information about the future evolutionary routes that subclonal populations might take. A greater understanding of the evolutionary timings and 'life histories' of tumors might shed light on the most clinically significant subclones and reveal common rules that govern tumor evolution both within and across cancer subtypes (Figure 5, Hiley et al., 2014). Consequently, serial characterization of tumors at multiple timepoints should be necessary in order to accurately capture the various temporal shifts that take place during clonal evolution. However, some drawbacks limit the large-scale adoption of parallel tumor biopsies for characterizing a neoplastic mass. First, tissue biopsies are invasive. Second, tumor tissues might be scarcely available

or else not suitable for providing a high yield or good quality of DNA for the new sequencing techniques. Moreover, there is the need of repeatable methods to monitor the tumor evolution over the disease progression in real time. These issues can be overcome by the use of liquid biopsy, now recognized as a powerful real-time approach for the comprehensive imaging of genomic heterogeneous tumors at given times (Chicard et al., 2018a; Venesio et al., 2018).

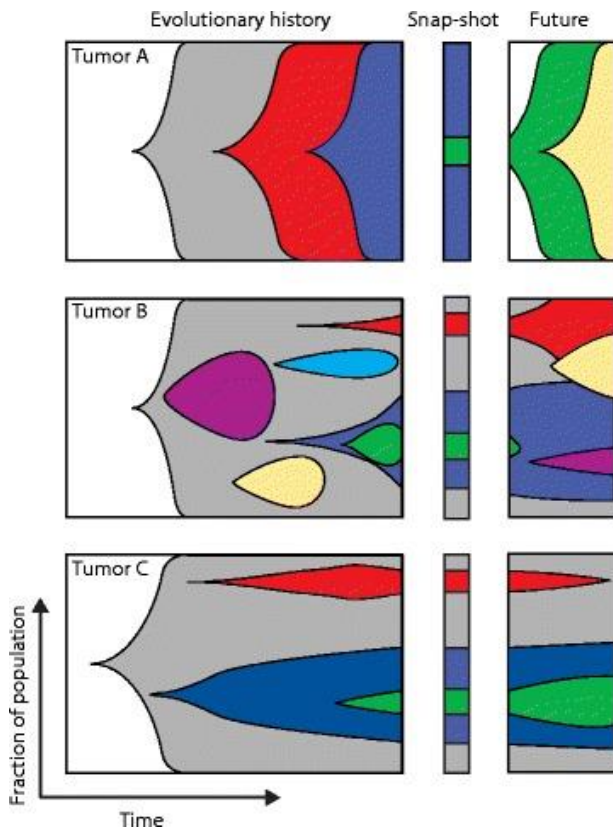


Figure 5 (Hiley et al., 2014): Evolution of three hypothetical tumors. The left panel shows the evolutionary history of each tumor, the middle panel represents a snapshot of the tumor at a given time, and the right panel shows the potential future development. Tumor A shows a linear evolution pattern; tumors B and C display a branched pattern. Single snapshots of Tumors B and C may suggest that they have identical evolutionary processes, but their past and future evolution actually follow different patterns.

2.2 Origins of intratumoral heterogeneity

2.2.1 Genomic instability

Genomic instability is defined as a process prone to genomic changes or an increased propensity for genomic alterations, that can be originated from exogenous factors (ultraviolet radiation, tobacco smoke) or aberrations in endogenous processes (DNA replication, DNA repair, oxidative stress). A particular way to study the mutational landscape of tumors is by the analysis of the biological processes generating these mutations. Different mutational processes often generate different combinations of mutation types, termed “signatures”. With the advent of NGS techniques, thousands of somatic mutations can now be identified in a single tumor sample, allowing to decipher mutational signatures even when several mutational processes are operative. In 2013, Alexandrov et al. developed an algorithm to extract mutational signatures from catalogues of somatic mutations. As part of the Pan-Cancer Analysis of Whole Genomes (PCAWG) Consortium of the International

Cancer Genome Consortium (ICGC) and The Cancer Genome Atlas (TCGA), Alexandrov et al. have characterized mutational signatures using 84,729,690 somatic mutations from 4,645 WGS and 19,184 WES sequences that encompass most types of cancer, and identified 49 single-base-substitution, 11 doublet-base-substitution, 4 clustered-base-substitution and 17 small insertion-and-deletion signatures (Alexandrov et al., 2020). For example, DNA cytosine deamination, resulting from upregulation of enzyme APOBEC3B, contributes to mutagenesis in approximately half of all human cancers. The APOBEC mutational signature is particularly enriched in the later stages of tumor development and becomes more prevalent after exposure to cytotoxic chemotherapy (Swanton et al., 2015). Signature 18 has predominantly been detected in neuroblastoma and is rare in most other cancers (Alexandrov et al., 2015). It has been causally associated with excessive generation of reactive oxygen species (ROS) (Pilati et al., 2017), which primarily induces C>A transversions. Signature 18 can be both an early event in neuroblastoma, causing truncal mutations, and an on-going mutational event causing relapse-specific mutations. Nevertheless, it seems there is an intrinsic and stable propensity of specific neuroblastoma tumors to either possess or lack the signature 18 mutational process (Brady et al., 2020).

Whereas genomic instability is not a major characteristic in neuroblastoma, changes in chromosome structure and number over time occur frequently, rather than point mutations. This process, termed chromosomal instability, arises from segregation errors that occur during cell division, which might promote genetic diversity by upsetting the balance between activation of oncogenes and tumor suppressors (Holland and Cleveland, 2009; Schleiermacher et al., 2010). Interestingly, in most cases, copy number alterations evolutionarily precede the acquisition of most point mutations in neuroblastoma, reinforcing the importance of copy number gains in early neuroblastoma pathogenesis (Brady et al., 2020).

2.2.2 Clonal evolution

Various models have been proposed to explain how clonal diversity is generated and maintained, although the more recognized is the clonal evolution and/or selection. This model, developed by Nowell in 1976, hypothesizes that tumor initiation is due to the stochastic accumulation of genetic changes in a previously normal cell, allowing it to become a tumor-causing cell and furthers its development to more malignant states. Thus, it is an evolutionary process in which the genomic instability of the expanding tumor population creates additional genetic diversity that is subjected to evolutionary selection pressures, resulting in the sequential emergence of increasingly genetically abnormal and heterogeneous subpopulations (Nowell, 1976). In addition, the appearance of branching evolution denotes the divergent propagation of multiple subclonal tumor cell populations that share a common ancestor. Many solid tumors adopt a branched pattern of evolution, whereas a linear pattern appears in certain hematological malignancies (Hiley et al., 2014).

Globally, clonal evolution can arise either stochastically or via distinct biological mechanism which can in turn generate treatment-sensitive and -resistant subclones. The elimination of sensitive subclones reduces the competitive forces imposed by cancer dominant subclones on minor

subclones. This so-called “competitive release” allows treatment-resistant minor subclones to repopulate and drive the relapsed tumor, which may be distinct from the treatment-naïve tumor. (Enriquez-Navas et al. 2016).

Nevertheless, the assumption that clonal subpopulations must always be in competition has been challenged by the results of studies showing that cooperation between distinctly different subclones might be necessary for tumor propagation or relapse. Indeed, cooperation can be metabolically costly but evolution and survival are more efficient, especially in a changing environment, when diversity and heterogeneity are high. Insights from patient’s tumors have revealed the presence of multiple independent neoplastic driver subclones that could re-establish tumor heterogeneity after therapy and lead to disease relapse. Furthermore, there is increasing evidence of transient clonal cooperation between neoplastic and benign subclones, which can also lead to tumor recurrence. (Tabassum and Polyak, 2015; Parsons, 2018; Esposito, 2019).

2.3 Evidences of clonal evolution in neuroblastoma

Many efforts have been put to unravel the evolutionary biology of neuroblastoma and the development of NGS techniques has allowed deciphering, at least in part, the complexity of neuroblastoma genetics. It is now well known that a diversity of populations of individual cancer cell clones coexist within a same tumor. Indeed, spatial heterogeneity with different clones within a neuroblastoma, or even differences in the genomic profile between different sites or between primary and metastatic sites, have been described, concerning *MYCN*, *SCA*, or mutations including *ALK* (Squire et al., 1996; Bellini et al., 2015; Chicard et al., 2016).

During treatment, clonal evolution may occur, as well as drug resistance (acquired drug resistance), leading to relapse if tumor cells are not fully eliminated by myeloablative and maintenance therapies. It remains a challenge to understand the complexity of the molecular events leading to the different biology of neuroblastoma development, especially in those that relapse. On the genomic level point of view, in relapse neuroblastomas there is a higher number of chromosome breakpoints (Schleiermacher et al., 2010) and homozygous deletion of *CDKN2A* is a recurrent event (Thompson et al., 2001). As already mentioned, the mutational load in neuroblastoma is characteristically low. The comparison of paired diagnosis and relapse neuroblastoma reveals that relapse tumors retain the majority of the mutations identified at diagnosis and that a small fraction ($\approx 10\%$) disappear from diagnosis to relapse (Schramm et al., 2015). Furthermore, relapse neuroblastomas show increased number of mutations, with specific enrichment in RAS/MAPK pathway mutations (including genes such as *ALK*, *NRAS*, *HRAS*, *NF1*, *FGFR1*, *PTPN11* and *BRAF*, Eleveld et al., 2015) and harbor new and distinct mutational signatures (Schramm et al., 2015). Thus, the mutational burden of relapse neuroblastoma is higher compared to the diagnosis (but remains low compared to other tumors, especially adult malignancies), and harbor specific events as well as shifts in mutational signatures. Interestingly, a significant number of mutations that appear at relapse are not *de novo* mutations but are present at the time of diagnosis at very subclonal level, with allele frequencies under

the detection limit of the sequencing technique, highlighting the importance of high-depth NGS techniques for the better understanding of this disease. This is a major finding, since these subclones present at relapse can be resistant to a particular treatment and then grow when therapy has eliminated the competitive subclones. In addition, *de novo* mutations at relapse may be induced by the treatment (Venkatesan et al., 2017). Thus, on one hand, the therapeutic intervention reduces the subclonal spectrum while, on the other hand, increases the total number of mutations at relapse.

Given the particular clonal architecture of a given tumor, a single tumor sample at a specific timepoint will give only partial information of the whole disease and will not give any information about the clonal evolution. Furthermore, a single sample will not inform on treatment responses and prediction of treatment failure upon individualized therapy. Indeed, inclusion of patient-specific genomic profiles for the selection of therapeutic targets would have to take into account sub-clonal genetic diversity. These technical limitations can be overcome by serial plasma samples for the study of clonal evolution by the analysis of cfDNA, which serves either for the determination of copy-number variations as well as SNVs. Indeed, modelization of mutated allele fractions in sequential cfDNA samples or neuroblastoma patients has been proven to allow the description of patterns of clonal evolution (Chicard et al., 2016, 2018a).

Taking advantage of their expertise in ctDNA analysis, the French national program MIC-CHADO (Molecular and Immunological Characterization of High-risk Childhood Cancer at Diagnosis, NCT03496402), promoted by the Institut Curie is being applied to children and adolescents with high-risk cancers at the time of diagnosis and is currently under investigation. Besides the searching for therapeutic targets, the principal objective is to study the clonal evolution based on sequential ctDNA analysis from the time of diagnosis in high-risk pediatric cancers, including high-risk neuroblastoma patients. Sequential ctDNA studies would further elucidate mechanisms of clonal evolution, tumor progression, and therapy resistance in high-risk pediatric cancers (Schleiermacher, 2020).

3. Molecular therapeutic targets

3.1 Precision medicine programs in Pediatric Oncology

Improvements in outcome for children and adolescents with cancer have been seen over the past 4 decades. Indeed, today more than 85% of these patients are alive 5 years after initial diagnosis. (Howlander et al., 2021). However, the overall success of pediatric oncology is largely due to excellent outcomes in the treatment of more common cancers and further major improvements in treatment for high-risk pediatric patients are imperative. This is the case of high-risk neuroblastoma, for which a ceiling has been reached in terms of treatment intensity and toxicity, and therefore novel strategies, such as targeted therapies, are needed.

Targeted treatment has been developed through the identification of disrupted pathways that drive the growth and progression of cancer, and the generation of specific and potent inhibitors of key proteins in these pathways. This strategy is most successful for the treatment of cancers that are dependent on key genetic alterations, which are referred to as 'oncogenic drivers', leading to aberrant proteins that are susceptible to be inactivated by specific molecules. Targeted therapies can be broadly divided into two classes: small molecules –predominantly tyrosine kinase– and monoclonal antibodies. The small molecules typically block pathways that are continuously activated in cancer cells. The tyrosine kinase inhibitors are the most common and work by inhibiting kinases that phosphorylate key proteins to activate signal transduction pathways. They are denoted by the suffix –nib, and are typically developed for oral administration. Monoclonal antibodies target cell surface molecules, usually receptors, or their ligands. Due to their large size, limited membrane permeability, and limited stability toward gastrointestinal protease activity, they are most often administered by intravenous injection.

The development of highly selective molecules, mostly and originally for adult diseases, targeting the specific proteins encoded by genetic alterations has had variable success to date. For example, the use of EGFR or ALK inhibitors in EGFR-mutated or ALK-rearranged non-small cell lung cancer (Pao et al., 2004; Kazandjian et al., 2014) or BRAF/MEK inhibitors in *BRAF*^{V600E}-positive melanoma (Chapman et al., 2011; Hauschild et al., 2012) has been a notable clinical benefit. This is in contrast with inconstant clinical activity of the same agents in other diseases despite similar molecular profiles, such as BRAF-inhibitors in *BRAF*^{V600E}-positive gliomas (Kaley et al., 2018; Nobre et al., 2020) In addition, the efficacy of targeted compounds has been limited due to the complexity of tumor biology and intratumor heterogeneity (Kummar et al., 2015) and the presence of primary or the emergence of acquired resistance mechanisms by selection pressure (Lin and Shaw, 2016). The development of NGS techniques, the identification of new drivers or most recently the analysis of circulating-free DNA (cfDNA), enable the better selection of patients and targeted drugs. Nevertheless, there is still limited understanding of the relevance of identified genomic events to define “actionable mutations” as strong biomarkers that can be successfully targeted (Carr et al., 2016). Indeed, in certain situations, blocking a particular pathway can induce adaptive changes in the cell, which will

lead to subsequent modifications, in such a way that the blockage of the molecule will be compensated.

In pediatric tumors, only few druggable targets exhibit high evidence of target-guided efficacy. A prototypic example is the implementation of the kinase inhibitor imatinib directed against *BCR-ABL1* fusions, which in clinical practice has revolutionized treatment of adult and pediatric chronic myeloid leukemia patients, leading to dramatically improved outcome with limited toxicities. In pediatric oncology, there is growing evidence that the use of BRAF inhibitors in *BRAF*^{V600E}-positive low-grade glioma results in robust and durable responses as well as increased progression-free survival (Nicolaidis et al., 2020; Nobre et al., 2020). *NTRK* fusions are oncogenic drivers of a histologically diverse group of pediatric tumors which can be successfully treated with NTRK inhibitors (Drilon et al., 2018). Finally, ALK inhibitors have demonstrated sustained overall responses in anaplastic large cell lymphomas and inflammatory myofibroblastic tumor harboring *ALK* fusions. The discovery of oncogenic activation of *ALK* in neuroblastoma suggested that this cancer could be potentially be treated with ALK inhibitors. However, whether these compounds could show survival benefit in *ALK*-driven neuroblastoma patients is uncertain and is currently under study.

Precision medicine trials, defined as the molecular profiling of tumors to identify targetable alterations, have been run for adult cancers since about 20 years (Phillips, 2020). While great efforts are being made to establish similar strategies in pediatric malignancies, a number of challenges have to be overcome to achieve the goal of molecular precision therapies in children with cancer (Worst et al., 2016; Harttrampf et al., 2017; Pincez et al., 2017). First, the mutation rate in pediatric tumors is low compared to adult malignancies and the mutation spectrum is heterogeneous in most entities. Considering the low incidence of pediatric tumors, the resulting low patient numbers is a challenge for the development of clinical trials. Second, many of the genetic alterations that are known to be drivers in pediatric cancers are currently not actionable by available drugs, such as alterations of *MYCN* or *TERT* in high risk neuroblastoma. Third, ethical considerations have to be taken into account (Fischer, 2018).

Indeed, the enrollment of pediatric patients in clinical trials has been subject of debate since years, which balances between the protection of children, and the need of research in pediatric diseases (Sammons and Starkey, 2012). Also, legal aspects, as the child is unable to provide legally binding consent, the parent(s)/legal representative are required to provide consent on the behalf of the child for participation. Finally, since molecular precision medicine studies using NGS techniques need the sequencing of germline DNA, there is no consent about how to manage potential germline variants identified, especially those of unknown clinical significance. Recognition of deleterious germline variants is essential not only for optimal care of the patient with cancer but also to initiate cascade genetic testing in at-risk family members who also may carry the familial mutation (DeLeonardis et al., 2019). Indeed, the use of genomic profiling has led to the discovery of potential germline abnormalities in approximately 10% of patients (Schrader et al., 2016; Zehir et al., 2017).

Several pilot pediatric oncology studies have explored the feasibility and use of genomics-driven precision medicine –two of them conducted in France–, and provided the foundation for pur-

suing this approach. The Institut Curie published their 1-year experience of prospective genetic analysis and molecular biology tumor board discussions for targeted therapies in pediatric solid tumors (Pincez et al., 2017). They studied 60 pediatric patients with poor prognosis or relapsed/refractory solid tumors in which tumor molecular profiling was performed with panel-based NGS and aCGH. The most recently available tumor tissue was analyzed but in the case in which there was inadequate material, a new biopsy was not requested and the initial diagnostic biopsy specimen was used. A potentially actionable finding was defined as a molecular alteration in a targetable gene known to be pathogenic. Molecular profiling was feasible in 58 patients, with 23 having a potentially actionable finding. Six of the 23 patients received a matched targeted therapy. Despite having a targetable lesion, four patients could not receive therapy owing to lack of available clinical trials with the agents. The Institut Gustave Roussy published also in 2017 a feasibility trial [Molecular screening for cancer treatment optimization (MOSCATO-01)] in which they prospectively characterized genomic alterations in recurrent or refractory solid tumors of pediatric patients to select a targeted therapy. Following treatment failure, patients underwent tumor biopsy or surgical resection of primary or metastatic tumor site. These newly acquired samples were analyzed by aCGH, panel based NGS, WES and RNAseq. Biological significance of the alterations and suggestion of most relevant targeted therapies available were discussed in a multidisciplinary tumor board. Seventy-five patients were included with 69 having a successful molecular analysis and 60% having an actionable alteration. Fourteen patients received 17 targeted therapies (Harttrampf et al., 2017).

In the light of these (and other) pilot studies, several trials at more large scale have been developed in several countries. The NCI-COG Pediatric MATCH (National Cancer Institute-Children Oncology Group Pediatric Molecular Analysis for Therapy Choice) trial (NCT03155620) is a nationwide umbrella-basket hybrid phase II trial at large cancer centers across the United States. This trial, which was open in 2017, enrolls children and adolescents with relapsed/refractory solid tumors, lymphomas, or histiocytoses, who are assigned to an experimental targeted treatment based on the genetic abnormalities determined by NGS targeted assay of more than 4000 different mutations (including SNVs, indels, copy number alterations and gene fusions) across more than 140 genes. The trial was developed to address the issue of whether a drug, targeted to a specific molecular abnormality, could produce responses or prolonged stable disease across the spectrum of cancer types in which the molecular abnormality is found. It was designed as a master protocol for molecular screening, with multiple associated phase 2 subprotocols or "arms" that could be added or closed without affecting the major trial. Currently, 12 subprotocols are assessing the efficacy of 12 targeted drugs, including HRAS, NTRK, FGFR, EZH2, ALK, BRAF, and PI3K/mTOR inhibitors, among others (Allen et al., 2017; Seibel et al., 2017).

The MAPPYACTS (Molecular Profiling for Pediatric and Young Adult Cancer Treatment Stratification, promoted by Gustave Roussy in France, NCT02613962) European program is being applied to children and adolescents with cancer at the time of relapse. This study started in 2016, has now included more than 750 pediatric patients with recurrent/refractory malignancies. Patients enrolled undergo tumor biopsy/surgery for molecular characterization by WES and RNAseq. Results are reviewed weekly in a molecular tumor board (MTB) followed by discussion with the treating physicians in a clinical MTB (Figure 6). From February 2016 to October 2018, 500 patients from France, Italy and

Ireland were included. Molecular profiling was performed in 88% of the patients and was contributive in 90 of them%. For 70% of the patients with contributive results, there was at least one genetic alteration that could represent a potential therapeutic target. Overall 448 treatment recommendations were given and involved mainly cell cycle checkpoint, PI3K/AKT/mTOR and RAF/MAPK, among others. Fifty-six patients were treated with a matched targeted agent, 48 of them in a clinical trial, mostly in their AcSé-ESMART trial (NCT02813135) (Berlanga et al., 2019). This proof-of-concept, phase I/II, multicenter, prospective basket trial was designed to explore targeting agents in a molecularly enriched cancer population (Gatz et al., 2019). The French national program MICCHADO (NCT03496402), besides the searching for therapeutic targets, adds a new parameter in the study of the genetic profiling of tumors, since it aims to study the clonal evolution based on sequential ctDNA analysis from the time of diagnosis in high-risk pediatric cancers. Sequential ctDNA studies would further elucidate mechanisms of clonal evolution, tumor progression, and therapy resistance (Schleiermacher, 2020).

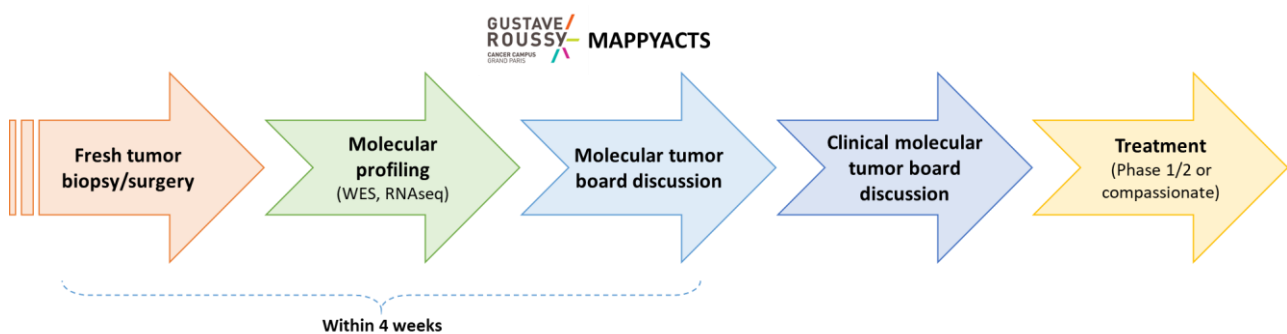


Figure 6: MAPPYACTS workflow.

Similarly, the 'Individualized Therapy for Relapsed Malignancies in Childhood' (INFORM) precision medicine study is a German program for children with high-risk relapsed/refractory malignancies, which aims to identify therapeutic targets on an individualized basis. The program consists of two major pillars: the INFORM registry providing a molecular screening platform and the INFORM2 series of exploratory biomarker-driven phase I/II trials, conducted through the European Innovative Therapies for Children with Cancer (ITCC) network. Sequencing techniques (WES, lcWGS and RNA sequencing) are complemented with methylation and expression microarray analyses. In a pilot phase, they reported the logistical and analytical pipelines used for rapid and comprehensive molecular profiling in a clinical setting. They developed a customized prioritization algorithm and subsequently discussed in an interdisciplinary molecular tumor board the potential targetability of genetic alterations. To date, more than 1300 patients have been enrolled. Turnaround time from sample receipt until first report averaged 25.4 days. Five-hundred twenty-five patients finished follow-up. They were enrolled in 72 centers in 8 countries. Potentially actionable targets of 'moderate' or higher priority were identified in approximately half of all patients. The distribution of the highest priority target per patient was: very high 8.0%, high 14.8%, moderate 20.3%, intermediate 23.6%, borderline 14.4%, low 2.5%, very low 1.0% and no actionable target 15.4%. Interestingly, most gene/pathway alterations were distributed across entities and not restricted to individual tumor types. One hundred and forty-nine patients received targeted treatment on the basis of identified targets, of which 20

had a very high priority target (mostly *ALK*, *BRAF* and *NRAS* mutations and *MET* and *NTRK*-fusions) (Worst et al., 2016; Pfister et al., 2020; van Tilburg et al., 2020).

These studies have clearly demonstrated the feasibility of technical and bioinformatics aspects. They need close collaboration between biologists, clinicians and bioinformaticians for the data interpretation, that goes beyond the simple identification of hotspot mutations of copy-number variations, but also their functional impact, and finally the proposition of pertinent targeted therapies according with the different pathologies. The prioritization algorithm identifies subgroups benefiting from molecularly matched targeted treatment. Generation of data on druggable alterations in relapsed pediatric tumors will provide a basis for designing interventional studies to address the need for biomarker-driven, early-phase trials for high-risk pediatric cancer patients. The fact that particular alterations were typically not restricted to individual entities supports the rationale of a cross-entity approach for these prospective studies. Nevertheless, several difficulties remain a challenge. First, the distinction between a driver or passenger mutation, or the interpretation of its potential real impact, is still subject to individual interpretation. Second, for the patients without a very high priority target further molecular and functional data should be incorporated in future programs. Another difficulty comes from the availability or not of a given drug. Whereas many efforts have been done from several groups (especially from the Innovative Therapies for Children with Cancer Consortium, ITCC) to promote early clinical trials in pediatric oncology, in many cases a particular targeted drug is not available, because of the lack of the corresponding clinical trial or slots in ongoing trials (Moreno, Pearson, et al., 2017). Thus, whereas pediatric precision medicine programs bring enormous hope for the cure of pediatric malignancies, major advances need still to be done, since the simply match of a molecular target to a specific drug, even if it proves clinical benefit, it is often followed by relapse or progression, and more studies are needed to understand the mechanisms of resistance and progression.

3.2 Targeted therapies for Neuroblastoma

The very poor prognosis of high-risk neuroblastoma largely justifies the search for new molecular targets and therapeutic strategies. Genome sequencing, transcriptomics and high-throughput genome analysis have revealed genetic alterations and disrupted pathways that are responsible for neuroblastoma growth and development. Many of these are being tested as druggable targets for patients with neuroblastoma. The use of molecular targeted therapy focused on genomic alterations and disrupted pathways represents a new approach for the treatment of NB that may result in improved efficacy and reduced toxicity. Several signaling pathways required for the growth and progression of neuroblastoma or that contribute to treatment resistance can be targeted by different compounds (Figure 7,(Zafar et al., 2021).

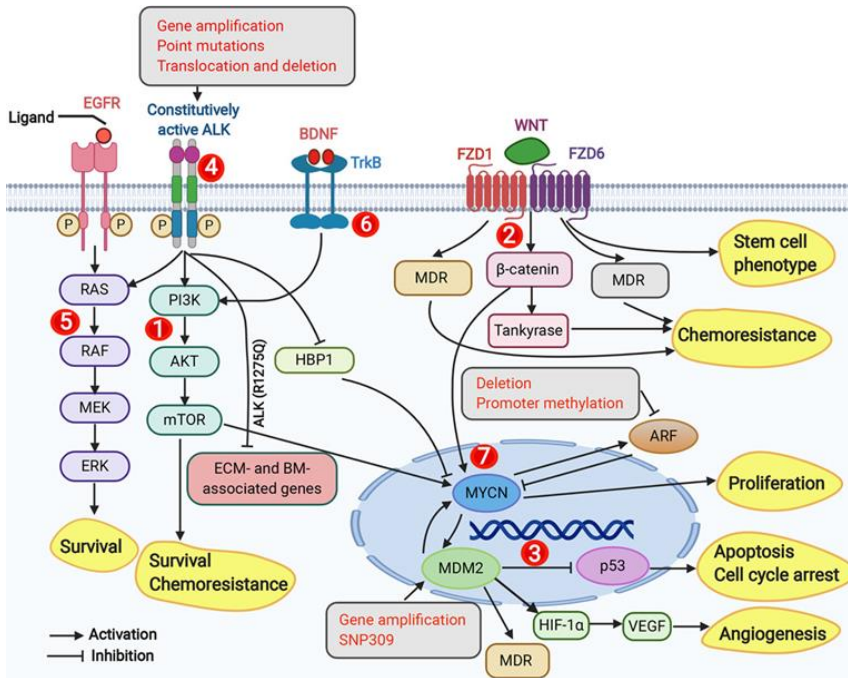


Figure 7 (Zafar et al., 2021): Overview of the molecular signaling pathways in NB. (1) PI3K/AKT/mTOR pathway promotes NB cell survival and chemoresistance. (2) Wnt signaling is involved in drug resistance and increases *MYCN* levels. (3) p53-MDM2 pathway: MDM2 inhibits p53 activity, promotes angiogenesis, increases *MYCN* translation and promotes drug resistance. Activated p53 is involved in apoptosis and growth arrest. (4) ALK signaling activates PI3K/AKT/mTOR, RAS-MAPK, and *MYCN* expression. *ALK* (R1275Q) mutation inhibits the expression of BM- and ECM-associated genes. (5) RAS-MAPK signaling promotes the survival of NB cells and is activated by EGFR signaling. (6) TrkB signaling activates the PI3K/AKT/mTOR signaling. (7) *MYCN* signaling promotes NB cell proliferation and activates MDM2 expression. Gray boxes in the figure represent genetic aberrations and promoter methylation, and yellow boxes represent downstream biological phenotypes

3.2.1 Genetic targets

3.2.1.1 Targeting ALK

Currently, the most evident druggable target for neuroblastoma is ALK. Point mutations and amplifications of *ALK* lead to the constitutive phosphorylation of ALK and increased kinase activity, as well as activation of other downstream signaling molecules, which results in enhanced survival, migration and proliferation of neuroblastoma (Janoueix-Lerosey et al., 2008; Mossé et al., 2008). The most extensively studied ALK inhibitor in neuroblastoma, crizotinib, is a small molecule competitive inhibitor of ALK and MET kinase activity and is FDA approved for use in adult patients with *ALK*-translocated non-small cell lung cancer (NSCLC). The ADVL0912 phase II trial involving crizotinib has been completed by the Children's Oncology Group (COG) in pediatric patients with relapsed/refractory *ALK*-driven neuroblastoma (NCT00939770). From 20 patients, objective responses were seen in 3 patients (1 patient with complete response and 2 with partial response) (Foster et al., 2021). Resistance is a real challenge with crizotinib and there is sufficient preclinical data to suggest that crizotinib synergizes with chemotherapy. Preclinical studies of crizotinib have demonstrated that neuroblastoma with the F1174L mutation, the second most frequent *ALK* mutation observed in neuroblastoma, is resistant to single agent crizotinib (Bresler et al., 2011). This resistance can be overcome when crizotinib is combined with a chemotherapy regimen including topotecan and cyclophosphamide (topo/cyclo). This was demonstrated in mouse xenografts harboring the F1174L mutation, in that mice treated with the combination of crizotinib plus topo/cyclo had rapid and sustained tumor regression with improved EFS compared to mice treated with single agent crizotinib or topo/cyclo alone (Krytska et al., 2016). A COG phase I trial evaluated the safety and toxicity of crizotinib in combination with topo/cyclo in children with relapsed and refractory solid tumors (NCT01606878, [Greengard et al., 2015](#)) and is conducting since 2017 the ANBL1531 phase III clinical trial to determine whether the addition of crizotinib to standard of care

therapy for high risk neuroblastoma improves survival for patients with *ALK*-driven neuroblastoma (NCT03126916).

The second-generation ALK inhibitors alectinib and ceritinib display activity toward crizotinib resistance mutations (Sakamoto et al., 2011; Friboulet et al., 2014). In 2014, the FDA approved ceritinib for crizotinib resistance *ALK*-fusion positive NSCLC patients. The CLDK378X2103 phase 1 study of ceritinib in children with *ALK* aberrant malignancies has been completed. From 30 patients with neuroblastoma, 6 had complete or partial responses (NCT01742286, (Schulte et al., 2020)). Despite the increased potency of ceritinib over crizotinib, resistance remains a challenge with single agent ceritinib. One potential approach to combating resistance is through the use of novel combinations. The combination of ceritinib and the CDK4/6 inhibitor, ribociclib, has been studied in preclinical models of *ALK* mutated neuroblastoma. In *ALK* mutated cell lines the combination was synergistic, whereas in xenografts, the combination resulted in complete and sustained tumor regression and prolonged EFS compared to either single agent alone (Wood et al., 2017). The Children's Hospital of Philadelphia is studying this combination in their Next Generation Personalized Neuroblastoma Therapy (NEPENTHE) trial (NCT02780128). In 2015 the FDA approved second-generation ALK inhibitor alectinib for *ALK*-fusion positive NSCLC patients who have progressed with crizotinib. As a single agent, alectinib was effective in inducing apoptosis in neuroblastoma cell lines with the *ALK* F1174L mutation (Lu et al., 2017). A case-report described a metastatic ALK-F1245C neuroblastoma case, where a partial clinical response was observed (Heath et al., 2018). A trial investigating alectinib for both adult and pediatric patients with *ALK* mutated or rearranged malignancies is currently enrolling patients (NCT03194893). The NCI-COG Pediatric MATCH phase II trial, which aims to classify patients into molecularly targeted treatments on the basis of genetic profiling, is using a second-generation ALK inhibitor ensartinib for patients with relapsed or refractory NB (NCT03155620).

Lorlatinib, a third-generation ROS1 and ALK inhibitor overcomes resistance to first and second generation ALK inhibitors (Zou et al., 2015) by its macrocyclic structure, which is associated with improved metabolic stability and low propensity for MDR efflux (Nagasaka et al., 2020). It has been found to be effective against neuroblastoma cells and against *ALK*-mutated PDX models, including crizotinib-resistant xenografts (Infarinato et al., 2016). These encouraging findings led to the NANT2015-02 phase I trial of lorlatinib for patients with *ALK*-driven neuroblastoma that is currently ongoing through the NANT consortium (NCT03107988) and has confirmed antineuroblastoma activity with minimal observed toxicity (Goldsmith et al., 2020). Furthermore, the COG phase III trial ANBL1531 mentioned above will be amended to replace Crizotinib by Lorlatinib. Finally, the international SIOPEN HR-NBL2 trial for first-line treatment of high-risk neuroblastoma will be amended to introduce Lorlatinib, and a design has been chosen to later perform meta-analysis of data from the ANBL1531 and HR-NBL2 trials (Schulte and Eggert, 2021).

3.2.1.2 Targeting MYCN

Many years of research have made evident that it is extremely difficult to find small molecule

inhibitors targeting transcription factors such as MYCN. An answer to this almost intractable problem could be the use of drugs that indirectly affect the transcriptional activity, the protein stability and the cofactors of MYCN (Sala, 2015; Liu et al., 2021).

TARGETING *MYCN* TRANSCRIPTION

Many mechanisms have been identified to be involved in the transcriptional regulation of MYCN. Soon after the discovery of the *MYCN* gene, it was found that retinoic acid (RA) treatment of both *MYCN*-amplified and non-amplified human neuroblastoma cell lines resulted in a down-regulation of *MYCN* expression at the mRNA level, and this preceded cell cycle arrest and implementation of a differentiation program (Thiele et al., 1985). This indicated that MYCN downregulation, at least partially, contributed to the biological effect of RA on neuroblastoma cells. Retinoid repression of *MYCN* transcription was a major motivation for the inclusion of 13 cis-retinoic acid during the consolidation phase of treatment for high-risk neuroblastomas (Reynolds et al., 2003). Retinoid regulation of MYCN represents one of the first strategies developed to target *MYCN* gene transcription and provides an example of indirect targeting of MYCN.

TARGETING *MYCN* PROTEIN STABILITY

MYCN is a short-lived protein whose stability is tightly regulated by different signaling pathways that target it for ubiquitin-mediated degradation by the proteasome. A major signaling pathway affecting MYCN protein stability occurs upon activation of PI3K/AKT/mTOR. Numerous inhibitors of the PI3K/AKT/mTOR pathway have been developed; however, the question still remains as to what the optimal target in this pathway is, as we will see later. PI3K activates Akt which phosphorylates GSK3 β , suppressing GSK3 β kinase activity. This results in decreased phosphorylation of MYCN-T58 which is critical for targeted degradation by the proteasome. As expected, inhibitors of PI3K destabilize the MYCN protein and suppress tumor growth in the TH-*MYCN*/GEMM NB model (Chesler et al., 2006).

Aurora A kinase (AURKA) inhibition is another secondary approach to inhibit MYCN, which is stabilized by AURKA, rendering MYCN less prone to degradation by the proteasome. AURKB has been confirmed as a direct transcriptional target of *MYCN*. Alisertib, an AURKA inhibitor, induced cell senescence and cell growth inhibition in IMR32 neuroblastoma cells and tumor growth inhibition in a xenograft mouse model (Yang et al., 2020). There were no clinical responses in neuroblastoma patients in a COG phase I clinical trial with alisertib for children with relapsed/refractory solid tumors (Mossé et al., 2012). Pre-clinical data suggest that MLN8237 synergizes with irinotecan and temozolomide and thus this combination was subsequently studied in children with relapsed or refractory neuroblastoma. The overall response rate in this combination phase 1 trial of 31.8% was encouraging; however, there are currently no ongoing trials investigating the use of this agent in neuroblastoma (DuBois et al., 2016). Perhaps targeting both AURKA and AURKB could provide a greater anti-tumor effect through the use of pan-aurora inhibitors. Tozasertib (VX680, MK-0457), a pan-aurora inhibitor, was found to have potent activity in a panel of drug-resistant neuroblastoma

cell lines (Michaelis et al., 2014). Although this agent has been studied in adult patients with malignancies, it has yet to be studied in pediatrics.

PLK1 is a serine/threonine kinase formally known as the polo-like kinase. The PLK1 inhibitor BI 2356 exhibits strong antitumor activity in NB cells *in vitro* and *in vivo*. PLK1 does not directly bind to the MYCN protein. Rather, it increases MYCN protein stability by destabilizing the FBXW7 ubiquitin ligase complex to counteract FBXW7-mediated degradation of MYCN. Importantly, *MYCN*-amplified tumor cells in neuroblastoma are more sensitive to treatment with PLK1 inhibitors than tumors with normal *MYCN* copy number, indicating that PLK1 inhibitors are potential therapeutics for *MYCN*-overexpressing cancers (Ackermann et al., 2011; Xiao et al., 2016).

TARGETING *MYCN* COFACTORS/COREGULATORS

Another explored strategy was targeting MYCN/MYC-associated factor X (Max) interactions. After amplification, MYCN forms heterodimers with Max to act as a transcription factor and promote neuroblastoma growth. Two compounds, 10058-F4 and 10074-G5, have been found to block heterodimerization, induce differentiation and apoptosis *in vitro* and growth suppression in xenografts models (Müller et al., 2014). Nevertheless, poor solubility and short half-lives of these agents currently available have limited their clinical development.

3.2.1.3 Targeting TRK

BDNF (brain-derived neurotrophic factor) is a growth factor that transmits its signal via tyrosine kinase receptor tropomyosin-related kinase B (TrkB) and promotes survival, and also confers chemoresistance to etoposide, doxorubicin and cisplatin by engaging the PI3/Akt/mTOR pathway (Ho et al., 2002). Elevated expression of TrkB is correlated with high-risk NB and poor survival, while increased TrkA expression is correlated with lower-risk NB and tumors that are prone to spontaneous regression (Brodeur, 1993). In preclinical models, Trk inhibitors GNF-4256 and AZD6918 slow the growth of xenograft tumors, and combining a Trk inhibitor with chemotherapeutic drugs leads to significantly better effects compared with treatment with either agent alone (Croucher et al., 2015; Li et al., 2015). Entrectinib, another inhibitor of TrkA/B/C which also inhibits ROS1 and ALK, and has been found to inhibit neuroblastoma tumor growth, while also augments the tumor growth inhibition of temozolomide when used in combination therapy in a xenograft mouse model (Iyer et al., 2016). Entrectinib is currently undergoing evaluation in a phase 1 clinical trial for children with recurrent or refractory solid tumors, with an arm specifically for neuroblastoma, but objective responses are almost only seen in patients carrying *NTRK* fusions (NCT02650401, [Desai et al., 2020](#)). Another clinical trial with a different TRK inhibitor, larotrectinib, enrolled both adult and pediatric patients with advanced solid tumors and brain tumors. Larotrectinib showed marked and durable antitumor activity in patients with TRK fusion-positive cancer, regardless of the age of the patient or of the tumor type (NCT02122913, [Drilon et al., 2018](#)). The pediatric MATCH trial is also investigating this agent; however, enrollment is limited to patients with actionable NTRK fusions, and thus is unlikely to enroll neuroblastoma patients (NCT03213704).

3.2.1.4 Targeting the p53/MDM2 pathway

In contrast to other malignancies, especially in adults, neuroblastomas rarely harbor *TP53* mutations. Nonetheless, there is evidence that p53 pathway inactivation, including mutations, often occurs at the time of neuroblastoma relapse and likely contributes to chemotherapy resistance (Tweddle et al., 2003; Carr-Wilkinson et al., 2010). Several mechanisms for this inactivation have been proposed including *MDM2* gene amplification or increased *MDM2* expression mediated by *MYCN* (Chen et al., 2009; Swarbrick et al., 2010; Veschi & Thiele, 2017). In addition, several chromosomal alterations commonly seen in neuroblastoma, including gain of 17q and LOH of 1p, alter p53 function. Thus, enhancing or reactivating the functional activity of p53 by targeting the p53-MDM2 pathway via MDM2 inhibitors may represent a plausible approach for neuroblastoma treatment. Indeed, inhibition of MDM2 has been the most extensively studied mechanism of restoring p53 activity in neuroblastoma (Khoo et al., 2014). Recently, it has been shown that the combination of the p53 and pRb pathway inhibitors does not lead to synergistic responses in neuroblastoma (Schubert et al., 2021)

The small molecule inhibitors nutlin-3 and MI-219 interact with MDM2 by mimicking the p53 N-terminal region, where MDM2 binds to p53. Preclinical investigation of these MDM2 inhibitors show that the effects depend on the *MYCN* status of the cells in that *MYCN* over-expression sensitizes the cells to MDM2 inhibition (Wang et al., 2006). Nutlin-3 activates p53 pathway in both chemosensitive and chemoresistant p53 wild-type neuroblastoma cells as well as inhibits tumor growth in neuroblastoma xenografts (Van Maerken et al., 2009). Both *in vitro* and *in vivo* studies of nutlin-3 have been promising as single agent and in combination with agents such as bevacizumab, venetoclax and temsirolimus (Barbieri et al., 2006; Maerken et al., 2006; Gamble et al., 2012; Van Goethem et al., 2017). Idasanutlin, a second generation nutlin, exhibits increased efficacy and lower toxicity than nutlin-3a and induces p53 activation and apoptosis in neuroblastoma cells (Lakoma et al., 2015). Its intravenous prodrug, RG7775, exhibits significant tumor growth inhibition alone and combined with temozolomide (Chen et al., 2019). Interestingly, other second-generation MDM2 inhibitors, such as RG7112 and NVP-CGM097, have shown to synergistically inhibit proliferation of *TP53* wild-type *ALK*-driven neuroblastoma cells *in vitro*, and to overcome resistance to *ALK* inhibitors by inducing apoptosis and preventing tumor relapse (Wang et al., 2017a; Miyazaki et al., 2018).

A recent publication has shown in neuroblastoma cell lines and xenografts that combining MDM2 inhibitor CGM097 combined with the BET inhibitor OTX015 resulted in *in vitro* p53 activation, decreased *MYCN* expression and synergistic increase in cell death, as well as *in vivo* significant delay in tumor growth and increase in prolonging survival (Maser et al., 2020).

3.2.1.5 Targeting VEGF

Apart from its functions in angiogenesis and vascular permeability, the autocrine signaling of VEGF plays a role in cancer stem cells, and the resistance of tumor cells to treatments (Carmeliet, 2005; Stanton et al., 2013). Increased expression of *VEGF* is found more frequently in high-risk

neuroblastoma compared with low-risk tumors (Eggert et al., 2000). Sunitinib, a receptor tyrosine kinase (RTK) inhibitor, impairs neuroblastoma growth and enhance the cytotoxic activity of chemotherapeutic drugs, as well as decreases *MYCN* and *VEGF* expression in neuroblastoma cells (Calero et al., 2014). mTOR inhibitors such as rapamycin, reduce VEGF-A secretion, inhibit mTOR and induce apoptosis and cell cycle arrest in neuroblastoma cells (Johnsen et al., 2008). Bortezomib, a proteasome inhibitor, decreases cellular proliferation and induces cell cycle arrest, as well as reduces in 75% the VEGF levels in treated tumors as compared with controls (Hamner et al., 2007). Finally, imatinib has also been found to inhibit the cellular growth of neuroblastoma both *in vitro* and *in vivo*. This inhibition of cellular growth is correlated with the decrease in expression of platelet-derived growth factor receptor alpha (*PDGFR*), c-kit, and *VEGFR* (Beppu et al., 2004).

3.2.1.6 Targeting PI3K/AKT/mTOR and RAS/MAPK pathways

AZD8055 is a dual inhibitor of mTORC1/2 and has been evaluated in preclinical neuroblastoma models. It has been found to suppress growth and induce apoptosis in neuroblastoma cell lines, and also decreases tumor growth in a xenograft model (Xu et al., 2018). The New Approaches to Neuroblastoma Therapy (NANT) consortium has conducted a phase 1 trial with SF1126, a pan-PI3K/mTOR inhibitor for relapsed or refractory neuroblastoma patients (NCT02337309). In addition, a phase 1/2 trial of the PI3K inhibitor, copanlisib, is currently ongoing through the COG and includes a cohort for patients with relapsed or refractory neuroblastoma (NCT03458728). Finally, combined targeting of AKT has been proposed as another potentially more successful approach to inhibiting this pathway. A phase 1/1b study has been conducted involving perifosine, an AKT inhibitor, for children with solid tumors (NCT00776867). This clinical study recruited 27 high-risk neuroblastoma patients, and only one patient had *MYCN*-amplified high-risk neuroblastoma, while none of the tumors had an *ALK* mutation in 21 tested patients (Kushner et al., 2017).

Although only 3–5% of primary neuroblastomas harbor mutations in the RAS-MAPK pathway, close to 80% of relapsed samples contain mutations in genes implicated in this pathway (Pugh et al., 2013; Eleveld et al., 2015a). Binimetinib, a MEK1/2 inhibitor, inhibits tumor growth and improves the survival of mouse models of neuroblastoma (Eleveld et al., 2015b) and exhibits synergistic effects with ribociclib (CDK 4/6 inhibitor), and suppresses the growth of tumors in a xenograft mice model (Hart et al., 2017). More recent preclinical studies have demonstrated the failure of monotherapy with MEK inhibition in *ALK*-addicted neuroblastoma due to increased feedback activation of other signaling pathways including PI3K/AKT pathway (Umopathy et al., 2017). There are several MEK inhibitors currently under clinical development. For instance, a phase I/IIa clinical trial (NCT02124772) is currently ongoing and recruiting patients to investigate trametinib monotherapy, and a combination of dabrafenib with trametinib, in cancer patients harboring *BRAF*^{V600E} mutations. This study includes an expansion cohort for children with relapsed or refractory neuroblastoma (NCT02124772). In addition, the NEPENTHE study at the Children’s Hospital of Philadelphia is studying the combination of ribociclib and trametinib for patients with relapsed neuroblastoma whose tumors harbor activating mutations in the RAS-MAPK or CDK4/6 pathway (NCT02780128).

3.2.2 Targeting epigenetics

Currently, most epigenetic drugs act at three main levels: (i) DNA methylation, which can be modulated by targeting of DNA methyltransferases (DNMT); (ii) histone modifications, such as acetylation and methylation, which can be targeted by inhibiting the enzymes responsible for these chemical changes; and (iii) blockage of the interpretation of these modifications by targeting epigenetic readers, among which proteins containing bromodomains are the most thoroughly characterized (Jubierre et al., 2018). In addition, the current notion that different cell identities exist in neuroblastoma (noradrenergic *vs.* mesenchymal, (Boeva et al., 2017; van Groningen et al., 2017), which might evolve from one to the other, and which could potentially constitute different reservoirs, might be a rationale for further epigenetic therapeutics.

3.2.2.1 Targeting DNA methyltransferases

Among the different DNA methyltransferases (DNMTs), *DNMT3A/B* has been found to have enhanced expression in high-risk neuroblastoma, especially in cisplatin-resistant cells. The DNMT inhibitor decitabine reduced their proliferation (Qiu et al., 2005) and increases sensitivity of neuroblastoma cells to chemotherapeutic drugs such as cisplatin, doxorubicin and etoposide (Charlet et al., 2012), thereby suggesting that a combination of 5-aza with standard therapies could lead to more effective and safer treatments. However, a phase I clinical study of decitabine with doxorubicin and cyclophosphamide showed that only low-doses of decitabine with this combination were tolerable and that those capable of producing clinically significant biologic effects were not well tolerated (George et al., 2010)

3.2.2.2 Targeting histone deacetylases

Histone acetylation and deacetylation exert a dynamic balance that controls gene transcription. Whereas histone acetylation is associated with active transcription, histone deacetylation is associated with transcriptional repression. Hypoacetylated nucleosomes usually result in tightly compacted chromatin, thereby restricting the access of transcription factors to their target DNA and leading to transcription repression. Histone deacetylases (HDACs) have an important function in regulating both DNA packaging in chromatin and gene transcription. *HDAC8* and *HDAC10* are overexpressed in high-risk neuroblastoma, and their inhibition significantly reduces the proliferation of neuroblastoma *in vitro* and *in vivo* (Oehme et al., 2009, 2013; Rettig et al., 2015). Moreover, the inhibition of HDCA8 and 10 was found to increase doxorubicin sensitivity (Zhao et al., 2017). Further, treatment with valproic acid (an HDAC inhibitor, HDACi) inhibits cellular proliferation and induces apoptosis and differentiation in neuroblastoma cells (Rocchi et al., 2005; Stockhausen et al., 2005). Other studies showed the therapeutic potential of valproic acid in combination with other drugs, such as ABT-510 (antiangiogenic) or OGX-01170 (inhibitor of clusterin), resulting in tumor growth impairment (Yang et al., 2007; Liu et al., 2009). Vorinostat, another HDACi, induces G2/M

phase arrest, followed by activation of the intrinsic apoptosis pathway (De los Santos et al., 2007) as well as decreases *MYCN* mRNA levels accompanied by cell apoptosis (Cortés et al., 2015). Vorinostat was also shown to impair VEGF secretion by neuroblastoma cells, thereby suggesting a potential antiangiogenic effect (Mühlethaler-Mottet et al., 2008). In addition, synergistic anticancer effects were observed when vorinostat was combined with the proteasome inhibitor MG132 in neuroblastoma SH-SY5Y cells (Wu et al., 2018). Recently, vorinostat and panobinostat (another HDACi) have been shown to induce autophagy in neuroblastoma cells at a transcriptional level. Combination of panobinostat with the lysosomal inhibitor chloroquine, which blocks autophagic flux, enhanced neuroblastoma cell death *in vitro* and suppresses tumor growth *in vivo* in a neuroblastoma zebrafish xenograft model (Körholz et al., 2021). Clinically, single agent vorinostat does not appear to be effective. The NANT consortium performed a phase 1 dose escalation study of vorinostat in combination with isotretinoin for patients with relapsed or refractory neuroblastoma. Although no objective responses were seen, 24% of patients had prolonged stable disease (Pinto et al., 2018). Vorinostat is also known to be a radiosensitizer, and thus was studied in combination with ¹³¹I-MIBG. A study through the NANT consortium was conducted to compare ¹³¹I-MIBG alone to ¹³¹I-MIBG plus the addition of vincristine and irinotecan or vorinostat (NCT02035137) and showed that the combination of vorinostat/MIBG had the highest response rate (DuBois et al., 2020). SIRT1 (class III HDACs), which transcription is induced by *MYCN*, can be pharmacologically inhibited by the SIRT1 inhibitor cambinol. This drug reduces tumor growth in murine *MYCN*-driven transgenic model of neuroblastoma (Marshall et al., 2011).

3.2.2.3 Targeting BET proteins

Another indirect targeting of *MYCN* includes the use of the bromodomain and extra-terminal domain (BET) family of proteins, which are transcriptional regulators of many genes, including *MYCN*. The BET family function as chromatin “readers” by binding to acetylated lysine residues. BET inhibitors (BETi) include JQ1, which downregulates *MYCN*, resulting in apoptosis and cell cycle arrest in neuroblastoma cells (Puissant et al., 2013). I-BET726 decreases cell growth and directly inhibits *MYCN* expression in neuroblastoma cells (Wyce et al., 2013). OTX015, has shown to suppress the expression of *MYCN* and reduce the viability in *MYCN*-amplified neuroblastoma cells and has potency against *MYCN*-amplified neuroblastoma xenografts (Henssen et al., 2016). Recent studies showed that the combination of a bromodomain inhibitor with a cyclin-dependent kinase 7 (CDK7) inhibitor, an AURKA inhibitor or an HDAC inhibitor is significantly more effective in suppressing *MYCN*-driven neuroblastoma tumor growth than either drug alone (Shahbazi et al., 2016; Durbin et al., 2018; Felgenhauer et al., 2018). It has been shown that BET bromodomain protein BRD4 promotes *TERT*-rearranged neuroblastoma cell proliferation through upregulating *TERT* expression. OTX015 and carfilzomib (a proteasome inhibitor) synergistically reduced *TERT* protein expression and induced *TERT*-rearranged neuroblastoma cell apoptosis, which was blocked by *TERT* overexpression. In mice xenografted with *TERT*-rearranged neuroblastoma cell lines or PDX tumor cells, OTX015 and carfilzomib synergistically blocked *TERT* expression, induced tumor cell apoptosis, suppressed tumor progression, and improved mouse survival, which was largely reversed by forced *TERT* overexpression (Chen et al., 2021).

3.2.2.4 Targeting DNA methyltransferases

EZH2, a methyltransferase and a member of the polycomb repressor complex 2 (PRC2) associates to MYCN to repress the neuroblastoma tumor suppressor gene *CLU* through a bivalent modification of the chromatin at the *CLU* promoter (Corvetta et al., 2013). In *MYCN*-amplified tumors, MYCN increases levels of EZH2 and components of the PRC2 complex leading to increased activity of PRC2-mediated transcriptional repression primarily of differentiation associated genes. Genomic or pharmacologic inhibition of EZH2 suppresses neuroblastoma growth *in vitro* and *in vivo* (Chen et al., 2018; Wang et al., 2012). The EZH2 inhibitor (EZH2i) tazemetostat, is currently under evaluation in pediatric patients with *SMARCB1*-negative tumors or recurrent synovial sarcoma but has not been specifically investigated in patients with neuroblastoma (NCT02601937, Chi et al., 2020).

3.2.3 Exploring synthetic lethal approaches

Synthetic lethality (SL) arises when a combination of deficiencies in the expression of two or more genes leads to cell death, whereas a deficiency in only one of these genes does not. The deficiencies can arise through mutations, epigenetic alterations or inhibitors of one of the genes. SL is an attractive therapy for cancer because inhibition of such a gene will only induce cell death in cells carrying the specific gene alteration.

MYCN activates both proliferative and apoptotic cellular responses. The proliferative response depends on cooperating apoptotic factors such as the antiapoptotic protein BCL2 (Fulda et al., 1999). BCL2 is highly expressed in neuroblastoma with high-level expression correlating with poor prognosis (Castle et al., 1993). It has been demonstrated that *MYCN*-amplified neuroblastoma cells are highly sensitive to BCL2 inhibitors navitoclax and venetoclax. Interestingly, Aurora Kinase A inhibitor alisertib cooperates with venetoclax to induce apoptosis and this drug combination was more effective in killing *MYCN*-amplified neuroblastoma cells *in vitro* and *in vivo* than either compound alone (Ham et al., 2016). Single agent venetoclax is currently being evaluated in a phase I trial for children with relapsed and refractory malignancies (NCT03236857). Navitoclax is also being studied (recruitment completed) in children with relapsed or refractory acute lymphoblastic leukemia/lymphoma; however, its use is limited by its side effect of thrombocytopenia (NCT03181126). Interestingly, in *MYCN*-amplified neuroblastoma, Polo-Like Kinase 1 (PLK1) and MYCN create a positive, feedforward activation loop essential for maintaining their high levels of expression. BCL2 antagonists have been shown to synergize with inhibitors of PLK1, such as BI6727 or BI2356 and may be an effective drug combination for neuroblastoma overexpressing *MYCN* (Xiao et al., 2016).

Another tumorigenic effect of MYCN in neuroblastoma is through the activation of transcription of genes involved in proliferation, including checkpoint kinase 1 (CHK1). This mechanism may contribute to the ability of *MYCN*-amplified neuroblastoma tumors to become refractory to standard chemotherapy (Cole et al., 2011). Conversely, tumor cells lacking DNA damage checkpoints during tumorigenesis or during cytotoxic therapy are highly sensitive to additional

genomic instability. MYCN induces replication stresses and DNA damage through excessive replication-fork firing. *MYCN*-overexpressing tumors are more sensitive to CHK1 inhibition. Another cell cycle related SL protein identified in *MYCN*-amplified neuroblastoma is CDK2. Knockdown of CDK2 or treatment with the CDK2 inhibitor roscovitine induces apoptosis in *MYCN*-amplified neuroblastoma cell lines but not in those with *MYCN* single copy. Thus, inhibition of CDK2 is synthetically lethal to neuroblastoma cells with overexpressed *MYCN* (Molenaar et al., 2009).

ATRX mutations and *MYCN* amplifications are mutually exclusive, suggesting a potential synthetic lethal condition. Induced overexpression of *MYCN* in *ATRX*-mutant neuroblastoma cell lines showed a marked loss of tumor cells. In addition, in the LSL-*MYCN* neuroblastoma GEMM no tumor develop when LSL-*MYCN*:Dbh-iCre neuroblastoma mice were crossed with *ATRX*^{flox} mice, demonstrating synthetic lethality between mutant *ATRX* and high levels of *MYCN* (Zeineldin et al., 2020). This is an example of rare synthetic lethality between an inactivated tumor suppressor and an activated oncogene. MYCN has been shown to play an apoptotic role in cancer cells under certain circumstances (Petroni et al., 2012). Thus, it is possible that under the stress of DNA replication, when *ATRX* is inactivated, high levels of MYCN induce an apoptotic cellular response. Therefore, *ATRX* targeting may be a therapeutic approach in *MYCN*-amplified neuroblastoma tumors. Alternative strategies that increase MYCN protein levels may lead to an SL situation in *ATRX*-mutant neuroblastoma cells.

The alternative lengthening of telomeres (ALT) pathway is a telomerase-independent mechanism of telomere length maintenance where telomeric DNA is replicated via homologous recombination. It is known that both loss of p53 function, as well as *ATRX* mutations, permit activation of the ALT pathway (Farooqi et al., 2014). It has recently been reported that inhibition of the ATR protein kinase disrupts the mechanism of ALT in ALT-positive cancer cells, resulting in cell death (Flynn et al., 2015). This suggest that ATR inhibitors may be a therapeutic strategy for ALT positive malignancies. These agents are currently being investigated in adults with cancer however, have not yet entered clinical trials in pediatrics.

Figures 8 and 9 depict the molecular targets of the drugs evaluated in preclinical studies and clinical trials.

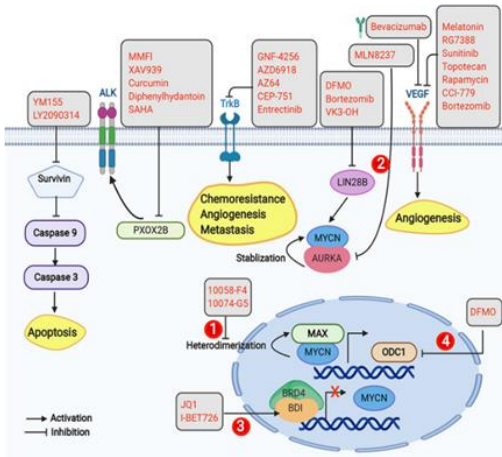


Figure 8 (Zafar et al., 2021): Targeted therapies involving genetic/protein aberrations in neuroblastoma. (1) Inhibition of MYCN/MAX heterodimerization. (2) Inhibition of Aurora A kinase. (3) Inhibition of BET proteins. (4) Inhibition of ODC1.

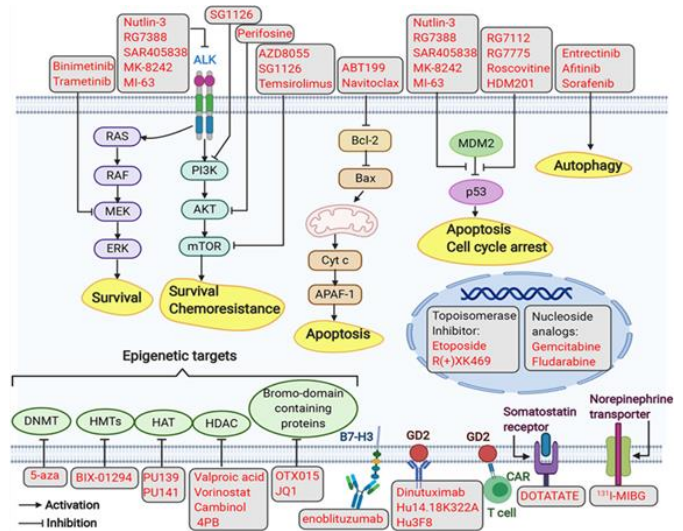


Figure 9 (Zafar et al., 2021): Approaches to targeted therapy involving different modalities in neuroblastoma: (1) small molecule inhibitors targeting signaling pathways (i.e., PI3K/AKT/mTOR, RAS-MAPK, p53-MDM2, Bcl-2, and ALK); (2) chemical inhibitors inducing autophagy; (3) immunotherapy employing monoclonal antibodies targeting GD2 and B7-H3, and using CAR-T cells targeting GD2; (4) targeting epigenetic regulators; (5) radiopharmaceuticals targeting NET (123I-MIBG) and the somatostatin receptor; (6) targeted therapy based on topoisomerase inhibitors or nucleoside analogs.

4. Drug sensitivity screening of anticancer compounds

Although targeting of specific genetic changes in defined patient subsets has been successful, there remain a significant number of cases where genomic analysis currently fails to identify effective drugs or applicable clinical trials. Even when targetable genomic alterations are discovered, patients do not always respond to therapy (Eng, 2021). Indeed, since cancer cells can have diverse potentially targetable genetic alterations, with different parallel activated pathways which may interact, and different available molecules may exist to target these alterations, the prediction of therapeutic responses remains a challenge. An understanding of the functionality of these alterations and the influence they have on treatment response would be necessary. The reasons given justify the search for new methods that allow testing a large number of molecules according to multiple biomarkers in different experimental models, which have resulted in massive compound screening systems.

Since more than two decades, several groups have developed screening systems to link drug sensitivity with genotype data using human tumor cell lines (Shoemaker et al., 1988; Weinstein et al., 1997; Shoemaker, 2006). With the development of NGS techniques, more precise data about pathogenic variants, copy number alterations and gene expression have been integrated in the screening pipelines. In the Cancer Cell Line Encyclopedia, 479 human cancer cell lines with compiled gene expression, copy number and targeted sequencing data were screened with 24 anticancer drugs (targeted and cytotoxic agents) to identify genetic, lineage, and gene-expression-based predictors of drug sensitivity (Barretina et al., 2012). Their main findings were that plasma cell lineage correlated with sensitivity to IGF1R inhibitors; *AHR* expression was associated with MEK inhibitor efficacy in *NRAS*-mutant lines; and *SLFN11* expression predicted sensitivity to topoisomerase inhibitors. A contemporary project screened 639 human cancer cell lines (with comprehensive genomic data) with 130 targeted and cytotoxic drugs. Some frequently mutated genes were associated with sensitivity (*BRAF* mutations to BRAF/MEK inhibitors, *HER2* amplifications to EGFR family inhibitors) or resistance (*TP53* or *RB1* mutations to MDM2 or CDK inhibitors, respectively) specific therapeutic agents. Unexpected relationships were revealed, including the marked sensitivity of Ewing's sarcoma cells harboring the *EWS-FLI1* gene translocation to PARP inhibitors (Garnett et al., 2012).

A more recent study of pharmacogenomic interactions in cancer links genotypes with cellular phenotypes with the purpose of targeting select cancer subpopulations (Iorio et al., 2016). Unfortunately, for many cancer types, traditional cell culture methodologies do not adequately model the biology of the native tumor. The high failure rate of preclinical compounds in clinical trials clearly demonstrates the limitations of existing preclinical models (Li et al., 2008). The accuracy of *in vitro* drug screens is therefore dependent on the optimization of cell culture tools that more closely mirror patient disease. This is the reason why other preclinical models have been developed for their use in high-throughput drug screenings, such as organoids or PDX-derived tumor cells (Bruna et al., 2016; Pauli et al., 2017; Stewart et al., 2017), coupled with genomic analysis from patient-derived tumor samples. These innovative approaches allow to compare the response of individual tumors to specific drugs in order to provide individualized recommendations to help guide patient care, as well

as to assess how individual tumors adapt in response to therapies and better understand the context in which these agents are efficient. From a clinical point of view, they can help to determine the next course of action for cases where standard clinical options have already been exhausted. In addition, results can be included in a database that relates drug sensitivity to tumor genetics to nominate potential therapeutic strategies even when only genomic data are available.

However, there is a remaining challenge in the transition from 'one-size-fits all' therapeutic approach to molecular personalized treatment: the development single-targeted drug resistance. Combinatorial therapy may be able to overcome this by targeting multiple cellular mechanisms involved in cancer cell growth and survival. Thus, while there is a high interest in drug combinations in cancer therapy, openly accessible datasets for drug combination responses are sparse. Few combinatorial high-throughput screens have been published with open access data (Crystal et al., 2014; Friedman et al., 2015; O'Neil et al., 2016; Au-Yeung et al., 2017; Holbeck et al., 2017; Flobak et al., 2019). The analysis of these data can be challenging, and experimental-computational pipelines are needed for the integration of automated screening techniques with advanced synergy scoring tools (He et al., 2018).

Finally, such strategies can lead to innovative clinical trials, such as the so-called "co-clinical trials". This concept was first established as a platform for translational research in cancer to cure acute promyelocytic leukemia (Nardella et al., 2011). The co-clinical trials use the advancement of preclinical models that can accurately replicate tumor heterogeneity, to conduct preclinical trials that parallel ongoing human phase I/II clinical trials. The main objective is to fast track the development of drugs to practice precision oncology, so that treatment can be tailored to patients, individually. The co-clinical trials are expected to reduce the disparity that exists between pre-clinical studies and clinical trials by conducting both studies in parallel, in contrast to the sequential order in the conventional drug development process.

Overall, neuroblastoma is a highly heterogeneous disease in both clinical and molecular point of views, which behavior is intimately related to the biology. High-risk neuroblastomas remain one of the tumors with the poorest survival in children, justifying all the current efforts in deciphering the phenomena related to treatment escapement and disease relapse. Our work aims at exploring the drug sensitivity by *ex vivo* approaches in order to highlight novel drug efficacies, the analysis of the clonal evolution under treatment, as well as giving new insights in the treatment of *ALK*-aberrant neuroblastoma.

II - Thesis objectives

High-risk neuroblastoma urgently needs improvements in patient outcome, since its overall survival still remain one of the poorest among all pediatric malignancies. Indeed, it accounts for about 15% of all children deaths due to cancer. While the majority of patients respond to primary standard chemotherapy, half of them undergo relapse, which is thereafter resistant to treatment. In addition, approximately 20% of patients progress early or are refractory to standard induction therapy. It is therefore crucial to improve our knowledge of the main difficulties that physicians face in the management of these patients: tumor relapse and treatment resistance.

To achieve this, first it is imperative to explore new treatment strategies, presumably in combination, to overcome treatment resistance, both primary and acquired. Based on the emergent personalized medicine approaches in pediatric oncology, the use of *in vitro* high-throughput drug screenings through the use of patient-derived xenografts (PDX)-derived tumor cells (PDTCs) enable the study of molecularly-matched targeted drug therapies, or the discovery of non-predicted treatment responses. We hypothesize that high-throughput drug screening on high-risk neuroblastoma PDX models will give us new insights into drug sensitivity and will allow us to highlight therapeutic classes that may be active in high-risk neuroblastoma treatment, with the ultimate goal of identifying therapeutically active drug combinations.

Second, from a therapeutic perspective, we need to better understand the process of clonal evolution in order to isolate the clones that would be able to determine the behavior of the tumor, in particular treatment resistance. Our hypothesis is that the study of the clonal evolution of high-risk neuroblastoma under targeted treatment is essential in the current context of development of new molecules and will represent a tool to highlight recurrent mechanisms, to subsequently predict the response to targeted treatments.

Third, in the current era of personalized medicine, this opens the door to targeted treatments, not only second but especially first line, in high-risk neuroblastoma. As only few strong biomarkers exist to predict tumor treatment responses, and *ALK* alterations are among them, we would like to explore the *in vitro* and *in vivo* efficacy of *ALK* inhibitors, alone or in combination, in *ALK*-aberrant neuroblastomas. We hypothesize that the study of *ALK* inhibitors in combination with chemotherapy or the exploration of novel combinations with other targeted treatments, could be a way to overcome resistance in *ALK*-aberrant neuroblastomas treated with *ALK* inhibitors.

To explore these different aspects, our work is divided in three parts:

1. The study of the *ex vivo* drug sensitivity of high-risk neuroblastoma by high-throughput drug screening of PDTCs, performed in collaboration with the Biophenics platform of the Institut Curie headed by Dr. Elaine Del Nery
2. The *in vivo* study of the clonal evolution of high-risk neuroblastoma under targeted therapies, by the use of PDX, performed in collaboration with the Laboratoire d'Investigations Précliniques of the Institut Curie conducted by Dr. Didier Decaudin.

3. The *in vivo* and *in vitro* study of combinatorial therapeutics for *ALK*-aberrant neuroblastoma, in collaboration with Dr. Sally George from the Institute of Cancer Research in London and Pr. Deborah Tweddle from the Translational & Clinical Research Institute in Newcastle.

III - Results

1. Study of the *in vitro* drug sensitivity of high-risk neuroblastoma

1.1 High-throughput drug screening in experimental neuroblastoma models

1.1.1 Scientific context

European clinical pediatric precision oncology platforms (INFORM, MAPPYACTS, iTHER) aim at providing a complete molecular profile at the time of relapse or progression, with an objective to match identified predictive biomarkers with relevant early clinical trials. More than one thousand cases of relapsed or high-risk pediatric cancers have been analyzed by applying NGS (WGS, WES, RNAseq) and microarray-based technologies (methylome, transcriptome). These programs have demonstrated the presence of actionable targets in about 60% of the tumors (Jones et al., 2019; van Tilburg et al., 2020). The term "actionable" refers to a detected molecular alteration or affected pathway in the patient's tumor and/or germline analysis which theoretically would be targetable by an approved or investigational agent, either directly or indirectly in the affected pathway. A low percentage, around 5%, harbors clinically proven predictive biomarkers such as *NTRK*-fusions (Pfaff et al., 2021) or *BRAF*^{V600E} mutations (Nobre et al., 2020), leading to clinically proven treatment. This is also the case for high-risk neuroblastoma, with 41% and 58% of tumors harboring at least one actionable variant at diagnosis *vs.* relapse, respectively (Schleiermacher et al., 2014; Padovan-Merhar et al., 2016), indicating significant currently unmet needs for this disease in precision medicine.

The Institut Curie is one of the six European partner centers of the ERAPerMed-funded COMPASS (Clinical implementation Of Multidimensional PhenotypicAI drug SenSitivities in paediatric precision oncology) project, in which the RTOP and the Biophenics drug-screening platform teams are involved. The scope of the COMPASS project is to improve current diagnostic and therapeutic approaches in pediatric precision oncology by establishing next generation drug sensitivity and resistance profiling coupled with bioinformatics integration of thorough genetic and epigenetic tumor profiles. The four main aims of the COMPASS consortium are: i) establish a standardized *ex vivo* drug response profiling platform to discover unexpected drug efficacies and drug re-positioning opportunities, ii) discover new biomarkers and molecular mechanisms for the drug efficacies seen, iii) generate a large-scale online data resource of drug efficacies with integrated omics data providing a basis for novel precision therapies for incurable pediatric tumors and iv) clinical translation. The task of the Institut Curie partner site in the COMPASS consortium is to apply *ex vivo* high-throughput drug-screening techniques across pediatric PDX models, including high-risk neuroblastoma.

1.1.2 Overall hypothesis and objectives

Our hypothesis is that this *ex vivo* platform could help to accelerate the identification of potential/unexpected drug efficacies for high-risk neuroblastoma in monotherapy and in combination. Indeed, we expect to bring out therapeutically active drug classes in high-risk neuroblastoma independently of its molecular profile or accordingly to particular genetic alterations, with the ultimate goal of finding active therapeutic combinations that could have a clinical impact in this disease. To achieve this, in a first step, we have employed a subset of cell lines exhibiting key genetic alterations found in pediatric tumors and then validated the approach in PDTc models. A part of the experiments was performed within the COMPASS project. All the experiments were performed in collaboration with the BioPhenics platform team of the Institut Curie headed by Elaine Del Nery. Altogether, in this first part of the PhD work, we describe, establish and validate the protocol for high-throughput drug screening in high-risk neuroblastoma.

1.1.3 Analysis of drug cytotoxicity

In order to study the drug cytotoxicity by high-throughput *in vitro* drug screenings in neuroblastoma cell lines and PDTcs, drug responses for each compound was based on the quantification of the cellular metabolic activity. The effect of drug treatment was determined by a well-known luminescent cell viability assay (CellTiter-Glo, CTG) (van de Wetering et al., 2015). This luminescence cell viability assay is a method of determining cytotoxicity and cell proliferation based on quantitation of the ATP present in metabolically active cells. The assay procedure involves the direct lysis of the cells with a detergent-based lysis buffer, resulting in ATP release that in turn reacts with added luciferin in the presence of luciferase, oxygen and magnesium to produce light. The emitted light is rapidly quantified with the use of a luminescence reader. The obtained luminescence signal is directly proportional to the amount of ATP as a metabolic marker present in the in culture and hence representative of cell viability.

Drug responses were represented and analyzed by (1) the half-maximal inhibitory concentration (IC_{50}), (2) the dose-response curve, and (3) the quantitative drug sensitivity score (DSS). The IC_{50} is the concentration of the drug causing 50% inhibition of the cell viability. The dose-response curve is a coordinate graph relating the percentage of cell viability (Y axis) with the drug concentration (X axis), which is usually indicated in a logarithmic scale. The DSS was developed by Yadav et al., 2014, for high-throughput drug testing experiments and represents the area under the dose-response curve normalized by the median area of the DMSO wells (removing the edges of the plate). These screenings often result in high-dimensional sample-dose-response matrices, with inherent measurement noise and technical variability, which hinders many down-stream analyses, such as those aimed at detecting differential drug sensitivities or clustering of patients and/or drugs based on their selective response patterns. To provide quantitative information about the degree of drug efficacy in a given model, this method integrates a multiparameter analysis, including the potency (the half-maximal effective concentration, EC_{50}), slope of the dose-response curve, the area under the curve, and the maximum effect of the drug, into the DSS metric. The lower the DSS, the higher is the cytotoxicity of the drug.

1.1.4 High-throughput drug screening using cell lines

To address the robustness and reproducibility of the COMPASS screening platform, a cross-laboratory validation study within the consortium was established. It consisted on the screening, by COMPASS partners, of a set of seven fully characterized pediatric cell lines –the COMPASS core model set– with the COMPASS core drug library provided by the FIMM partner site. This library consisted of 75 clinically approved cancer drugs (Supplementary Table 1, in Appendix), including standard-of-care and small molecule targeted therapies. In COMPASS, drugs were pre-printed on three ‘ready-to-screen’ 384-well plates (384-wp) in 5 concentrations each as 10-fold serial dilutions with technical in-plate duplicates of each. The COMPASS drug plate layout design included negative (DMSO) and positive (staurosporine) controls used for data normalization, as well as an assay control drug (BzCL) also used as a phenotypical and training control for 3D-image processing. The COMPASS drug plate layout is shown in Figure 10.

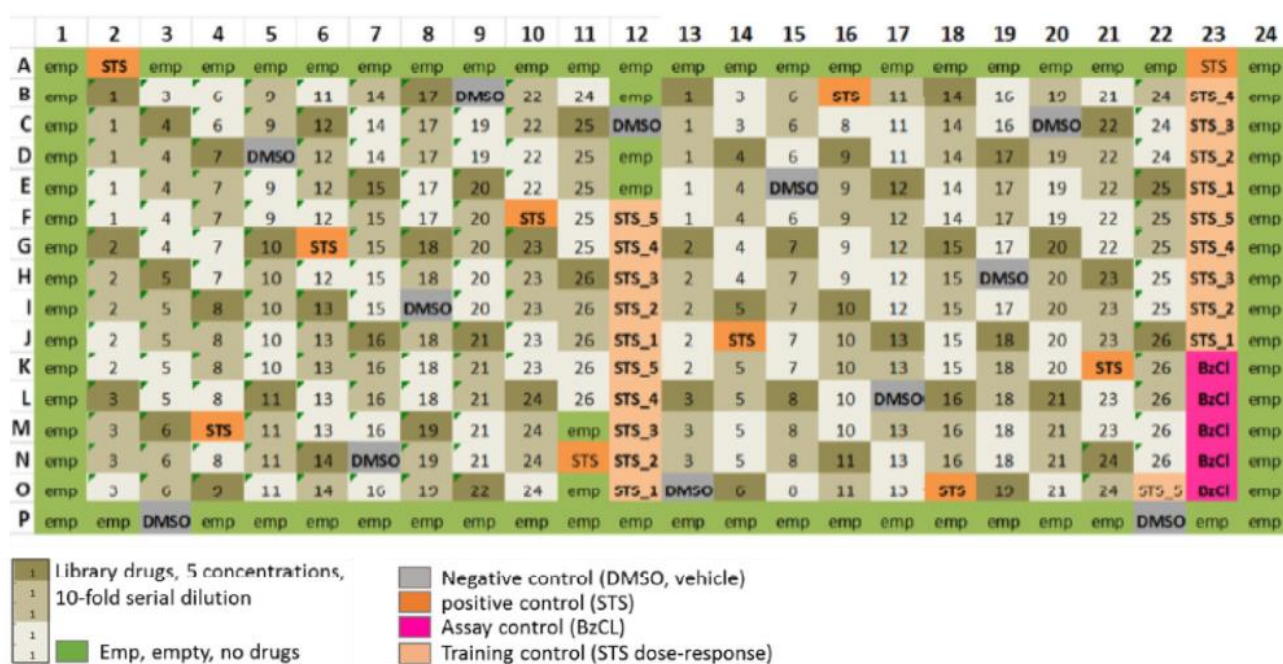


Figure 10: COMPASS core drug library and drug plate layout design

At D0, cell lines were seeded (500 cells in 25 μ L per well) directly into the 384-wp provided by the FIMM. Cells were incubated 72 hours (37°C, 5% CO₂) and then the metabolic read-out by CTG was performed at D3.

The core model cell lines (described in Table 2) were selected based on known molecular characteristics and vulnerabilities with known clinical benefit (i.e. *NTRK* fusion with response to NTRK inhibitors; *ALK* fusion with response to ALK inhibitors) and cover different entities (neuroblastoma, sarcoma or brain tumor). While used to evaluate the predictive value of the drug response profiling platform, the COMPASS core models also served as internal standards and positive controls for predicted drug response, allowing for inter-laboratory cross-validation studies.

Cell line	Tumor entity	Molecular alteration	Predicted active drugs	Screening replicates	Pearson's correlation (<i>r</i>)
BT40	Pilocytic astrocytoma	<i>BRAF</i> -V600E mutation <i>TP53</i> mutation	BRAF _i (vemurafenib, dabrafenib), MEK _i (selumetinib, trametinib)	2	0.82
SJ-GBM2	High-grade glioma	<i>MET</i> fusion, <i>MYC</i> amp, <i>TP53</i> mutation	MET _i (foretinib, cabozantinib, merestinib), HDAC _i (entinostat)	2	0.89
I070_004	Inflammatory myofibroblastic tumor	<i>ETV6-NTRK3</i> fusion	NTRK _i (larotrectinib, entrectinib)	2	0.94
NB1643	Neuroblastoma	<i>ALK</i> R1275Q mutation <i>BCL2</i> overexpression	ALK _i (lorlatinib) BCL2 _i (venetoclax, navitoclax)	1	
SMS-KCNR	Neuroblastoma	<i>ALK</i> F1174L mutation, <i>BCL2</i> overexpression	ALK _i (lorlatinib), BCL2 _i (venetoclax, navitoclax)	2	0.87
NCI-H3112	Lung cancer	<i>ALK</i> fusion	ALK _i (lorlatinib)	NS	
HD-MB03	Medulloblastoma gr. 3	<i>MYC</i> amplification	HDAC _i	3	0.93*

Table 2: COMPASS core model cell lines, their main molecular alterations and predicted active drugs. Correlation between replicates show the Pearson's correlation coefficient between independent replicates.

* This value represents the median Pearson's correlation of the comparison between 3 replicates. The individual values are 0.93, 0.914 and 0.972 for HD-MB03-R1 vs. HD-MB03-R2, HD-MB03-R1 vs. HD-MB03-new and HD-MB03-R2 vs. HD-MB03-new respectively.

We screened cell lines in two independent technical replicates (two different screenings with the same cell model, same cell batch) for BT40, SJ-GBM2, I070_004, SMS-KCNR and HD-MB3. For cell line NB1643, one single screening was performed and for HD-MB03 a supplementary biological replicate was performed with a different cell batch. NCI-H3112 was not screened due to delays in transportation from NCI repository. We observed that DSS values across all drugs and models tested were highly correlated between replicates, with median Pearson's correlation coefficient of 0.89 [0.82-0.94] (table 2).

Drugs predicted as active in their corresponding cell line were identified as hits in most of cases: of 7 therapeutic classes predicted, 6 showed specific cytotoxicity in the cells carrying the corresponding predictive therapeutic target. For example, BRAF inhibitors vemurafenib and dabrafenib and MEK inhibitors selumetinib, cobimetinib and trametinib emerged as active drugs in *BRAF*^{V600E} mutated BT40 cell line. MET inhibitors foretinib, cabozantinib and merestinib emerged as specific hits in *MET* translocated SJ-GBM2 cell line. The *ETV6-NTRK3* fusion harbored by I070_004 was a good predictor of response for NTRK inhibitors entrectinib and larotrectinib. Foretinib, in addition to MET, also targets TRK, conferring specific sensitivity of I070_004 to this molecule. MEK inhibitors were also selectively cytotoxic against I070_004. Lorlatinib showed specific cytotoxicity for *ALK* mutant cell lines NEM1643 and SMS-KCNR. *BCL-2* overexpression harbored by SMS-KCNR conferred specific sensitivity to Bcl-2 inhibitors navitoclax and venetoclax. HDAC inhibitors did not induced the expected specific cytotoxicity against SJ-GBM2 and HD-MB03, as it was predicted by their *MYC* amplification (Ecker et al., 2017; Shofuda and Kanemura, 2021). Interestingly, SJ-GBM2 and I070_004 cells harbored specific resistance to MDM2 inhibitors idasanutlin and amg-232, as expected by their *TP53* mutation (Jung et al., 2016). These findings are summarized in Figure 11 as a clustering heatmap based on the DSS.

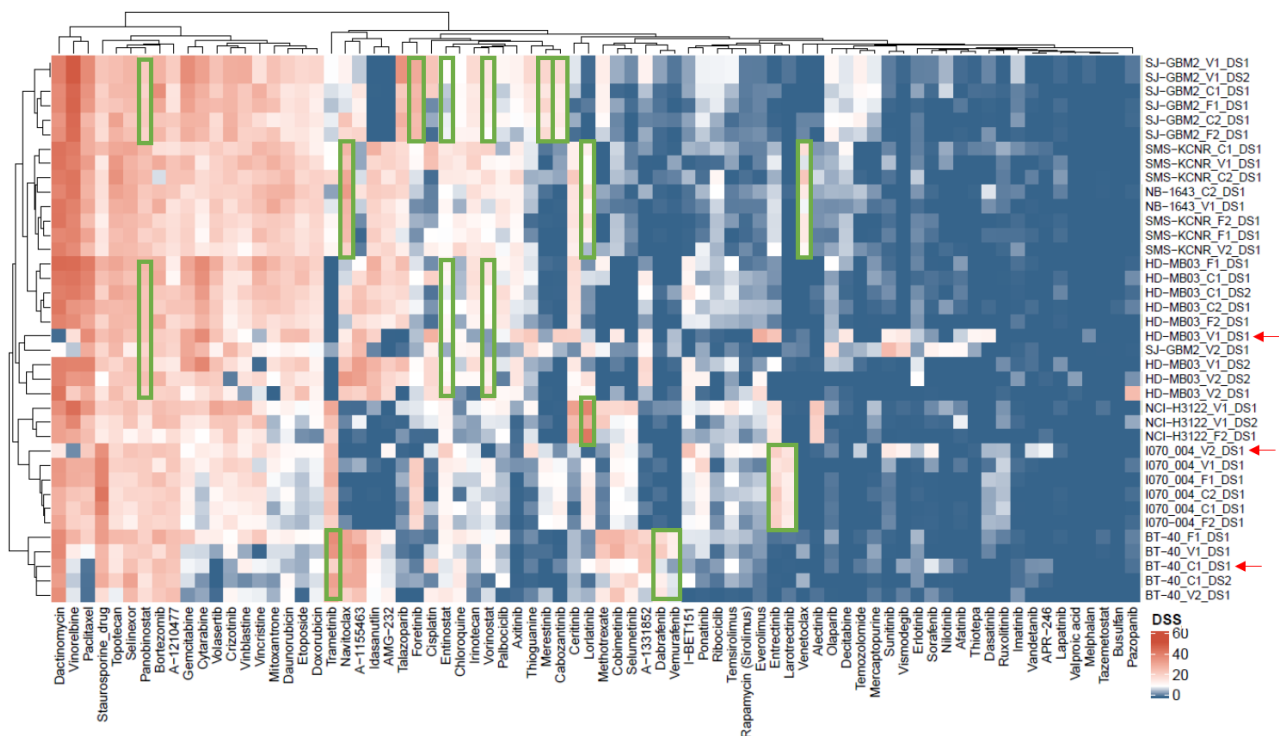


Figure 12: hierarchical clustering across different cell lines and screening centers based on the drug sensitivity score (DSS). C: Curie; V: DKFZ; F: FIMM; C1, C2, V1, V2, F1 and F2 refer to the cell line batch (biological replicates) from each institution; DS1 and DS2 refer to screen numbers (technical replicates). Green boxes indicate expected hits based on cell molecular alterations. Red arrows indicate screen outliers.

In conclusion, these results are a proof-of-concept of the robustness of the assay and the comparability of platforms between COMPASS partner sites. Given the robustness and reproducibility of the COMPASS approach and the screening procedure established within the high throughput BioPhenics platform, this approach was then used for further *in vitro* drug screens in neuroblastoma.

1.1.5 High-throughput drug screening using PDTC models

1.1.5.1 High-risk neuroblastoma PDX models

Xenografts based on traditional cancer cell lines have been used for decades to evaluate drug cytotoxicity, and although these models can provide valuable data, cell lines that have adapted to the *in vitro* environment often differ from the original tumor developed in patients. Specially, the use of fetal bovine serum in the culture medium can lead to cell differentiation and significant genetic alterations (Lee et al., 2006). Gene expression profiling has further demonstrated that cell lines obtained from diverse tumors resemble each other more than the corresponding clinical samples from which they were derived and serum-cultured cell lines can lose drug resistance mechanisms (Gillet et al., 2011). Although cell line-derived xenografts have contributed to the identification and testing of many classical cytotoxic drugs, these models tend to be less predictive of the action of targeted therapies (Johnson et al., 2001).

PDXs are generated by immediate subcutaneous/orthotopic implantation of patient’s tumor

fragments into immunodeficient mice without any prior *in vitro* culture step. The interest in PDXs has increased since the last years due to the limitations of classical xenografts and the development of personalized cancer medicines based on genomic profiling. PDXs recapitulate the histopathological hallmarks, genetic pathways, mutational patterns, expression profiles as well as proteomic profiles of the corresponding patient's tumors (Hidalgo et al., 2014; Huang et al., 2017; Stewart et al., 2017; Rokita et al., 2019). In addition, PDX models recapitulate better than cell lines the intratumor genetic heterogeneity, which is of special interest in neuroblastoma (Braekeveldt et al., 2018; Kamili et al., 2020; Tucker et al., 2021). Once a PDX has been established, tumors can be serially passaged to next-generation recipients and these models generally retain their molecular features after serial passaging (Hidalgo et al., 2014). Major applications of PDXs include drug testing/screening, biomarker discovery and exploration of treatment resistance. Several studies have shown that results derived from PDXs parallel clinical outcomes (Malaney et al., 2014; Rosfjord et al., 2014).

In the Institut Curie, a biobank of 16 molecularly characterized high-risk neuroblastoma PDXs with known genetic profiles and at least one actionable mutation (range 1-4) is available. The majority have been established in the Institut Curie by Dr. Didier Surdez and others by the collaboration with other institutions (Birgit Georger from Institut Gustave Roussy within the MAPPYACTS program and Angel M. Carcaboso from Hospital Sant Joan de Déu in Barcelona). Thirteen models were established at relapse and 3 models at diagnosis. Almost all derived from stage 4 disease, with and without *MYCN* amplifications. They harbored a wide range of additional somatic genetic abnormalities including *ALK* mutations or amplifications, *TP53* or *ATRX* mutations.

Table 3 summarizes the 16 high-risk neuroblastoma PDX models available in our institution and their main clinical and molecular features. Ethical considerations of *in vivo* experimentation are described in section 2.2.2.

HR-NB PDX MODELS	CLINICAL DATA				SOMATIC GENETIC ALTERATIONS						EXPERIMENTS	
	PDX established	Stage	Gender	Dx-PDX delay (m)	<i>MYCN</i>	<i>ALK</i>	<i>TP53</i>	<i>ATRX</i>	Other relevant somatic genetic abnormalities	<i>Ex vivo</i>	<i>In vivo</i>	
GR-NB4	Relapse	4	F	22	A	A	WT	WT	CDKN2A/B homo del	Yes	Yes	
GR-NB5	Relapse	4	M	48	A	WT	WT	WT		Yes		
GR-NB7	Relapse	4	M	18	A	WT	WT	WT	Focal losses of <i>ATM</i> , <i>RAD51</i> and <i>PTEN</i>			
GR-NB10	Relapse	4	M	30	WT	WT	c.555+1G >A	WT	High mutational load, <i>NF1</i> mut+LOH, <i>PTEN</i> mut+LOH,	Yes	Yes	
IC-pPDX-17	Relapse	3	F	8	WT	WT	WT	c.5242G>A	<i>CDK4</i> amp, <i>MDM2</i> amp, <i>ETV1</i> mut, <i>PDGFB</i> mut, ALT+	Yes	Yes	
IC-pPDX-63	Relapse	4	M	14	A	WT	WT	WT	<i>SRC</i> mut	Yes		
IC-pPDX-75	Relapse	4	F	84	WT	F1174L	WT	c.6391C>T		Yes	Yes	
IC-pPDX-109	Relapse	4	M	24	A	WT	WT	WT	<i>SMARC4</i> mut, <i>HRAS</i> mut		Yes	
IC-pPDX-112	Diagnosis	4	M	0	A	A	WT	WT	High mutational load	Yes		
HSJD-NB-003	Diagnosis	4	F	0	WT	WT	WT	WT	<i>PIK3R3</i> mut	Yes		
HSJD-NB-004 ^f	Diagnosis	4	F	0	A	WT	c.517G>T	WT	<i>ARID1A</i> mut, <i>NF1</i> mut	Yes		
HSJD-NB-005 ^f	Relapse	4	F	5	A	WT	c.517G>T	WT	<i>ARID1A</i> mut, <i>NF1</i> mut, <i>ROS1</i> mut	Yes	Yes	
HSJD-NB-007	Relapse	4	M	27	A	WT	WT	WT	<i>PIK3CD</i> mut, <i>PTCH1</i> mut	Yes		
HSJD-NB-009	Relapse	4	M	31	WT	E1419K	WT	WT	<i>MYC</i> mut	Yes		
HSJD-NB-011	Relapse	4	M	15	A	I1171N	WT	WT		Yes		
HSJD-NB-012	Relapse	4	M	8	A	F1174C	WT	WT			Yes	

Table 3: summary of the clinical and molecular characteristics of the 16 high-risk neuroblastoma (HR-NB) patient-derived xenografts available in our institution. Delay diagnosis-PDX is the time between the diagnosis of neuroblastoma and the establishment of the PDX. We also indicate whether each PDX was used for *ex vivo* drug screenings, *in vivo* study of the clonal evolution or *in vivo* efficacy of ALK inhibitors. Mut: mutation; LOH: loss-of-heterozygosity; ALT+: alternative lengthening of telomeres phenotype; Dx: diagnosis.

^f Models HSJD-NB-004 and HSJD-NB-005 were established from the same patient at diagnosis and relapse, respectively.

The set of PDXs described above constitute a living biobank that reflects the overall heterogeneity of neuroblastoma with different genetic subtypes of high-risk neuroblastoma. We have used dissociated cells from the established high-risk neuroblastoma PDXs for high-throughput drug screening.

1.1.5.2 Obtaining PDTCs

PDTCs can be systematically and consistently generated from PDXs and retain their genomic features, making them an excellent model system for high-throughput drug screens (Bruna et al., 2016). PDTCs are obtained from PDXs by mechanical and enzymatic dissociation. Once dissociated, high-risk neuroblastoma PDTCs can be cultured in serum-free stem-cell (SC) conditions to retain their immature and undifferentiated phenotype (Persson et al., 2017).

We established a “ready-to-dissociate” biobank of cryopreserved high-risk neuroblastoma PDX tumors. For viable PDTC generation, we used a dissociation protocol adapted from Stewart et al., 2017, which included a first step of mechanical dissociation with sterile scalpels and then enzymatic dissociation by trypsin (10 mg/ml) and type II collagenase (275 U/mg). The tube was then placed in a warm 37°C water bath for 60 min. Dissociation was stopped by adding Soybean Trypsin Inhibitor (10 mg/ml). Deoxyribonuclease I (2 mg/ml) and magnesium chloride (1 M) are added in equal amounts. Tumor suspension was filtered with a 40 µm cell strainer and then centrifuged at 500g for 5 minutes. Supernatant was discarded and cell pellet was resuspended in PBS-minus/10%FBS for cell counting. The suspension was then re-centrifuged and resuspended in serum-free SC medium (Bate-Eya et al., 2014), which contained Dulbecco’s Modified Eagle Medium/Nutrient Mixture F-12 (DMEM/F12) supplemented with 40 ng/ml basic fibroblast growth factor (bFGF), 20 ng/ml epidermal growth factor (EGF), 1× B27 supplement and 500 U/ml of penicillin/streptomycin.

1.1.5.3 Experimental pipeline

We tested the use of PDTCs as a pre-clinical drug-screening platform. A selection of 13 different high-risk neuroblastoma PDX models were screened (see table 3). After PDX tumor dissociation (described in the previous section), cells in SC medium were plated by robotic seeding in 384-well plates (384-wp) at a concentration of 20,000 cells in 40 µL per well (final concentration $5 \cdot 10^5$ cells/mL), at D0. Cells were then incubated for 24 hours (37°C, 5% CO₂) and drugs at several concentrations were added at D1 by robotic drug dispensing. Drug-treated cells were then incubated for 72 hours (37°C, 5% CO₂) until D4, when cell viability was measured by CTG luminescent assay. Figure 13 schematically describes the experimental pipeline.

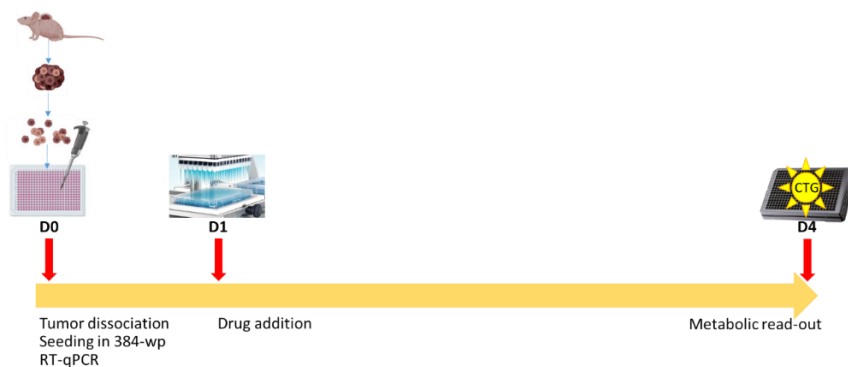


Figure 13: schematic description of the experimental pipeline of the high-throughput drug screening with PDTCs.

Among the 13 screened high-risk neuroblastoma PDX models, 11 were screened with the COMPASS drug library and 10 with an in-house drug library. Eight models were screened with both libraries (see table 4). The COMPASS library contained the same drugs and concentrations as the one used in the COMPASS core set screenings (section 1.1.4). The in-house library consisted on 55 compounds (listed in Supplementary Table 1) including both approved cancer treatments and approved/non-approved drugs targeting key cancer pathways. Sixteen drugs are present in both libraries.

HR-NB PDX model	Drug library
<i>GR-NB4</i>	Both
<i>GR-NB5</i>	COMPASS
<i>GR-NB10</i>	Both
<i>IC-pPDX-17</i>	Both
<i>IC-pPDX-63</i>	Both
<i>IC-pPDX-75</i>	In-house
<i>IC-pPDX-112</i>	In-house
<i>HSJD-NB-003</i>	Both
<i>HSJD-NB-004</i>	Both
<i>HSJD-NB-005</i>	Both
<i>HSJD-NB-007</i>	COMPASS
<i>HSJD-NB-009</i>	COMPASS
<i>HSJD-NB-011</i>	Both

Table 4: Summary of the high-risk neuroblastoma (HR-NB) PDX models screened with the in-house library, the COMPASS library or both.

There were some technical differences in drug preparation between the COMPASS and the in-house library screenings. The COMPASS 384-wp designed by the FIMM for cell line screening could not be adapted to our PDX screening protocol. A dedicated 384-wp containing the drugs at a volume of 100 nL/well was then provided allowing compound dilution directly using the FIMM master drug plates. Twenty μ L of media were added and then 10 μ L of this dilution were dispensed in the cells to have the aimed final concentration of drug in each well. For the in-house library screening, the drugs were received at 10 mM and serially diluted on the cells plates at the desired final concentrations.

The in-house drug library was screened in two independent biological replicates (same model, different passages, different mice), whereas a single screening on PDTCs was performed with the COMPASS library. A total of 10 PDX models were tested in monotherapy with the in-house library (55 compounds, 12 dilutions, biological duplicates) and 11 models tested with the COMPASS library (75 compounds, 5 dilutions, technical duplicates), generating a total of 21,450 data points for 2,750 drug tests.

To address the question of the proportion of human *vs.* murine cells in our dissociated cell suspension, an aliquot of non-plated cells of each PDX model was used for RNA extraction and RT-qPCR, targeting the housekeeping *TBP* gene using both specific human and murine primers, as well as common primers to the human and mouse forms of the gene (Bieche et al., 2014). The average proportion of human *vs.* murine cells was 92% and 8% respectively (Figure 14).



Figure 14: Proportion of human and murine cells in PDX-derived tumor cell suspension after dissociation across the different screened models. H%: human fraction; %M: murine fraction.

One significant limitation of these analyses is that the measurements on drug responses (IC_{50} and DSS) did not account for cell division rates across the different PDX models. Growth rate inhibition metrics have been shown to provide more-reliable measurements of sensitivity to cancer drugs (Hafner et al., 2016). Nevertheless, we have been able to make several observations that attest to the value of the drug screening results obtained despite this caveat.

1.1.5.4 Screening of PDX models with the COMPASS core drug library

Eleven high-risk neuroblastoma PDX models were screened with the COMPASS library, as well as five Ewing sarcoma and 2 rhabdoid tumor models. Here we show the results for the neuroblastoma models.

High-risk neuroblastoma models showed broad resistance to most drugs included in the library. The most commonly used broad-spectrum chemotherapeutics were the most active compounds in these models. Models GR-NB5 and IC-pPDX-63 showed an enhanced chemosensitivity compared to others. Interestingly, busulfan, melphalan and thiotepa did not show any *ex vivo* cytotoxicity across the different models (Figure 15).

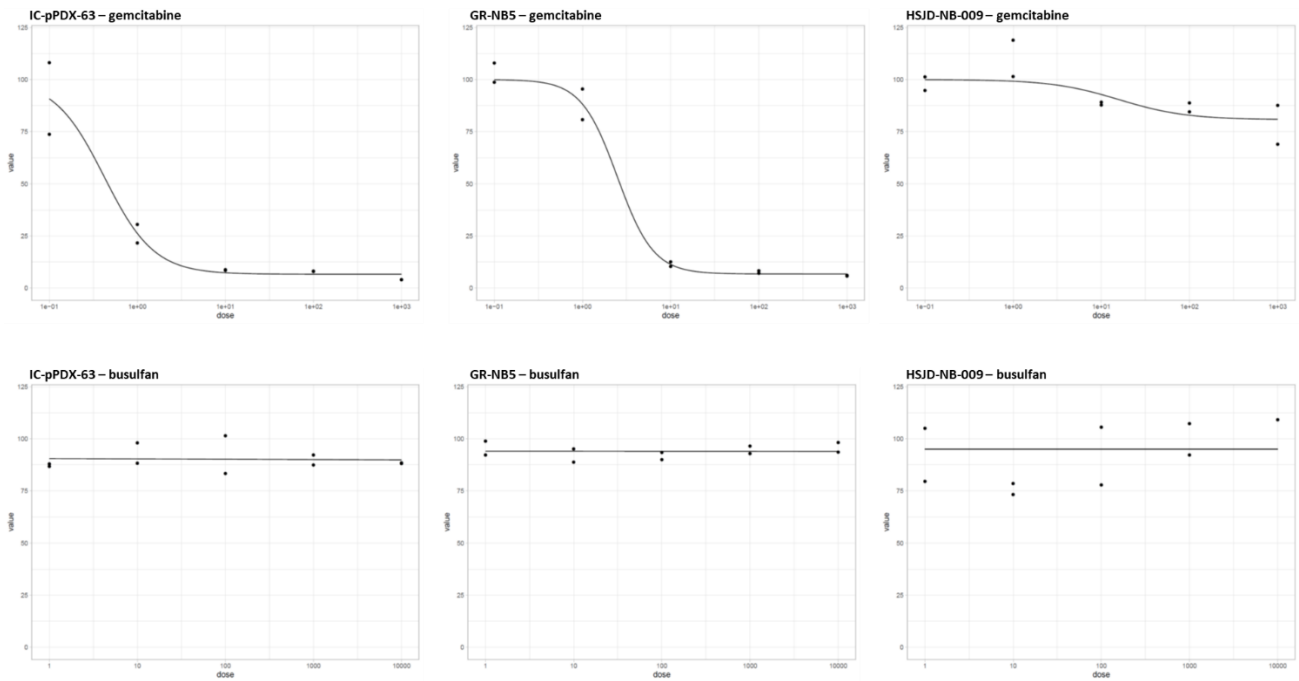


Figure 15: Dose-response curves showing enhanced cytotoxicity of models IC-pPDX-63 and GR-NB5 to gemcitabine, which is not routinely used for high-risk neuroblastoma treatment, compared to HSJD-NB-009. high-risk neuroblastoma models were broadly resistant to some chemotherapeutic compounds such as busulfan, which is used in the intensification phase of high-risk neuroblastoma treatment.

Interestingly, models GR-NB5 and IC-pPDX-63 were selectively sensitive to PARP inhibitors olaparib and talazoparib compared to other models (figure 16). Neither of the two PDX models carried an 11q-deletion (Sanmartín et al., 2017).

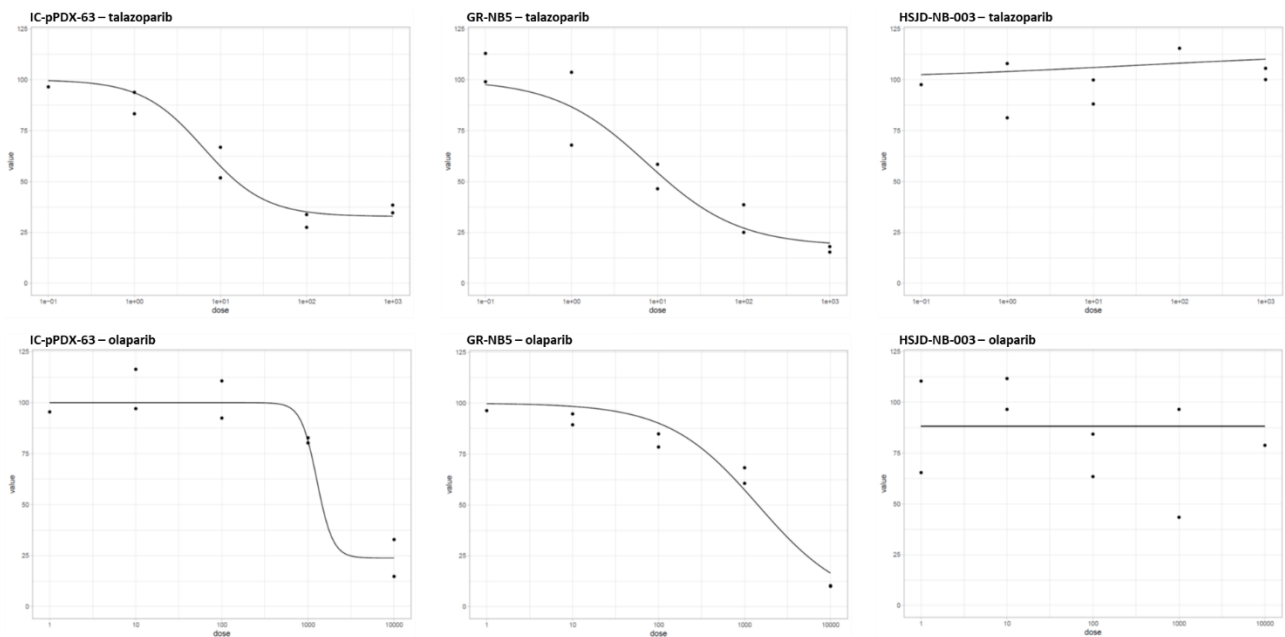


Figure 16: Dose-response curves showing selectivity of PARP inhibitors olaparib and talazoparib against models IC-pPDX-63 and GR-NB5 compared to HSJD-NB-003.

Figure 17 shows in a hierarchical clustering the efficacy of the COMPASS drug library across the different screened high-risk neuroblastoma models. Overall, there is a low efficacy across the different screened models, but importantly some models have a distinct drug response profile highlighting the importance of these investigations.

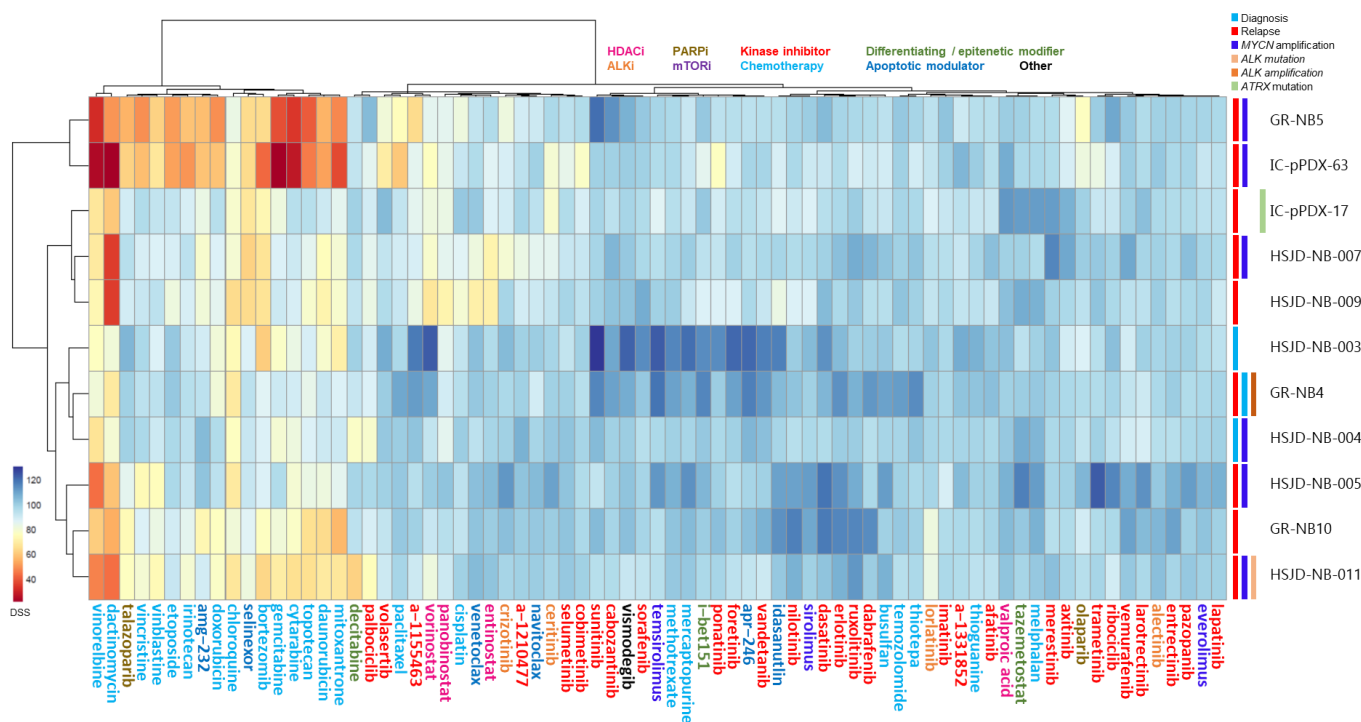


Figure 17: hierarchical clustering of the COMPASS library drug screening across different PDX models based on the drug sensitivity score (DSS). On the bottom are listed the 75 compounds included in the COMPASS drug library. The color code for drugs is defined in the top left panel. On the right, are listed the different PDX models screened. In the top right panel are described the main characteristics harbored by the different PDX models, indicated as a color bar next to the PDX identifications.

1.1.5.5 Screening of PDX models using an in-house drug library

The in-house library consisted of 55 compounds including both approved cancer treatments and approved/non-approved drugs targeting key cancer pathways. This library was enriched in epigenetic targeted drugs and differentiating/epigenetic modifiers such as HDACi, BETi or EZH2i (listed in Supplementary Table 1). In this library, drugs were diluted in 12 concentrations each as 3-fold serial dilutions (from 10,000 nM to 0.056 nM).

As for the COMPASS library screening, the effect of drug treatment on cell viability was determined by CTG and drug responses represented and analyzed by the dose-response curve and the quantitative DSS. The robustness of our approach of high-throughput drug screening on PDX models was supported by the high correlation between biological replicates across the different models tested based on DSS values, with a median Pearson's correlation coefficient of 0.95 [0.85-0.996] (Figure 18).

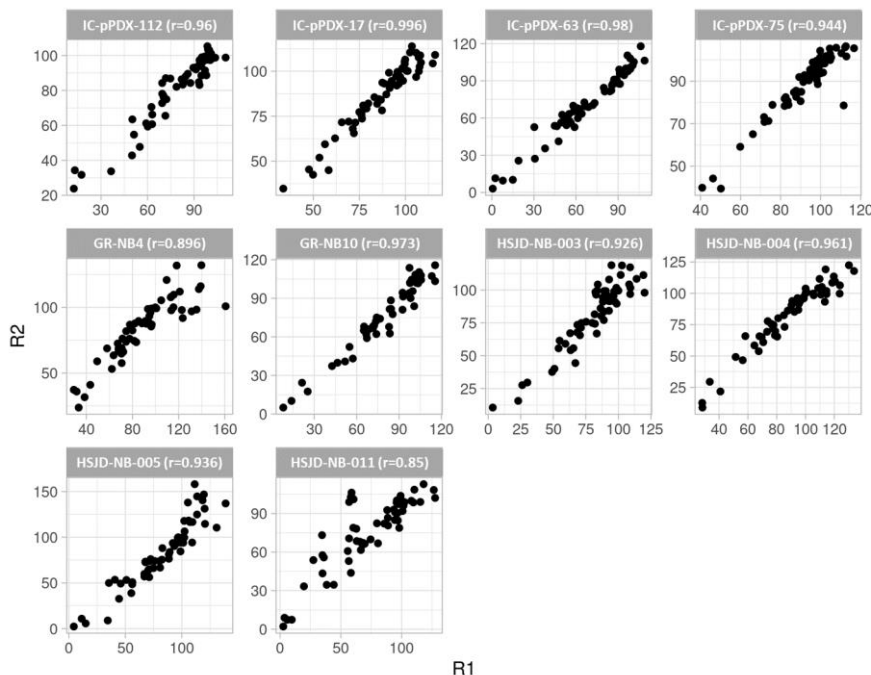


Figure 18: DSS scatterplots showing Pearson's correlation between biological duplicates R1 and R2 (independent experiments, same PDX model, different passages) of the in-house library screening across 10 PDX models.

Globally, the 10 PDX models showed significant resistance to most drugs included in the library, although some important differences were observed. Models IC-pPDX17 and IC-pPDX-75 were globally more resistant, whereas IC-pPDX-63 or HSJD-NB-011 showed higher drug sensitivity compared to other models. A group of four compounds showed high cytotoxicity across all models: cudc-907, quisinostat, panobinostat and trichostatin, all HDACi. Overall, HDACi were the group of compounds that showed highest cytotoxicity. Interestingly, ALK inhibitor ceritinib (which also inhibits IGF-1R) showed wide cytotoxicity across models, as well as BIX 01294 (inhibitor of G9a histone methyltransferase). Some compounds were differentially more cytotoxic depending on the PDX model. For example, AZD1480 (JAK1/2 inhibitor) was significantly more toxic against HSJD-NB-011 compared to the other models, or zm447439 showed higher cytotoxicity in IC-pPDX-63 compared to others (Figure 19).

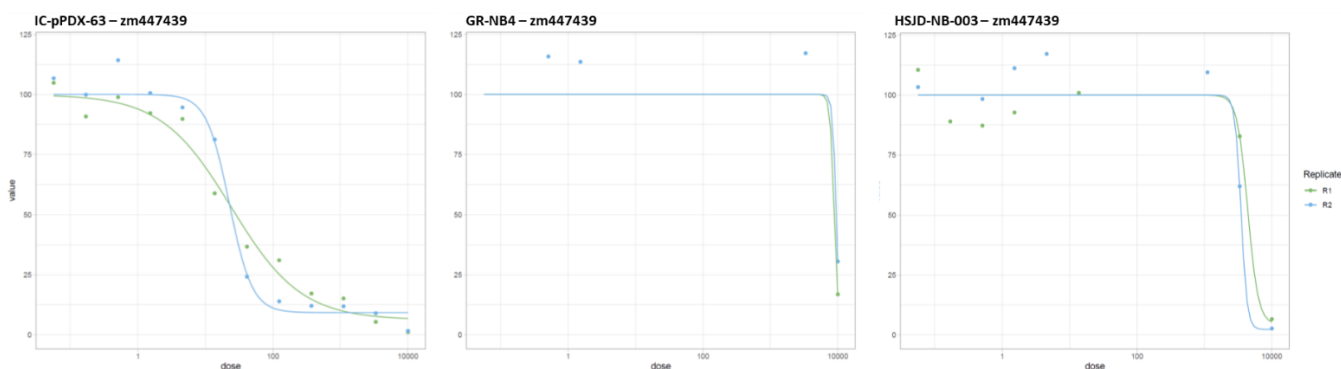


Figure 19: Dose-response curves showing enhanced cytotoxicity of Aurora kinase A/B inhibitor zm447439 against model IC-pPDX-63 compared to models GR-NB4 and HSJD-NB-003.

Concerning chemotherapy compounds, the different models were globally sensitive to doxorubicin, globally resistant to carboplatin, and showed model-dependent sensitivity for etoposide, with IC-pPDX-63 being very sensitive and IC-pPDX-75 and HSJD-NB-004 very resistant to this drug (Figure 20).

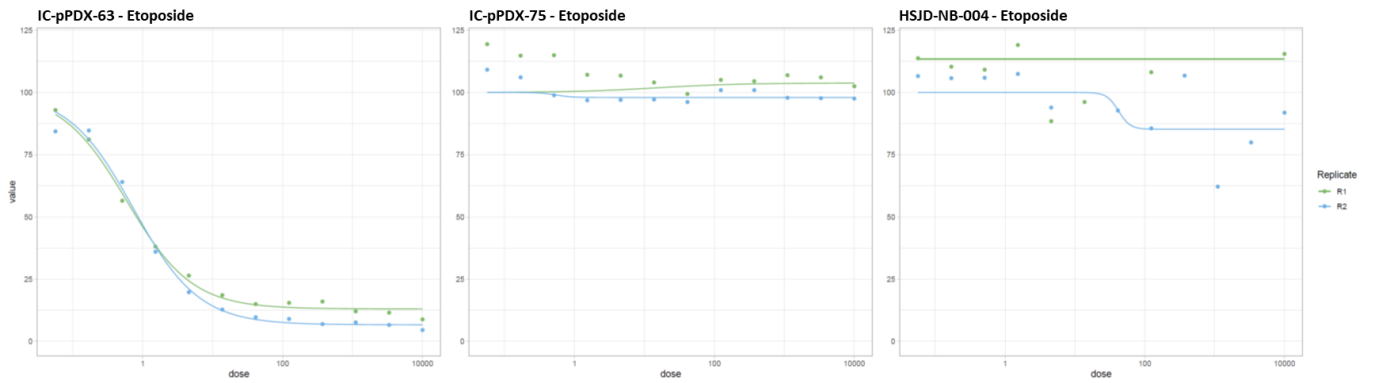


Figure 20: Dose-response curves showing model-dependent cytotoxicity of Etoposide against models IC-pPDX-63, HSJD-NB-004 and IC-pPDX-75.

Analysis of DSS data for compounds targeting the same pathway or within a same therapeutic class showed again that HDACi were the therapeutic class that showed lower DSS across the different models, followed by chemotherapy (Figure 21).

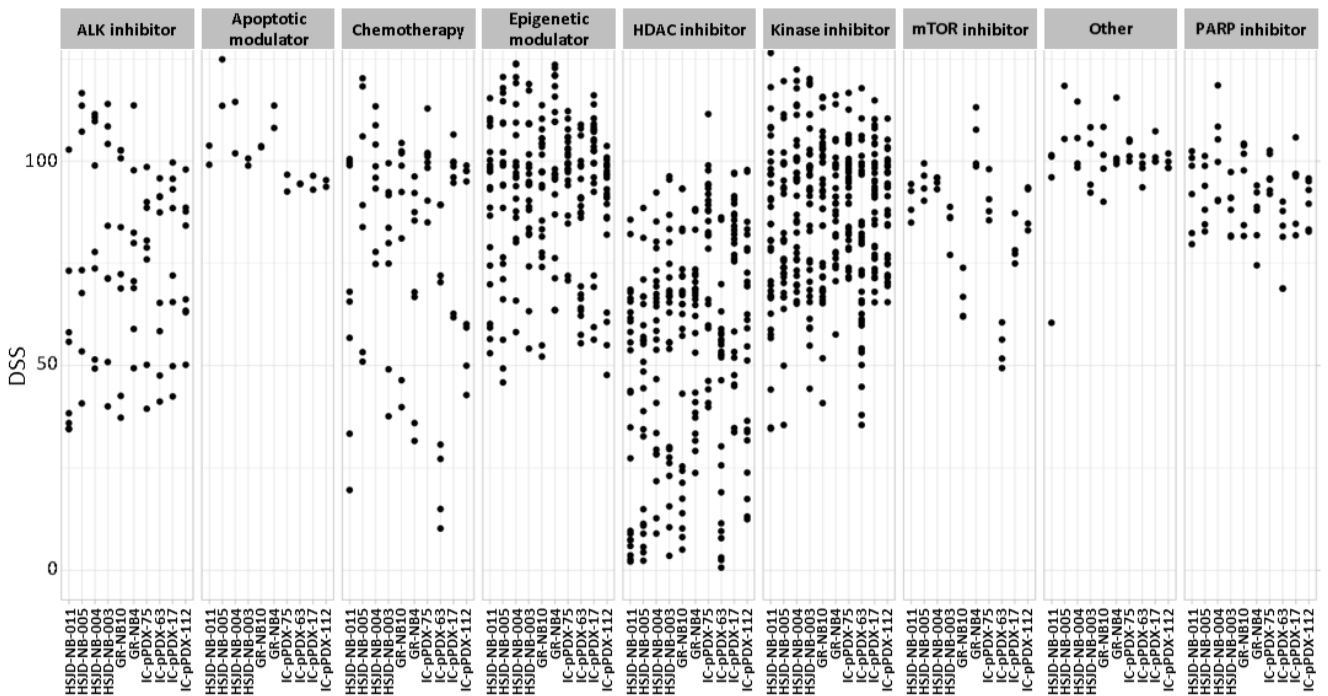


Figure 21: Drug sensitivity score (DSS) distribution across the ten PDX models screened according to the drug therapeutic class.

We then looked for the expected drug sensitivities according to the molecular characteristics of the different models. ALK inhibitor lorlatinib appeared as a hit in *ALK* aberrant models (HSJD-NB-011, GR-NB4 and IC-pPDX-75). CDK4/6 inhibitor ribociclib did not show specific cytotoxicity against *CDK4* amplified IC-pPDX-17 model, nor did trametinib (MEK inhibitor) or tazemetostat (EZH2 inhibitor) against *NF1* mutated GR-NB10 and *ARID1A* mutated HSJD-NB-005 models, respectively. The results of the screening of the in-house library are summarized as a heatmap in Figure 22.

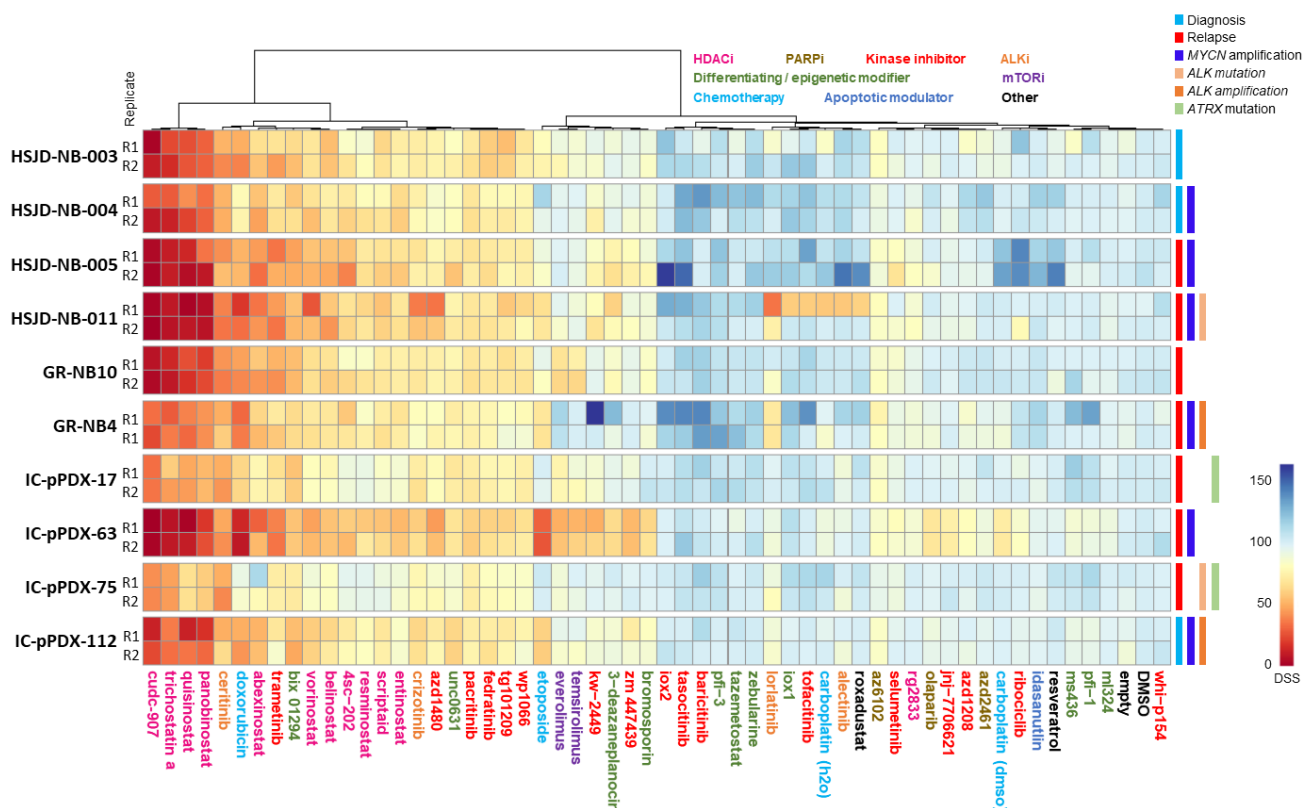


Figure 22: Hierarchical clustering across the high-risk neuroblastoma PDX models screened by the in-house library based on their drug sensitivity score (DSS) for each drug. On the bottom are listed the 55 compounds included in our in-house drug library. On the left, are listed the different PDX models screened. The color code for drugs is defined in the top left panel. In the top right panel are described the main characteristics harbored by the different PDX models, indicated as a color bar in the right. R1: replicate 1; R2: replicate 2.

1.1.5.6 Common drugs to the in-house and COMPASS libraries

We then wanted to compare the cytotoxicity of the drugs found in both libraries, namely our in-house and the COMPASS libraries for the models screened with both libraries. There were 16 common drugs (alectinib, ceritinib, crizotinib, doxorubicin, entinostat, etoposide, everolimus, idasanutlin, lorlatinib, olaparib, panobinostat, ribociclib, tazemetostat, temsirolimus, trametinib and vorinostat) and eight PDX models (HSJD-NB-003, (HSJD-NB-004, HSJD-NB-005, HSJD-NB-011, GR-NB10, GR-NB4, IC-pPDX-17 and IC-pPDX-63) screened with both libraries.

The comparative analysis of the cytotoxicity of common drugs to both libraries showed significant differences between in-house biological replicates and the COMPASS library screening, especially for panobinostat, ceritinib, doxorubicin, vorinostat, entinostat, trametinib, crizotinib and etoposide. For all these molecules, the cytotoxicity obtained with the in-house library screening was higher compared to the COMPASS', which showed almost no cytotoxicity for these molecules (figure 23).

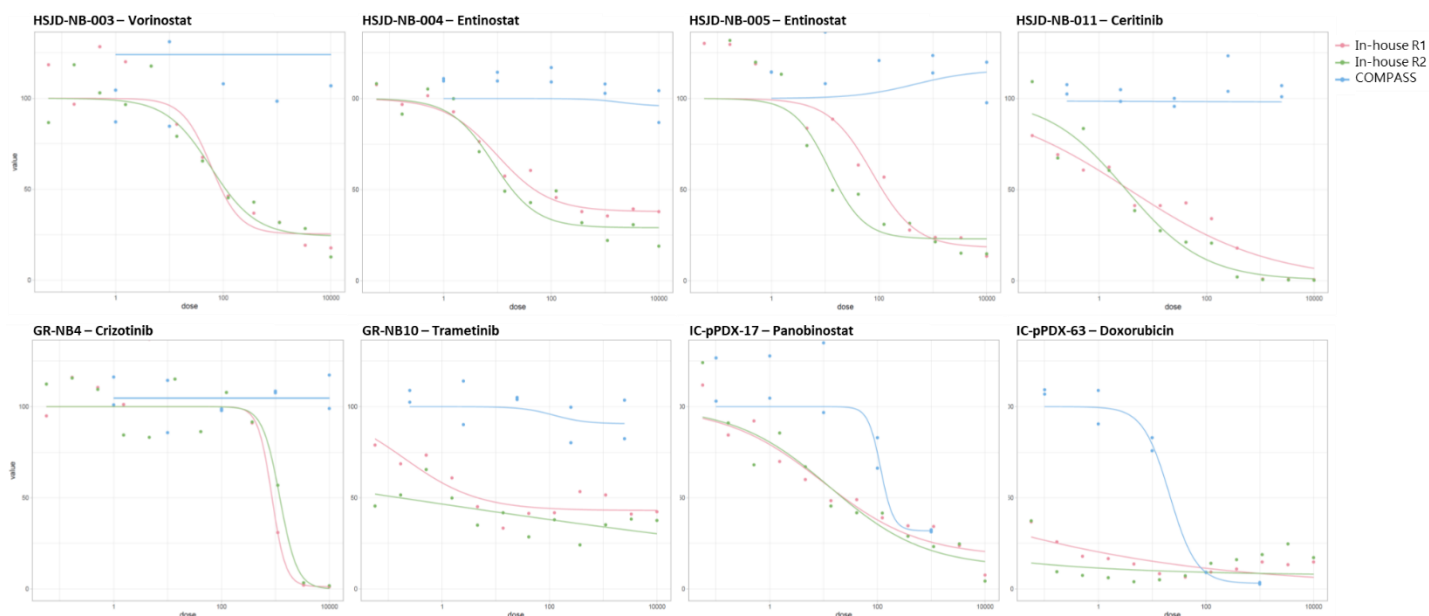


Figure 23: Drug-response curves of several drugs common to the COMPASS and in-house libraries in the eight models screened with both libraries. R1: replicate 1; R2: replicate 2.

Further explorations are needed to understand the differences obtained between different screenings: new experiments are ongoing to rule out technical difficulties which could explain these issues.

1.1.5.7 Concluding remarks

These data show that it is possible to perform *ex vivo* high-throughput drug screening using short-term cultures of high-risk neuroblastoma PDXs. Results were highly reproducible for the in-house screening. We identified HDACi as a group of compounds that are highly cytotoxic across the different high-risk neuroblastoma PDTC models

Most of the drugs predicted as hits based on the molecular profiling of the cell lines were confirmed. This was not the case in *ex vivo* PDTC screenings, in which the predicted active drugs did not always induce the expected cytotoxicity. This highlights the heterogeneous nature of single biomarker/drug-response associations, particularly in neuroblastoma, and suggest that integrative analysis of molecular and drug response data are more informative. Further improvements are expected in the future using new drug-response metrics that are insensitive to cell division rates (Hafner et al., 2016).

These results also highlight the challenges of comparability between drug screenings when slight technical parameters change, which could play a major role in the final output, and further underline the importance of alignment and harmonization of techniques especially when considering moving this into clinical applications.

1.1.6 Use of PDTCs to test chemo-drug combinations

1.1.6.1 Experimental pipeline

Combination therapies are increasingly being used as an approach to combat development of resistance in cancer treatment. We aimed at exploring the combination of chemotherapy and targeted agents in seven high-risk neuroblastoma PDX models (GR-NB4, GR-NB10, IC-pPDX-75, HSJD-NB-003, HSJD-NB-004, HSJD-NB-005 and HSJD-NB-011), with the intention that the addition of chemotherapy to targeted agents would increase their cytotoxicity.

First, we designed 3 matrixes combining chemotherapy compounds doxorubicin, etoposide and carboplatin with each other, in 11 concentrations each as 3-fold serial dilutions (from 10,000 nM to 0.017 nM) (Figure 24). We performed a single experience without internal technical replicates. We screened the six PDX models following the same design than described previously: dissociation and plating a D0, drug addition at D1 and metabolic readout at D4.

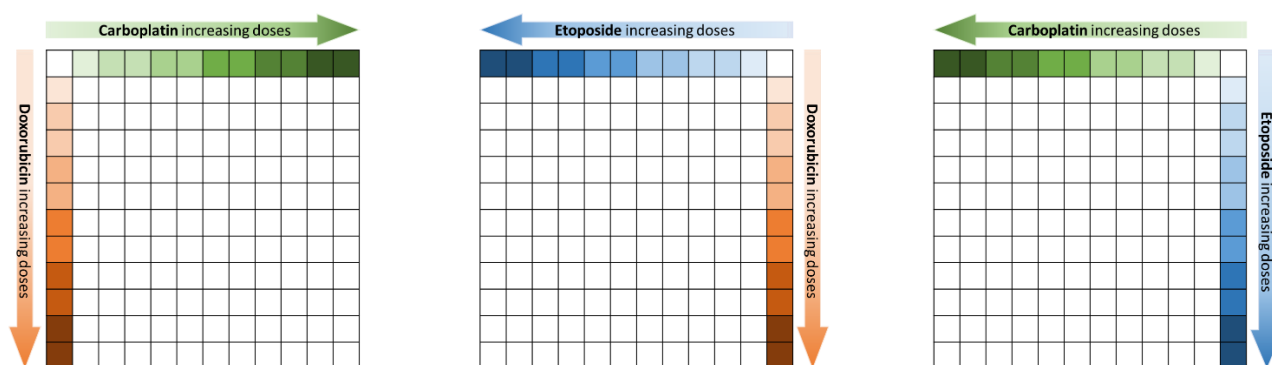


Figure 24: figure showing schematically the matrixes for chemotherapy combination.

The results of the chemotherapy combination screening are shown in Figure 25. Chemosensitivity varied across models, but overall this experiment confirmed the global sensitivity to doxorubicin, resistance to carboplatin and model-dependent sensitivity to etoposide described in section 1.1.5.5. We then searched for the combined concentrations of chemotherapy compounds that resulted in 80% of cell viability, to be further combined with relevant targeted compounds in a dose-response manner.

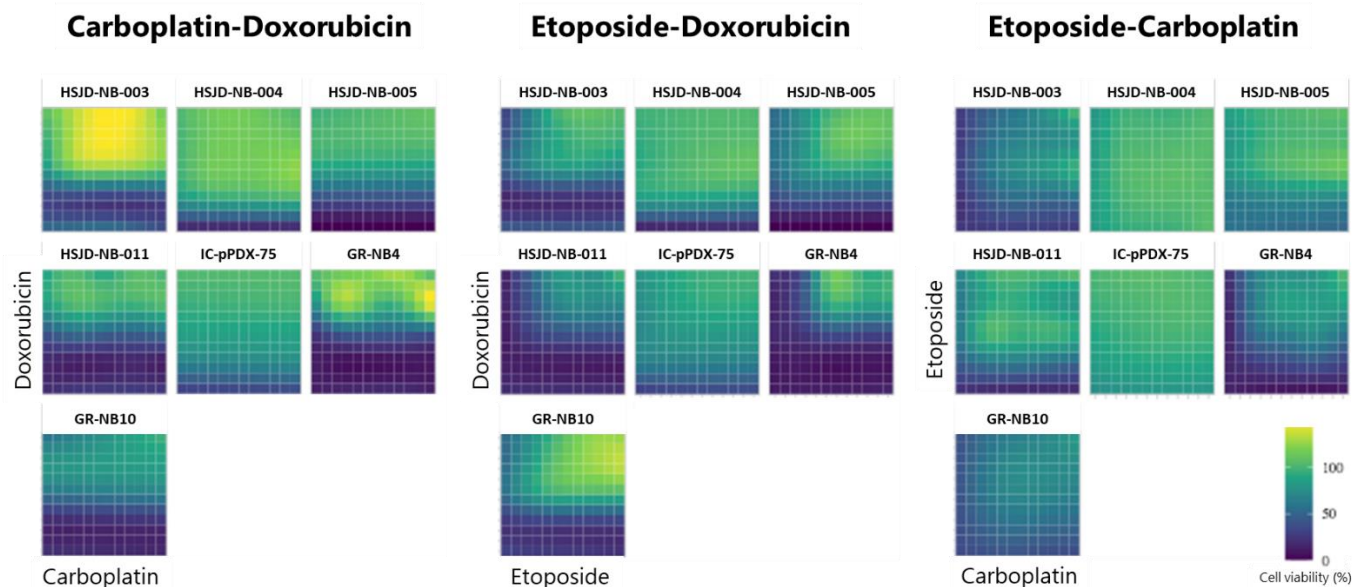


Figure 25: figure showing schematically the matrixes for chemotherapy combination.

For each PDX model, we chose the concentration that corresponded to 80% of cell viability based on the results of the chemotherapy association experiment. Selected doses are shown in Table 5 for models HSJD-NB-004, HSJD-NB-005, HSJD-NB-011, IC-pPDX-75, GR-NB4 and GR-NB10, since chemotherapy-targeted drug combination screenings were performed in these six models.

	HSJD-NB-004	HSJD-NB-005	HSJD-NB-011	IC-pPDX-75	GR-NB4	GR-NB10
[Carboplatin– Doxorubicin]	3,333 : 370.37	370.37 : 41.15	41.15 : 4.57	1,111 : 123.46	41.15 : 4.57	13.72 : 1.52
[Carboplatin – Etoposide]	10,000 : 3,333	370.37 : 123.46	1.52 : 0.51	10,000 : 3,333	13.72 : 4.57	13.72 : 4.57
[Etoposide – Doxorubicin]	3,333 : 1,111	126.46 : 41.15	1.52 : 0.51	123.46 : 41.15	13.72 : 4.57	123.46 : 41.15

Table 5: Combined concentrations (expressed in nM) of chemotherapy compounds leading to 80% of cell viability that were chosen for combination with targeted drugs.

We then proceeded to combine chemotherapy (using the fixed dose of both compounds described above in table 5) with targeted agents. Targeted agents were screened in a dose-response manner in 12 concentrations each as 3-fold serial dilutions (from 10,000 nM to 0.056 nM). We performed a single experiment with internal technical duplicates. The experimental pipeline was, also, dissociation and plating a D0, drug addition at D1 and metabolic readout at D4. For technical reasons, we had to regroup the screens. Thus, the chosen targeted agents for combination with chemotherapy were:

- For HSJD-NB-011, IC-pPDX-75 and GR-NB4 *ALK* aberrant models we screened the *ALK* inhibitors crizotinib and lorlatinib as well as the *MDM2* inhibitor idasanutlin (since in the last part of the thesis we are interested in *MDM2* inhibitors in neuroblastoma). The *HDAC* inhibitors belinostat and entinostat were added to the screening to complete the 384-wp.
- For HSJD-NB-004 and HSJD-NB-005 and GR-NB10, we screened the *EZH2* inhibitor tazemetostat (according to the *ARID1A* mutation of HSJD-NB-004 and HSJD-NB-005), the *MEK* inhibitor

trametinib and the mTOR inhibitor temsirolimus (according to the *NF1* mutation+LOH of GR-NB10). Entinostat and Lorlatinib were added to the screening to complete the plate and as controls since they were used for the *ALK*-aberrant models.

1.1.6.2 Analysis of the chemotherapy-targeted drug combinations in PDTC

The expected enhanced cytotoxicity of the [chemotherapy + targeted drug] combination depended on the cytotoxicity of chemotherapy combination alone. Indeed, we observed that the expected cell viability of 80% of chemo alone was only achieved for some chemo combinations in some models (figure 26), whereas for others, cell viability was significantly higher than 80%. Concretely, in IC-pPDX-75 the selected carboplatin-etoposide combination reached a median of 76.3% of cell viability, and carboplatin-doxorubicin and etoposide-doxorubicine attained 87.2% and 87.9% respectively. For models GR-NB10 and HSJD-NB-004, the etoposide-doxorubicin combination resulted in 81.9% and 65.4% of median cell viability respectively, whereas the other chemo combinations were near 100%. In HSJD-NB-005, all chemo combinations resulted in median cell viabilities slightly higher than 80%, with etoposide-doxorubicin and carboplatin-etoposide at 83.1% and 85.6% respectively, but only 93% for carboplatin-doxorubicin). Finally, for models GR-NB4 and HSJD-NB-011, the median cell viability of the different chemo combinations was near 100%.

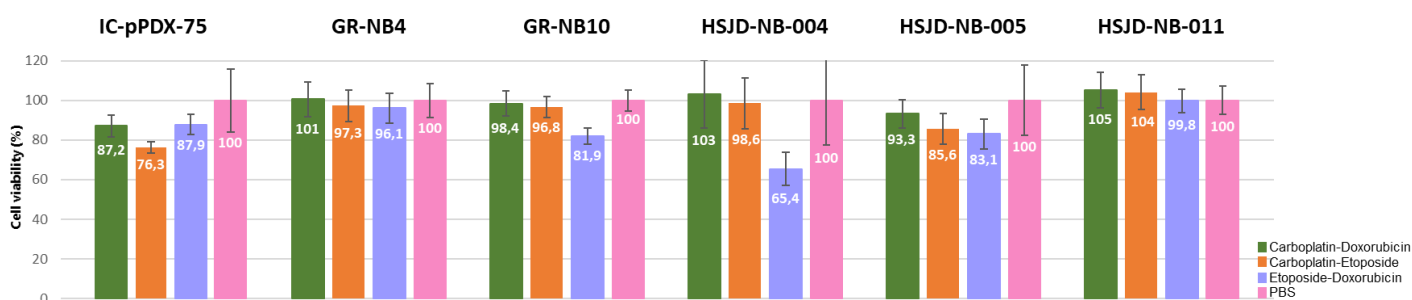


Figure 26: Barplots showing the cell viability corresponding to the different chemotherapy compounds combined with each other.

Consequently, we noticed that when the expected cell viability of chemotherapy alone did not reach 80%, no differences in dose-response curves of the associated targeted compounds were observed (figure 27). Concretely, in IC-pPDX-75 the addition of carboplatin-etoposide to the targeted drugs (belinostat, entinostat, crizotinib, lorlatinib and idasanutlin) showed enhanced cytotoxicity compared to carboplatin-doxorubicin and etoposide-doxorubicin. Furthermore, the associations of [carboplatin-doxorubicin + targeted drug] and [etoposide-doxorubicine + targeted drug], were significantly more cytotoxic than the targeted drugs alone. On the other hand, in models GR-NB10 and HSJD-NB-004, etoposide-doxorubicin enhanced the cytotoxicity of the 4 associated targeted drugs (entinostat, tazemetostat, temsirolimus and trametinib), but the other chemotherapy combinations were not significantly different than the targeted drug alone. Interestingly, in HSJD-NB-005, carboplatin-etoposide and etoposide-doxorubicin enhanced the cytotoxicity of entinostat, tazemetostat and lorlatinib but not temsirolimus and trametinib. Finally, in models GR-NB4 or HSJD-NB-011, the association was not more cytotoxic than the targeted drug alone (curves are superposed).

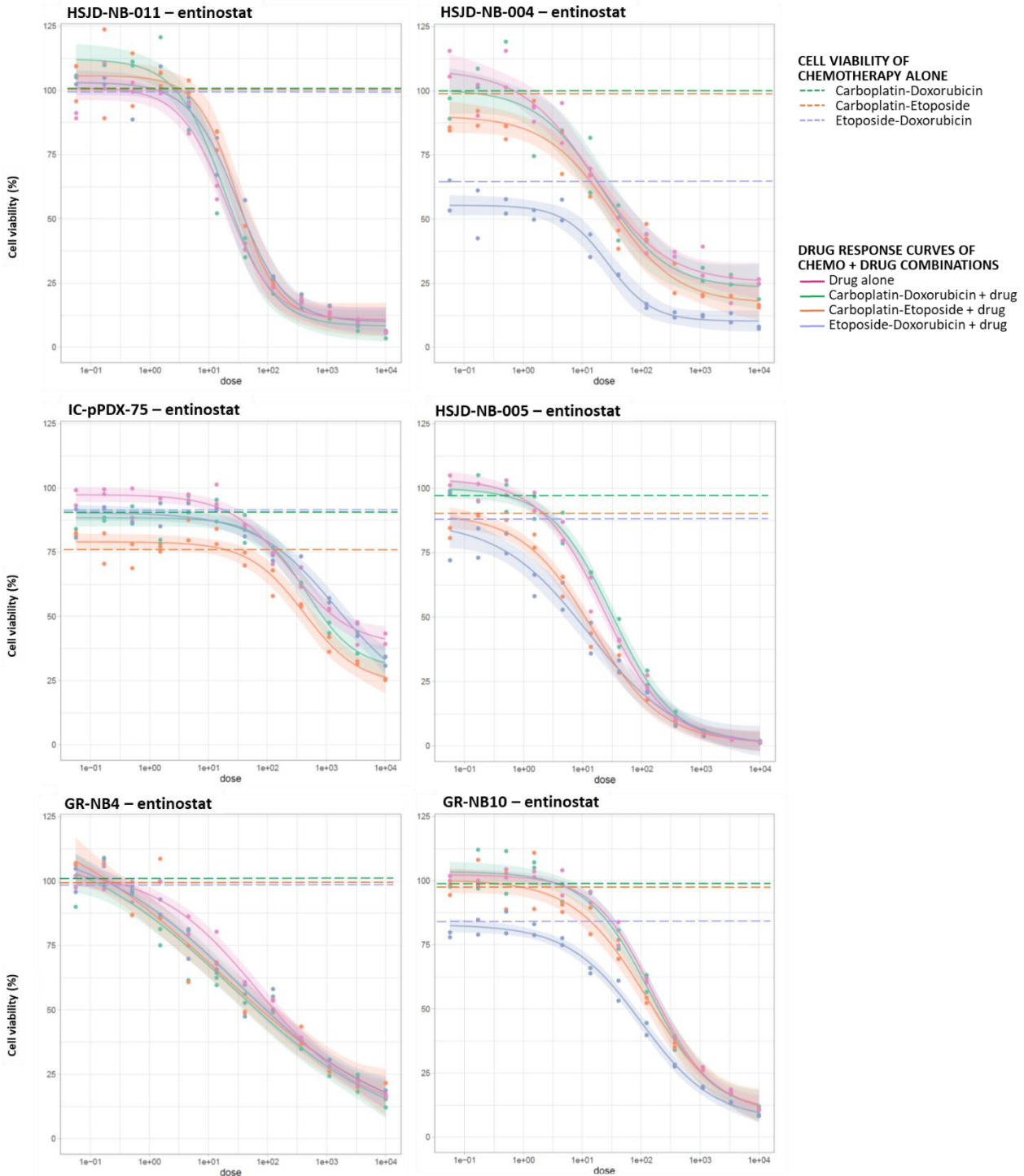


Figure 27: Dose response curves of chemo-drug combinations corresponding to models IC-pPDX-75, GR-NB10, HSJD-NB-004, HSJD-NB-005, GR-NB4 and HSJD-NB-011 for entinostat (HDAC inhibitor). Dot lines show the cell viability of the chemotherapy alone. Shadows surrounding the curves represent the confidence interval for each curve: if intervals do not overlap, the differences between curves are significant.

The results of the chemo-drug combination experiences are summarized in figure 28 as a heatmap based on the DSS: the addition of chemotherapy to the targeted drug was more cytotoxic than the drug alone only when the cell viability of chemotherapy alone was lower than 80% (as shown in figure 26).

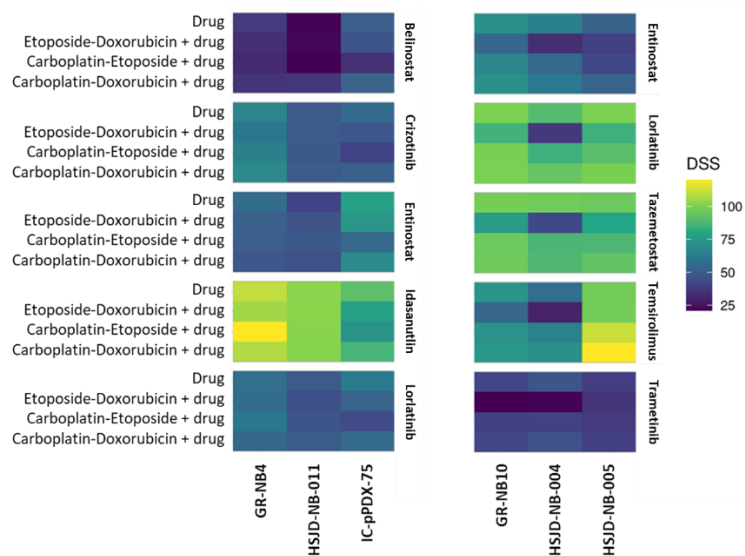


Figure 28: Heatmap based on the DSS for each chemo-drug combination and the corresponding PDX model.

1.1.6.3 Concluding remarks

We observed an additive effect of chemotherapy combined with targeted drugs when the chosen dose of chemotherapy was significantly cytotoxic itself (i.e. cell viability lower than 80% according to combination matrix assay). In the remaining cases, since the selected doses of chemotherapy did not correspond to the expected 80% of cell viability, this additive effect on the targeted compounds was not observed. New efforts must be done to improve the dose selection for chemotherapy compounds.

1.2 G-quadruplex structures as potential targets in high risk neuroblastoma

1.2.1 Scientific context

Overcoming chemoresistance is one of the major challenges in high-risk neuroblastoma. Despite intensive treatments (including standard chemotherapy, surgery, high-dose chemotherapy with stem cell rescue and maintenance treatment including anti-GD2 immunotherapy), after an initial response, over half of all patients undergo relapse of the disease that is subsequently resistant to treatment, with an overall survival after relapse which reaches 0-5% after 12 months (Moreno et al., 2017b). With the aim of improving the outcome of this group of patients, several strategies are being studied, the most of them trying to target different tumor cell specific genetic events with matched targeted agents (Matthay et al., 2012). There is now long experience with targeted treatments such as tyrosine kinase inhibitors in adult malignancies but these molecules, administered most frequently until recently as single agents, are associated in most cases with secondary resistance and disease progression (Konieczkowski et al., 2018). Thus, it is urgent to develop other innovating mechanistic strategies, including the identification of tumor cell specific vulnerabilities, to face chemoresistance and increase the survival of this group of patients with very poor outcome.

With the exception of *MYCN* gene amplifications and *ALK* mutations, few genetic abnormalities are recurrent in NB (Pugh et al., 2013). A group of genetic defects, representing 10-15% of high-risk neuroblastoma, involves the *ATRX* ("Alpha Thalassemia/mental Retardation syndrome X-linked") gene, including inactivating mutations or focal deletions (Pugh et al., 2013; Zeineldin et al., 2020). *ATRX* inactivating mutations and *MYCN* amplifications have been shown to be mutually exclusive in neuroblastoma (Ackermann et al., 2018; Zeineldin et al., 2020). *ATRX* is a protein that is part of the SWI/SNF2 Chromatin Remodeling Complex (SWItch/Sucrose Non Fermentable). In combination with the DAXX (death domain associated protein) transcription cofactor, it maintains the genomic stability of the cell by depositing histone H3.3 in telomeres and pericentromeric heterochromatin (Lewis et al., 2010). Approximately 17% of high-risk neuroblastoma maintain their telomeres through a telomerase-independent Alternative Lengthening of Telomeres (ALT) process, involving direct homologous recombination (Ackermann et al., 2018). Recent studies have shown the existence of a strong correlation between the appearance of an ALT phenotype and the presence of mutations inactivating the *ATRX* gene (Amorim et al., 2016). Despite loss-of-function mutations of *ATRX* are the most frequent events associated with ALT, they are observed only in 55% of ALT-positive neuroblastomas. Other events associated to ALT in neuroblastoma are somatic mutations in *TP53* pathway genes (*TP53*, *CREBBP*, *ATM*, *ATR*, *CDKN2A*, and *MDM2*), deletions in *PTPRD*, *CDK4* amplifications and loss of chr11q (Hartlieb et al., 2021).

ATRX binds widely across the genome at sites featuring tandem repeats and CpG islands (Law et al., 2010). Many such loci are GC-rich and susceptible to form G-quadruplex structures (G4). G4 are labile non-B DNA or RNA structures known to form obstacles to multiple nuclear processes including DNA replication and transcription, and are present in large number at telomeres due to their G-rich sequences. A large proportion of *ATRX* target sites are predicted to adopt these G4-DNA

structures, leading to the concept that ATRX might facilitate replication in the presence of G4 or by preventing their formation (Watson et al., 2013). It has also been shown that a consequence of loss of ATRX function is an increased frequency of these G4, causing DNA damage (Whitehouse I., Cell, 2010), and that ATRX-null cells have difficulty in resolving them (Wang et al., 2019). It is also likely that the presence of G4 in telomeric DNA favors the ALT phenotype by presenting a barrier to the replication fork, causing fork stalling, collapse and subsequent restart by the homologous recombination DNA-repair mechanism (Clynes et al., 2015). This has been recently confirmed in neuroblastoma: the loss of ATRX in the nucleus causes a deficiency in the repair mechanisms by homologous recombination and a deterioration of the replication fork in this disease. Furthermore, the combination of iPARP inhibitors and DNA damaging agents (such as irinotecan) was effective in preclinical models of neuroblastoma (George et al., 2020).

Interestingly, the G4 structures mentioned above can represent therapeutic targets. In oncology, the first G4-ligands (G4-L) were developed to stabilize the G4 structures present mostly at telomeres in order to inhibit telomerase activity (reactivated in many cancer cells), leading to the telomere shortening and cell senescence. As G4 structures have been found in many sequences outside the telomeres, G4-L were then designed as novel anticancer agents to target non-telomeric restricted G4 structures (Monchaud and Teulade-Fichou, 2008). One recent publication reported that 1/ in *in vitro* and *in vivo* experiments, ATRX deficiency in normal human astrocytes and *ATRX*-mutant glioma selectively enhanced DNA damage and cell death following chemical G4 stabilization, and 2/ G4 stabilization synergized with DNA-damaging therapies, including chemotherapeutic agents (Wang et al., 2019). This would be the result of a synthetic lethal mechanism: G4s are normally resolved by both ATRX-dependent and ATRX-independent mechanisms to mitigate DNA damage in cells. In the setting of ATRX deficiency, DNA damage increases but its lethal effects are dampened by ATRX-independent G4 resolution, maintaining cellular viability. However, concurrent G4 stabilization impairs these salvage pathways, further enhancing DNA damage and inducing cell death by synthetic lethality in the ATRX-deficient context (Figure 29). Nevertheless, the therapeutic potential based on the synthetic lethality resulting from the stabilization of G4 structures in ATRX-deficient tumors has not been enough explored, particularly in high-risk neuroblastoma .

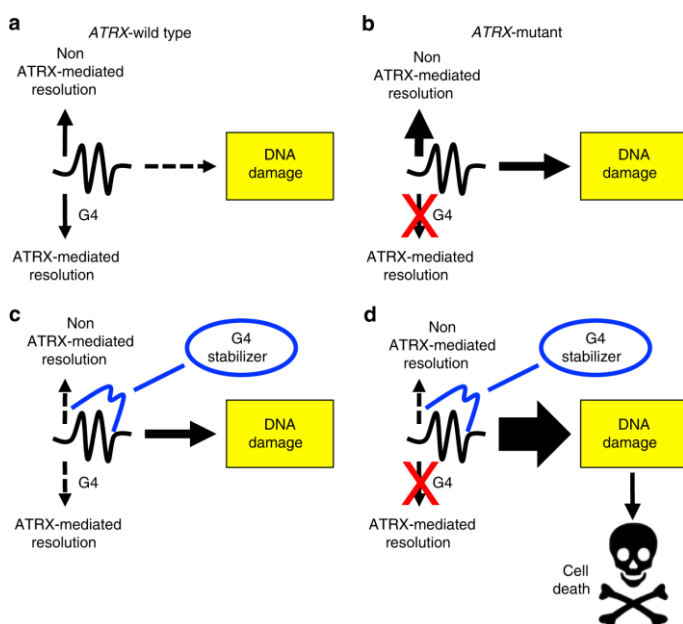


Figure 29 (Wang et al., 2019): Selectively targeting G4s in the ATRX-deficient context. Both ATRX-dependent and ATRX-independent mechanisms resolve G4s to mitigate DNA damage in cells (a). When the activity of ATRX is absent, DNA damage is higher its cytotoxic effects are dampened by ATRX-independent G4 resolution, thus maintaining cellular viability (b). Concurrent G4 stabilization impairs these salvage pathways (c, d), enhancing DNA damage and inducing cell death in the ATRX-deficient context

The two G4-L that are currently in clinical development in adults are quarfloxin and CX-5461. Three trials with quarfloxin (phase I NCT00955292 and NCT00955786 for advanced solid tumors and phase II NCT00780663 for neuroendocrine carcinoma) have completed the recruitment (an additional phase II trial NCT00485966, for patients with relapsed or refractory B-cell chronic lymphocytic leukemia was withdrawn prior to patient enrollment). One phase I trial is currently ongoing with CX-5461 for advanced solid tumors (NCT02719977).

To date only limited data on G4-L in neuroblastoma is available. The efficacy of two small G4-L molecules, quarfloxin and CX-5461, has been studied in this disease, showing efficacy, both *in vitro* and *in vivo*, of these molecules in high-risk neuroblastoma models overexpressing *MYCN* without mutation of *ATRX* (Hald et al., 2019). Treatment of neuroblastoma cells with quarfloxin or CX-5461 suppressed *MYCN* expression, induced DNA damage, and activated p53 followed by cell cycle arrest or apoptosis. In addition, CX-5461 repressed the growth of established *MYCN*-amplified neuroblastoma xenograft tumors in nude mice. Thus, this work opens new perspectives for targeting the “undruggable” *MYCN*. Indeed, it has been extremely difficult to develop a specific inhibitor that directly targets MYCN protein in high-risk neuroblastoma (Sala, 2015).

This work was performed in collaboration with Pierre Verrelle, who inspired the project, and Marie-Paule Fichou-Teulade who provided us with a precious G4-L library.

1.2.2 Hypotheses and objectives

In the context of *ATRX* deficiency, there is a specific therapeutic vulnerability by which the stabilization of the G4 structures induces cell death by a mechanism of synthetic lethality due to replication stress and DNA damage. According to our hypothesis, G4-L molecules may be potential specific effective molecules for the treatment of *ATRX*-deficient high-risk neuroblastoma, based on the exploitation of the synthetic lethality, but also for *MYCN*-amplified neuroblastoma through a mechanism that is not yet fully elucidated. In addition, we want to explore whether the pre-treatment with G4-L could sensitize high-risk neuroblastoma cells (either *ATRX*-mutated or *MYCN*-amplified) by fixing G4 structures, so that concomitant treatment with DNA-damaging chemotherapy agents should induce cell death by a synthetic lethal mechanism. Thus, our proof-of-concept project aims at demonstrating the effectiveness of small molecules G4-L to overcome resistance to conventional chemotherapy in high-risk neuroblastoma.

Thus, the two main objectives of our study are:

- 1. To determine the *in vitro* selective sensitivity of high-risk neuroblastoma cells to a panel of G4-L according to their *ATRX* and *MYCN* status.**

For this, high-risk neuroblastoma cell lines representative of different phenotypes, depending on the *ATRX* mutational profile, the *MYCN* amplification and other markers (Table 1) will be used. *ATRX*-deficient cells are sensitive to DNA damage and cell death after chemical stabilization of G4 structures secondary to a mechanism of synthetic lethality due to

replication stress and DNA damage. We also want to explore in an innovative and novel way the sensitivity of high-risk neuroblastoma in a *MYCN*-amplified *ATRX*-wild type context.

2. To *in vitro* study whether, once pretreated with G4-L, chemoresistant *ATRX*-defective or *MYCN*-amplified high-risk neuroblastoma cells can be re-sensitized to standard chemotherapy.

According to this, we hypothesize that, by treating cells with low doses of G4-L (80% inhibitory concentration, IC_{80}), cells can be re-sensitized to chemotherapy compounds to which they were previously resistant, based on a mechanism of synthetic lethality, and therefore overcome chemoresistance.

1.2.3 Phenotype of high-risk neuroblastoma cell lines and PDX models.

First, we characterized the 31 high-risk neuroblastoma cell lines available in our laboratory with respect to their ALT phenotype, as well as a subset of our PDX models. We used the c-circle assay (Henson et al., 2017), which is based on detection of the c-circles. As mentioned, ALT involves recombination-dependent DNA replication and generates large increases in telomere length, consistent with either a long, linear telomeric template or a rolling mechanism, giving rise these circular single-stranded DNA c-circles. Two cell lines, CHLA-90 and SK-N-FI (with and without *ATRX* mutations, respectively), as well as *ATRX*-mutated PDX IC-pPDX-17 harbor an ALT phenotype (Figure 30).

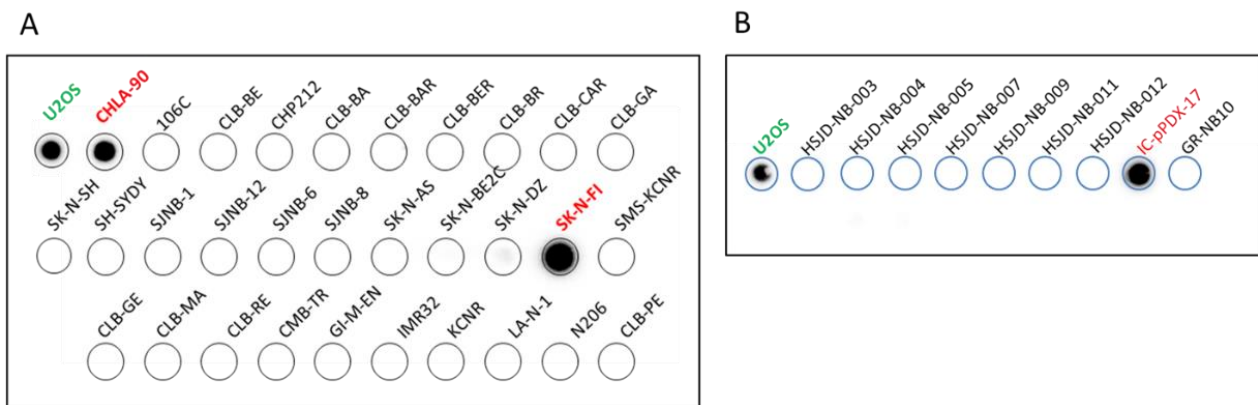


Figure 30: C-circle assay of a panel of 31 high-risk neuroblastoma cell lines (A), as well as 9 high-risk neuroblastoma patient-derived xenografts (B). CHLA-90 and SK-N-FI cell lines as well as IC-pPDX-17 harbor an ALT phenotype. U2OS osteosarcoma cell line is used as a c-circle positive control.

We also assessed the *ATRX* expression in a subset of cell lines, since in clinical practice the absence of *ATRX* nuclear expression is used as a reliable surrogate marker of ALT phenotype (Heaphy et al., 2011) (Figure 31). The study of *ATRX* expression by identification of *ATRX* foci was performed by immunofluorescence using anti-*ATRX* antibody and confocal microscopy.

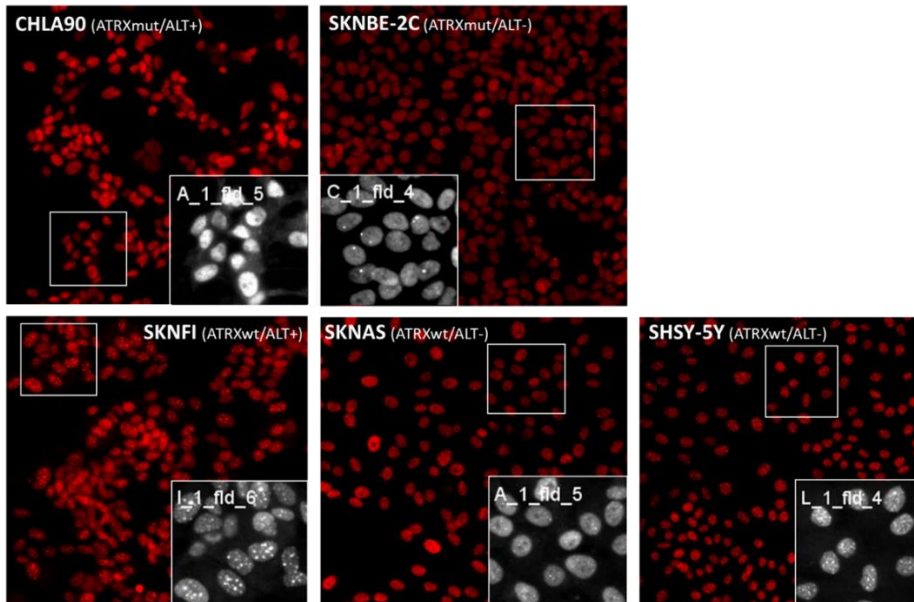


Figure 31: ATRX expression by immunofluorescence in 5 high-risk neuroblastoma cell lines. The presence of nuclear foci indicates a normal expression of ATRX. The absence of nuclear foci in the CHLA-90 cell line indicates that the deletion of the ATRX exon 9 in this cell line causes a loss of expression of the protein.

Table 6 summarizes the *MYCN*, *ATRX* and ALT status in 31 neuroblastoma cell lines and in a subset of our PDX models.

Model	Cell line or PDX	Established at	<i>MYCN</i> status	<i>ATRX</i> status	ATRX expression by IF	ALT status
106C	Cell line	MD	Amplified	WT		ALT (-)
CLB-BE	Cell line	Relapse	Amplified	WT		ALT (-)
CHP212	Cell line	MD	Amplified	WT		ALT (-)
CLB-BA	Cell line	Diagnosis	Amplified	WT		ALT (-)
CLB-BAR	Cell line	Relapse	Amplified	WT		ALT (-)
CLB-BER	Cell line	Relapse	Amplified	WT		ALT (-)
CLB-BR	Cell line	Relapse	Amplified	WT		ALT (-)
CLB-CAR	Cell line	Relapse	Amplified	WT		ALT (-)
CLB-GA	Cell line	Relapse	WT	WT		ALT (-)
CLB-GE	Cell line	Relapse	Amplified	WT		ALT (-)
CLB-MA	Cell line	Relapse	Amplified	WT		ALT (-)
CLB-RE	Cell line	Relapse	Amplified	WT		ALT (-)
CLB-TR	Cell line	Relapse	Amplified	WT		ALT (-)
GI-M-EN	Cell line	Relapse	WT	WT		ALT (-)
IMR-32	Cell line	Diagnosis	Amplified	WT		ALT (-)
SMS-KCNR	Cell line		Amplified	WT		ALT (-)
LA-N-1	Cell line	Relapse	Amplified	WT		ALT (-)
KELLY/N206	Cell line	MD	Amplified	WT		ALT (-)
CLB-PE	Cell line	MD	Amplified	WT		ALT (-)
SH-SY-5Y	Cell line	Relapse	WT	WT	Expressed	ALT (-)
SJNB-1	Cell line	MD	WT	WT		ALT (-)
SJNB-12	Cell line	MD	WT	WT		ALT (-)
SJNB-6	Cell line	MD	Amplified	WT		ALT (-)
SJNB-8	Cell line	MD	Amplified	WT		ALT (-)
SK-N-AS	Cell line	Relapse	WT	WT	Expressed	ALT (-)
SK-N-BE-2C	Cell line	Relapse	Amplified	p.Asn717Lys	Expressed	ALT (-)
SK-N-DZ	Cell line	MD	Amplified	WT		ALT (-)
SK-N-FI	Cell line	MD	WT	WT	Expressed	ALT (+)

SK-N-SH	Cell line	MD	WT	WT		ALT (-)
TR14	Cell line	Relapse	Amplified	WT		ALT (-)
CHLA-90	Cell line		WT	Partial del exon 9	Not expressed	ALT (+)
HSJD-NB-003	PDX	Diagnosis	WT	WT		ALT (-)
HSJD-NB-004	PDX	Diagnosis	Amplified	WT		ALT (-)
HSJD-NB-005	PDX	Relapse	Amplified	WT		ALT (-)
HSJD-NB-007	PDX	Relapse	Amplified	WT		ALT (-)
HSJD-NB-009	PDX	Relapse	WT	WT		ALT (-)
HSJD-NB-011	PDX	Relapse	Amplified	WT		ALT (-)
HSJD-NB-012	PDX	Relapse	Amplified	WT		ALT (-)
IC-pPDX-17	PDX	Relapse	WT	p.Gly1748Arg		ALT (+)
GR-NB10	PDX	Relapse	Amplified	WT		ALT (-)

Table 6: Characteristics of 31 HR-NB cell lines and 9 PDX models with respect to their *MYCN*, *ATRX* and ALT status. In bold are highlighted the cell lines that were used for our first experiments. For these cell lines, we performed IF for *ATRX* expression. IF: immunofluorescence; del: deletion

Below, we will describe the experiments that we carried-out in a subset of 5 high-risk neuroblastoma cell lines: CHLA-90, SK-N-FI, SK-N-BE-2C, SK-N-AS and SHSY-5Y.

1.2.4 Experimental workflow

The ultimate goal of this project is to assess the functional role of G4-L as “chemosensitizers”. We expected to identify an enhanced cytotoxic effect of the tested chemotherapeutic drugs by previous cell incubation with our panel of G4-L at low doses. For this purpose, we planned to incubate cells at D1 with a non-lethal dose (IC₈₀) of G4-L (determined in section 1.2.7) and 4 days later (D5) to add chemotherapy drugs to cells at several concentrations to perform dose-response curves (see figure X). Adding the chemotherapy 4 days later assures the at least 2 doubling population time (DPT), in order to stabilize the DNA structures. A metabolic read-out by CTG is performed at D7.

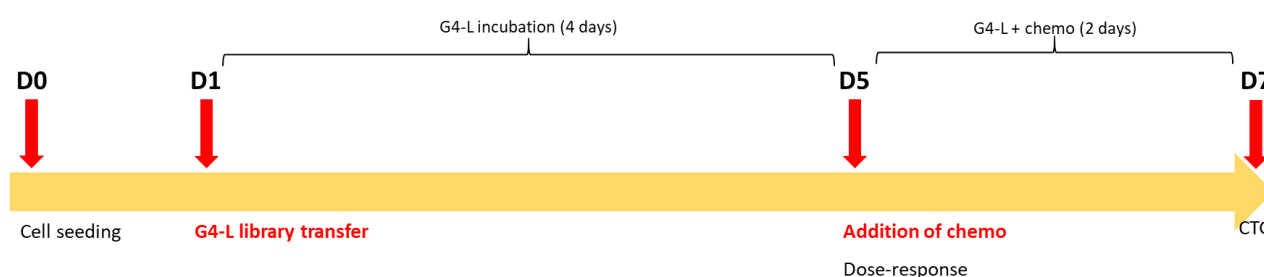


Figure 32: Goal experimental workflow.

All data generated during these experiments were analyzed using in-house bioinformatics and biostatistics in order to rank differential G4-L activities from dose-response synthetic lethality screens. Our hit selection method aimed to combine the different dose-response curve parameters and DSS metrics to ensure that relevant G4-L compounds were selected based on the synthetic lethal vulnerability. This methodology helped us to prioritize differentially active compounds, together with the manual inspection of the dose responses of the selected compounds at each step of the selection

process, and was critical for the final hit selection.

Before running this experimental workflow, several setting-up experiences needed to be done:

1. Grow study and population doubling time estimation in 384-wp (section 1.2.5)
2. Evaluation of chemoresistance to DNA-damaging agents across cell lines (section 1.2.6)
3. Studies of cytotoxicity of G4-L compounds alone (section 1.2.7)

All experiments were performed in biological triplicates and are described in the next sections.

1.2.5 Growth study and population doubling time estimation in 384-wp

Some pilot experiments were performed in order to check the number of cells to be seeded and their resistance to automated pipetting, as well as optimization of cell proliferation assays in multi-well plate format. We also wanted to evaluate the differential proliferative capacity across the high-risk neuroblastoma cell models we evaluated the dynamics of the cell culture development in 384-wp by calculating the population doubling time (PDT), which is the average time it takes a cell population to double in the log-phase/exponential phase, i.e. during linear growth. This task was very important although neglected in the current literature since G4-L compounds must be incubated with cells during at least 2 PDTs in order to stabilize the DNA structures.

Cell line cultures were prepared according standard protocols established for each cell line, detached using TrypLE dissociation reagent and viable cells automatically counted (Cellometer, Nexcelom). Cells were seeded in 384-wp (culture-treated, flat bottom, optically clear, Perkin Elmer) at 4 different densities in 40 μ l of cell medium. Plates were let at room temperature (RT) for 30 minutes before incubating at 37°C overnight to attach. The pre-incubation at RT minimizes thermal gradients while the cells are settling to the bottom of assay plates, thus allowing a more even distribution of cells within the well. Cell counts were monitored for 4 days using the fluorescent nuclei dye Hoechst 33342 added directly to the wells for 30 minutes at 37 °C and 5% CO₂. Then high-speed automated confocal imaging system (INCell 6500 HS, GE Healthcare) was used to acquire two random image fields in each well using a 10X objective. For each image, the total number of nuclei present in the image was automated counted using the INCell analyzer software algorithm, and the total/sum number of cells of the two image-fields calculated. Total cell count was then reported as mean values per well. For each cell type and condition, growth curves were plotted using GraphPad Prism software using the number of cells *vs.* days of culture and the PDT calculate from the linear part of the curve using the following equation:

$$(t_2 - t_1) / 3,32 \times (\log n_2 - \log n_1)$$

where t is time and n number of cells at the time interval 1-2. Figure 33 shows the proliferation assay and population doubling time for our 5 selected cell lines.

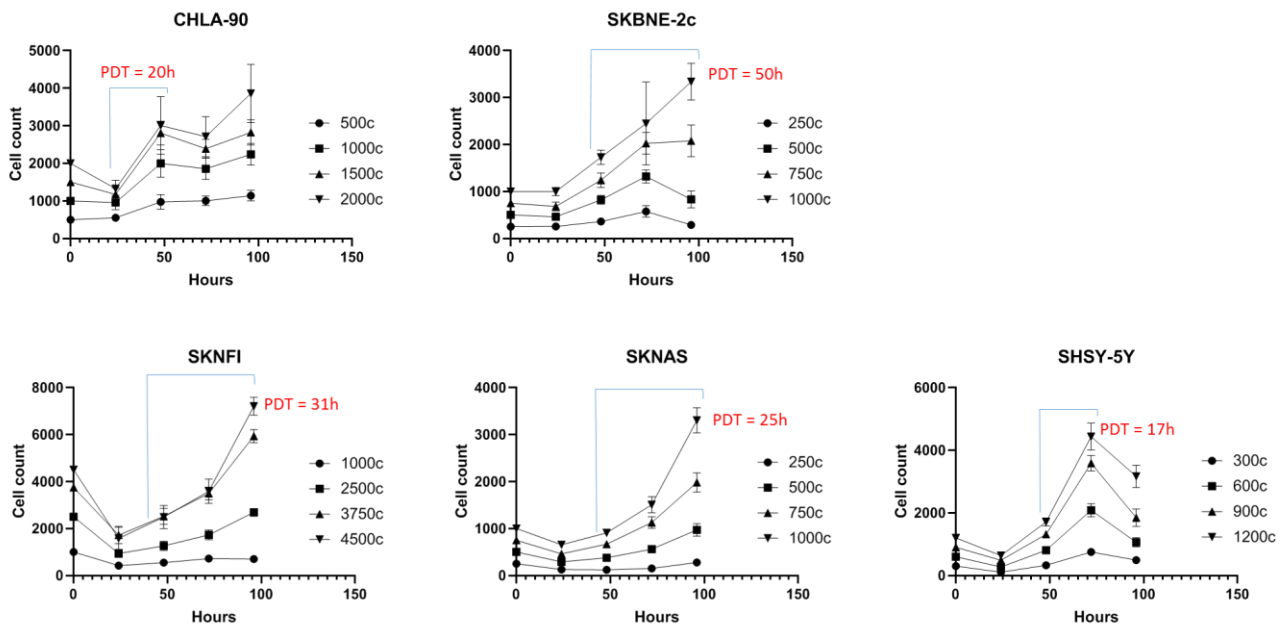


Figure 33: estimation of the population doubling time across our 5 selected high-risk neuroblastoma cell lines.

The PDT of the different cell lines ranged between 17 and 50 hours, meaning that 4 days was the minimum G4-L incubation time to have at least 2 doublings for each line. This is the reason why the G4-L incubation time was established at 4 days before in our goal experience workflow.

1.2.6 Evaluation of chemoresistance in 5 high-risk neuroblastoma cell lines

Resistance to conventional chemotherapy is a hallmark of high-risk neuroblastoma following relapse. In order to evaluate whether G4-L are able to revert drug resistance in high-risk neuroblastoma, we first needed to evaluate the level of *in vitro* chemoresistance to DNA-damaging agents of our selected high-risk neuroblastoma cell lines. The cytotoxic activity of three DNA-damaging agents used in high-risk neuroblastoma chemotherapy in standard clinical protocols (doxorubicin, etoposide, carboplatin) were evaluated using cell proliferation assays previously described in section 1.2.5. Cells were seeded and dose-dependently stimulated or treated with cell media only (control).

In order to exclude that the hypothetical chemoresistance was due to an efflux pump-mediated multi-drug resistance (MDR), we performed a preliminary experiment in cell lines consisting of adding doxorubicin (10 μ M) to the cell medium and visualizing the nuclei after 48h incubation by confocal microscopy taking advantage of the fluorescence properties of doxorubicin. Thus, if doxorubicin was identified in cell nuclei, this would be indicative that MDR might not be implicated in the observed chemoresistance. On the other hand, if doxorubicin was not identified in cell nuclei, MDR could be responsible of chemoresistance and this/these cell line(s) would be excluded for further experiments. We could identify doxorubicin-labelled nuclei in all cell lines, indicating that MDR is probably not implicated in the potential chemoresistance of the cell lines (figure 34).

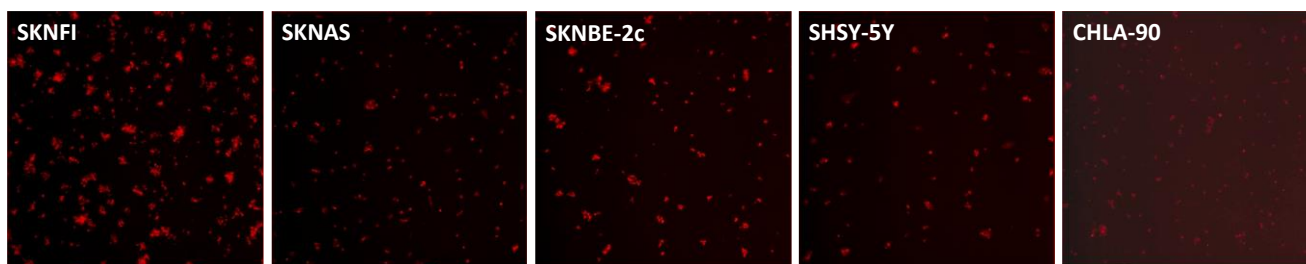


Figure 34: Doxorubicin (10 μ M) was added to the cell medium and doxorubicin labelled-nuclei were visualized by INCell 6500 10X confocal fluorescence microscopy, thus confirming that MDR was not responsible for the chemoresistance to carboplatin in this group of cell lines.

Experimental workflow for evaluation of cell line chemoresistance (figure 35): On D0, cells were seeded. On D1, cells were treated with 0.5% DMSO (solvent control mimicking G4-L addition) and on D5 serially diluted doxorubicin, etoposide or carboplatin were added to cells at 8 concentrations from 10 μ M to 4.57 nM. Chemotherapy compounds were diluted in PBS and the pipetting steps were automatized (Tecan) for increased robustness. Cells were then incubated with compounds at 37°C for 48h with no further changes of media or re-addition of compounds. Cell viability was assessed on D7 by fluorescence microscopy (as previously described in section 1.2.5) and CTG.

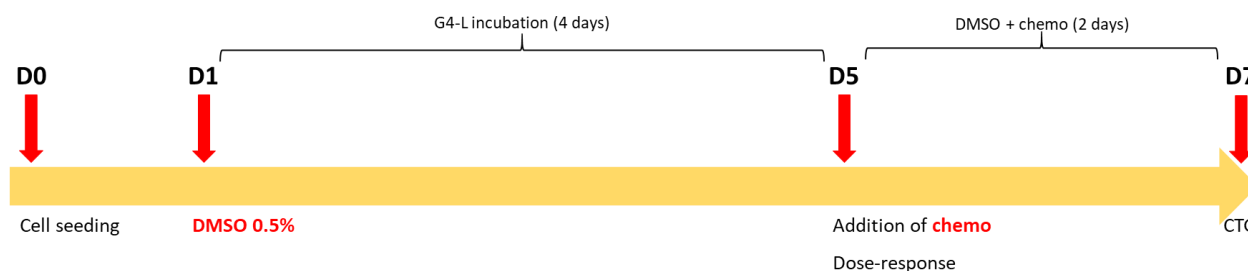


Figure 35: Experimental workflow for evaluation of cell line chemoresistance.

For dose-response data analysis, the dose-response curves were fitted in order to establish a response profile for each drug. In our protocol, the compound activity is normalized on a per-plate basis by dividing the value in each well by the median value of the DMSO control wells (100% cell viability). For each compound, a fourth parameter Hill curve log-logistic model was then fitted on the pooled replicate data with the R package drc22.

Cell lines were completely resistant to carboplatin. Etoposide showed limited cytotoxicity at the highest doses and doxorubicin was globally cytotoxic across the different cell lines (Figure 36).

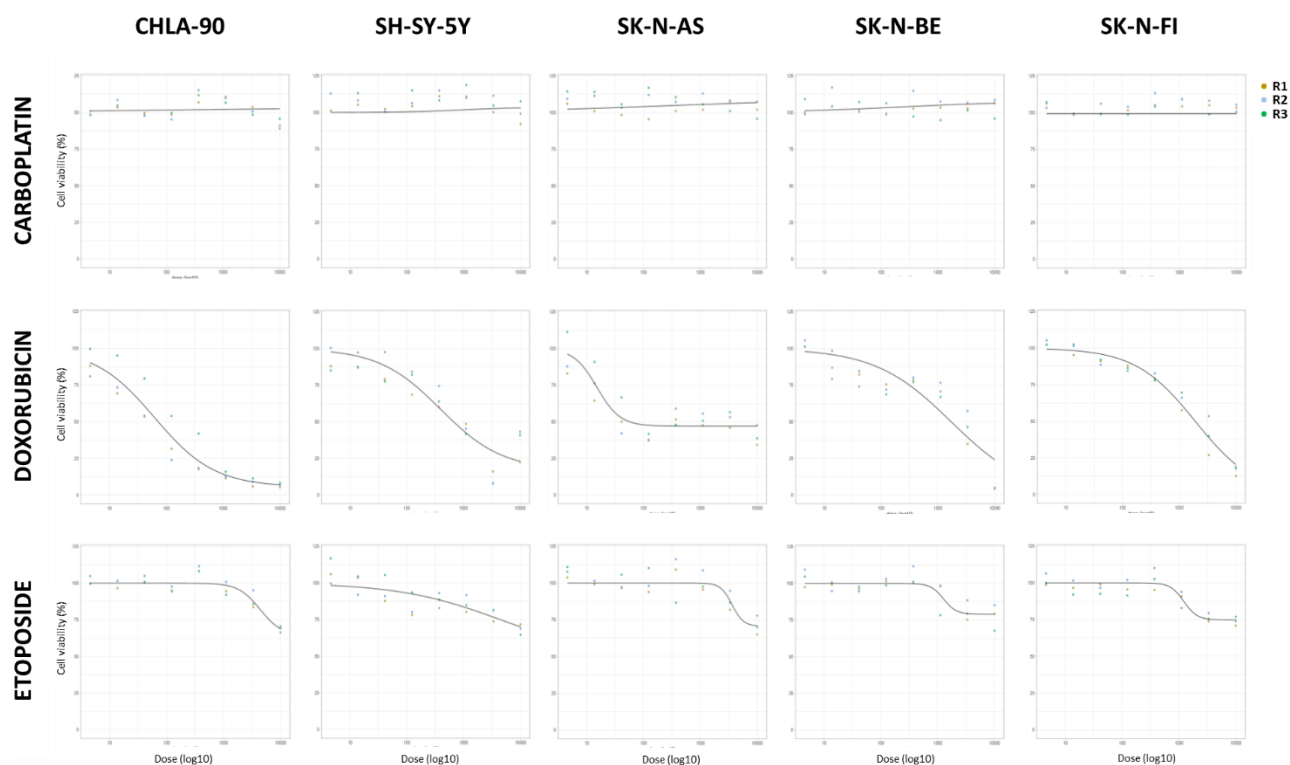


Figure 36: Dose-response curves of carboplatin, etoposide and doxorubicin across the 5 selected neuroblastoma cell lines.

1.2.7 Studies of cytotoxicity of G4-L compounds alone

A home-made collection of 55 G4-L was provided by a collaboration with Dr Marie-Paule Teulade-Fichou, leader of the CMBC team (Chimie et Modélisation pour la Biologie du Cancer) of the Institut Curie. Compounds were arrayed in 96-well plate that served as a master plate compound library. The G4-L stock compound library guaranteed a collection of standardized compounds used as common "reference material" for assessing the performance of each G4-L and providing a common compound stock to support meaningful experimental comparisons. This focused collection covered the five main chemical families of G4-L developed by Marie-Paule Teulade-Fichou laboratory over the past decade. In detail these 5 classes are:

- 1) **The PhenDC family** comprising derivatives of the PhenDC3 chemotype (bisquinolinium Phenanthroline DiCarboxamide). PhenDC3 is the best G4 ligand developed so far and considered worldwide the G4 gold standard. It displays a high affinity (nanomolar Kd) for all G4 and exhibits exquisite selectivity for G4 over all other DNA and RNA structures. This is attributed to the size of the PhenDC3 skeleton that matches perfectly with that of a G quartet thereby maximizing the interaction. This compound has been used extensively as a G4 probe in numerous cancer cell lines as well as in yeast (*S. Cerevisiae*) to promote G4 formation and induce G4 related effects (De Cian et al., 2007; Piazza et al., 2010; Lista et al., 2017).
- 2) **The PDC family** comprises derivatives of the PDC-360A-chemotype (bisquinolinium Pyridine DiCarboxamide). These are analogues of the PhenDC family with a pyridine core, they display very close properties for G4 targeting although possessing slightly lower binding affinity. The PDC series offers advantages in term of pharmacological properties as the derivatives are less

hydrophobic than their PhenDC counterparts. In addition it is easily derivatizable to add functionalities (De Cian et al., 2007; Verga et al., 2014).

- 3) **The HetDH family** (N-acylhydrazone with a heterocyclic core) comprises derivatives of the chemotypes PhenDH and PyDH. These are analogues of PhenDC and PDC but harbor N-acylhydrazone linkers instead of carboxamide linkers. Due to this chemical modification the compounds retain the properties of G4 binding but may show in some cases lower cellular toxicity (Reznichenko et al., 2019).
- 4) **The M-ttpty family** comprises Platinum (II) or Copper(II) complexes derived from the tolyterpyridine chemotype. This compound belongs to the first generation of metal complexes developed for targeting G4 structures. They offer the unique advantage to establish highly stable crosslinking adducts with G4 structures due to the presence of the metallic cation (e.g. Pt(II)). In addition the platinum derivatives have shown radiosensitizing properties (confirmed in animal models) and resulting in part from G4 targeting and telomeric dysfunctions (Bertrand et al., 2007; Merle et al., 2015).
- 5) **The ArPol family** comprises Aromatic Polycyclic compounds exemplified by the TrisQ chemotype (Trisquinalozinium). These cationic compounds possess planar rigid skeletons with a star shape that provides G4 affinity whilst preventing interaction with double-stranded DNA. Therefore the TrisQ series exhibits a high selectivity for G4 with minimized off-target effects (comparable to PhenDC3) (Bertrand et al., 2011).

This original collection is unique both in terms of structure diversity and in terms of knowledge and data that have been accumulated over the years on the chemical, pharmacological and cellular properties of these five classes. Finally, a set of commercially available compounds considered benchmarks or clinical reference for targeting G4 and validated in cells have been added to the home-made G4-L collection. These are Pyridostatin (PDS), N-mesomethylporphyrin (NMM), Quarfloxin and CX5461 (Seimiya, 2020).

We sought to study the cytotoxicity of G4-L alone in our selected 5 high-risk neuroblastoma cells to evaluate the selective efficacy of G4-L in ATRX-defective or *MYCN*-amplified context. The compounds were added to high-risk neuroblastoma cells at eight different concentrations in 3-fold dilutions covering a 10,000-fold concentration range from 10 μ M to 4.57 nM. The compounds were dispensed in each well to keep the final DMSO concentration no higher than 0.5% in the cell culture medium. As the negative control, DMSO was added to the wells to give final concentrations of 0.5% DMSO when the concentration of G4-L was 10 μ M.

Experimental workflow for the studies of cytotoxicity of G4-L alone (figure 37). Cell lines were seeded on D0 at the previously determined density and treated on D1 with the G4-L library. The compounds were diluted in DMSO and the pipetting steps were automatized (Tecan) for increased robustness. On D5, cell medium was added to the plates to mimic chemotherapy addition. Forty-eight hours later, on D7, Hoechst stain was added at 1/500 in the wells for 30 minutes and cell nuclei will be counted by fluorescence microscopy and its paired image analysis software (INCell 6500 HS, GE Healthcare). Cell viability was determined by CTG. Dose-response data analysis was performed as for chemotherapy compound screening. G4-L compound activity was summarized by computing a DSS.

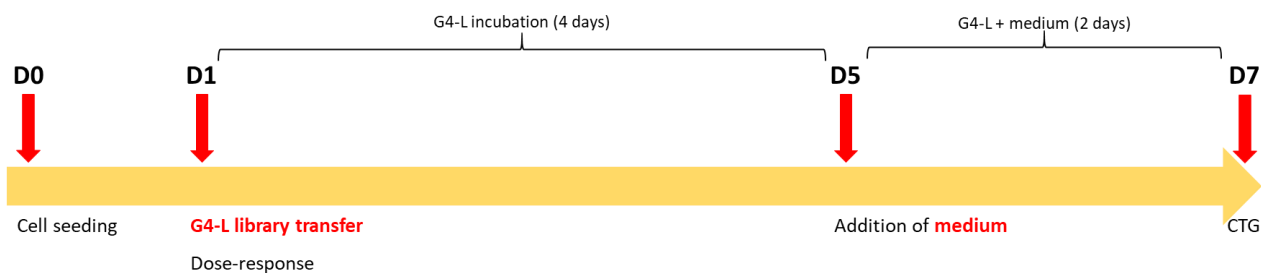


Figure 37: Experimental workflow for evaluation of G4-L cytotoxicity.

We observed a good correlation between triplicates in luminescence values across all models tested (median $R^2 = 0.836$ [0.719-0.906]) (Figure 38).

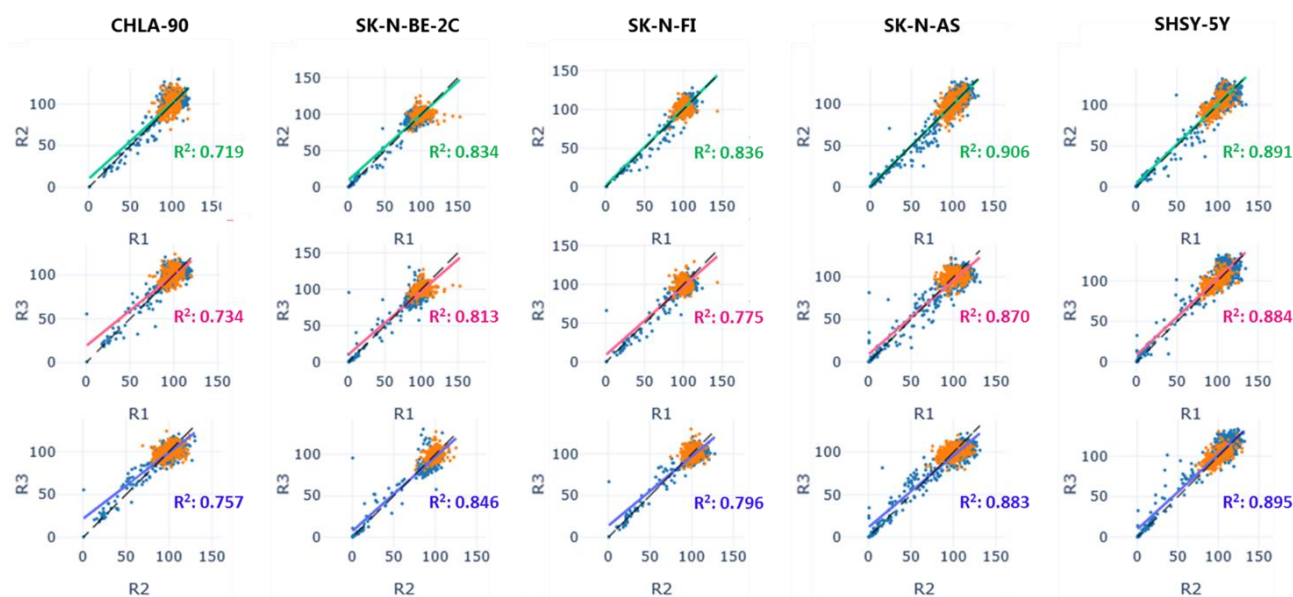


Figure 38: Coefficient of determination between triplicates in luminescence values across the 5 cell lines tested.

The analysis of the cytotoxicity of the G4-L library showed that a group of 3 compounds (el203, pt-ttpt and ra0941) induced important cytotoxicity across all the models. Furthermore, a group of compounds (fhy491, phendc3, pds, or20, or35, or40, or41, or42, or127 and or128) was selectively cytotoxic against the SK-N-AS cell line exclusively. CHLA-90 or SK-N-FI, the ALT-positive cell lines, did not show selective sensitivity to the G4-L library (Figure 39). Quarfloxine and CX-5461, the two G4-L in clinical development, showed different cytotoxicity across the different cell lines: CX-5461 was very cytotoxic against SH-SY-5Y and SK-N-BE-2C, moderately cytotoxic against SK-N-AS and not very cytotoxic against SK-N-FI and CHLA-90. Quarfloxine was cytotoxic against SK-N-BE-2C and SK-N-AS only at higher concentrations.

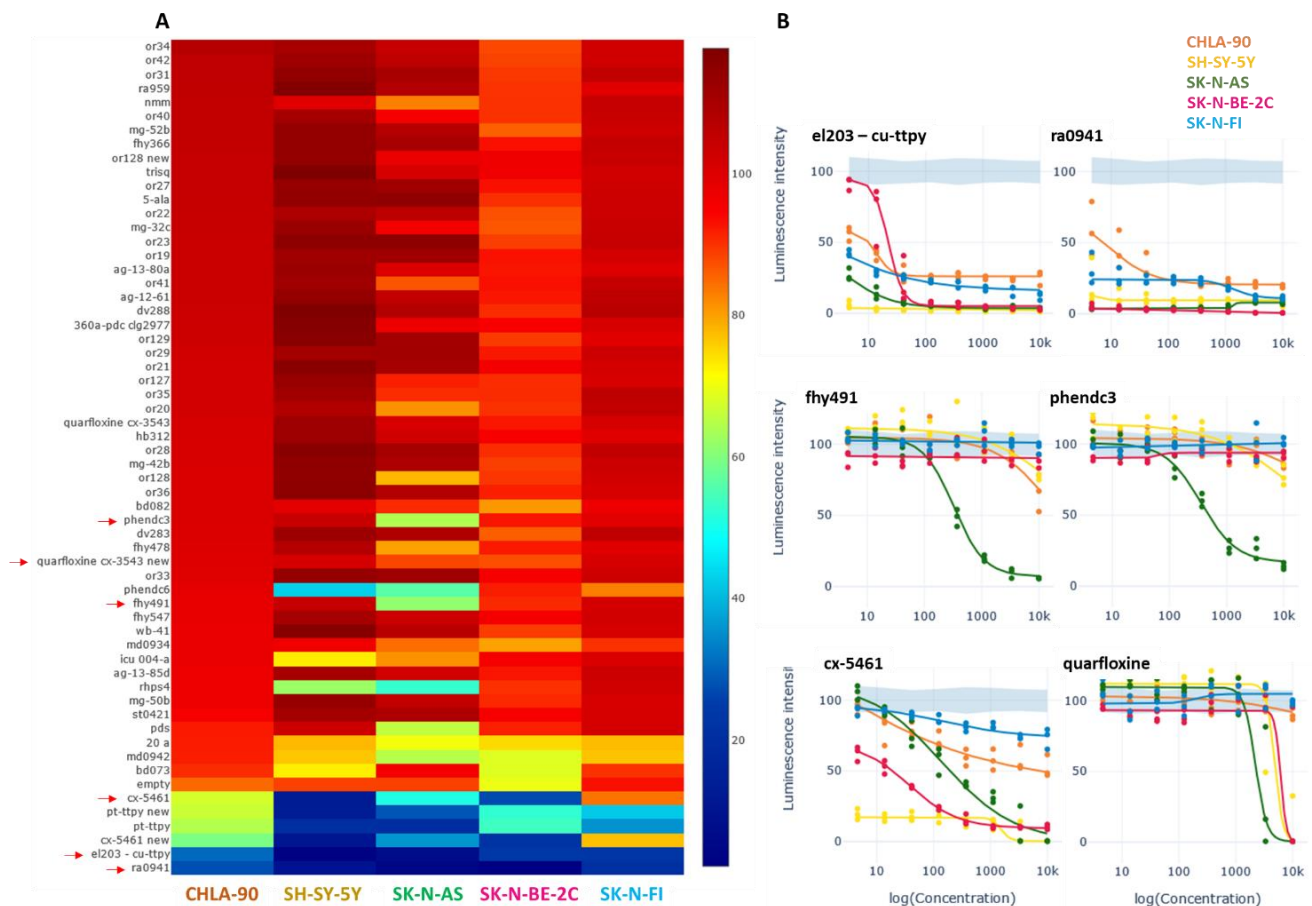


Figure 39: (A) Heatmap showing the activity of the G4-L against our 5 selected cell lines according to the DSS. (B) Several examples of dose-response curves of a selection of G4-L. The compounds el203 and ra0941 (top) induced important cytotoxicity across all the models. The compounds fhy491 and phendc3 (middle) were selectively cytotoxic against the SK-N-AS cell line. The activity of cx-5461 and quarfloxine, the two G4-ligand in clinical development, are shown in the bottom.

1.2.8 Next steps

Some additional experiments are planned to complete this project.

1. All these experiments will be **extended to a subset of MYCN amplified high-risk neuroblastoma cell lines** to be more representative of this genetic alteration.
2. Once these experiments completed, we will be able to perform our experiment with combinations of G4-L and chemotherapy agents.
3. In all instances, following the demonstration of specific vulnerability of ATRX-deficient or MYCN-amplified high-risk neuroblastoma to small G4-L molecules, correlative and **mechanistical studies** will be performed, in addition to the study of cell viability.
 1. Since ATRX deficiency impairs G4 resolution, inducing DNA damage, we will perform 2 tests which are a highly specific and sensitive molecular markers for monitoring DNA damage (Verga et al., 2014). First, the **quantitation of gamma-H2AX (γ -H2AX)** by fluorescence microscopy: DNA double-strand breaks (DSBs) are produced at sites of DNA damage. One of the initial responses to the DSB is phosphorylation of histone H2AX protein that forms γ -H2AX foci. Each DSB site is believed to correspond to one microscopic γ -H2AX focus. These

foci repair over a period of 2 days and can be followed microscopically by the IF γ -H2AX assay that immunostains the phosphorylated H2AX histone represented as γ -H2AX. Both the intensity of the fluorescence at individual DSB sites and the number of γ -H2AX foci is directly proportional to the amount of DSB produced. Second, the **quantitation of 53BP1**: during DSB repair, cells recruit different proteins to the damaged sites in a manner dependent on local chromatin structure, DSB location in the nucleus, and the repair pathway entered. 53BP1 is one of the important players participating in repair pathway decision of the cell. Whereas γ -H2AX foci describe the shape and size of a chromatin locus with damaged DNA, 53BP1 foci provide information on the formation of foci during the recruitment of proteins for repair.

2. The selected combined modalities will be also evaluated for their ability to induce **cell cycle dysregulation by flow cytometry studies after BrdU incorporation**. This method is based on the use of Bromodeoxyuridine (BrdU) as a DNA precursor and its detection by the quenching of the fluorescence intensity of DNA-bound fluorochromes, and indicates the fraction of cells synthesizing DNA. The level of fluorescence is used to distinguish different phases of the cell cycle. BrdU is incorporated into DNA during replication and anti-BrdU antibodies are used for staining in order to measure level of DNA synthesis by flow cytometry.
3. This proof-of-concept project aims at demonstrating the specific vulnerability of ATRX-deficient or *MYCN*-amplified high-risk neuroblastoma to small G4-L, and that chemotherapy resistance can be overcome. This study will then **lead to further *ex vivo* and *in vivo* preclinical experiments using high-risk neuroblastoma PDX models**. As mentioned, nine PDXs have been explored on their ALT phenotype (Table 6), the remaining will be screened. The experience within the COMPASS-ERAPerMed consortium has allowed us to implement and validate high-throughput screening techniques in high-risk neuroblastoma and other pediatric cancers, in cell lines and PDX-derived tumor cells. For the following step of validation, we have the possibility to perform *in vivo* experiments for drug validation thanks to the Laboratoire d'Investigations Précliniques (LIP) of our institution.

1.2.9 Concluding remarks

The screening of the G4-L library developed by Marie-Paule Teulade-Fichou laboratory has shown different cytotoxic effects, with a group of 3 compounds (el203, pt-ttpty and ra0941) inducing enhanced cytotoxicity against all the 5 cell lines screened. Interestingly, the SK-N-AS cell line showed specific sensitivity to another group of compounds (fhy491, phendc3, pds, or20, or35, or40, or41, or42, or127 and or128) which were selectively cytotoxic against this cell line. This cell line is ALT-negative and *MYCN*-WT, and harbors an intermediate cell identity state between adrenergic and mesenchymal state (Boeva et al., 2017). It should be interesting to further investigate why this cell line harbors this differential sensitivity to selected G4-L.

The expected selective sensitivity of ALT positive cell lines (*ATRX*-mutant CHLA-90 and *ATRX*-WT SK-N-FI) to G4-L was not confirmed in our group of screened neuroblastoma cell lines. Nevertheless, our ultimate goal is to address the question of the overcoming resistance to chemotherapy by sensitization with G4-L. The experiments of combination of G4-L and

chemotherapy are needed to answer to this question.

Thus, we propose to overcome the chemoresistance of tumor cells by the administration of a non-toxic dose of G4-L molecule, acting by a SL mechanism. Indeed, based on our hypothesis, if only low doses of G4-L are required for cell line sensitization, and low doses of CT are needed for cell death, when translating this into clinical practice, low doses with low toxic side effects should be expected, therefore reducing the chemotherapy side effects.

2. Clonal evolution of high-risk NB under targeted therapies

2.1 Scientific context

In high-risk neuroblastoma, the occurrence of intra tumor genetic heterogeneity has long been suggested, and more recently, NGS techniques have confirmed the presence of different clones characterized by distinct genetic alterations. These observations suggest the existence of “multiclonal” heterogeneous cellular populations, sometimes sharing common ancestors characterized by early genetic events that have determined their malignant transformation. In neuroblastoma, genetic heterogeneity concerns both copy number alterations and SNVs. The importance of this intra-tumor heterogeneity (ITH) lies in its association to tumor maintenance, progression and treatment resistance, likely because of selection of treatment resistant cooperating clones, with the progressive emergence of subclones. Different dimensions in ITH have been described. First, spatial genetic ITH, where distinct tumor cell genotypes coexist in different regions of the same tumor. Second, temporal genetic ITH has been observed when comparing primary (treatment naïve) with matched relapsed NBs. Indeed, relapsed NBs are enriched in mutations predicted to activate the RAS-MAPK pathway, and these mutations reside within major relapsed neuroblastoma subclones (Bellini et al., 2015a; Eleveld et al., 2015a). In addition, some SNVs detected by WES in relapsed tumors are below the WES detection limit in the primary tumor, meaning that these mutations were already present at very low frequencies in the pretreated primary tumors, but their allelic frequencies were significantly higher at relapse.

This spatial and temporal genetic ITH are intimately connected, demonstrated by the fact that mutations present in the major clone at relapse have their origin in subclones of the primary tumor. This has led to the description of four different evolutionary trajectories over different anatomic areas (Karlsson et al., 2018). The most common pattern consists of subclones with few mutations confined to a single tumor region. The second most common is a stable coexistence, over vast areas, of clones characterized by changes in chromosome numbers. This is contrasted by a third, less frequent, pattern where a clone with driver mutations or structural chromosome rearrangements expands to encompass all other clones in a region. The fourth and rarest pattern is the local emergence of a massive regional chromosomal instability triggered by inactivation of the p53 pathway. The presence in the primary tumor of the two latter patterns are strong predictors of high-risk disease and poor outcome in neuroblastoma as well as other pediatric cancers.

If we try to translate these findings into clinical practice, what is observed is that while homogeneous tumors are frequently cured by conventional chemotherapy, cure is not achievable in cancers that are highly heterogeneous because they already contain some cells that might be therapy resistant due to genetic, epigenetic, phenotypic or environmentally-mediated mechanisms. The expansion of subclonal populations under selective pressure is believed to contribute to the phenomenon of resistance to targeted cancer therapy and it has been shown that genetically heterogeneous tumors, comprised of multiple subclonal populations, tend to be associated with

poorer patient survival than tumors harboring low/moderate levels of intratumor heterogeneity (Morris et al., 2016).

In a therapeutically perspective, it is of major importance to characterize the clones that could be responsible of the tumor behavior, by their role in the processes of tumor initiation, metastatic extension, treatment resistance or relapse. The description of deterministic events in these processes could lead to anticipate the evolution of the tumor under treatment or during the follow-up by early detection of relevant subclones. First line therapeutic strategies for the treatment of high-risk neuroblastoma currently consist of multimodal intensive therapies combining conventional and high dose chemotherapy, surgery, radiotherapy, immunotherapy with anti-GD₂ monoclonal antibody and retinoic acid. The very poor prognosis of high-risk neuroblastoma justifies the exploration of new therapeutic approaches and the identification of genetic alterations might orient towards integration of molecular targeted therapies in frontline treatment. Although neuroblastoma is characterized by an overall genetic heterogeneity with few recurrent biomarkers, actionable targets might be identified in 30-50% of all cases (Jones et al., 2019; van Tilburg et al., 2020).

Beyond this genetic ITH, there is also a transcriptional/epigenetic ITH, with two distinct cell-type states of neuroblastoma cells, called mesenchymal (undifferentiated) and adrenergic, that exist within the same tumor. These cells are genetically identical but differ in their transcriptional and epigenetic landscape (Boeva et al., 2017; van Groningen et al., 2017). Also, heterogeneity in the tumor microenvironment, including extracellular matrix, stromal cells and immune cells, also contribute to tumor progression in neuroblastoma (Blavier et al., 2020; Joshi, 2020).

The experience with targeted therapies in adults has shown that after a first phase of disease response, even complete remission, tumors often develop therapeutic escape with disease progression under targeted treatment. The potential mechanisms of resistance after initial sensibility to targeted therapies remain to be fully elucidated. In addition to genetic events, other mechanisms might be involved in resistance after initial sensitivity to targeted therapies. The most plausible hypothesis suggests three mechanisms (Konieczkowski et al., 2018). First, and the most common, the reactivation of the original effectors downstream of the drug target. Pathway reactivation mechanisms include drug target alterations (e.g., mutation, amplification or alternate splicing), which render the target insensitive to drug inhibition, as well as recruitment of upstream, parallel, and downstream effectors, which re-activate index pathway effectors. An example of the pathway reactivation mechanism is the acquisition of *de novo* *ALK*^{F1174L} mutation in *ALK*-translocated cancers treated with ALK inhibitors (Sasaki et al., 2010). Second, the pathway bypass, a mechanism that circumvent the index signaling pathway as a whole, conferring resistance without reactivation of the original intermediary signaling effectors. This mechanism uses alternate parallel effectors to bypass the inhibited effectors, converging on the original downstream oncogenic output. Pathway bypass mechanisms can reactivate fundamental oncogenic transcriptional or translational outputs through engagement of alternative intermediary effectors. In neuroblastoma, this mechanism has been described to underly acquired resistance to ALK inhibitors in *ALK*^{F1174L}-driven neuroblastoma by the overexpression and GAS6-mediated activation of a TAM family RTK, AXL. This change was associated with activation of the MAPK signaling pathway and the development of an epithelial-to-mesenchymal transition phenotype (Debruyne et al., 2016). Finally, the pathway indifference, an

alternative cellular state (transcriptional or otherwise) that is independent of the index oncogenic pathway and that confers drug resistance despite continued inhibition of the index drug target and its downstream outputs. An example for this resistance mechanism in neuroblastoma is the aberrant upregulation of *BORIS* gene, which promotes chromatin interactions in *ALK*-mutated, *MYCN*-amplified neuroblastoma cells that develop resistance to *ALK* inhibition. These cells are reprogrammed to a distinct phenotypic state during the acquisition of resistance, resulting in loss of *MYCN* expression followed by overexpression of *BORIS* and a concomitant switch in cellular dependence from *MYCN* to *BORIS*. The resultant *BORIS*-regulated alterations in chromatin looping lead to the formation of super-enhancers that drive the ectopic expression of a subset of proneural transcription factors that ultimately define the resistance phenotype (Debruyne et al., 2019).

The integration of new targeted strategies even in first line treatment of high-risk neuroblastoma is currently being discussed to improve the overall survival of these patients. Among these, the identification of somatic alterations of *ALK* in neuroblastoma (such as amplifications and activating mutations) opens the door to new therapeutic opportunities by the use of *ALK* inhibitors (Trigg and Turner, 2018; Bellini et al., 2021, *in press*). Furthermore, it has been shown that about 30% of neuroblastomas have genomic CNAs affecting G1-S regulating genes. Strategies leading to restore a control of cell cycle at G1-S phase by direct inhibition of CDK4/6 could have vested interest in this disease (Rader et al., 2013; Rihani et al., 2015; Georger et al., 2017). Another promising way comes from the known antagonism between SWI/SNF and PRC2 complexes, meaning that EZH2 inhibitors could be a good candidate for NB (Wilson et al., 2010). Finally, neuroblastomas are enriched in RAS/MAPK pathway mutations at relapse, which could represent “druggable” targets (Eleveld et al., 2015a; Valencia-Sama et al., 2020). It is likely that introducing targeted therapies will lead to modification of genetic events and enable study of clonal evolution.

Based on the above, we hypothesize that treating mouse PDX models in order to induce (partial) response, followed by tumor regrowth, will enable the study of mechanisms of tumor development and resistance by the analysis of genetic events by WES. Our objectives are:

- To analyze how clones behave under the pressure of the different treatments received and compared them with each other
- To study the global mutational rate after treatment and if differences exist compared to non-treated PDXs
- To try to infer plausible resistance mechanisms
- To use the cfDNA as a surrogate of tumor DNA for the study of clonal evolution under targeted therapies in PDX models.

In this part of the PhD project, we have studied the genetic ITH at a DNA level, and analyzed how the different clones evolve under treatment, including targeted therapies. To do so, we have carried-out several *in vivo* experiments with different high-risk neuroblastoma PDX models and treated them with targeted drugs (according to genetic abnormalities of the PDXs) and/or chemotherapy. The *in vivo* experiments have been carried-out in collaboration with the Laboratoire d'Investigations Précliniques of the Institut Curie, headed by Dr. Didier Decaudin.

2.2 *In vivo* experiments for the study of clonal evolution under treatment

2.2.1 Experimental pipeline

For the study of the clonal evolution under targeted therapies, we have performed 6 independent *in vivo* experiences with 6 different PDX models (shown in table 7).

HR-NB PDX MODELS	SOMATIC GENETIC ALTERATIONS					Chosen target	Targeted drug	Sequenced samples
	<i>MYCN</i>	<i>ALK</i>	<i>P53</i>	<i>ATRX</i>	Other			
GR-NB4	A	A	WT			<i>ALK</i>	Lorlatinib	Tumor / cfDNA
GR-NB10	WT	WT	c.555+1G>A		<i>NF1</i> mut+LOH	<i>NF1</i>	Trametinib	Tumor / cfDNA
IC-pPDX-17	WT	WT	WT	c.5242G>A	<i>CDK4</i> amp	<i>CDK4</i>	Ribociclib	Tumor / cfDNA
IC-pPDX-75	WT	F1174L	WT	c.6391C>T		<i>ALK</i>	Lorlatinib	Tumor
IC-pPDX-109	A	WT	WT		<i>HRAS</i> mut	<i>HRAS</i>	Trametinib	Tumor
HSJD-NB-005	A	WT	c.517G>T		<i>ARID1A</i> mut	<i>ARID1A</i>	Tazemetostat	Tumor

Table 7: PDX models used for the *in vivo* study of the clonal evolution of high-risk neuroblastoma (HR-NB) under targeted therapies.

In each experiment, *Swiss Nude* mice were engrafted in the interscapular fat pad. Eight mice per group were planned to ensure at least 6 treated mice per experimental arm, to consequently guarantee statistical significance. When the tumor volume reached 150-200 mm³, animals were randomized in 6 groups, corresponding to the 6 experimental treatment arms of each experiment. Mouse weight and tumor volume were determined 3 times a week. Mice were sacrificed when tumor reached the ethical size (\approx 1,500-2,000 mm³). At the end of the experiment, tumor DNA and paired cfDNA were whole-exome sequenced. Intermediate cfDNA samples were collected for targeted sequencing. The experimental pipeline is described in Figure 40.

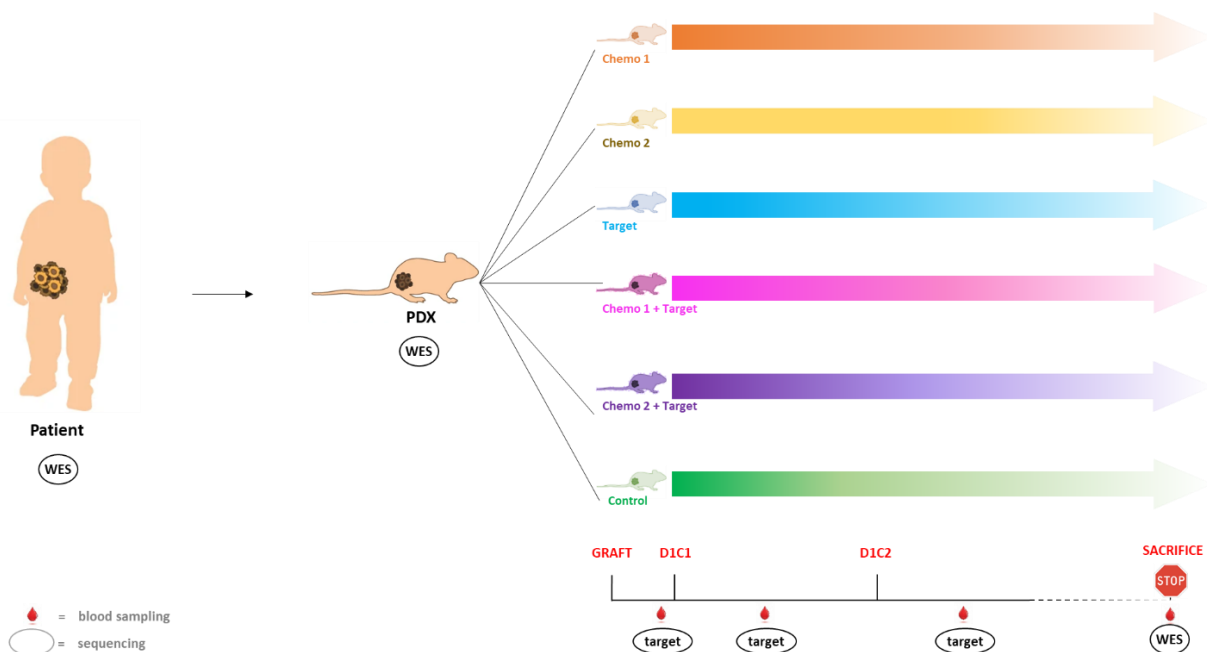


Figure 40: experimental pipeline used for the *in vivo* study of the clonal evolution of high-risk neuroblastoma under targeted therapies. Animals were randomized in 6 groups, corresponding to the 6 experimental treatment arms. Mice were sacrificed when tumor reached the ethical size. Blood samples were obtained at different intermediate time-points for targeted sequencing of cfDNA. Tumors and blood samples were collected at sacrifice for whole-exome sequencing (WES) on tumor and cfDNA respectively.

2.2.2 Ethical considerations of *in vivo* experimentation

The use of the mouse model remains essential for the outcome of this project: it represents an integrated biological model with a physiological whole context system, in contrast to *in vitro* models. For PDX establishment, tumor tissue was obtained after informed consent provided by the patients' legal guardians. All animal experiments complied with current European/French legislation (articles R.214-87 to R.214-126 of the Decree n°2013-118 of February 1st) and were carried out in accredited animal facilities of the Institut Curie.

The animal well-being was be monitored through strict scale endpoints. Following international recommendations, experiments were stopped before any animal suffering or when the tumor volume reached 1500 to 2000 mm³. The number of mice used considered the reduction principle. In order to reduce its number, whenever possible experiments were pooled to limit the number of control groups. In addition, data obtained from control groups could be used for future projects and leftover tumor material was stored for further projects.

All procedures were approved by the Institutional Review Board of the Institut Curie. This project was approved by the Ethics Committee of the Institut Curie and the Ministry of Higher Education, Research and Innovation, with reference number AFAPIS #13980.2018030813227748 v2.

2.2.3 Treatment schedules

Engrafted mice were randomized into 6 experimental arms depending on the treatment regimen and received 2 cycles of treatment. Mice were treated with standard chemotherapy, targeted agents or both. Targeted therapy was selected according to tumor genetic abnormalities identified in the primary tumor and PDX by molecular characterization using WES (100X, filtered on the germline) and RNAseq, with targetable alterations and therapeutic options determined according to MAPPYACTS, NCI-MATCH and INFORM algorithms (Worst et al., 2016). Doses are described below:

1. **Chemo 1:** Etoposide-Cisplatin
 - Etoposide 12 mg/kg IP at D1, D2, D3 (cycle 1) and D22, D23, D24 (cycle 2)
 - Cisplatin 6 mg/kg IP at D1 and D22
2. **Chemo 2:** Doxorubicin-Cyclophosphamide
 - Doxorubicin 2 mg/kg IP at D1 and D22
 - Cyclophosphamide 100 mg/kg IP at D1 and D22
3. **Targeted agents** were administrated orally 5/7 days from D1 to D42. Depending on the PDX model, mice received:
 - IC-pPDX-17: Ribociclib 75 mg/kg
 - IC-pPDX-75: Lorlatinib 10 mg/kg
 - IC-pPDX-109: Trametinib 0.4 mg/kg from D1 to D5 and 0.2 mg/kg from D8 to D42
 - GR-NB4: Lorlatinib 10 mg/kg

- GR-NB10: Trametinib 0.4 mg/kg from D1 to D5 and 0.2 mg/kg from D8 to D42
- HSJD-NB-005 (*ARID1A* mutation): Tazemetostat 100 mg/kg

4. Chemo 1 + Targeted agent
5. Chemo 2 + Targeted agent
6. Control group

2.2.4 *In vivo* treatment efficacy

Although it was not our primary objective, the efficacy of the different treatments tested was studied in the different PDX models used for the study of the clonal evolution.

2.2.4.1 Determination of the treatment efficacy

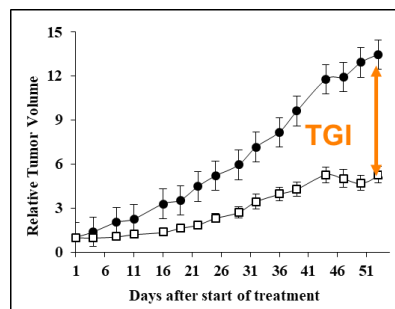
Some concepts are described here for the analysis of the treatment efficacy, such as relative tumor volume, tumor growth inhibition, overall response rate. Statistical significance of differences observed between the individual RTVs corresponding to the treated mice and control groups was calculated by the two-tailed Student's t test (Némati et al., 2010).

Tumor Growth Inhibition (TGI) determination:

- Tumor volume (V) was measured as $V = a \times b \times b/2$, where a and b are the largest and smallest perpendicular tumor diameters, respectively.
- Relative tumor volume (RTV), is calculated as $RTV = (V_x/V_1)$, where V_x is the tumor volume on day x and V_1 is the tumor volume at initiation of therapy (day 1).
- Growth curves were obtained by plotting the mean values of RTV on the Y-axis against time.

$$TGI (\%) = 1 - (RTV_t/RTV_c)$$

where RTV_t is the relative tumor volume of the treated mouse and RTV_c the median of RTV of the corresponding control group at a time corresponding to the end of treatment. Fifty percent TGI was considered to be the limit for a meaningful biological effect.



$$\Rightarrow TGI (\%) = 100 - (5.3/13.5) = 61\%$$

Overall response rate (ORR) determination:

- The objective is to evaluate the response to treatment according to individual mouse variability.

$$\text{ORR} = [(\text{RTV}) - 1]$$

- The relative tumor volume variation (RTVV) of each treated mouse is calculated as

$$\text{RTVV} = [(\text{RTVt}/\text{RTVc}) - 1]$$

- A tumor was considered as responding to therapy when the ORR was lower than -0.5.

Probability of progression

- Based on the time it takes for the tumor to double (RTV2) or quadruple (RTV4) in size for each mouse

2.2.4.2 Analysis of treatment efficacy

For the study of clonal evolution, targeted therapies were selected based on the molecular profile of the PDX. Targeted therapies exhibited different efficacies depending on the model. Indeed, lorlatinib, which resulted in high TGI (91%) in *ALK*-amplified model GR-NB4 (Figure 41), did not show any efficacy in *ALKF1174L*-mutated IC-pPDX-75 (TGI 28%). Trametinib showed significant antitumor efficacy on *HRAS*-mutated IC-pPDX-109, with a TGI of 60%, whereas in GR-NB10 model carrying an *NF1* mutation associated to a LOH, the efficacy was low (TGI 49%). Ribociclib, a CDK4 inhibitor, showed significant efficacy against CDK4-amplified IC-pPDX-17 model, with a TGI of 61%.

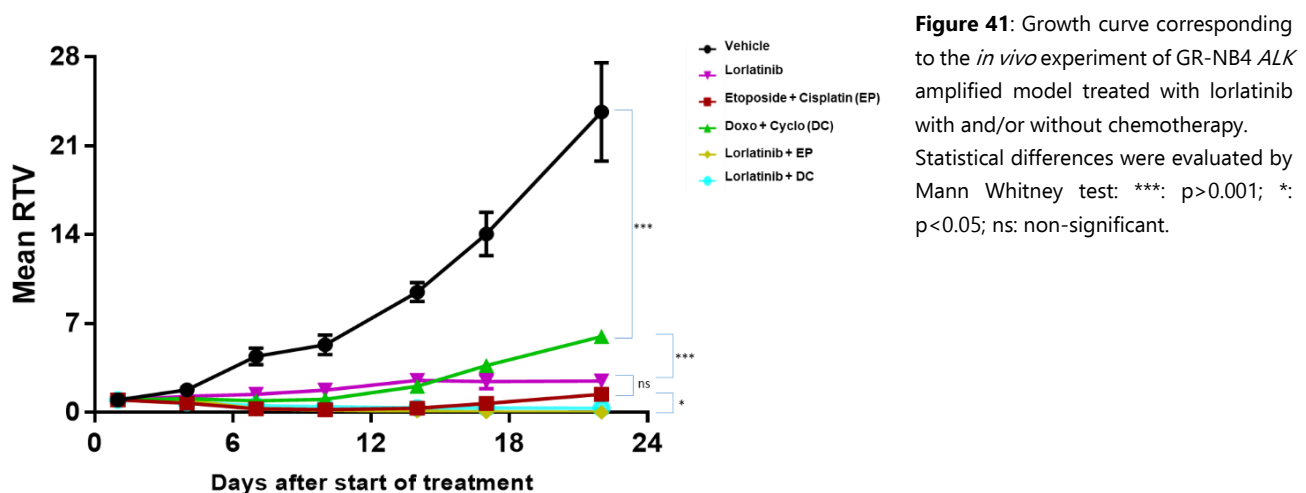


Figure 41: Growth curve corresponding to the *in vivo* experiment of GR-NB4 *ALK* amplified model treated with lorlatinib with and/or without chemotherapy. Statistical differences were evaluated by Mann Whitney test: ***: $p > 0.001$; *: $p < 0.05$; ns: non-significant.

Concerning chemotherapies, etoposide-cisplatin were efficient in models GR-NB4 and IC-pPDX109 (TGI 93.7% and 67% respectively) and doxorubicin-cyclophosphamide against models IC-pPDX-17 and GR-NB4 (TGI 70% and 76% respectively). The addition of a targeted treatment to chemotherapy was significantly more efficient than chemotherapy alone in models GR-NB4 (when lorlatinib was added to both chemotherapies), GR-NB10 (when trametinib was added to doxorubicin-

cyclophosphamide) and IC-pPDX-109 (when lorlatinib was added to doxorubicin-cyclophosphamide). In models IC-pPDX-17 and IC-pPDX-75, the addition of targeted therapy (ribociclib and lorlatinib, respectively) did not add any significant efficacy to any of the two chemotherapies.

Finally, we could find that GR-NB4 was globally sensitive to all treatments, whereas IC-pPDX-75 was globally very resistant. These results are summarized in table 8.

	TUMOR GROWTH INHIBITION (%)						
	Day of analysis	Targeted therapy	Etop-Cisplat (EP)	Doxo-Cyclo (DC)	Target + EP	Target + DC	
IC-pPDX-17	16	Ribociclib	61	43	70	73	78
IC-pPDX-75	25	Lorlatinib	28	39	35	62	62
IC-pPDX-109	37	Trametinib	61	67	47	78	63
GR-NB4	22	Lorlatinib	91	93.7	76	99.9	98
GR-NB10	15	Trametinib	49	53	58	75	79

Table 8: Tumor growth inhibition in the different PDX models tested according to the different arms of treatment performed for clonal evolution *in vivo* experiments. Etop-Cisplat: etoposide-cisplatin; Doxo-Cyclo: doxorubicin-cyclophosphamide.

The charts with the comprehensive analysis of treatment efficacies corresponding to each model are shown in Appendix 2.

2.2.5 Prediction of the *in vivo* response

Based on the results of the *ex vivo* screenings on PDTs described in Results section 2.2.4.2, we sought to evaluate if the *ex vivo* drug toxicity could predict the *in vivo* responses previously described in Results section 2.5. Overall, five PDX models were screened both *ex vivo* and *in vivo*: IC-pPDX-75, IC-pPDX-17, HSJD-NB-005, GR-NB4 and GR-NB10 (see table 3 in section 1.1.5.1 for molecular alterations).

In Table 9 we have summarized the comparisons between DSS in *ex vivo* drug screening and TGI obtained in the *in vivo* experiments. In summary, *ex vivo* screenings were good predictors of the *in vivo* response for all experimental arms in models HSJD-NB-005 (*ARID1A* mutated, treated with tazemetostat +/- chemotherapy) and IC-pPDX-75 (*ALK*^{F1174L}, treated with lorlatinib +/- chemotherapy). In model IC-pPDX-17, the *in vitro* cytotoxicity of the drugs was a good predictor of their corresponding *in vivo* efficacy, whereas ribociclib, which did not show significant *in vitro* cytotoxicity, was significantly efficient *in vivo*. The same occurred for GR-NB4: while cytotoxicity *in vitro* for chemotherapy corresponded well to *in vivo* responses, the poor cytotoxicity of lorlatinib *in vitro* did not correspond with the good *in vivo* response of the drug. Finally, for GR-NB10 there were no good correspondences between *in vitro* and *in vivo* experiments, for both trametinib and chemotherapy.

	<i>Ex vivo</i> (drug sensitivity score)				<i>In vivo</i> (tumor growth inhibition)			
	Targeted	Doxorubicin	Etoposide	Carbolatin	Targeted	Doxo-Cyclo	Etop-Cisplat	
GR-NB4	Lorlatinib	60	30	60	70	91%	76%	93%
GR-NB10	Trametinib	40	40	70	100	49%	58%	53%
IC-pPDX-17	Ribociclib	90	65	90	90	61%	70%	43%
IC-pPDX-75	Lorlatinib	80	70	100	100	29%	35%	39%
HSJD-NB-005	Tazemetostat	100	40	80	100	22%	78%	48%

Table 9: Comparative study of the ex vivo activity and in vivo efficacy in different neuroblastoma PDX models.

2.2.6 Tumor DNA sampling, processing and sequencing

PDX tumor tissue was flash-frozen after dissection and stored at -80°C. PDX tumor DNA was extracted by using the QIAamp DNA Mini Kit. DNA concentration after extraction was measured by Qubit fluorometric assay with dsDNA BR Assay Kit. Tumor DNA was fragmented and then libraries constructed using Kapa Library Preparation Kit Illumina platforms (Kapa Biosystems) with Indexed Adapters included in SeqCap EZ Human Exome Kit v3.0 (Nimblegen Roche Sequencing). The manufacturer's protocol was modified according to Chicard et al., 2018. For exome capture of PDXs, SeqCap EZ Exome Enrichment Kit v3.0 (Nimblegen Roche Sequencing) was performed according to the manufacturer's protocol, using Illumina Hi-seq2500 leading to paired-ends 100x100 bp (expected coverage: 100X).

Paired patient's tumor DNA and germline DNA was available for all PDXs and was whole-exome sequenced by Agilent SureSelect Human All Exon v5. Tumor DNA from patients was obtained from the same tumor specimen that was used to establish the corresponding PDX excepting for GR-NB10. In this particular case enrolled in the MAPPYACTS program (NCT02613962), the patient's tumor DNA sequenced corresponded to a later timepoint with respect to the establishment of the PDX.

In the experiments performed on IC-pPDX-17, GR-NB4 and GR-NB10, two tumors were sequenced per treatment arm, whereas in the experiments on IC-pPDX-75 and IC-pPDX-109 only one tumor per experimental arm was sequenced.

2.2.7 Bioinformatics pipeline

Bioinformatics analysis were performed in collaboration with bioinformatician Elnaz Saberi-Ansari. Following sequencing, first the WES fastq files were aligned. After filtering the alignment reads, several computational analyses were performed, including quality controls, prediction of the ploidy and cellularity, copy-number variation analysis and mutation calling. Finally, the observations were validated by a biologist (figure 41).

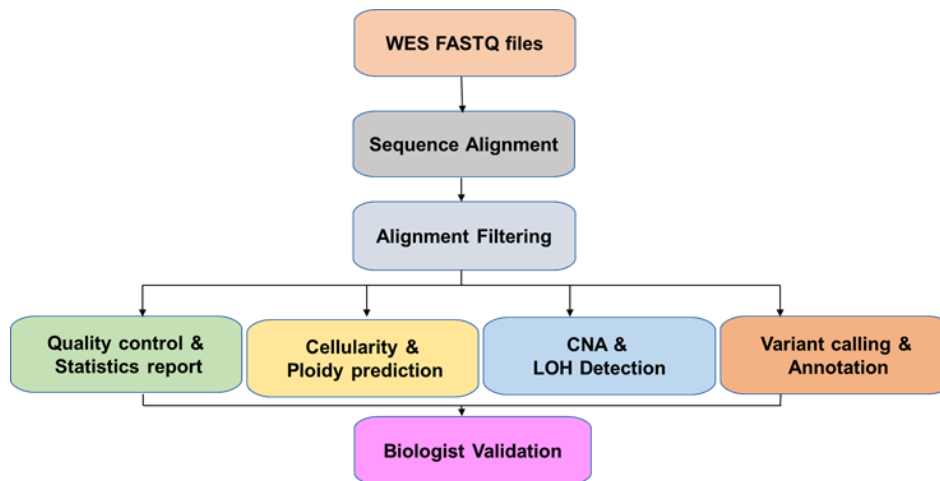


Figure 41: General overview of the bioinformatics pipeline for PDX sequencing analysis. CNA: copy-number analysis; LOH: loss-of-heterozygosity.

Except for PDX samples, fastq files were aligned on GRCh37 human genome reference using Bwa-mem. Uniquely mapped reads with mapping quality more than 20 were extracted. For PDX samples, a hybrid of GRCh37 and GRCm38 reference was used and reads uniquely mapped to human chromosomes with mapping quality more than 20 were extracted. Finally, duplicate reads were removed. Coverage analysis was done using MOSDEPTH and GATK4. For copy number analysis, Sequenza and FACETS were used and purity and the ploidy of each samples were extracted from Sequenza results (Figure 42).

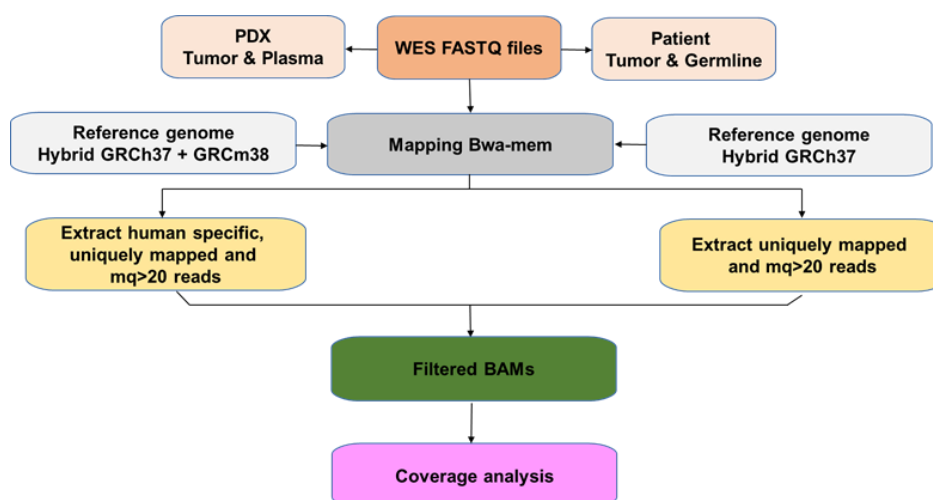


Figure 42: Schematic representation of the alignment pipeline for PDX sequencing samples and exclusion of mouse reads.

Mutect2 was used for variants calling. The paired calling mode and the jointcalling mode were used in parallel and the mutations resulting from both analyses were merged. The mutations were filtered using Filter Mutect2 calls and annotated using VEP. Only the variants matching the following criteria were retained: the coverage should be more than 20X, variant supporting reads should be more than 10X in tumor and cfDNA with at least one forward and one reverse read, VAF >0.01, predicted as deleterious by SIFT or PolyPhen, and frequency less than 0.001 in the population. Germline variants were filtered out if they had ≥ 1 read in germline sample. Finally, all the variants were validated by visual inspection using Integrated Genome Viewer (IGV) (Figure 43).

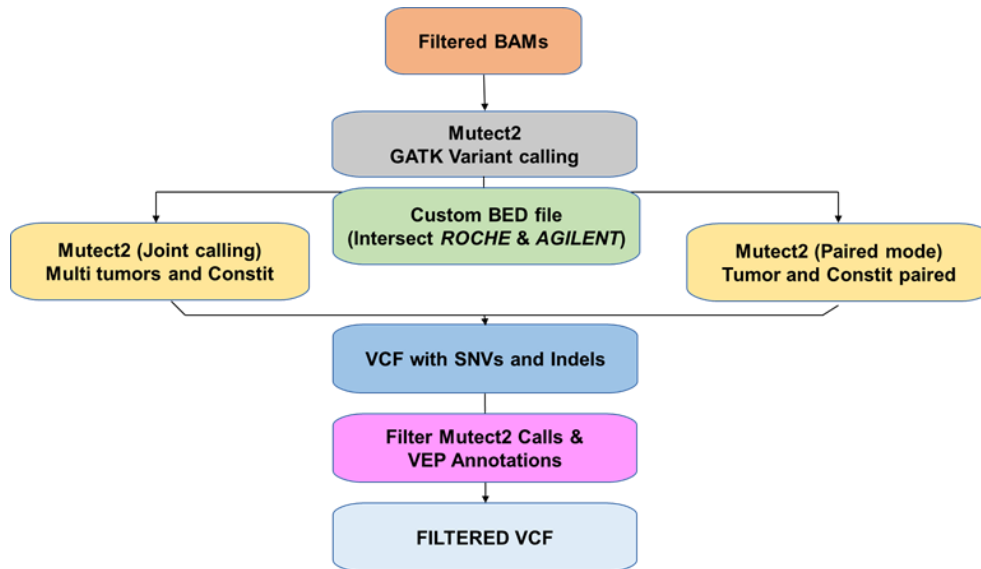


Figure 43: Schematic representation of the bioinformatics pipeline for variant calling.

Mean coverage of tumors varied between 29 and 97 reads. Four tumor samples from GR-NB4 had very low coverage (due to low purity) and could not be analyzed: both tumors from etoposide-cisplatin-lorlatinib group, one sample from doxorubicin-cyclophosphamide-lorlatinib and one sample from etoposide-cisplatin group (table 10).

	Mean coverage (X)		Mean number of variants
	Tumors	cfDNA	
IC-pPDX-17	97	20	70
IC-pPDX-75	43	NA	107
IC-pPDX-109	46	NA	85
GR-NB4	29*	9	31
GR-NB10	28	19	611

Table 10: Mean coverage of tumors and corresponding cfDNA samples and mean number of variants across the different PDX models.

* Four samples were not contributive due to low coverage issues and could not be analyzed. When eliminating these samples, mean coverage increased to 33 X.

2.3 Analysis of the clonal evolution of NB under treatment by WES

We have studied the genetic intratumor heterogeneity at a DNA level and search for evidence of clonal evolution under treatment, including targeted therapies (according to genetic abnormalities of the PDXs) and/or chemotherapy.

2.3.1 Study of the variability

As in the experiments performed on IC-pPDX-17, GR-NB4 and GR-NB10 two tumors were sequenced per treatment arm, this allowed us to study the variability based on the analysis of the VAF of SNVs between tumors belonging to the same treatment arm, as well as to compare control tumors with their corresponding patient's tumor.

Mutational pattern of tumors corresponding to the same treatment arm as well as control arm were very similar, with a median Pearson's correlation coefficient of 0.95 [0.84-0.99]. Figure 44 illustrates variability between tumors for model IC-pPDX-17.

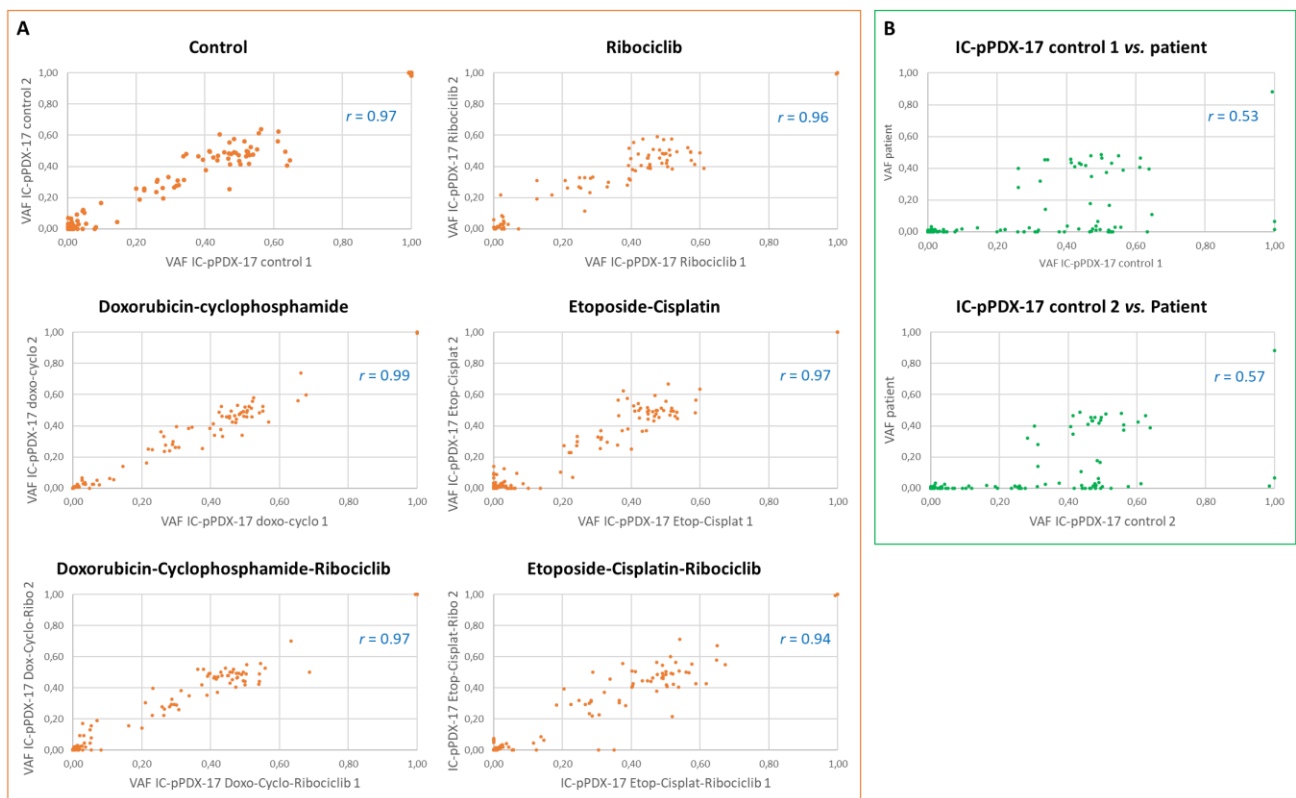


Figure 44 Study of the variability between tumors in IC-pPDX-17 model. (A) shows the correlations between both tumors belonging to the same treatment arm. (B) shows the correlation between PDX control tumors and the patient's tumor. *r* indicates the Pearson's correlation coefficient.

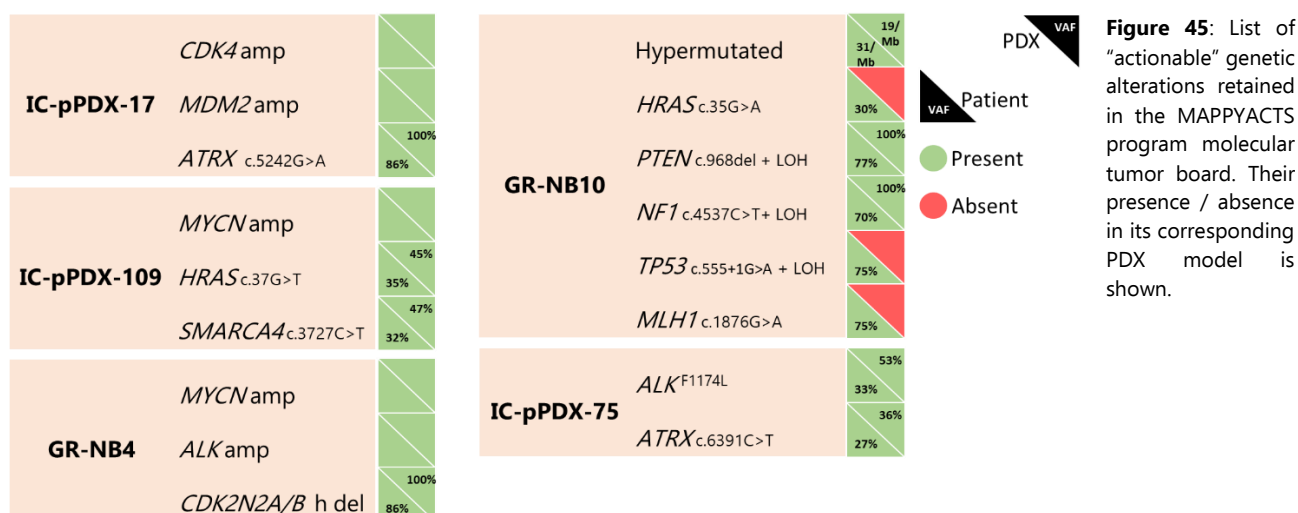
The Pearson's correlation between PDX tumors belonging to the etoposide-cisplatin treatment group of GR-NB4 model was quite low ($r=0.84$) compared to the others. This is explained by coverage issues, since the mean sequencing coverage was 6 reads for one of the tumors,

compared to 27 reads for the other tumor. In addition, the comparison between PDX tumors was not possible in the doxorubicin-cyclophosphamide-target and etoposide-cisplatin-target treatment groups of GR-NB4 model also for coverage issues: in the first case because one of the tumors had a mean coverage of 0 reads, rendering comparison impossible; in the second case, both tumors had no coverage (mean 0 reads). These results are summarized in table 11.

	Pearson's correlation coefficient (<i>r</i>)							
	Control 1 vs Patient	Control 2 vs Patient	Control	Target	Doxo-Cyclo	Doxo-Cyclo-Target	Etop-Cisplat	Etop-Cisplat-Target
IC-pPDX-17 P7	0,53	0,57	0,97	0,96	0,99	0,97	0,97	0,94
GR-NB4 P5	0,70	0,71	0,93	0,93	0,96	NA	0,84	NA
GR-NB10 P8	0,23	0,22	0,93	0,88	0,90	0,96	0,92	0,95
IC-pPDX-75 P11	0,29							
IC-pPDX-109 P5	0,80							

Table 11: Pearson's correlation between tumors. For all models, control tumors were compared with patients' tumors. For PDX models IC-pPDX-17, GR-NB4 and GR-NB10, for which two tumors were sequenced per experimental arm, Pearson's correlation between both tumors of the same experimental treatment arm are also shown. NA: not applicable (since at least one sample had no coverage); P: PDX passage.

The analysis of the variability between PDX control tumors and patient's tumors showed decreased correlations. Models GR-NB4 and IC-pPDX-109 showed higher similarities with their corresponding patient's tumors compared to the other models. This analysis is biased due to different sequencing technologies (Roche vs. Agilent) and fastq files alignment between PDXs and patient's tumors (see section 2.2.6). In addition, in the case of GR-NB10, the patient's tumor sequenced corresponded to a later timepoint in the patient's evolution compared to the tumor from which the PDX was established. Despite this, all the genetic alterations that were retained in the MAPPYACTS molecular tumor board (these 5 PDX were established within this program) could also be identified in PDX tumors, excepting for GR-NB10. In that case, it means that the mutations present in the patient's tumor and absent in the PDX are events that occurred at a later timepoint in the patient but not in the PDX (Figure 45).



2.3.2 How clones evolve under treatment

We then compared, for each experiment, SNVs from each treatment group against control group (non-treated mice), to study how the variants were modified after treatment. Variants were classified in “persistent” (when present in both treatment and control groups), “emerging” (if they appeared in a given treatment group and were absent in control group) or “disappearing” (if they were present in controls but absent in treated mice of a given treatment group). For persistent variants, we also noted the variants for which the VAF significantly increased (“increasing”) or decreased (“shrinking”).

The study of the VAF density showed superposable profiles between tumors. The total number of variants did not statistically differ between treated vs non-treated tumors of a same model (figure 46). We did not observe significantly increased or decreased number of SNVs associated to a specific treatment group. These three statements were not fulfilled for 4 samples from GR-NB4 (from groups doxorubicin-cyclophosphamide-lorlatinib, etoposide-cisplatin and etoposide-cisplatin-lorlatinib), because of low coverage issues (mean coverage <25 reads), which were excluded from the analysis. Based on the VAF distribution, we analyzed the SNVs in three distinct groups: first, the clonal variants (VAF $\geq 20\%$), second the SNVs with VAFs between $\geq 5\%$ and $< 20\%$ and finally SNVs with VAF $< 5\%$, near to the background sequencing noise. Overall, most of variants were clonal with a median proportion of clonal variants of 64% [40-76], whereas the subclonal or very subclonal ones had median percentages of 17% [15-20] and 18% [8-40], respectively.

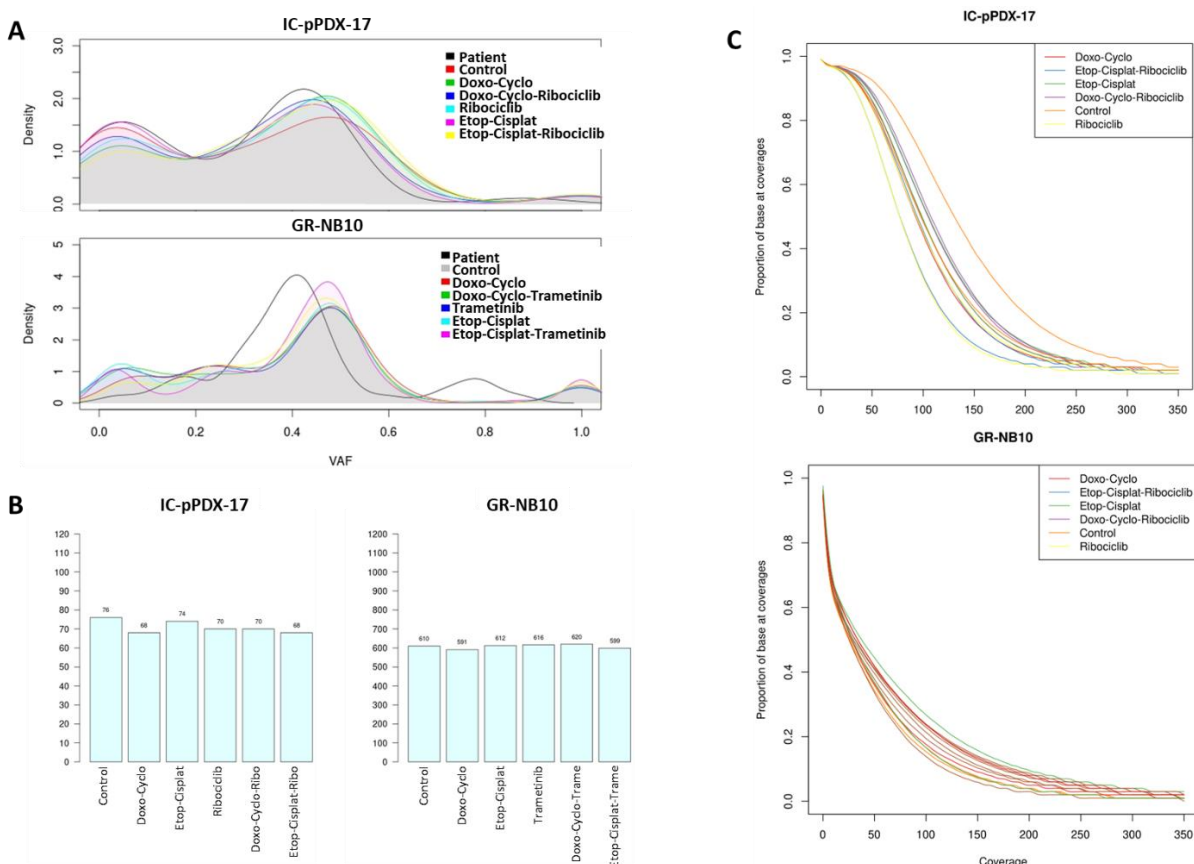


Figure 46: Referred to IC-pPDX-17 and GR-NB10 models. (A) Density plot of the variant allele fraction (VAF) of the different SNVs, showing superposable profiles across samples. (B) Total number of variants per treatment arm (2 tumors were sequenced per experimental arm). No significant differences exist between groups. (C) Coverage plots.

At a clonal level, almost all variants persisted across models after treatment, with a median of 64 persistent variants per model. Few variants emerged in specific treatment groups. Interestingly, in IC-pPDX-17, two variants emerged in the target-etoposide-cisplatin treatment group. These 2 variants were missense *HDAC4* (p.Pro64Leu) and truncating *STAG2* (p.Arg305Ter) mutations. HDAC4 belongs to class II of the histone deacetylase alpha family. It possesses histone deacetylase activity and represses transcription when tethered to a promoter. HDAC4 does not bind DNA directly, but through transcription factors MEF2C and MEF2D. HDACs are overexpressed and mutated in various solid and hematologic malignancies and play key roles in tumorigenesis (Lee et al., 2017). Furthermore, *STAG2*, a subunit of the cohesin complex which regulates the separation of sister chromatids during cell division, is frequently inactivated by mutations in cancer. Targeted inactivation of this gene results in chromatid cohesion defects and aneuploidy, suggesting that genetic disruption of cohesin is a cause of aneuploidy in human cancer (Mondal et al., 2019). Emergent variants in this and other models are summarized in Table 12. In GR-NB4, any variant emerged in treated mice.

		Emergent variants at clonal level			Bibliographic reference	
		Gene name	Genomic position	VAF		
IC-pPDX-17	DC	No emergent variant				
	EP	No emergent variant				
	Target	No emergent variant				
	Target-DC	No emergent variant				
	Target-EP	<i>HDAC4</i>	c.191C>T	30%	Histone deacetylase	(Lee et al., 2017)
		<i>STAG2</i>	c.913C>T	35%	Subunit of cohesin complex	(Mondal et al., 2019)
IC-pPDX-75	DC	<i>NUBPL</i>	c.7A>G	42%	Nucleotide binding protein like	(Wang et al., 2017b)
	EP	<i>NUBPL</i>	c.7A>G	48%	Nucleotide binding protein like	(Wang et al., 2017b)
		<i>ZBTB10</i>	c.96+1340G>C	22%	Zinc finger - BTB domain containing 10	
	Target	<i>NUBPL</i>	c.7A>G	42%	Nucleotide binding protein like	(Wang et al., 2017b)
	Target-DC	<i>NUBPL</i>	c.7A>G	41%	Nucleotide binding protein like	(Wang et al., 2017b)
Target-EP	<i>NUBPL</i>	c.7A>G	40%	Nucleotide binding protein like	(Wang et al., 2017b)	
IC-pPDX-109	DC	<i>HSPB11</i>	c.292G>C	22%	Prognostic marker in high-grade glioma	(Cheng et al., 2016)
	EP	<i>SMG7</i>	c.2545dup	21%	Nonsense-mediated mRNA decay	(Park et al., 2019)
		<i>PPP1R13B</i>	c.544C>T	21%	Apoptosis regulation via p53 interaction	
	Target	<i>SMG7</i>	c.2545dup	31%	Nonsense-mediated mRNA decay	(Park et al., 2019)
		<i>ZIM2</i>	c.1146G>T	22%	Zinc finger imprinted 2	
Target-DC	No emergent variant					
Target-EP	<i>SMG7</i>	c.2545dup	39%	Nonsense-mediated mRNA decay	(Park et al., 2019)	
GR-NB10	DC	<i>AHSA2</i>	c.89C>A	21%	Prognostic marker in colon cancer	(Han et al., 2020)
		<i>SLC4A7</i>	c.3230T>C	24%	Sodium bicarbonate cotransporter	
	EP	<i>EXPH5</i>	c.4483dup	59%	Member of the synaptotagmin-like protein	
		<i>SIX3</i>	c.38A>G	25%	Negative regulator of the Wnt pathway	(Carlin et al., 2012)
		<i>TMEM70</i>	c.541G>A	36%	Mitochondrial membrane protein	
		<i>MIS18A</i>	c.335-1G>T	40%	Kinetochore Protein A, cancer survival predictor	(Zhang et al., 2016)
	Target	<i>SIK3</i>	c.3445C>A	40%	Salt-inducible kinases, role in tumorigenesis	(Sun et al., 2020)
		<i>TOP3A</i>	c.989T>A	50%	Topoisomerase III alpha	
		<i>APBB1IP</i>	c.1130C>A	28%	Role in tumor immunity	(Ge et al., 2021)
		<i>POLE</i>	c.1362G>T	21%	DNA polymerase epsilon, familial cancer	(Mur et al., 2020)
	Target-DC	<i>ZZEF1</i>	c.2308A>T	24%	Histone reader	(Yu et al., 2021)
		<i>MARS2</i>	c.584T>C	22%	Mitochondrial methionyl-tRNA synthetase	
	<i>LUM</i>	c.206A>G	22%	Prognostic factor in gastric cancer	(Chen et al., 2020)	
Target-EP	<i>TRIO</i>	c.1207C>T	25%	Poomotes actin cytoskeleton reorganization		

Table 12: Emergent variants at clonal level according to specific treatment groups. DC: doxorubicin-cyclophosphamide, EP: etoposide-cisplatin; VAF: variant-allele fraction

GR-NB10 deserves a separate paragraph. This is a model derived from a neuroblastoma with hypermutation profile, with a mean number of 608 mutations per sample (Bhalshankar J., ANR 2021). This model carried a *MSH6* germline variant of unknown significance (p.His1317Arg). *MSH6* is a component of the post-replicative DNA mismatch repair system (MMR) and mutations in this gene result in a strong mutator phenotype known as microsatellite instability (MSI). MSI secondary to germline mutation in DNA MMR proteins is the molecular fingerprint of Lynch syndrome, while epigenetic inactivation of these genes is more commonly found in sporadic MSI tumors. Lynch syndrome, also known as hereditary nonpolyposis colorectal cancer (HNPCC), is an autosomal dominant genetic condition associated with a high risk of colon cancer as well as other cancers including endometrial cancer (second most common), ovary, stomach, small intestine, hepatobiliary tract, upper urinary tract, brain, and skin. MSI occurs at different frequencies across malignancies and its signatures may differ among different cancer types: instability may concern different loci in different cancer types (Chang et al., 2018). In a pan-cancer study focused on hypermutation, the only pediatric cancer types that involved cases of ultrahypermutation (>100 mutations/Mb) were malignant gliomas, colorectal cancers, and leukemias/lymphomas (Campbell et al., 2017). In neuroblastoma, which overall has a low mutation frequency, it is known that high mutational burden is related with poorer overall survival. Nevertheless, germline events in the MMR pathway and other mechanisms of hypermutation are exceedingly rare in neuroblastoma (Hwang et al., 2019). In this model, also the majority of the variants persisted after treatment at a clonal level, with a median of 545 persistent variants [529-555] per treatment group. A median number of 2 variants [1-5] emerged in treated mice in this model, compared to median 1 emergent variant [0-3] in the remaining models. Interestingly, in the doxorubicin-cyclophosphamide-trametinib group, a *POLE* variant emerged at a clonal level. Also, more variants were lost in treated groups with respect to controls in this model, with a median of 5 disappearing variants [3-9] compared to the other models (median 0, [0-1]).

At subclonal level (VAF 5-20%), the number of variants were more homogeneously distributed between groups, meaning that subclones either emerged, disappeared or persisted similarly, with some differences depending on the model. In model IC-pPDX-17, the median number of emergent, disappearing and persistent variants, including persistent increasing and shrinking, little varied (between 2 and 4). For models IC-pPDX-75 and IC-pPDX-109, the variants were similarly emergent, disappearing or persistent, with lower total number of variants corresponding to persistent increasing (median 1 for both models) or shrinking (median 1 and 2, respectively). In GR-NB4 model, there was a particular enrichment of persistent subclonal variants compared to other models. For hypermutated model GR-NB10, there was an enhanced number of SNVs that persisted with a shrinking VAF.

For very subclonal SNVs (VAF <5%), some differences were observed depending on each PDX model. In models IC-pPDX-17 and GR-NB4, the majority of the variants persisted (median 22 and 29 respectively), with low number of emerging (median 0 and 1 respectively) or persistent increasing/shrinking (median 0 for both models). In models IC-pPDX-75 and IC-pPDX-109, the variants were more frequently emerging (median 6 and 8 respectively) or disappearing (median 5 and 7 respectively) than persistent. In GR-NB10, the majority of the variants persisted but an important number (median 23) emerged. All these findings are summarized in the next Table 13.

		CLONAL (VAF ≥20%)					SUBCLONAL (VAF ≥5 - <20%)					VERY SUBCLONAL (VAF <5%)					
		Emergent	Disappearing	Persistent	Increasing	Shrinking	Emergent	Disappearing	Persistent	Increasing	Shrinking	Emergent	Disappearing	Persistent	Increasing	Shrinking	
IC-pPDX-17	Doxo-Cyclo	0	0	59	0	1	1	3	3	2	3	1	10	21	0	0	
	Etop-Cisplat	0	0	60	0	0	4	3	4	5	3	0	3	32	0	0	
	Target	0	0	59	2	0	4	3	3	2	2	0	0	12	0	0	
	Target-DC	0	0	56	1	2	3	1	5	3	4	0	2	26	0	0	
	Target-EP	2	0	58	1	0	3	3	4	1	5	0	5	22	0	0	
	Total number Median		0	0	59	1	0	3	3	4	2	3	0	3	22	0	0
		301 (59%)					77 (15%)					134 (26%)					
IC-pPDX-75	Doxo-Cyclo	1	0	76	5	5	5	11	5	0	0	6	5	3	1	3	
	Etop-Cisplat	2	0	78	4	3	11	7	8	1	3	10	7	2	1	2	
	Target	1	0	78	5	5	6	11	6	0	1	6	5	4	1	3	
	Target-DC	1	1	70	7	6	7	5	9	2	3	5	4	4	4	3	
	Target-EP	1	2	81	3	3	7	9	6	1	1	2	6	2	0	4	
	Total number Median		1	0	78	5	5	7	9	6	1	1	6	5	3	1	3
		438 (67%)					125 (19%)					93 (14%)					
IC-pPDX-109	Doxo-Cyclo	1	1	62	5	0	1	7	2	0	2	8	4	4	1	3	
	Etop-Cisplat	1	1	63	4	0	2	6	3	2	3	7	5	3	4	0	
	Target	3	0	64	5	0	5	9	3	1	1	5	9	1	2	0	
	Target-DC	0	0	65	6	0	10	8	2	1	2	8	7	1	1	1	
	Target-EP	1	0	65	5	0	15	8	3	1	0	14	7	2	1	0	
	Total number Median		1	0	64	5	0	5	8	3	1	2	8	7	2	1	0
		352 (64%)					97 (18%)					98 (18%)					
GR-NB4	Doxo-Cyclo	0	0	31	2	3	3	0	14	3	2	1	9	30	0	0	
	Etop-Cisplat	0	0	31	8	1	1	0	12	1	4	1	12	20	0	0	
	Target	0	0	30	3	3	0	0	16	3	3	0	8	30	0	0	
	Target-DC	0	1	28	12	0	0	5	4	2	6	5	8	27	0	0	
	Total number Median		0	0	30.5	5.5	2	0.5	0	13	2.5	3.5	1	8.5	28.5	0	0
			153 (40%)					79 (20%)					151 (40%)				
GR-NB10	Doxo-Cyclo	2	3	529	41	38	16	17	12	11	42	23	1	35	0	0	
	Etop-Cisplat	4	9	534	42	11	27	30	19	19	38	18	10	34	0	0	
	Target	2	5	553	46	10	13	14	17	27	32	24	7	35	0	0	
	Target-DC	5	3	555	10	15	9	17	37	11	45	25	4	54	0	0	
	Target-EP	1	5	545	23	17	28	20	23	16	46	18	9	6	10	10	
	Total number Median		2	5	545	41	15	16	17	19	16	42	23	7	35	0	0
		3008 (77%)					586 (15%)					323 (8%)					

Table 13 Number of variants that emerged, disappeared or persisted in each treatment group (“emerging”, “disappearing”, “persistent”, respectively) compared with the control group (non-treated mice) of a given PDX model, classified by their variant allele fraction (VAF) (clonal, subclonal and very subclonal). The persistent variants which variant allele frequency (VAF) significantly increased or decreased are (“increasing” or “shrinking”, respectively) also shown. The framed number corresponds to the total number of variants according to the clonal/subclonal/very subclonal groups in a given PDX model, with its proportion among the total number of mutations in brackets. Target-EP group of model GR-NB4 could not be analyzed because the whole-exome sequencing of these tumors was not contributive. Doxo-Cyclo (DC): doxorubicin-cyclophosphamide; Etop-Cisplat (DP): etoposide-cisplatin.

In summary, at a clonal level, the majority of the variants persisted across the different PDX models and treatment groups. We could identify few novel variants that emerged after treatment: of especial interest are the *STAG2* and *HDAC4* variants that emerged in the etoposide-cisplatin-target group of IC-pPDX-17. At a subclonal and very subclonal levels, differences were observed across models. Whereas in IC-pPDX-17, IC-pPDX-75 and IC-pPDX109 the variants persisted, disappeared or emerged homogeneously at a subclonal level, GR-NB4 had a majority number of persistent variants. At a very subclonal level, the SNVs in IC-pPDX-17 and GR-NB4 models were mostly persistent, whereas in IC-pPDX-75 and IC-pPDX-109 predominantly emerged or disappeared. GR-NB10, a hypermutated PDX model, showed important number of SNVs that significantly reduced their VAF at subclonal level after treatment; at very subclonal level the variants were mostly persistent and emerging.

In conclusion, model GR-NB4 was the most stable, with enhanced number of clones and subclones that persisted, whereas models IC-pPDX-75 and IC-pPDX109 showed greater variability, with more dynamic variants and higher number of variants emerging or disappearing. Finally, IC-pPDX-17 and GR-NB10 showed an intermediate profile of variability, with higher number of persistent variants at clonal and very subclonal levels, but enhanced variability at subclonal level. Interestingly, these are positively correlated with the efficacy of treatments in these models: GR-NB4 model, which was the most stable, showed higher sensitivity to treatments (mean TGI across treatment groups of 88.5%), whereas models IC-pPDX-75 and IC-pPDX109, the most variable, showed increased resistance to treatments (mean TGI: 45.2% and 61% respectively). Finally, IC-pPDX-17 and GR-NB10 models; with an intermediate degree of variability showed intermediate drug sensitivity profile, with TGI of 65% and 63% respectively.

These data are generated from bulk samples, which are composed of mixtures of cancer subpopulations, as well as normal cells. Novel subclonal reconstruction approaches combining machine learning with theoretical population genetics are able to separate those subpopulations in a sample and reconstruct their evolutionary history. These approaches minimize the confounding factors of non-evolutionary methods, leading to more accurate recovery of the evolutionary history of human cancers (Caravagna et al., 2020). In the next section we will describe some preliminary analysis based in novel bioinformatics approaches enabling the evolutionary subclonal reconstruction.

2.3.3 Modelization of clonal evolution

The detection of mutations belonging to each clone in a tumor depends on several factors such as sequencing depth and quality, tumor cellularity and mutation copy-number. The expansion of each clone over the life of a tumor is encoded in the allele frequency of somatic mutations. To characterize the clonal composition of a tumor, initially the VAF must be converted to a cancer cell fraction (CCF), which is the fraction of cancer cells within which the variant is present. Events appearing in all cancer cells (CCF = 100%) are considered clonal and events appearing in a subset of

cells (CCF < 100%) are considered subclonal and part of an ongoing expansion. Estimating the cancer cell fraction of events is challenging, as the observed variant allele frequency depends on the amount of normal cell admixture (purity) and local copy number (Cmero et al., 2020). Thus, taking in account the CCF and more advanced bioinformatics analyses, it is possible to infer the clonal evolution under treatment based in novel modelization methods of clonal architecture.

The modelization study of clonal evolution is objective of detailed work within a PhD thesis (Jaydutt Bhalshankar). We will give here the overview.

2.3.3.1 Bioinformatics analysis

In collaboration with bioinformatician Jaydutt Bhalshankar, WES was performed on PDX samples in the study. An average 110X depth of coverage per sample was observed after preprocessing of mapped BAM files. Poor quality samples with less than 30X of mean coverage were removed from the clonal evolution analysis. Joint variant calling was performed using Mutect2. Paired patient germline, treated and untreated (control) PDX tumor samples were pooled together for variant analysis. After initial filtering of variants (SNVs and Indels) a list of good quality somatic variants was obtained for each paired treated and untreated sample independently. Somatic Allele specific copy number analysis and purity estimation was performed using Sequenza tool. SNVs and Indels were mapped to copy number segmentation genomic region using Bedtools.

Clonal evolution modelization study was performed between untreated (control) and treated PDX sample as per study design. All somatic variants with combined depth of coverage $\geq 30X$ in control and treated PDX samples and VAF ≥ 0.05 (5%) in either or both samples were selected for the clonal inference. For clonal estimation and subpopulations of cancer cells identification, variants were first clustered using Pyclone-VI tool using beta-binomial distribution. Then clonal grouping, reordering and inferring consensus of phylogeny or evolution trees were performed using ClonEvol R package. Plotting of the figures was done by using R statistical environment and packages such as FishPlot, ggplot and ClonEvol.

2.3.3.2 Insights in clonal architecture and evolution after treatment

We could perform some preliminary analysis to try to reconstruct the clonal evolution before and after treatment by comparing the treated tumors *vs.* the controls (non-treated mice). For model GR-NB4, doxorubicin+cyclophosphamide treatment did not affect the clone architecture, whereas lorlatinib alone or combined with chemotherapy induced the expansion and shrinking of several clones (Figure 47). Since variant calling was performed based on joint calling between controls and treatment samples, the modeled clonal architecture varies between controls, whereas they are the same tumors. In model IC-pPDX-17, clones evolved similarly independently of the treatment they received (Figure 48).

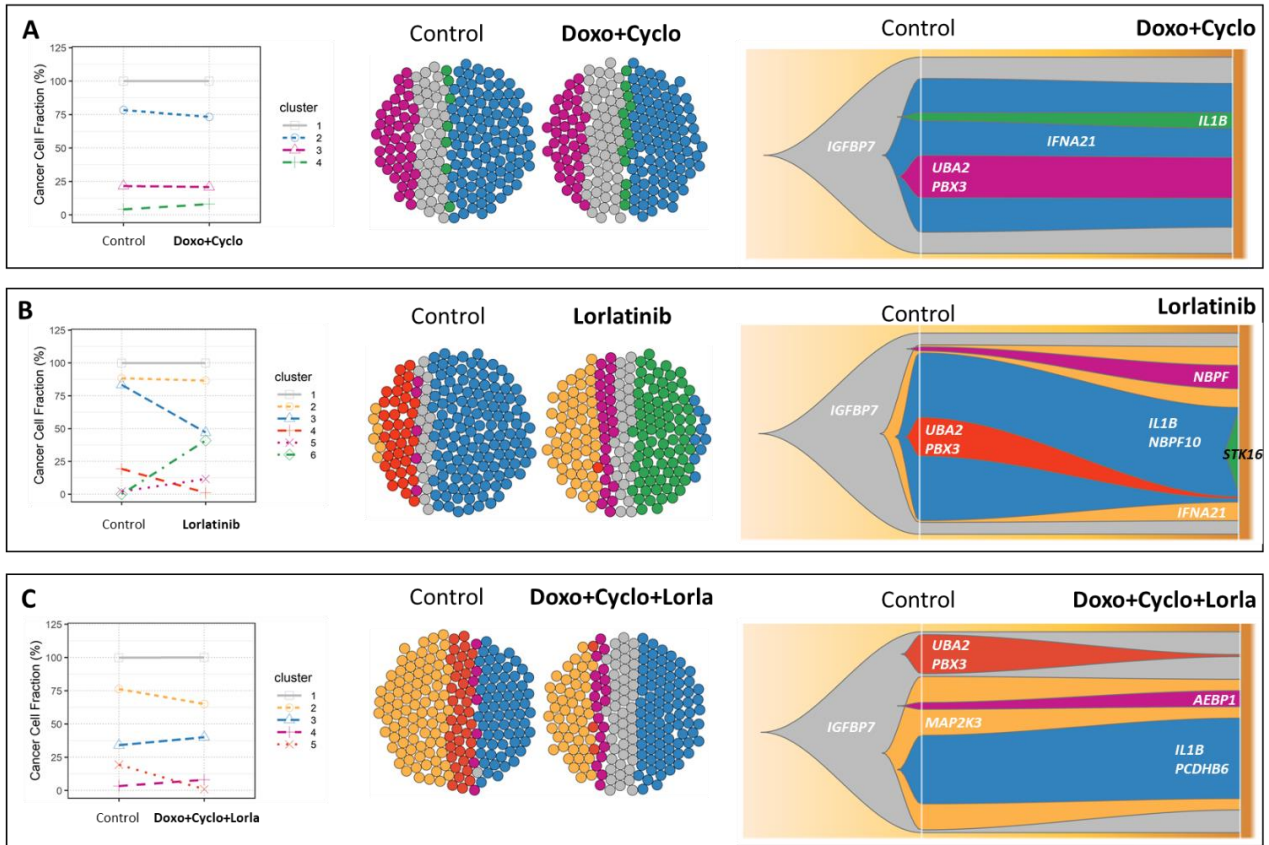


Figure 47: Clonal evolution of GR-NB4 model after (A) doxorubicin-cyclophosphamide (doxo+cyclo), (B) lorlatinib and (C) doxorubicin-cyclophosphamide-lorlatinib (doxo+cyclo+lorla). Since variant calling was performed based on joint calling, clonal architecture varies between controls, whereas they are the same tumors.

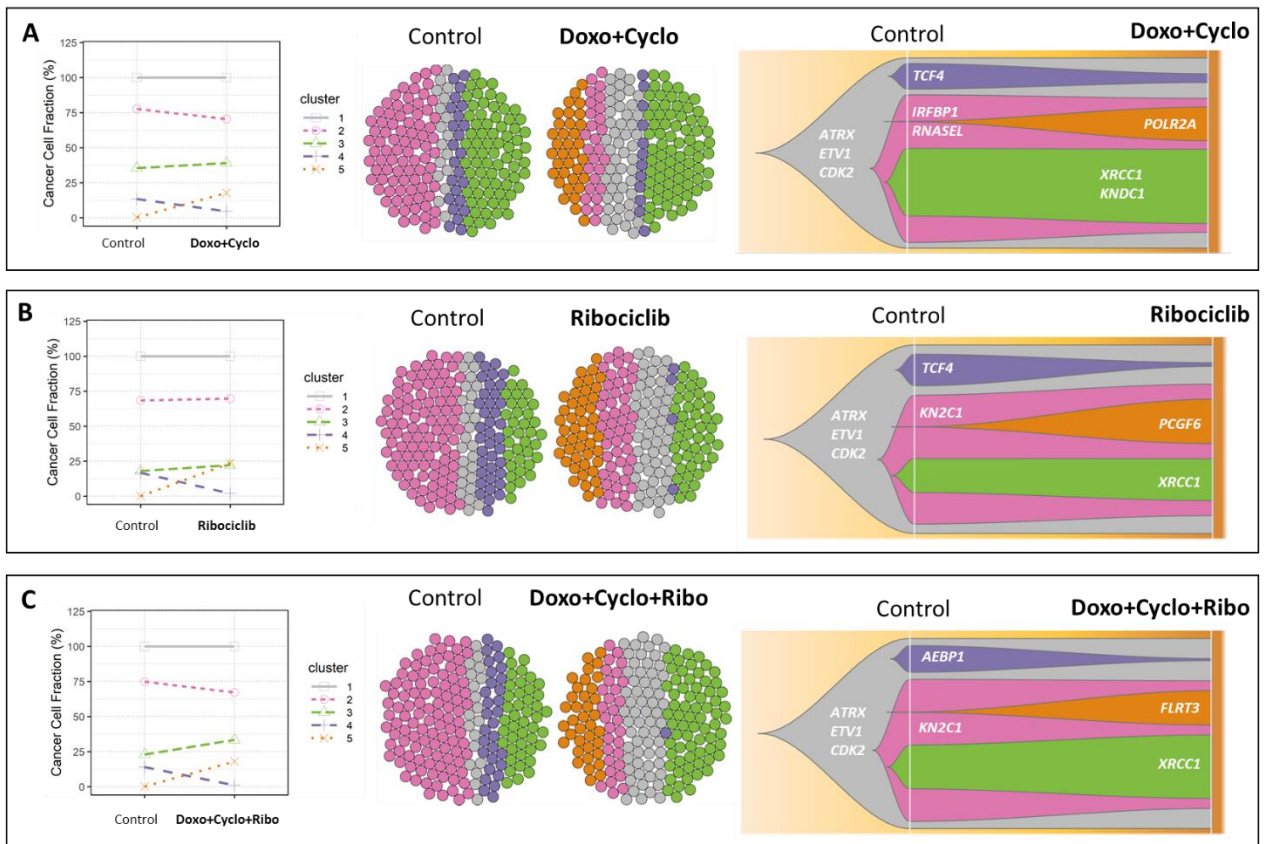


Figure 48: Clonal evolution of IC-pDX-17 model after (A) doxorubicin-cyclophosphamide (doxo+cyclo), (B) Ribociclib and (C) doxorubicin-cyclophosphamide-Ribociclib (doxo+cyclo+lora), showing similar evolutions despite different treatments.

Overall, we are able to highlight modifications, in some cases specific after targeted therapies. Bioinformatics analysis beyond the scope of the work of this Thesis is ongoing. The integration of more detailed bioinformatics will allow us to further give an overview and look in detail at genetic events. The exploration of clonal architecture and evolution across different PDX models and under several treatment arms will allow us to understand how clones evolve under different therapeutic pressures.

Beyond these findings, further work is needed to better understand the mechanisms of clonal evolution and treatment resistance. In fact, our results are based on a unique timepoint in the evolution of the tumor, at the time of sacrifice, when the tumor has fully escaped to treatment. It could be of interest to decipher the successive events that occur progressively during the treatment, which could lead to resistance. For this purpose, the analysis of the cfDNA could give us precious chronologic information of these genetic events. In addition, since our PDX models grow quite fast, this method could give us the opportunity to perform more prolonged treatments and follow the genetic events for longer, by the study of the cfDNA. Thus, we have performed several feasibility experiments which prove that it is possible to use the cfDNA as a surrogate of tumor DNA for the analysis of tumor-related genetic alterations and the study of clonal evolution which are described in the next *Perspectives* section.

2.4 Perspectives: cfDNA as a surrogate of tumor DNA in PDX models

As clonal evolution can be tracked over time by the analysis of tumor-related mutations in cfDNA, we collected blood samples at different timepoints during the *in vivo* experiments in order to confirm that the analysis of cfDNA in the plasma of PDX mice enables the study of the temporal heterogeneity and clonal evolution during treatment. In this section, we will describe the feasibility of the study of cfDNA analysis in mice PDX.

Cell-free DNA (cfDNA) consists of small DNA fragments released into the bloodstream by various processes such as tumor cell apoptosis or necrosis (Schwarzenbach et al., 2011a). The mean fragment length of cfDNA is 150–200 base pair-long, which corresponds to the length of a nucleosome. Both circulating tumor DNA (ctDNA) and normal genomic DNA (gDNA) are fractions of the total cfDNA. The analysis of cfDNA enables the detection of tumor-specific genetic alterations in patients with cancer. Indeed, cfDNA is distinguished from gDNA by the presence of cancer-related mutations. Genetic and epigenetic modifications, such as copy number alterations, mutations, and methylation can be detected in the ctDNA (Schwarzenbach et al., 2008a). It is of special utility for the sequential analysis of molecular alterations in solid tumors to limit the number of tissue biopsies for the study of temporal heterogeneity, providing an extremely specific biomarker for cancer that can be detected and tracked over time. Neuroblastoma is one of the pediatric tumors that generate the highest amounts of ctDNA, enabling the study of clonal evolution by the analysis of ctDNA in this disease (Chicard et al., 2018a). Taking advantage of our *in vivo* experiments on clonal evolution under targeted therapies in PDX models, we performed serial mice blood samples during the treatment in order to address the question of the study of the clonal evolution by the analysis of the cfDNA in mice bearing PDX tumors.

2.4.1 Blood sampling and processing

Mice blood samples were retrieved in EDTA tubes at different intermediate timepoints: before treatment (when tumor measured $\approx 3 \times 3$ mm), at day 10 of cycle 1 (D10C1) and at day 10 of cycle 2 (D10C2). A blood sample at final time point was also obtained at sacrifice. Blood samples were taken from the retro-orbital sinus for non-terminal procedures and by intracardiac puncture at the time of sacrifice. Blood volumes were aimed at approximately 100 μL and 1 mL for intermediate and final timepoints, in order to obtain 50 μL and 500 μL of plasma, respectively. Mouse blood was centrifuged within 2 to 4 hours after collection at 1,500 rpm for 15 minutes and then at 20,000 for 2 minutes, in order to separate the plasma from the pellet. Plasma samples were aliquoted and frozen at -20°C until cfDNA extraction. Overall, 781 blood samples were retrieved (556 at intermediate timepoints and 225 at sacrifice). The median plasma volume collected was 56 μL [8-185] and 380 μL [60-700] for intermediate and final timepoints, respectively.

2.4.2 cfDNA extraction, qualification and sequencing

CfDNA was extracted by using the QIAamp MinElute Virus Spin Kit (special for very low DNA concentrations) and cfDNA concentration was measured by Qubit fluorometric assay with dsDNA HS Assay Kit. The total cfDNA concentration per mL of mouse plasma was calculated. After extraction, quality control of extracted cfDNA was performed by capillary electrophoresis using Fragment Analyzer (Advanced Analytical®) with cfDNA quality expressed as the 150-200-bp fragment fraction. Median plasma cfDNA concentration was 1,337 ng/mL, 1,710 ng/mL, 1,497 ng/mL and 383 ng/mL for pre-treatment, D10C1, D10C2 and final timepoints, respectively (Figure 49).

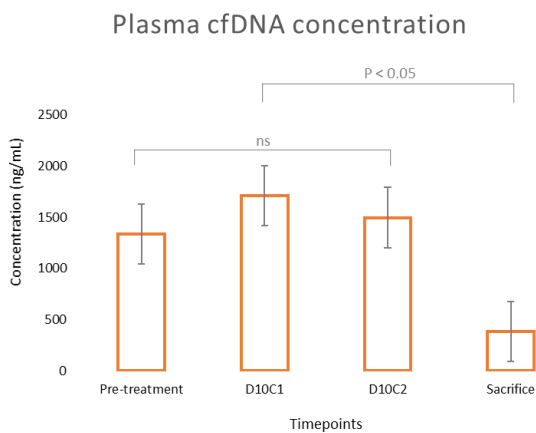


Figure 49: CfDNA concentration in plasma according to the different timepoints of blood sampling. No significant differences existed between intermediate timepoints, i.e. pre-treatment, day 10 of cycle 1 (D10C1) and day 10 of cycle 2 (D10C2). CfDNA concentration at sacrifice was significantly lower compared to intermediate timepoints.

The differences observed in plasma cfDNA concentration between intermediate and final timepoints were more likely due to the blood collection technique (retro-orbital sinus *vs.* intracardiac puncture) than to ctDNA content in cfDNA, since the retro-orbital sinus technique generates more hemolysis than intracardiac puncture (Regan et al., 2016), and then gDNA contamination (Figure 50).

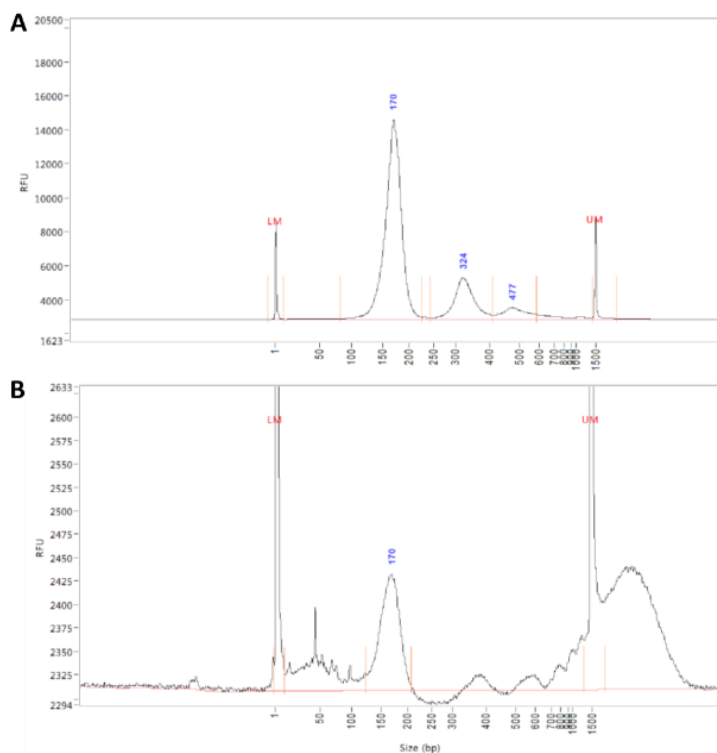


Figure 50: Capillary electrophoresis profiles of two mouse plasma cfDNA samples. (A) CfDNA from plasma sample obtained at sacrifice. The peak observed at ≈ 150 bp (170 bp in this particular example) corresponds to cfDNA. Additional peaks at ≈ 300 and ≈ 450 bp are often observed, corresponding to di- and tri-nucleotide-associated cfDNA. (B) CfDNA from plasma sample obtained at an intermediate timepoint. The peak corresponding to cfDNA is observed at 170 pb. A big peak of more than 1500 bp is observed in this sample, corresponding to a huge amount of genomic DNA contamination. LM and UM correspond to lower and upper size markers.

CfDNA from final timepoints of the experiments on models IC-pPDX-17, GR-NB4 and GR-NB10 were whole-exome sequenced as described in section 2.2.6 (without previous cfDNA fragmentation, accounting for the mean cfDNA fragment size of 160 bp). Median cfDNA input for library construction was 73 ng [30-200]. Mean depth-of-coverage for cfDNA samples corresponding to models IC-pPDX-17, GR-NB4 and GR-NB10 was 20, 9 and 19 reads respectively (table 10 in section 2.2.7).

2.4.3 Feasibility study in one cfDNA sample

We then compared a single cfDNA sample from IC-pPDX-17 model with its corresponding PDX tumor DNA and patient's tumor DNA. The analysis of copy-number profiles showed superposable cfDNA and tumor DNA profiles, in which we can clearly identify the 2q loss, the 7p gain and 7q loss, the amplicon in chr12, the chr15 loss, or two amplicons in chr22, among others. We then look for the study of SNVs and the comparison of the variants between IC-pPDX-17 tumor *vs.* cfDNA. The VAFs of SNVs identified in cfDNA and tumor DNA were highly correlated ($r = 0.95$). When comparing patient's tumor and cfDNA with IC-pPDX-17 tumor and cfDNA, we could identify a high concordance between PDX and patient's tumor, with 60 variants common to the four samples. Specific variants to patient's tumor/cfDNA and the corresponding PDX tumor/cfDNA were also identified. These results are illustrated in Figure 51.

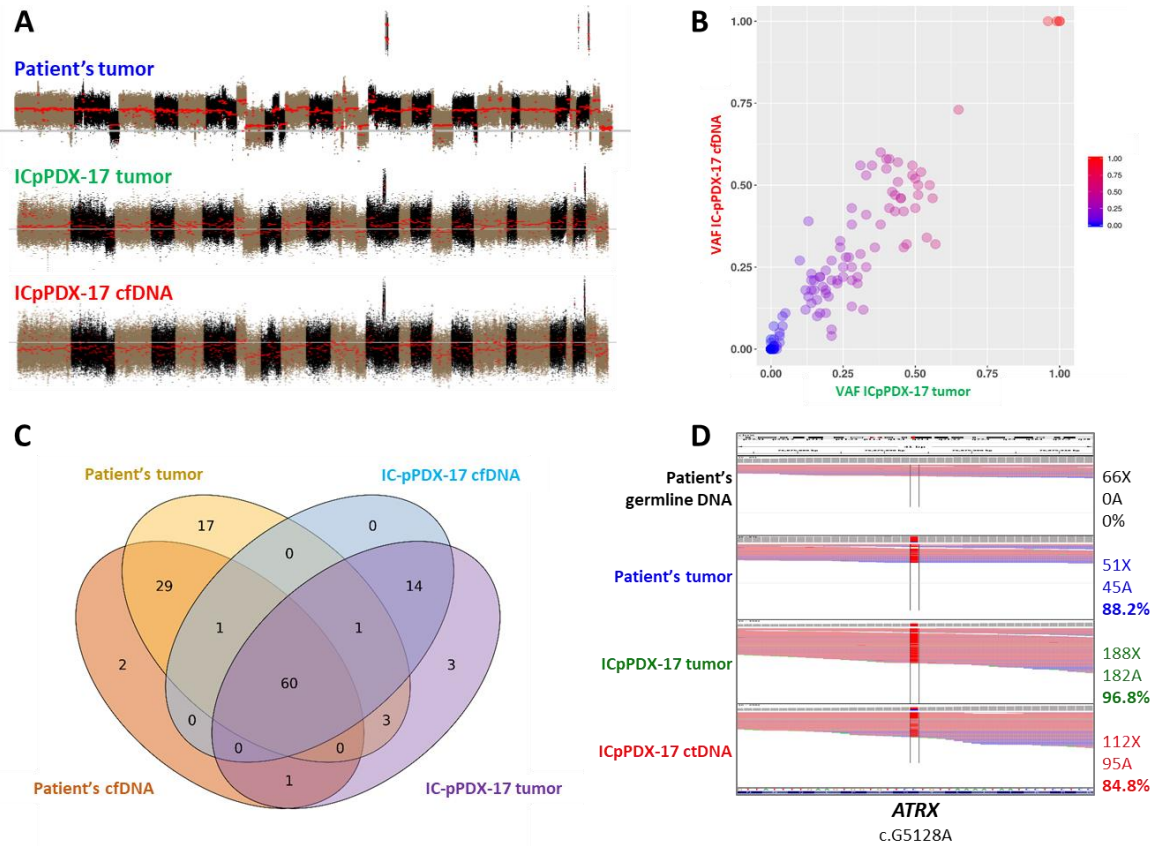


Figure 51: Whole-exome sequencing (WES) enables the study of copy-number alterations and single-nucleotide variations in PDX tumor and cfDNA of IC-pPDX-17. (A) Figure comparing the copy-number profiles of patient's tumor and corresponding PDX tumor DNA and cfDNA. (B) Linear correlation between variant allele fractions (VAFs) identified in tumor DNA vs cfDNA. (C) Venn diagram showing the common and specific variants of PDX tumor and cfDNA and patient tumor and cfDNA. (D) Integrative Genome Viewer image showing the *ATRX* c.G5128A variant carried by patient's tumor and corresponding PDX tumor DNA and cfDNA with similar allele frequencies. X: total depth at this position; A: number of alternative reads supporting the mutation; %: variant allele fraction of this single-nucleotide variation.

This feasibility study confirms that the analysis of mouse PDX cfDNA by WES can be exploited and is a useful tool to infer copy-number profiles and to study SNVs. These findings are the base and justify the use of cfDNA from mouse PDX for further studies on the clonal evolution under treatment.

2.4 Concluding remarks

Our studies show the close similarity between different tumors from the same PDX. Previous studies have shown that PDX models retain the main genetic features of their corresponding patient's tumor, highlighting the biological relevance of the PDX model in translational research (Bruna et al., 2016; Braekeveldt et al., 2018; Kamili et al., 2020). Although we could not confirm this for all the models, since sequencing technologies and fastq alignments for PDXs and corresponding patients' tumors were different, we could highlight close similarities for some models and their corresponding patient's tumor. Indeed, the variants retained for the patients in the MAPPYACTS molecular tumor board were also found in the corresponding PDX derived from patient's tumors.

The study of the clonal evolution under treatment allowed us to make several observations. First, we found that the total number of SNVs in treated mice was not higher than in non-treated mice, contrary to that could be expected. The patients from which PDX were derived received an average of 36 months of treatment before PDX establishment, and our PDXs were treated during 6 weeks, this is probably too short an interval of time to observe a significant number of new mutations in treated mice with respect with non-treated. We also did not find any difference in the number of variants between the different treatment groups.

The study of the VAF density showed that SNVs followed a particular distribution, despite minor differences between models. In all cases, there was a group of subclonal variants with VAFs around 5%, a second group of clonal variants with VAFs around 50% and a third minor group of clonal with 100% VAF. Whereas the majority of clonal variants persisted independently of PDX model or the treatment group, we observed an important variability in the group of subclonal and very subclonal variants across models. Interestingly, we found a number of actionable mutations with VAFs <5% in almost all the models, including *MAP3K7* emerging variant in ribociclib group of IC-pPDX-17, *VEGF* and *SMARCA2* persistent variants in GR-NB4, *RARA* persistent variant in IC-pPDX-75 or *CXCR1*, *MAP4K2* and *ARID1B* emerging and *MAPK13* and *CDK2AP1* persistent variants in GR-NB10 model.

Also, the analysis of clonal evolution under treatment allowed us to see that high-risk neuroblastoma PDX models with higher clonal variability after treatment showed increased treatment resistance, whereas models with more stable (persistent) clones, were more sensitive to the treatment.

We could perform some preliminary analysis for the reconstruction of clonal evolution before and after treatment and we are able to highlight modifications specific after targeted therapies for certain cases. More detailed bioinformatics analysis is ongoing to give an overview and look in detail at genetic events.

Finally, we have confirmed that the analysis of mouse PDX cfDNA by WES can be exploited to infer copy-number profiles and SNVs for further studies on the clonal evolution under treatment.

3. Combinatorial therapeutics for ALK-aberrant neuroblastoma

3.1 Scientific context

ALK mutations are identified in approximately 10% of newly diagnosed neuroblastomas (Janoueix-Lerosey et al., 2008; Mossé et al., 2008) and *ALK* amplifications (De Brouwer et al., 2010) in 1-2% of the cases. Furthermore, the incidence of *ALK* mutations increases in relapsed neuroblastomas, accounting for about 20% of the relapsed cases (Schleiermacher et al., 2014; Eleveld et al., 2015b; Padovan-Merhar et al., 2016). Three mutation hotspots in its kinase domain (F1174, R1275 and F1245) represent 85% of all forms of *ALK* mutation (Bresler et al., 2011). Together with *ALK* amplifications, these gain-of-function aberrations lead to the phosphorylation of ALK and constitutive increased kinase activity, as well as activation of downstream signaling molecules (such as PI3K-AKT, JAK-STAT and MAPK pathways), which results in enhanced survival, migration and proliferation of neuroblastoma (Janoueix-Lerosey et al., 2008; Mossé et al., 2008). These findings largely justify the efforts towards the study of ALK inhibition as a therapeutic target in neuroblastoma.

The most extensively studied ALK inhibitor in neuroblastoma, crizotinib, is a small molecule competitive inhibitor of ALK and MET kinase activity and was the first FDA approved for use in adult patients with *ALK*-translocated non-small cell lung cancer (NSCLC). The ADVL0912 phase II trial involving crizotinib has been completed by the Children's Oncology Group (COG) in pediatric patients with relapsed/refractory *ALK*-driven neuroblastoma (NCT00939770). Nevertheless, only 3 of 20 patients showed objective responses (1 patient with complete response and 2 with partial response) (Foster et al., 2021), mainly explained by the intrinsic resistance of F1174 and F1245 hotspot mutations to crizotinib (Bresler et al., 2011) and the inability to reach the concentrations of crizotinib needed to overcome the competing ATP affinity. Preclinical studies showed that this resistance can be overcome when crizotinib is combined with chemotherapy (Krytska et al., 2016), which was the rationale for the COG ANBL1531 phase III trial evaluating whether the addition of crizotinib to standard of care therapy for high risk neuroblastoma improves survival for patients with *ALK*-driven neuroblastoma (NCT03126916).

Resistance is a real challenge with crizotinib and new-generation ALK inhibitors have been developed to overcome both the intrinsic and *de novo* resistance. Lorlatinib, a third-generation ROS1 and ALK inhibitor has shown to exert significant preclinical activity against xenograft and patient-derived xenograft (PDX) models harbouring all hotspot mutations (Infarinato et al., 2016). These findings led to the NANT2015-02 phase I trial of lorlatinib for patients with *ALK*-driven neuroblastoma that is currently ongoing through the NANT consortium (NCT03107988) with encouraging preliminary results (Goldsmith et al., 2020). Furthermore, the COG phase III trial ANBL1531 mentioned above will be amended to replace Crizotinib by Lorlatinib. Finally, the international SIOPEN HR-NBL2 trial for first-line treatment of high-risk neuroblastoma will be amended to introduce Lorlatinib, and a

design has been chosen to later perform meta-analysis of data from the ANBL1531 and HR-NBL2 trials (Figure 52, Schulte & Eggert, 2021).

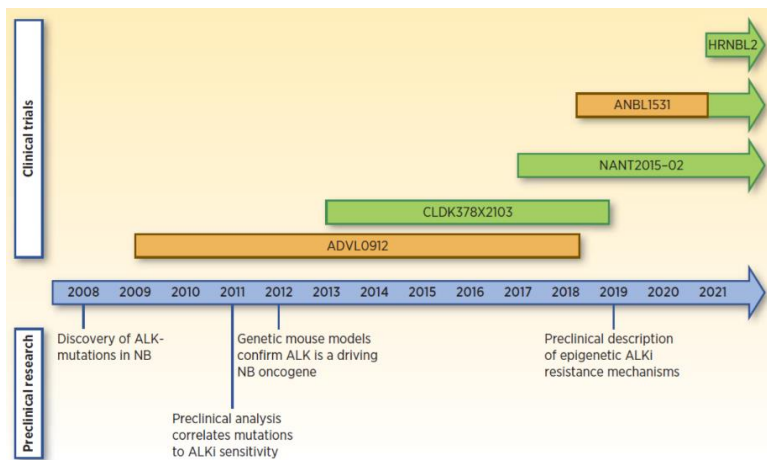


Figure 52 (Schulte and Eggert, 2021): Overview of the translational timeline from discovery of *ALK*-activating alterations and preclinical research in neuroblastoma into ALK inhibitor (ALKi) treatment. Orange indicates clinical trial with first-generation ALKi. Green indicates trials with second- or third-generation ALKi.

- ADVL0912: Crizotinib, relapse/refractory NB.
- CLDK378X2103: Ceritinib, relapse/refractory NB.
- NANT2015-02: Lorlatinib, relapse/refractory NB.
- ANBL1531: Crizotinib, first-line therapy. Crizotinib was subsequently replaced by Lorlatinib, via amendment.
- HRNBL2: Lorlatinib, introduced in ongoing trial via amendment, first-line therapy.

Recent works have shown that it is also possible to overcome resistance to ALK inhibition by activating the p53-MDM2 pathway (Miyazaki et al., 2018; Wang et al., 2017). In contrast to other malignancies, mostly in adults, neuroblastomas rarely harbor *TP53* mutations. Nevertheless, there is evidence of p53 pathway inactivation in a high proportion of neuroblastomas at the time of relapse that would likely contribute to chemotherapy resistance (Carr-Wilkinson et al., 2010). Several mechanisms for this inactivation have been proposed, including increased MDM2 expression mediated by *MYCN* or *MDM2* gene amplification (Chen et al., 2009; Swarbrick et al., 2010; Veschi and Thiele, 2017). Thus, enhancing or reactivating the functional activity of p53 by targeting the p53-MDM2 pathway via MDM2 inhibitors may represent a plausible approach for neuroblastoma treatment.

In this study, we have explored the *in vitro* and *in vivo* activity of ALK inhibitors alone and in combination with chemotherapy in various *ALK*-aberrant preclinical models of neuroblastoma including *in vitro* (cell lines), *ex vivo* (PDX-derived tumor cells, PDTs), and *in vivo* (genetically engineered mouse models, GEMMs, and PDX) models. These models were also used to study the activity of the combination of ALK and MDM2 inhibition for the treatment of *ALK*-mutated or amplified neuroblastomas.

Due to COVID-19 pandemic restrictions, several experiments were delayed and could not yet be included in the following draft, especially the in vivo experiments that in some cases had to be interrupted (institutional and ministerial decrees). Following the possibility to partially re-start these experiments, after the summer 2020, these experiments required additional time also because laboratory work was only possible at half-capacity. This is the reason why the manuscript lacks some of the figure panels or a stronger conclusion. These experiments are ongoing and are planned to be finished by the end of June 2021. The manuscript will be submitted for mid-July.

TITLE: COMBINATORIAL THERAPEUTICS FOR ALK-ABERRANT NEUROBLASTOMA

AUTHORS:

Irene Jiménez^{1,2†}, Lindi Chen^{3†}, Elizabeth R. Tucker^{4†}, Elizabeth Calton⁴, Evon Poon⁴, Barbara Martins Da Costa⁴, Karen Barker⁴, Elaine Del Nery⁵, Pierre Gestraud⁶, Angela Bellini^{1,2}, Jaydutt Bhalshankar^{1,2}, Yasmine Iddir^{1,2}, Elnaz Saberi-Ansari^{1,2}, Alexandra Saint-Charles^{1,2}, Birgit Georger⁷, Eugenia Da Costa⁷, Didier Decaudin⁸, Fariba Nemati⁸, Angel M. Carcaboso⁹, Didier Surdez³, Eve Lapouble¹⁰, Olivier Delattre³, Louis Chesler⁴, Gudrun Schleiermacher^{1,2‡}, Deborah A. Tweddle^{3‡}, Sally L. George^{4‡}

†These authors contributed equally to this work

‡These authors contributed equally to this work

AFFILIATIONS:

1 SiRIC RTOP (Recherche Translationnelle en Oncologie Pédiatrique); Translational Research Department, Institut Curie Research Center, PSL Research University, Institut Curie, Paris, France

2 INSERM U830, Equipe Labellisée Ligue contre le Cancer, PSL Research University, Institut Curie Research Center, Paris, France

3 Wolfson Childhood Cancer Research Centre; Newcastle Centre for Cancer, Translational & Clinical Research Institute, Newcastle University, Newcastle upon Tyne, United Kingdom.

4 Pediatric Tumour Biology; Division of Clinical Studies; The Institute of Cancer Research, Cotswold Road, London, SM2 5NG, United Kingdom.

5 Biophenics Laboratory, Institut Curie, Paris, France

6 Bioinformatics platform, Institut Curie, Paris, France

7 Gustave Roussy Cancer Center, Department of Pediatric and Adolescent Oncology, Université Paris-Saclay, Villejuif, France

8 Laboratoire d'Investigations Précliniques, Institut Curie, Paris, France

9 Hospital Sant Joan de Déu, Barcelona, Spain

10 Somatic Genetics Unit, Institut Curie, Paris, France

***Corresponding author.** Sally George
Pediatric Tumour Biology, Division of Clinical Studies
The Institute of Cancer Research, London, UK
E-mail address: sally.george@icr.ac.uk

KEY WORDS: Neuroblastoma; ALK-mutation; ALK-amplification; ALK inhibitors; idasanutlin

INTRODUCTION

Neuroblastoma is an embryonal tumor that arises in the developing sympathetic nervous system and is the most common cancer diagnosed during the first year of life. The clinical behavior of neuroblastoma is dramatically heterogeneous, from spontaneous and complete regression (1,2) to very aggressive tumors. Indeed, high-risk forms of neuroblastoma have a 5-year overall survival of 50% despite advances in treatment over the last 30 years (3) and account approximately 15% of all childhood cancer deaths (4), meaning that still many efforts need to be done in order to increase disease survival.

This diverse clinical presentation and course depend highly on the tumor biology. Few recurrent molecular alterations have been described in neuroblastoma, some of which are correlated to poor outcome. *MYCN* amplifications (5–7), *TERT* promoter rearrangements (8–10), loss-of-function (LoF) *ATRX* mutations (11,12) and *ALK* activating mutations and amplifications (Bellini et al., 2021, in press) are the most recognized. Both *MYCN* amplifications and *TERT* rearrangements lead to telomere maintenance by induction of telomerase, whereas *ATRX* LoF mutations induce telomere maintenance by activation of the alternative lengthening of telomeres (ALT) pathway. These three conditions identify three almost non-overlapping groups of high-risk neuroblastomas, each associated with very poor prognosis (10,13). As driver oncogenic events, these alterations could represent potential therapeutic targets for neuroblastoma.

ALK activating mutations are identified in approximately 10% of newly diagnosed neuroblastomas (14,15) and *ALK* amplifications (16) in 1-2% of the cases. Furthermore, the incidence of *ALK* mutations increases in relapsed neuroblastomas, occurring in about 20% of relapsed cases (17–19). Three mutation hotspots in its kinase domain (F1174, R1275 and F1245) represent 85% of all forms of *ALK* mutations (20). Together with *ALK* amplifications, these gain-of-function alterations lead to the phosphorylation of *ALK* and constitutive increased kinase activity, as well as activation of downstream signaling molecules (such as PI3K-AKT, JAK-STAT and MAPK pathways), which results in enhanced survival, migration and proliferation of neuroblastoma (14,15). In addition, germline *ALK* mutations are cause of hereditary neuroblastoma, which account for 1-2% of all neuroblastoma cases (14,15,21). These findings largely justify the efforts towards the study of *ALK* inhibition as a therapeutic target in neuroblastoma, especially taking in account the germline *ALK* mutated cases.

The most extensively studied *ALK* inhibitor in neuroblastoma, crizotinib, is a small molecule competitive inhibitor of *ALK* and *MET* kinase activity and was the first FDA approved for use in adult patients with *ALK*-translocated non-small cell lung cancer (NSCLC). A phase II trial involving crizotinib has been completed by the Children's Oncology Group (COG) in pediatric patients with relapsed/refractory *ALK*-driven neuroblastoma (NCT00939770). Only 3 of 20 patients showed objectives responses (22), mainly explained by the intrinsic resistance of F1174 and F1245 hotspots mutations to crizotinib (20) and the inability to reach adequate concentrations. Preclinical studies showed that crizotinib resistance can be overcome when crizotinib is combined with chemotherapy (23), which was the rationale for the COG phase I trial combining crizotinib with topotecan and cyclophosphamide in children with relapsed and refractory solid tumors (NCT01606878) (24).

Resistance following treatment with crizotinib remains a major challenge and new-generation *ALK* inhibitors have been developed to overcome both the intrinsic and de novo resistance. Lorlatinib, a

third-generation ROS1 and ALK inhibitor has shown to exert significant preclinical activity against xenograft and patient-derived xenograft (PDX) models harboring all hotspot mutations (25). These findings led to a phase I trial of lorlatinib for patients with *ALK*-driven neuroblastoma that is currently ongoing through the NANT consortium (NCT03107988) with encouraging preliminary results (26).

Furthermore, recent works have shown that it is also possible to overcome resistance to ALK inhibition by activating the p53-MDM2 pathway (27,28). In contrast to other malignancies, mostly in adults, neuroblastomas rarely harbor *TP53* mutations. Nevertheless, there is evidence of p53 pathway inactivation in a high proportion of neuroblastomas, especially at the time of relapse, that would likely contribute to chemotherapy resistance (29). Several mechanisms for this inactivation have been proposed, including MYCN-mediated MDM2 overexpression or MDM2 gene amplification (Chen et al., 2009; Swarbrick et al., 2010; Veschi & Thiele, 2017). Thus, enhancing or reactivating the functional activity of p53 by targeting the p53-MDM2 pathway via MDM2 inhibitors may represent a plausible approach for neuroblastoma treatment.

We now hypothesize that combining ALK inhibitors with chemotherapy or with other targeted drugs, such as MDM2 inhibitors, will lead to enhanced efficacy in neuroblastoma and, thus ultimately in a clinical setting, to a better patient survival. In this work, the *in vitro* and *in vivo* activity of ALK inhibitors has been explored alone and in combination with chemotherapy in various *ALK*-mutated or amplified preclinical models of neuroblastoma, including *in vitro* (cell lines), *ex vivo* (PDX-derived tumor cells, PDTCs), and *in vivo* (genetically engineered mouse models, GEMMs, and PDX) models. These models were also used to study the activity of the combination of ALK and MDM2 inhibition for the treatment of *ALK*-aberrant neuroblastomas. The ultimate goal of this work is to define novel therapeutic combinations for *ALK*-aberrant neuroblastoma patients that could eventually find their place and been explored in potential future pediatric early clinical trials.

MATERIALS AND METHODS

In this collaborative project, the experiments on cell lines were performed by the Wolfson Childhood Cancer Research Centre team in Newcastle, headed by Pr. Deborah Tweddle. The experiments on GEMM were performed by the Institute of Cancer Research team in London, headed by Dr Sally George. Finally, the experiments on PDX and PDTCs were carried out by the Institut Curie team, under the direction of Dr Gudrun Schleiermacher.

Treatment of *ALK* aberrant neuroblastoma cell lines

Human neuroblastoma cell lines were cultured in RPMI 1640 (Sigma) supplemented with 10% v/v Fetal Calf Serum (FCS; Gibco/Life Technologies Ltd, Paisley, UK) (Supplementary Table 2) (30). Cell lines were authenticated using STR genotyping and/or cytogenetic analyses. Cell lines were sequenced for *ALK* by Sanger sequencing (exons 20-29) and *ALK* amplification was assessed by FISH and/or SNP array, the latter analyzed using Nexus Biodiscovery software. The list of cell lines is detailed in Supplementary table 1.

The MDM2 antagonist idasanutlin was kindly provided by Hoffman la-Roche/Genentech. All other compounds were purchased from Selleck Chemicals (Strattech Scientific Ltd, Newmarket, UK). All compounds were dissolved in dimethyl sulfoxide (DMSO) (Sigma-Aldrich). Seventy-two-hour XTT growth inhibition assays with determination of the concentration required to inhibit growth by 50% (GI₅₀) and median effect analysis were performed as previously described (31). Synergy and Combination Index (CI) values were determined using CalcuSyn v2 (Biosoft, Cambridge, UK). Flow cytometry and caspase 3/7 assays were performed as previously described and according to manufacturer's protocols (32).

Determination of PDX genomic alterations

Sequencing. ALK-aberrant PDX models are described in Supplementary Table 2. All PDX tumors and paired patient germline DNA were whole-exome sequenced (WES) by Agilent SureSelect Human All Exon v5 or Nimblegen Roche Sequencing SeqCap EZ MedExome Kit according to manufacturer's protocols (paired-ends 100x100 bp, expected coverage 100 X).

Bioinformatics sequencing pipeline. For PDX samples, fastq files were aligned using Bwa-mem on a hybrid GRCh37-GRCm38 (human-mouse) reference genome. Reads exclusively mapped to human chromosomes with mapping quality more than 20 were extracted. For human samples, fastq files were aligned on GRCh37 human genome reference and uniquely mapped reads with mapping quality more than 20 were extracted. Finally, duplicate reads were removed. Coverage analysis was done using MOSDEPTH and GATK4. For copy number analysis, Sequenza and FACETS were used and purity and the ploidy of each samples were extracted from Sequenza results. Mutect2 was used for variants calling. The mutations were filtered using Filter Mutect2 calls and annotated using VEP. Only the variants matching the following criteria were retained: the coverage should be more than 20X, variant supporting reads should be more than 10 in tumor and cfDNA with at least one forward and one reverse read, less than 2 reads in germline sample, VAF >0.01, predicted as deleterious by SIFT or PolyPhen, and frequency less than 0.001 in the population.

Ex vivo drug screenings on PDTC models

Obtaining PDTCs from PDX tumors. For viable PDTC generation, we used a dissociation protocol adapted from Stewart et al., 2017 (33), which included a first step of PDX tumor mechanical dissociation with sterile scalpels and then enzymatic dissociation by trypsin (10 mg/ml) and type II collagenase (275 U/mg, Worthington Biochemical). The tube was then placed in a warm 37°C water bath for 60 min. Dissociation was stopped by adding Soybean Trypsin Inhibitor (10 mg/ml, Sigma). Deoxyribonuclease I (2 mg/ml, Sigma) and magnesium chloride (1 M) were added in equal amounts. Tumor suspension was filtered with a 40 µm cell strainer and then centrifuged at 500g for 5 minutes. Supernatant was discarded and cell pellet was resuspended in PBS-minus/10%FBS for cell counting. The suspension was then re-centrifuged and resuspended in serum-free stem-cell (SC) medium (34), which contained Dulbecco's Modified Eagle Medium/Nutrient Mixture F-12 (DMEM/F12, Gibco) supplemented with 40 ng/ml basic fibroblast growth factor (bFGF), 20 ng/ml epidermal growth factor (EGF), 1× B27 supplement (Gibco) and 500 U/ml of penicillin/streptomycin.

Experimental pipeline. The same experimental pipeline was used for all drug screens in PDTCs. All compounds were purchased from Selleck Chemicals (Strattech Scientific Ltd, Newmarket, UK). After PDX tumor dissociation, cells in SC medium were plated by robotic seeding in 384-well plates (384-wp) at a concentration of 20,000 cells in 40 μ L per well. Drugs dissolved in DMSO (Sigma-Aldrich) were added to cells 24 hours after plating (day 1) by robotic drug dispense. Cells were then incubated for 72 hours until day 4, when cell viability was measured by CellTiter Glo (Promega) luminescent assay.

Monotherapy drug screening. For monotherapy drug screening, we performed high-throughput drug screening on PDTCs with a commercial drug library (Selleck Chemicals) consisting on 55 compounds including ALK inhibitors crizotinib, alectinib, ceritinib, and lorlatinib and MDM2 inhibitor idasanutlin. Drugs were diluted in 12 concentrations each as 3-fold serial dilutions (from 10,000 nM to 0.056 nM) and screened in two independent biological replicates (two different experiments, same PDX model, different PDX passages with high correlations (Supplementary figure 1). Only the results on ALK inhibitors and idasanutlin are shown in this study.

Chemo-chemo combinations. For chemo-chemo combinations in PDTCs, we designed 3 matrixes combining chemotherapy compounds doxorubicin, etoposide and carboplatin with each other (doxorubicin-etoposide, carboplatin-etoposide, doxorubicin-carboplatin), in 11 concentrations each as 3-fold serial dilutions (from 10,000 nM to 0.17 nM). We then chose, for each PDTc model, the combined concentrations of chemotherapy compounds that resulted in 80% of cell viability (Supplementary figure 2). The selected concentrations were then used for chemo-drug combinations.

Chemo-drug combinations. For chemo-drug combinations in PDTCs, cells were treated with the selected dose of chemotherapy compounds leading to 80% of cell viability and combined with targeted agents in a dose-response manner (12 concentrations each as 3-fold serial dilutions from 10,000 nM to 0.056 nM).

Analysis of drug responses in PDTCs. Drug responses were represented by the dose-response curve and the quantitative drug sensitivity score (DSS), as described by Yadav et al. (35).

***In vivo* experiments with GEMMs**

All experiments, including the breeding of transgenic animals, were performed in accordance with the local ethical review panel, the UK Home Office Animals (Scientific procedures) Act 1986, the ARRIVE (Animal Research: Reporting of In Vivo Experiments) guidelines (36) and the UK NCRI guideline (37). Th-*ALK*^{F1174L}/*MYCN* tumor-bearing animals were enrolled into therapeutic trials when their abdominal tumors reached 5 mm in diameter according to palpation.

Short-term studies. For short-term studies volumetric MRI was performed as previously described (38), with each animal under-going imaging on day 1 and day 3. The tumor volume at each time point was then calculated. For in vivo oral dosing on day 1-3, crizotinib was dissolved in sterile water with 10% Tween 20. Ceritinib was dissolved into 0.5% methylcellulose, 0.5% Tween 80 with sterile water. Alectinib was dissolved in 10% DMSO, 10% cremophor, 15% PEG400, 15% HPCD, 0.02N HCl in sterile water. Lorlatinib was dissolved into 0.5% methylcellulose, 0.5% Tween 80 with sterile water. Two

hours following the final dose of compound, tumor tissue was excised and snap frozen prior to analysis.

Longer-term survival studies. For longer-term survival studies tumor volume was monitored by daily palpation, and the animal was sacrificed when Home Office Licence limits were reached to record survival. Dosing of compounds was continuous for maximum of 56 doses. Mice receiving VAC chemotherapy regimen were treated intraperitoneally at day 1 with the following doses: vincristine: 0.015 mg/kg; doxorubicin: 0.7 mg/kg; cyclophosphamide: 28 mg/kg. In this regimen, Lorlatinib was commenced from day 2 at 10 mg/kg orally. Mice were sacrificed 2 hours following the final dose of Lorlatinib and any remaining tumor tissue collected for pharmacodynamic studies.

Pharmacodynamic studies on GEMM tumors. Snap frozen tumors were lysed in 5% CHAPS buffer and quantitation of ALK and pY1586 ALK was performed using immunoassay as previously described (39).

PDX *in vivo* experiments

PDX treatments. Swiss Nude mice (Charles River) were engrafted in the interscapular fat pad. Ten mice per group were engrafted per experimental arm to ensure at least 5 treated mice and 3 PDX tumors for pharmacodynamics studies. Treatments started when tumor reached 150-200 mm³. All mice received VAC chemotherapy regimen intraperitoneally (IP) at day 1 (D1) with the following doses: vincristine: 0.015 mg/kg; doxorubicin: 0.7 mg/kg; cyclophosphamide: 28 mg/kg. For efficacy studies, mice received idasanutlin and lorlatinib orally at 75 mg/kg/dose from D1 and 10 mg/kg/dose from day 2 (D2), respectively, 5 days per week. Targeted therapies were pursued until tumor ethical size, when tumor reached 2,000 mm³. For pharmacodynamic studies, mice received VAC chemotherapy at D1, idasanutlin at D1 and D2, and lorlatinib at D2 and D3 (all drugs at the doses described above). Mice were sacrificed at D3, 4 hours after the second dose of lorlatinib, for pharmacodynamic studies.

Antitumor efficacy assessment on PDX tumors. Tumor volumes were calculated by measuring two perpendicular diameters with callipers. Each tumor volume (V) was calculated according to the following formula: $V = a \times b^2 / 2$, where a and b are the largest and smallest perpendicular tumor diameters. Relative tumor volumes (RTV) were calculated from the following formula: $RTV = (V_x/V_1)$, where V_x is the tumor volume on day x and V₁ is the tumor volume at initiation of therapy (D1). Growth curves were obtained by plotting the mean values of RTV on the Y axis against time (X axis, expressed as days after start of treatment). Antitumor activity was evaluated according to tumor growth inhibition (TGI), calculated according to the following formula: $\text{percent GI} = 1 - (RTV_t / RTV_c \times 100)$, where RTV_t is the median RTV of treated mice and RTV_c is the median RTV of controls, both at a given time point when the antitumor effect was optimal. Fifty percent TGI was considered to be the limit for a meaningful biological effect. Statistical significance of differences observed between the individual RTVs corresponding to the treated mice and control groups was calculated by the two-tailed Student's t test.

Pharmacodynamics studies on PDX tumors. Tumors were extracted at D3 of treatment, 4 hours after the second dose of lorlatinib. Immunohistochemistry was performed for Ki67 (Abcam ab15580) and

cleaved caspase-3 (Cell Signaling #9661) in order to assess for cell proliferation and apoptosis, respectively. Western blotting was carried out for ALK, pY1586 ALK, ERK1/2, pERK1/2, AKT, pAKT from Cell Signaling Technology Inc. and MYCN, MDM2, p53, p21 and GAPDH, as previously described (31,39).

RESULTS

ALK inhibitors in monotherapy

Pre-clinical evaluation of ALK inhibitors in ALK aberrant neuroblastoma models

Given the poorer prognostic impact of *ALK* amplifications and clonal *ALK* mutations in high-risk neuroblastoma patients, we sought to further study the pre-clinical efficacy of ALK inhibitors in neuroblastoma models. In a first step, GI₅₀ values for ALK inhibitors TAE-684, crizotinib, alectinib, ceritinib and lorlatinib were determined in a panel of neuroblastoma cell lines of varying ALK status using 72h XTT assays. *ALK* status of cell lines was determined from a combination of previously published literature and our own FISH/SNP array and sequencing analyses (Supplementary table 1). Sensitivity to the tested ALK inhibitors with the exception of lorlatinib correlated with the presence and type of *ALK* alteration (i.e. mutation or amplification) (Fig. 1 A-E). Cell lines with *ALK* alterations were in general less sensitive to lorlatinib than crizotinib, with a much wider range of reported GI₅₀ values also seen for lorlatinib.

We next quantified *in vitro* inhibition of ALK activation using an immunoassay by the different ALK inhibitors in *ALK* mutant and *ALK* amplified neuroblastoma cell lines and found that in contrast to the *in vitro* sensitivity, lorlatinib was the most effective inhibitor of ALK phosphorylation (figure 1f), raising the possibility that *in vitro* sensitivity to ALK inhibitors as determined by cell inhibition growth may not be an accurate predictor of ALK dephosphorylation and then of *in vivo* activity (39).

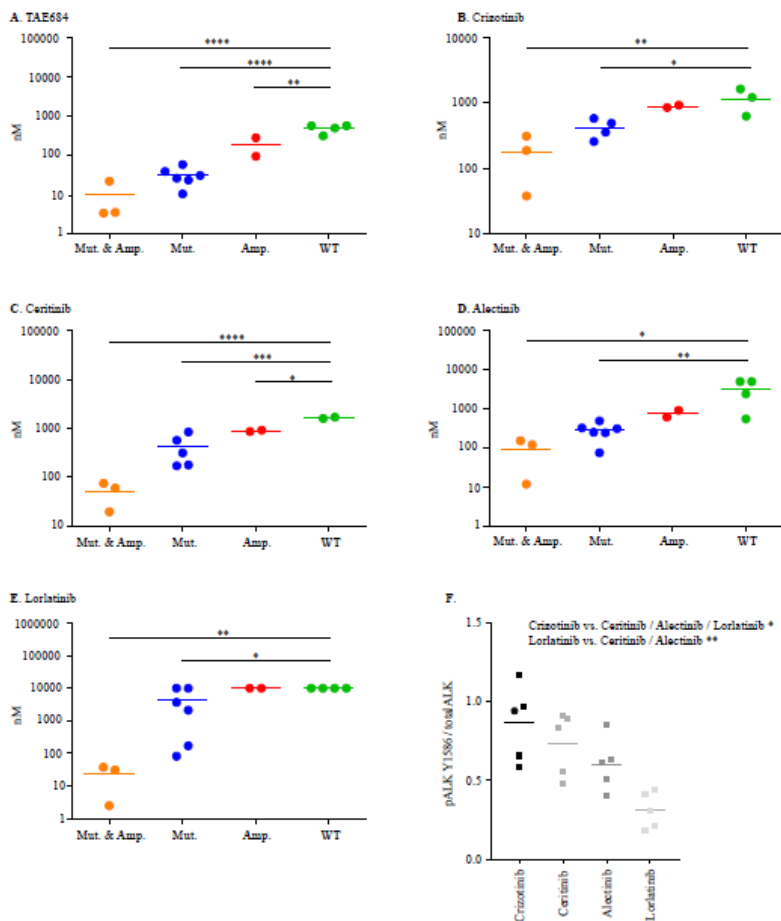


Figure 1. ALK mutant or amplified neuroblastoma cell lines are significantly more sensitive to targeted ALK inhibition versus ALK wild-type lines, and Lorlatinib is the most potent ALK inhibitor tested. Seventy-two-hour GI₅₀ values for ALK inhibitors. A, TAE-684, B, Crizotinib, C, Ceritinib, D, Alectinib and E, Lorlatinib in a panel of neuroblastoma cell lines. Cell lines were grouped based on the type of *ALK* alteration. Statistically significant differences were determined by one-way ANOVA with Bonferroni post-hoc tests and paired testing versus WT. $P \leq 0.05$ (*); 0.01 (**); 0.001 (***) 0.0001 (****). F, NB cell lines treated with 20nM of indicated inhibitor for 3 hours, and lysates subjected to ALK immunoassay for total ALK and pY1586 ALK. Statistically significant differences determined by paired, two-tailed t-test. $P \leq 0.05$ (*); 0.01 (**).

To evaluate the *in vivo* efficacy of ALK inhibitors, we performed a short-term response assessment study for four different ALK inhibitors in the Th-*ALK*^{F1174L}/*MYCN* GEMM model of ALK mutant neuroblastoma. Th-*ALK*^{F1174L}/*MYCN* double transgenic animals develop spontaneous abdominal neuroblastomas at a shorter latency and 100% penetrance, compared to their Th-*MYCN* littermates, indicating that the addition of ALKF1174L plays a key role in tumorigenesis in this model (40). Tumor-bearing Th-*ALK*^{F1174L}/*MYCN* mice, which had been treated with lorlatinib showed the greatest reduction in tumor volume, over a 3-day interventional dosing schedule (Fig. 2A). When tumors were harvested for immunoassay testing of ALK and pY1586 ALK status, it was found that alectinib had an equivalent effect to lorlatinib on the reduction of pY1586ALK/ALK in the tumor cells, suggesting that the tumor volume response observed in these animals following lorlatinib treatment, may be due to a secondary off-target effect of lorlatinib, not shared with alectinib (Fig. 2B). Treatment of Th-*MYCN* heterozygous mice with these inhibitors also resulted in tumor volume decrease over three days of therapy, attesting to the non-ALK activity of these compounds (Supplementary figure 3).

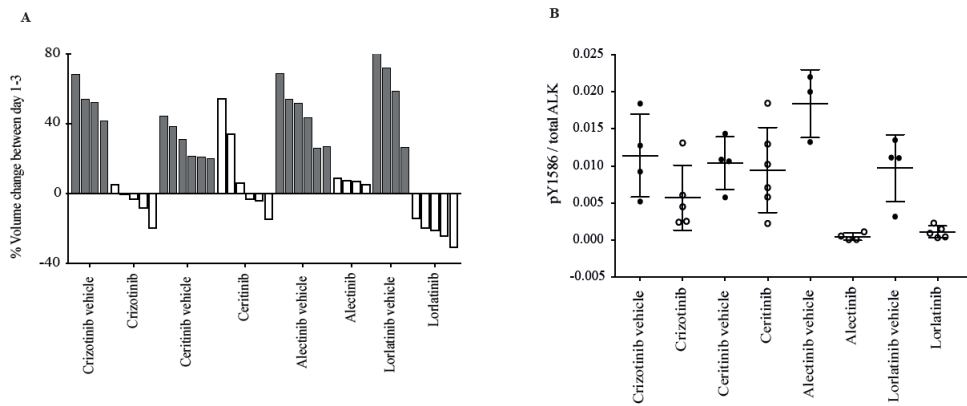


Figure 2. 3-Day treatment of Th- $ALK^{F1174L}/MYCN$ tumor-bearing animals with Lorlatinib results in tumor regression with evidence of ALK dephosphorylation. In vivo analysis of a panel of ALK inhibitors including crizotinib, ceritinib, alectinib and lorlatinib was carried out using the Th- $ALK^{F1174L}/MYCN$ model. Tumor-bearing Th- $ALK^{F1174L}/MYCN$ mice, were treated with the indicated inhibitor over a 3-day interventional dosing schedule. Tumors were harvested for immunoassay testing of ALK and pY1586 ALK status.

Ex vivo evaluation of ALK inhibitors in PDTC models

A selection of five PDX models carrying *ALK* alterations were screened: GR-NB4 and IC-pPDX-112 carried *ALK* amplifications, and IC-pPDX-75, HSJD-NB-011 and HSJD-NB-012 carried ALK^{F1174L} , ALK^{1171N} and ALK^{F1174C} mutations, respectively (Supplementary table 2). Interestingly, the patient from whom the IC-pPDX-75 model was derived received crizotinib treatment for 12 months before the establishment of the PDX model.

PDTCs were treated with the ALK inhibitors alectinib, ceritinib, crizotinib and lorlatinib. Drug responses were represented by the quantitative drug sensitivity score (DSS) (35), which integrates a multiparameter analysis, including the potency (the half-maximal effective concentration, EC_{50}), slope of the dose–response curve, the area under the curve (AUC), and the maximum effect of the drug. In PDTC models, while DSS values of lorlatinib were higher than those of ceritinib or similar to crizotinib, only lorlatinib showed significantly higher cytotoxicity (lower DSS values) in *ALK*-aberrant PDTC models compared to wild-type models (Fig. 3A).

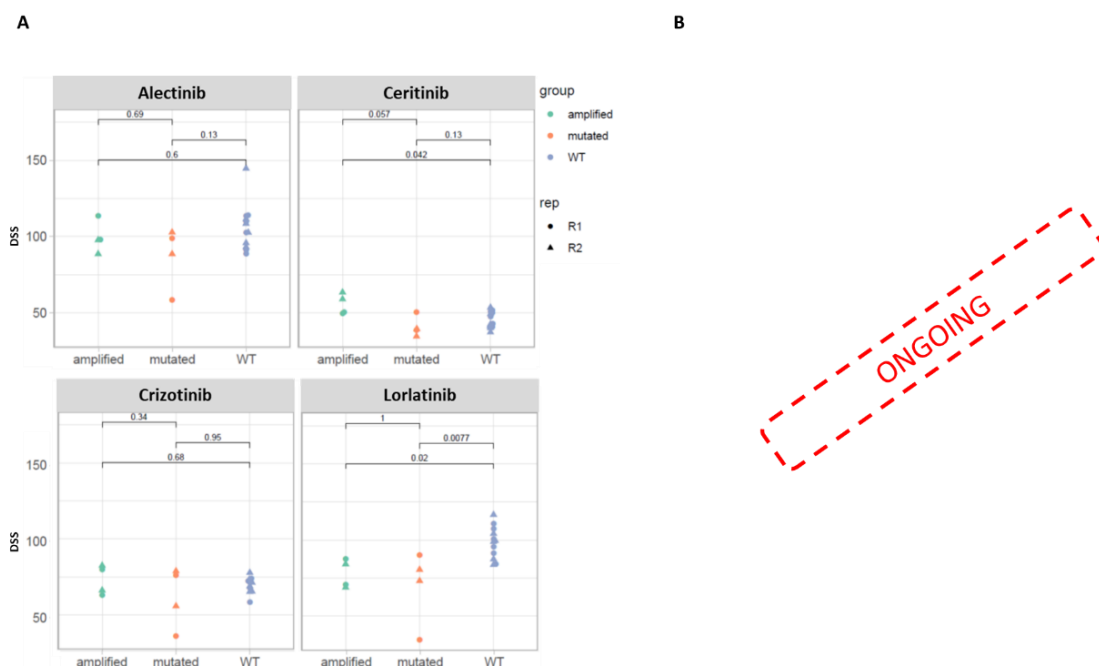


Figure 3: *ALK* aberrant neuroblastoma PDX-derived tumor cell (PDTC) models are significantly more sensitive to lorlatinib than *ALK* wild-type, and combining *ALK* inhibitors with chemotherapy show additive effect in these models. A, Study of the cell viability by the analysis of the drug sensitivity score (DSS) after treatment by alectinib, ceritinib and crizotinib *ALK* inhibitors in *ALK*-mutant and amplified PDTC models. B, Study of the cell viability of lorlatinib associated or not with chemotherapy in *ALK*-mutant and amplified PDTC models. The cell viability of chemotherapy alone is shown in dotted lines. The combination of chemotherapy and lorlatinib is shown in solid lines. Rep: replicate; R1: replicate 1; R2 replicate 2.

ALK inhibitors combined with chemotherapy

Combinatorial treatments in PDTC models

We then aimed at exploring the combination of chemotherapy and lorlatinib in high-risk neuroblastoma PDX models, based on the hypothesis that the addition of chemotherapy to lorlatinib would increase its cytotoxicity. First, we combined chemotherapy compounds doxorubicin, etoposide and carboplatin with each other in combinatorial matrixes (Supplementary figure 1), and then chose, for each PDTC model, the combined concentrations of chemotherapy compounds that resulted in 80% of cell viability (IC₈₀), to be further combined with lorlatinib in a dose-response manner. We then proceed to combine chemotherapy with lorlatinib (Fig. 3B).

Synergy between Lorlatinib and chemotherapy in the Th-*ALK*^{F1174L}/*MYCN* model

We next evaluated whether concurrent *ALK* inhibition could increase the efficacy of conventional multi-agent chemotherapy regimens representative of those used in clinical practice. We found that the addition of lorlatinib to multi-agent (vincristine, doxorubicin (A), cyclophosphamide – VAC) chemotherapy significantly increased survival in the Th-*ALK*^{F1174L}/*MYCN* neuroblastoma genetically engineered murine model (GEMM) but not in the Th-*MYCN* GEMM (Fig. 4A). Notably, animals treated with lorlatinib alone exhibited no survival advantage against vehicle controls. To facilitate a representative, reproducible model that is more efficient for multi-arm multiagent clinical trials we next created a murine allograft model by implanting Th-*ALK*^{F1174L}/*MYCN* tumors into animals with the same genetic background. We show that tumor onset is predictable in Th-*ALK*^{F1174L}/*MYCN* allografts, and that levels of *ALK* activation are maintained in the allograft model (Supplementary figure 4). We then treated Th-*ALK*^{F1174L}/*MYCN* allografts with either VAC chemotherapy alone or in combination with either crizotinib or lorlatinib. No benefit was demonstrated when crizotinib was added to conventional chemotherapy, however a significant survival benefit was demonstrated when lorlatinib was added to VAC chemotherapy (Fig. 4B). Taken together, this data shows that lorlatinib is an effective inhibitor of *ALK* activation in neuroblastoma GEMMs and, in a model of *ALK*^{F1174L} mutant neuroblastoma, clear pre-clinical efficacy is demonstrated when lorlatinib is combined with induction type chemotherapy.

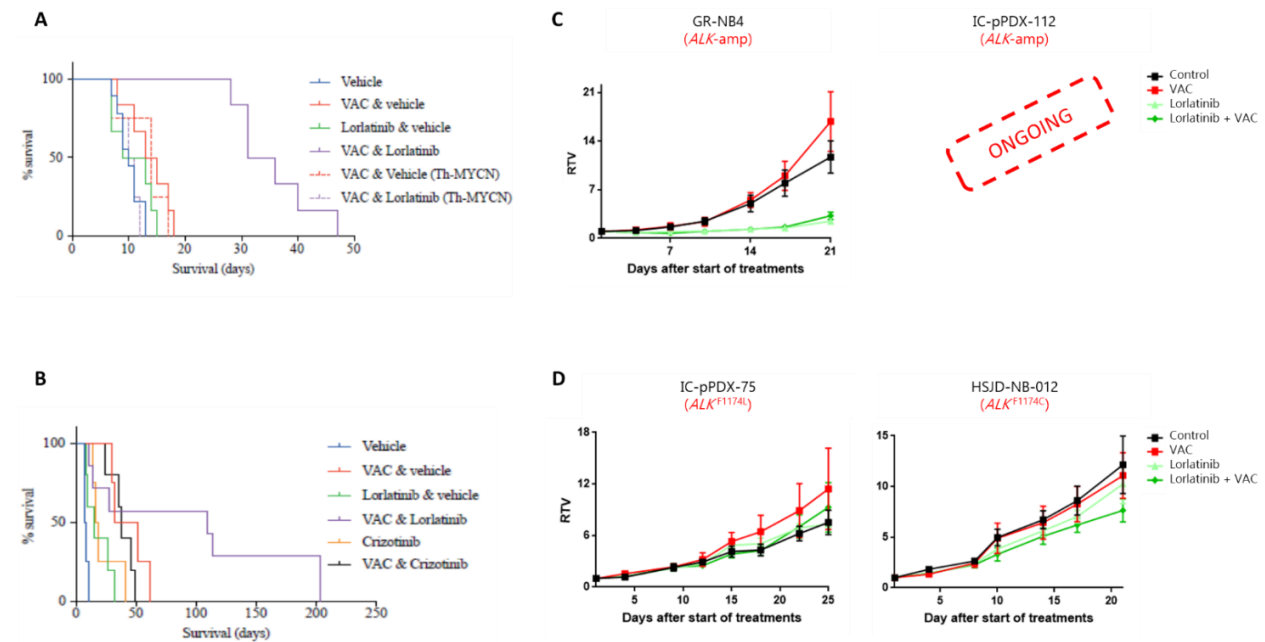


Figure 4: VAC chemotherapy in combination with Lorlatinib leads to significantly enhanced survival in preclinical GEMMs of *ALK^{F1174L}/MYCN* neuroblastoma. A, survival study of Lorlatinib, with and without VAC chemotherapy in Th-*ALK^{F1174L}/MYCN* and Th-*MYCN* GEMM. B, Survival study of Lorlatinib or Crizotinib with and without VAC chemotherapy in Th-*ALK^{F1174L}/MYCN* allografts. C, Growth curves showing the activity of lorlatinib alone or combined with 1-day VAC chemotherapy in *ALK*-amplified and (D) *ALK*-mutant PDX models.

ALK-amplified high-risk neuroblastoma PDX model respond significantly to Lorlatinib

We then aimed to further investigate the efficacy of lorlatinib alone or combined with 1-day VAC chemotherapy regimen in two *ALK*-amplified and two *ALK*-mutant (*ALK^{F1174L}* and *ALK^{F1174C}*) PDX models (Supplementary table 1). Treatment schedules and doses were the same as used in GEMM models. In *ALK*-amplified GR-NB4 model, lorlatinib alone showed significant activity (TGI 99%). The addition of VAC did not significantly increase the efficacy of lorlatinib alone (Fig. 4C). On the other hand, both *ALK*-mutant PDX models were completely resistant to lorlatinib, both alone or combined with VAC (Fig. 4D). Pharmacodynamics studies were performed at D3.

ALK inhibitors combined with MDM2 inhibitor idasanutlin

Idasanutlin synergizes with ALK inhibitors in TP53 wild-type and ALK mutant neuroblastoma cell lines.

Whilst the combination of lorlatinib with chemotherapy will be soon introduced into upfront therapy for high-risk *ALK*-aberrant neuroblastoma, combinatorial approaches that might be suitable for this sub-group of patients following relapse and chemotherapy-resistance are still warranted. To this end, this study also investigated combinations of *ALK* inhibitors with *MDM2* inhibitors, which have previously been suggested as potential strategies to overcome resistance to *ALK* inhibitors (27,28). *MDM2* antagonists have recently emerged as a potential therapeutic option in neuroblastoma. In *TP53*-wild-type and *ALK*-aberrant neuroblastoma cell lines including a previously unreported *MDM2* and *ALK* amplified cell line (Supplementary Figure 5) and 2 *ALK* mutant and amplified cell lines (Supplementary

Table 1), median-effect-analysis demonstrated a synergistic interaction between idasanutlin and ALK inhibitors, TAE-684 and alectinib *in vitro* (Figure 5A & B). Further assessment showed that the combination treatment lead to enhanced levels of apoptosis as evident by the greater proportion of sub-G1 events and caspase 3/7 activity as determined using FACS and caspase 3/7 assays (Figure 5C-F) (41).

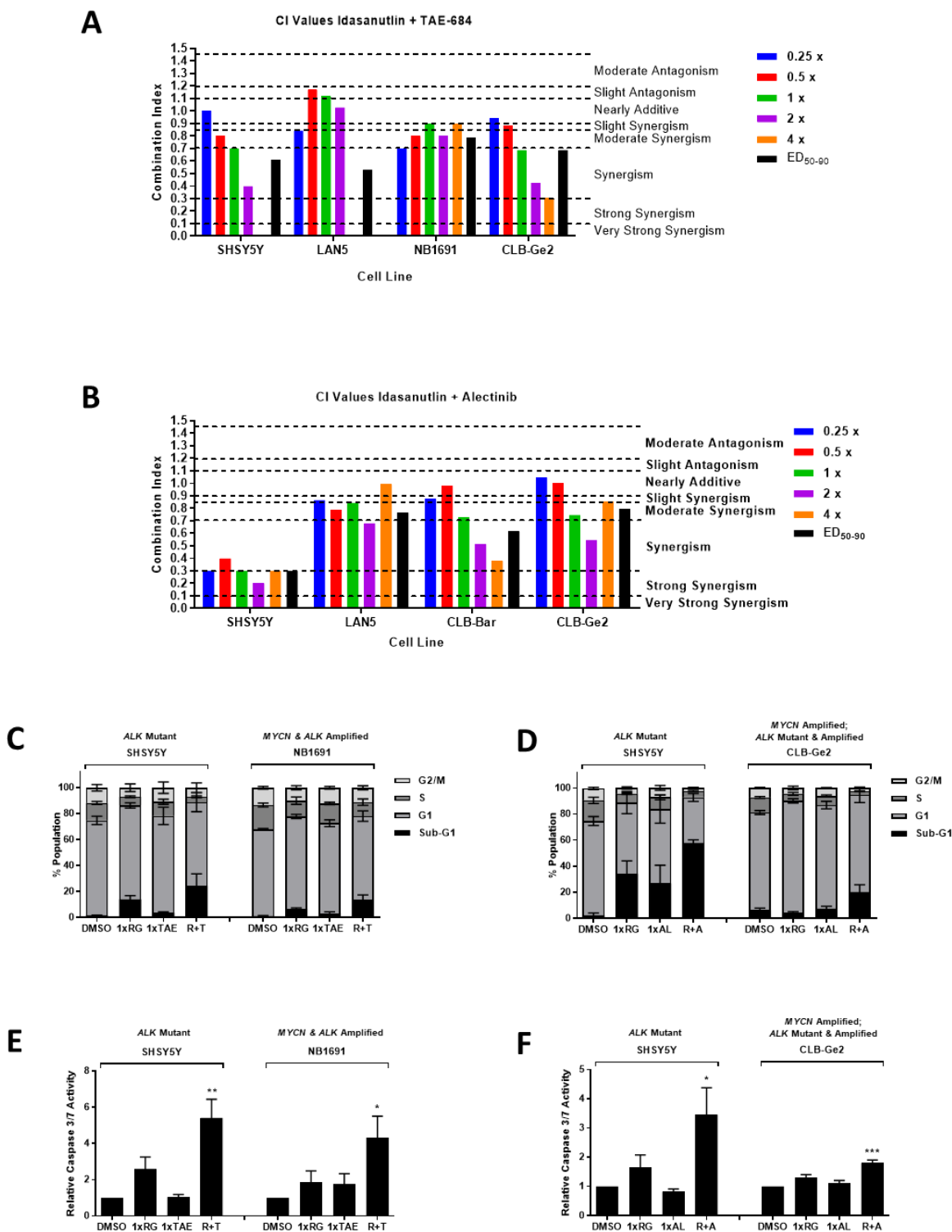


Figure 5: Idasanutlin synergises with ALK inhibitors in *TP53* wild-type and *ALK* mutant neuroblastoma cell lines. CI values at each constant 1:1 ratio combination and average of CI values at ED50, ED75 and ED90 of Idasanutlin in combination with A) TAE-684 and B) Alectinib. Functional analysis Idasanutlin in combination with TAE-684 and Alectinib using sub-G1 and cell cycle phase distribution (C & D), and caspase 3/7 activity (E & F). RG, Idasanutlin; TAE, TAE-684; R+T, Idasanutlin + TAE-684; AL, Alectinib; R+A, Idasanutlin + Alectinib.

Lorlatinib synergises with idasanutlin in ALK-amplified neuroblastoma PDX model

We studied the efficacy of lorlatinib in combination with idasanutlin in two *ALK*-amplified and two *ALK*-mutant models. In the *ALK*-amplified GR-NB4 model, whereas idasanutlin alone had a reduced effect on TGI (36%), the combination of lorlatinib and idasanutlin showed impressive synergy with complete remission at the time of the statistical analysis (D24) for this experimental arm. On the other hand, both *ALK* mutant models were completely resistant to the combination as well as both drugs in monotherapy. Pharmacodynamics were performed at D3.

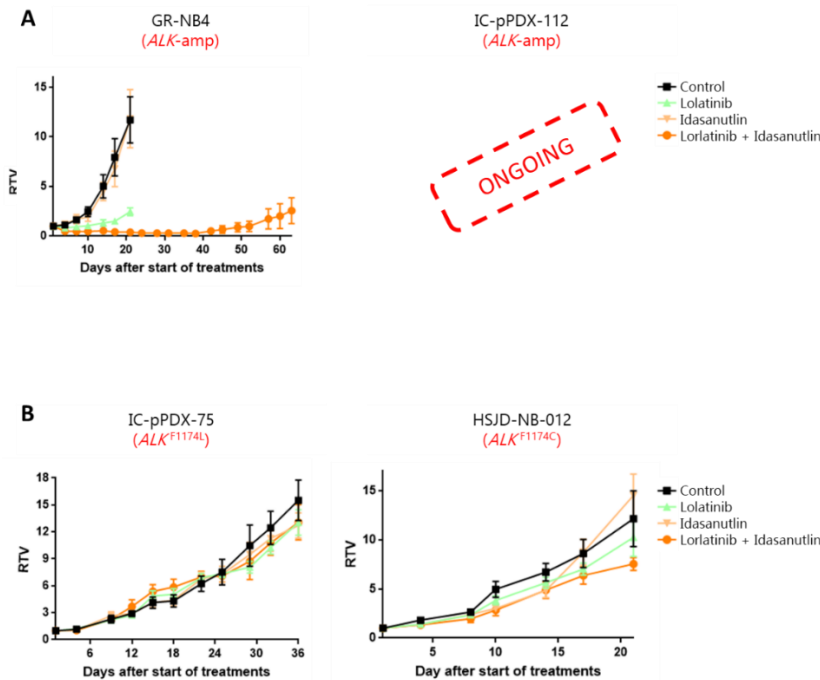


Figure 6: Synergy between lorlatinib and idasanutlin in *ALK*-amplified PDX model. Growth curves corresponding to A, 2 *ALK*-amplified and B, 2 *ALK*-mutant PDX models treated by lorlatinib combined with idasanutlin.

DISCUSSION

High-risk neuroblastoma patients still have very poor prognosis despite scaling treatment intensity over the last 30 years, with a 5-year overall survival increased from 29% to 50% in patients diagnosed in the 90's and 2005-2010 respectively (3). The goal of this study is to give robust preclinical insights in the activity of *ALK* inhibitors in combination with chemotherapy or other targeted agents in neuroblastomas carrying mutations or amplifications in this gene.

The ongoing International Society of Paediatric Oncology European Neuroblastoma (SIOPEN) trial HRNBL2 for first-line treatment of high-risk neuroblastoma has been amended to introduce lorlatinib in upfront treatment of patients with *ALK*-aberrant high-risk neuroblastoma. Also, the Children's Oncology Group has amended the ANBL1531 phase III trial to replace crizotinib by lorlatinib. Since 2008, when the role of *ALK* in neuroblastoma was first described (14,15,42,43), the progression in the study of *ALK* inhibitors in neuroblastoma has grown as the result not only of doors opened by the development of these drugs in adult malignancies, but also of close and well-planned collaborations in the scientific neuroblastoma community (44).

Preclinical studies in *ALK*-aberrant neuroblastomas have shown the intrinsic resistance of *ALK*^{F1174} and *ALK*^{F1245}, two of the 3 main hotspots, to crizotinib (20,45). Lorlatinib, a third-generation *ALK* inhibitor overcomes resistance to first and second generation *ALK* inhibitors by its macrocyclic structure with optimized physicochemical properties, which are associated with improved metabolic stability, blood-brain barrier permeability and low propensity for multi-drug resistance (MDR) efflux (46–48).

Cell lines with *ALK* alterations were in general less sensitive to lorlatinib than to crizotinib and other *ALK* inhibitors based on growth inhibition assays. This data is in direct contrast with both previously reported *in vivo* data and the differential clinical response data to crizotinib and lorlatinib seen in *ALK*-mutant relapsed/refractory neuroblastoma (25,49). Despite these GI_{50} data in cell lines, lorlatinib showed the highest inhibition of *ALK* phosphorylation in cell lines, which could reflect that *in vitro* cytotoxicity of *ALK* inhibitors may not be an accurate predictor of their *in vivo* activity. Indeed, lorlatinib showed the greatest *in vivo* reduction in tumor volume over a 3-day interventional dosing schedule in *ALK*^{F1174L}/*MYCN* GEMMs although alectinib had a similar effect to lorlatinib on *ALK* dephosphorylation in tumor cells, suggesting off-target effects of lorlatinib which could lead to its enhanced efficacy compared to alectinib. Furthermore, whereas VAC chemotherapy or lorlatinib alone did not show any survival advantage, the association of both were synergistic and induced significantly increased survival in the Th-*ALK*^{F1174L}/*MYCN* neuroblastoma model.

The interest in PDXs has increased since the last years due to the development of personalized cancer medicines based on genomic profiling and have drastically improve the predictive power of preclinical therapeutic studies (50). In addition, PDX and PDTTC models recapitulate better than cell lines the intratumor genetic heterogeneity, which is of special interest in neuroblastoma. Similar to cell lines, *in ex vivo* screening of PDTTC models, whereas ceritinib was more active and crizotinib showed similar activity than lorlatinib in *ALK*-aberrant models, lorlatinib was the only *ALK* inhibitor to show statistically significant enhanced cytotoxicity in *ALK*-aberrant models compared to wild-type, reinforcing the hypothesis of off-targets of ceritinib or crizotinib. *In vivo* studies showed high efficacy of lorlatinib alone in GR-NB4 *ALK*-amplified model, whereas the addition of chemotherapy did not increase the tumor growth inhibition and chemotherapy alone was totally ineffective. This is maybe due to the low doses of chemotherapy chosen for these experiments (lower doses and lower number of treatment cycles than usually done in our PDX models): VAC doses were voluntarily low to reveal a potential synergy between chemotherapy and lorlatinib, nevertheless, they were too low to be efficient even alone. The *ALK*^{F1174L} and *ALK*^{F1174C} mutated models were totally resistant to both lorlatinib and chemotherapy, alone or in combination.

In view of the future amended HRNBL2 protocol combining lorlatinib with chemotherapy in *ALK*-aberrant high-risk neuroblastoma patients, we then investigated the possibility whether combined *ALK* and MDM2 inhibition might be relevant for *ALK*-aberrant neuroblastoma patients following relapse, as *ALK* and MDM2 inhibitors have already been explored as potential strategies to overcome resistance to *ALK* inhibitors (27,28). In *TP53*-wild-type and *ALK*-aberrant (mutated, amplified or both) cell lines, the combination of idasanutlin and *ALK* inhibitors was revealed as synergistic and induced enhanced levels of apoptosis.

REFERENCES

1. Brodeur GM. Spontaneous regression of neuroblastoma. *Cell Tissue Res.* 2018;372:277–86.
2. Hero B, Simon T, Spitz R, Ernestus K, Gnekow AK, Scheel-Walter H-G, et al. Localized infant neuroblastomas often show spontaneous regression: results of the prospective trials NB95-S and NB97. *J Clin Oncol Off J Am Soc Clin Oncol.* 2008;26:1504–10.
3. Pinto NR, Applebaum MA, Volchenboum SL, Matthay KK, London WB, Ambros PF, et al. Advances in Risk Classification and Treatment Strategies for Neuroblastoma. *J Clin Oncol.* 2015;33:3008–17.
4. Park JR, Eggert A, Caron H. Neuroblastoma: Biology, Prognosis, and Treatment. *Hematol Oncol Clin North Am.* 2010;24:65–86.
5. Brodeur GM, Seeger RC, Schwab M, Varmus HE, Bishop JM. Amplification of N-myc in untreated human neuroblastomas correlates with advanced disease stage. *Science.* 1984;224:1121–4.
6. Schwab M, Alitalo K, Klempnauer KH, Varmus HE, Bishop JM, Gilbert F, et al. Amplified DNA with limited homology to myc cellular oncogene is shared by human neuroblastoma cell lines and a neuroblastoma tumour. *Nature.* 1983;305:245–8.
7. Seeger RC, Brodeur GM, Sather H, Dalton A, Siegel SE, Wong KY, et al. Association of multiple copies of the N-myc oncogene with rapid progression of neuroblastomas. *N Engl J Med.* 1985;313:1111–6.
8. Ackermann S, Cartolano M, Hero B, Welte A, Kahlert Y, Roderwieser A, et al. A mechanistic classification of clinical phenotypes in neuroblastoma. *Science.* 2018;362:1165–70.
9. Peifer M, Hartwig F, Roels F, Drexler D, Gattlgruber M, Menon R, et al. Telomerase activation by genomic rearrangements in high-risk neuroblastoma. *Nature.* 2015;526:700–4.
10. Valentijn LJ, Koster J, Zwijnenburg DA, Hasselt NE, van Sluis P, Volckmann R, et al. TERT rearrangements are frequent in neuroblastoma and identify aggressive tumors. *Nat Genet. Nature Publishing Group;* 2015;47:1411–4.
11. Cheung N-KV, Zhang J, Lu C, Parker M, Bahrami A, Tickoo SK, et al. Association of age at diagnosis and genetic mutations in patients with neuroblastoma. *JAMA.* 2012;307:1062–71.
12. Hartlieb SA, Sieverling L, Nadler-Holly M, Ziehm M, Toprak UH, Herrmann C, et al. Alternative lengthening of telomeres in childhood neuroblastoma from genome to proteome. *Nat Commun. Nature Publishing Group;* 2021;12:1269.
13. Zeineldin M, Federico S, Chen X, Fan Y, Xu B, Stewart E, et al. MYCN amplification and ATRX mutations are incompatible in neuroblastoma. *Nat Commun.* 2020;11:913.
14. Janoueix-Lerosey I, Lequin D, Brugières L, Ribeiro A, de Pontual L, Combaret V, et al. Somatic and germline activating mutations of the ALK kinase receptor in neuroblastoma. *Nature.* 2008;455:967–70.
15. Mossé YP, Laudenslager M, Longo L, Cole KA, Wood A, Attiyeh EF, et al. Identification of ALK as a major familial neuroblastoma predisposition gene. *Nature.* 2008;455:930–5.
16. De Brouwer S, De Preter K, Kumps C, Zabrocki P, Porcu M, Westerhout EM, et al. Meta-analysis of neuroblastomas reveals a skewed ALK mutation spectrum in tumors with MYCN amplification. *Clin Cancer Res Off J Am Assoc Cancer Res.* 2010;16:4353–62.
17. Schleiermacher G, Javanmardi N, Bernard V, Leroy Q, Cappo J, Rio Frio T, et al. Emergence of new ALK mutations at relapse of neuroblastoma. *J Clin Oncol Off J Am Soc Clin Oncol.* 2014;32:2727–34.
18. Eleveld TF, Oldridge DA, Bernard V, Koster J, Daage LC, Diskin SJ, et al. Relapsed neuroblastomas show frequent RAS-MAPK pathway mutations. *Nat Genet.* 2015;47:864–71.

19. Padovan-Merhar OM, Raman P, Ostrovnaya I, Kalletla K, Rubnitz KR, Sanford EM, et al. Enrichment of Targetable Mutations in the Relapsed Neuroblastoma Genome. *PLoS Genet* [Internet]. 2016 [cited 2021 Apr 8];12. Available from: <https://www.ncbi.nlm.nih.gov/pmc/articles/PMC5172533/>
20. Bresler SC, Wood AC, Haglund EA, Courtright J, Belcastro LT, Plegaria JS, et al. Differential inhibitor sensitivity of anaplastic lymphoma kinase variants found in neuroblastoma. *Sci Transl Med*. 2011;3:108ra114.
21. Bourdeaut F, Ferrand S, Brugières L, Hilbert M, Ribeiro A, Lacroix L, et al. ALK germline mutations in patients with neuroblastoma: a rare and weakly penetrant syndrome. *Eur J Hum Genet*. 2012;20:291–7.
22. Foster JH, Voss SD, Hall DC, Minard CG, Balis FM, Wilner K, et al. Activity of Crizotinib in Patients with ALK-Aber- rant Relapsed/Refractory Neuroblastoma: A Children’s Oncology Group Study (ADVL0912). *Clin Cancer Res* [Internet]. American Association for Cancer Research; 2021 [cited 2021 May 11]; Available from: <https://clincancerres.aacrjournals.org/content/early/2021/04/13/1078-0432.CCR-20-4224>
23. Krytska K, Ryles HT, Sano R, Raman P, Infarinato NR, Hansel TD, et al. Crizotinib Synergizes with Chemotherapy in Preclinical Models of Neuroblastoma. *Clin Cancer Res Off J Am Assoc Cancer Res*. 2016;22:948–60.
24. Greengard EG, Mosse YP, Liu X, Ahern CH, Minard C, Blaney S, et al. Safety and tolerability of crizotinib in combination with chemotherapy for relapsed or refractory solid tumors or anaplastic large cell lymphoma: a Children’s Oncology Group phase I consortium study. *J Clin Oncol*. Wolters Kluwer; 2015;33:10058–10058.
25. Infarinato NR, Park JH, Krytska K, Ryles HT, Sano R, Szigety KM, et al. The ALK/ROS1 Inhibitor PF-06463922 Overcomes Primary Resistance to Crizotinib in ALK-Driven Neuroblastoma. *Cancer Discov*. 2016;6:96–107.
26. Goldsmith KC, Kayser K, Groshen SG, Chioda M, Thurm HC, Chen J, et al. Phase I trial of lorlatinib in patients with ALK-driven refractory or relapsed neuroblastoma: A New Approaches to Neuroblastoma Consortium study. *J Clin Oncol*. Wolters Kluwer; 2020;38:10504–10504.
27. Wang HQ, Halilovic E, Li X, Liang J, Cao Y, Rakiec DP, et al. Combined ALK and MDM2 inhibition increases anti-tumor activity and overcomes resistance in human ALK mutant neuroblastoma cell lines and xenograft models. *eLife*. 2017;6.
28. Miyazaki M, Otomo R, Matsushima-Hibiya Y, Suzuki H, Nakajima A, Abe N, et al. The p53 activator overcomes resistance to ALK inhibitors by regulating p53-target selectivity in ALK-driven neuroblastomas. *Cell Death Discov*. 2018;4:56.
29. Carr-Wilkinson J, O’Toole K, Wood KM, Challen CC, Baker AG, Board JR, et al. High Frequency of p53/MDM2/p14ARF Pathway Abnormalities in Relapsed Neuroblastoma. *Clin Cancer Res Off J Am Assoc Cancer Res*. 2010;16:1108–18.
30. Chen L, Humphreys A, Turnbull L, Bellini A, Schleiermacher G, Salwen H, et al. Identification of different ALK mutations in a pair of neuroblastoma cell lines established at diagnosis and relapse. *Oncotarget*. 2016;7:87301–11.
31. Chen L, Rousseau RF, Middleton SA, Nichols GL, Newell DR, Lunec J, et al. Pre-clinical evaluation of the MDM2-p53 antagonist RG7388 alone and in combination with chemotherapy in neuroblastoma. *Oncotarget*. Impact Journals; 2015;6:10207–21.
32. Pre-clinical evaluation of the MDM2-p53 antagonist RG7388 alone and in combination with chemotherapy in neuroblastoma. - PubMed - NCBI [Internet]. [cited 2019 Nov 25]. Available from: <https://www.ncbi.nlm.nih.gov.proxy.insermbiblio.inist.fr/pubmed/?term=Rapha%C3%ABl+Rousseau+chen+L+2015>
33. Stewart E, Federico SM, Chen X, Shelat AA, Bradley C, Gordon B, et al. Orthotopic Patient-Derived Xenografts of Pediatric Solid Tumors. *Nature*. 2017;549:96–100.
34. Bate-Eya LT, Ebus ME, Koster J, den Hartog IJM, Zwijnenburg DA, Schild L, et al. Newly-derived neuroblastoma cell lines propagated in serum-free media recapitulate the genotype and phenotype of primary neuroblastoma tumours. *Eur J Cancer*. 2014;50:628–37.

35. Yadav B, Pemovska T, Szwajda A, Kuleskiy E, Kontro M, Karjalainen R, et al. Quantitative scoring of differential drug sensitivity for individually optimized anticancer therapies. *Sci Rep. Nature Publishing Group*; 2014;4:5193.
36. Kilkenny C, Browne WJ, Cuthill IC, Emerson M, Altman DG. Improving bioscience research reporting: the ARRIVE guidelines for reporting animal research. *PLoS Biol.* 2010;8:e1000412.
37. Workman P, Aboagye EO, Balkwill F, Balmain A, Bruder G, Chaplin DJ, et al. Guidelines for the welfare and use of animals in cancer research. *Br J Cancer. Cancer Research UK*; 2010;102:1555–77.
38. Jamin Y, Tucker ER, Poon ES, Popov S, Vaughan L, Boulton JKR, et al. Evaluation of Clinically Translatable Magnetic Resonance Imaging Biomarkers of Therapeutic Response in the TH-MYCN Transgenic Mouse Model of Neuroblastoma. *Radiology.* 2013;266:130–40.
39. Tucker ER, Tall JR, Danielson LS, Gowan S, Jamin Y, Robinson SP, et al. Immunoassays for the quantification of ALK and phosphorylated ALK support the evaluation of on-target ALK inhibitors in neuroblastoma. *Mol Oncol.* 2017;11:996–1006.
40. Berry T, Luther W, Bhatnagar N, Jamin Y, Poon E, Sanda T, et al. The ALK(F1174L) mutation potentiates the oncogenic activity of MYCN in neuroblastoma. *Cancer Cell.* 2012;22:117–30.
41. Chen L, Pastorino F, Berry P, Bonner J, Kirk C, Wood KM, et al. Preclinical evaluation of the first intravenous small molecule MDM2 antagonist alone and in combination with temozolomide in neuroblastoma. *Int J Cancer.* 2019;144:3146–59.
42. George RE, Sanda T, Hanna M, Fröhling S, Luther W, Zhang J, et al. Activating mutations in ALK provide a therapeutic target in neuroblastoma. *Nature.* 2008;455:975–8.
43. Chen Y, Takita J, Choi YL, Kato M, Ohira M, Sanada M, et al. Oncogenic mutations of ALK kinase in neuroblastoma. *Nature.* 2008;455:971–4.
44. Schulte JH, Eggert A. ALK Inhibitors in Neuroblastoma: A Sprint from Bench to Bedside. *Clin Cancer Res.* 2021;clincanres.0627.2021.
45. Bresler SC, Weiser DA, Huwe PJ, Park JH, Krytska K, Ryles H, et al. ALK mutations confer differential oncogenic activation and sensitivity to ALK inhibition therapy in neuroblastoma. *Cancer Cell.* 2014;26:682–94.
46. Zou HY, Friboulet L, Kodack DP, Engstrom LD, Li Q, West M, et al. PF-06463922, an ALK/ROS1 Inhibitor, Overcomes Resistance to First and Second Generation ALK Inhibitors in Preclinical Models. *Cancer Cell.* 2015;28:70–81.
47. Johnson TW, Richardson PF, Bailey S, Brooun A, Burke BJ, Collins MR, et al. Discovery of (10R)-7-Amino-12-fluoro-2,10,16-trimethyl-15-oxo-10,15,16,17-tetrahydro-2H-8,4-(metheno)pyrazolo[4,3-h][2,5,11]-benzoxadiazacyclopentadecine-3-carbonitrile (PF-06463922), a Macrocyclic Inhibitor of Anaplastic Lymphoma Kinase (ALK) and c-ros Oncogene 1 (ROS1) with Preclinical Brain Exposure and Broad-Spectrum Potency against ALK-Resistant Mutations. *J Med Chem. American Chemical Society*; 2014;57:4720–44.
48. Nagasaka M, Ge Y, Sukari A, Kukreja G, Ou S-HI. A user's guide to lorlatinib. *Crit Rev Oncol Hematol.* 2020;151:102969.
49. Guan J, Tucker ER, Wan H, Chand D, Danielson LS, Rueth K, et al. The ALK inhibitor PF-06463922 is effective as a single agent in neuroblastoma driven by expression of ALK and MYCN. *Dis Model Mech.* 2016;9:941–52.
50. Tucker ER, George S, Angelini P, Bruna A, Chesler L. The Promise of Patient-Derived Preclinical Models to Accelerate the Implementation of Personalised Medicine for Children with Neuroblastoma. *J Pers Med [Internet].* 2021 [cited 2021 May 16];11. Available from: <https://www.ncbi.nlm.nih.gov/pmc/articles/PMC8065808/>

SUPPLEMENTARY TABLES

Supplementary table 1: list of cell lines screened for crizotinib, TAE-684, ceritinib alectinib and lorlatinib ALK inhibitors.

Cell Line	MYCN	TP53	ALK	ALK Status reference	Crizotinib (nM)	TAE-684 (nM)	Ceritinib (nM)	Alectinib (nM)	Lorlatinib (nM)
Diagnosis									
CLB-Ge2	Amp	WT	Amp; F1174V	Janoueix-Lerosey <i>et al</i> (2008), Nature	188 ± 21	21.6 ± 3.6	59.7 ± 5.1	119.8 ± 21	30.7 ± 7.7
IMR32	Amp	WT	Partial amp	De Brouwer <i>et al</i> (2010), Clin Can Res	934.3 ± 68.2	94.0 ± 32.4	862.6 ± 86.5	609.9 ± 20.65	>10µM
LAN5	Amp	WT	R1275Q	Chen <i>et al</i> (2008), Nature	258.4 ± 38.9	10.3 ± 0.3	170.1 ± 55.2	74.3 ± 11.9	81.4 ± 30.9
NB69	Non-amp	WT	WT	Chen <i>et al.</i> (2008), Nature	634.3 ± 26.8	570.0 ± 36.7	ND	548 ± 31.8	>10µM
NBLW	Amp	WT	R1275L	Chen <i>et al</i> , Oncotarget, 2016	584.0 ± 41.6	38.5 ± 3.9	842.5 ± 91.5	488.5 ± 49.1	>10µM
Relapse/Post-treatment									
CHLA136	Amp	WT	WT	Koneru <i>et al</i> (2020), Can Res	ND	314.7 ± 36.3	ND	>5µM	>10µM
CLB-BAR-Rec	Amp	WT	Amp; Del Ex4-11	Cazes <i>et al</i> (2012), Cancer Res	311.5 ± 28.4	3.4 ± 1.1	74.5 ± 10.1	151.7 ± 9.8	37.2 ± 11.7
GIMEN	Non-amp	WT	WT	De Brouwer <i>et al</i> (2010), Clin Can Res	1655.5 ± 320.5	500.0 ± 61.7	1594.7 ± 184.3	>5µM	>10µM
LAN1	Amp	Mut	F1174L	Chen <i>et al</i> (2008), Nature; George <i>et al</i> (2008), Nature	ND	25.8 ± 9.6	ND	243.6 ± 17.4	3436.2 ± 1361.9
LAN6	Non-amp	WT	D1091N	George <i>et al</i> (2008), Nature	ND	23.1 ± 3.8	567.8 ± 67.8	322.8 ± 55.1	>10µM
NB-1*	Amp	WT	Amp; Del Ex2-3	Okubo <i>et al</i> (2012), Oncogene	37.5 ± 5.9	3.3 ± 1.6	19.4 ± 4.1	11.7 ± 2.1	2.5 ± 0.3
NB1691	Amp	WT	Amplified	This study	857.5 ± 51.9	280.1 ± 81.3	916.4 ± 45.6	914.5 ± 59.7	>10µM
NBLW-R	Amp	WT	F1174L	Chen <i>et al</i> (2016) Oncotarget	494.2 ± 43.5	30.2 ± 5.3	176.8 ± 28.4	307.3 ± 18.3	169.9 ± 20.6
NGP	Amp	WT	CNG	Li <i>et al.</i> , 2010, J Natl Cancer Inst	783.0 ± 157.5	179.3 ± 10.9	627.4 ± 78.9	609.1 ± 77.3	>10µM
SHSY5Y	Non-amp	WT	F1174L	George <i>et al</i> 2008, Nature	358.0 ± 49.5	57.4 ± 16.8	313 ± 77.7	249.5 ± 44.4	3674.8 ± 990.3
SKNAS	Non-amp	Mut	WT	De Brouwer <i>et al</i> (2010), Clin Can Res	1230.3 ± 128.3	570.9 ± 91.2	1697.3 ± 249.7	2425.9 ± 142.2	>10µM
SKnBe2C	Amp	Mut	CNG (sub pop)	Cazes <i>et al</i> (2012), Cancer Res	987.7 ± 13.71	119.8 ± 14.5	363.6 ± 60.4	665.5 ± 38.9	>10µM
TR14	Amp	WT	CNG	Cazes <i>et al</i> (2012), Cancer Res	ND	97.8 ± 30.4	ND	186.3 ± 64.6	>10µM

* assume post treatment as established from patient who died from disseminated disease

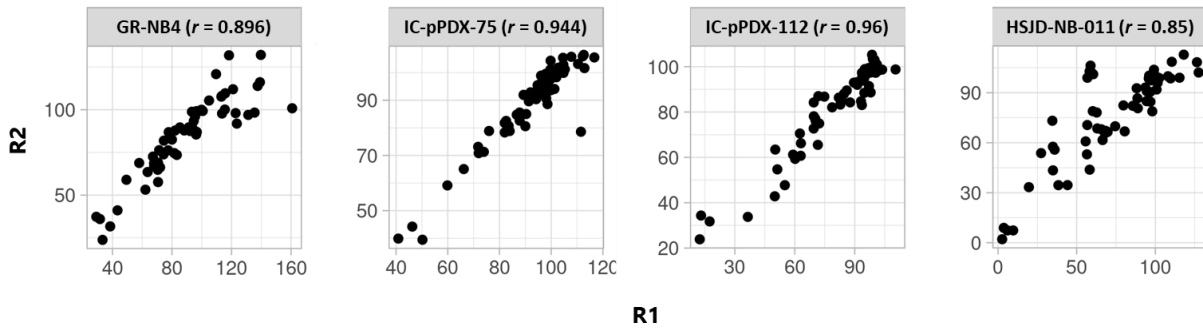
WT, wild type; Mut, mutant; Del, deletion, ND, not determined

Supplementary table 2: summary of the clinical and molecular characteristics of the five *ALK*-aberrant high-risk neuroblastoma (HR-NB) patient-derived xenografts. We also indicate whether each PDX was used for *ex vivo* high throughput drug screenings or *in vivo* efficacy of *ALK* inhibitors. *ALKi*: *ALK* inhibitors; *VAF*: variant allele fraction; *TERT* overexpr: *TERT* gene overexpression; *ALT*: alternative lengthening of telomeres; *NA*: not applicable; *WT*: wild-type.

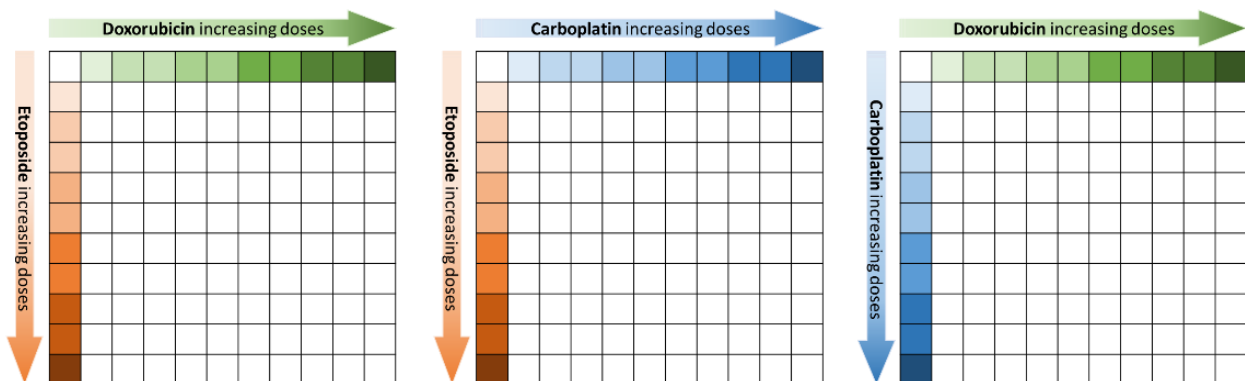
<i>ALK</i> -aberrant HR-NB PDX MODELS	CLINICAL DATA				SOMATIC GENETIC ALTERATIONS							EXPERIMENT S	
	PDX timepoint	Stage	Gender	Previous <i>ALKi</i>	<i>MYCN</i>	<i>ALK</i> (<i>VAF</i>)	<i>TP53</i>	<i>ATRX</i> (<i>VAF</i>)	<i>TERT</i> overexpr	<i>ALT</i>	Other relevant somatic genetic abnormalities	<i>Ex vivo</i>	<i>In vivo</i>
GR-NB4	Relapse	4	F		A	A	WT	WT	Ongoing	NA	CDKN2A/B homo del	Yes	Yes
IC-pPDX-75	Relapse	4	F	Crizotinib	WT	F1174L (65%)	WT	c.6391C> T (34%)	Ongoing	Ongoing		Yes	Yes
IC-pPDX-112	Diagnosis	4	M		A	A	WT	WT	Ongoing	NA	High mutational load	Yes	Yes
HSJD-NB-011	Relapse	4	M		A	I1171N (80%)	WT	WT	Ongoing	Negative		Yes	No
HSJD-NB-012	Relapse	4	M		A	F1174C (30%)	WT	WT	Ongoing	Negative		Yes	Yes

SUPPLEMENTARY FIGURES

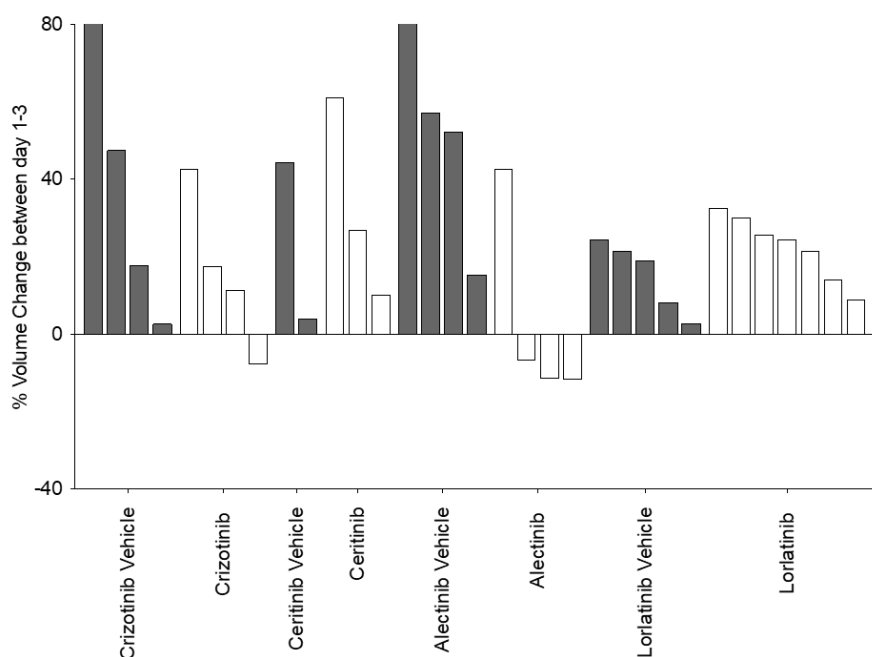
Supplementary figure 1: Correlations between independent high-throughput drug screenings on PDX-derived tumour cells (two different experiments, same PDX model, different passages). The Pearson's correlation coefficient (r) is indicated. R1: replicate 1; R2: replicate 2.



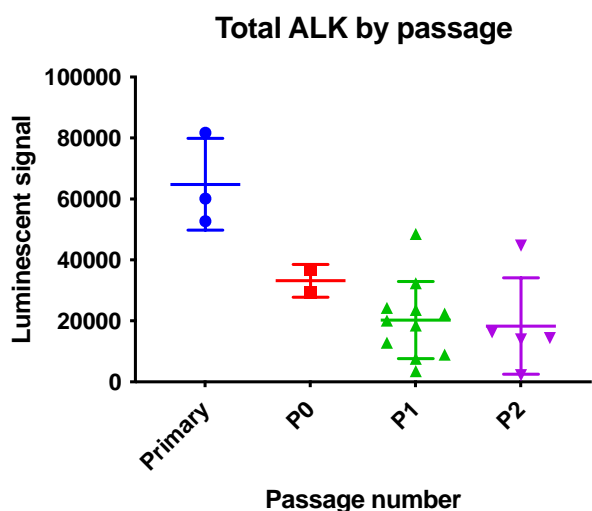
Supplementary figure 2: schematic representation of matrixes designed for chemo-chemo combinations.



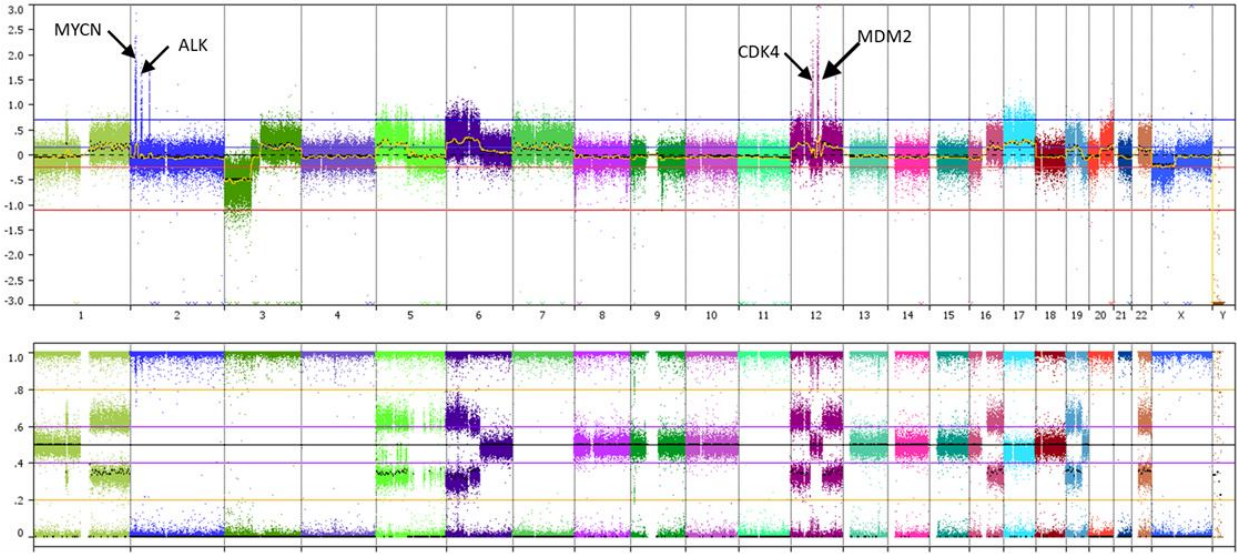
Supplementary figure 3: 3-Day treatment of Th-*MYCN* tumour-bearing animals with ALK inhibitor panel. *In vivo* analysis of a panel of ALK inhibitors including crizotinib, ceritinib, alectinib and lorlatinib was carried out using the Th-*MYCN* model. Tumour-bearing Th-*MYCN* mice, were treated with the indicated inhibitor over a 3-day interventional dosing schedule.



Supplementary figure 4: Total ALK expression of Th-*ALK^{F1174L}/MYCN* primary GEMM tumour compared to allografts. *Ex vivo* analysis of total ALK expression using immunoassay of tumour lysates from untreated Th-*ALK^{F1174L}/MYCN* GEMM primary tumour in 129svj mice, and Th-*ALK^{F1174L}/MYCN* subcutaneous allograft tumours in 129svj wild-type mice.



Supplementary Figure 5: SNP array of NB1691 cell line showing the *ALK* amplification.



3.3 Next steps

Several experiments are ongoing in order to complete this collaborative work and submit the draft for publication:

1. *In vivo* efficacy studies with the *ALK* amplified IC-pPDX-112 PDX model treated with lorlatinib alone or combined with VAC chemotherapy
2. *In vivo* efficacy studies with the *ALK* amplified IC-pPDX-112 PDX model treated with lorlatinib alone or combined with lorlatinib
3. Pharmacodynamics studies after 3-day treatment with lorlatinib +/- chemotherapy for the 4 PDX models tested:
 - 3.1. Immunohistochemistry: Ki-67, cleaved-caspase 3, ALK
 - 3.2. Western blot analyses: ALK, pALK, ERK1/2, pERK1/2, AKT, pAKT, MYCN
4. Pharmacodynamics studies after 3-day treatment with lorlatinib +/- idasanutlin for the 4 PDX models tested:
 - 4.1. Immunohistochemistry: Ki-67, cleaved-caspase 3, ALK, p53, p21
 - 4.2. Western blot analyses: ALK, pALK, ERK1/2, pERK1/2, AKT, pAKT, MYCN, p53, p21, PUMA
5. Exploration of expression data of PDX to look for TERT overexpression or additional events explaining the overall resistance of IC-pPDX-75 and HSJD-NB-012 models
6. Exploration of the ALT phenotype in the IC-pPDX-75 (non-*MYCN* amplified) model

Once these experiments completed, we would have additional efficacy and mechanistical data to draw more robust conclusions for this collaborative work. These experiments are ongoing and are planned to be finished by the end of June 2021. The manuscript will be submitted for mid-July.

IV - Discussion and perspectives

In vitro drug sensitivities in neuroblastoma

Neuroblastoma is a highly heterogeneous pediatric cancer both clinically and biologically. Indeed, its clinical behavior is intimately linked to its biology. From a molecular point of view, few genes are recurrently altered at a somatic level, such as *MYCN*, *ALK*, *TERT* and *ATRX*, but have profound clinical implications in patient outcome. High-risk neuroblastoma, which is widely recognized as any neuroblastoma harboring *MYCN* amplification or metastatic neuroblastoma diagnosed in children older than 12 months, has very poor prognosis (overall survival 50%) and remains almost incurable in the relapse/refractory situation. Many efforts are being made towards searching for new prognostic (for patient stratification) and predictive (to find new molecular targets for novel treatment strategies) biomarkers.

Molecular precision medicine programs have shown that the simple match of a molecular target to a specific drug has proven its relevance, but for a limited number of tumors and targets, and many efforts need to be done to implement combined methods, including WGS, WES, RNAseq, methylation profiles, associated to high-throughput drug screenings and machine learning approaches, in order to explore and predict new drug efficacies. The COMPASS Consortium, in which the RTOP team and the BioPhenics platform of the Institut Curie participate, aims at exploring this integrative approach in 6 European centers. Many efforts have been done to homogenize screening protocols and have shown remarkably reproducibility in cell line high-throughput drug screenings between the different platforms of the Consortium.

As PDX models are being widely used for the study of new drug sensitivities, either *ex vivo* and *in vivo* (Gao et al., 2015), and since it is urgent to find new drug efficacies, we have performed drug sensitivity studies of neuroblastoma on PDTCs by a high-throughput drug screening approach in collaboration with the BioPhenics platform of the Institut Curie. Indeed, the Institut Curie has a wide panel of molecularly characterized high-risk neuroblastoma PDX models that we have used for these screenings. Due to the paucity of recurrent somatic mutations in neuroblastoma, suggesting a possible role for epigenetic alterations in driving this cancer, we tested a drug library with more than 50 compounds enriched in epigenetic targeted drugs. Our experiments showed high reproducibility in biological replicates with different tumors of a same PDX model. HDAC inhibitors emerged as the most active compound family across our 11 neuroblastoma PDXs models tested. Indeed, a recent study using a genome-wide *MYCN* target gene screen by ChIP-seq combined with a phenotypic screen of small molecule epigenetic targeting compounds revealed global *MYCN*-epigenetic interactions. Numerous epigenetic proteins were identified as *MYCN* targets, such as HDAC2, CBX8 and CREBBP. The library screen targeting epigenetic proteins revealed broad susceptibility of neuroblastoma cells to all classes of epigenetic regulators, including HDACi (Krstic et al., 2021). In our screening, four compounds, cudc-907, quisinostat, panobinostat and trichostatin, showed the most cytotoxic effects. Indeed, quisinostat and panobinostat have been found to induce autophagy and cell death when combined with lysosomal inhibitor chloroquine (Kommalapati et al., 2020;

Körholz et al., 2021). In addition, a case report showed that Panobinostat had been successfully used for the treatment of a refractory metastatic neuroblastoma associated to chemotherapy (Zareifar et al., 2020). Finally, trichostatin has been shown to increase neuroblastoma cell differentiation, associated with the nucleocytoplasmic shuttling of HDACs (Jang et al., 2018). Thus, further *in vivo* screenings with HDAC inhibitors alone and in combination with other molecules, including chemotherapy are needed to advance in the exploration of new therapeutic combinations relevant for high-risk neuroblastoma that could lead to early clinical trials.

There is a high consensus that the improvement of high-risk neuroblastoma survival will need combined treatments to overcome resistance, one of the major issues in the treatment of this disease. We have explored the combinations of chemotherapy and targeted drugs by high-throughput screening methods, showing the additive effect of chemotherapy combined with targeted drugs. Interestingly, high-throughput combination drug screening have already shown high concordance between *ex vivo* PDTc and *in vivo* PDX responses in other diseases such as melanoma (Ice et al., 2020). It will be necessary to deepen into these combination approaches at high-throughput level to explore novel multiple combinations that could demonstrate their relevance in the treatment of high-risk neuroblastoma and which could find their place in further clinical trials.

The ultimate aim of these experiments is to advance in the exploration of consistent ways to the development of co-clinical trials for high-risk neuroblastoma that parallel ongoing human phase I/II clinical trials. By conducting both studies in parallel, their main objective is to fast track the development of drugs to practice molecular precision oncology. In addition, synchronizing treatments in mice and patients allows real-time integration of data, provides predictive guidance for treatment using genetic and molecular criteria and has shown to rapidly identify mechanisms of resistance and effective new combination therapies (Lunardi and Pandolfi, 2015).

Furthermore, in an additional attempt to explore novel drug sensitivity profiles of neuroblastoma, we screened a library of 55 compounds that fix the G4 structures of nucleic acids, the so-called G4-L, across 5 well molecularly characterized high-risk neuroblastoma cell lines. These agents are supposed to induce synthetic lethality in the context of *ATRX* loss-of-function, which characteristically leads to an alternative lengthening of telomere status, by the stabilization of G4 structures, which cannot be solved by dysfunctional *ATRX* (Wang et al., 2019). In addition, a synthetic lethal mechanism could also be a result of the combination of DNA-damaging agents with the stabilization of G4 structures by G4-L. Therefore, we also aimed at exploring the relevance of the combination of G4-L with chemotherapy. We have found that 3 G4-L compounds were broadly highly cytotoxic across all the cell lines, including but not specifically *ATRX*-deficient cells. Interestingly, 10 compounds showed impressive activity against the SK-N-AS cell line, *MYCN*-, *ATRX*- and *ALT*-wild type, which needs to be further explored. Indeed, this cell line has neither *ATRX* LoF mutations or *ALT* phenotype, but harbors an intermediate epigenetic identity status between adrenergic and mesenchymal state which could explain that this specific epigenetic targeting has this remarkably activity (Boeva et al., 2017).

In vivo studies of clonal evolution in neuroblastoma

While the precision medicine approaches increase the probability of success, it partially neglects the evidence that virtually all tumor responses are followed by the emergence of resistance, and therefore, treatment failure. Thus, precision medicine needs to deal with the complex evolutionary dynamics that govern emergence and proliferation of resistant phenotypes (Gallaher et al., 2018). Indeed, it is well accepted that clonal dynamics associate with major events in tumor progression including oncogenesis, progression and treatment resistance (McPherson et al., 2018). During clonal evolution the acquired mutations can be categorized into those that do not provide any benefit to cancer progression and therefore are selectively neutral (passenger mutations), those that are disadvantageous for the cancer cell and therefore are subjected to negative selection (deleterious mutations), and those that increase survival or proliferation, conferring a selective advantage during tumor evolution (driver mutations) (Rampias, 2020). In addition to oncogene activation, other hallmarks linked to driver mutations are those of escape from apoptosis and senescence (*TP53* mutations), the replication immortality (*TERC* mutations) and the induction of angiogenesis (*VHL* mutations)

Exploring how clones evolve under treatment in PDX models, we have found that clonal events remain stable after treatment across the different models. Differences arise at subclonal and very subclonal level: certain models remain quite stable after treatment in their subclonal architecture, whereas others harbor a higher propensity for new SNVs to emerge or preexistent variants to disappear after treatment. In addition, these models with higher variability seem more resistant to treatment than the more stable ones, which respond better to treatment. Further work needs to be done to explore whether the emergence or disappearance (as well as significant increasing or shrinking of persistent variants) in a particular treatment arm is linked to a particular pathway or is enriched in a particular family of cellular processes.

These findings highlight the importance of subclonal and very subclonal events in the behavior of the tumors. Variants with low VAFs can be due to low tumor purity but can also be treatment-induced mutations, and, interestingly, it has been shown that a significant fraction of clinically actionable variants have low VAFs (Shin et al., 2017). Indeed, we found a number of actionable mutations with VAFs <5% in almost all the models, including *MAP3K7*, *VEGF*, *SMARCA2*, *RARA*, *CXCR1*, *MAP4K2*, *ARID1B* and *CDK2AP1*. In this sense, it has been shown that the measurement of subclonal architectures has clinical relevance, since subclone multiplicity and other measures of intratumor heterogeneity have been reported as prognostic biomarkers (Andor et al., 2016). Indeed, minor clones can expand rapidly, conferring tumor aggressiveness and metastatic potential (Tew et al., 2020). Therefore, it is crucial to ensure that subclonal reconstruction is accurate. This is the reason why important efforts have been directed towards the implementation of subclonal reconstruction methods that combine data-driven machine-learning with theoretical population genetics. This is in contrast to purely data-driven approaches that lack an underlying evolutionary model (Caravagna et al., 2020).

Indeed, the intra tumoral heterogeneity can be used to identify the temporal order of acquired mutation acquisition as is known that the temporal and spatial dynamics of clones may affect

the clinical course of certain diseases. An example of this are *JAK2* and *TET2* mutations in myeloproliferative disorders. If a *TET2* mutation is acquired first, there is an expansion of hematopoietic stem and progenitor cells, blocking expansion of erythroid progenitors until cells acquire a *JAK2* mutation. Conversely, if a *JAK2* mutation is acquired first, megakaryocyte number increases, with no expansion of the hematopoietic stem and progenitor cells until a *TET2* mutation is acquired (Ortmann et al., 2015; McGranahan and Swanton, 2017). In melanoma, selective gain of mutated *BRAF* alleles occurs as an early event, whereas whole-genome duplication occurs as a late truncal event (Birkeland et al., 2018).

We have found an increased clonal variability of certain PDX models, which could reflect an enhanced genomic instability that would explain their clinical behavior. Indeed, certain mutational signatures are source of genomic instability, such as the APOBEC mutational signature, which is particularly enriched in the later stages of tumor development (Swanton et al., 2015). Furthermore, several chemotherapies (such as cisplatin, cyclophosphamide or temozolomide) can activate APOBEC3, and can potentially promote APOBEC3 mutagenesis (Kanu et al., 2016). In neuroblastoma, mutational signature 18, causally associated with reactive oxygen species, is the most common cause of driver point mutations and appears early and is continuous throughout disease evolution (Brady et al., 2020). Thus, the exploration of these or other mutational signatures could help to understand the underlying mechanisms of variable genomic instability of these models and to understand their differential response to treatment, including targeted agents. It would be also necessary to deepen into the mutational processes and signatures leading to hypermutator phenotype in our hypermutated GR-NB10 model.

It is likely that this variability in subclonal distribution is a fine balance between chemotherapy-induced competitive release, which allows treatment-resistant minor subclones to repopulate and drive the relapsed tumor, and chemotherapy-induced mutagenesis. Further bioinformatics approaches are planned to model clonal evolution and architecture (Caravagna et al., 2020), since although emergence of resistance mechanisms in cancer cells to therapy is probably inevitable, proliferation of the resistant phenotypes would not and could be delayed with sufficient understanding of the underlying ecoevolutionary dynamics (Gatenby and Brown, 2018). Conventional cancer treatment strategies are based on the maximum tolerated dose (MTD), assuming that maximum patient benefit is achieved through maximum killing of tumor cells. Indeed, standard MTD therapy can cure homogeneous tumors consisting almost entirely of sensitive cells (Gallaher et al., 2018). However, in heterogeneous tumors, the elimination of therapy-sensitive populations accelerates the emergence of resistant clones. Thus, in tumors that are not curable by conventional MTD therapy, evolution-guided treatment strategies, also known as adaptive therapy, could find their place. The goal of adaptive therapy is to maintain a controllable stable tumor burden by allowing a significant population of treatment-sensitive cells to survive. These, in turn, suppress proliferation of the resistant populations (West et al., 2020). Indeed, experimental studies have shown that adaptive therapy can enforce prolonged tumor control (Enriquez-Navas et al., 2016) and that metronomic therapy can efficiently control drug-sensitive and -resistant clone balance, while achieving control of tumor progression (Bondarenko et al., 2021).

Nevertheless, all these explorations performed through bulk sequencing can provide

information about cancer biology and prognosis, but cannot accurately distinguish which mutations occur in the same clone, precisely measure clonal complexity, or definitively elucidate the order of mutations. To analyze the clonal architecture of tumors, single-cell DNA (scDNA) approaches have demonstrated their capacity to provide information about the molecular sequence of events that drive tumor transformation and evolution and insights in how mutational combinations contribute to clonal dominance. The major relevance of this approach is the possibility to detect newly-transformed clones that emerge and may inform the use of therapies that target these clones before they achieve clonal dominance (Lim et al., 2020; Miles et al., 2020). Indeed, scDNA analyses are currently ongoing in our laboratory on the same neuroblastoma PDX models that we have used for the study of clonal evolution, and will be part of a common publication with the results of this PhD work.

Our *in vivo* experiences in clonal evolution have allowed us to create an important biobank of tumors (DMSO and flash-frozen) and plasma samples which are a precious collection of biological tissues that can be used for further investigations, for both genetics but also mechanistical studies of pathway activation, metabolomics or proteomics. With this, in addition to scDNA, single-cell RNA data provided by Isabell Janoueix will allow us to look at the expression of particular genetic events that could be useful to understand the mechanisms of clonal evolution and/or drug sensitivities.

ALK preclinical studies in neuroblastoma

The goal of this study was to give robust preclinical insights in the activity of ALK inhibitors in combination with chemotherapy or other targeted agents in neuroblastomas carrying mutations or amplifications in this gene. The ongoing SIOPEN HRNBL2 and the COG's ANBL1531 trials for first-line treatment of high-risk neuroblastoma have been amended to introduce lorlatinib in upfront treatment of patients with *ALK*-aberrant high-risk neuroblastoma.

While cell lines with ALK alterations were less sensitive to lorlatinib than to crizotinib and other ALK inhibitors, lorlatinib showed the highest *in vitro* inhibition of ALK phosphorylation and the greatest *in vivo* reduction in tumour volume. Altogether, this reflects that *in vitro* cytotoxicity of ALK inhibitors may not be an accurate predictor of their *in vivo* activity. In GEMM models, whereas VAC chemotherapy or lorlatinib alone did not show any survival advantage, the association of both were synergistic and induced significantly increased survival in the Th-*ALK*^{F1174L}/*MYCN* neuroblastoma model. In PDX models, lorlatinib alone showed high efficacy in GR-NB4 *ALK*-amplified model. The *ALK*^{F1174L} and *ALK*^{F1174C} mutated models were totally resistant to both lorlatinib and chemotherapy, alone or in combination.

In view of the future amended HRNBL2 protocol combining lorlatinib with chemotherapy in *ALK*-aberrant high-risk neuroblastoma patients, we then investigated the possibility whether combined ALK and MDM2 inhibition might be relevant for *ALK*-aberrant neuroblastoma patients following relapse, as ALK and MDM2 inhibitors have already been explored as potential strategies to overcome resistance to ALK inhibitors (Wang et al., 2017a, 2; Miyazaki et al., 2018). In *TP53*-wild-type and *ALK*-aberrant (mutated, amplified or both) cell lines, the combination of idasanutlin and ALK

inhibitors was revealed as synergistic and induced enhanced levels of apoptosis. *In vivo*, an ALK-amplified model showed impressive synergistic effects with the combination of lorlatinib and idasanutlin, whereas both ALK^{F1174L} and ALK^{F1174C} mutated models did not show any response to the combination.

Due to COVID19 pandemic restrictions, this part of the PhD work was interrupted at several times. Current experiments are ongoing to provide stronger conclusions. Experiments are ongoing and are planned to be finished by the end of June 2021. The manuscript will be submitted for mid-July.

Publication strategies

Different publications will result from this thesis:

1. The *ex vivo* drug screenings performed within the COMPASS consortium will be part of a common publication with all members of the consortium.
2. The study of the clonal evolution under targeted therapies will be part of a common publication with the work of Jaydutt Bhalshankar and Angela Bellini on single-cell DNA sequencing for the study of subclonal evolution.
3. The work on *ALK*-aberrant neuroblastoma and ALK inhibitory combinatorial treatments is planned in collaboration with Dr. Sally George from the Institute of Cancer Research in London and Pr. Deborah Tweddle from the Translational & Clinical Research Institute in Newcastle.

V - Conclusion

High-risk neuroblastoma patients remain a challenge for clinicians. It is therefore crucial to improve our knowledge of the main difficulties that physicians face in the management of these patients: tumor relapse and treatment resistance. With this work, we have tried to give new insights on the drug sensitivity and clonal evolution of high-risk neuroblastoma. All this work is fruit of close collaborations with different colleagues within the Institut Curie and with other partners in France and Europe. This PhD project would not have been possible without them.

First, we have shown that high-risk neuroblastoma PDX models show particular *ex vivo* sensitivity to HDAC inhibitors, which will need preclinical *in vivo* confirmation. Second, from a therapeutic perspective, our study of the *in vivo* clonal evolution of high-risk neuroblastoma in PDX models under targeted treatment has allowed us to show how clones vary after treatment and that PDX models with lower variability are more sensitive to treatment, whereas models which clones emerge or disappear more easily, show an intrinsic resistance to treatment. Third, we wanted to give new insights in ALK inhibitory treatment in view of the future amended first-line HRNBL2 protocol combining upfront lorlatinib and chemotherapy for *ALK*-aberrant high-risk neuroblastoma patients. Lorlatinib has shown the most effective ALK inhibitory activity both *in vitro* and *in vivo*. The combination of lorlatinib and idasanutlin showed impressive synergy in an *ALK* amplified model, which could be use in case of relapse or treatment resistance.

References

- Ackermann, S., Cartolano, M., Hero, B., Welte, A., Kahlert, Y., Roderwieser, A., et al. (2018). A mechanistic classification of clinical phenotypes in neuroblastoma. *Science* 362, 1165–1170. doi:10.1126/science.aat6768.
- Ackermann, S., Goeser, F., Schulte, J. H., Schramm, A., Ehemann, V., Hero, B., et al. (2011). Polo-like kinase 1 is a therapeutic target in high-risk neuroblastoma. *Clin. Cancer Res. Off. J. Am. Assoc. Cancer Res.* 17, 731–741. doi:10.1158/1078-0432.CCR-10-1129.
- Alexandrov, L. B., Kim, J., Haradhvala, N. J., Huang, M. N., Tian Ng, A. W., Wu, Y., et al. (2020). The repertoire of mutational signatures in human cancer. *Nature* 578, 94–101. doi:10.1038/s41586-020-1943-3.
- Allen, C. E., Laetsch, T. W., Mody, R., Irwin, M. S., Lim, M. S., Adamson, P. C., et al. (2017). Target and Agent Prioritization for the Children’s Oncology Group—National Cancer Institute Pediatric MATCH Trial. *JNCI J. Natl. Cancer Inst.* 109. doi:10.1093/jnci/djw274.
- Amorim, J. P., Santos, G., Vinagre, J., and Soares, P. (2016). The Role of ATRX in the Alternative Lengthening of Telomeres (ALT) Phenotype. *Genes* 7. doi:10.3390/genes7090066.
- Andor, N., Graham, T. A., Jansen, M., Xia, L. C., Aktipis, C. A., Petritsch, C., et al. (2016). Pan-cancer analysis of the extent and consequences of intra-tumor heterogeneity. *Nat. Med.* 22, 105–113. doi:10.1038/nm.3984.
- Asgharzadeh, S., Pique-Regi, R., Sposto, R., Wang, H., Yang, Y., Shimada, H., et al. (2006). Prognostic significance of gene expression profiles of metastatic neuroblastomas lacking MYCN gene amplification. *J. Natl. Cancer Inst.* 98, 1193–1203. doi:10.1093/jnci/djj330.
- Asgharzadeh, S., Salo, J. A., Ji, L., Oberthuer, A., Fischer, M., Berthold, F., et al. (2012). Clinical significance of tumor-associated inflammatory cells in metastatic neuroblastoma. *J. Clin. Oncol. Off. J. Am. Soc. Clin. Oncol.* 30, 3525–3532. doi:10.1200/JCO.2011.40.9169.
- Attiyeh, E. F., London, W. B., Mossé, Y. P., Wang, Q., Winter, C., Khazi, D., et al. (2005). Chromosome 1p and 11q Deletions and Outcome in Neuroblastoma. *N. Engl. J. Med.* 353, 2243–2253. doi:10.1056/NEJMoa052399.
- Au-Yeung, G., Lang, F., Azar, W. J., Mitchell, C., Jarman, K. E., Lackovic, K., et al. (2017). Selective Targeting of Cyclin E1-Amplified High-Grade Serous Ovarian Cancer by Cyclin-Dependent Kinase 2 and AKT Inhibition. *Clin. Cancer Res.* 23, 1862–1874. doi:10.1158/1078-0432.CCR-16-0620.
- Barbieri, E., Mehta, P., Chen, Z., Zhang, L., Slack, A., Berg, S., et al. (2006). MDM2 inhibition sensitizes neuroblastoma to chemotherapy-induced apoptotic cell death. *Mol. Cancer Ther.* 5, 2358–2365. doi:10.1158/1535-7163.MCT-06-0305.
- Barretina, J., Caponigro, G., Stransky, N., Venkatesan, K., Margolin, A. A., Kim, S., et al. (2012). The Cancer Cell Line Encyclopedia enables predictive modelling of anticancer drug sensitivity. *Nature* 483, 603–607. doi:10.1038/nature11003.
- Bate-Eya, L. T., Ebus, M. E., Koster, J., den Hartog, I. J. M., Zwijnenburg, D. A., Schild, L., et al. (2014). Newly-derived neuroblastoma cell lines propagated in serum-free media recapitulate the genotype and phenotype of primary neuroblastoma tumours. *Eur. J. Cancer* 50, 628–637. doi:10.1016/j.ejca.2013.11.015.

- Bellini, A., Bernard, V., Leroy, Q., Frio, T. R., Pierron, G., Combaret, V., et al. (2015a). Deep Sequencing Reveals Occurrence of Subclonal ALK Mutations in Neuroblastoma at Diagnosis. *Clin. Cancer Res.* 21, 4913–4921. doi:10.1158/1078-0432.CCR-15-0423.
- Bellini, A., Bernard, V., Leroy, Q., Frio, T. R., Pierron, G., Combaret, V., et al. (2015b). Deep Sequencing Reveals Occurrence of Subclonal ALK Mutations in Neuroblastoma at Diagnosis. *Clin. Cancer Res.* 21, 4913–4921. doi:10.1158/1078-0432.CCR-15-0423.
- Bellini, A., Bessoltane-Bentahar, N., Bhalshankar, J., Clement, N., Raynal, V., Baulande, S., et al. (2019). Study of chromatin remodeling genes implicates SMARCA4 as a putative player in oncogenesis in neuroblastoma. *Int. J. Cancer* 145, 2781–2791. doi:https://doi.org/10.1002/ijc.32361.
- Beppu, K., Jaboine, J., Merchant, M. S., Mackall, C. L., and Thiele, C. J. (2004). Effect of imatinib mesylate on neuroblastoma tumorigenesis and vascular endothelial growth factor expression. *J. Natl. Cancer Inst.* 96, 46–55. doi:10.1093/jnci/djh004.
- Berbegall, A. P., Bogen, D., Pötschger, U., Beiske, K., Bown, N., Combaret, V., et al. (2018). Heterogeneous MYCN amplification in neuroblastoma: a SIOP Europe Neuroblastoma Study. *Br. J. Cancer* 118, 1502–1512. doi:10.1038/s41416-018-0098-6.
- Berlanga, P., Schleiermacher, G., Lacroix, L., Pierron, G., Beaumais, T. A. de, Chicard, M., et al. (2019). Abstract CT081: Pediatric precision medicine program in recurrent tumors: Results of the first 500 patients included in the European MAPPYACTS molecular profiling trial. *Cancer Res.* 79, CT081–CT081. doi:10.1158/1538-7445.AM2019-CT081.
- Berry, J. L., Xu, L., Kooi, I., Linn Murphree, A., Prabakar, R. K., Reid, M., et al. (2018). Genomic cfDNA Analysis of Aqueous Humor in Retinoblastoma Predicts Eye Salvage: The Surrogate Tumor Biopsy for Retinoblastoma. *Mol. Cancer Res. MCR* 16, 1701–1712. doi:10.1158/1541-7786.MCR-18-0369.
- Bertrand, H., Bombard, S., Monchaud, D., and Teulade-Fichou, M.-P. (2007). A platinum-quinacridine hybrid as a G-quadruplex ligand. *J. Biol. Inorg. Chem. JBIC Publ. Soc. Biol. Inorg. Chem.* 12, 1003–1014. doi:10.1007/s00775-007-0273-3.
- Bertrand, H., Granzhan, A., Monchaud, D., Saettel, N., Guillot, R., Clifford, S., et al. (2011). Recognition of G-quadruplex DNA by triangular star-shaped compounds: with or without side chains? *Chem. Weinh. Bergstr. Ger.* 17, 4529–4539. doi:10.1002/chem.201002810.
- Bhang, H. C., Ruddy, D. A., Krishnamurthy Radhakrishna, V., Caushi, J. X., Zhao, R., Hims, M. M., et al. (2015). Studying clonal dynamics in response to cancer therapy using high-complexity barcoding. *Nat. Med.* 21, 440–448. doi:10.1038/nm.3841.
- Bidard, F.-C., Madic, J., Mariani, P., Piperno-Neumann, S., Rampanou, A., Servois, V., et al. (2014). Detection rate and prognostic value of circulating tumor cells and circulating tumor DNA in metastatic uveal melanoma. *Int. J. Cancer* 134, 1207–1213. doi:10.1002/ijc.28436.
- Bieche, I., Vacher, S., Vallerand, D., Richon, S., Hatem, R., De Plater, L., et al. (2014). Vasculature analysis of patient derived tumor xenografts using species-specific PCR assays: evidence of tumor endothelial cells and atypical VEGFA-VEGFR1/2 signalings. *BMC Cancer* 14, 178. doi:10.1186/1471-2407-14-178.
- Birkbak, N. J., and McGranahan, N. (2020). Cancer Genome Evolutionary Trajectories in Metastasis. *Cancer Cell* 37, 8–19. doi:10.1016/j.ccell.2019.12.004.
- Birkeland, E., Zhang, S., Poduval, D., Geisler, J., Nakken, S., Vodak, D., et al. (2018). Patterns of genomic evolution in advanced melanoma. *Nat. Commun.* 9, 2665. doi:10.1038/s41467-018-05063-1.

- Blavier, L., Yang, R.-M., and DeClerck, Y. A. (2020). The Tumor Microenvironment in Neuroblastoma: New Players, New Mechanisms of Interaction and New Perspectives. *Cancers* 12. doi:10.3390/cancers12102912.
- Boeva, V., Louis-Brennetot, C., Peltier, A., Durand, S., Pierre-Eugène, C., Raynal, V., et al. (2017). Heterogeneity of neuroblastoma cell identity defined by transcriptional circuitries. *Nat. Genet.* 49, 1408–1413. doi:10.1038/ng.3921.
- Bollati, V., and Baccarelli, A. (2010). Environmental epigenetics. *Heredity* 105, 105–112. doi:10.1038/hdy.2010.2.
- Bondarenko, M., Le Grand, M., Shaked, Y., Raviv, Z., Chapuisat, G., Carrère, C., et al. (2021). Metronomic Chemotherapy Modulates Clonal Interactions to Prevent Drug Resistance in Non-Small Cell Lung Cancer. *Cancers* 13, 2239. doi:10.3390/cancers13092239.
- Bourdeaut, F., Ferrand, S., Brugières, L., Hilbert, M., Ribeiro, A., Lacroix, L., et al. (2012). ALK germline mutations in patients with neuroblastoma: a rare and weakly penetrant syndrome. *Eur. J. Hum. Genet.* 20, 291–297. doi:10.1038/ejhg.2011.195.
- Bown, N., Cotterill, S., Lastowska, M., O'Neill, S., Pearson, A. D., Plantaz, D., et al. (1999). Gain of chromosome arm 17q and adverse outcome in patients with neuroblastoma. *N. Engl. J. Med.* 340, 1954–1961. doi:10.1056/NEJM199906243402504.
- Brady, S. W., Liu, Y., Ma, X., Gout, A. M., Hagiwara, K., Zhou, X., et al. (2020). Pan-neuroblastoma analysis reveals age- and signature-associated driver alterations. *Nat. Commun.* 11. doi:10.1038/s41467-020-18987-4.
- Braekeveldt, N., von Stedingk, K., Fransson, S., Martinez-Monleon, A., Lindgren, D., Axelson, H., et al. (2018). Patient-Derived Xenograft Models Reveal Intratumor Heterogeneity and Temporal Stability in Neuroblastoma. *Cancer Res.* 78, 5958–5969. doi:10.1158/0008-5472.CAN-18-0527.
- Bresler, S. C., Weiser, D. A., Huwe, P. J., Park, J. H., Krytska, K., Ryles, H., et al. (2014). ALK mutations confer differential oncogenic activation and sensitivity to ALK inhibition therapy in neuroblastoma. *Cancer Cell* 26, 682–694. doi:10.1016/j.ccell.2014.09.019.
- Bresler, S. C., Wood, A. C., Haglund, E. A., Courtright, J., Belcastro, L. T., Plegaria, J. S., et al. (2011). Differential inhibitor sensitivity of anaplastic lymphoma kinase variants found in neuroblastoma. *Sci. Transl. Med.* 3, 108ra114. doi:10.1126/scitranslmed.3002950.
- Brodeur, G. M. (1993). TRK-a expression in neuroblastomas: a new prognostic marker with biological and clinical significance. *J. Natl. Cancer Inst.* 85, 344–345. doi:10.1093/jnci/85.5.344.
- Brodeur, G. M. (2018). Spontaneous regression of neuroblastoma. *Cell Tissue Res.* 372, 277–286. doi:10.1007/s00441-017-2761-2.
- Brodeur, G. M., Seeger, R. C., Schwab, M., Varmus, H. E., and Bishop, J. M. (1984). Amplification of N-myc in untreated human neuroblastomas correlates with advanced disease stage. *Science* 224, 1121–1124. doi:10.1126/science.6719137.
- Bruna, A., Rueda, O. M., Greenwood, W., Batra, A. S., Callari, M., Batra, R. N., et al. (2016). A Biobank of Breast Cancer Explants with Preserved Intra-tumor Heterogeneity to Screen Anticancer Compounds. *Cell* 167, 260–274.e22. doi:10.1016/j.cell.2016.08.041.
- Calero, R., Morchon, E., Johnsen, J. I., and Serrano, R. (2014). Sunitinib Suppress Neuroblastoma Growth through Degradation of MYCN and Inhibition of Angiogenesis. *PLOS ONE* 9, e95628.

doi:10.1371/journal.pone.0095628.

- Campbell, B. B., Light, N., Fabrizio, D., Zatzman, M., Fuligni, F., de Borja, R., et al. (2017). Comprehensive Analysis of Hypermutation in Human Cancer. *Cell* 171, 1042–1056.e10. doi:10.1016/j.cell.2017.09.048.
- Campbell, K., Naranjo, A., Hibbitts, E., Gastier-Foster, J. M., Bagatell, R., Irwin, M. S., et al. (2020). Association of heterogeneous MYCN amplification with clinical features, biological characteristics and outcomes in neuroblastoma: A report from the Children's Oncology Group. *Eur. J. Cancer* 133, 112–119. doi:10.1016/j.ejca.2020.04.007.
- Caravagna, G., Heide, T., Williams, M. J., Zapata, L., Nichol, D., Chkhaidze, K., et al. (2020). Subclonal reconstruction of tumors by using machine learning and population genetics. *Nat. Genet.* 52, 898–907. doi:10.1038/s41588-020-0675-5.
- Carlin, D., Sepich, D., Grover, V. K., Cooper, M. K., Solnica-Krezel, L., and Inbal, A. (2012). Six3 cooperates with Hedgehog signaling to specify ventral telencephalon by promoting early expression of Foxg1a and repressing Wnt signaling. *Dev. Camb. Engl.* 139, 2614–2624. doi:10.1242/dev.076018.
- Carmeliet, P. (2005). VEGF as a key mediator of angiogenesis in cancer. *Oncology* 69 Suppl 3, 4–10. doi:10.1159/000088478.
- Carr, T. H., McEwen, R., Dougherty, B., Johnson, J. H., Dry, J. R., Lai, Z., et al. (2016). Defining actionable mutations for oncology therapeutic development. *Nat. Rev. Cancer* 16, 319–329. doi:10.1038/nrc.2016.35.
- Carr-Wilkinson, J., O'Toole, K., Wood, K. M., Challen, C. C., Baker, A. G., Board, J. R., et al. (2010). High Frequency of p53/MDM2/p14ARF Pathway Abnormalities in Relapsed Neuroblastoma. *Clin. Cancer Res. Off. J. Am. Assoc. Cancer Res.* 16, 1108–1118. doi:10.1158/1078-0432.CCR-09-1865.
- Castle, V. P., Heidelberger, K. P., Bromberg, J., Ou, X., Dole, M., and Nuñez, G. (1993). Expression of the apoptosis-suppressing protein bcl-2, in neuroblastoma is associated with unfavorable histology and N-myc amplification. *Am. J. Pathol.* 143, 1543–1550.
- Cescon, D. W., Bratman, S. V., Chan, S. M., and Siu, L. L. (2020). Circulating tumor DNA and liquid biopsy in oncology. *Nat. Cancer* 1, 276–290. doi:10.1038/s43018-020-0043-5.
- Chang, L., Chang, M., Chang, H. M., and Chang, F. (2018). Microsatellite Instability: A Predictive Biomarker for Cancer Immunotherapy. *Appl. Immunohistochem. Mol. Morphol.* 26, e15–e21. doi:10.1097/PAI.0000000000000575.
- Chapman, P. B., Hauschild, A., Robert, C., Haanen, J. B., Ascierto, P., Larkin, J., et al. (2011). Improved survival with vemurafenib in melanoma with BRAF V600E mutation. *N. Engl. J. Med.* 364, 2507–2516. doi:10.1056/NEJMoa1103782.
- Charlet, J., Schneckenger, M., Brown, K. W., and Diederich, M. (2012). DNA demethylation increases sensitivity of neuroblastoma cells to chemotherapeutic drugs. *Biochem. Pharmacol.* 83, 858–865. doi:10.1016/j.bcp.2012.01.009.
- Chaussade, A., Millot, G., Wells, C., Brisse, H., Laé, M., Savignoni, A., et al. (2019). Correlation between RB1 germline mutations and second primary malignancies in hereditary retinoblastoma patients treated with external beam radiotherapy. *Eur. J. Med. Genet.* 62, 217–223. doi:10.1016/j.ejmg.2018.07.017.
- Chen, J., Nelson, C., Wong, M., Tee, A. E., Liu, P. Y., La, T., et al. (2021). Targeted Therapy of TERT-Rearranged Neuroblastoma with BET Bromodomain Inhibitor and Proteasome Inhibitor Combination Therapy.

Clin. Cancer Res. Off. J. Am. Assoc. Cancer Res. 27, 1438–1451. doi:10.1158/1078-0432.CCR-20-3044.

- Chen, L., Alexe, G., Dharia, N. V., Ross, L., Iniguez, A. B., Conway, A. S., et al. (2018). CRISPR-Cas9 screen reveals a MYCN-amplified neuroblastoma dependency on EZH2. *J. Clin. Invest.* 128, 446–462. doi:10.1172/JCI90793.
- Chen, L., Pastorino, F., Berry, P., Bonner, J., Kirk, C., Wood, K. M., et al. (2019). Preclinical evaluation of the first intravenous small molecule MDM2 antagonist alone and in combination with temozolomide in neuroblastoma. *Int. J. Cancer* 144, 3146–3159. doi:10.1002/ijc.32058.
- Chen, X., Li, X., Hu, X., Jiang, F., Shen, Y., Xu, R., et al. (2020). LUM Expression and Its Prognostic Significance in Gastric Cancer. *Front. Oncol.* 10. doi:10.3389/fonc.2020.00605.
- Chen, Z., Lin, Y., Barbieri, E., Burlingame, S., Hicks, J., Ludwig, A., et al. (2009). Mdm2 deficiency suppresses MYCN-Driven neuroblastoma tumorigenesis in vivo. *Neoplasia N. Y. N* 11, 753–762. doi:10.1593/neo.09466.
- Cheng, W., Li, M., Jiang, Y., Zhang, C., Cai, J., Wang, K., et al. (2016). Association between small heat shock protein B11 and the prognostic value of MGMT promoter methylation in patients with high-grade glioma. *J. Neurosurg.* 125, 7–16. doi:10.3171/2015.5.JNS142437.
- Chesler, L., Schlieve, C., Goldenberg, D. D., Kenney, A., Kim, G., McMillan, A., et al. (2006). Inhibition of phosphatidylinositol 3-kinase destabilizes Mycn protein and blocks malignant progression in neuroblastoma. *Cancer Res.* 66, 8139–8146. doi:10.1158/0008-5472.CAN-05-2769.
- Cheung, N.-K. V., Zhang, J., Lu, C., Parker, M., Bahrami, A., Tickoo, S. K., et al. (2012). Association of age at diagnosis and genetic mutations in patients with neuroblastoma. *JAMA* 307, 1062–1071. doi:10.1001/jama.2012.228.
- Chévez-Barrios, P., Eagle, R. C., Krailo, M., Piao, J., Albert, D. M., Gao, Y., et al. (2019). Study of Unilateral Retinoblastoma With and Without Histopathologic High-Risk Features and the Role of Adjuvant Chemotherapy: A Children's Oncology Group Study. *J. Clin. Oncol.* 37, 2883–2891. doi:10.1200/JCO.18.01808.
- Chi, S. N., Bourdeaut, F., Laetsch, T. W., Fouladi, M., Macy, M. E., Makin, G. W., et al. (2020). Phase I study of tazemetostat, an enhancer of zeste homolog-2 inhibitor, in pediatric pts with relapsed/refractory integrase interactor 1-negative tumors. *J. Clin. Oncol.* 38, 10525–10525. doi:10.1200/JCO.2020.38.15_suppl.10525.
- Chicard, M., Boyault, S., Daage, L. C., Richer, W., Gentien, D., Pierron, G., et al. (2016). Genomic Copy Number Profiling Using Circulating Free Tumor DNA Highlights Heterogeneity in Neuroblastoma. *Clin. Cancer Res.* 22, 5564–5573. doi:10.1158/1078-0432.CCR-16-0500.
- Chicard, M., Colmet-Daage, L., Clement, N., Danzon, A., Bohec, M., Bernard, V., et al. (2018a). Whole-Exome Sequencing of Cell-Free DNA Reveals Temporo-spatial Heterogeneity and Identifies Treatment-Resistant Clones in Neuroblastoma. *Clin. Cancer Res. Off. J. Am. Assoc. Cancer Res.* 24, 939–949. doi:10.1158/1078-0432.CCR-17-1586.
- Chicard, M., Colmet-Daage, L., Clement, N., Danzon, A., Bohec, M., Bernard, V., et al. (2018b). Whole-Exome Sequencing of Cell-Free DNA Reveals Temporo-spatial Heterogeneity and Identifies Treatment-Resistant Clones in Neuroblastoma. *Clin. Cancer Res. Off. J. Am. Assoc. Cancer Res.* 24, 939–949. doi:10.1158/1078-0432.CCR-17-1586.
- Cingolani, P., Platts, A., Wang, L. L., Coon, M., Nguyen, T., Wang, L., et al. (2012). A program for annotating and predicting the effects of single nucleotide polymorphisms, SnpEff: SNPs in the genome of

Drosophila melanogaster strain w1118; iso-2; iso-3. *Fly (Austin)* 6, 80–92. doi:10.4161/fly.19695.

- Clynes, D., Jelinska, C., Xella, B., Ayyub, H., Scott, C., Mitson, M., et al. (2015). Suppression of the alternative lengthening of telomere pathway by the chromatin remodelling factor ATRX. *Nat. Commun.* 6, 7538. doi:10.1038/ncomms8538.
- Cmero, M., Yuan, K., Ong, C. S., Schröder, J., Corcoran, N. M., Papenfuss, T., et al. (2020). Inferring structural variant cancer cell fraction. *Nat. Commun.* 11, 730. doi:10.1038/s41467-020-14351-8.
- Cohn, S. L., Pearson, A. D. J., London, W. B., Monclair, T., Ambros, P. F., Brodeur, G. M., et al. (2009). The International Neuroblastoma Risk Group (INRG) Classification System: An INRG Task Force Report. *J. Clin. Oncol.* 27, 289–297. doi:10.1200/JCO.2008.16.6785.
- Cole, K., J, H., M, L., Ce, H., Mr, R., K, B., et al. (2011). RNAi screen of the protein kinome identifies checkpoint kinase 1 (CHK1) as a therapeutic target in neuroblastoma. *Proc. Natl. Acad. Sci. U. S. A.* 108. doi:10.1073/pnas.1012351108.
- Cooper, M. J., Steinberg, S. M., Chatten, J., Evans, A. E., and Israel, M. A. (1992). Plasticity of neuroblastoma tumor cells to differentiate along a fetal adrenal ganglionic lineage predicts for improved patient survival. *J. Clin. Invest.* 90, 2402–2408.
- Cortés, C., Kozma, S. C., Tauler, A., and Ambrosio, S. (2015). MYCN concurrence with SAHA-induced cell death in human neuroblastoma cells. *Cell. Oncol. Dordr.* 38, 341–352. doi:10.1007/s13402-015-0233-9.
- Corvetta, D., Chayka, O., Gherardi, S., D'Acunto, C. W., Cantilena, S., Valli, E., et al. (2013). Physical interaction between MYCN oncogene and polycomb repressive complex 2 (PRC2) in neuroblastoma: functional and therapeutic implications. *J. Biol. Chem.* 288, 8332–8341. doi:10.1074/jbc.M113.454280.
- Croucher, J. L., Iyer, R., Li, N., Molteni, V., Loren, J., Gordon, W. P., et al. (2015). TrkB Inhibition by GNF-4256 Slows Growth and Enhances Chemotherapeutic Efficacy in Neuroblastoma Xenografts. *Cancer Chemother. Pharmacol.* 75, 131–141. doi:10.1007/s00280-014-2627-1.
- Crystal, A. S., Shaw, A. T., Sequist, L. V., Friboulet, L., Niederst, M. J., Lockerman, E. L., et al. (2014). Patient-derived models of acquired resistance can identify effective drug combinations for cancer. *Science* 346, 1480–1486. doi:10.1126/science.1254721.
- Dagogo-Jack, I., and Shaw, A. T. (2018). Tumour heterogeneity and resistance to cancer therapies. *Nat. Rev. Clin. Oncol.* 15, 81–94. doi:10.1038/nrclinonc.2017.166.
- Daniel, P., Sabri, S., Chaddad, A., Meehan, B., Jean-Claude, B., Rak, J., et al. (2019). Temozolomide Induced Hypermutation in Glioma: Evolutionary Mechanisms and Therapeutic Opportunities. *Front. Oncol.* 9. doi:10.3389/fonc.2019.00041.
- De Brouwer, S., De Preter, K., Kumps, C., Zabrocki, P., Porcu, M., Westerhout, E. M., et al. (2010). Meta-analysis of neuroblastomas reveals a skewed ALK mutation spectrum in tumors with MYCN amplification. *Clin. Cancer Res. Off. J. Am. Assoc. Cancer Res.* 16, 4353–4362. doi:10.1158/1078-0432.CCR-09-2660.
- De Cian, A., Delemos, E., Mergny, J.-L., Teulade-Fichou, M.-P., and Monchaud, D. (2007). Highly efficient G-quadruplex recognition by bisquinolinium compounds. *J. Am. Chem. Soc.* 129, 1856–1857. doi:10.1021/ja067352b.
- De los Santos, M., Zambrano, A., and Aranda, A. (2007). Combined effects of retinoic acid and histone deacetylase inhibitors on human neuroblastoma SH-SY5Y cells. *Mol. Cancer Ther.* 6, 1425–1432. doi:10.1158/1535-7163.MCT-06-0623.

- Debruyne, D. N., Bhatnagar, N., Sharma, B., Luther, W., Moore, N. F., Cheung, N.-K., et al. (2016). ALK inhibitor resistance in ALKF1174L-driven neuroblastoma is associated with AXL activation and induction of EMT. *Oncogene* 35, 3681–3691. doi:10.1038/onc.2015.434.
- Debruyne, D. N., Dries, R., Sengupta, S., Seruggia, D., Gao, Y., Sharma, B., et al. (2019). BORIS promotes chromatin regulatory interactions in treatment-resistant cancer cells. *Nature* 572, 676–680. doi:10.1038/s41586-019-1472-0.
- Decock, A., Ongenaert, M., Vandesompele, J., and Speleman, F. (2011). Neuroblastoma epigenetics: From candidate gene approaches to genome-wide screenings. *Epigenetics* 6, 962–970. doi:10.4161/epi.6.8.16516.
- Dehainault, C., Michaux, D., Pagès-Berhouet, S., Caux-Moncoutier, V., Doz, F., Desjardins, L., et al. (2007). A deep intronic mutation in the RB1 gene leads to intronic sequence exonisation. *Eur. J. Hum. Genet. EJHG* 15, 473–477. doi:10.1038/sj.ejhg.5201787.
- DeLeonardis, K., Hogan, L., Cannistra, S. A., Rangachari, D., and Tung, N. (2019). When Should Tumor Genomic Profiling Prompt Consideration of Germline Testing? *J. Oncol. Pract.* 15, 465–473. doi:10.1200/JOP.19.00201.
- Depuydt, P., Boeva, V., Hocking, T. D., Cannoodt, R., Ambros, I. M., Ambros, P. F., et al. (2018). Genomic Amplifications and Distal 6q Loss: Novel Markers for Poor Survival in High-risk Neuroblastoma Patients. *J. Natl. Cancer Inst.* 110, 1084–1093. doi:10.1093/jnci/djy022.
- Desai, A. V., Robinson, G. W., Basu, E. M., Foster, J., Gauvain, K., Sabnis, A., et al. (2020). Updated entrectinib data in children and adolescents with recurrent or refractory solid tumors, including primary CNS tumors. *J. Clin. Oncol.* 38, 107–107. doi:10.1200/JCO.2020.38.15_suppl.107.
- Dimaras, H., and Corson, T. W. (2019). Retinoblastoma, the visible CNS tumor: A review. *J. Neurosci. Res.* 97, 29–44. doi:https://doi.org/10.1002/jnr.24213.
- Dimaras, H., Khetan, V., Halliday, W., Orlic, M., Prigoda, N. L., Piovesan, B., et al. (2008). Loss of RB1 induces non-proliferative retinoma: increasing genomic instability correlates with progression to retinoblastoma. *Hum. Mol. Genet.* 17, 1363–1372. doi:10.1093/hmg/ddn024.
- Dong, R., Yang, R., Zhan, Y., Lai, H.-D., Ye, C.-J., Yao, X.-Y., et al. (2020). Single-Cell Characterization of Malignant Phenotypes and Developmental Trajectories of Adrenal Neuroblastoma. *Cancer Cell* 38, 716–733.e6. doi:10.1016/j.ccell.2020.08.014.
- Drilon, A., Laetsch, T. W., Kummar, S., DuBois, S. G., Lassen, U. N., Demetri, G. D., et al. (2018). Efficacy of Larotrectinib in TRK Fusion-Positive Cancers in Adults and Children. *N. Engl. J. Med.* doi:10.1056/NEJMoa1714448.
- Duan, X.-F., and Zhao, Q. (2018). TERT-mediated and ATRX-mediated Telomere Maintenance and Neuroblastoma. *J. Pediatr. Hematol. Oncol.* 40, 1–6. doi:10.1097/MPH.0000000000000840.
- DuBois, S. G., Granger, M., Groshen, S. G., Tsao-Wei, D., Shamirian, A., Czarnecki, S., et al. (2020). Randomized phase II trial of MIBG versus MIBG/vincristine/irinotecan versus MIBG/vorinostat for relapsed/refractory neuroblastoma: A report from the New Approaches to Neuroblastoma Therapy Consortium. *J. Clin. Oncol.* 38, 10500–10500. doi:10.1200/JCO.2020.38.15_suppl.10500.
- DuBois, S. G., Marachelian, A., Fox, E., Kudgus, R. A., Reid, J. M., Groshen, S., et al. (2016). Phase I Study of the Aurora A Kinase Inhibitor Alisertib in Combination With Irinotecan and Temozolomide for Patients With Relapsed or Refractory Neuroblastoma: A NANT (New Approaches to Neuroblastoma Therapy) Trial. *J. Clin. Oncol. Off. J. Am. Soc. Clin. Oncol.* 34, 1368–1375. doi:10.1200/JCO.2015.65.4889.

- Durbin, A. D., Zimmerman, M. W., Dharia, N. V., Abraham, B. J., Iniguez, A. B., Weichert-Leahey, N., et al. (2018). Selective gene dependencies in MYCN-amplified neuroblastoma include the core transcriptional regulatory circuitry. *Nat. Genet.* 50, 1240–1246. doi:10.1038/s41588-018-0191-z.
- Ecker, J., Oehme, I., Selt, F., Kool, M., Chavez, L., Hohloch, J., et al. (2017). MEDU-20. TARGETING OF MYC BY HDAC INHIBITION IN MYC AMPLIFIED GROUP 3 MEDULLOBLASTOMA. *Neuro-Oncol.* 19, iv41–iv42. doi:10.1093/neuonc/nox083.170.
- Eggert, A., Ikegaki, N., Kwiatkowski, J., Zhao, H., Brodeur, G. M., and Himelstein, B. P. (2000). High-level expression of angiogenic factors is associated with advanced tumor stage in human neuroblastomas. *Clin. Cancer Res. Off. J. Am. Assoc. Cancer Res.* 6, 1900–1908.
- Eleveld, T. F., Oldridge, D. A., Bernard, V., Koster, J., Daage, L. C., Diskin, S. J., et al. (2015a). Relapsed neuroblastomas show frequent RAS-MAPK pathway mutations. *Nat. Genet.* 47, 864–871. doi:10.1038/ng.3333.
- Eleveld, T. F., Oldridge, D. A., Bernard, V., Koster, J., Daage, L. C., Diskin, S. J., et al. (2015b). Relapsed neuroblastomas show frequent RAS-MAPK pathway mutations. *Nat. Genet.* 47, 864–871. doi:10.1038/ng.3333.
- Eng, C. (2021). BRAF Mutation in Colorectal Cancer: An Enigmatic Target. *J. Clin. Oncol.* 39, 259–261. doi:10.1200/JCO.20.03043.
- Enriquez-Navas, P. M., Kam, Y., Das, T., Hassan, S., Silva, A., Foroutan, P., et al. (2016). Exploiting evolutionary principles to prolong tumor control in preclinical models of breast cancer. *Sci. Transl. Med.* 8, 327ra24. doi:10.1126/scitranslmed.aad7842.
- Esposito, A. (2019). Cooperation of partially-transformed clones: an invisible force behind the early stages of carcinogenesis. *bioRxiv*, 431478. doi:10.1101/431478.
- Fardin, P., Barla, A., Mosci, S., Rosasco, L., Verri, A., Versteeg, R., et al. (2010). A biology-driven approach identifies the hypoxia gene signature as a predictor of the outcome of neuroblastoma patients. *Mol. Cancer* 9, 185. doi:10.1186/1476-4598-9-185.
- Farooqi, A. S., Dagg, R. A., Choi, L. M. R., Shay, J. W., Reynolds, C. P., and Lau, L. M. S. (2014). Alternative lengthening of telomeres in neuroblastoma cell lines is associated with a lack of MYCN genomic amplification and with p53 pathway aberrations. *J. Neurooncol.* 119, 17–26. doi:10.1007/s11060-014-1456-8.
- Felgenhauer, J., Tomino, L., Selich-Anderson, J., Bopp, E., and Shah, N. (2018). Dual BRD4 and AURKA Inhibition Is Synergistic against MYCN-Amplified and Nonamplified Neuroblastoma. *Neoplasia N. Y. N* 20, 965–974. doi:10.1016/j.neo.2018.08.002.
- Fischer, M. (2018). Targeted Therapies in Pediatric Oncology. *Drug Res.* 68, S14. doi:10.1055/a-0733-0816.
- Flobak, Å., Niederdorfer, B., Nakstad, V. T., Thommesen, L., Klinkenberg, G., and Lægreid, A. (2019). A high-throughput drug combination screen of targeted small molecule inhibitors in cancer cell lines. *Sci. Data* 6, 237. doi:10.1038/s41597-019-0255-7.
- Flynn, R. L., Cox, K. E., Jeitany, M., Wakimoto, H., Bryll, A. R., Ganem, N. J., et al. (2015). Alternative lengthening of telomeres renders cancer cells hypersensitive to ATR inhibitors. *Science* 347, 273–277. doi:10.1126/science.1257216.
- Foster, J. H., Voss, S. D., Hall, D. C., Minard, C. G., Balis, F. M., Wilner, K., et al. (2021). Activity of Crizotinib in Patients with ALK-Aberrant Relapsed/Refractory Neuroblastoma: A Children’s Oncology Group Study

(ADVL0912). *Clin. Cancer Res.* doi:10.1158/1078-0432.CCR-20-4224.

- Fransson, S., Martinez-Monleon, A., Johansson, M., Sjöberg, R.-M., Björklund, C., Ljungman, G., et al. (2020). Whole-genome sequencing of recurrent neuroblastoma reveals somatic mutations that affect key players in cancer progression and telomere maintenance. *Sci. Rep.* 10, 22432. doi:10.1038/s41598-020-78370-7.
- Friboulet, L., Li, N., Katayama, R., Lee, C. C., Gainor, J. F., Crystal, A. S., et al. (2014). The ALK inhibitor ceritinib overcomes crizotinib resistance in non-small cell lung cancer. *Cancer Discov.* 4, 662–673. doi:10.1158/2159-8290.CD-13-0846.
- Friedman, A. A., Amzallag, A., Pruteanu-Malinici, I., Baniya, S., Cooper, Z. A., Piris, A., et al. (2015). Landscape of Targeted Anti-Cancer Drug Synergies in Melanoma Identifies a Novel BRAF-VEGFR/PDGFR Combination Treatment. *PLoS ONE* 10, e0140310. doi:10.1371/journal.pone.0140310.
- Fulda, S., Lutz, W., Schwab, M., and Debatin, K. M. (1999). MycN sensitizes neuroblastoma cells for drug-induced apoptosis. *Oncogene* 18, 1479–1486. doi:10.1038/sj.onc.1202435.
- Gallaher, J. A., Enriquez-Navas, P. M., Luddy, K. A., Gatenby, R. A., and Anderson, A. R. A. (2018). Spatial heterogeneity and evolutionary dynamics modulate time to recurrence in continuous and adaptive cancer therapies. *Cancer Res.* 78, 2127–2139. doi:10.1158/0008-5472.CAN-17-2649.
- Gamble, L. D., Kees, U. R., Tweddle, D. A., and Lunec, J. (2012). MYCN sensitizes neuroblastoma to the MDM2-p53 antagonists Nutlin-3 and MI-63. *Oncogene* 31, 752–763. doi:10.1038/onc.2011.270.
- Gao, H., Korn, J. M., Ferretti, S., Monahan, J. E., Wang, Y., Singh, M., et al. (2015). High-throughput screening using patient-derived tumor xenografts to predict clinical trial drug response. *Nat. Med.* 21, 1318–1325. doi:10.1038/nm.3954.
- Garcia, I., Mayol, G., Ríos, J., Domenech, G., Cheung, N.-K. V., Oberthuer, A., et al. (2012). A three-gene expression signature model for risk stratification of patients with neuroblastoma. *Clin. Cancer Res. Off. J. Am. Assoc. Cancer Res.* 18, 2012–2023. doi:10.1158/1078-0432.CCR-11-2483.
- Garnett, M. J., Edelman, E. J., Heidorn, S. J., Greenman, C. D., Dastur, A., Lau, K. W., et al. (2012). Systematic identification of genomic markers of drug sensitivity in cancer cells. *Nature* 483, 570–575. doi:10.1038/nature11005.
- Gatenby, R., and Brown, J. (2018). The Evolution and Ecology of Resistance in Cancer Therapy. *Cold Spring Harb. Perspect. Med.* 8. doi:10.1101/cshperspect.a033415.
- Gatz, S. A., Rubino, J., Rossoni, C., Andre, N., Aerts, I., Thebaud, E., et al. (2019). AcSé-ESMART: European Proof of Concept Therapeutic Stratification Trial of Molecular Anomalies in Relapsed or Refractory Tumors in Children and Adolescents—Arm D: Olaparib and irinotecan. *J. Clin. Oncol.* 37, 10047–10047. doi:10.1200/JCO.2019.37.15_suppl.10047.
- Ge, Q., Li, G., Chen, J., Song, J., Cai, G., he, Y., et al. (2021). Immunological Role and Prognostic Value of APBB1IP in Pan-Cancer Analysis. *J. Cancer* 12, 595–610. doi:10.7150/jca.50785.
- Gelli, E., Pinto, A. M., Somma, S., Imperatore, V., Cannone, M. G., Hadjistilianou, T., et al. (2019). Evidence of predisposing epimutation in retinoblastoma. *Hum. Mutat.* 40, 201–206. doi:https://doi.org/10.1002/humu.23684.
- Georger, B., Bourdeaut, F., DuBois, S. G., Fischer, M., Geller, J. I., Gottardo, N. G., et al. (2017). A Phase I Study of the CDK4/6 Inhibitor Ribociclib (LEE011) in Pediatric Patients with Malignant Rhabdoid Tumors, Neuroblastoma, and Other Solid Tumors. *Clin. Cancer Res. Off. J. Am. Assoc. Cancer Res.* 23, 2433–

2441. doi:10.1158/1078-0432.CCR-16-2898.

- George, R. E., Lahti, J. M., Adamson, P. C., Zhu, K., Finkelstein, D., Ingle, A. M., et al. (2010). Phase I study of decitabine with doxorubicin and cyclophosphamide in children with neuroblastoma and other solid tumors: a Children's Oncology Group study. *Pediatr. Blood Cancer* 55, 629–638. doi:10.1002/pbc.22607.
- George, R. E., Sanda, T., Hanna, M., Fröhling, S., Luther, W., Zhang, J., et al. (2008). Activating mutations in ALK provide a therapeutic target in neuroblastoma. *Nature* 455, 975–978. doi:10.1038/nature07397.
- George, S. L., Lorenzi, F., King, D., Hartlieb, S., Campbell, J., Pemberton, H., et al. (2020). Therapeutic vulnerabilities in the DNA damage response for the treatment of ATRX mutant neuroblastoma. *EBioMedicine* 59, 102971. doi:10.1016/j.ebiom.2020.102971.
- Gerlinger, M., Horswell, S., Larkin, J., Rowan, A. J., Salm, M. P., Varela, I., et al. (2014). Genomic architecture and evolution of clear cell renal cell carcinomas defined by multiregion sequencing. *Nat. Genet.* 46, 225–233. doi:10.1038/ng.2891.
- Gerrish, A., Stone, E., Clokie, S., Ainsworth, J. R., Jenkinson, H., McCalla, M., et al. (2019). Non-invasive diagnosis of retinoblastoma using cell-free DNA from aqueous humour. *Br. J. Ophthalmol.* doi:10.1136/bjophthalmol-2018-313005.
- Gillet, J.-P., Calcagno, A. M., Varma, S., Marino, M., Green, L. J., Vora, M. I., et al. (2011). Redefining the relevance of established cancer cell lines to the study of mechanisms of clinical anti-cancer drug resistance. *Proc. Natl. Acad. Sci. U. S. A.* 108, 18708–18713. doi:10.1073/pnas.1111840108.
- Goldsmith, K. C., Kayser, K., Groshen, S. G., Chioda, M., Thurm, H. C., Chen, J., et al. (2020). Phase I trial of lorlatinib in patients with ALK-driven refractory or relapsed neuroblastoma: A New Approaches to Neuroblastoma Consortium study. *J. Clin. Oncol.* 38, 10504–10504. doi:10.1200/JCO.2020.38.15_suppl.10504.
- Greengard, E. G., Mosse, Y. P., Liu, X., Ahern, C. H., Minard, C., Blaney, S., et al. (2015). Safety and tolerability of crizotinib in combination with chemotherapy for relapsed or refractory solid tumors or anaplastic large cell lymphoma: a Children's Oncology Group phase I consortium study. *J. Clin. Oncol.* 33, 10058–10058. doi:10.1200/jco.2015.33.15_suppl.10058.
- Gröbner, S. N., Worst, B. C., Weischenfeldt, J., Buchhalter, I., Kleinheinz, K., Rudneva, V. A., et al. (2018). The landscape of genomic alterations across childhood cancers. *Nature* 555, 321–327. doi:10.1038/nature25480.
- Hafner, M., Niepel, M., Chung, M., and Sorger, P. K. (2016). Growth rate inhibition metrics correct for confounders in measuring sensitivity to cancer drugs. *Nat. Methods* 13, 521–527. doi:10.1038/nmeth.3853.
- Hald, Ø. H., Olsen, L., Gallo-Oller, G., Elfman, L. H. M., Løkke, C., Kogner, P., et al. (2019). Inhibitors of ribosome biogenesis repress the growth of MYCN-amplified neuroblastoma. *Oncogene* 38, 2800–2813. doi:10.1038/s41388-018-0611-7.
- Ham, J., Costa, C., Sano, R., Lochmann, T. L., Sennott, E. M., Patel, N. U., et al. (2016). Exploitation of the Apoptosis-Primed State of MYCN-Amplified Neuroblastoma to Develop a Potent and Specific Targeted Therapy Combination. *Cancer Cell* 29, 159–172. doi:10.1016/j.ccell.2016.01.002.
- Hamner, J. B., Dickson, P. V., Sims, T. L., Zhou, J., Spence, Y., Ng, C. Y., et al. (2007). Bortezomib inhibits angiogenesis and reduces tumor burden in a murine model of neuroblastoma. *Surgery* 142, 185–191. doi:10.1016/j.surg.2007.04.012.

- Han, S. W., Ahn, J. Y., Lee, S., Noh, Y. S., Jung, H. C., Lee, M. H., et al. (2020). Gene expression network analysis of lymph node involvement in colon cancer identifies AHSA2, CDK10, and CWC22 as possible prognostic markers. *Sci. Rep.* 10, 7170. doi:10.1038/s41598-020-63806-x.
- Hanahan, D., and Weinberg, R. A. (2011). Hallmarks of Cancer: The Next Generation. *Cell* 144, 646–674. doi:10.1016/j.cell.2011.02.013.
- Hao, J.-J., Lin, D.-C., Dinh, H. Q., Mayakonda, A., Jiang, Y.-Y., Chang, C., et al. (2016). Spatial intratumoral heterogeneity and temporal clonal evolution in esophageal squamous cell carcinoma. *Nat. Genet.* 48, 1500–1507. doi:10.1038/ng.3683.
- Harbst, K., Lauss, M., Cirenajwis, H., Isaksson, K., Rosengren, F., Törngren, T., et al. (2016). Multiregion Whole-Exome Sequencing Uncovers the Genetic Evolution and Mutational Heterogeneity of Early-Stage Metastatic Melanoma. *Cancer Res.* 76, 4765–4774. doi:10.1158/0008-5472.CAN-15-3476.
- Hart, L. S., Rader, J., Raman, P., Batra, V., Russell, M. R., Tsang, M., et al. (2017). Preclinical Therapeutic Synergy of MEK1/2 and CDK4/6 Inhibition in Neuroblastoma. *Clin. Cancer Res. Off. J. Am. Assoc. Cancer Res.* 23, 1785–1796. doi:10.1158/1078-0432.CCR-16-1131.
- Hartlieb, S. A., Sieverling, L., Nadler-Holly, M., Ziehm, M., Toprak, U. H., Herrmann, C., et al. (2021). Alternative lengthening of telomeres in childhood neuroblastoma from genome to proteome. *Nat. Commun.* 12, 1269. doi:10.1038/s41467-021-21247-8.
- Harttrampf, A. C., Lacroix, L., Deloger, M., Deschamps, F., Puget, S., Auger, N., et al. (2017). Molecular Screening for Cancer Treatment Optimization (MOSCATO-01) in Pediatric Patients: A Single-Institutional Prospective Molecular Stratification Trial. *Clin. Cancer Res.* 23, 6101–6112. doi:10.1158/1078-0432.CCR-17-0381.
- Hauschild, A., Grob, J.-J., Demidov, L. V., Jouary, T., Gutzmer, R., Millward, M., et al. (2012). Dabrafenib in BRAF-mutated metastatic melanoma: a multicentre, open-label, phase 3 randomised controlled trial. *The Lancet* 380, 358–365. doi:10.1016/S0140-6736(12)60868-X.
- He, L., Kuleskiy, E., Saarela, J., Turunen, L., Wennerberg, K., Aittokallio, T., et al. (2018). Methods for High-throughput Drug Combination Screening and Synergy Scoring. *Methods Mol. Biol. Clifton NJ* 1711, 351–398. doi:10.1007/978-1-4939-7493-1_17.
- Heaphy, C. M., de Wilde, R. F., Jiao, Y., Klein, A. P., Edil, B. H., Shi, C., et al. (2011). Altered telomeres in tumors with ATRX and DAXX mutations. *Science* 333, 425. doi:10.1126/science.1207313.
- Heath, J. A., Campbell, M. A., Thomas, A., and Solomon, B. (2018). Good clinical response to alectinib, a second generation ALK inhibitor, in refractory neuroblastoma. *Pediatr. Blood Cancer* 65, e27055. doi:10.1002/pbc.27055.
- Henson, J. D., Lau, L. M., Koch, S., Martin La Rotta, N., Dagg, R. A., and Reddel, R. R. (2017). The C-Circle Assay for alternative-lengthening-of-telomeres activity. *Methods San Diego Calif* 114, 74–84. doi:10.1016/j.jymeth.2016.08.016.
- Henssen, A., Althoff, K., Odersky, A., Beckers, A., Koche, R., Speleman, F., et al. (2016). Targeting MYCN-Driven Transcription By BET-Bromodomain Inhibition. *Clin. Cancer Res. Off. J. Am. Assoc. Cancer Res.* 22, 2470–2481. doi:10.1158/1078-0432.CCR-15-1449.
- Hero, B., Simon, T., Spitz, R., Ernestus, K., Gnekow, A. K., Scheel-Walter, H.-G., et al. (2008). Localized infant neuroblastomas often show spontaneous regression: results of the prospective trials NB95-S and NB97. *J. Clin. Oncol. Off. J. Am. Soc. Clin. Oncol.* 26, 1504–1510. doi:10.1200/JCO.2007.12.3349.

- Hidalgo, M., Amant, F., Biankin, A. V., Budinská, E., Byrne, A. T., Caldas, C., et al. (2014). Patient-derived xenograft models: an emerging platform for translational cancer research. *Cancer Discov.* 4, 998–1013. doi:10.1158/2159-8290.CD-14-0001.
- Hiley, C., de Bruin, E. C., McGranahan, N., and Swanton, C. (2014). Deciphering intratumor heterogeneity and temporal acquisition of driver events to refine precision medicine. *Genome Biol.* 15, 453. doi:10.1186/s13059-014-0453-8.
- Ho, R., Eggert, A., Hishiki, T., Minturn, J. E., Ikegaki, N., Foster, P., et al. (2002). Resistance to chemotherapy mediated by TrkB in neuroblastomas. *Cancer Res.* 62, 6462–6466.
- Hoehner, J. C., Gestblom, C., Hedborg, F., Sandstedt, B., Olsen, L., and Pålman, S. (1996). A developmental model of neuroblastoma: differentiating stroma-poor tumors' progress along an extra-adrenal chromaffin lineage. *Lab. Investig. J. Tech. Methods Pathol.* 75, 659–675.
- Holbeck, S. L., Camalier, R., Crowell, J. A., Govindharajulu, J. P., Hollingshead, M., Anderson, L. W., et al. (2017). The National Cancer Institute ALMANAC: A Comprehensive Screening Resource for the Detection of Anticancer Drug Pairs with Enhanced Therapeutic Activity. *Cancer Res.* 77, 3564–3576. doi:10.1158/0008-5472.CAN-17-0489.
- Holland, A. J., and Cleveland, D. W. (2009). Boveri revisited: chromosomal instability, aneuploidy and tumorigenesis. *Nat. Rev. Mol. Cell Biol.* 10, 478–487. doi:10.1038/nrm2718.
- Hong, F. D., Huang, H. J., To, H., Young, L. J., Oro, A., Bookstein, R., et al. (1989). Structure of the human retinoblastoma gene. *Proc. Natl. Acad. Sci. U. S. A.* 86, 5502–5506. doi:10.1073/pnas.86.14.5502.
- Howlander, N., Noone, A., Krapcho, M., Miller, D., Brest, A., Yu, M., et al. (2021). SEER Cancer Statistics Review, 1975–2018. *SEER*. Available at: https://seer.cancer.gov/csr/1975_2018/index.html.
- Hu, Z., and Curtis, C. (2020). Looking backward in time to define the chronology of metastasis. *Nat. Commun.* 11, 3213. doi:10.1038/s41467-020-16995-y.
- Huang, K.-L., Li, S., Mertins, P., Cao, S., Gunawardena, H. P., Ruggles, K. V., et al. (2017). Proteogenomic integration reveals therapeutic targets in breast cancer xenografts. *Nat. Commun.* 8, 14864. doi:10.1038/ncomms14864.
- Hwang, W. L., Wolfson, R. L., Niemierko, A., Marcus, K. J., DuBois, S. G., and Haas-Kogan, D. (2019). Clinical Impact of Tumor Mutational Burden in Neuroblastoma. *J. Natl. Cancer Inst.* 111, 695–699. doi:10.1093/jnci/djy157.
- Ice, R. J., Chen, M., Sidorov, M., Le Ho, T., Woo, R. W. L., Rodriguez-Brotons, A., et al. (2020). Drug responses are conserved across patient-derived xenograft models of melanoma leading to identification of novel drug combination therapies. *Br. J. Cancer* 122, 648–657. doi:10.1038/s41416-019-0696-y.
- Infarinato, N. R., Park, J. H., Krytska, K., Ryles, H. T., Sano, R., Szigety, K. M., et al. (2016). The ALK/ROS1 Inhibitor PF-06463922 Overcomes Primary Resistance to Crizotinib in ALK-Driven Neuroblastoma. *Cancer Discov.* 6, 96–107. doi:10.1158/2159-8290.CD-15-1056.
- Inomistova, M., Khranovska, N., and Skachkova, O. (2019). "Chapter 2 - Role of Genetic and Epigenetic Alterations in Pathogenesis of Neuroblastoma," in *Neuroblastoma*, ed. S. K. Ray (Academic Press), 23–41. doi:10.1016/B978-0-12-812005-7.00002-3.
- Iorio, F., Knijnenburg, T. A., Vis, D. J., Bignell, G. R., Menden, M. P., Schubert, M., et al. (2016). A Landscape of Pharmacogenomic Interactions in Cancer. *Cell* 166, 740. doi:10.1016/j.cell.2016.06.017.

- Iraci, N., Diolaiti, D., Papa, A., Porro, A., Valli, E., Gherardi, S., et al. (2011). A SP1/MIZ1/MYCN repression complex recruits HDAC1 at the TRKA and p75NTR promoters and affects neuroblastoma malignancy by inhibiting the cell response to NGF. *Cancer Res.* 71, 404–412. doi:10.1158/0008-5472.CAN-10-2627.
- Iyer, R., Wehrmann, L., Golden, R. L., Naraparaju, K., Croucher, J. L., MacFarland, S. P., et al. (2016). Entrectinib is a Potent Inhibitor of Trk-Driven Neuroblastomas in a Xenograft Mouse Model. *Cancer Lett.* 372, 179–186. doi:10.1016/j.canlet.2016.01.018.
- Jamal-Hanjani, M., Wilson, G. A., McGranahan, N., Birkbak, N. J., Watkins, T. B. K., Veeriah, S., et al. (2017). Tracking the Evolution of Non-Small-Cell Lung Cancer. *N. Engl. J. Med.* 376, 2109–2121. doi:10.1056/NEJMoa1616288.
- Jang, B.-G., Choi, B., Kim, S., Lee, J.-Y., and Kim, M.-J. (2018). Trichostatin A and Sirtinol Regulate the Expression and Nucleocytoplasmic Shuttling of Histone Deacetylases in All-Trans Retinoic Acid-Induced Differentiation of Neuroblastoma Cells. *J. Mol. Neurosci.* 64, 501–511. doi:10.1007/s12031-018-1050-1.
- Janoueix-Lerosey, I., Lequin, D., Brugières, L., Ribeiro, A., de Pontual, L., Combaret, V., et al. (2008). Somatic and germline activating mutations of the ALK kinase receptor in neuroblastoma. *Nature* 455, 967–970. doi:10.1038/nature07398.
- Janoueix-Lerosey, I., Schleiermacher, G., Michels, E., Mosseri, V., Ribeiro, A., Lequin, D., et al. (2009). Overall genomic pattern is a predictor of outcome in neuroblastoma. *J. Clin. Oncol. Off. J. Am. Soc. Clin. Oncol.* 27, 1026–1033. doi:10.1200/JCO.2008.16.0630.
- Jansky, S., Sharma, A. K., Körber, V., Quintero, A., Toprak, U. H., Wecht, E. M., et al. (2021). Single-cell transcriptomic analyses provide insights into the developmental origins of neuroblastoma. *Nat. Genet.*, 1–11. doi:10.1038/s41588-021-00806-1.
- Jiménez, I., Chicard, M., Colmet-Daage, L., Clément, N., Danzon, A., Lapouble, E., et al. (2019a). Circulating tumor DNA analysis enables molecular characterization of pediatric renal tumors at diagnosis. *Int. J. Cancer* 144, 68–79. doi:10.1002/ijc.31620.
- Jiménez, I., Chicard, M., Colmet-Daage, L., Clément, N., Danzon, A., Lapouble, E., et al. (2019b). Circulating tumor DNA analysis enables molecular characterization of pediatric renal tumors at diagnosis. *Int. J. Cancer* 144, 68–79. doi:10.1002/ijc.31620.
- Johnsen, J. I., Segerström, L., Orrego, A., Elfman, L., Henriksson, M., Kågedal, B., et al. (2008). Inhibitors of mammalian target of rapamycin downregulate MYCN protein expression and inhibit neuroblastoma growth in vitro and in vivo. *Oncogene* 27, 2910–2922. doi:10.1038/sj.onc.1210938.
- Johnson, B. E., Mazor, T., Hong, C., Barnes, M., Aihara, K., McLean, C. Y., et al. (2014). Mutational Analysis Reveals the Origin and Therapy-Driven Evolution of Recurrent Glioma. *Science* 343, 189–193. doi:10.1126/science.1239947.
- Johnson, J. I., Decker, S., Zaharevitz, D., Rubinstein, L. V., Venditti, J. M., Schepartz, S., et al. (2001). Relationships between drug activity in NCI preclinical in vitro and in vivo models and early clinical trials. *Br. J. Cancer* 84, 1424–1431. doi:10.1054/bjoc.2001.1796.
- Jones, D. T. W., Banito, A., Grünewald, T. G. P., Haber, M., Jäger, N., Kool, M., et al. (2019). Molecular characteristics and therapeutic vulnerabilities across paediatric solid tumours. *Nat. Rev. Cancer* 19, 420–438. doi:10.1038/s41568-019-0169-x.
- Joshi, S. (2020). Targeting the Tumor Microenvironment in Neuroblastoma: Recent Advances and Future

Directions. *Cancers* 12. doi:10.3390/cancers12082057.

- Jubierre, L., Jiménez, C., Rovira, E., Soriano, A., Sábado, C., Gros, L., et al. (2018). Targeting of epigenetic regulators in neuroblastoma. *Exp. Mol. Med.* 50, 1–12. doi:10.1038/s12276-018-0077-2.
- Jung, J., Lee, J. S., Dickson, M. A., Schwartz, G. K., Le Cesne, A., Varga, A., et al. (2016). TP53 mutations emerge with HDM2 inhibitor SAR405838 treatment in de-differentiated liposarcoma. *Nat. Commun.* 7. doi:10.1038/ncomms12609.
- Kaley, T., Touat, M., Subbiah, V., Hollebecque, A., Rodon, J., Lockhart, A. C., et al. (2018). BRAF Inhibition in BRAFV600-Mutant Gliomas: Results From the VE-BASKET Study. *J. Clin. Oncol.* 36, 3477–3484. doi:10.1200/JCO.2018.78.9990.
- Kamili, A., Gifford, A. J., Li, N., Mayoh, C., Chow, S.-O., Failes, T. W., et al. (2020). Accelerating development of high-risk neuroblastoma patient-derived xenograft models for preclinical testing and personalised therapy. *Br. J. Cancer* 122, 680–691. doi:10.1038/s41416-019-0682-4.
- Kanu, N., Cerone, M. A., Goh, G., Zalmas, L.-P., Bartkova, J., Dietzen, M., et al. (2016). DNA replication stress mediates APOBEC3 family mutagenesis in breast cancer. *Genome Biol.* 17, 185. doi:10.1186/s13059-016-1042-9.
- Karlsson, J., Valind, A., Holmquist Mengelbier, L., Bredin, S., Cornmark, L., Jansson, C., et al. (2018). Four evolutionary trajectories underlie genetic intratumoral variation in childhood cancer. *Nat. Genet.* 50, 944–950. doi:10.1038/s41588-018-0131-y.
- Kazandjian, D., Blumenthal, G. M., Chen, H.-Y., He, K., Patel, M., Justice, R., et al. (2014). FDA Approval Summary: Crizotinib for the Treatment of Metastatic Non-Small Cell Lung Cancer With Anaplastic Lymphoma Kinase Rearrangements. *The Oncologist* 19, e5–e11. doi:10.1634/theoncologist.2014-0241.
- Khoo, K. H., Hoe, K. K., Verma, C. S., and Lane, D. P. (2014). Drugging the p53 pathway: understanding the route to clinical efficacy. *Nat. Rev. Drug Discov.* 13, 217–236. doi:10.1038/nrd4236.
- Knudson, A. G., and Strong, L. C. (1972). Mutation and cancer: neuroblastoma and pheochromocytoma. *Am. J. Hum. Genet.* 24, 514–532.
- Koboldt, D. C., Zhang, Q., Larson, D. E., Shen, D., McLellan, M. D., Lin, L., et al. (2012). VarScan 2: somatic mutation and copy number alteration discovery in cancer by exome sequencing. *Genome Res.* 22, 568–576. doi:10.1101/gr.129684.111.
- Kommalapati, V. K., Kumar, D., and Tangutur, A. D. (2020). Inhibition of JNJ-26481585-mediated autophagy induces apoptosis via ROS activation and mitochondrial membrane potential disruption in neuroblastoma cells. *Mol. Cell. Biochem.* 468, 21–34. doi:10.1007/s11010-020-03708-8.
- Konieczkowski, D. J., Johannessen, C. M., and Garraway, L. A. (2018). A Convergence-Based Framework for Cancer Drug Resistance. *Cancer Cell* 33, 801–815. doi:10.1016/j.ccell.2018.03.025.
- Körholz, K., Ridinger, J., Kronic, D., Najafi, S., Gerloff, X. F., Frese, K., et al. (2021). Broad-Spectrum HDAC Inhibitors Promote Autophagy through FOXO Transcription Factors in Neuroblastoma. *Cells* 10, 1001. doi:10.3390/cells10051001.
- Kothari, P., Marass, F., Yang, J. L., Stewart, C. M., Stephens, D., Patel, J., et al. (2020). Cell-free DNA profiling in retinoblastoma patients with advanced intraocular disease: An MSKCC experience. *Cancer Med.* 9, 6093–6101. doi:10.1002/cam4.3144.

- Krstic, A., Konietzny, A., Halasz, M., Cain, P., Oppermann, U., Kolch, W., et al. (2021). A Chemo-Genomic Approach Identifies Diverse Epigenetic Therapeutic Vulnerabilities in MYCN-Amplified Neuroblastoma. *Front. Cell Dev. Biol.* 9, 612518. doi:10.3389/fcell.2021.612518.
- Krytska, K., Ryles, H. T., Sano, R., Raman, P., Infarinato, N. R., Hansel, T. D., et al. (2016). Crizotinib Synergizes with Chemotherapy in Preclinical Models of Neuroblastoma. *Clin. Cancer Res. Off. J. Am. Assoc. Cancer Res.* 22, 948–960. doi:10.1158/1078-0432.CCR-15-0379.
- Kummar, S., Williams, P. M., Lih, C.-J., Polley, E. C., Chen, A. P., Rubinstein, L. V., et al. (2015). Application of Molecular Profiling in Clinical Trials for Advanced Metastatic Cancers. *JNCI J. Natl. Cancer Inst.* 107. doi:10.1093/jnci/djv003.
- Kushner, B. H., Cheung, N.-K. V., Modak, S., Becher, O. J., Basu, E. M., Roberts, S. S., et al. (2017). A phase I/Ib trial targeting the Pi3k/Akt pathway using perifosine: Long-term progression-free survival of patients with resistant neuroblastoma. *Int. J. Cancer* 140, 480–484. doi:10.1002/ijc.30440.
- Ladenstein, R., Pötschger, U., Pearson, A. D. J., Brock, P., Luksch, R., Castel, V., et al. (2017). Busulfan and melphalan versus carboplatin, etoposide, and melphalan as high-dose chemotherapy for high-risk neuroblastoma (HR-NBL1/SIOPEN): an international, randomised, multi-arm, open-label, phase 3 trial. *Lancet Oncol.* 18, 500–514. doi:10.1016/S1470-2045(17)30070-0.
- Ladenstein, R., Pötschger, U., Valteau-Couanet, D., Luksch, R., Castel, V., Yaniv, I., et al. (2018). Interleukin 2 with anti-GD2 antibody ch14.18/CHO (dinutuximab beta) in patients with high-risk neuroblastoma (HR-NBL1/SIOPEN): a multicentre, randomised, phase 3 trial. *Lancet Oncol.* 19, 1617–1629. doi:10.1016/S1470-2045(18)30578-3.
- Lakoma, A., Barbieri, E., Agarwal, S., Jackson, J., Chen, Z., Kim, Y., et al. (2015). The MDM2 small-molecule inhibitor RG7388 leads to potent tumor inhibition in p53 wild-type neuroblastoma. *Cell Death Discov.* 1, 1–9. doi:10.1038/cddiscovery.2015.26.
- Law, M. J., Lower, K. M., Voon, H. P. J., Hughes, J. R., Garrick, D., Viprakasit, V., et al. (2010). ATR-X syndrome protein targets tandem repeats and influences allele-specific expression in a size-dependent manner. *Cell* 143, 367–378. doi:10.1016/j.cell.2010.09.023.
- Lee, D. H., Ryu, H.-W., Won, H.-R., and Kwon, S. H. (2017). Advances in epigenetic glioblastoma therapy. *Oncotarget* 8, 18577–18589. doi:10.18632/oncotarget.14612.
- Lee, E. Y., Bookstein, R., Young, L. J., Lin, C. J., Rosenfeld, M. G., and Lee, W. H. (1988). Molecular mechanism of retinoblastoma gene inactivation in retinoblastoma cell line Y79. *Proc. Natl. Acad. Sci. U. S. A.* 85, 6017–6021. doi:10.1073/pnas.85.16.6017.
- Lee, J., Kotliarova, S., Kotliarov, Y., Li, A., Su, Q., Donin, N. M., et al. (2006). Tumor stem cells derived from glioblastomas cultured in bFGF and EGF more closely mirror the phenotype and genotype of primary tumors than do serum-cultured cell lines. *Cancer Cell* 9, 391–403. doi:10.1016/j.ccr.2006.03.030.
- Lewis, P. W., Elsaesser, S. J., Noh, K.-M., Stadler, S. C., and Allis, C. D. (2010). Daxx is an H3.3-specific histone chaperone and cooperates with ATRX in replication-independent chromatin assembly at telomeres. *Proc. Natl. Acad. Sci. U. S. A.* 107, 14075–14080. doi:10.1073/pnas.1008850107.
- Li, A., Walling, J., Kotliarov, Y., Center, A., Steed, M. E., Ahn, S. J., et al. (2008). Genomic Changes and Gene Expression Profiles Reveal That Established Glioma Cell Lines Are Poorly Representative of Primary Human Gliomas. *Mol. Cancer Res.* 6, 21–30. doi:10.1158/1541-7786.MCR-07-0280.
- Li, Z., Zhang, Y., Tong, Y., Tong, J., and Thiele, C. J. (2015). Trk inhibitor attenuates the BDNF/TrkB-induced protection of neuroblastoma cells from etoposide in vitro and in vivo. *Cancer Biol. Ther.* 16, 477–483.

doi:10.1080/15384047.2015.1016659.

- Lim, B., Lin, Y., and Navin, N. (2020). Advancing Cancer Research and Medicine with Single-Cell Genomics. *Cancer Cell* 37, 456–470. doi:10.1016/j.ccell.2020.03.008.
- Lin, J. J., and Shaw, A. T. (2016). Resisting Resistance: Targeted Therapies in Lung Cancer. *Trends Cancer* 2, 350–364. doi:10.1016/j.trecan.2016.05.010.
- Linn Murphree, A. (2005). Intraocular retinoblastoma: the case for a new group classification. *Ophthalmol. Clin. N. Am.* 18, 41–53, viii. doi:10.1016/j.ohc.2004.11.003.
- Lista, M. J., Martins, R. P., Billant, O., Contesse, M.-A., Findakly, S., Pochard, P., et al. (2017). Nucleolin directly mediates Epstein-Barr virus immune evasion through binding to G-quadruplexes of EBNA1 mRNA. *Nat. Commun.* 8, 16043. doi:10.1038/ncomms16043.
- Liu, T., Liu, P. Y., Tee, A. E. L., Haber, M., Norris, M. D., Gleave, M. E., et al. (2009). Over-expression of clusterin is a resistance factor to the anti-cancer effect of histone deacetylase inhibitors. *Eur. J. Cancer Oxf. Engl.* 1990 45, 1846–1854. doi:10.1016/j.ejca.2009.03.002.
- Liu, Z., Chen, S. S., Clarke, S., Veschi, V., and Thiele, C. J. (2021). Targeting MYCN in Pediatric and Adult Cancers. *Front. Oncol.* 10. doi:10.3389/fonc.2020.623679.
- Lodrini, M., Oehme, I., Schroeder, C., Milde, T., Schier, M. C., Kopp-Schneider, A., et al. (2013). MYCN and HDAC2 cooperate to repress miR-183 signaling in neuroblastoma. *Nucleic Acids Res.* 41, 6018–6033. doi:10.1093/nar/gkt346.
- Lohmann, D. R., and Gallie, B. L. (2004). Retinoblastoma: revisiting the model prototype of inherited cancer. *Am. J. Med. Genet. C Semin. Med. Genet.* 129C, 23–28. doi:10.1002/ajmg.c.30024.
- London, W. B., Castel, V., Monclair, T., Ambros, P. F., Pearson, A. D. J., Cohn, S. L., et al. (2011). Clinical and biologic features predictive of survival after relapse of neuroblastoma: a report from the International Neuroblastoma Risk Group project. *J. Clin. Oncol. Off. J. Am. Soc. Clin. Oncol.* 29, 3286–3292. doi:10.1200/JCO.2010.34.3392.
- London, W. b., Castleberry, R. p., Matthay, K. k., Look, A. t., Seeger, R. c., Shimada, H., et al. (2005). Evidence for an Age Cutoff Greater Than 365 Days for Neuroblastoma Risk Group Stratification in the Children's Oncology Group. *J. Clin. Oncol.* 23, 6459–6465. doi:10.1200/JCO.2005.05.571.
- Look, A. T., Hayes, F. A., Shuster, J. J., Douglass, E. C., Castleberry, R. P., Bowman, L. C., et al. (1991). Clinical relevance of tumor cell ploidy and N-myc gene amplification in childhood neuroblastoma: a Pediatric Oncology Group study. *J. Clin. Oncol. Off. J. Am. Soc. Clin. Oncol.* 9, 581–591. doi:10.1200/JCO.1991.9.4.581.
- Lopez, G., Conkrite, K. L., Doepner, M., Rathi, K. S., Modi, A., Vaksman, Z., et al. (2020). Somatic structural variation targets neurodevelopmental genes and identifies SHANK2 as a tumor suppressor in neuroblastoma. *Genome Res.* 30, 1228–1242. doi:10.1101/gr.252106.119.
- Lu, J., Guan, S., Zhao, Y., Yu, Y., Woodfield, S. E., Zhang, H., et al. (2017). The second-generation ALK inhibitor alectinib effectively induces apoptosis in human neuroblastoma cells and inhibits tumor growth in a TH-MYCN transgenic neuroblastoma mouse model. *Cancer Lett.* 400, 61–68. doi:10.1016/j.canlet.2017.04.022.
- Lunardi, A., and Pandolfi, P. P. (2015). A co-clinical platform to accelerate cancer treatment optimization. *Trends Mol. Med.* 21, 1–5. doi:10.1016/j.molmed.2014.10.008.

- Maerken, T. V., Speleman, F., Vermeulen, J., Lambertz, I., Clercq, S. D., Smet, E. D., et al. (2006). Small-Molecule MDM2 Antagonists as a New Therapy Concept for Neuroblastoma. *Cancer Res.* 66, 9646–9655. doi:10.1158/0008-5472.CAN-06-0792.
- Malaney, P., Nicosia, S. V., and Davé, V. (2014). One mouse, one patient paradigm: New avatars of personalized cancer therapy. *Cancer Lett.* 344, 1–12. doi:10.1016/j.canlet.2013.10.010.
- Malikic, S., Jahn, K., Kuipers, J., Sahinalp, S. C., and Beerenwinkel, N. (2019). Integrative inference of subclonal tumour evolution from single-cell and bulk sequencing data. *Nat. Commun.* 10, 2750. doi:10.1038/s41467-019-10737-5.
- Maris, J. M., Mosse, Y. P., Bradfield, J. P., Hou, C., Monni, S., Scott, R. H., et al. (2008). Chromosome 6p22 locus associated with clinically aggressive neuroblastoma. *N. Engl. J. Med.* 358, 2585–2593. doi:10.1056/NEJMoa0708698.
- Marshall, G. M., Liu, P. Y., Gherardi, S., Scarlett, C. J., Bedalov, A., Xu, N., et al. (2011). SIRT1 promotes N-Myc oncogenesis through a positive feedback loop involving the effects of MKP3 and ERK on N-Myc protein stability. *PLoS Genet.* 7, e1002135. doi:10.1371/journal.pgen.1002135.
- Martin, M. (2011). Cutadapt removes adapter sequences from high-throughput sequencing reads. *EMBnet J.* 17, 10. doi:10.14806/ej.17.1.200.
- Maser, T., Zagorski, J., Kelly, S., Ostrander, A., Goodyke, A., Nagulapally, A., et al. (2020). The MDM2 inhibitor CGM097 combined with the BET inhibitor OTX015 induces cell death and inhibits tumor growth in models of neuroblastoma. *Cancer Med.* 9, 8144–8158. doi:10.1002/cam4.3407.
- Matthay, K., Atkinson, J. B., Stram, D. O., Selch, M., Reynolds, C. P., and Seeger, R. C. (1993). Patterns of relapse after autologous purged bone marrow transplantation for neuroblastoma: a Childrens Cancer Group pilot study. *J. Clin. Oncol. Off. J. Am. Soc. Clin. Oncol.* 11, 2226–2233. doi:10.1200/JCO.1993.11.11.2226.
- Matthay, K., George, R. E., and Yu, A. L. (2012). Promising therapeutic targets in neuroblastoma. *Clin. Cancer Res. Off. J. Am. Assoc. Cancer Res.* 18, 2740–2753. doi:10.1158/1078-0432.CCR-11-1939.
- Matthay, K. K., Maris, J. M., Schleiermacher, G., Nakagawara, A., Mackall, C. L., Diller, L., et al. (2016a). Neuroblastoma. *Nat. Rev. Dis. Primer* 2, 16078. doi:10.1038/nrdp.2016.78.
- Matthay, K., Maris, J. M., Schleiermacher, G., Nakagawara, A., Mackall, C. L., Diller, L., et al. (2016b). Neuroblastoma. *Nat. Rev. Dis. Primer* 2, 1–21. doi:10.1038/nrdp.2016.78.
- Matthay, K., Villablanca, J. G., Seeger, R. C., Stram, D. O., Harris, R. E., Ramsay, N. K., et al. (1999). Treatment of high-risk neuroblastoma with intensive chemotherapy, radiotherapy, autologous bone marrow transplantation, and 13-cis-retinoic acid. Children’s Cancer Group. *N. Engl. J. Med.* 341, 1165–1173. doi:10.1056/NEJM199910143411601.
- McEvoy, J., Nagahawatte, P., Finkelstein, D., Richards-Yutz, J., Valentine, M., Ma, J., et al. (2014). RB1 gene inactivation by chromothripsis in human retinoblastoma. *Oncotarget* 5, 438–450. doi:10.18632/oncotarget.1686.
- McGranahan, N., and Swanton, C. (2017). Clonal Heterogeneity and Tumor Evolution: Past, Present, and the Future. *Cell* 168, 613–628. doi:10.1016/j.cell.2017.01.018.
- McPherson, A. W., Chan, F. C., and Shah, S. P. (2018). Observing Clonal Dynamics across Spatiotemporal Axes: A Prelude to Quantitative Fitness Models for Cancer. *Cold Spring Harb. Perspect. Med.* 8, a029603. doi:10.1101/cshperspect.a029603.

- Merle, P., Gueugneau, M., Teulade-Fichou, M.-P., Müller-Barthélémy, M., Amiard, S., Chautard, E., et al. (2015). Highly efficient radiosensitization of human glioblastoma and lung cancer cells by a G-quadruplex DNA binding compound. *Sci. Rep.* 5, 16255. doi:10.1038/srep16255.
- Michaelis, M., Selt, F., Rothweiler, F., Löschmann, N., Nüsse, B., Dirks, W. G., et al. (2014). Aurora kinases as targets in drug-resistant neuroblastoma cells. *PLoS One* 9, e108758. doi:10.1371/journal.pone.0108758.
- Miles, L. A., Bowman, R. L., Merlinsky, T. R., Csete, I. S., Ooi, A. T., Durruthy-Durruthy, R., et al. (2020). Single-cell mutation analysis of clonal evolution in myeloid malignancies. *Nature* 587, 477–482. doi:10.1038/s41586-020-2864-x.
- Misale, S., Di Nicolantonio, F., Sartore-Bianchi, A., Siena, S., and Bardelli, A. (2014). Resistance to anti-EGFR therapy in colorectal cancer: from heterogeneity to convergent evolution. *Cancer Discov.* 4, 1269–1280. doi:10.1158/2159-8290.CD-14-0462.
- Miyazaki, M., Otomo, R., Matsushima-Hibiya, Y., Suzuki, H., Nakajima, A., Abe, N., et al. (2018). The p53 activator overcomes resistance to ALK inhibitors by regulating p53-target selectivity in ALK-driven neuroblastomas. *Cell Death Discov.* 4, 56. doi:10.1038/s41420-018-0059-0.
- Molenaar, J. J., Ebus, M. E., Geerts, D., Koster, J., Lamers, F., Valentijn, L. J., et al. (2009). Inactivation of CDK2 is synthetically lethal to MYCN over-expressing cancer cells. *Proc. Natl. Acad. Sci. U. S. A.* 106, 12968–12973. doi:10.1073/pnas.0901418106.
- Molenaar, J. J., Koster, J., Zwijnenburg, D. A., van Sluis, P., Valentijn, L. J., van der Ploeg, I., et al. (2012). Sequencing of neuroblastoma identifies chromothripsis and defects in neuritogenesis genes. *Nature* 483, 589–593. doi:10.1038/nature10910.
- Monchaud, D., and Teulade-Fichou, M.-P. (2008). A hitchhiker's guide to G-quadruplex ligands. *Org. Biomol. Chem.* 6, 627–636. doi:10.1039/b714772b.
- Monclair, T., Brodeur, G. M., Ambros, P. F., Brisse, H. J., Cecchetto, G., Holmes, K., et al. (2009). The International Neuroblastoma Risk Group (INRG) staging system: an INRG Task Force report. *J. Clin. Oncol. Off. J. Am. Soc. Clin. Oncol.* 27, 298–303. doi:10.1200/JCO.2008.16.6876.
- Mondal, G., Stevers, M., Goode, B., Ashworth, A., and Solomon, D. A. (2019). A requirement for STAG2 in replication fork progression creates a targetable synthetic lethality in cohesin-mutant cancers. *Nat. Commun.* 10, 1686. doi:10.1038/s41467-019-09659-z.
- Moreno, L., Pearson, A. D. J., Paoletti, X., Jimenez, I., Geoerger, B., Kearns, P. R., et al. (2017a). Early phase clinical trials of anticancer agents in children and adolescents - an ITCC perspective. *Nat. Rev. Clin. Oncol.* 14, 497–507. doi:10.1038/nrclinonc.2017.59.
- Moreno, L., Rubie, H., Varo, A., Le Deley, M. C., Amoroso, L., Chevance, A., et al. (2017b). Outcome of children with relapsed or refractory neuroblastoma: A meta-analysis of ITCC/SIOPEN European phase II clinical trials. *Pediatr. Blood Cancer* 64, 25–31. doi:10.1002/pbc.26192.
- Morgenstern, D. A., Pötschger, U., Moreno, L., Papadakis, V., Owens, C., Ash, S., et al. (2018). Risk stratification of high-risk metastatic neuroblastoma: A report from the HR-NBL-1/SIOPEN study. *Pediatr. Blood Cancer* 65, e27363. doi:https://doi.org/10.1002/pbc.27363.
- Morris, L. G. T., Riaz, N., Desrichard, A., Şenbabaoğlu, Y., Hakimi, A. A., Makarov, V., et al. (2016). Pan-cancer analysis of intratumor heterogeneity as a prognostic determinant of survival. *Oncotarget* 7, 10051–10063. doi:10.18632/oncotarget.7067.

- Mossé, Y. P., Deyell, R. J., Berthold, F., Nagakawara, A., Ambros, P. F., Monclair, T., et al. (2014). Neuroblastoma in older children, adolescents and young adults: a report from the International Neuroblastoma Risk Group project. *Pediatr. Blood Cancer* 61, 627–635. doi:10.1002/psc.24777.
- Mossé, Y. P., Laudenslager, M., Longo, L., Cole, K. A., Wood, A., Attiyeh, E. F., et al. (2008). Identification of ALK as a major familial neuroblastoma predisposition gene. *Nature* 455, 930–935. doi:10.1038/nature07261.
- Mossé, Y. P., Lipsitz, E., Fox, E., Teachey, D. T., Maris, J. M., Weigel, B., et al. (2012). Pediatric phase I trial and pharmacokinetic study of MLN8237, an investigational oral selective small-molecule inhibitor of Aurora kinase A: a Children’s Oncology Group Phase I Consortium study. *Clin. Cancer Res. Off. J. Am. Assoc. Cancer Res.* 18, 6058–6064. doi:10.1158/1078-0432.CCR-11-3251.
- Mühlethaler-Mottet, A., Meier, R., Flahaut, M., Bourlond, K. B., Nardou, K., Joseph, J.-M., et al. (2008). Complex molecular mechanisms cooperate to mediate histone deacetylase inhibitors anti-tumour activity in neuroblastoma cells. *Mol. Cancer* 7, 55. doi:10.1186/1476-4598-7-55.
- Müller, I., Larsson, K., Frenzel, A., Oliynyk, G., Zirath, H., Prochownik, E. V., et al. (2014). Targeting of the MYCN Protein with Small Molecule c-MYC Inhibitors. *PLOS ONE* 9, e97285. doi:10.1371/journal.pone.0097285.
- Munier, F. L. (2014). Classification and Management of Seeds in Retinoblastoma Ellsworth Lecture Ghent August 24th 2013. *Ophthalmic Genet.* 35, 193–207. doi:10.3109/13816810.2014.973045.
- Mur, P., García-Mulero, S., del Valle, J., Magraner-Pardo, L., Vidal, A., Pineda, M., et al. (2020). Role of POLE and POLD1 in familial cancer. *Genet. Med.* 22, 2089–2100. doi:10.1038/s41436-020-0922-2.
- Nagasaka, M., Ge, Y., Sukari, A., Kukreja, G., and Ou, S.-H. I. (2020). A user’s guide to lorlatinib. *Crit. Rev. Oncol. Hematol.* 151, 102969. doi:10.1016/j.critrevonc.2020.102969.
- Nam, A. S., Chaligne, R., and Landau, D. A. (2021). Integrating genetic and non-genetic determinants of cancer evolution by single-cell multi-omics. *Nat. Rev. Genet.* 22, 3–18. doi:10.1038/s41576-020-0265-5.
- Nardella, C., Lunardi, A., Patnaik, A., Cantley, L. C., and Pandolfi, P. P. (2011). The APL Paradigm and the “Co-Clinical Trial” Project. *Cancer Discov.* 1, 108–116. doi:10.1158/2159-8290.CD-11-0061.
- Némati, F., Sastre-Garau, X., Laurent, C., Couturier, J., Mariani, P., Desjardins, L., et al. (2010). Establishment and Characterization of a Panel of Human Uveal Melanoma Xenografts Derived from Primary and/or Metastatic Tumors. *Clin. Cancer Res.* 16, 2352–2362. doi:10.1158/1078-0432.CCR-09-3066.
- Newman, A. M., Bratman, S. V., To, J., Wynne, J. F., Eclow, N. C. W., Modlin, L. A., et al. (2014). An ultrasensitive method for quantitating circulating tumor DNA with broad patient coverage. *Nat. Med.* 20, 548–554. doi:10.1038/nm.3519.
- Nguyễn, L. B., Diskin, S. J., Capasso, M., Wang, K., Diamond, M. A., Glessner, J., et al. (2011). Phenotype Restricted Genome-Wide Association Study Using a Gene-Centric Approach Identifies Three Low-Risk Neuroblastoma Susceptibility Loci. *PLOS Genet.* 7, e1002026. doi:10.1371/journal.pgen.1002026.
- Nicolaides, T., Nazemi, K. J., Crawford, J., Kilburn, L., Minturn, J., Gajjar, A., et al. (2020). Phase I study of vemurafenib in children with recurrent or progressive BRAFV600E mutant brain tumors: Pacific Pediatric Neuro-Oncology Consortium study (PNOC-002). *Oncotarget* 11, 1942–1952. doi:10.18632/oncotarget.27600.
- Nobre, L., Zapotocky, M., Ramaswamy, V., Ryall, S., Bennett, J., Alderete, D., et al. (2020). Outcomes of BRAF

V600E Pediatric Gliomas Treated With Targeted BRAF Inhibition. *JCO Precis. Oncol.*, 561–571. doi:10.1200/PO.19.00298.

Nowell, P. C. (1976). The clonal evolution of tumor cell populations. *Science* 194, 23–28. doi:10.1126/science.959840.

Oberthuer, A., Hero, B., Berthold, F., Juraeva, D., Faldum, A., Kahlert, Y., et al. (2010). Prognostic impact of gene expression-based classification for neuroblastoma. *J. Clin. Oncol. Off. J. Am. Soc. Clin. Oncol.* 28, 3506–3515. doi:10.1200/JCO.2009.27.3367.

Oberthuer, A., Juraeva, D., Hero, B., Volland, R., Sterz, C., Schmidt, R., et al. (2015). Revised Risk Estimation and Treatment Stratification of Low- and Intermediate-Risk Neuroblastoma Patients by Integrating Clinical and Molecular Prognostic Markers. *Clin. Cancer Res.* 21, 1904–1915. doi:10.1158/1078-0432.CCR-14-0817.

Oehme, I., Deubzer, H. E., Lodrini, M., Milde, T., and Witt, O. (2009). Targeting of HDAC8 and investigational inhibitors in neuroblastoma. *Expert Opin. Investig. Drugs* 18, 1605–1617. doi:10.1517/14728220903241658.

Oehme, I., Linke, J.-P., Böck, B. C., Milde, T., Lodrini, M., Hartenstein, B., et al. (2013). Histone deacetylase 10 promotes autophagy-mediated cell survival. *Proc. Natl. Acad. Sci. U. S. A.* 110, E2592–2601. doi:10.1073/pnas.1300113110.

O’Neil, J., Benita, Y., Feldman, I., Chenard, M., Roberts, B., Liu, Y., et al. (2016). An Unbiased Oncology Compound Screen to Identify Novel Combination Strategies. *Mol. Cancer Ther.* 15, 1155–1162. doi:10.1158/1535-7163.MCT-15-0843.

Ortmann, C. A., Kent, D. G., Nangalia, J., Silber, Y., Wedge, D. C., Grinfeld, J., et al. (2015). Effect of Mutation Order on Myeloproliferative Neoplasms. <http://dx.doi.org/10.1056/NEJMoa1412098>. doi:10.1056/NEJMoa1412098.

Osajima-Hakomori, Y., Miyake, I., Ohira, M., Nakagawara, A., Nakagawa, A., and Sakai, R. (2005). Biological role of anaplastic lymphoma kinase in neuroblastoma. *Am. J. Pathol.* 167, 213–222. doi:10.1016/S0002-9440(10)62966-5.

Padovan-Merhar, O. M., Raman, P., Ostrovskaya, I., Kalletla, K., Rubnitz, K. R., Sanford, E. M., et al. (2016). Enrichment of Targetable Mutations in the Relapsed Neuroblastoma Genome. *PLoS Genet.* 12. doi:10.1371/journal.pgen.1006501.

Pao, W., Miller, V., Zakowski, M., Doherty, J., Politi, K., Sarkaria, I., et al. (2004). EGF receptor gene mutations are common in lung cancers from “never smokers” and are associated with sensitivity of tumors to gefitinib and erlotinib. *Proc. Natl. Acad. Sci.* 101, 13306–13311. doi:10.1073/pnas.0405220101.

Park, J. R., Eggert, A., and Caron, H. (2010). Neuroblastoma: Biology, Prognosis, and Treatment. *Hematol. Oncol. Clin. North Am.* 24, 65–86. doi:10.1016/j.hoc.2009.11.011.

Park, J. R., Kreissman, S. G., London, W. B., Naranjo, A., Cohn, S. L., Hogarty, M. D., et al. (2016). A phase III randomized clinical trial (RCT) of tandem myeloablative autologous stem cell transplant (ASCT) using peripheral blood stem cell (PBSC) as consolidation therapy for high-risk neuroblastoma (HR-NB): A Children’s Oncology Group (COG) study. *J. Clin. Oncol.* 34, LBA3–LBA3. doi:10.1200/JCO.2016.34.15_suppl.LBA3.

Park, J., Seo, J.-W., Ahn, N., Park, S., Hwang, J., and Nam, J.-W. (2019). UPF1/SMG7-dependent microRNA-mediated gene regulation. *Nat. Commun.* 10, 4181. doi:10.1038/s41467-019-12123-7.

- Parsons, B. L. (2018). Multiclonal tumor origin: Evidence and implications. *Mutat. Res. Mutat. Res.* 777, 1–18. doi:10.1016/j.mrrev.2018.05.001.
- Pauli, C., Hopkins, B. D., Prandi, D., Shaw, R., Fedrizzi, T., Sboner, A., et al. (2017). Personalized In Vitro and In Vivo Cancer Models to Guide Precision Medicine. *Cancer Discov.* 7, 462–477. doi:10.1158/2159-8290.CD-16-1154.
- Peifer, M., Hertwig, F., Roels, F., Drexler, D., Gattgruber, M., Menon, R., et al. (2015). Telomerase activation by genomic rearrangements in high-risk neuroblastoma. *Nature* 526, 700–704. doi:10.1038/nature14980.
- Persson, C. U., von Stedingk, K., Bexell, D., Merselius, M., Braekeveldt, N., Gisselsson, D., et al. (2017). Neuroblastoma patient-derived xenograft cells cultured in stem-cell promoting medium retain tumorigenic and metastatic capacities but differentiate in serum. *Sci. Rep.* 7, 10274. doi:10.1038/s41598-017-09662-8.
- Petroni, M., Veschi, V., Gulino, A., and Giannini, G. (2012). Molecular mechanisms of MYCN-dependent apoptosis and the MDM2-p53 pathway: an Achilles' heel to be exploited for the therapy of MYCN-amplified neuroblastoma. *Front. Oncol.* 2, 141. doi:10.3389/fonc.2012.00141.
- Pfaff, E., Adam de Beaumais, T., Marchais, A., van Tilburg, C. M., Blattner-Johnson, M., Dirksen, U., et al. (2021). NTRK Alterations in Pediatric High-Risk Malignancies Identified Through European Clinical Sequencing Programs Constitute Promising Drug Targets. *JCO Precis. Oncol.*, 450–454. doi:10.1200/PO.20.00417.
- Pfister, S. M., Jones, D. T., Jones, B. C., Prakash, B. G., Blattner-Johnson, M., Pfaff, E., et al. (2020). Abstract SY09-01: A comprehensive European approach to precision pediatric cancer medicine. *Cancer Res.* 80, SY09-SY09-01. doi:10.1158/1538-7445.AM2020-SY09-01.
- Phillips, C. J. (2020). Precision Medicine and its Imprecise History. *Harv. Data Sci. Rev.* 2. doi:10.1162/99608f92.3e85b56a.
- Piazza, A., Boulé, J.-B., Lopes, J., Mingo, K., Largy, E., Teulade-Fichou, M.-P., et al. (2010). Genetic instability triggered by G-quadruplex interacting Phen-DC compounds in *Saccharomyces cerevisiae*. *Nucleic Acids Res.* 38, 4337–4348. doi:10.1093/nar/gkq136.
- Pincez, T., Clément, N., Lapouble, E., Pierron, G., Kamal, M., Bieche, I., et al. (2017). Feasibility and clinical integration of molecular profiling for target identification in pediatric solid tumors. *Pediatr. Blood Cancer* 64. doi:10.1002/pbc.26365.
- Pinto, N., DuBois, S. G., Marachelian, A., Diede, S. J., Taraseviciute, A., Glade Bender, J. L., et al. (2018). Phase I study of vorinostat in combination with isotretinoin in patients with refractory/recurrent neuroblastoma: A new approaches to Neuroblastoma Therapy (NANT) trial. *Pediatr. Blood Cancer* 65, e27023. doi:10.1002/pbc.27023.
- Pinto, N. R., Applebaum, M. A., Volchenboum, S. L., Matthay, K. K., London, W. B., Ambros, P. F., et al. (2015). Advances in Risk Classification and Treatment Strategies for Neuroblastoma. *J. Clin. Oncol.* 33, 3008–3017. doi:10.1200/JCO.2014.59.4648.
- Pugh, T. J., Morozova, O., Attiyeh, E. F., Asgharzadeh, S., Wei, J. S., Auclair, D., et al. (2013). The genetic landscape of high-risk neuroblastoma. *Nat. Genet.* 45, 279–284. doi:10.1038/ng.2529.
- Puissant, A., Frumm, S. M., Alexe, G., Bassil, C. F., Qi, J., Chanthery, Y. H., et al. (2013). Targeting MYCN in neuroblastoma by BET bromodomain inhibition. *Cancer Discov.* 3, 308–323. doi:10.1158/2159-8290.CD-12-0418.

- Qiu, Y.-Y., Mirkin, B. L., and Dwivedi, R. S. (2005). Inhibition of DNA methyltransferase reverses cisplatin induced drug resistance in murine neuroblastoma cells. *Cancer Detect. Prev.* 29, 456–463. doi:10.1016/j.cdp.2005.05.004.
- Rader, J., Russell, M. R., Hart, L. S., Nakazawa, M. S., Belcastro, L. T., Martinez, D., et al. (2013). Dual CDK4/CDK6 inhibition induces cell-cycle arrest and senescence in neuroblastoma. *Clin. Cancer Res. Off. J. Am. Assoc. Cancer Res.* 19, 6173–6182. doi:10.1158/1078-0432.CCR-13-1675.
- Rampias, T. (2020). Exploring the Eco-Evolutionary Dynamics of Tumor Subclones. *Cancers* 12, 3436. doi:10.3390/cancers12113436.
- Regan, R. D., Fenyk-Melody, J. E., Tran, S. M., Chen, G., and Stocking, K. L. (2016). Comparison of Submental Blood Collection with the Retroorbital and Submandibular Methods in Mice (*Mus musculus*). *J. Am. Assoc. Lab. Anim. Sci. JAALAS* 55, 570–576.
- Rettig, I., Koeneke, E., Trippel, F., Mueller, W. C., Burhenne, J., Kopp-Schneider, A., et al. (2015). Selective inhibition of HDAC8 decreases neuroblastoma growth in vitro and in vivo and enhances retinoic acid-mediated differentiation. *Cell Death Dis.* 6, e1657. doi:10.1038/cddis.2015.24.
- Reynolds, C. P., Matthay, K. K., Villablanca, J. G., and Maurer, B. J. (2003). Retinoid therapy of high-risk neuroblastoma. *Cancer Lett.* 197, 185–192. doi:10.1016/s0304-3835(03)00108-3.
- Reznichenko, O., Quillévéré, A., Martins, R. P., Loaëc, N., Kang, H., Lista, M. J., et al. (2019). Novel cationic bis(acylhydrazones) as modulators of Epstein-Barr virus immune evasion acting through disruption of interaction between nucleolin and G-quadruplexes of EBNA1 mRNA. *Eur. J. Med. Chem.* 178, 13–29. doi:10.1016/j.ejmech.2019.05.042.
- Rihani, A., Vandesompele, J., Speleman, F., and Van Maerken, T. (2015). Inhibition of CDK4/6 as a novel therapeutic option for neuroblastoma. *Cancer Cell Int.* 15, 76. doi:10.1186/s12935-015-0224-y.
- Robinson, J. T., Thorvaldsdóttir, H., Wenger, A. M., Zehir, A., and Mesirov, J. P. (2017). Variant Review with the Integrative Genomics Viewer. *Cancer Res.* 77, e31–e34. doi:10.1158/0008-5472.CAN-17-0337.
- Rocchi, P., Tonelli, R., Camerin, C., Purgato, S., Fronza, R., Bianucci, F., et al. (2005). p21Waf1/Cip1 is a common target induced by short-chain fatty acid HDAC inhibitors (valproic acid, tributyrin and sodium butyrate) in neuroblastoma cells. *Oncol. Rep.* 13, 1139–1144.
- Rodriguez-Galindo, C., Orbach, D. B., and VanderVeen, D. (2015). Retinoblastoma. *Pediatr. Clin. North Am.* 62, 201–223. doi:10.1016/j.pcl.2014.09.014.
- Rokita, J. L., Rathi, K. S., Cardenas, M. F., Upton, K. A., Jayaseelan, J., Cross, K. L., et al. (2019). Genomic Profiling of Childhood Tumor Patient-Derived Xenograft Models to Enable Rational Clinical Trial Design. *Cell Rep.* 29, 1675–1689.e9. doi:10.1016/j.celrep.2019.09.071.
- Rosfjord, E., Lucas, J., Li, G., and Gerber, H.-P. (2014). Advances in patient-derived tumor xenografts: from target identification to predicting clinical response rates in oncology. *Biochem. Pharmacol.* 91, 135–143. doi:10.1016/j.bcp.2014.06.008.
- Rushlow, D. E., Mol, B. M., Kennett, J. Y., Yee, S., Pajovic, S., Thériault, B. L., et al. (2013). Characterisation of retinoblastomas without RB1 mutations: genomic, gene expression, and clinical studies. *Lancet Oncol.* 14, 327–334. doi:10.1016/S1470-2045(13)70045-7.
- Saarinen-Pihkala, U. M., Jahnukainen, K., Wikström, S., Koivusalo, A., Karikoski, R., Sariola, H., et al. (2013). Ultrahigh-risk group within the high-risk neuroblastoma category. *J. Pediatr. Hematol. Oncol.* 35, e254–259. doi:10.1097/MPH.0b013e318287326b.

- Sakamoto, H., Tsukaguchi, T., Hiroshima, S., Kodama, T., Kobayashi, T., Fukami, T. A., et al. (2011). CH5424802, a selective ALK inhibitor capable of blocking the resistant gatekeeper mutant. *Cancer Cell* 19, 679–690. doi:10.1016/j.ccr.2011.04.004.
- Sala, A. (2015). Editorial: Targeting MYCN in Pediatric Cancers. *Front. Oncol.* 4. doi:10.3389/fonc.2014.00330.
- Salk, J. J., Schmitt, M. W., and Loeb, L. A. (2018). Enhancing the accuracy of next-generation sequencing for detecting rare and subclonal mutations. *Nat. Rev. Genet.* 19, 269–285. doi:10.1038/nrg.2017.117.
- Salviat, F., Gauthier-Villars, M., Carton, M., Cassoux, N., Lumbroso-Le Rouic, L., Dehainault, C., et al. (2020). Association Between Genotype and Phenotype in Consecutive Unrelated Individuals With Retinoblastoma. *JAMA Ophthalmol.* 138, 843–850. doi:10.1001/jamaophthalmol.2020.2100.
- Sammons, H. M., and Starkey, E. S. (2012). Ethical issues of clinical trials in children. *Paediatr. Child Health* 22, 47–50. doi:10.1016/j.paed.2011.04.011.
- Sanmartín, E., Muñoz, L., Piqueras, M., Sierol, J. A., Berlanga, P., Cañete, A., et al. (2017). Deletion of 11q in Neuroblastomas Drives Sensitivity to PARP Inhibition. *Clin. Cancer Res.* 23, 6875–6887. doi:10.1158/1078-0432.CCR-17-0593.
- Sasaki, T., Okuda, K., Zheng, W., Butrynski, J., Capelletti, M., Wang, L., et al. (2010). The neuroblastoma-associated F1174L ALK mutation causes resistance to an ALK kinase inhibitor in ALK-translocated cancers. *Cancer Res.* 70, 10038–10043. doi:10.1158/0008-5472.CAN-10-2956.
- Schleiermacher, G. (2020). Abstract IA06: New strategies for multidimensional molecular characterization and follow-up of high-risk pediatric cancers. *Cancer Res.* 80, IA06–IA06. doi:10.1158/1538-7445.PEDCA19-IA06.
- Schleiermacher, G., Janoueix-Lerosey, I., Ribeiro, A., Klijanienko, J., Couturier, J., Pierron, G., et al. (2010). Accumulation of segmental alterations determines progression in neuroblastoma. *J. Clin. Oncol. Off. J. Am. Soc. Clin. Oncol.* 28, 3122–3130. doi:10.1200/JCO.2009.26.7955.
- Schleiermacher, G., Javanmardi, N., Bernard, V., Leroy, Q., Cappo, J., Rio Frio, T., et al. (2014). Emergence of new ALK mutations at relapse of neuroblastoma. *J. Clin. Oncol. Off. J. Am. Soc. Clin. Oncol.* 32, 2727–2734. doi:10.1200/JCO.2013.54.0674.
- Schrader, K. A., Cheng, D. T., Joseph, V., Prasad, M., Walsh, M., Zehir, A., et al. (2016). Germline Variants in Targeted Tumor Sequencing Using Matched Normal DNA. *JAMA Oncol.* 2, 104–111. doi:10.1001/jamaoncol.2015.5208.
- Schramm, A., Köster, J., Assenov, Y., Althoff, K., Peifer, M., Mahlow, E., et al. (2015). Mutational dynamics between primary and relapse neuroblastomas. *Nat. Genet.* 47, 872–877. doi:10.1038/ng.3349.
- Schubert, N. A., Schild, L., van Oirschot, S., Keller, K. M., Alles, L. K., Vernooij, L., et al. (2021). Combined targeting of the p53 and pRb pathway in neuroblastoma does not lead to synergistic responses. *Eur. J. Cancer* 142, 1–9. doi:10.1016/j.ejca.2020.10.009.
- Schulte, J. H., and Eggert, A. (2021). ALK Inhibitors in Neuroblastoma: A Sprint from Bench to Bedside. *Clin. Cancer Res.*, clincanres.0627.2021. doi:10.1158/1078-0432.CCR-21-0627.
- Schulte, J. H., Moreno, L., Ziegler, D. S., Marshall, L. V., Zwaan, C. M., Irwin, M., et al. (2020). Final analysis of phase I study of ceritinib in pediatric patients with malignancies harboring activated anaplastic lymphoma kinase (ALK). *J. Clin. Oncol.* 38, 10505–10505. doi:10.1200/JCO.2020.38.15_suppl.10505.
- Schwab, M., Alitalo, K., Klempnauer, K. H., Varmus, H. E., Bishop, J. M., Gilbert, F., et al. (1983). Amplified DNA

with limited homology to myc cellular oncogene is shared by human neuroblastoma cell lines and a neuroblastoma tumour. *Nature* 305, 245–248. doi:10.1038/305245a0.

- Schwarzenbach, H., Hoon, D. S. B., and Pantel, K. (2011a). Cell-free nucleic acids as biomarkers in cancer patients. *Nat. Rev. Cancer* 11, 426–437. doi:10.1038/nrc3066.
- Schwarzenbach, H., Hoon, D. S. B., and Pantel, K. (2011b). Cell-free nucleic acids as biomarkers in cancer patients. *Nat. Rev. Cancer* 11, 426–437. doi:10.1038/nrc3066.
- Schwarzenbach, H., Stoeckl, J., Pantel, K., and Goekkurt, E. (2008a). Detection and monitoring of cell-free DNA in blood of patients with colorectal cancer. *Ann. N. Y. Acad. Sci.* 1137, 190–196. doi:10.1196/annals.1448.025.
- Schwarzenbach, H., Stoeckl, J., Pantel, K., and Goekkurt, E. (2008b). Detection and monitoring of cell-free DNA in blood of patients with colorectal cancer. *Ann. N. Y. Acad. Sci.* 1137, 190–196. doi:10.1196/annals.1448.025.
- Seeger, R. C., Brodeur, G. M., Sather, H., Dalton, A., Siegel, S. E., Wong, K. Y., et al. (1985). Association of multiple copies of the N-myc oncogene with rapid progression of neuroblastomas. *N. Engl. J. Med.* 313, 1111–1116. doi:10.1056/NEJM198510313131802.
- Seibel, N. L., Janeway, K., Allen, C. E., Chi, S. N., Cho, Y.-J., Glade Bender, J. L., et al. (2017). Pediatric oncology enters an era of precision medicine. *Curr. Probl. Cancer* 41, 194–200. doi:10.1016/j.crrproblcancer.2017.01.002.
- Seimiya, H. (2020). Crossroads of telomere biology and anticancer drug discovery. *Cancer Sci.* 111, 3089–3099. doi:10.1111/cas.14540.
- Shahbazi, J., Liu, P. Y., Atmadibrata, B., Bradner, J. E., Marshall, G. M., Lock, R. B., et al. (2016). The Bromodomain Inhibitor JQ1 and the Histone Deacetylase Inhibitor Panobinostat Synergistically Reduce N-Myc Expression and Induce Anticancer Effects. *Clin. Cancer Res. Off. J. Am. Assoc. Cancer Res.* 22, 2534–2544. doi:10.1158/1078-0432.CCR-15-1666.
- Shields, C. L., Schoenberg, E., Kocher, K., Shukla, S. Y., Kaliki, S., and Shields, J. A. (2013). Lesions simulating retinoblastoma (pseudoretinoblastoma) in 604 cases: results based on age at presentation. *Ophthalmology* 120, 311–316. doi:10.1016/j.optha.2012.07.067.
- Shin, H.-T., Choi, Y.-L., Yun, J. W., Kim, N. K. D., Kim, S.-Y., Jeon, H. J., et al. (2017). Prevalence and detection of low-allele-fraction variants in clinical cancer samples. *Nat. Commun.* 8, 1377. doi:10.1038/s41467-017-01470-y.
- Shoemaker, R. H. (2006). The NCI60 human tumour cell line anticancer drug screen. *Nat. Rev. Cancer* 6, 813–823. doi:10.1038/nrc1951.
- Shoemaker, R. H., Monks, A., Alley, M. C., Scudiero, D. A., Fine, D. L., McLemore, T. L., et al. (1988). Development of human tumor cell line panels for use in disease-oriented drug screening. *Prog. Clin. Biol. Res.* 276, 265–286.
- Shofuda, T., and Kanemura, Y. (2021). HDACs and MYC in medulloblastoma: how do HDAC inhibitors control MYC-amplified tumors? *Neuro-Oncol.* 23, 173–174. doi:10.1093/neuonc/noaa292.
- Squire, J., Thorner, P., Marrano, P., Parkinson, D., Ng, Y., Gerrie, B., et al. (1996). Identification of mycn copy number heterogeneity by direct fish analysis of neuroblastoma preparations. *Mol. Diagn.* 1, 281–289. doi:10.1016/S1084-8592(96)70010-3.

- Stanton, M. J., Dutta, S., Zhang, H., Polavaram, N. S., Leontovich, A. A., Hönscheid, P., et al. (2013). Autophagy control by the VEGF-C/NRP-2 axis in cancer and its implication for treatment resistance. *Cancer Res.* 73, 160–171. doi:10.1158/0008-5472.CAN-11-3635.
- Stewart, E., Federico, S. M., Chen, X., Shelat, A. A., Bradley, C., Gordon, B., et al. (2017). Orthotopic Patient-Derived Xenografts of Pediatric Solid Tumors. *Nature* 549, 96–100. doi:10.1038/nature23647.
- Stiller, C. A., and Parkin, D. M. (1992). International variations in the incidence of neuroblastoma. *Int. J. Cancer* 52, 538–543. doi:10.1002/ijc.2910520407.
- Stockhausen, M.-T., Sjölund, J., Manetopoulos, C., and Axelson, H. (2005). Effects of the histone deacetylase inhibitor valproic acid on Notch signalling in human neuroblastoma cells. *Br. J. Cancer* 92, 751–759. doi:10.1038/sj.bjc.6602309.
- Sun, Y., Liu, P. Y., Scarlett, C. J., Malyukova, A., Liu, B., Marshall, G. M., et al. (2014). Histone deacetylase 5 blocks neuroblastoma cell differentiation by interacting with N-Myc. *Oncogene* 33, 2987–2994. doi:10.1038/onc.2013.253.
- Sun, Z., Jiang, Q., Li, J., and Guo, J. (2020). The potent roles of salt-inducible kinases (SIKs) in metabolic homeostasis and tumorigenesis. *Signal Transduct. Target. Ther.* 5, 1–15. doi:10.1038/s41392-020-00265-w.
- Swanton, C., McGranahan, N., Starrett, G. J., and Harris, R. S. (2015). APOBEC Enzymes: Mutagenic Fuel for Cancer Evolution and Heterogeneity. *Cancer Discov.* 5, 704–712. doi:10.1158/2159-8290.CD-15-0344.
- Swarbrick, A., Woods, S. L., Shaw, A., Balakrishnan, A., Phua, Y., Nguyen, A., et al. (2010). miR-380-5p represses p53 to control cellular survival and is associated with poor outcome in MYCN-amplified neuroblastoma. *Nat. Med.* 16, 1134–1140. doi:10.1038/nm.2227.
- Tabassum, D. P., and Polyak, K. (2015). Tumorigenesis: it takes a village. *Nat. Rev. Cancer* 15, 473–483. doi:10.1038/nrc3971.
- Tew, B. Y., Legendre, C., Schroeder, M. A., Triche, T., Gooden, G. C., Huang, Y., et al. (2020). Patient-derived xenografts of central nervous system metastasis reveal expansion of aggressive minor clones. *Neuro-Oncol.* 22, 70–83. doi:10.1093/neuonc/noz137.
- Thiele, C. J., Reynolds, C. P., and Israel, M. A. (1985). Decreased expression of N-myc precedes retinoic acid-induced morphological differentiation of human neuroblastoma. *Nature* 313, 404–406. doi:10.1038/313404a0.
- Thole, T. M., Toedling, J., Sprüssel, A., Pfeil, S., Savelyeva, L., Capper, D., et al. (2020). Reflection of neuroblastoma intratumor heterogeneity in the new OHC-NB1 disease model. *Int. J. Cancer* 146, 1031–1041. doi:https://doi.org/10.1002/ijc.32572.
- Thompson, P. M., Maris, J. M., Hogarty, M. D., Seeger, R. C., Reynolds, C. P., Brodeur, G. M., et al. (2001). Homozygous Deletion of CDKN2A (p16INK4a/p14ARF) but not within 1p36 or at Other Tumor Suppressor Loci in Neuroblastoma. *Cancer Res.* 61, 679–686.
- Trigg, R. M., and Turner, S. D. (2018). ALK in Neuroblastoma: Biological and Therapeutic Implications. *Cancers* 10. doi:10.3390/cancers10040113.
- Trochet, D., Bourdeaut, F., Janoueix-Lerosey, I., Deville, A., de Pontual, L., Schleiermacher, G., et al. (2004). Germline mutations of the paired-like homeobox 2B (PHOX2B) gene in neuroblastoma. *Am. J. Hum. Genet.* 74, 761–764. doi:10.1086/383253.

- Tucker, E. R., George, S., Angelini, P., Bruna, A., and Chesler, L. (2021). The Promise of Patient-Derived Preclinical Models to Accelerate the Implementation of Personalised Medicine for Children with Neuroblastoma. *J. Pers. Med.* 11. doi:10.3390/jpm11040248.
- Tweddle, D. A., Pearson, A. D. J., Haber, M., Norris, M. D., Xue, C., Flemming, C., et al. (2003). The p53 pathway and its inactivation in neuroblastoma. *Cancer Lett.* 197, 93–98. doi:10.1016/S0304-3835(03)00088-0.
- Umapathy, G., Guan, J., Gustafsson, D. E., Javanmardi, N., Cervantes-Madrid, D., Djos, A., et al. (2017). MEK inhibitor trametinib does not prevent the growth of anaplastic lymphoma kinase (ALK)-addicted neuroblastomas. *Sci. Signal.* 10. doi:10.1126/scisignal.aam7550.
- Valencia-Sama, I., Ladumor, Y., Kee, L., Adderley, T., Christopher, G., Robinson, C. M., et al. (2020). NRAS Status Determines Sensitivity to SHP2 Inhibitor Combination Therapies Targeting the RAS-MAPK Pathway in Neuroblastoma. *Cancer Res.* 80, 3413–3423. doi:10.1158/0008-5472.CAN-19-3822.
- Valentijn, L. J., Koster, J., Zwijnenburg, D. A., Hasselt, N. E., van Sluis, P., Volckmann, R., et al. (2015). TERT rearrangements are frequent in neuroblastoma and identify aggressive tumors. *Nat. Genet.* 47, 1411–1414. doi:10.1038/ng.3438.
- Van Goethem, A., Yigit, N., Moreno-Smith, M., Vasudevan, S. A., Barbieri, E., Speleman, F., et al. (2017). Dual targeting of MDM2 and BCL2 as a therapeutic strategy in neuroblastoma. *Oncotarget* 8, 57047–57057. doi:10.18632/oncotarget.18982.
- van Groningen, T., Koster, J., Valentijn, L. J., Zwijnenburg, D. A., Akogul, N., Hasselt, N. E., et al. (2017). Neuroblastoma is composed of two super-enhancer-associated differentiation states. *Nat. Genet.* 49, 1261–1266. doi:10.1038/ng.3899.
- Van Maerken, T., Ferdinande, L., Taideman, J., Lambertz, I., Yigit, N., Vercruyse, L., et al. (2009). Antitumor activity of the selective MDM2 antagonist nutlin-3 against chemoresistant neuroblastoma with wild-type p53. *J. Natl. Cancer Inst.* 101, 1562–1574. doi:10.1093/jnci/djp355.
- van Tilburg, C. M., Pfaff, E., Pajtler, K. W., Langenberg, K. P. S., Fiesel, P., Jones, B. C., et al. (2020). The pediatric precision oncology study INFORM: Clinical outcome and benefit for molecular subgroups. *J. Clin. Oncol.* 38, LBA10503–LBA10503. doi:10.1200/JCO.2020.38.18_suppl.LBA10503.
- Venesio, T., Siravegna, G., Bardelli, A., and Sapino, A. (2018). Liquid Biopsies for Monitoring Temporal Genomic Heterogeneity in Breast and Colon Cancers. *Pathobiology* 85, 146–154. doi:10.1159/000473882.
- Venkatesan, S., Swanton, C., Taylor, B. S., and Costello, J. F. (2017). Treatment-Induced Mutagenesis and Selective Pressures Sculpt Cancer Evolution. *Cold Spring Harb. Perspect. Med.* 7. doi:10.1101/cshperspect.a026617.
- Verga, D., Hamon, F., Poyer, F., Bombard, S., and Teulade-Fichou, M.-P. (2014). Photo-cross-linking probes for trapping G-quadruplex DNA. *Angew. Chem. Int. Ed Engl.* 53, 994–998. doi:10.1002/anie.201307413.
- Vermeulen, J., De Preter, K., Naranjo, A., Vercruyse, L., Van Roy, N., Hellemans, J., et al. (2009). Predicting outcomes for children with neuroblastoma using a multigene-expression signature: a retrospective SIOPEN/COG/GPOH study. *Lancet Oncol.* 10, 663–671. doi:10.1016/S1470-2045(09)70154-8.
- Veschi, V., and Thiele, C. J. (2017). High-SETD8 inactivates p53 in neuroblastoma. *Oncoscience* 4, 21–22. doi:10.18632/oncoscience.344.
- Volik, S., Alcaide, M., Morin, R. D., and Collins, C. (2016). Cell-free DNA (cfDNA): Clinical Significance and Utility in Cancer Shaped By Emerging Technologies. *Mol. Cancer Res. MCR* 14, 898–908.

doi:10.1158/1541-7786.MCR-16-0044.

- Wang, C., Liu, Z., Woo, C.-W., Li, Z., Wang, L., Wei, J. S., et al. (2012). EZH2 Mediates epigenetic silencing of neuroblastoma suppressor genes CASZ1, CLU, RUNX3, and NGFR. *Cancer Res.* 72, 315–324. doi:10.1158/0008-5472.CAN-11-0961.
- Wang, H. Q., Halilovic, E., Li, X., Liang, J., Cao, Y., Rakiec, D. P., et al. (2017a). Combined ALK and MDM2 inhibition increases antitumor activity and overcomes resistance in human ALK mutant neuroblastoma cell lines and xenograft models. *eLife* 6. doi:10.7554/eLife.17137.
- Wang, K., Li, M., and Hakonarson, H. (2010). ANNOVAR: functional annotation of genetic variants from high-throughput sequencing data. *Nucleic Acids Res.* 38, e164–e164. doi:10.1093/nar/gkq603.
- Wang, P., Greiner, T. C., Lushnikova, T., and Eischen, C. M. (2006). Decreased Mdm2 expression inhibits tumor development induced by loss of ARF. *Oncogene* 25, 3708–3718. doi:10.1038/sj.onc.1209411.
- Wang, Y., Wu, N., Sun, D., Sun, H., Tong, D., Liu, D., et al. (2017b). NUBPL, a novel metastasis-related gene, promotes colorectal carcinoma cell motility by inducing epithelial-mesenchymal transition. *Cancer Sci.* 108, 1169–1176. doi:10.1111/cas.13243.
- Wang, Y., Yang, J., Wild, A. T., Wu, W. H., Shah, R., Danussi, C., et al. (2019). G-quadruplex DNA drives genomic instability and represents a targetable molecular abnormality in ATRX-deficient malignant glioma. *Nat. Commun.* 10, 943. doi:10.1038/s41467-019-08905-8.
- Watson, L. A., Solomon, L. A., Li, J. R., Jiang, Y., Edwards, M., Shin-ya, K., et al. (2013). Atrx deficiency induces telomere dysfunction, endocrine defects, and reduced life span. *J. Clin. Invest.* 123, 2049–2063. doi:10.1172/JCI65634.
- Weinstein, J. N., Myers, T. G., O'Connor, P. M., Friend, S. H., Fornace, A. J., Kohn, K. W., et al. (1997). An Information-Intensive Approach to the Molecular Pharmacology of Cancer. *Science* 275, 343–349. doi:10.1126/science.275.5298.343.
- West, J., You, L., Zhang, J., Gatenby, R. A., Brown, J. S., Newton, P. K., et al. (2020). Towards Multidrug Adaptive Therapy. *Cancer Res.* 80, 1578–1589. doi:10.1158/0008-5472.CAN-19-2669.
- Wilson, B. G., Wang, X., Shen, X., McKenna, E. S., Lemieux, M. E., Cho, Y.-J., et al. (2010). Epigenetic antagonism between polycomb and SWI/SNF complexes during oncogenic transformation. *Cancer Cell* 18, 316–328. doi:10.1016/j.ccr.2010.09.006.
- Wood, A. C., Krytska, K., Ryles, H. T., Infarinato, N. R., Sano, R., Hansel, T. D., et al. (2017). Dual ALK and CDK4/6 Inhibition Demonstrates Synergy against Neuroblastoma. *Clin. Cancer Res. Off. J. Am. Assoc. Cancer Res.* 23, 2856–2868. doi:10.1158/1078-0432.CCR-16-1114.
- Worst, B. C., van Tilburg, C. M., Balasubramanian, G. P., Fiesel, P., Witt, R., Freitag, A., et al. (2016). Next-generation personalised medicine for high-risk paediatric cancer patients - The INFORM pilot study. *Eur. J. Cancer Oxf. Engl.* 1990 65, 91–101. doi:10.1016/j.ejca.2016.06.009.
- Wu, J.-C., Jiang, H.-M., Yang, X.-H., and Zheng, H.-C. (2018). ING5-mediated antineuroblastoma effects of suberoylanilide hydroxamic acid. *Cancer Med.* 7, 4554–4569. doi:10.1002/cam4.1634.
- Wyce, A., Ganji, G., Smitheman, K. N., Chung, C., Korenchuk, S., Bai, Y., et al. (2013). BET Inhibition Silences Expression of MYCN and BCL2 and Induces Cytotoxicity in Neuroblastoma Tumor Models. *PLoS ONE* 8. doi:10.1371/journal.pone.0072967.
- Xiao, D., Yue, M., Su, H., Ren, P., Jiang, J., Li, F., et al. (2016). Polo-like Kinase-1 Regulates Myc Stabilization and

Activates a Feedforward Circuit Promoting Tumor Cell Survival. *Mol. Cell* 64, 493–506. doi:10.1016/j.molcel.2016.09.016.

Xu, D.-Q., Toyoda, H., Yuan, X.-J., Qi, L., Chelakkot, V. S., Morimoto, M., et al. (2018). Anti-tumor effect of AZD8055 against neuroblastoma cells in vitro and in vivo. *Exp. Cell Res.* 365, 177–184. doi:10.1016/j.yexcr.2018.02.032.

Yang, Q., Tian, Y., Liu, S., Zeine, R., Chlenski, A., Salwen, H. R., et al. (2007). Thrombospondin-1 peptide ABT-510 combined with valproic acid is an effective antiangiogenesis strategy in neuroblastoma. *Cancer Res.* 67, 1716–1724. doi:10.1158/0008-5472.CAN-06-2595.

Yang, Y., Ding, L., Zhou, Q., Fen, L., Cao, Y., Sun, J., et al. (2020). Silencing of AURKA augments the antitumor efficacy of the AURKA inhibitor MLN8237 on neuroblastoma cells. *Cancer Cell Int.* 20, 9. doi:10.1186/s12935-019-1072-y.

Yates, L. R., Gerstung, M., Knappskog, S., Desmedt, C., Gundem, G., Van Loo, P., et al. (2015). Subclonal diversification of primary breast cancer revealed by multiregion sequencing. *Nat. Med.* 21, 751–759. doi:10.1038/nm.3886.

Yu, Y., Tencer, A., Xuan, H., Kutateladze, T. G., and Shi, X. (2021). ZZEF1 is a Histone Reader and Transcriptional Coregulator of Krüppel-Like Factors. *J. Mol. Biol.* 433, 166722. doi:10.1016/j.jmb.2020.11.021.

Yuan, S., Norgard, R. J., and Stanger, B. Z. (2019). Cellular Plasticity in Cancer. *Cancer Discov.* 9, 837–851. doi:10.1158/2159-8290.CD-19-0015.

Zafar, A., Wang, W., Liu, G., Wang, X., Xian, W., McKeon, F., et al. (2021). Molecular targeting therapies for neuroblastoma: Progress and challenges. *Med. Res. Rev.* 41, 961–1021. doi:https://doi.org/10.1002/med.21750.

Zareifar, S., Shakibzad, N., Zekavat, O. R., Bordbar, M., and Shahriari, M. (2020). Successful treatment of refractory metastatic neuroblastoma with panobinostat in combination with chemotherapy agents and iodine-131-meta-iodobenzylguanidine therapy. *J. Oncol. Pharm. Pract. Off. Publ. Int. Soc. Oncol. Pharm. Pract.* 26, 481–486. doi:10.1177/1078155219852670.

Zehir, A., Benayed, R., Shah, R. H., Syed, A., Middha, S., Kim, H. R., et al. (2017). Mutational landscape of metastatic cancer revealed from prospective clinical sequencing of 10,000 patients. *Nat. Med.* 23, 703–713. doi:10.1038/nm.4333.

Zeineldin, M., Federico, S., Chen, X., Fan, Y., Xu, B., Stewart, E., et al. (2020). MYCN amplification and ATRX mutations are incompatible in neuroblastoma. *Nat. Commun.* 11, 913. doi:10.1038/s41467-020-14682-6.

Zhang, J., Benavente, C. A., McEvoy, J., Flores-Otero, J., Ding, L., Chen, X., et al. (2012). A novel retinoblastoma therapy from genomic and epigenetic analyses. *Nature* 481, 329–334. doi:10.1038/nature10733.

Zhang, W., Mao, J.-H., Zhu, W., Jain, A. K., Liu, K., Brown, J. B., et al. (2016). Centromere and kinetochore gene misexpression predicts cancer patient survival and response to radiotherapy and chemotherapy. *Nat. Commun.* 7, 12619. doi:10.1038/ncomms12619.

Zhao, G., Wang, G., Bai, H., Li, T., Gong, F., Yang, H., et al. (2017). Targeted inhibition of HDAC8 increases the doxorubicin sensitivity of neuroblastoma cells via up regulation of miR-137. *Eur. J. Pharmacol.* 802, 20–26. doi:10.1016/j.ejphar.2017.02.035.

Zou, H. Y., Friboulet, L., Kodack, D. P., Engstrom, L. D., Li, Q., West, M., et al. (2015). PF-06463922, an ALK/ROS1 Inhibitor, Overcomes Resistance to First and Second Generation ALK Inhibitors in

Appendix

Appendix 1: Supplementary table 1

List of the drugs used for PDTC high-throughput drug screening included in the in-house library, COMPASS library or both.

DRUG NAME	TYPE	PUTATIVE TARGET	LIBRARY
3-Deazaneplanocin A	Differentiating/ epigenetic modifier	EZH2	In-house
4SC-202	HDAC inhibitor	HDAC-I, LSD1	In-house
A-1155463	Kinase inhibitor	BCL-XL	COMPASS
A-1210477	Kinase inhibitor	MCL-1	COMPASS
A-1331852	Kinase inhibitor	BCL-XL	COMPASS
Abexinostat	HDAC inhibitor	HDAC-I, HDAC-II	In-house
Afatinib	Kinase inhibitor	EGFR	COMPASS
Alectinib	ALK inhibitor	ALK	Both
AMG-232	Apoptotic modulator	MDM2	COMPASS
APR-246	Apoptotic modulator	p53 activator	COMPASS
Axitinib	Kinase inhibitor	VEGFR, PDGFR, KIT	COMPASS
AZ6102	PARP inhibitor	TNKS1, TNKS2	In-house
AZD1208	Kinase inhibitor	Pim	In-house
AZD1480	Kinase inhibitor	JAK1, JAK2	In-house
AZD2461	PARP inhibitor	PARP1	In-house
Baricitinib	Kinase inhibitor	JAK1, JAK2	In-house
Belinostat	HDAC inhibitor	HDAC-I, HDAC-II, HDAC-IV	In-house
BIX 01294	Differentiating/ epigenetic modifier	G9a	In-house
Bortezomib	Chemotherapy	26S subunit proteasome	COMPASS
Bromosporin	Differentiating/ epigenetic modifier	BRD2, BRD4, BRD9, CECR2	In-house
Busulfan	Chemotherapy	Alkylating agent	COMPASS
Cabozantinib	Kinase inhibitor	VEGFR2, Met, FLT3, Tie2, Kit, Ret	COMPASS
Carboplatin	Chemotherapy	Alkylating agent	In-house
Ceritinib	ALK inhibitor	ALK	Both
Chloroquine	Chemotherapy	Antimalaria agent; chemo/radiosensitizer	COMPASS
Cisplatin	Chemotherapy	Alylating agent	COMPASS
Cobimetinib	Kinase inhibitor	MEK1, MEK2	COMPASS
Crizotinib	ALK inhibitor	ALK	Both
CUDC-907	HDAC inhibitor	HDAC, PI3K	In-house
Cytarabine	Chemotherapy	Antimetabolite	COMPASS
Dabrafenib	Kinase inhibitor	BRAF V600E	COMPASS
Dactinomycin	Chemotherapy	RNA-DNA synthesis inhibitor	COMPASS
Dasatinib	Kinase inhibitor	Abl, Src, Kit, EphR	COMPASS
Daunorubicin	Chemotherapy	Topoisomerase II inhibitor	COMPASS
Decitabine	Differentiating/ epigenetic modifier	Cytidine analog	COMPASS
Doxorubicin	Chemotherapy	Intercalating agent	Both
Entinostat	HDAC inhibitor	HDAC-I	Both

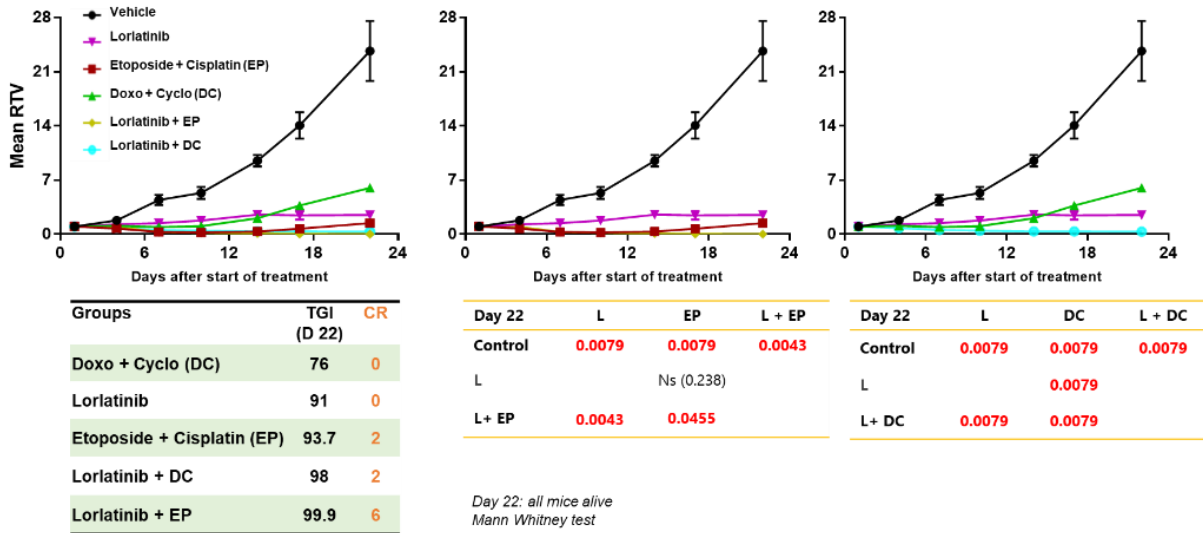
Entrectinib	Kinase inhibitor	TRK, ROS1, ALK	COMPASS
Erlotinib	Kinase inhibitor	EGFR	COMPASS
Etoposide	Chemotherapy	Topoisomerase inhibitor	Both
Everolimus	mTOR inhibitor	mTOR	Both
Fedratinib	Kinase inhibitor	JAK2	In-house
Foretinib	Kinase inhibitor	MET, VEGFR2	COMPASS
Gemcitabine	Chemotherapy	Antimetabolite	COMPASS
I-BET151	Differentiating/ epigenetic modifier	BRD2, BRD3, BRD4, BRD9	COMPASS
Idasanutlin	Apoptotic modulator	MDM2	Both
Imatinib	Kinase inhibitor	Abl, Kit, PDGFRB	COMPASS
IOX1	Differentiating/ epigenetic modifier	2OG, JMJD	In-house
IOX2	Kinase inhibitor	PHD2	In-house
Irinotecan	Chemotherapy	Topoisomerase I inhibitor	COMPASS
JNJ-7706621	Kinase inhibitor	AURKA, AURKB, CDK1, CDK2	In-house
KW-2449	Kinase inhibitor	FLT3, ABL, AURK	In-house
Lapatinib	Kinase inhibitor	HER2, EGFR	COMPASS
Larotrectinib	Kinase inhibitor	TRK	COMPASS
Lorlatinib	ALK inhibitor	ALK	Both
Melphalan	Chemotherapy	Alkylating agent	COMPASS
Mercaptopurine	Chemotherapy	Antimetabolite	COMPASS
Merestinib	Kinase inhibitor	Met inhibitor	COMPASS
Methotrexate	Chemotherapy	Antimetabolite; Anti-folate	COMPASS
Mitoxantrone	Chemotherapy	Topoisomerase II inhibitor	COMPASS
ML324	Differentiating/ epigenetic modifier	JMJD2	In-house
MS436	Differentiating/ epigenetic modifier	PMRT	In-house
Navitoclax	Apoptotic modulator	Bcl-2/Bcl-xL inhibitor	COMPASS
Nilotinib	Kinase inhibitor	Abl	COMPASS
Olaparib	PARP inhibitor	PARP1	Both
Paclitaxel	Chemotherapy	Mitotic inhibitor	COMPASS
Pacritinib	Kinase inhibitor	JK2	In-house
Palbociclib	Kinase inhibitor	DK4/6 inhibitor	COMPASS
Panobinostat	HDAC inhibitor	Pan-HDAC	Both
Pazopanib	Kinase inhibitor	VEGFR inhibitor	COMPASS
PFI-1	Differentiating/ epigenetic modifier	BRD4, BRD2	In-house
PFI-3	Differentiating/ epigenetic modifier	SMARCA2/4	In-house
Ponatinib	Kinase inhibitor	Broad TK inhibitor	COMPASS
Quisinostat	HDAC inhibitor	HDAC-I, HDAC-II	In-house
Resminostat	HDAC inhibitor	HDAC-VI	In-house
Resveratrol	Other	Natural Antioxidant	In-house
RG2833	HDAC inhibitor	HDAC-I, HDAC-III	In-house
Ribociclib	Kinase inhibitor	CDK4, CDK6	Both
Roxadustat	Other	HIF	In-house
Ruxolitinib	Kinase inhibitor	JAK1, JAK2	COMPASS
Scriptaid	HDAC inhibitor	HDAC-I	In-house
Selinexor	Apoptotic modulator	CRM1 inhibitor	COMPASS
Selumetinib	Kinase inhibitor	MEK1, MEK2, ERK1, ERK2	In-house
Selumetinib	Kinase inhibitor	MEK1, MEK2	COMPASS
Sirolimus	mTOR inhibitor	mTOR	COMPASS
Sorafenib	Kinase inhibitor	BRAF, FGFR-1, VEGFR-2/3, PDGFR β , KIT, FLT3	COMPASS

Sunitinib	Kinase inhibitor	Broad T inhibitor	COMPASS
Talazoparib	PARP inhibitor	PARP1, PARP2	COMPASS
Tasocitinib	Kinase inhibitor	JAK2	In-house
Tazemetostat	Differentiating/ epigenetic modifier	EZH2	Both
Temozolomide	Chemotherapy	Alkylating agent	COMPASS
Temsirolimus	mTOR inhibitor	mTOR	Both
TG101209	Kinase inhibitor	JAK2	In-house
Thioguanine	Chemotherapy	Antimetabolite, Purine analog	COMPASS
Thiotepa	Chemotherapy	Alkylating agent	COMPASS
Tofacitinib Citrate	Kinase inhibitor	JAK2	In-house
Topotecan	Chemotherapy	Topoisomerase I inhibitor	COMPASS
Trametinib	Kinase inhibitor	MEK1, MEK2	Both
Trichostatin	HDAC inhibitor	HDAC-I, HDAC-II	In-house
UNC0631	Differentiating/ epigenetic modifier	G9a	In-house
Valproic acid	HDAC inhibitor	HDAC	COMPASS
Vandetanib	Kinase inhibitor	VEGFR, EGFR, RET	COMPASS
Vemurafenib	Kinase inhibitor	B-Raf(V600E)	COMPASS
Venetoclax	Apoptotic modulator	Bcl-2-selective inhibitor	COMPASS
Vinblastine	Chemotherapy	Mitotic inhibitor	COMPASS
Vincristine	Chemotherapy	Mitotic inhibitor	COMPASS
Vinorelbine	Chemotherapy	Mitotic inhibitor	COMPASS
Vismodegib	Other	Smothered (Hh) inhibitor	COMPASS
Volasertib	Kinase inhibitor	PLK1	COMPASS
Vorinostat	HDAC inhibitor	HDAC-I	Both
WHI-P154	Kinase inhibitor	JAK3	In-house
WP1066	Kinase inhibitor	STAT3, JAK2	In-house
Zebularine	Differentiating/ epigenetic modifier	Cytidine analog	In-house
ZM447439	Kinase inhibitor	AURKA, AURKB	In-house

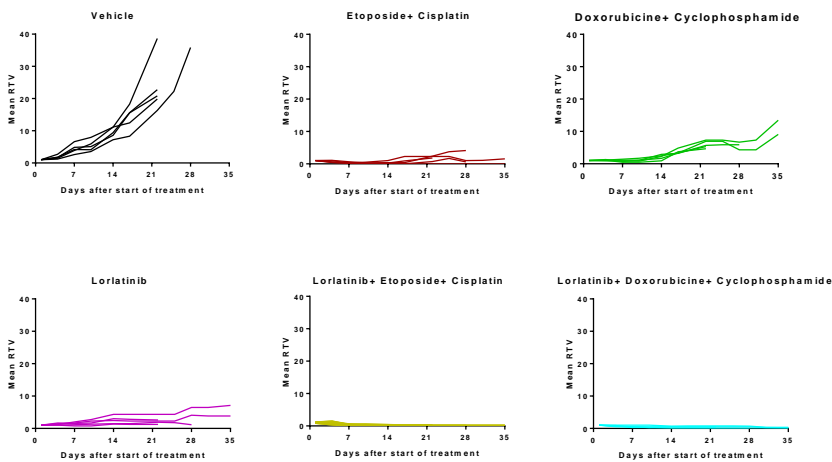
Appendix 2: treatment efficacy charts

Model GR-NB4

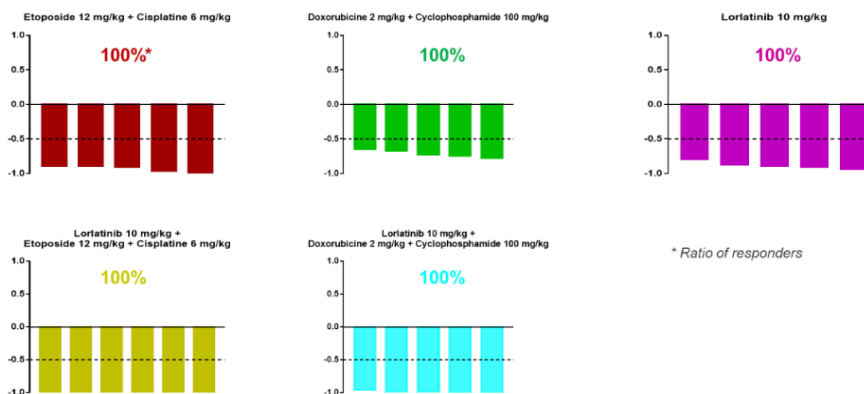
Relative tumor volume (mean)



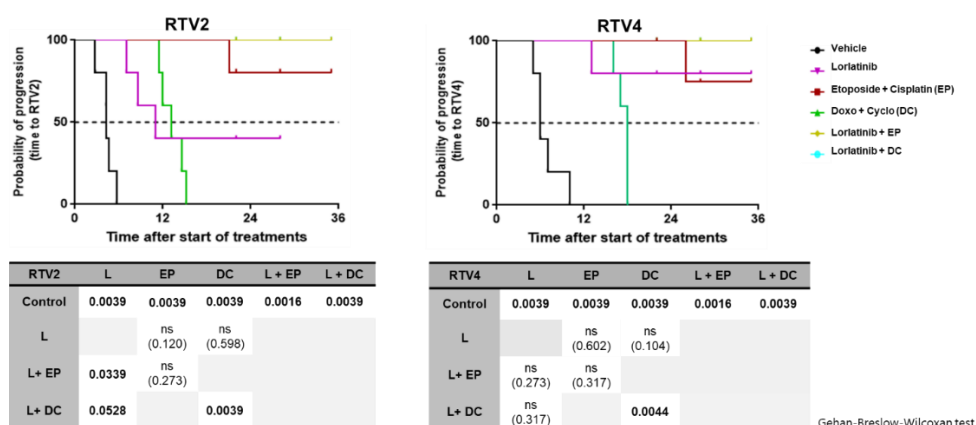
Individual RTV



Individual ORR



Probability of progression (RTV2 and RTV4)



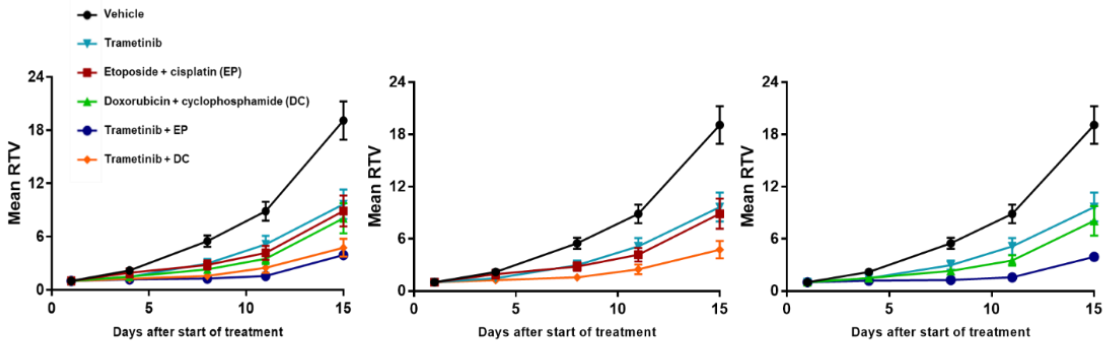
Conclusions

This *in vivo* experiment was interrupted early due to COVID-19, but available conclusion could be formulated, as follow:

- Lorlatinib alone showed significant efficacy on GR-NB4, with a TGI of 91%.
- Combination of lorlatinib with cisplatin-etoposide increased significantly the efficacy of chemotherapy alone or lorlatinib alone (six complete responses were obtained compared to two for chemotherapy alone)
- Combination of lorlatinib with doxorubicin-cyclophosphamide significantly increased the antitumor efficacy of chemotherapy alone or lorlatinib alone (two complete responses were obtained in the group combining lorlatinib with doxorubicin + cyclophosphamide).

These results showed that lorlatinib alone was highly efficient in the GR-NB4 model and that combination of lorlatinib with either doxorubicine-cyclophosphamide or etoposide-cisplatin significantly increased its antitumor efficiency and complete response rates.

Relative tumor volume (mean)

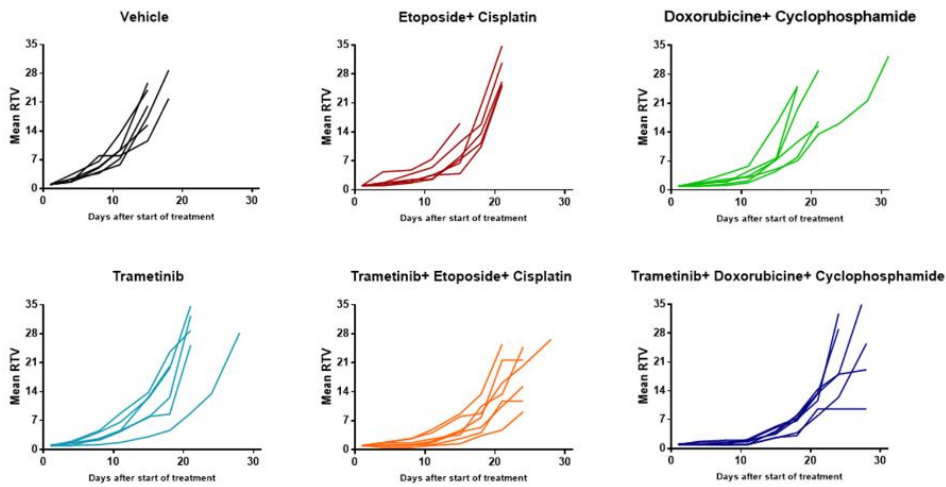


Groups	TG (day 15)
Trametinib	49
Etoposide + cisplatin (EP)	53
Doxorubicin + cyclophosphamide (DC)	58
Trametinib + EP	75
Trametinib+ DC	79

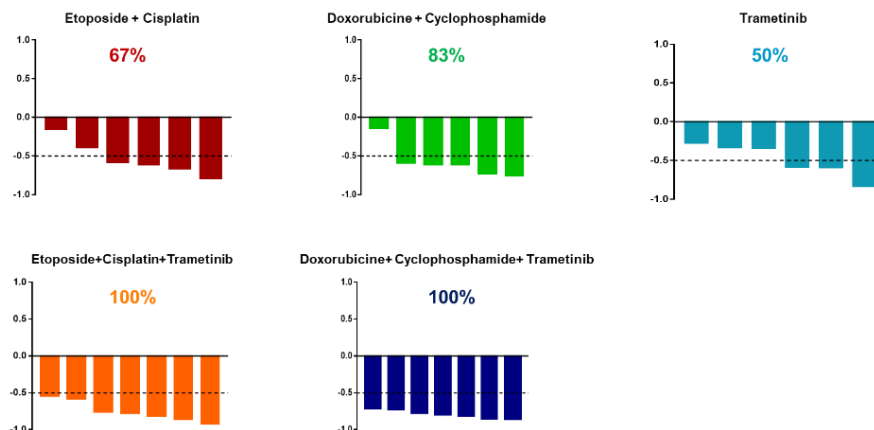
d15	T	EP	T + EP
Control	0.0152	0.0087	0.0012
T		ns (0.623)	
T + EP	ns (0.0798)	ns (0.1096)	

d15	T	DC	T + DC
Control	0.0152	0.0087	0.0012
T		ns (0.329)	
T + CD	0.0221	0.0082	

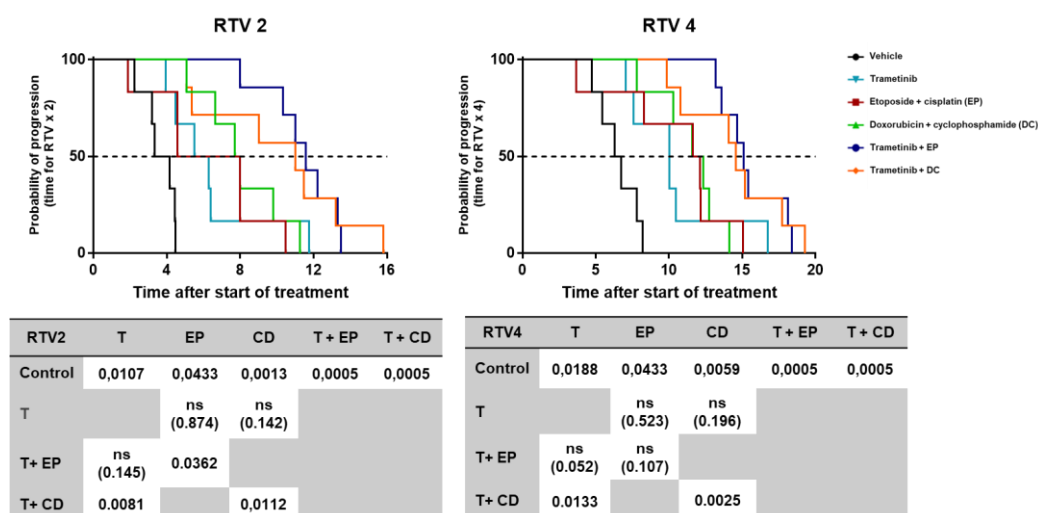
Individual RTV



Individual ORR



Probability of progression (RTV2 and RTV4)



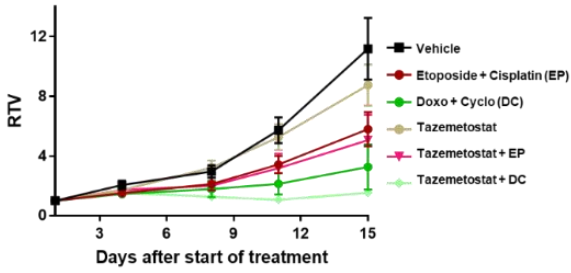
Conclusions

This *in vivo* experiment was interrupted early due to COVID-19, but available conclusion could be formulated, as follow:

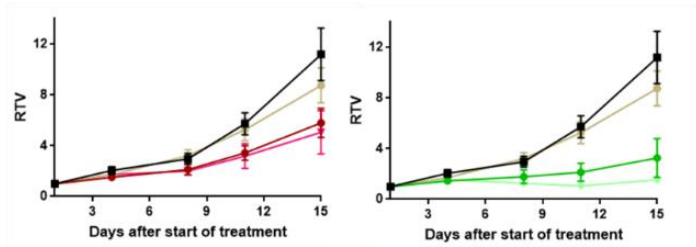
- Trametinib alone showed low efficacy on GR-NB10 model, with a TGI of 49%
- Combination of trametinib with cisplatin-etoposide was not more efficient than chemotherapy or trametinib alone
- Combination of trametinib with doxorubicin-cyclophosphamide was significantly more efficient than trametinib or chemotherapy alone, even at the early state of experiment

These results showed that trametinib alone was slightly efficient in the GR-NB10 model and that its combination with doxorubicine-cyclophosphamide significantly increased its antitumor efficacy, but not with etoposde-cisplatin.

Relative tumor volume (mean)

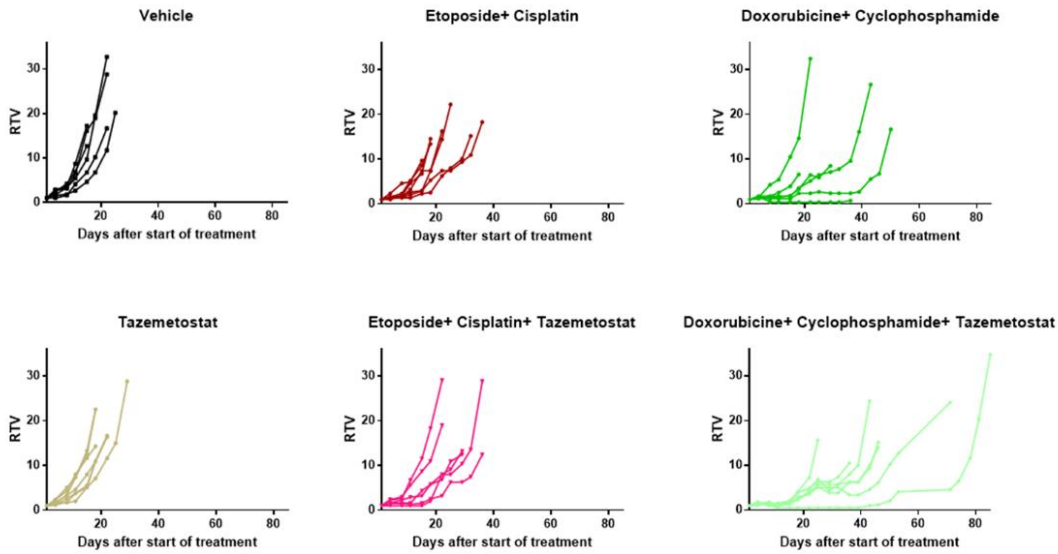


Groups	TGI (day 15)
Tazemetostat	22
Etoposide + Cisplatin	48
Doxorubicin + Cyclophosphamide	71
Tazemetostat+ Etoposide + Cisplatin	55
Tazemetostat+ doxorubicin+ cyclo	86

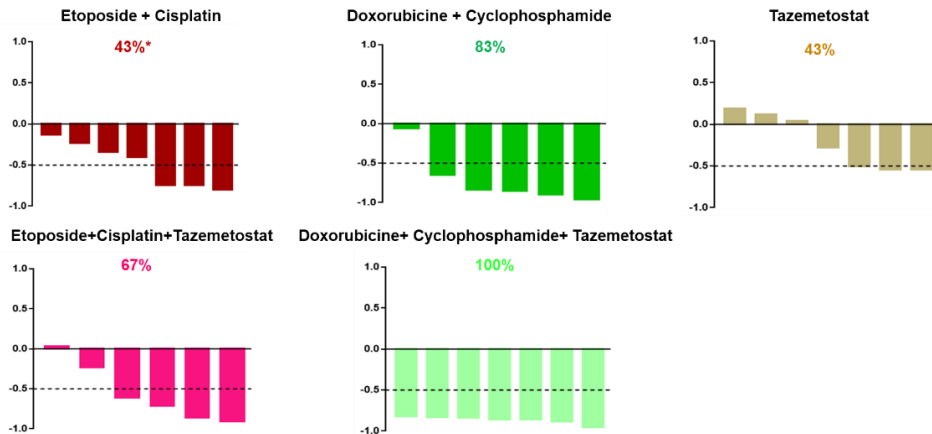


Day 15	TAZ	EP	TAZ+ EP	Day 15	TAZ	CD	TAZ+CD
Control	ns 0.4452	ns 0.0798	0.0411	Control	ns 0.4452	0.0152	0.0012
TAZ		ns 0.2086		TAZ		0.014	
TAZ+ EP	ns 0.0734	ns 0.8357		TAZ+ CD	0.0006	ns 0.8357	

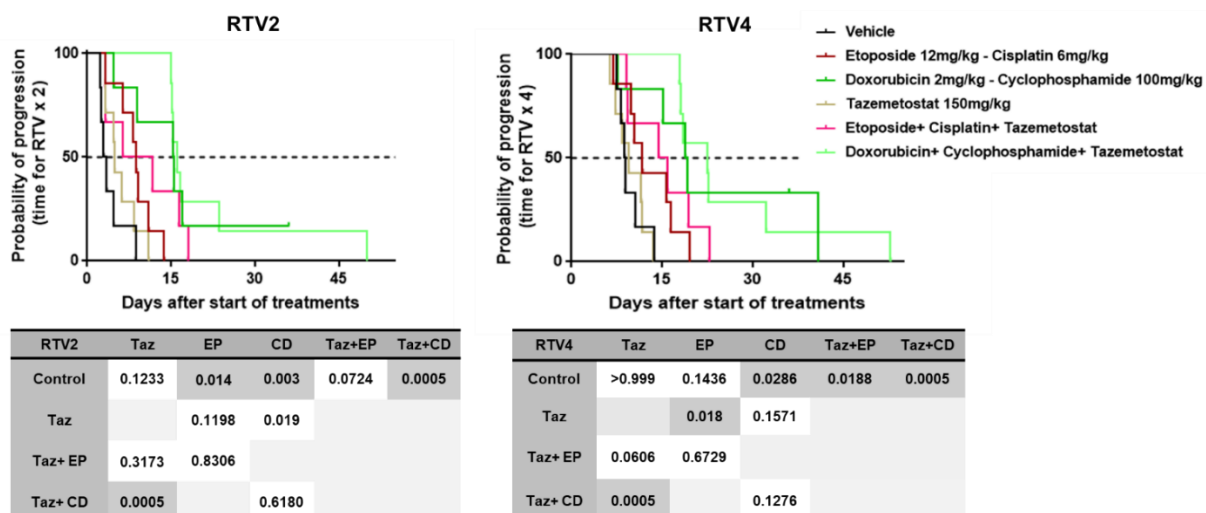
Individual RTV



Individual ORR



Probability of progression (RTV2 and RTV4)



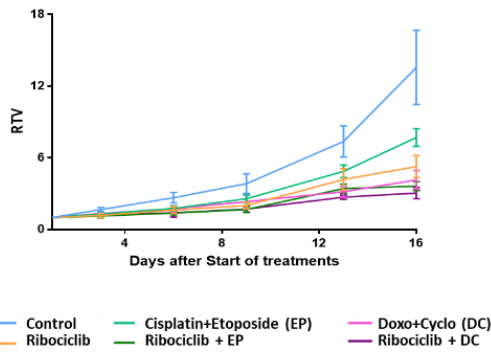
Conclusions

This *in vivo* experiment allowed us to draw the following conclusions concerning treatment efficacy:

- Tazemetostat alone showed no efficacy on HSJD-NB-005 PDX, with a TGI of 22%.
- Combination of tazemetostat with cisplatin + etoposide did not increase the efficacy of cisplatin + etoposide or tazemetostat alone; but this combination increased the number of responders compared to tazemetostat alone or cisplatin + etoposide alone.
- Combination of tazemetostat with doxorubicin + cyclophosphamide significantly increased the antitumor efficacy of tazemetostat ($p = 0.0006$) but not the antitumor effect of doxorubicin + cyclophosphamide alone.

All results showed that (1) tazemetostat was no efficiency in the NB005 neuroblastoma PDX and that combination of Tazemetostat with doxorubicine + cyclophosphamide or etoposide+ cisplatin didn't increase significantly antitumor efficiency of chemotherapies.

Relative tumor volume (mean)

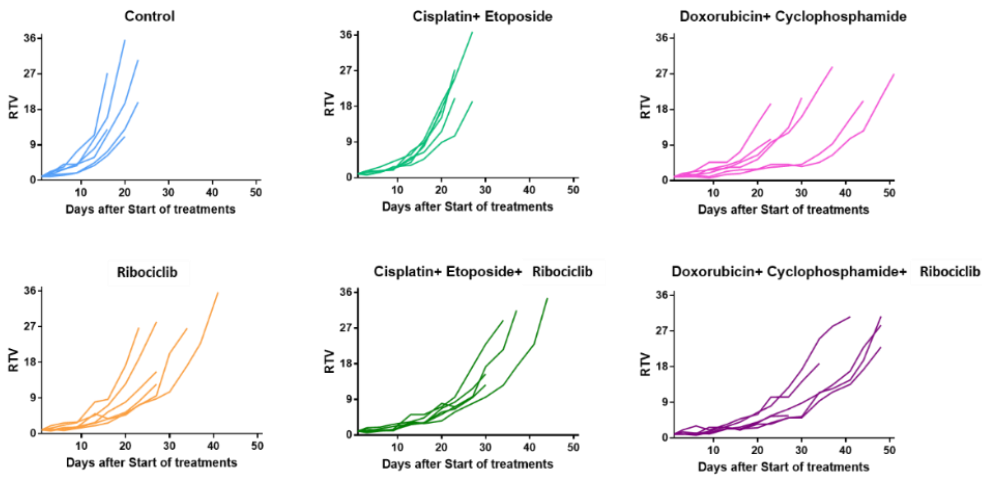


D16	Control	Ribociclib	Etoposide + Cisplatin	Doxo + Cycloph.
Ribociclib	$p = 0,0152$			
Etoposide + Cisplatin (EP)	NS			
Doxo + Cyclophosphamide (DC)	$p = 0,0043$			
Ribociclib + EP	$p = 0,022$	NS	NS*	
Ribociclib + DC	$p = 0,0022$	NS		NS

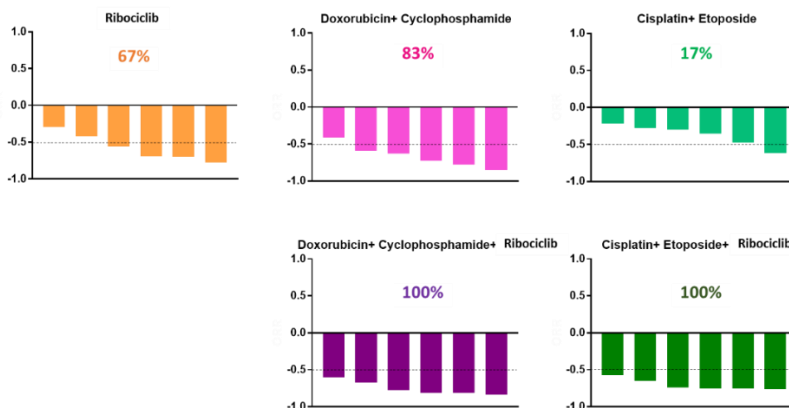
Groups	TGI (D 22)
Ribociclib	61
Etoposide + Cisplatin (EP)	43
Doxo + Cyclophosphamide (DC)	70
Ribociclib + EP	73
Ribociclib + DC	78

* At day 20, $p = 0,0022$.

Individual RTV



Individual ORR



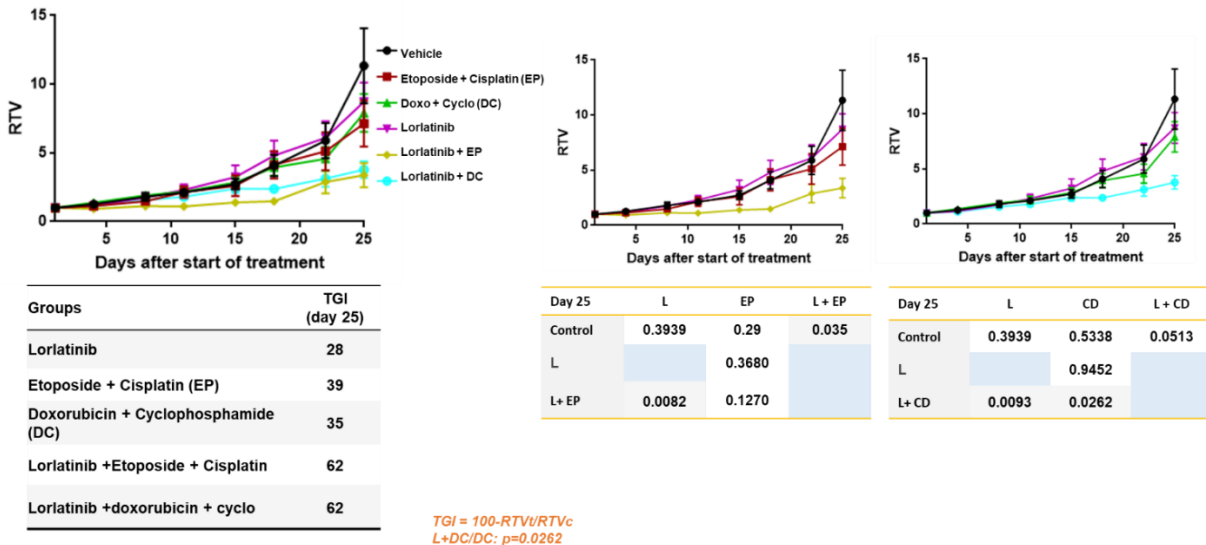
Conclusions

This *in vivo* experiment allowed us to draw the following conclusions concerning treatment efficacy:

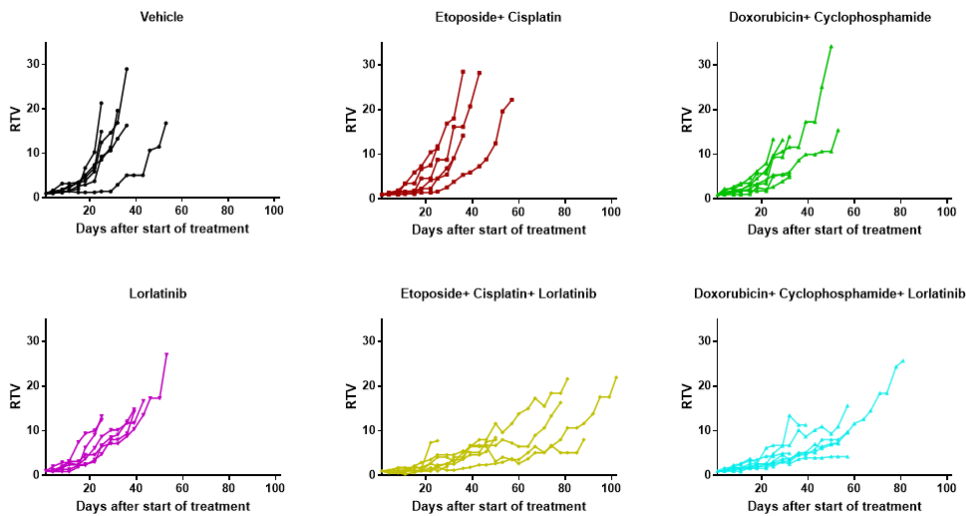
- Ribociclib alone showed significant efficacy on IC-pPDX-17, with a TGI of 61%.
- Combination of doxorubicin and cyclophosphamide to Ribociclib was not significantly more efficient than chemotherapy or ribociclib alone
- Combination of Cisplatin and Etoposide to Ribociclib was not significantly more efficient than chemotherapy or ribociclib alone, but showed a significant increase of TGI at day 20.

These results showed that Ribociclib was significantly efficient in IC-pPDX-17 PDX and that its combination with cisplatin / etoposide significantly increased chemotherapy efficiency.

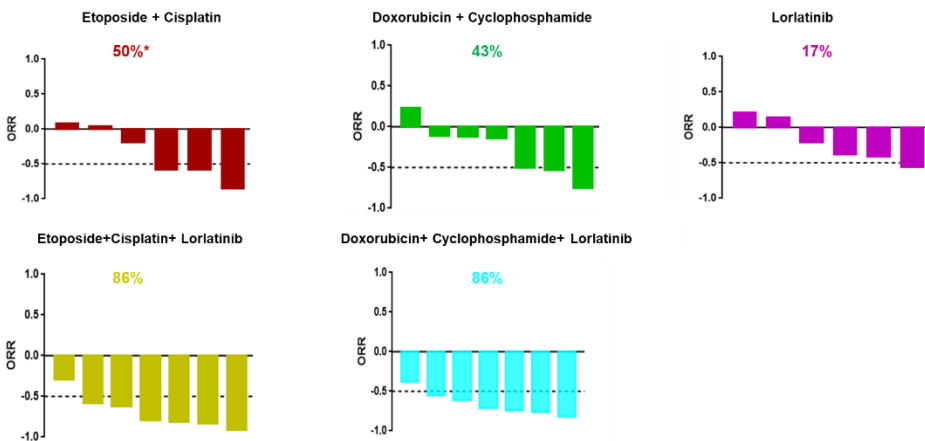
Relative tumor volume (mean)



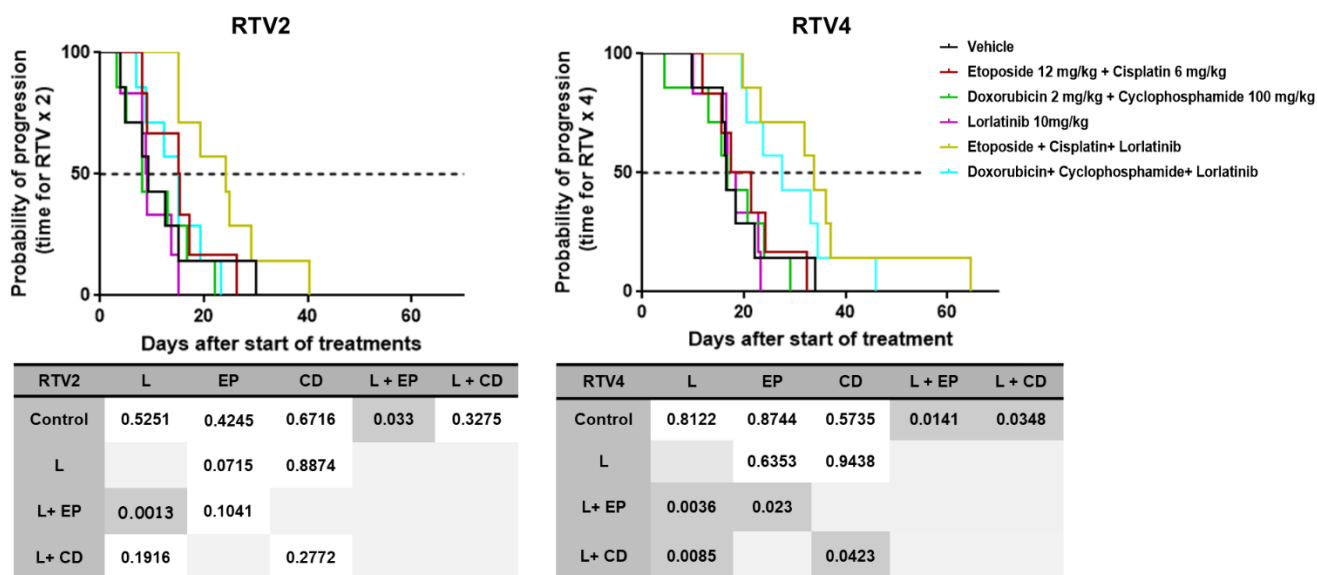
Individual RTV



Individual ORR



Probability of progression (RTV2 and RTV4)



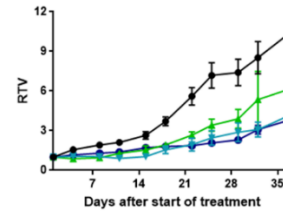
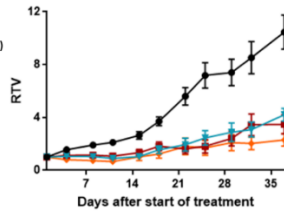
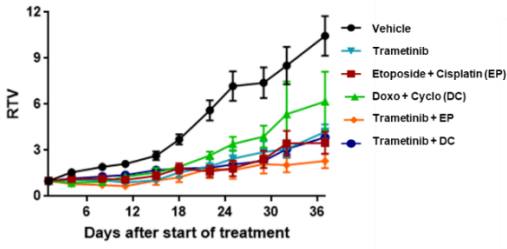
Conclusions

This *in vivo* experiment allowed us to draw the following conclusions concerning treatment efficacy:

- Lorlatinib alone showed no efficacy on IC-pPDX-75 model, with a TGI of 28%.
- Combination of lorlatinib with cisplatin + etoposide increased the efficacy of lorlatinib alone but not chemotherapies.
- Combination of lorlatinib with doxorubicin + cyclophosphamide significantly increased the antitumor efficacy of lorlatinib or doxorubicin + cyclophosphamide alone.

All results showed that (1) lorlatinib alone was not efficient in the IC-pPDX-75 neuroblastoma model and that (2) combination of lorlatinib with both doxorubicine + cyclophosphamide or etoposide+ cisplatin increased their antitumor efficiency.

Relative tumor volume (mean)



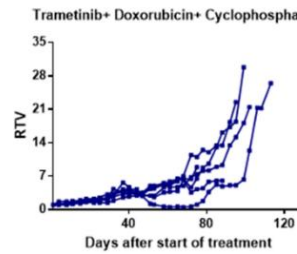
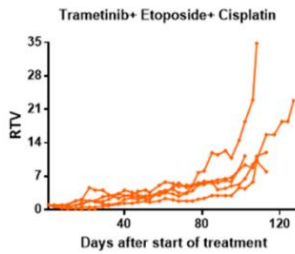
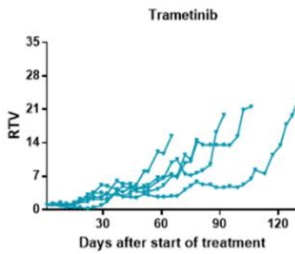
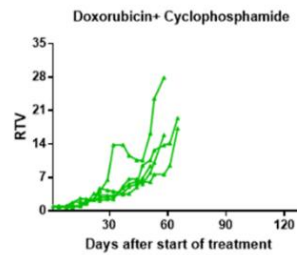
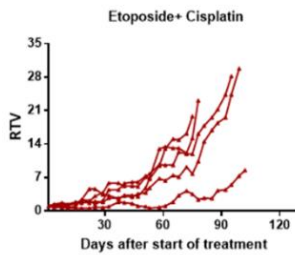
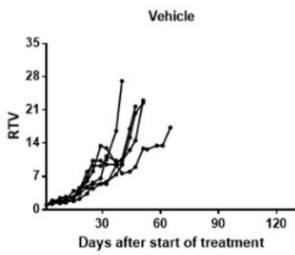
Groups	TGI* (day 37)
Trametinib	60
etoposide + cisplatin (EP)	67
doxorubicin + cyclophosphamide (DC)	41
Trametinib+ etoposide + cisplatin	78
Trametinib+ doxorubicin + cyclo	63*

d37	T	EP	T + EP
Control	0.0025	0.0025	0.0025
T+ EP	0.0317	0.3095	ns

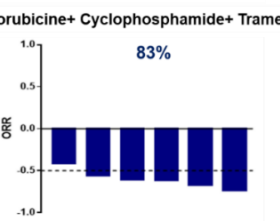
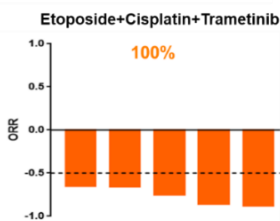
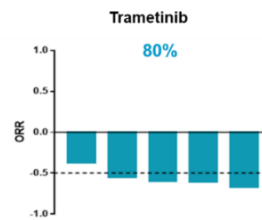
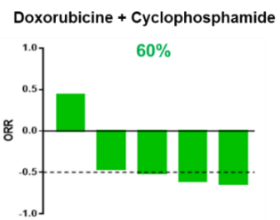
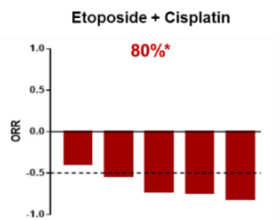
d37	T	CD	T + CD
Control	0.0025	0.048	0.0012
T+ CD	ns	ns	0.5368
			0.3290

TGI=100-RTV_T/RTV_C
 * DC/DC+T: P<0.0018

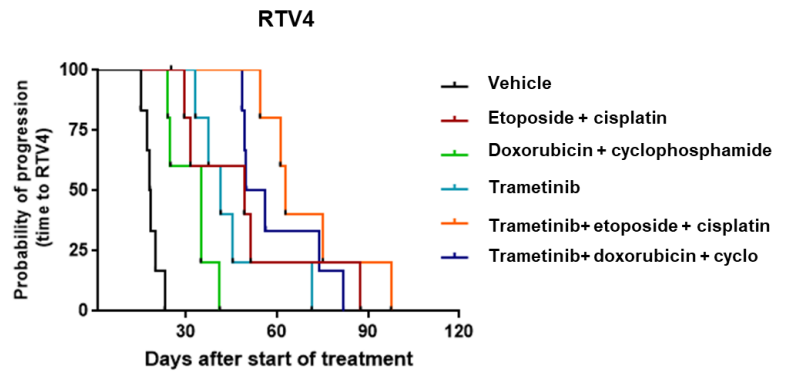
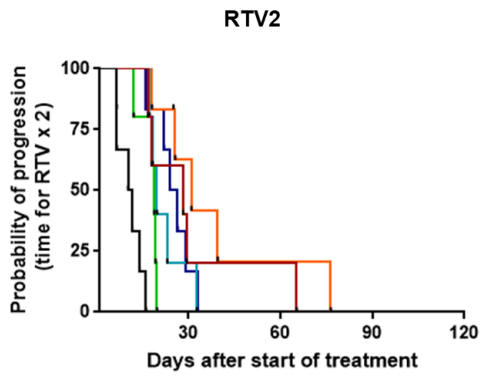
Individual RTV



Individual ORR



Probability of progression (RTV2 and RTV4)



RTV2	T	EP	CD	T + EP	T + CD
Control	0.0034	0.0034	0.014	0.0013	0.003
T		ns 0.757	ns 0.2971		
T + EP	ns 0.1019	ns 0.3306			
T + CD	ns 0.3573		0.0310		

RTV4	T	EP	CD	T + EP	T + CD
Control	0.0034	0.0034	0.0034	0.0013	0.0013
T		ns 0.917	ns 0.0684		
T + EP	0.0382	ns 0.0652			
T + CD	0.0310		0.0017		

Conclusions

This *in vivo* experiment allowed us to draw the following conclusions concerning treatment efficacy:

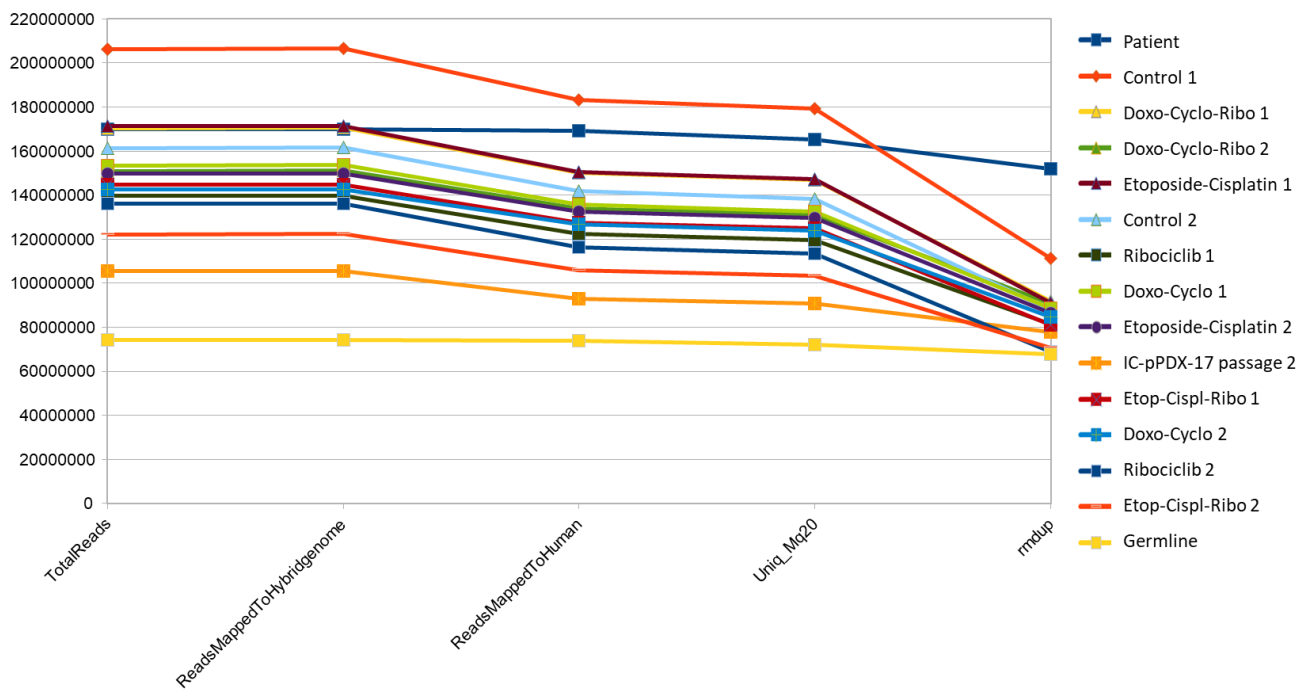
- Trametinib alone showed significant antitumor efficacy on IC-pPDX-109, with a TGI of 60%.
- Combination of trametinib with cisplatin + etoposide was significantly more efficient than Trametinib alone ($p=0.0317$) but not more than cisplatin + etoposide alone.
- The addition of doxorubicin + cyclophosphamide to trametinib was not more efficient than trametinib alone.

All results showed that trametinib alone was efficient in the IC-pPDX-109 neuroblastoma PDX and that its combination with Etoposide+Cisplatin significantly increased their antitumor efficacy.

Appendix 3: whole-exome sequencing quality control

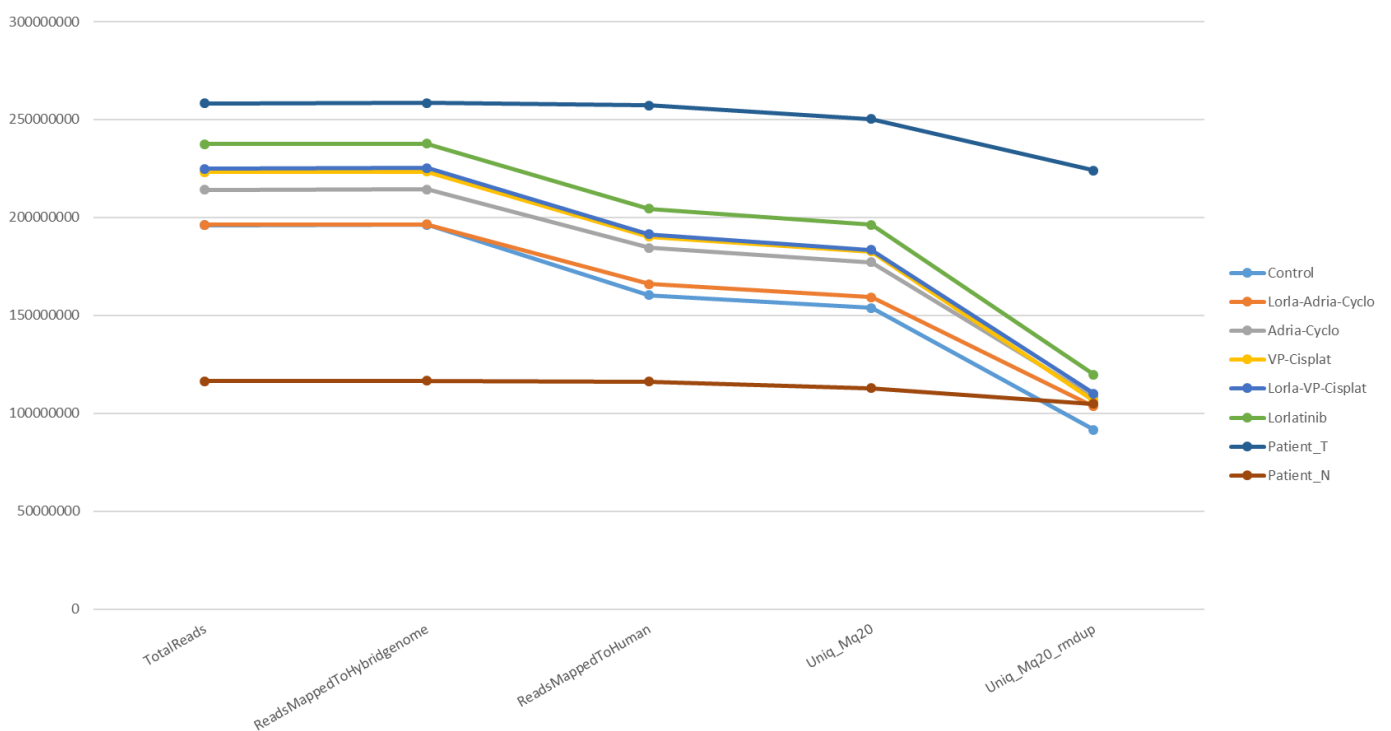
Model IC-pPDX-17

IC-pPDX-17 COVERAGE ANALYSIS



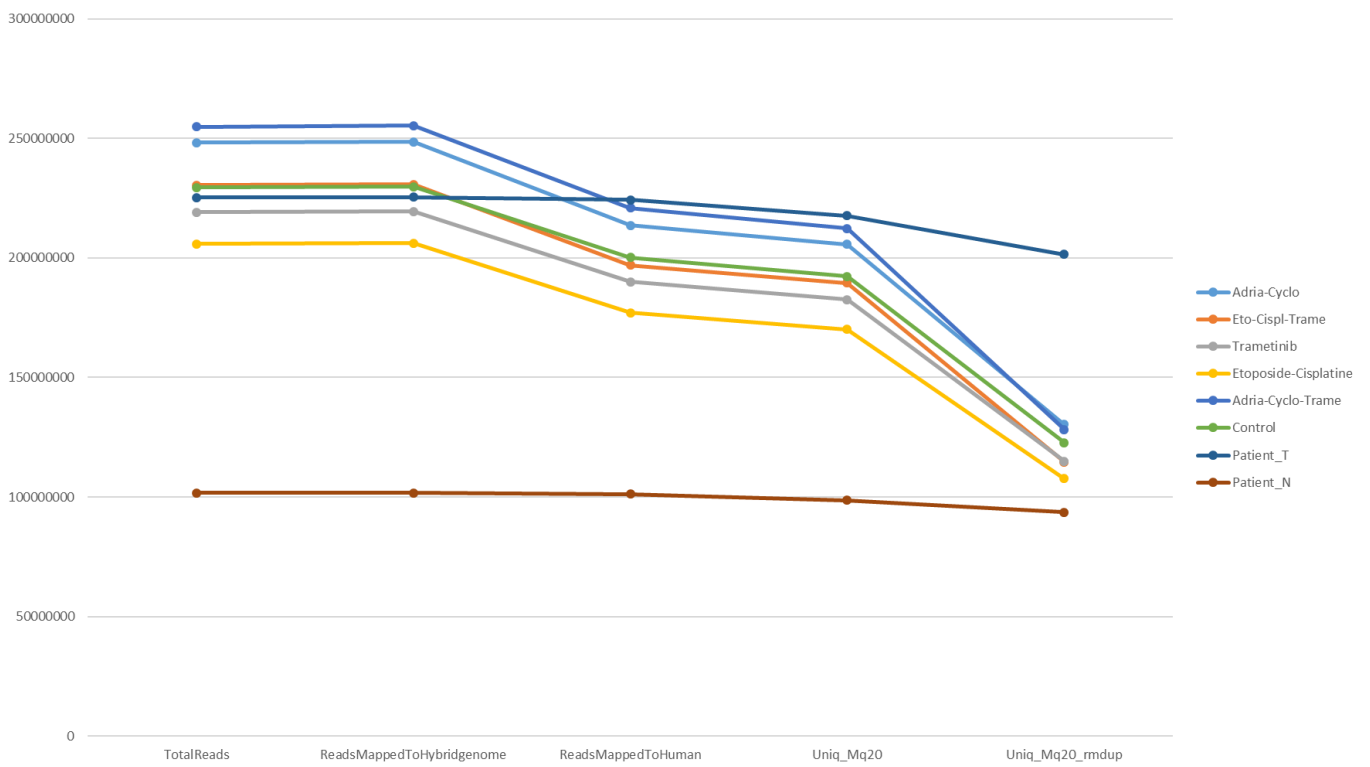
Model IC-pPDX-75

IC-pPDX-75 COVERAGE ANALYSIS



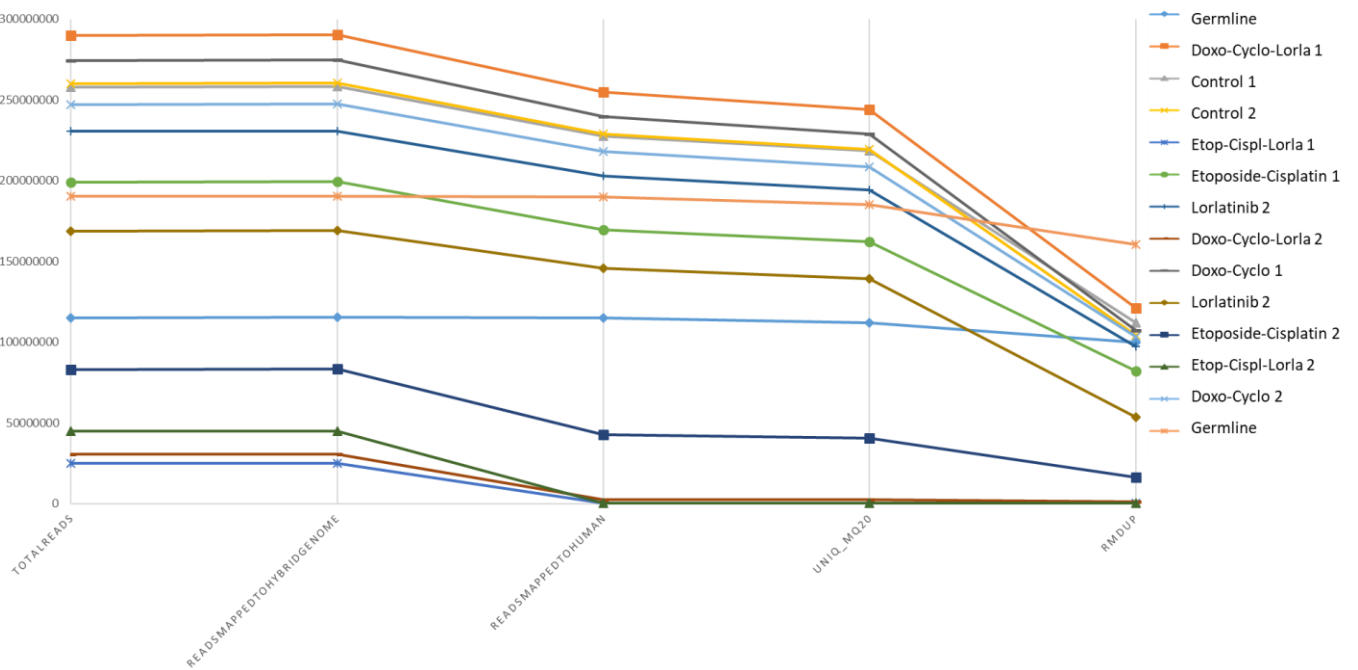
Model IC-pPDX-109

IC-pPDX-109 COVERAGE ANALYSIS



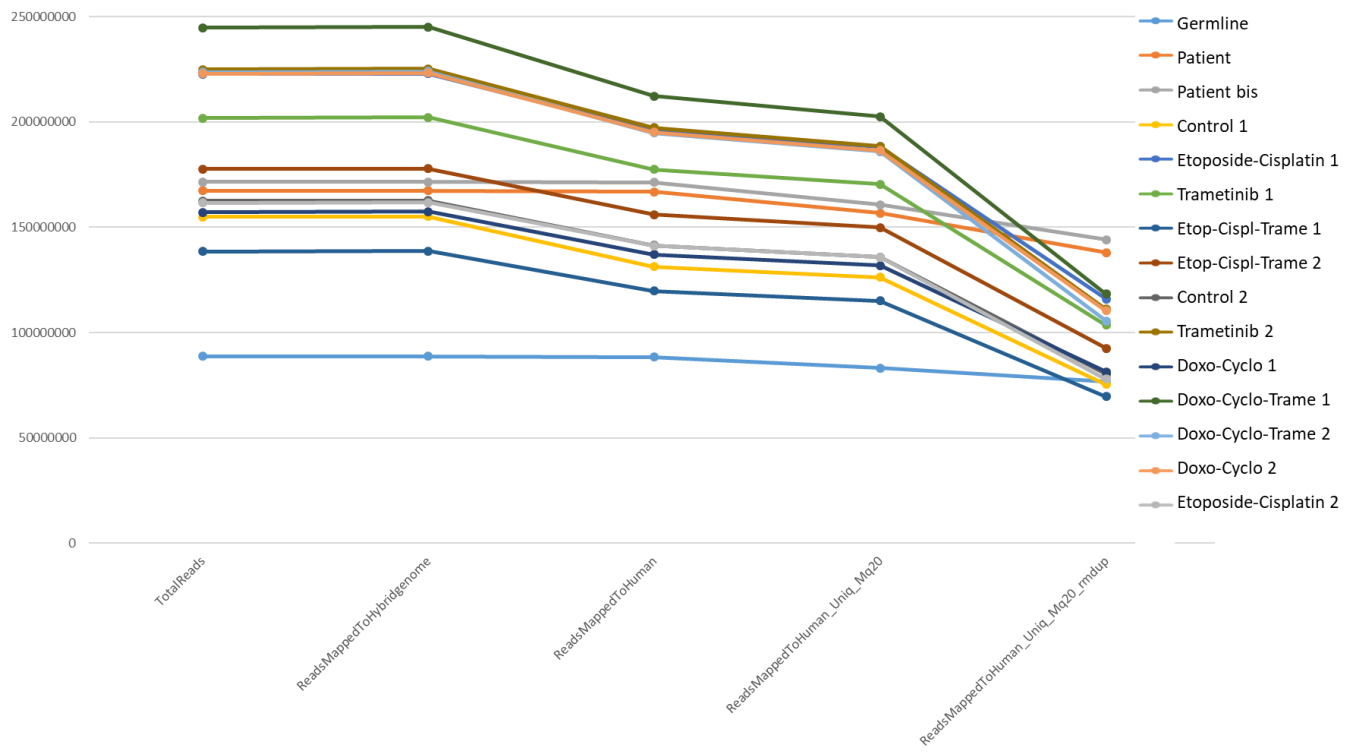
Model GR-NB4

GR-NB4 COVERAGE ANALYSIS



Model GR-NB10

GR-NB 10 COVERAGE ANALYSIS



Circulating tumor DNA analysis enables molecular characterization of pediatric renal tumors at diagnosis

Irene Jiménez^{1,2,3,4}, Mathieu Chicard^{1,2,3,4}, Léo Colmet-Daage^{1,2,3,4}, Nathalie Clément^{1,3,4}, Adrien Danzon^{1,2,3,4}, Eve Lapouble⁵, Gaëlle Pierron⁵, Mylène Bohec⁶, Sylvain Baulande⁶, Dominique Berrebi⁷, Paul Fréneaux^{4,8}, Aurore Coulomb^{9,10}, Louise Galmiche-Rolland¹¹, Sabine Sarnacki^{12,13}, Georges Audry^{10,14}, Pascale Philippe-Chomette¹⁵, Hervé J. Brisse^{4,16}, François Doz^{1,4,13}, Jean Michon^{1,4}, Olivier Delattre^{1,2,4} and Gudrun Schleiermacher^{1,2,3,4}

¹SIREDO Oncology Center (Care, Innovation and research for children and AYA with cancer), Institut Curie, Paris, France

²INSERM U830, Laboratoire de Génétique et Biologie des Cancers, Research Center, Institut Curie, Paris, France

³SiRIC RTOP « Recherche Translationnelle en Oncologie Pédiatrique », Institut Curie, Paris, France

⁴PSL Research University, Paris, France

⁵Somatic Genetics Unit, Institut Curie, Paris, France

⁶Research Center, Institut Curie, Institut Curie Genomics of Excellence (ICGex) Platform, Paris, France

⁷Service de Pathologie, Hôpital Robert Debré, APHP, Paris, France

⁸Service de Pathologie, Hospital Group, Institut Curie, Paris, France

⁹Service de Pathologie, Hôpital Armand Trousseau, APHP, Paris, France

¹⁰Université Pierre et Marie Curie, Paris, France

¹¹Service de Pathologie, Hôpital Necker, APHP, Paris, France

¹²Département de Chirurgie Pédiatrique, Hôpital Necker, APHP, Paris, France

¹³Université Paris Descartes, Paris, France

¹⁴Département de Chirurgie Pédiatrique, Hôpital Armand Trousseau, APHP, Paris, France

¹⁵Département de Chirurgie Pédiatrique, Hôpital Robert Debré, APHP, Paris, France

¹⁶Département d'Imagerie, Hospital Group, Institut Curie, Paris, France

Circulating tumor DNA (ctDNA) is a powerful tool for the molecular characterization of cancer. The most frequent pediatric kidney tumors (KT) are Wilms' tumors (WT), but other diagnoses may occur. According to the SIOP strategy, in most countries pediatric KT have a presumptive diagnosis of WT if they are clinically and radiologically compatible. The histologic confirmation is established after post-chemotherapy nephrectomy. Thus, there is a risk for a small fraction of patients to receive neoadjuvant chemotherapy that is not adapted to the disease. The aim of this work is to perform molecular diagnosis of pediatric KT by tumor genetic characterization based on the analysis of ctDNA. We analyzed ctDNA extracted from plasma samples of 18 pediatric patients with KT by whole-exome sequencing and compared the results to their matched tumor and germline DNA. Copy number alterations (CNAs) and single nucleotide variations (SNVs) were analyzed. We were able to detect tumor cell specific genetic alterations—CNAs, SNVs or both—in ctDNA in all patients except in one (for whom the plasma sample was obtained long after nephrectomy). These results open the door to new applications for the study of ctDNA with regards to the molecular diagnosis of KT, with a possibility of its usefulness for adapting the treatment early after diagnosis, but also for disease monitoring and follow up.

Key words: circulating tumor DNA, cell-free DNA, Pediatrics, Kidney tumors, Wilms' tumors, Renal tumors

Abbreviations: CCSK: Clear Cell sarcoma of the kidney; cfDNA: Cell-free DNA; CNAs: Copy number alterations; ctDNA: Circulating tumor DNA; DDS: Denys-Drash syndrome; GATK: Genome Analysis Toolkit; ITD: Internal Tandem Duplications; KT: Kidney Tumors; LOH: Loss of heterozygosity; MAF: Mutated allele fraction; RCC: Renal cell carcinoma; RMC: Renal medullary carcinoma; RTK: Rhabdoid tumor of the kidney; SIOP: International Society of Pediatric Oncology; SNVs: Single-nucleotide variations; WAGR: Wilms' tumor-aniridia-genitourinary anomaly-retardation syndrome; WES: Whole-exome sequencing; WT: Wilms' tumor

Additional Supporting Information may be found in the online version of this article.

Grant sponsor: Annenberg Foundation; **Grant sponsor:** Association Meghanora; **Grant sponsor:** Fondation Nelia et Amadeo Barletta; **Grant sponsor:** Agence Nationale de la Recherche; **Grant numbers:** INCa-DGOS- 4654; **Grant sponsor:** Institut Curie; **Grant numbers:** ANR-10-EQPX-03

DOI: 10.1002/ijc.31620

History: Received 11 Dec. 2017; Accepted 11 May 2018;

Online 19 Jun 2018

Correspondence to: Gudrun Schleiermacher, Institut Curie, SIREDO Oncology Center (Care, Innovation and research for children and AYA with cancer), INSERM U830, PSL Research University, 26 rue d'Ulm, Paris, Cedex 05 75248, France, E-mail: gudrun.schleiermacher@curie.fr; Tel: 00 33 (0)1 44 32 45 50

What's new?

The analysis of cell-free DNA (cfDNA) in pediatric patients with kidney tumors is of interest for the molecular diagnosis and early identification of aggressive disease subtypes. In this study, significant amounts of circulating tumor DNA (ctDNA) were successfully isolated from pediatric patients with malignant kidney tumors. Accurate copy number profile and mutation calling to identify specific tumor cell genetic alterations was performed with whole-exome sequencing using only low volumes of blood ($\geq 100 \mu\text{L}$) and low amounts of cfDNA ($\geq 4 \text{ ng}$). The findings suggest that ctDNA analysis can facilitate the molecular diagnosis of specific subtypes of pediatric kidney tumors, potentially enabling earlier treatment.

Introduction

Circulating tumor DNA (ctDNA), a fraction of the total cell free DNA (cfDNA), consists of small 150–200 base pair-long DNA fragments and is released into the bloodstream by various processes such as apoptosis or necrosis.¹ CtDNA reflects tumor cell specific genetic alterations, and its usefulness as liquid biopsy is based on the possibility of non-invasive and iterative sampling. It might be especially useful in tumors for which tumor samples—for histologic or genetic analyses—are difficult to obtain, or for which a biopsy is not usually performed at diagnosis, as is the case for a large proportion of pediatric patients with kidney tumors treated according to the *International Society of Pediatric Oncology* (SIOP) protocols.²

Malignant kidney tumors (KT) comprise about 5% of childhood cancers, with Wilms' tumor (WT) accounting for approximately 90% of all cases.³ In pediatric patients, other primary KT are rare and are mainly represented by congenital mesoblastic nephroma, clear cell sarcoma of the kidney (CCSK), rhabdoid tumor of the kidney (RTK), renal medullary carcinoma (RMC) or renal cell carcinoma (RCC).

The genetic landscape of pediatric KT depends on each subtype (Supporting Information Table 1). WT harbor recurrent but non-specific genetic abnormalities, with *WT1*, *CTNNB1* and *WTX* occurring in about one-third of WT.⁴ *TP53* mutations and focal *MYCN* copy number gain are associated with the more aggressive diffuse anaplastic form of WT.^{5,6} Other genetic somatic abnormalities include mutations in microRNA-processing genes (such as *DROSHA* and *DICER1*) and *SIX1/2*⁷ mutations. WT exhibit a relatively low number of recurrent copy number alterations (CNAs), as well as loss of heterozygosity (LOH), some of which are related to patient outcome. LOH at chromosomes 1p, 11q, 16q and 22q have been correlated with poor prognosis^{8–11}; more specifically allele loss involving 1p and 16q have been associated with increased risk of relapse in favorable-histology WT⁸; LOH on 11p predicts relapse in very low-risk WT treated with surgery alone in children <2 years¹². Loss of chromosomes 4q and 14q has been frequently found in diffuse anaplastic WT⁵. Furthermore, WT can also occur in a context of genetic predisposition, such as the WT-aniridia-genitourinary anomaly-retardation (WAGR) syndrome and the Denys–Drash syndrome (DDS), due to *WT1* constitutional deletions or missense mutations¹³ respectively.

According to the SIOP strategy for the management of pediatric KT, these patients are initially treated as WT if clinical and radiological features are compatible with a presumptive diagnosis of WT, since the majority of pediatric KT are WT and the risks associated with a surgical or percutaneous biopsy are thought to be not negligible. In this overall treatment strategy, the histologic diagnosis is confirmed after neoadjuvant chemotherapy and nephrectomy. Thus, there is a risk for a fraction of pediatric patients with KT to receive a neoadjuvant chemotherapy that is not adapted to the disease.

The aim of this study was to analyze the ctDNA obtained at the time of diagnosis in pediatric patients with malignant KT, in order to identify tumor cell specific genetic alterations with the objective of confirmation of histological diagnosis. Since most cases harbor non-specific but recurrent genetic abnormalities, a whole-exome sequencing (WES) was used to search for copy-number alterations and mutation calling, instead of a targeted gene sequencing approach. We hypothesize that the identification of tumor-cell specific genetic alterations in ctDNA might be useful for the upfront management of these patients in the context of a presumptive diagnosis.

Materials and Methods**Patients**

This is a retrospective, monocentric, feasibility study. Pediatric patients with non-hematopoietic renal masses were included in this study if a plasma sample was available at the time of diagnosis or relapse ($n = 18$ patients; Table 1). Plasma samples were collected between March 2012 and January 2017. Histologic diagnosis was established after biopsy for 2 patients (patients #1 and #2) and after nephrectomy for the 16 remaining patients. Plasma samples were obtained at the time of diagnosis (before starting the treatment) for 13 patients with WT and 1 patient with nephrogenic rests (in the context of WAGR syndrome). For four patients, plasma samples were collected in the following specific situations: for patient #1 the plasma sample was obtained at the time of a local and metastatic progression; for patient #2 plasma was collected at the time of a metastatic muscle relapse; for patient #6, the plasma sample was obtained 16 days after primary nephrectomy; for patient #9 plasma was collected 27 days after nephrectomy following preoperative chemotherapy. Patients were treated in the SIREDO Oncology Center of the Institut Curie (Paris,

Table 1. Summary of patients' and sample's characteristics.

Patient	Clinical information				Sample characteristics				Time point of WES		Tumor fraction estimated by Sequenza				
	Age at diagnosis (y)	Syndromic context	Volume of primary tumor at the time of plasma sampling (mL)	Diagnosis	Histologic subtype/risk according to SIOP (only WT)	Local stage after neoadjuvant CT (only WT)	Follow-up		Quantity of cfDNA in plasma (ng of cfDNA per mL of plasma)	Quality of cfDNA (200 bp peak ratio)	cfDNA input for library (ng)	Tumor	cfDNA fraction in cfDNA	Tumor fraction in tumor tissue	
							Delay diagnosis-relapse (m)	Status at last news							
1	2.0	No	912	Metastatic RCC	NA	NA	17	DOD	2,000	30.96	84.2%	56.8	At local and metastatic relapse	36%	38%
2	0.4	No	42	Metastatic CCSK	NA	NA	17	PD	550	150.55	8.5%	65	At metastatic relapse	NC	32%
3	4.3	No	127	Metastatic WT	Mixed / IR	Stage II	NA	CR	600	34.32	62.3%	20	At diagnosis	30%	92%
4	2.9	No	1,258	Localized WT	Stromal / IR	Stage II	NA	CR	750	271.68	14.1%	100	At diagnosis	23%	30%
5	1.1	WAGR	¥	Nephro-genic rests	NA	NA	NA	CR	100	536.40	22.2%	50	At diagnosis	23%	-
6	0.3	No	0	Localized WT	Blastemal / *	Stage II *	NA	CR	650	36.66	48%	20	After primary nephrectomy	18%	17%
7	5.2	No	489	Localized WT	Stromal / IR	Stage II	NA	CR	850	82.16	80.9%	30	At diagnosis	11%	94%
8	3.8	No	1,260	Metastatic WT	Blastemal anaplastic / HR	Stage III	6	DOD	850	546.35	38%	200	At diagnosis	61%	96%
9	3.5	No	0	Localized CCSK	NA	NA	NA	CR	800	1,332	12.1%	500	After neoadjuvant chemo and nephrectomy	NC	65%
10	0.9	DDS	1,710	Localized WT	Mixed / IR	Stage I	NA	CR	500	71.14	100%	20	At diagnosis	57%	25%
11	4.2	No	2,444	Localized WT	Regressive / IR	Stage I	NA	CR	550	7.99	4%	4	At diagnosis	14%	90%
12	2.2	No	448	Localized WT	Regressive / IR	Stage III	NA	CR	400	2,286	79.4%	100	At diagnosis	84%	86%
13	7.4	No	204	Localized WT	Regressive / IR	Stage II	NA	CR	600	88.20	37.3%	50	At diagnosis	29%	-
14	1.0	No	1,097	Localized WT	Stromal / IR	Stage II	NA	CR	800	643.50	46%	200	At diagnosis	42%	93%
15	2.1	No	206	Localized WT	Mixed / IR	Stage II	NA	CR	850	57.60	18.3%	38	At diagnosis	26%	10%
16	1.2	No	727	Localized WT	Stromal / IR	Stage II	NA	CR	800	262.80	18.5%	200	At diagnosis	49%	92%
17	0.7	No	1,224	Localized WT	Mixed / IR	Stage II	NA	CR	450	816.00	64.2%	200	At diagnosis	32%	13%
18	2.5	No	380	Localized WT	Mixed / IR	Stage I	NA	CR	1,050	586.29	44.4%	200	At diagnosis	21%	96%

cfDNA: cell-free DNA. ctDNA: circulating tumor DNA. WT: Wilms tumor. CCSK: Clear-cell sarcoma of the kidney. RCC: Renal cell carcinoma. DDS: Denys-Drash syndrome. WAGR: Wilms-aniridia-genitourinary-retardation syndrome. DOD: dead of disease. CR: complete remission. PD: progressive disease. NA: not applicable. SIOP: International Society of Pediatric Oncology. IR: intermediate risk. HR: high risk. CI: chemotherapy. (y): years. (m): months. (°): Plasma sample obtained after primary nephrectomy, thus, histologic risk and local stage have no prognostic value. (¥): Not a tumor but nephrogenic rests. NC: non contributive.

France). Clinical characteristics of patients were recorded. Patients were included and samples were collected following written informed consent obtained from parents/guardians according to national law. The institutional ethics committee (“Comité de Revue Institutionnel”) of the Institut Curie authorized this study (reference OBS 160051).

Tumor samples and DNA extraction

Tumor samples containing >30% of viable tumor cells were requested. Tumor tissue was obtained for 16 of 18 patients: for patients #1 and #2 after biopsy and for the remaining 14 patients after nephrectomy. Tumor samples could not be obtained for patients #5 and #13, with WT and nephrogenic rests respectively. DNA from tumor samples was extracted according to standard procedures.

Plasma sample collection and processing

Left over blood samples of patients collected on EDTA tubes for routine full blood count analyses was retrieved with a maximum delay of 24 h after venipuncture: of a total of 2–5 ml of blood samples (on EDTA) for full blood count, left over volumes of 200 µL–2 mL were retrieved in the laboratory for research purposes. For this feasibility study, no specific additional blood sample was collected. Blood was centrifuged at 2,000 rpm for 10 min. Plasma and pellet were carefully separated, aliquoted and stored at –80 °C until cfDNA and germline DNA extraction.

cfDNA purification and quantification

cfDNA was extracted from 100 µL–2 mL of plasma and purified using the QIAmp Circulating Nucleic Acid Kit (Qiagen) with the QiaVac24s system. cfDNA concentration in plasma was determined by Qubit fluorometric assay (Invitrogen) with dsDNA High Sensitivity Assay Kit. Quality control of extracted cfDNA was performed by capillary electrophoresis using 2100Bioanalyzer (Agilent) with the High Sensitivity DNA chip. CfDNA quality was expressed as the ≈200 bp fragment fraction of the overall DNA quantity obtained upon extraction of DNA from plasma, in order to take into account only the fraction corresponding to cfDNA and not potentially contaminating DNA from blood cells (Supporting Information Fig. 4).

Whole-exome sequencing of tumor and germline DNA

Tumor and germline genomic DNA were fragmented by using Covaris technology. WES was performed on tumor and paired germline DNA using the SeqCap EZ MedExome Kit (Nimblegen Roche Sequencing) according to manufacturer procedures.

Whole-exome sequencing on cfDNA

cfDNA sequencing libraries were prepared with Kapa Library Preparation Kit (Kapa Biosystems) with Indexed Adapters included in Roche Nimblegen SeqCap EZ. The manufacturer’s protocol was slightly modified: the duration of the ligation was increased to 16 h as previously published.¹⁴ Ten microliters of Pre LM-PCR oligo 1&2 (5 µM) on 9 cycles of Pre-

Captured LM-PCR and 99 µL of SeqCap EZ Purification Beads (1.8x) were used for clean-up of the amplified sample library. Library quantification was determined by Qubit fluorometric assay (Invitrogen) with dsDNA High Sensitivity Assay Kit. Library quality was verified by capillary electrophoresis using LabChip GXII Touch HT. Exome capture was performed with Seq Cap EZ MedExome. WES was performed in trios of cfDNA, tumor and germline DNA by paired-ends (PE) 100x100 bp Illumina HiSeq2500 technology, for an expected coverage of 100X.

Bioinformatics detection of variations

Following sequencing, reads were aligned with Bowtie2¹⁵ on genome build Hg19 allowing up to 4% of mismatches. Bam files were pre-processed according to the Genome Analysis Toolkit (GATK) recommendations.¹⁶ Targeted bam files were pre-processed without removing duplicates. Variant calling was performed in parallel using 5 variant callers: Unified Genotyper, Haplotype Caller, Samtools-0.1.18, MuTect-1.1.7 and MuTect2.^{17–19} Annovar-v2013–07–29 with cosmic-v64 and dbsnp-v137 were used for the annotation and RefSeq for the structural annotation. Single nucleotide variations (SNVs) with a quality <30, a depth of coverage <20 in tumor or plasma samples or < 2 reads supporting the variant were filtered out. Only missense, splice sites and non-synonymous coding variations were kept. In order to filter out polymorphisms, variants reported in more than 1% of the population in the 1,000 genomes (1000gApr1_2012) or Exome Sequencing Project (ESP6500) were discarded. Deleterious effects were predicted by MutationTaster,²⁰ LRT,²¹ Polyphen2,²² and SIFT.²³ In addition, variants supported by >5 reads on germline DNA were discarded. Copy number profiles were computed with VarScan.v2.3.5²⁴ and DNACopy-1.42.0.²⁵ Sequenza²⁶ tool was used for the analysis of copy-neutral LOH. We explored structural variants including insertions, deletions, inversions, tandem duplications using pindel-0.2.5a3 with standard parameters.²⁷ The genetic alterations observed in cfDNA were compared to those identified in the tumor and germline samples. Tumor-cell fraction in the tumor sample and ctDNA fraction in cfDNA were estimated using Sequenza,²⁶ which is able to estimate correctly the ploidy in samples with tumor content higher than 30%, with inaccurate results obtained in samples harboring <30% of tumor content.

Based on Sequenza tumor fraction estimation and the frequency of mutant reads with respect to total reads for each position, we estimated the mutated allele fraction (MAF) for each SNV in both cfDNA and tumor DNA. Events with MAF ≥20% or < 20% were considered to be at major or minor tumor cell fraction, respectively.

Results

Patients’ and samples’ characteristics

Eighteen patients (7 males, 11 females) with renal masses and available plasma sample were identified. Median age at diagnosis was 2.2 years [0.3–7.4]. Histologic diagnoses were

Table 2. Comparative analysis of copy number profile and single nucleotide variations in tumor DNA and circulating tumor DNA (ctDNA).

Patient	Germline events	Structural variants detected in tumor DNA	Copy number analysis		CNAs in ctDNA only, tumor DNA only or both	Analysis of the SNVs		Representative main genetic abnormalities detected in cfDNA (yes/no)
			Copy number profile			SNVs in ctDNA only, tumor DNA only or both	SNVs in ctDNA only, tumor DNA only or both	
			ctDNA	Tumor				
1		SPL/TFE3 fusion	Silent	Dynamic	Chromothripsis chr 19		GLDC, HEPH1, UACA, ATP13A1, ACRT1, CDH18, SLC34A1, TAAR1, CDR2L	No
2		BCOR ITD	Silent	Silent	NA		IFNA10 RABGAP1L, ARAP3, VTI1A, SORL1, OSBPL7 GPN1, ARNTL2, TMEM74B	No
3			Dynamic	Dynamic	7p-, 7q+		NBPF10, PAX3, IGSF10, PLEKHG3 TMEM131 PCDHA1, NAT16,	No
4			Dynamic	Dynamic	1q+, 4(ptel-p15.33)+, 6+, 7+, 8+, 10+, 12p+, 22+ 21(q22.3-qtel)-		LRIF1, CTNMB1 , PPARGC1A, BCLAF1, KIAA1244, ACTL6B, LRRCC1, ZNF517, PLCE1 DPY19L4, PKD2L1, LTBR, PLK1 ADAMTS10, MAP4K1, PPP1R3D	Yes
5	11p13 deletion		Silent	-	NA		DENND4B, LATS1, PSMD11	No
6			Silent	Silent	NA		CCDC97 MSH6, DLC1 KPRP, R3HDM1, MLLT1	No
7			Dynamic	Dynamic	12+, 18+		MYCN , CTNMB1 , LHFPL5, KIAA0355, KIRREL2, SNX21 CPD, TBC1D17 IKBK, OR5I1	Yes
8			Dynamic	Dynamic	3+, 7p-, 7q+, 8+, 12+, 16q-, 17(ptel-p12)-, 17(p12-p11.2)+, 20p-17p(11.2)+, 18p-, 20(p11.23-q11.21)+, 20(q11.21-q13.33)+, 22-, 10 breakpoints on chr 18q 8(q23.1-qtel)-, 18-, 20q+, 12 breakpoints on chr 4, 5 breakpoints on chr 10q		LRP1B, PCDH10, HRCT1, FAM86C1, GOLGA6L1, AKAP13, TP53 , NTN1, POTE ZIC4, GRM5, MED13L, DMD GALR1	Yes
9		BCOR ITD	Silent	Dynamic	1q+, 10q-		USP17L11, MYO10, MOK, ZNF629	Yes
10	WT1 mutation		Dynamic	Dynamic	7p-, 7q+ LOH chr 11p		VAV3, CTNMB1 , POTE CTDSPL, CTDSPL, ARID1B , GRIPAP1	Yes

(Continues)

Table 2. Continued

Patient	Germline events	Structural variants detected in tumor DNA	Copy number analysis		Analysis of the SNVs		Representative main genetic abnormalities detected in cfDNA (yes/no)
			Copy number profile	Copy number profile	SNVs in ctDNA only, tumor DNA only or both	SNVs in ctDNA only, tumor DNA only or both	
11			Dynamic	Dynamic	7p-, 7q+		Yes
						DROSHA KIF1B, TRABD2A, SPEG, CACNA2D2, IRX4, SLC16A10, KCND2, C8orf48, NUDT18, EGR3, SLC25A37, FAM83H, HECTD4, SIX1 , GOLGA6L1, NRN1L, NPB, TRIP10, C19orf57, CHST7, SSX1, ARMCX3, CT47B1 MMP14, PDILT, ZNF728	
12			Dynamic	Dynamic	3+, LOH chr 4, 6+, LOH chr 8, 8+, 9+, LOH chr 11, 12+, 12(p12.1-p11.1)+, LOH chr 17, 18p-, 19q+		Yes
						SCN1A, EBLN2, STX18, FBP6, MS4A12, SLC22A12, ABCG9, SDK2, PRMT2 PALM, SLP1	
13			Dynamic	-	18+ LOH chr 11p		Yes
						CRB1, SF3B1, GPR123, PLCB2, MYH1, RAD51C, U2AF1, ZFX, LTN1, ATP6AP1	
14	WT1 mutation		Dynamic	Dynamic	LOH chr 11p, LOH chr 19q		Yes
			Silent	Silent	NA		Yes
						TMEM247, CTNMB1 , MPHOSPH8, THAP11 WDFY1, PRR5L, HNRNPUL2, DICER1 , MEX3C CHCHD5, SCTR, CTNMB1 , ARIH2OS, RFK, ARDC1 ACTN2, NUP155, ANKRD18A	
16			Dynamic	Dynamic	LOH chr 11p LOH chr 3p		Yes
						CTNMB1 , WT1 , SAFB2 VANGL1, CTNMB1 , XPO7	
17			Silent	Silent	NA		Yes
						YBX2, MLL1 , TRIB3 ANKRD36B, WDFY4 NASP, HEATR1, MFSD2B, SLC26A6, ALDH1L1, RPS3A, TLL1, DDX60, GTF2H4, KIF6, GABRR2, DNAH11, MET, MEST, PRKAG2, ZFXH4, ASTN2, ANO1, SART3, CCDC63, DNAH10, TLN2, MAP1LC3B, ERN1, RNF213, MIDN, BCR, CARD10, NROB1, IQSEC2	
18			Silent	Dynamic	1(p36.11-p35.2)-, 9(q22.31-q22.32)+, 11(p11.2-q11)-, 11(q23.1-q23.3)-		No
						MUC4, B4GALNT1, MTUS2, SUPT5H, MYT1, CABIN1 DKK2, SLC6A3, RASGRP2, SPDYC, MCRS1, CRYM, THAP11, LRRCS9, REXO1, ANGP1L4 MAP6, SETD1B, VASH1, KIAA2022	

cfDNA: cell-free DNA. LOH: loss-of-heterozygosity. Chr: chromosome. SNVs: single nucleotide variations. CNAs: copy number alterations. (-): Tumor DNA not available. NA: not applicable. BCOR ITD: BCOR internal tandem duplications.

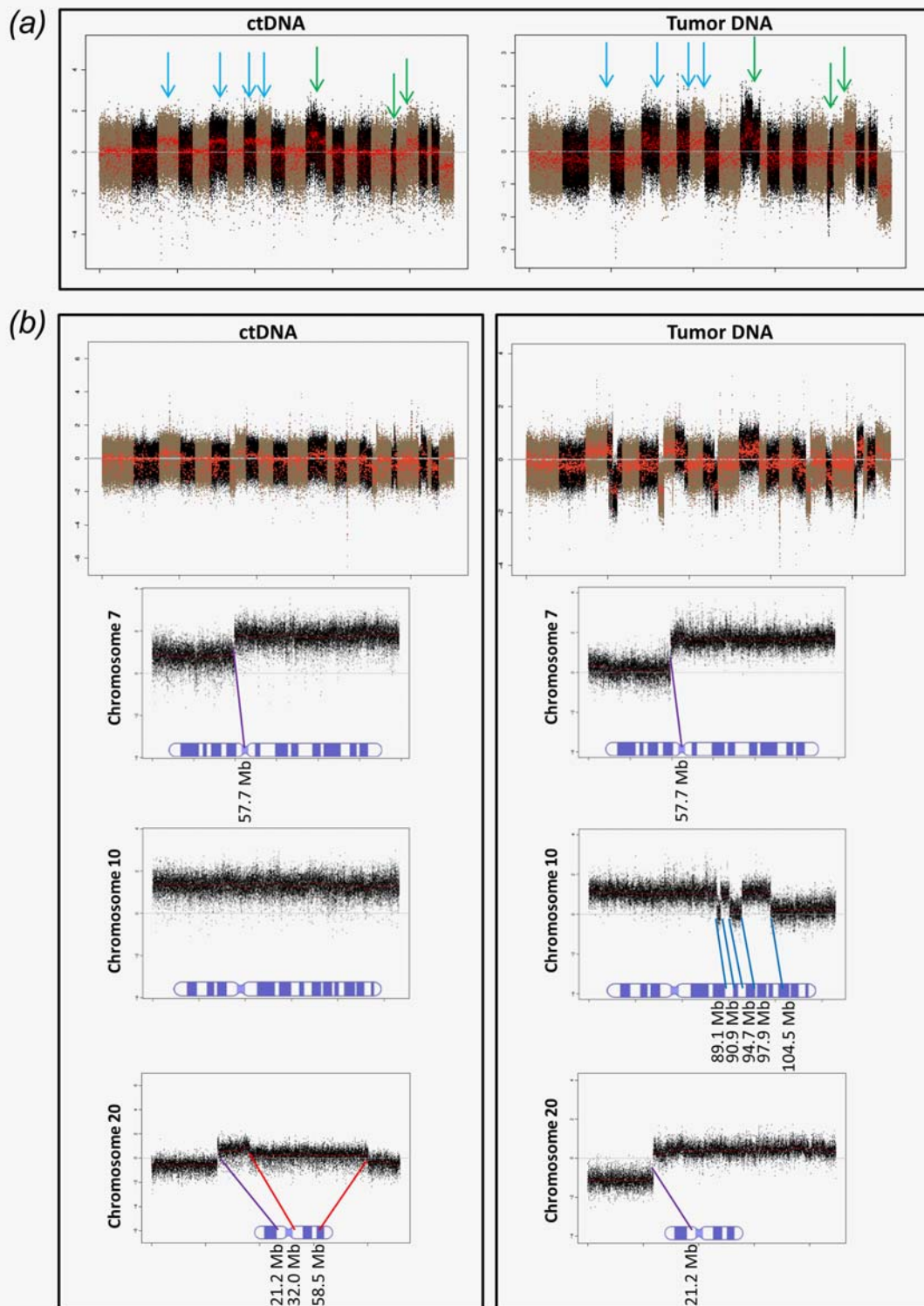


Figure 1. Comparative analysis of copy-number profiles performed by WES on tumor DNA and circulating tumor DNA (ctDNA) using VarScan tool. (a) Tumor DNA and ctDNA of patient #12 share the same copy-number abnormalities (CNAs). Blue arrows indicate gains of chromosomes 3, 6, 8 and 9; green arrows show segmental abnormalities such as gain of 12(p12.1-p11.1), 18p loss and 19q gain. (b) Tumor DNA and ctDNA copy-number profiles of patient #8 and details on chromosomes 7, 10 and 20. Some abnormalities are shared by tumor DNA and ctDNA (purple lines on chromosomes 7 and 20), and others are specific to tumor DNA (blue lines on chromosome 10) or ctDNA (red lines on chromosome 20), illustrating the clonal heterogeneity. Breakpoints positions on different chromosomes are shown.

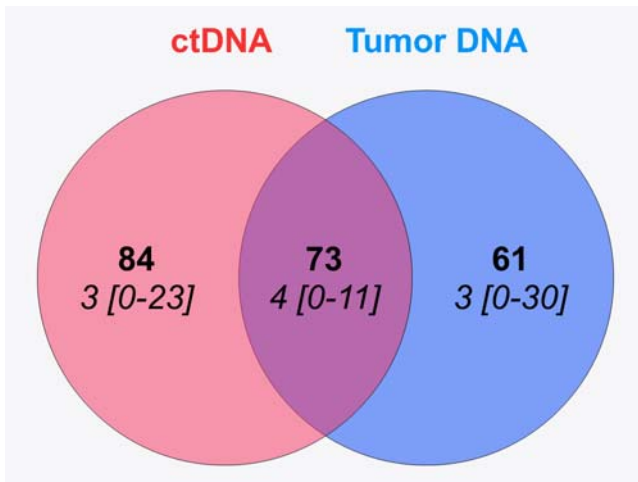


Figure 2. Venn diagram of single nucleotide variations (SNVs) detected by WES in ctDNA, tumor DNA and both. Absolute number of SNVs in all patients is marked in bold; median number of SNVs per patient is marked in italics (intervals in square brackets). [Color figure can be viewed at wileyonlinelibrary.com]

available for all patients (Table 1), with 17 of 18 patients having malignant renal tumors (14 WT, 2 CCSK and 1 RCC) and 1 patient with intralobar nephrogenic rests in the context of WAGR syndrome (patient #5). One patient with localized WT had phenotypic findings consistent with Denys–Drash syndrome (patient #10).

The median time of freezing between the storage of plasma sample and cfDNA extraction was 15.7 months [1.9–47.5]. Volume of plasma samples ranged between 100 and 2,000 μ L (median 700 μ L). After extraction, median concentration of cfDNA in plasma was 206.67 ng/mL [7.99–2,286]. cfDNA input for library construction ranged between 4 and 500 ng (median 60.9 ng). WES of trios of tumor, germline and cfDNA was performed in 16 cases. In two cases (patients #5 and #13), only cfDNA and paired germline DNA were sequenced (Tables 1 and 2).

Sequencing quality control

The analysis of the depth of coverage showed that 80% of the target was covered at more than 20X (Supporting Information Fig. 1). Analysis based on the Sequenza tool showed a median of 76% [10–96] of tumor cells in the primary tumor sample and a median of 29% [11–84] of ctDNA fraction in the cfDNA (Table 2).

Copy number alterations in ctDNA by WES

Copy number analysis of the cfDNA samples resulted in 10 dynamic and 8 silent copy number profiles (Table 2). Among the 10 cases with dynamic copy number profile on cfDNA (all of them were WT), 9 had also a dynamic copy number profile on tumor DNA; in the remaining case tumor DNA was not available. Among the 8 cases with silent copy

number profile on cfDNA, their paired tumor copy number profiles were also silent in 4 cases; 3 had a dynamic copy number profile on tumor DNA; in the remaining case tumor DNA was not available. Altogether, in 13 of 18 cases (72.2%), the dynamics of the cfDNA copy number profile corresponded to the dynamics of the tumor DNA copy number profile.

Comparative analysis of paired dynamic copy number profiles of cfDNA and tumor DNA showed closely related profiles (Table 2 and Supporting Information Table 2), with a majority of CNAs identical in both samples of a given patient (Fig. 1a). Interestingly, in some cases, cfDNA showed additional CNAs that were not present in tumor DNA and conversely (Fig. 1b), with a median of 2 [1–12] common CNAs, 0 [0–18] cfDNA-specific and 0 [0–19] tumor-specific CNAs. In addition to CNAs, 12 copy neutral LOH were observed in 6 cases.

Looking specifically for CNAs in ctDNA suggestive of WT, 4 cases harbored 7p loss and 7q gain, 4 showed LOH on chromosome 11p, 1 patient showed loss of chromosome 16q and 1 patient showed gain of chromosome 1q. In summary, 8 of 14 patients with WT showed CNAs suggestive of WT on ctDNA.

Furthermore, some structural variants were found in tumors with other histotypes than WT: we were able to find *BCOR* internal tandem duplications (ITD) in tumor DNA of patients #2 and #9 with metastatic and localized CCSK respectively. These structural variants detected with Pindel bioinformatics tool could not be identified in ctDNA likely due to poor or absent tumor fraction content in cfDNA (Table 2). The RCC of patient #1 was carrier of a *SPL/TFE3* translocation detected by quantitative reverse transcription PCR in the tumor sample at the time of diagnosis, which was not identifiable by WES in cfDNA.

Analysis of the single nucleotide variations

SNV analysis was able to detect SNVs in cfDNA in all cases except in patient #9 (whose plasma was obtained 27 days after post-chemotherapy nephrectomy). Among these 17 patients, a total of 157 SNVs were detected in cfDNA, of which 84 were specific to cfDNA and 73 were common with tumor DNA (Figs. 3a and 3b and Supporting Information Fig. 2), with a median of 8 [0–23] SNVs in cfDNA per patient.

Looking more specifically at cfDNA results of patients with WT (Table 2 and Supporting Information table 3) several key mutations were detected, such as tumor cell specific somatic *CTNNB1* mutations found in the cfDNA in 6 of 14 (42.9%) patients. In addition to the *CTNNB1* mutation, patient #7 harbored a *MYCN* mutation (COSM35624), patient #10 a mutation in *ARID1B* gene and patient #16 a *WT1* frameshift insertion. As expected, a *TP53* mutation (COSM43559) was detected in ctDNA in patient #8 with the very high-risk metastatic anaplastic WT (Fig. 3a). Mutations in miRNA processing genes were found in ctDNA of patient #15 (*DICER1*) and #11 (*DROSHA*) (Fig. 3b), who was also carrier of a *SIX1* mutation in ctDNA. Altogether, for 9 out of 14 cases (64.3%) at least 1 tumor cell specific SNV in WT-characteristic genes was clearly identified in the cfDNA. Importantly, in some

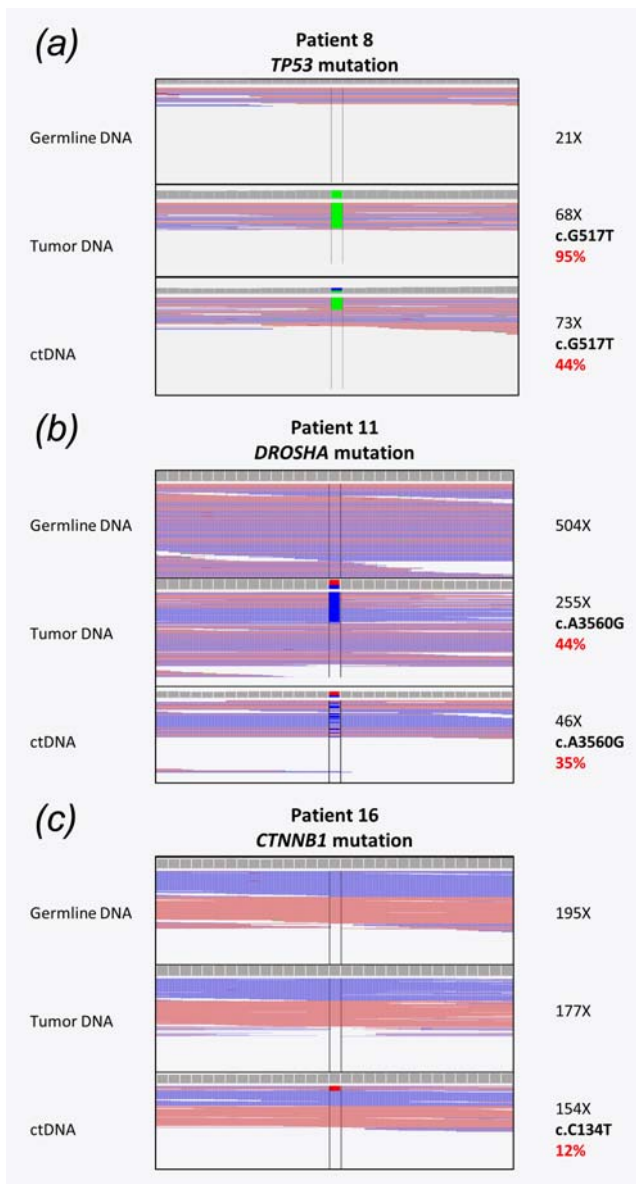


Figure 3. Three examples of single nucleotide variations (SNVs) by Integrated Genome Viewer. (a) and (b): *TP53* and *DROSHA* mutations in patients #8 and #11 respectively were detected in both tumor DNA and ctDNA. (c): in patient #16, a *CTNNB1* mutation was found in ctDNA only. X: total number of reads for a given position. In red, the percentage of alternative reads supporting the variation among the total number of reads.

cases, genetic alterations were specific to cfDNA and not seen in the primary tumor. For example, patients #10, #11 and #15 showed relevant *ARID1B*, *SIX1* and *CTNNB1* mutations respectively in cfDNA only and not in tumor DNA (Table 2). Patient #16 harbored a combined *WT1* and *CTNNB1* mutation in both tumor and cfDNA, and an additional *CTNNB1* mutation in cfDNA only (Fig. 3c).

To assess the frequency of somatic mutational events, we estimated the MAF for each SNV position: 120 of the

157 SNVs (76.4%) detected in ctDNA and 108 of the 134 SNVs (80.6%) identified in tumor DNA were estimated to occur at major tumor cell fraction (i.e. SNVs with a MAF $\geq 20\%$). On the other hand, 37 of 157 SNVs (23.6%) in ctDNA and 26 of 134 SNVs (19.4%) in tumor DNA were estimated to occur at minor (<20%) tumor cell fraction (Supporting Information Table 3). Interestingly, 6 of the 7 *CTNNB1* mutations occurred at major tumor cell fraction in cfDNA, as well as the *TP53* mutation of patient #8, the *DICER1* mutation of patient #15 and the *DROSHA* and *SIX1* mutations of patient #11.

Furthermore, germline genetic abnormalities were confirmed in patients with syndromic WT, as expected: patient #5 with WAGR syndrome harbored a constitutional microdeletion in chromosome 11p13 encompassing *WT1* and patient #10 with DDS showed a germline *WT1* mutation. We unexpectedly detected a germline *WT1* mutation in patient #14 without genitourinary abnormalities, consistent with previous reports indicating that 2–5% of patients with non-syndromic WT might harbor constitutional *WT1* mutations.^{4,28} Tumors of patients #10 and #14 harbored somatic *CTNNB1* mutations, illustrating that there is a highly significant association between *WT1* and *CTNNB1* somatic mutations.²⁹ In these two patients, *CTNNB1* mutations were found in exon 3, as reported previously in WT that have lost *WT1*.³⁰

Concerning patients with non-WT kidney tumors, patient #1 with RCC showed somatic SNVs in cfDNA in 5 genes, common to tumor DNA. Interestingly, we detected SNVs at 7 different positions in the ATPase domain of a single gene (*ATP13A1*). Six of these 7 SNVs were confirmed by Sanger sequencing (Supporting Information Fig. 3). Five SNVs were identified in ctDNA of patient #2 with localized CCSK, with 1 SNV specific to ctDNA and 5 common to tumor DNA. We did not detect any SNV in ctDNA of patient #9.

Altogether, we were able to detect tumor cell specific, somatic, genetic alterations—CNAs, SNVs or both—in ctDNA in 10 (55.6%), 17 (94.4%) and 17 (94.4%) of the 18 patients of our cohort, respectively. Thus, tumor cell specific alterations in the ctDNA were found in all patients but one (for whom the plasma sample was obtained long after nephrectomy).

Discussion and Perspectives

The study of ctDNA is a promising noninvasive method for the molecular diagnosis and monitoring of tumors. It is of special interest in pediatric KT, for which histologic confirmation is not a standard practice before starting the treatment in many countries. Although only left over samples from routine full blood counts were used in this study, significant amounts of cfDNA with significant percentages of ctDNA could be isolated for a majority of patients. CtDNA higher than in adult cancers have been reported in other pediatric cancers such as neuroblastoma.^{31,32} We now demonstrate that also in pediatric KT at the time of diagnosis significant quantities of ctDNA can be isolated. We did not find any correlation between

ctDNA levels and tumor volume, metastatic stage nor histologic subtype of WT. This is probably due to the overall large volume of WT and important degree of necrosis in most cases, allowing the release of significant amounts of ctDNA.

Some technical issues may affect the analysis and have to be taken in account for the interpretation of the results. First, we worked with very low plasma volumes (as low as 100 μ L) or cfDNA input (as low as 4 ng). Nevertheless, we were able to detect specific tumor cell genetic abnormalities in plasma in all cases but one. This was possible because the sensitivity of our technique enables the detection of CNAs with a proportion of 20%, and of SNVs with a proportion of 5%, of ctDNA in overall cfDNA.¹⁴ Another relevant point is that left over blood of patients was retrieved in EDTA tubes within 24 h after venipuncture. Thus, there is a possibility of germline genomic DNA contamination in plasma samples that increases background noise and interferes with the molecular analysis. To avoid genomic DNA contamination and prevent disturbing of the results, the blood sample centrifugation should ideally be done within the 2 h after sampling.³³ However, the experimental procedure of library construction enables specifically the selection of small DNA fragments for sequencing, hence limiting the genomic DNA contamination in subsequent experimental steps (Supporting Information Fig. 4). Furthermore separate analysis of germline DNA enables to detect constitutional alterations separately and thus to clearly distinguish germline from somatic specific genetic events. In this sense, another issue that may affect the analysis of ctDNA is the potential presence of germline alterations, which should not to be missed during the interpretation of mutational data, especially during the SNVs filtering. Thus, we have to take in account whether a genetic alteration is also present in the germline, such as *WT1* mutations or intragenic deletions, but also *DICER1*, *DROSHA*, *DGCR8*, *XPO5*, *DIS3L2* or *FBXW7* mutations^{7,34–36} in WT, or *SMARCB1* abnormalities in RTK. Finally, in 10 of 18 cases, Sequenza tool estimated a fraction of ctDNA in cfDNA lower than 30%. This has to be taken in account in the interpretation of the data because the tool estimates correctly the ploidy when tumor content is higher than 30%, meaning that for lower tumor fractions we cannot formally conclude in case of negative results.

With regard to the copy number analysis, the profiles obtained in cfDNA were consistent with tumor DNA's (i.e. dynamic or silent in both samples) in 13 of the 16 cases (81.3%) for whom both cfDNA and tumor DNA were available. Importantly, tumors did not harbor a significantly higher number of CNAs after chemotherapy compared to ctDNA extracted before treatment. In 3 other cases (patients #1, #9 and #18), copy number profiles were silent in cfDNA but dynamic in tumor DNA. The absence of tumor cell specific CNAs in cfDNA in the presence of CNAs in tumor DNA might be due to different situations. First, in the absence of tumor mass, no ctDNA in the cfDNA is expected. This was the case of patient #9, whose plasma was collected after

nephrectomy when the patient was in clinical remission, explaining that no CNAs (nor SNVs) were found in cfDNA. Secondly, the absence of CNAs in cfDNA might suggest either an intratumor heterogeneity (with only a small fraction of tumor cells harboring these CNAs), or that these CNAs should have appeared secondarily in the tumor and were not present at the time of plasma sampling. Finally, the presence of high content of normal DNA in cfDNA, with a low ctDNA fraction, can potentially interfere in the bioinformatics interpretation and make it difficult to perform an accurate copy number analysis. These last three hypothesis could explain that in cases #1 and #18 CNAs in cfDNA could not be identified but some SNVs were detectable.

Concerning the analysis of SNVs, tumor cell specific variations were detected in cfDNA of all patients except one (patient #9, for whom the sample had been obtained when in complete remission). Focusing on patients with WT, somatic tumor cell specific *CTNNB1* alterations were found in ctDNA in more than one third of the cases (5 of 14), including two patients with germline *WT1* mutations. Interestingly, we found 3 non germline SNVs in the ctDNA of patient #5 with nephrogenic rests in the context of a WAGR syndrome, illustrating that nephrogenic rests may represent clonal precursor lesions derived from a transformed renal stem cell³⁷ that can be detected by analysis of cfDNA. Hence, the identification of tumor specific SNVs could be of importance with regards to surveillance and management of such lesions.

Some mutational events in tumor DNA were found to be at lower MAF than expected based on tumor fraction in tumor tissue. This might be explained by the presence of subclonal events occurring in only a small fraction of the overall tumor cell population. For ctDNA, events occurring at minor or major tumor cell fraction might be due to the variable pattern of ctDNA release into the blood between different tumor cell subclones. A good illustration of this issue is patient #14, who harbored a *CTNNB1* mutation at subclonal level in tumor DNA whereas it was found at major tumor cell fraction in cfDNA (Supporting Information Table 3).

Altogether, we were able to detect tumor cell genetic abnormalities in ctDNA by the presence of CNAs, SNVs or both in all patients except in patient #9 (17 of 18 patients, 94.4%). For this patient we can conclude that there was no tumor fraction in cfDNA, because of the total lack of tumor cell genetic alterations in cfDNA. Interestingly, in some cases genetic alterations were specific to cfDNA but not seen in the primary tumor (examples of patients #11, #15 and #16). This might be explained by the presence of intra tumor heterogeneity, with cellular populations releasing ctDNA not included in the tumor fragment analyzed at diagnosis or after surgery. Furthermore, in case of metastatic disease such heterogeneity could also suggest the hypothesis of heterogeneity between the primary tumor and the metastatic site, which might also release ctDNA. Our study indicates that among the total number of somatic SNVs identified, 76.4% occurred at a major

and 23.6% at minor tumor cellular fraction in cfDNA. This illustrates the pertinence of the study of cfDNA, which provides a different view of genetic alterations compared to the analysis of a small tumor fragment.

We sought to assess whether cfDNA analysis could allow us to identify the histologic tumor type of pediatric KT. Among the 14 patients with WT, in 12 of 14 cases (85.7%) tumor-cell specific alterations—CNAs, SNVs or both—highly suggestive of this disease were detected in cfDNA. The 2 WT for which no WT characteristic molecular abnormalities were detected in ctDNA included 2 localized tumors. First, patient #6 for whom the plasma sample was extracted 16 days after primary nephrectomy and whose tumor and cfDNA harbored a silent copy number profile and tumor cell specific SNVs in cfDNA but non suggestive of WT. Second, patient #18 with a silent copy number profile and several non-WT characteristic SNVs in ctDNA. Regarding other histotypes (CCSK and RCC), no characteristic genetic abnormalities suggestive of the corresponding KT subtype could be identified in cfDNA. In particular, we failed to detect the *BCOR* ITD of CCSKs (due to poor or absent tumor fraction content in cfDNA) and the *SPL/TFE3* translocation of the RCC. In this last case, it was due to the intrinsic characteristics of our sequencing technique. WES does not allow the identification of translocations (whereas indels are correctly detected), and this is a limit our approach. To overcome this issue, an additional sequencing technique, such as low-coverage whole-genome sequencing, could be implemented to detect chromosomal rearrangements in cfDNA. This technique is not expensive and could be a means to increase the discriminative power of our approach.

In conclusion, we demonstrate here the feasibility of ctDNA analysis to identify tumor cell specific genetic alterations in pediatric KT, in particular CNAs, SNVs and small indels based on a

ctDNA WES sequencing technique. This may be of interest to address distinct clinical questions. Firstly, this technique may be of interest by contributing to the diagnosis by molecular characterization of KT when an upfront biopsy was not performed. Furthermore, the early identification of the more aggressive subtypes, such as the anaplastic WT—based on the detection of *TP53* mutations—or other histotypes such as RTK—by the identification of *SMARCB1* alterations—could represent a useful tool to adapt the treatment early after diagnosis in these poor-prognosis diseases. Indeed, this work is a good basis for the development of a prospective study leading to the analysis of cfDNA in patients with KT by a panel of genes characteristic of each KT subtype, enabling to suggest the histologic diagnosis and guide the upfront management of pediatric patients with KT. Such a panel should incorporate biomarkers to enable screening for SNVs in genes recurrently altered in WT and other pediatric KT, as well as recurrently occurring CNAs and LOH. Secondly, prospective studies may also enable to determine the sensitivity of this technique for disease monitoring and follow up, which is particularly relevant in a disease where second line efficient salvage treatment options should be implemented early as soon as relapse is detected.

Acknowledgments

High-throughput sequencing has been performed by the ICGex NGS platform of the Institut Curie supported by the grants ANR-10-EQPX-03 (Equipex) and ANR-10-INBS-09-08 (France Génomique Consortium) from the Agence Nationale de la Recherche (“Investissements d’Avenir” program), by the Cancerpole Ile-de-France and by the SiRIC-Curie program - SiRIC Grant “INCa-DGOS- 4654”.

We would like to thank the tumor BioBanks of the Assistance Publique—Hôpitaux de Paris (APHP) hospitals Necker-Enfants Malades, Armand Trousseau, Robert Debré and Bicêtre.

This study was supported by the Annenberg Foundation, the Nelia and Amadeo Barletta Foundation (FNAB), and the Meghanora Association.

References

- Schwarzenbach H, Hoon DS, Pantel K. Cell-free nucleic acids as biomarkers in cancer patients. *Nat Rev Cancer* 2011;11:426–37.
- Tournade MF, Com-Nougue C, de Kraker J, et al. Optimal duration of preoperative therapy in unilateral and nonmetastatic Wilms' tumor in children older than 6 months: results of the Ninth International Society of Pediatric Oncology Wilms' Tumor Trial and Study. *J Clin Oncol* 2001;19:488–500.
- Pastore G, Znaor A, Spreafico F, et al. Malignant renal tumours incidence and survival in European children (1978–1997): Report from the Automated Childhood Cancer Information System project. *European Journal of Cancer* 2006;42:2103–14.
- Ruteshouser EC, Robinson SM, Huff V. Wilms tumor genetics: mutations in *WT1*, *WTX*, and *CTNBN1* account for only about one-third of tumors. *Genes Chromosomes Cancer* 2008;47:461–70.
- Williams RD, Al-Saadi R, Natrajan R, et al. Molecular profiling reveals frequent gain of *MYCN* and anaplasia-specific loss of 4q and 14q in Wilms tumor. *Genes Chromosomes Cancer* 2011;50:982–5.
- Maschietto M, Williams RD, Chagtai T, et al. *TP53* mutational status is a potential marker for risk stratification in Wilms tumour with diffuse anaplasia. *PLoS ONE* 2014;9(10):e109924.
- Wegert J, Ishaque N, Vardapour R, et al. Mutations in the *SIX1/2* pathway and the *DROSHA/DGCR8* miRNA microprocessor complex underlie high-risk blastemal type Wilms tumors. *Cancer Cell* 2015;27:298–311.
- Grundy PE, Breslow NE, Li S, et al. Loss of heterozygosity for chromosomes 1p and 16q is an adverse prognostic factor in favorable-histology Wilms tumor: a report from the National Wilms Tumor Study Group. *J Clin Oncol* 2005;23:7312–21.
- Wittmann S, Zirn B, Alkassar M, et al. Loss of 11q and 16q in Wilms tumors is associated with anaplasia, tumor recurrence, and poor prognosis. *Genes Chromosomes Cancer* 2007;46:163–70.
- Messahel B, Williams R, Ridolfi A, et al. Allele loss at 16q defines poorer prognosis Wilms tumour irrespective of treatment approach in the UKW1-3 clinical trials: a Children's Cancer and Leukaemia Group (CCLG) Study. *Eur J Cancer* 2009;45:819–26.
- Klamt B, Schulze M, Thate C, et al. Allele loss in Wilms tumors of chromosome arms 11q, 16q, and 22q correlate with clinicopathological parameters. *Genes Chromosomes Cancer* 1998;22:287–94.
- Perlman EJ, Grundy PE, Anderson JR, et al. *WT1* mutation and 11P15 loss of heterozygosity predict relapse in very low-risk wilms tumors treated with surgery alone: a children's oncology group study. *J Clin Oncol* 2011;29:698–703.
- Royer-Pokora B, Beier M, Henzler M, et al. Twenty-four new cases of *WT1* germline mutations and review of the literature: genotype/phenotype correlations for Wilms tumor development. *Am J Med Genet A* 2004;127A:249–57.
- Chicard M, Colmet Daage L, Clement N, et al. Whole exome sequencing of cell-free DNA reveals temporo-spatial heterogeneity and identifies treatment-resistant clones in neuroblastoma. *Clin Cancer Res* 2017.

15. Langmead B, Salzberg SL. Fast gapped-read alignment with Bowtie 2. *Nat Methods* 2012;9:357–9.
16. Van der Auwera GA, Carneiro MO, Hartl C, et al. From FastQ data to high confidence variant calls: the Genome Analysis Toolkit best practices pipeline. *Curr Protoc Bioinformatics* 2013;43:11 0 1–33.
17. Cibulskis K, Lawrence MS, Carter SL, et al. Sensitive detection of somatic point mutations in impure and heterogeneous cancer samples. *Nat Biotechnol* 2013;31:213–9.
18. McKenna A, Hanna M, Banks E, et al. The Genome Analysis Toolkit: a MapReduce framework for analyzing next-generation DNA sequencing data. *Genome Res* 2010;20:1297–303.
19. Li H, Handsaker B, Wysoker A, et al. The Sequence Alignment/Map format and SAMtools. *Bioinformatics* 2009;25:2078–9.
20. Schwarz JM, Cooper DN, Schuelke M, et al. MutationTaster2: mutation prediction for the deep-sequencing age. *Nat Methods* 2014;11:361–2.
21. Chun S, Fay JC. Identification of deleterious mutations within three human genomes. *Genome Res* 2009;19:1553–61.
22. Adzhubei IA, Schmidt S, Peshkin L, et al. A method and server for predicting damaging missense mutations. *Nat Methods* 2010;7:248–9.
23. Kumar P, Henikoff S, Ng PC. Predicting the effects of coding non-synonymous variants on protein function using the SIFT algorithm. *Nat Protoc* 2009;4:1073–81.
24. Koboldt DC, Zhang Q, Larson DE, et al. VarScan 2: somatic mutation and copy number alteration discovery in cancer by exome sequencing. *Genome Res* 2012;22:568–76.
25. Seshan VE, Olshen AB. DNACopy: DNA copy number data analysis. R package version 1.48.0. *Bioconductor* 2016.
26. Favero F, Joshi T, Marquard AM, et al. Sequenza: allele-specific copy number and mutation profiles from tumor sequencing data. *Ann Oncol* 2015;26:64–70.
27. Ye K, Schulz MH, Long Q, et al. Pindel: a pattern growth approach to detect break points of large deletions and medium sized insertions from paired-end short reads. *Bioinformatics* 2009;25:2865–71.
28. Little SE, Hanks SP, King-Underwood L, et al. Frequency and heritability of WT1 mutations in nonsyndromic Wilms' tumor patients: a UK Children's Cancer Study Group Study. *J Clin Oncol* 2004;22:4140–6.
29. Maiti S, Alam R, Amos CI, et al. Frequent association of beta-catenin and WT1 mutations in Wilms tumors. *Cancer Res* 2000;60:6288–92.
30. Li CM, Kim CE, Margolin AA, et al. CTNNB1 mutations and overexpression of Wnt/beta-catenin target genes in WT1-mutant Wilms' tumors. *Am J Pathol* 2004;165:1943–53.
31. Chicard M, Boyault S, Colmet Daage L, et al. Genomic Copy Number Profiling Using Circulating Free Tumor DNA Highlights Heterogeneity in Neuroblastoma. *Clin Cancer Res* 2016;22:5564–73.
32. Bettegowda C, Sausen M, Leary RJ, et al. Detection of circulating tumor DNA in early- and late-stage human malignancies. *Sci Transl Med* 2014;6:224ra24.
33. Combaret V, Iacono I, Bellini A, et al. Detection of tumor ALK status in neuroblastoma patients using peripheral blood. *Cancer Med* 2015;4:540–0.
34. Rakheja D, Chen KS, Liu Y, et al. Somatic mutations in DROSHA and DICER1 impair micro-RNA biogenesis through distinct mechanisms in Wilms tumours. *Nat Commun* 2014;2:4802.
35. Walz AL, Ooms A, Gadd S, et al. Recurrent DGCR8, DROSHA, and SIX homeodomain mutations in favorable histology Wilms tumors. *Cancer Cell* 2015;27:286–97.
36. Williams RD, Al-Saadi R, Chagtai T, et al. Subtype-specific FBXW7 mutation and MYCN copy number gain in Wilms' tumor. *Clin Cancer Res* 2010;16:2036–45.
37. Coppes MJ, Haber DA, Grundy PE. Genetic events in the development of Wilms' tumor. *N Engl J Med* 1994;331:586–90.

Bromodomain and extraterminal protein inhibitors in pediatrics: A review of the literature

Irene Jiménez¹ | André Baruchel^{2,3,4} | François Doz^{1,5} | Johannes Schulte⁶

¹Département d'Oncologie Pédiatrique, Adolescents et Jeunes Adultes de l'Institut Curie, Paris, France

²Service d'hémo-immunologie de l'Hôpital Universitaire Robert Debré, Paris, France

³Institut Universitaire d'Hématologie, Centre Hayem, Hôpital Saint-Louis, Paris, France

⁴Professor of Pediatrics, Université Paris-Diderot, Paris, France

⁵Professor of Pediatrics, Sorbonne Paris Cité, Université Paris-Descartes, Paris, France

⁶Department of Pediatric Oncology/Hematology, Charité-Universitätsmedizin Berlin, Berlin, Germany

Correspondence

François Doz, Département d'Oncologie pédiatrique, adolescents et jeunes adultes de l'Institut Curie, 26 rue d'Ulm, Paris 75005, France.
 Email: francois.doz@curie.net

Grant sponsor: Nelia and Amadeo Barletta Foundation; Grant sponsor: OncoEthix Pharma.

Abstract

The last few years have seen the identification of pharmacologic approaches to target bromodomain and extraterminal (BET) proteins for cancer treatment. These proteins have an essential role in gene transcription regulation by binding acetylated lysine residues on histone tails, activating gene transcription. BET inhibitors have been tested in preclinical models including pediatric malignancies and several adult clinical trials are ongoing. Since the development of new drugs in pediatric cancer has long lagged behind programs for adults, the aim of this review is to show the importance of these therapies in pediatric malignancies to support their development in pediatric oncology/hematology.

KEYWORDS

BET inhibitors, bromodomain, epigenetics, pediatrics

1 | INTRODUCTION: EPIGENETICS AND BROMODOMAIN AND EXTRATERMINAL PROTEINS

The field of epigenetics studies genetic modifications not encoded in the DNA sequence but the factors that affect how cells express genes. DNA methylation, histone modification, and nucleosome remodeling are some examples of epigenetic modifications. At least 16 different classes of histone modifications have been described to date¹ and acetylation is the most common and explored mechanism, inducing chromatin structure modifications that affect gene transcription. Examples of epigenetic targets are the enzymes that catalyze the deacetylation of histones, which are inhibited by the commonly used drug vorinostat.

The last few years have seen the identification of bromodomain and extraterminal (BET) proteins as critical mediators of transcription.

Bromodomains (BRDs), which are present on BET proteins, are highly conserved functional domains that recognize and bind acetylated lysine residues on histone tails. For this reason, BET proteins have been labeled as “readers,” in contrast to two other groups of proteins known as “writers and “erasers.” Writers and erasers respectively add or remove an acetyl group to transition from closed to open chromatin, and vice versa, in order to access or repress the genetic information. The four members of this family, BRD2, BRD3, BRD4, and BRDT, activate transcription via recruitment of polymerases and transcription factors (TFs) and play a fundamental role in transcriptional elongation, promoting G1 gene expression, and cell cycle progression.²

A well-studied member of the BET family is BRD4, which plays a key role in Pol II-dependent transcription during interphase. This activity is mediated primarily by its ability to recruit positive transcription elongation factor b (P-TEFb) and the Mediator complex to a promoter by contacting acetylated chromatin,³ thus promoting transcriptional elongation. Through this activity, BRD4 is shown to act as a transcriptional coactivator of many cellular genes, especially genes involved in the G1 phase of the cell cycle (during which the cell grows and synthesizes proteins required for DNA replication), such as *MYC*, *BCL2*, and *CDK2*.⁴ (Fig. 1A). While the P-TEFb level displays no major change through the cell cycle, the interaction of P-TEFb with BRD4

Abbreviations: AML, acute myeloid leukemia; AL, acute leukemia; B-ALL, B-cell acute lymphoblastic leukemia; BBB, blood-brain barrier; BET1, BET inhibitors; BET, bromodomain and extraterminal; BL, Burkitt's lymphoma; BRD, bromodomain; DLBCL, diffuse large B-cell lymphoma; DLT, dose-related toxicity; HGG, high-grade glioma; NMC, NUT midline carcinoma; NUT, nuclear protein in testis; P-TEFb, positive transcription elongation factor b; SHH, sonic hedgehog; Smo, smoothened; T-ALL, T-cell acute lymphoblastic leukemia; TF, transcription factor

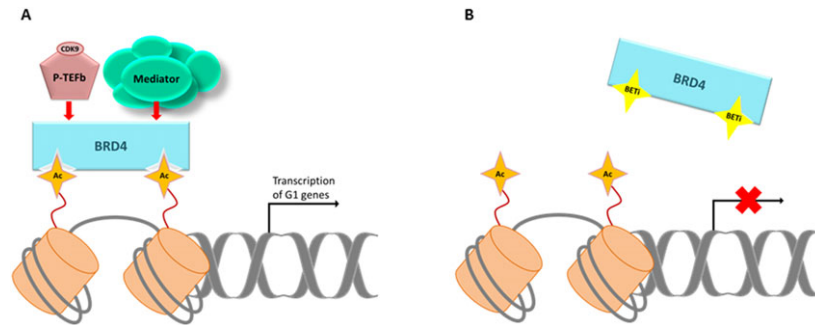


FIGURE 1 Protein–protein interactions involving BRD4 and mechanism of action of BET inhibitors. (A) BRD4 binds to acetylated lysine residues on histone tails and recruits candidate effectors as Mediator and P-TEFb (with its catalytic subunit, CDK9) and regulates G1 genes transcription by DNA polymerase II. (B) BET inhibitors interfere with the interaction between the bromodomain of BRD4 and acetylated lysines on histone tails and repress gene transcription. BETi, BET inhibitor; Ac, acetylated lysine residues; and P-TEFb, positive transcription elongation factor b

dramatically increases in cells progressing from late mitosis to early G1. All this together has given a strong rationale to hypothesize that BET proteins are involved in cancer molecular events.

2 | BET INHIBITORS IN PEDIATRIC AND YOUNG ADULT CANCER: PRECLINICAL DATA

Motivated by the above-mentioned rationale, several teams have developed different drugs that target BET proteins (Fig. 1B) with different affinities. The fusion between *BRD4* and nuclear protein in testis (*NUT*) gene leads to a BRD4–NUT oncoprotein responsible for the highly aggressive undifferentiated squamous cell carcinomas known as NUT midline carcinoma (NMC).⁵ This malignancy provided a clear rationale for the development and initial therapeutic evaluation of BET inhibitors (BETi): JQ1 was the first BRD inhibitor to be described in 2010 by Filippakopoulos et al.,⁶ who showed that JQ1 engaged the binding site of BET bromodomains in a way that mimics the binding mode of acetylated lysine residues, displaced BRD4 from nuclear chromatin in cells and induced differentiation and apoptosis in NMC cells, as well as antitumor efficacy in xenograft models. Since then, several molecules have been developed in preclinical studies mainly in adult malignancies but in some cases also in pediatric cancer models.^{7,8} Details concerning *in vitro* and *in vivo* models, including cell lines, inhibitory concentration 50%, and mouse models, are shown in Table 1.

2.1 | BETi in pediatric hematological malignancies

The first approach of JQ1 to pediatric malignancies was performed in pediatric acute myeloid leukemia (AML) cell lines.⁹ MLL fusion leukemia is an example of epigenetic deregulation: MLL is a histone methyltransferase (actually a “writer”) that activates transcription by adding a methyl group to histone residues. Leukemia-associated translocations lead to a rearrangement of *MLL* with several partners that are mostly critical components of the initiation and transcription elongation complexes SEC and PAFc. Zuber et al.¹⁰ tested three primary *MLL*-rearranged pediatric AML cell lines, all sensitive to JQ1,

which triggered cell cycle arrest and apoptosis. *In vivo* experiments showed that JQ1 had leukemia-specific effects, denoted by a delay in disease progression and significantly extended survival in treated mice.

MYC is a master TF of cell proliferation and has been considered for a long time a compelling therapeutic target because of its implication in a wide range of human malignancies. However, inhibition of *MYC* function has been challenging because of the diverse mechanisms driving its aberrant expression and the challenge of disrupting protein–DNA interactions. A paradigm for *MYC* dysregulation is offered by Burkitt’s lymphoma (BL), where chromosomal translocations leading to immunoglobulin gene–*MYC* fusion are the crucial initiating oncogenic events. JQ1 has been shown to reduce *MYC* expression by releasing BET proteins from *MYC* locus, indicating that BET proteins directly regulate *MYC* gene expression. JQ1 has also shown antitumor activity in xenograft mouse models of BL,¹¹ with significantly slower tumors growth and higher survival compared with vehicle-treated controls.

In that context, Da Costa et al.¹² studied JQ1 BRD inhibition in pediatric B-cell acute lymphoblastic leukemia (B-ALL) with common cytogenetic abnormalities (e.g., hyperdiploidy, t(12;21), t(1;19), and *MLL* rearrangements): JQ1 showed cytotoxic effect on patient-derived pediatric B-ALL cells (by downregulation of multiple prosurvival genes and apoptosis-mediated cell death) and in mouse xenografts (by a significant reduction in tumor load when combined with dexamethasone, even in a dexamethasone-resistant cell line xenograft model), independent of the phenotype. Given that cytogenetic profiles of primary B-ALL samples did not influence the response to JQ1, they addressed the issue of transcriptional markers of sensitivity to BET inhibition in primary B-ALL samples and showed that the cytotoxic response correlated with the downregulation of *MYC* transcription and reduction of *MYC* stability.

Other oncogenic pathways involving *MYC* are *NOTCH1* mutations, which are present in about 55% of patients with T-cell acute lymphoblastic leukemia (T-ALL).¹³ Notch1 regulates leukemic proliferation by directly stimulating *MYC* and cyclin D3 expression. Roderick et al.¹⁴ studied whether *MYC* inhibition results in efficient targeting of T-ALL-initiating cells. They showed that JQ1 downregulates *MYC*

TABLE 1 Preclinical studies evaluating BET inhibitors in pediatric malignancies

Disease	BET inhibitor	Reference	In vitro models		In vivo mouse models (cell line engrafted or GEMM model)
			Cell lines	Median IC ₅₀ [range]	
Hematological malignancies					
BL	JQ1	Mertz et al. ¹¹	Human BL cell line <i>Raji</i>	NA	Human CLX (<i>Raji</i>)
Pediatric AML	JQ1	Zuber et al. ¹⁰	Three patient-derived pediatric MLL-rearranged AML cell lines	174 nM [163–345]	Mouse allograft (MLL-AF9/ <i>Nras</i> ^{G12D})
Pediatric B-ALL	JQ1	Da Costa et al. ¹²	Twenty-six patient-derived pediatric B-ALL cell lines	1,800 nM [0.106–34,172]	Human CLX (REF, patient-derived B-ALL cell line)
Pediatric T-ALL	JQ1	Roderick et al. ¹⁴	Mouse T-ALL cell line <i>Tal1/Lmo2</i> Seven patient-derived pediatric T-ALL cell lines	NA Average: 380 nM [149–868]	NOTCH1-mutated GEMM (<i>Tal1/Lmo2</i>)
DLBCL	JQ1	Trabucco et al. ¹⁷	Human DLBCL cell lines OCI-Ly18, RC-K8, SU-DHL-4, SU-DHL-5, SU-DHL-6, SU-DHL-10, HBL-1, HLY-1, OCI-Ly8, OCI-Ly3, OCI-Ly10	Range: [25–160] nM	Human CLX (OCI-Ly8)
DLBCL	OTX015	Boi et al. ¹⁸	Human DLBCL cell lines DOHH2, HBL1, Karpas 422, OCI-Ly1, OCI-Ly10, OCI-Ly2, OCI-Ly3, OCI-Ly7, OCI-Ly8, Val, RCK8, Riva, SU-DHL-10, SU-DHL-2, SU-DHL-4, SU-DHL-5, SU-DHL-6, SU-DHL-7, TMD8, U-2932, WSU-DLCL2	195 nM [70–1,500]	Human CLX (SU-DHL-2)
AL	OTX015	Coudé et al. ¹⁵	Human ALL cell lines JURKAT, RS4-11, TOM-1, BV-173 Human AML cell lines K562, HL60, NOMO-1, KG1, KG1a, HEL, OCI-AML3, NB4, KASUMI Patient-derived ALL and AML cell lines	147 Nm [34–249] 233 nM [17–11,342] NA	
Brain tumors					
GB	JQ1	Cheng et al. ²⁶	Primary GB xenograft lines T4105, T4302, T4597, GBM6, GBM8, GBM10, GBM12, GBM16, GBM22, GBM29, GBM43, GBM46 Human GB cell lines VU10369, VU10827, VU11014	300 nM [60–2,000]	Human CLX (T4302, T4597)
GB	i-BET151	Pastori et al. ²⁵	Human GB cell lines U87MG, A172, SW1783	1,120 nM [1,050–1,280]	Human CLX (U87MG)
MYCa MB	JQ1	Henssen et al. ²⁷	Human MYCa MB cell lines HD-MB3, D-283	78 and 477 nM	Human CLX (HD-MB3)
MYCa MB	JQ1	Bandopadhyay et al. ²⁹	Human MYCa MB cell lines D283, D425, D556, D458 Patient-derived MYCa MB cell lines MB002, MB004	264 nM [221–322] 555 and 683 nM	Human CLX (MB002)
MYCa MB	JQ1	Venkataraman et al. ²⁸	Human MYCa MB cell lines D283, D425, D458	NA	Human CLX (Daoy)
SHH-driven MB	i-BET151	Long et al. ³¹			PTCH1-mutated GEMM (<i>Ptc^{+/−}</i>)
SHH-driven MB	JQ1	Tang et al. ³²	Patient-derived MB cell lines RCMB025 (SU-FU-mutated), RCMB018 (MYCN amplified)	NA	Mouse allograft (Med1-MB, SmoWT-MB, SmoD477G-MB)

(continues)

TABLE 1 (Continued)

Disease	BET inhibitor	Reference	In vitro models		In vivo mouse models (cell line engrafted or GEMM model)
			Cell lines	Median IC ₅₀ [range]	
Neuroblastoma					
MYCNa NB	JQ1	Puissant et al. ¹⁹	Human MYCNa NB cell lines BE(2)-C, Kelly, LAN-1, NGP	560 nM [430–590]	Human CLX (BE(2)-C, SH-SY5Y) MYCNa NB GEMM (TH-MYCN)
MYCNa NB	I-BET726	Wyce et al. ²⁰	Human MYCNa NB cell lines LA-N-1, Kelly, LA1-55n, BE(2)-M17, BE(2)-C, KanTS, IMR32, LA-N-2, SK-N-BE(2), CHP-134, CHP-212, LA1-5s, SK-N-DZ	75 nM [2–460]	Human CLX (CHP-212, SK-N-AS)
MYCNa NB	JQ1	Lee et al. ²²	Human MYCNa NB cell lines BE(2)-C, IMR-32, BE(2)-M17, SK-N-DZ	NA	Human CLX (BE(2)-C)
MYCNa NB	OTX015	Henssen et al. ²¹	Human NB cell lines Chp-134, IMR-5, IMR-32, SK-N-BE, and SK-N-BE	NA	Human CLX (IMR-5)
Other solid tumors					
NMC	JQ1	Filippakopoulos and co-workers ²³	Patient-derived BRD4-NUT NMC cell line 11060	4 nM	Human CLX (NMC797)
OS	JQ1	Lamoureaux et al. ³³	Human OS cell lines MG63, SaOS2, U2OS, KHOS, MNNG/HOS, SJSa-1, SJSa-1, 143B, G-292, CAL72	5.476 μM [0.268–9772]	Human CLX (HOS) mouse allograft (POS-1)
OS	JQ1 I-BET726 I-BET151	Baker et al. ³⁴	Murine OS cell lines POS-1 and MOS-J Murine OS cell lines 494H, 493H, 716H, 148L, 148I, 98Sc, 89R, 494L, 493L, 148L, 98L	NA JQ1: 136 nM [50–406]; I-BET151: 561 nM [166–1,120] I-BET726: 943 nM [278–1,845]	Mouse allograft (494H)
ES	JQ1	Jacques et al. ³⁶	Human OS cell lines OS17, Os9, MG63, SAOS2, U2OS, SJSa-1	1.387 nM [0.109–4.911]	Human CLX (TC71)
MPNST	JQ1	Patel et al. ³⁷	Human ES cell lines A673, TC32, SKES-1, SK-N-MC, RDES, EW24, TC71, A673-1c, ASP14, EW7, IOR/BRZ Human MPNST cell line S462 Murine NF1-P53-mutated MPNST cell lines	NA <400 nM	Mouse allograft (sMPNST)

IC₅₀, inhibitory concentration 50%; BL, Burkitt's lymphoma; AML, acute myeloid leukemia; ALL, acute lymphoblastic leukemia; AL, acute leukemia; DLBCL, diffuse large B-cell lymphoma; GB, glioblastoma; MB, medulloblastoma; MYCa MB, MYC-amplified medulloblastoma; SHH-driven MB, sonic hedgehog driven medulloblastoma; NB, neuroblastoma; MYCNa NB, MYCN-amplified neuroblastoma; NMC, NUT midline carcinoma; OS, osteosarcoma; ES, Ewing sarcoma; MPNST, malignant peripheral nerve sheath tumor; CLX, cell line derived xenograft; GEMM, genetically engineered mouse model; NA, not available.

and induces cell cycle arrest and apoptosis in murine *Notch1*-mutated T lymphoblastic transgenic cells and pediatric T-ALL cells, including treatment refractory, both *in vitro* and in mouse transplanted models. Silencing of *MYC* resulted in significant increases in overall survival in the *in vivo* models.

OTX015, a JQ1 analog authorized for clinical use in human trials, has also shown its *in vitro* effects in acute leukemia (AL), both lymphoblastic and myeloblastic. Coudé et al.¹⁵ assessed the effects of OTX015 on cell proliferation, cell cycle, and apoptosis in a representative panel of ALL and AML cell lines and in leukemic patient-derived samples, and observed similar cell cycle arrest in the G1/S transition and apoptosis rates as previously reported for JQ1. Significant growth inhibition was found in six of nine AML cell lines and all four ALL cell lines tested. A decrease in *MYC* expression was observed in the majority of the cell lines as well as in primary AL samples when treated with OTX015.

BRD inhibition has also been studied in diffuse large B-cell lymphoma (DLBCL), for which three subtypes differing in molecular and clinical features have been identified (activated B-cell like, germinal center B-cell like, and primary mediastinal B-cell lymphoma). *MYC* rearrangements (roughly 10% of DLBCL) and increased protein levels of *MYC* (about 30% of DLBCL) confer a negative prognostic impact to standard therapy including rituximab regimens,¹⁶ suggesting that targeting *MYC* may be beneficial for these patients. Trabucco et al.¹⁷ found antitumor activity of JQ1 in human DLBCL cell lines, independently of their molecular subtypes, by inducing either apoptosis or senescence. Suppression of *MYC* was also seen in cell lines, regardless of their natural, chromosomally translocated or gene-amplified *MYC* loci. In mouse models, JQ1 suppressed the growth of DLBCL-engrafted cells and improved the survival of tumor-bearing mice but was not sufficient to cure the disease. Trabucco et al.¹⁷ hypothesized that bioavailability, especially the relative low half-life of JQ1 in plasma, could explain this issue. More recently, Boi et al.¹⁸ reported the preclinical activity of OTX015 in DLBCL. OTX015 showed *in vitro* antiproliferative and proapoptotic effects with *MYC* downregulation. *In vivo*, OTX015 induced a significant reduction in the growth of lymphoma xenografts compared with control vehicle.

2.2 | BETi in neuroblastoma

In neuroblastoma, BETi have recently generated considerable excitement based on its ability to block transcription of *MYCN*, a key driver of neuroblastoma tumorigenesis whose amplification status is a marker of poor prognosis. In preclinical studies, JQ1, OTX015, and I-BET726 have shown to induce cell cycle arrest and apoptosis, as well as downregulation of *MYCN* expression in neuroblastoma cell lines.^{19–21} In murine models, the three drugs showed therapeutic activity by inhibiting neuroblastoma tumor growth and significantly prolonging survival. This effect was applicable for I-BET726 in both mice carrying *MYCN*-amplified and *MYCN*-nonamplified neuroblastomas. Lee et al.²² observed in a recent study that, in addition to its antitumor activity, JQ1 induced neuronal differentiation in cell lines and mouse models of *MYCN*-amplified neuroblastomas by showing morphologic changes and expression of neural differentiation markers.

2.3 | BETi in brain tumors

Although there are no publications comparing the blood–brain barrier (BBB) permeability to the different BETi, some data are available concerning this issue. JQ1 has shown to have a good permeability across BBB ($AUC_{\text{brain}}/AUC_{\text{plasma}} = 98\%$).²³ There is also a good permeability for OTX015, which shows tumor levels 7- to 15-fold higher than that in normal tissues,²⁴ but it is unlikely that I-BET151 is brain penetrant due to its high polar surface area.²⁵

High-grade glioma (HGG) is an aggressive malignant brain tumor with generally poor outcome. Two substantial advances have been achieved in the last few years regarding their molecular biology. First, the identification of V600E *BRAF* mutations in a subset of HGG, thus targetable by *BRAF* inhibitors, and second, the description of driver mutations in histone H3.3 without therapeutic implications to date. Two preclinical studies with both JQ1 and I-BET151 have been recently published. JQ1 was shown by Cheng et al.²⁶ to have *in vitro* antineoplastic effects by compromising cellular proliferation and survival of glioblastoma (GB) cells due to selective targeting of BET proteins. Downregulation of *MYC* observed in sensitive cells was rather modest but more intense than that for insensitive cells. In the first *in vivo* assay, JQ1-treated mice showed a better survival compared with nontreated mice. In another experiment, the growth rate and sizes of JQ1-treated tumors were slightly higher than those of the control arm, but treated tumors appeared to progress at a slower rate while treatment continued and thus were soon overgrown by tumors in the control arm. Pastori et al.²⁵ showed that I-BET151 reduced GB cell proliferation and was as effective as temozolomide to reduce tumor size in xenografts, suggesting that I-BET151 analogs that cross the BBB may be an effective GB treatment.

Medulloblastoma is the most common malignant pediatric brain tumor and still represents a significant clinical challenge, especially for subgroup 3 with *MYC* amplification and sonic hedgehog (SHH) subtype harboring *MYCN* amplification, both with extremely poor prognosis. Based on the previous preclinical studies with BETi in *MYC*-driven malignancies, several teams have studied the usefulness of JQ1 in *MYC*-driven medulloblastoma, showing *in vitro* reduction of cell viability and proliferation, induction of apoptosis and senescence, and downregulation of *MYC* and *MYC* target expression. Tumors grew significantly slower in JQ1-treated mice compared with the vehicle control group.^{27–29}

In the SHH subtype, when not bound by hedgehog ligand, PTCH1 inhibits the pathway signaling protein smoothed (Smo). Once bound by ligand, PTCH1 allows Smo to positively regulate mobilization of GLI2 to the nucleus, where GLI2 transactivates the *GLI1* promoter. GLI1 and GLI2 directly transactivate the transcription of hedgehog target genes, several of which are involved in proliferation, such as *MYCN* and *CCND1*.³⁰ Long et al.³¹ showed *in vitro* that I-BET151 abrogates *GLI1* transcription by reducing the association of BRD4 with the proximal regulatory region of the *GLI1* locus. In a *PTCH1*-mutated medulloblastoma model, I-BET151 induced tumor growth attenuation through inhibition of hedgehog signaling, reducing the levels of GLI1, compared with vehicle-treated mice. Tang et al.³² showed markedly cell viability decrease in response to JQ1 in SHH medulloblastoma cell

lines including one SUFU-mutated and one MYCN-amplified cell lines. In *in vivo* models, JQ1-treated mice had a significant reduction in tumor growth as well as an increase in overall survival. MYCN was consistently downregulated by JQ1 in all SHH-driven models studied, suggesting that decreased MYCN levels in SHH-driven tumors reflect the role of GLI in directly transactivating the MYCN promoter.

2.4 | BETi in other pediatric and young adult solid tumors

As already mentioned, NMC was the first malignancy showing the anti-tumor effects of JQ1 *in vivo* and *in vitro*,⁶ and provided a strong rationale to target BET proteins in human cancer. Osteosarcoma is the most frequent malignant primary bone tumor type in children and young adults and have poor prognosis owing to its propensity to metastasize. Lamoureux et al.³³ showed *in vitro* that BRD4 is present on the MYC and RUNX2 promoter region and that JQ1 antiproliferative activity results in the downregulation of these two genes in osteosarcoma cells. They observed a strong reduction in viability of osteosarcoma cells with JQ1, irrespective of whether the oncogenic driver was MYC or RUNX2, and antitumor effects by reducing the average tumor volume and prolonging survival of mouse models. The authors unexpectedly found that JQ1 is a potent inhibitor of osteoblast and osteoclast differentiation. Baker et al.³⁴ showed the antiproliferative activity of JQ1, I-BET151, and I-BET726 in osteosarcoma cell cultures. Interestingly, they did not find MYC downregulation with JQ1 in their *in vitro* models, but corroborated robust reductions of RUNX2, which is emerging as a potential oncogene in osteosarcoma.³⁵ Ewing sarcoma is characterized by chromosomal translocations, and the most common case is the translocation t(11; 22) that yields the EWS-FLI1 chimeric TF. Jacques et al.³⁶ found that JQ1 directly represses EWS-FLI1, induces G1-phase cell cycle arrest, and inhibits cell viability in all Ewing sarcoma cell lines studied. *In vivo*, JQ1 showed therapeutic effects by significantly reducing tumor growth and prolonging overall survival in mouse xenografts, with repression of EWS-FLI1 expression. Malignant peripheral nerve sheath tumors are very aggressive sarcomas that mainly develop in neurofibromatosis type 1 patients. It is typically chemo- and radioresistant and its prognosis is almost invariably fatal. Patel et al.³⁷ showed that BRD4 regulates cyclin D1 expression and thus cell cycle progression, and JQ1 induces apoptosis by induction of proapoptotic Bim protein and downregulation of antiapoptotic protein BCL-2.

3 | PREDICTIVE BIOMARKERS

A prerequisite to successful targeted cancer therapy is not only the availability of targeted compounds but also the presence of robust biomarkers that predict responsiveness of tumors to a specific compound or class of compounds. To identify predictive biomarkers of responsiveness to the JQ1, Puissant et al.¹⁹ analyzed more than 600 tumor cell lines. Indeed, among the cell lines most responsive to JQ1 treatment were neuroblastoma cell lines with MYCN amplification, pointing to the fact that MYCN could be a biomarker predicting response to BETi. However, only four of 99 sensitive cell lines

were MYCN amplified, meaning that other biomarkers of sensitivity for BET inhibition remain to be defined. Based on the above-mentioned preclinical data, MYC amplification, NOTCH1 activation, PTCH1 mutations, BRD4-NUT fusion protein, and MLL or MYC fusion proteins should also be explored as predictors of response to BETi. Taking into consideration that the function of BET proteins depends on the cell context-dependent patterns of histone modifications and BETi have likely pleiotropic effects, further efforts to define predictive biomarkers in different tumor entities or context-independent general patterns should be undertaken.

4 | ALTERNATIVE STRATEGIES TO TARGET BRD4-DEPENDANT GENE TRANSCRIPTION

While direct inhibition of BRD4 (and other BET family members) is an efficient way to suppress transcription, inhibition of proteins that are recruited by BET proteins to drive transcription could be an alternative. Indeed, inhibition of CDK7, a factor that phosphorylates Pol II, efficiently inhibits BET protein-driven transcription and phenocopies the effect of the BETi JQ1.³⁸ Furthermore, inhibition of CDK9, the catalytic subunit of P-TEFb, should also quite effectively inhibit BRD4-driven transcription. The differences between BET, CDK7, and CDK9 inhibitors remain to be determined, but it is tempting to speculate that these compounds could also act synergistically and/or might also be used to overcome or prevent resistance.

5 | SEARCHING FOR THE MECHANISMS OF RESISTANCE

Since the effectiveness of targeted therapies is often limited by the development of resistance, several groups have studied the resistance of different cancer cell populations to BETi. In the first published study focusing on BET inhibition resistance,³⁹ pancreatic cancer cells developing resistance to JQ1 showed cross-resistance to I-BET151 and were insensitive to BRD4 downregulation, maintaining expression of MYC. More recently, in triple negative breast cancer cells with acquired resistance to BET inhibition, a strong association with hyperphosphorylation of BRD4 was highlighted.⁴⁰ In a genetically engineered model of B-cell lymphoma, upregulation of BCL-2 and activation of the RAS pathway were observed in both intrinsically and acquired resistant tumors to JQ1 inhibition, as well as the activation of the RAS pathway conferred primary resistance to JQ1.⁴¹

6 | COMBINING BET INHIBITORS WITH OTHER ANTICANCER THERAPIES: THE PRECLINICAL DATA

Some BETi have been tested in combination with other anticancer therapies in preclinical models of pediatric diseases. In particular JQ1 has been shown to sensitize B-ALL cells to dexamethasone, *in*

TABLE 2 List of clinical trials with BET inhibitors in cancer (from www.clinicaltrials.gov, last update: September 20, 2016)

Compound/company	Status	Clinical phase	Age (years)	Disease	Identifier	Estimated completion date
FT-1101/Forma Therapeutics	Recruiting	I	≥ 18	AML Myelodysplastic syndrome	NCT02543879	August 2018
CPI-0610/Constellation Pharmaceuticals	Recruiting	I	≥18	Lymphoma	NCT01949883	November 2016
	Recruiting	I	≥18	Multiple myeloma	NCT02157636	December 2016
	Recruiting	I	≥18	Acute leukemia Myelodysplastic syndrome Myelodysplastic neoplasms Myeloproliferative neoplasms Myelofibrosis	NCT02158858	January 2017
GSK525762/GSK	Recruiting	I	≥18	Hematologic malignancies	NCT01943851	July 2019
	Recruiting	I	≥16	NUT midline carcinoma Solid tumors	NCT01587703	May 2020
GSK2820151/GSK	Not yet recruiting	I	≥18	Advanced solid tumors	NCT02630251	February 2018
OTX015/OncoEthix	Active, not recruiting	I	≥18	AML Acute lymphoblastic leukemia Multiple myeloma DLBCL	NCT01713582	November 2016
	Active, not recruiting	I	≥18	NUT midline carcinoma TN breast cancer NSC lung cancer with rearranged ALK gene/fusion protein or KRAS mutation Castration-resistant prostate cancer Pancreatic ductal adenocarcinoma	NCT02259114	November 2016
	Terminated	I/II	≥18	Glioblastoma multiforme	NCT02296476	October 2015
	Withdrawn	I/II	≥18	AML (in combination with azacitidine)	NCT02303782	March 2016
BMS-986158/Bristol-Myers Squibb	Recruiting	I/II	≥18	Advanced solid tumors	NCT02419417	December 2018
TEN-010/Tensha Therapeutics	Recruiting	I	≥18	AML Myelodysplastic syndrome	NCT02308761	June 2017
	Recruiting	I	≥18	Advanced solid tumors	NCT01987362	August 2017
BAY 1238097/Bayer	Terminated	I	≥18	Advanced cancer	NCT02369029	January 2016
ABBV-075/AbbVie	Recruiting	I	≥18	Advanced solid tumors	NCT02391480	May 2018
MK-8628/Merck	Recruiting	I	≥18	AML DLBCL	NCT02698189	January 2018
	Recruiting	I	≥16 ≥18	NUT midline carcinoma Triple negative breast cancer Non-small cell lung cancer Castration-resistant prostate cancer	NCT02698176	February 2018
ZEN003694/Zenith Epigenetics	Recruiting	I	≥18	Metastatic castration-resistant prostate cancer	NCT02705469	April 2018
	Not yet recruiting	I	≥18	Metastatic castration-resistant prostate cancer (in combination with enzalutamide)	NCT02711956	April 2018
INCB054329/Incyte Corporation	Recruiting	I/II	≥18	Advanced cancer	NCT02431260	February 2018
INCB057643/Incyte Corporation	Recruiting	I/II	≥18	Advanced solid tumors or hematologic malignancies	NCT02711137	July 2018

DLBCL: Diffuse large B cell lymphoma. TN: triple negative. NSC: Non-small cell. AML: Acute Myeloid Leukemia.

vitro and *in vivo*, including dexamethasone-resistant cell lines. Dexamethasone also acted synergistically even in cell lines that responded well to both drugs individually.¹² In osteosarcoma cell lines, JQ1 showed additive effects with doxorubicin (suggesting that JQ1 could chemosensitize osteosarcoma cells to standard therapy) and synergistic effects with CDK inhibitors flavopiridol and dinaciclib.³⁴ OTX015 has been tested in *AML1-ETO* AML cell line¹⁵ combined with other epigenetic modifying drugs, such as panobinostat (histone deacetylase inhibitor) and azacitidine (hypomethylating agent): simultaneous treatments lead to additive effects while a strong synergy was observed with a sequential treatment with azacitidine followed by OTX015. This drug has also been tested in combination with several anticancer agents in a panel of five DLBCL cell lines.¹⁸ In particular, strong synergism was observed in all the cell lines when combined with everolimus (mTOR inhibitor). Other agents such as idelalisib (PI3K-delta inhibitor), vorinostat (histone deacetylase inhibitor), rituximab (CD20 monoclonal antibody), decitabine (hypomethylating agent), and lenalidomide (immunomodulant) also showed synergistic effects with OTX015.

7 | POTENTIAL SPECIFIC SIDE EFFECTS IN THE PEDIATRIC POPULATION

It is known that the four *BET* genes are expressed during spermatogenesis, and the testis-specific gene *BRDT* is essential for spermatogenesis. Loss of the first BRD of *BRDT* results in improper spermatid elongation and severely defective sperm,⁴² meaning that BETi could potentially have deleterious effects in fertility. As *BRDT* is not expressed in mitotically dividing spermatogonia, *BRDT* inhibition would not affect the spermatogonial stem cell, hence making this fertility impairment reversible, but no information is available concerning potential long-term effects in organisms under development, such as the pediatric population; another issue that is not yet explored concerns children's growth. As JQ1 has been shown to inhibit osteoblast and osteoclast differentiation,³³ there could be a theoretical effect with growth impairment or bone remodeling. A third potential side effect concerns the relationship between *BET* proteins and viruses. Some publications have shown the involvement of *BET* proteins in viral infections such as HIV (but also papillomavirus or Epstein-Barr virus), in which *BRD4* could act as a transcriptional repressor of HIV, preventing virus reactivation from latency.⁴³ Thus, BETi could potentially promote HIV transcription and reactivation in HIV-positive patients. Because of this theoretical side effect, HIV screening should be possibly included in clinical trials with BETi.

8 | CLINICAL EXPERIENCE WITH BET INHIBITORS IN CANCER

Based on the promising effects seen in preclinical studies, several early clinical trials started in 2013 to evaluate the safety and efficacy of BETi in human cancer (Table 2), with 22 early trials have been registered to date (last update September 2016). These trials are focused

on hematological malignancies (10 of 22) and solid tumors (eight of 22), but also on selected tumors such as NMC, GB, triple negative breast cancer, nonsmall cell lung cancer with rearranged *ALK* gene/fusion protein or *KRAS* mutation, castration-resistant prostate cancer, and pancreatic ductal adenocarcinoma. In total, 13 registered molecules are being tested in 22 early clinical trials. All of them include patients older than 18 years with the exception of two trials using GSK525762 and MK-8628 (previously known as OTX015) respectively, which are being tested in patients older than 16.

The first clinical data concerning BETi were produced during a phase I trial with OTX015^{44,45} in two groups of relapsed/refractory adult hematologic malignancies: advanced AL and lymphoma or multiple myeloma. In patients with AL, the observed dose-limiting toxicities (DLTs) were grade 3 diarrhea and grade 3 fatigue. Three patients achieved complete remission (CR) or CR with incomplete recovery of platelets lasting 2–5 months, and two additional patients had partial blast clearance. In nonleukemic patients, the most prevalent adverse event was thrombocytopenia. DLTs included thrombocytopenia, gastrointestinal events, fatigue, and hyponatremia. Three patients with DLBCL achieved durable objective responses (two CR and one partial response); six additional patients (two with DLBCL and four with indolent lymphomas) had evidence of clinical activity, but none met the criteria of objective response. Although the numbers are still relatively small, OTX015 appears to be tolerable in these patient populations. Pharmacokinetic analyses of this trial have been published,⁴⁶ confirming the oral availability of the drug. Otherwise, antitumor activity of OTX015 in NMC was reported in a recent publication⁴⁷ in four patients with advanced NMC with confirmed *BRD4-NUT* fusions.

9 | DISCUSSION

BETi have shown a quite interesting preclinical activity in pediatric malignancies *in vivo* models. The interest of the scientific community for this group of molecules is clearly shown by the current clinical development in adults but no clinical study to date has been conceived for children. The elements that make *BET* a particularly exciting target are due in part to the opportunity they offer to indirectly target the previously “undruggable” oncogenes *MYC* or *MYCN*. In pediatrics, this potentially opens the door to a group of diseases with very poor prognosis, such as *MYCN*-amplified neuroblastoma or *MYC*-driven medulloblastoma. With the above-mentioned preclinical rationale, other high-risk diseases may also benefit from these new targeted drugs, such as HGG, metastatic sarcoma, and *MLL*-rearranged leukemia. All these elements clearly justify the development of a phase I/II clinical trial in Pediatrics, which urges now for children with high-risk cancer.

An important point to consider is how BETi could be introduced in treatment protocols based on synergistic preclinical findings. Combinations with cytotoxic drugs may be possible taking in account primarily the potential additive hematological and digestive toxicities, which seem to be the more prevalent at the sight of the published data. No preclinical data are available concerning combination with

immunotherapy agents. Furthermore, two early clinical trials have been developed in adults with BETi in combination with other anti-cancer therapies. In particular, a trial with OTX015 in combination with azacitidine for patients with newly diagnosed AML not candidate for standard intensive induction therapy was registered, but withdrawn prior to enrollment. Based on preclinical data in castration-resistant prostate cancer,⁴⁸ one early clinical trial will be opened soon with ZEN003694 BETi in combination with the second-generation antiandrogen agent, enzalutamide (Table 2). Further prospective clinical studies are needed also to assess whether BETi should be introduced in induction or maintenance therapy protocols.

Finally, several issues that still remain to be elucidated are long-term effects in children, the establishment of predictive biomarkers, and the identification of resistance mechanisms. It seems crucial to clearly define these aspects to streamline introduction of BETi in the multimodal treatment of pediatric cancer patients.

In conclusion, because the development of new drugs in pediatric cancer has long lagged behind development programs for adults with cancer, the authors wish to encourage the industry in partnership with academic institutions to develop these molecules in pediatric oncology/hematology.

CONFLICT OF INTEREST

The authors declare that there is conflict of interest.

AUTHORS' CONTRIBUTIONS

François Doz: investigator for GSK and Bayer clinical trials.

REFERENCES

- Dawson MA, Kouzarides T. Cancer epigenetics: From mechanism to therapy. *Cell*. 2012;150:12–27.
- Yang Z, He N, Zhou Q. Brd4 recruits P-TEFb to chromosomes at late mitosis to promote G1 gene expression and cell cycle progression. *Mol Cell Biol*. 2008;28:967–976.
- Jang MK, Mochizuki K, Zhou M, et al. The bromodomain protein Brd4 is a positive regulatory component of P-TEFb and stimulates RNA polymerase II-dependent transcription. *Mol Cell*. 2005;19:523–534.
- Mochizuki K, Nishiyama A, Jang MK, et al. The bromodomain protein Brd4 stimulates G1 gene transcription and promotes progression to S phase. *J Biol Chem*. 2008;283:9040–9048.
- French CA. NUT midline carcinoma. *Cancer Genet Cytogenet*. 2010;203:16–20.
- Filippakopoulos P, Qi J, Picaud S, et al. Selective inhibition of BET bromodomains. *Nature*. 2010;468:1067–1073.
- Filippakopoulos P, Knapp S. Targeting bromodomains: Epigenetic readers of lysine acetylation. *Nat Rev Drug Discov*. 2014;13:337–356.
- Jung M, Gelato KA, Fernandez-Montalvan A, et al. Targeting BET bromodomains for cancer treatment. *Epigenomics*. 2015;7:487–501.
- Krivtsov AV, Armstrong SA. MLL translocations, histone modifications and leukaemia stem-cell development. *Nat Rev Cancer*. 2007;7:823–833.
- Zuber J, Shi J, Wang E, et al. RNAi screen identifies Brd4 as a therapeutic target in acute myeloid leukaemia. *Nature*. 2011;478:524–528.
- Mertz JA, Conery AR, Bryant BM, et al. Targeting MYC dependence in cancer by inhibiting BET bromodomains. *Proc Natl Acad Sci USA*. 2011;108:16669–16674.
- Da Costa D, Agathangelou A, Perry T, et al. BET inhibition as a single or combined therapeutic approach in primary paediatric B-precursor acute lymphoblastic leukaemia. *Blood Cancer J*. 2013;3:e126.
- Weng AP, Ferrando AA, Lee W, et al. Activating mutations of NOTCH1 in human T cell acute lymphoblastic leukemia. *Science*. 2004;306:269–271.
- Roderick JE, Tesell J, Shultz LD, et al. c-Myc inhibition prevents leukemia initiation in mice and impairs the growth of relapsed and induction failure pediatric T-ALL cells. *Blood*. 2014;123:1040–1050.
- Coude MM, Braun T, Berrou J, et al. BET inhibitor OTX015 targets BRD2 and BRD4 and decreases c-MYC in acute leukemia cells. *Oncotarget*. 2015;6:17698–17712.
- Horn H, Ziepert M, Becher C, et al. MYC status in concert with BCL2 and BCL6 expression predicts outcome in diffuse large B-cell lymphoma. *Blood*. 2013;121:2253–2263.
- Trabucco SE, Gerstein RM, Evens AM, et al. Inhibition of bromodomain proteins for the treatment of human diffuse large B-cell lymphoma. *Clin Cancer Res*. 2015;21:113–122.
- Boi M, Gaudio E, Bonetti P, et al. The BET Bromodomain inhibitor OTX015 affects pathogenetic pathways in preclinical B-cell tumor models and synergizes with targeted drugs. *Clin Cancer Res*. 2015;21:1628–1638.
- Puissant A, Frumm SM, Alexe G, et al. Targeting MYCN in neuroblastoma by BET bromodomain inhibition. *Cancer Discov*. 2013;3:308–323.
- Wyce A, Ganji G, Smitheman KN, et al. BET inhibition silences expression of MYCN and BCL2 and induces cytotoxicity in neuroblastoma tumor models. *PLoS ONE*. 2013;8:e72967.
- Henssen A, Althoff K, Odersky A, et al. Targeting MYCN-driven transcription By BET-bromodomain inhibition. *Clin Cancer Res*. 2016;22:2470–2481.
- Lee S, Rellinger EJ, Kim KW, et al. Bromodomain and extraterminal inhibition blocks tumor progression and promotes differentiation in neuroblastoma. *Surgery*. 2015;158:819–826.
- Matzuk MM, McKeown MR, Filippakopoulos P, et al. Small-molecule inhibition of BRDT for male contraception. *Cell*. 2012;150:673–684.
- Berenguer-Daize C, Astorgues-Xerri L, Odore E, et al. OTX015 (MK-8628), a novel BET inhibitor, displays in vitro and in vivo antitumor effects alone and in combination with conventional therapies in glioblastoma models. *Int J Cancer*. 2016;139:2047–2055.
- Pastori C, Daniel M, Penas C, et al. BET bromodomain proteins are required for glioblastoma cell proliferation. *Epigenetics*. 2014;9:611–620.
- Cheng Z, Gong Y, Ma Y, et al. Inhibition of BET bromodomain targets genetically diverse glioblastoma. *Clin Cancer Res*. 2013;19:1748–1759.
- Henssen A, Thor T, Odersky A, et al. BET bromodomain protein inhibition is a therapeutic option for medulloblastoma. *Oncotarget*. 2013;4:2080–2095.
- Venkataraman S, Alimova I, Balakrishnan I, et al. Inhibition of BRD4 attenuates tumor cell self-renewal and suppresses stem cell signaling in MYC driven medulloblastoma. *Oncotarget*. 2014;5:2355–2371.
- Bandopadhyay P, Bergthold G, Nguyen B, et al. BET bromodomain inhibition of MYC-amplified medulloblastoma. *Clin Cancer Res*. 2014;20:912–925.
- Liu A, Wang B, Niswander LA. Mouse intraflagellar transport proteins regulate both the activator and repressor functions of Gli transcription factors. *Development*. 2005;132:3103–3111.

31. Long J, Li B, Rodriguez-Blanco J, et al. The BET bromodomain inhibitor I-BET151 acts downstream of smoothed protein to abrogate the growth of hedgehog protein-driven cancers. *J Biol Chem*. 2014;289:35494–35502.
32. Tang Y, Gholamin S, Schubert S, et al. Epigenetic targeting of Hedgehog pathway transcriptional output through BET bromodomain inhibition. *Nat Med*. 2014;20:732–740.
33. Lamoureux F, Baud'huin M, Rodriguez Calleja L, et al. Selective inhibition of BET bromodomain epigenetic signalling interferes with the bone-associated tumour vicious cycle. *Nat Commun*. 2014;5:3511.
34. Baker EK, Taylor S, Gupte A, et al. BET inhibitors induce apoptosis through a MYC independent mechanism and synergise with CDK inhibitors to kill osteosarcoma cells. *Sci Rep*. 2015;5:10120.
35. Lucero CM, Vega OA, Osorio MM, et al. The cancer-related transcription factor Runx2 modulates cell proliferation in human osteosarcoma cell lines. *J Cell Physiol*. 2013;228:714–723.
36. Jacques C, Lamoureux F, Baud'huin M, et al. Targeting the epigenetic readers in Ewing sarcoma inhibits the oncogenic transcription factor EWS/Fli1. *Oncotarget*. 2016;7:24125–24140.
37. Patel AJ, Liao CP, Chen Z, et al. BET bromodomain inhibition triggers apoptosis of NF1-associated malignant peripheral nerve sheath tumors through Bim induction. *Cell Rep*. 2014;6:81–92.
38. Chipumuro E, Marco E, Christensen CL, et al. CDK7 inhibition suppresses super-enhancer-linked oncogenic transcription in MYCN-driven cancer. *Cell*. 2014;159:1126–1139.
39. Kumar K, Raza SS, Knab LM, et al. GLI2-dependent c-MYC upregulation mediates resistance of pancreatic cancer cells to the BET bromodomain inhibitor JQ1. *Sci Rep*. 2015;5:9489.
40. Shu S, Lin CY, He HH, et al. Response and resistance to BET bromodomain inhibitors in triple-negative breast cancer. *Nature*. 2016;529:413–417.
41. Hogg SJ, Newbold A, Vervoort SJ, et al. BET inhibition induces apoptosis in aggressive B-cell lymphoma via epigenetic regulation of BCL-2 family members. *Mol Cancer Ther*. 2016;15:2030–2041.
42. Berkovits BD, Wolgemuth DJ. The role of the double bromodomain-containing BET genes during mammalian spermatogenesis. *Curr Top Dev Biol*. 2013;102:293–326.
43. Belkina AC, Denis GV. BET domain co-regulators in obesity, inflammation and cancer. *Nat Rev Cancer*. 2012;12:465–477.
44. Amorim S, Stathis A, Gleeson M, et al. Bromodomain inhibitor OTX015 in patients with lymphoma or multiple myeloma: A dose-escalation, open-label, pharmacokinetic, phase 1 study. *Lancet Haematol*. 2016;3:e196–e204.
45. Berthon C, Raffoux E, Thomas X, et al. Bromodomain inhibitor OTX015 in patients with acute leukaemia: A dose-escalation, phase 1 study. *Lancet Haematol*. 2016;3:e186–e195.
46. Odore E, Lokiec F, Cvitkovic E, et al. Phase I population pharmacokinetic assessment of the oral bromodomain inhibitor OTX015 in patients with haematologic malignancies. *Clin Pharmacokinet*. 2016;55:397–405.
47. Stathis A, Zucca E, Bekradda M, et al. Clinical response of carcinomas harboring the BRD4-NUT oncoprotein to the targeted bromodomain inhibitor OTX015/MK-8628. *Cancer Discov*. 2016;6:492–500.
48. Asangani IA, Dommeti VL, Wang X, et al. Therapeutic targeting of BET bromodomain proteins in castration-resistant prostate cancer. *Nature*. 2014;510:278–282.

How to cite this article: Jiménez I, Baruchel A, Doz F, Schulte J. Bromodomain and extraterminal protein inhibitors in pediatrics: A review of the literature. *Pediatr Blood Cancer*. 2017;64:e26334. <https://doi.org/10.1002/pbc.26334>



Pediatric Patient With Renal Cell Carcinoma Treated by Successive Antiangiogenics Drugs: A Case Report and Review of the Literature

Irene Jiménez, MD,*† Hervé J. Brisse, MD,‡ Paul Fréneaux, MD,§
Sabine Sarnacki, MD, PhD,|| Jean Michon, MD,* Daniel Orbach, MD,*
Gaelle Pierron, PhD,¶|| Nathalie Clément, PhD,† François Doz, MD, PhD,*#
Bernard Escudier, MD, PhD,** and Gudrun Schleiermacher, MD, PhD*††

Summary: Antiangiogenic drugs are currently standard of care in adults with renal cell carcinoma (RCC), including translocation RCC. Although antitumor activity and toxicity profile are well known in adults, few data have been reported in children. Here we present the case of a patient diagnosed at 2 years old with a metastatic translocation RCC, consecutively treated with 5 tyrosine kinase inhibitors during 6 years. The antitumor activity and toxic effects are described, and a brief review of the literature is presented.

Key Words: antiangiogenics, tyrosine kinase inhibitors, VEGF, renal cell carcinoma, children

(*J Pediatr Hematol Oncol* 2017;39:e279–e284)

Since angiogenesis has been defined as one of the hallmarks of cancer, numerous antiangiogenic agents have been developed and integrated into treatment algorithms in adults. The tumor-associated neovasculature mainly depends on the vascular endothelial growth factor (VEGF) signaling pathway, which is basically represented by the VEGF and the VEGF receptor (VEGFR), an intracellular tyrosine kinase receptor. Antiangiogenic agents are sought to regulate new vessel formation and to induce vascular normalization¹ by blocking the ligand or the receptor in the VEGF signaling pathway. Bevacizumab, a monoclonal antibody, specifically binds to circulating VEGFA. The tyrosine kinase receptors VEGFR1, VEGFR2, and VEGFR3 can be inhibited by small molecule tyrosine kinase inhibitors (TKIs) such as sorafenib, sunitinib, pazopanib or axitinib, which work at an intracellular level.

VEGF pathway targeted agents have shown activity in adult patients with metastatic renal cell carcinoma (mRCC) and antiangiogenic therapy has become the standard treatment for this disease.^{2,3} As they have been used for several years, the toxicity profile of these drugs is well known in adults but data concerning antitumor activity and toxicity of these drugs in pediatric cancer is very limited. Indeed, in most cases, they have only completed pediatric phase I evaluation but have not yet found their place in upfront treatment strategies. As these agents might move to a more prominent place in the treatment of pediatric cancers, study of not only their short-term effects, but also their medium and long-term toxicity profiles in children and adolescents is crucial. The few studies published to date show that the majority of the adverse events are common in adults and children, but some specific toxicities have been described in the pediatric population and have also to be taken into account.

RCCs represent only 3% to 5% of renal masses in children and although they are commonly classified according to the WHO classification of renal tumors in adults, some RCCs (about 25%) show heterogenous features that do not sit comfortably in either of the 2 main morphologic subgroups, papillary and clear-cell RCCs.⁴ However, this grouping predates molecular characterization of RCC and many studies have shown that most RCCs in children can be sub classified according to specific genetic translocations, including Xp11 translocation RCC, a subtype that was introduced in 2004 as a genetically distinct entity into the WHO classification of renal tumors. This leads to fusion between the *TFE3* transcription factor gene (located in chromosome Xp11.2) to different fusion partners as *PRCC* in t(X;1)(p11.2;q21), *ASPL* in t(X;17)(p11.2;q25), *PSF* in t(X;1)(p11.2;p34), *CLTC* in t(X;17)(p11;q23), and *LUC7L3* in t(X;17)(p11;q21).⁵ Large surgical resection is the mainstay of therapy for localized RCC, given its intrinsic resistance to chemotherapy and radiation therapy. In the metastatic setting, antiangiogenic treatments might be proposed in children, as it is in adults.⁶ We report on the long-term use of antiangiogenic therapy in a pediatric patient with RCC, focusing on the late effects of this drug in this young child.

CASE HISTORY

We present the case of a 2-year-old girl admitted for a right kidney tumor diagnosed in the context of serious fatigue, abdominal distension, hypertension, and microscopic hematuria. The abdominal computed tomography (CT) scan showed an heterogenous tumor measuring 7.5 × 10.5 × 11.5 cm (Fig. 1A) of the

Received for publication July 25, 2016; accepted December 12, 2016.
From the Departments of *Pediatric Oncology, Adolescents and Young Adults; †Translational Research; ‡Radiology; §Pathology; ¶Somatic Genetics; ††INSERM U830 Research Center, Institut Curie; ||Department of Pediatric Surgery, Necker Enfants-Malades Hospital, Assistance Publique; #Department of Pediatrics, University of Paris-Descartes, Sorbonne Paris Cité, Paris; and **Department of Cancer Medicine, Gustave Roussy, Cancer Campus, Grand Paris, University of Paris-Sud, Villejuif, France.
Supported by Nelia et Amadeo Barletta Foundation, Meghanora Association, Annenberg Foundation.
I.J. received grants from the Nelia et Amadeo Barletta Foundation.
The remaining authors declare no conflict of interest.
Reprints: Gudrun Schleiermacher, MD, PhD, Department of Pediatric Oncology, Adolescents and Young Adults, Institut Curie, 26 rue d'Ulm, 75005, Paris, France (e-mail: gudrun.schleiermacher@curie.fr).
Copyright © 2017 Wolters Kluwer Health, Inc. All rights reserved.

right kidney with large areas of necrosis, and multiple lymph nodes involving the right renal pedicle, the median retroperitoneum and the contralateral renal pedicle. The liver was unremarkable and the chest CT showed few lung nodules interpreted as metastases (Fig. 1B). A core needle biopsy of the renal tumor was performed, showing the features of RCC in its clear cell variant with strong TFE3 staining. The somatic molecular analysis by reverse transcriptase polymerase chain reaction confirmed the presence of an *ASPL/TFE3* translocation.

As the patient presented with a metastatic and loco-regional extension of the disease, she was not eligible for a primary surgical resection and received first-line chemotherapy by oxaliplatin-gemcitabine. No radiologic response was observed after 2 months of treatment. A second-line treatment was delivered with sunitinib (25 mg/m² once daily). Evaluation after 3 months of treatment showed a local partial response (PR) on primary tumor (50% of volume reduction), a pulmonary stable disease (SD) and the occurrence of multiple calcified micronodules within the liver. These images were interpreted as calcification of liver micro-metastases probably already present at diagnosis but not visible on initial CT because of their very small size. In the first 3 months of treatment, the most significant adverse events were transient macroscopic hematuria, hypertension (controlled with increasing doses of nifedipine), hypothyroidism (needing hormonal replacement therapy), hair depigmentation, and failure to thrive with normal levels of IGF1 (Fig. 2). Evaluation after 6 and 9 months showed a

slowly locoregional and metastatic progressive disease (PD), and it was decided to double the dose of sunitinib. Two weeks after the dose escalation, the patient developed an acute glomerular and tubular dysfunction with creatinine increase, metabolic acidosis and proteinuria, which led to definitely discontinue the TKI treatment. After stopping sunitinib, creatinine returned to normal values but metabolic acidosis and proteinuria persisted.

A third-line treatment was then proposed with sorafenib. The starting dose was 400 mg/m² bid but was decreased to 200 mg/m² bid 1 week after starting treatment due to uncontrolled hypertension, despite higher doses of nifedipine and addition of captopril. After 6 months of treatment, the tumor evaluation showed pulmonary SD and local PR (30% of volume) that afterward remained stable during 2.5 years. Several previously detected toxicities remained (such as hypertension, hypothyroidism, metabolic acidosis, and growth impairment), but proteinuria increased requiring higher doses of angiotensin-converting enzyme inhibitor therapy. After 3 years of treatment it was decided to discontinue sorafenib because of the SD and the reluctances about the unknown long-term adverse events of this recent treatment in children. Interestingly, during the treatment discontinuation, the patient showed growth acceleration (ie, 4 cm in 4 mo) (Fig. 2).

Four months after discontinuation, a new loco-regional PD occurred and sorafenib was reintroduced (at 200 mg/m² bid). The disease showed a slow local and metastatic progression and sorafenib was definitely stopped after 9 months.

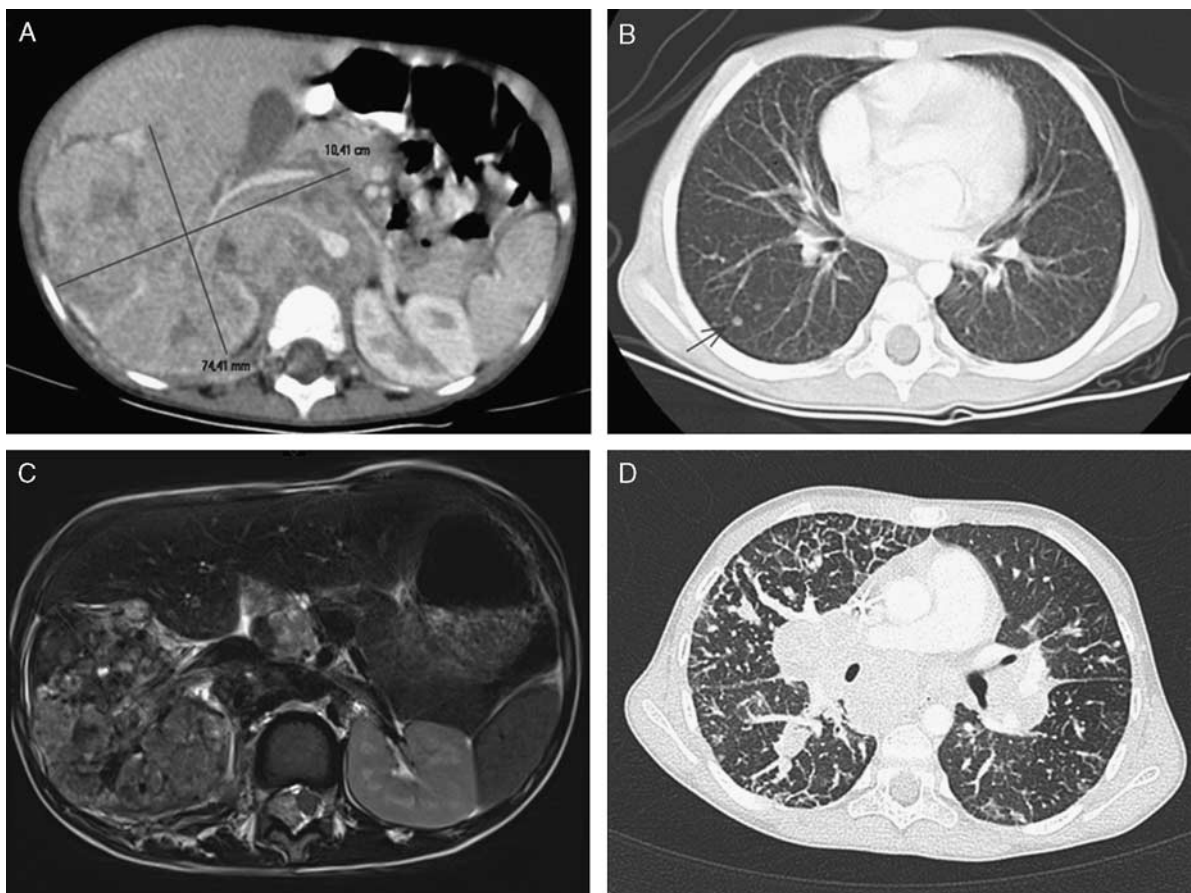


FIGURE 1. Imaging at diagnosis of renal cell carcinoma and after 9 years of treatment. A, Abdominal computed tomography (CT) scan at diagnosis showing the heterogenous tumor of the right kidney measuring 10.5 × 7.5 cm in the axial plane, with retroperitoneal lymph node invasion. B, Chest CT at diagnosis showing lung metastases of the right lower lobe (arrow). C, Abdominal magnetic resonance imaging after 9 years of treatment showing the right renal tumor measuring 9.5 × 7.5 cm in the axial plane, adjacent lymphadenopathies, and epidural extension. D, Chest CT 9 years after treatment demonstrating disease progression (carcinomatous lymphangitis with hilar and mediastinal lymph nodes invasion).

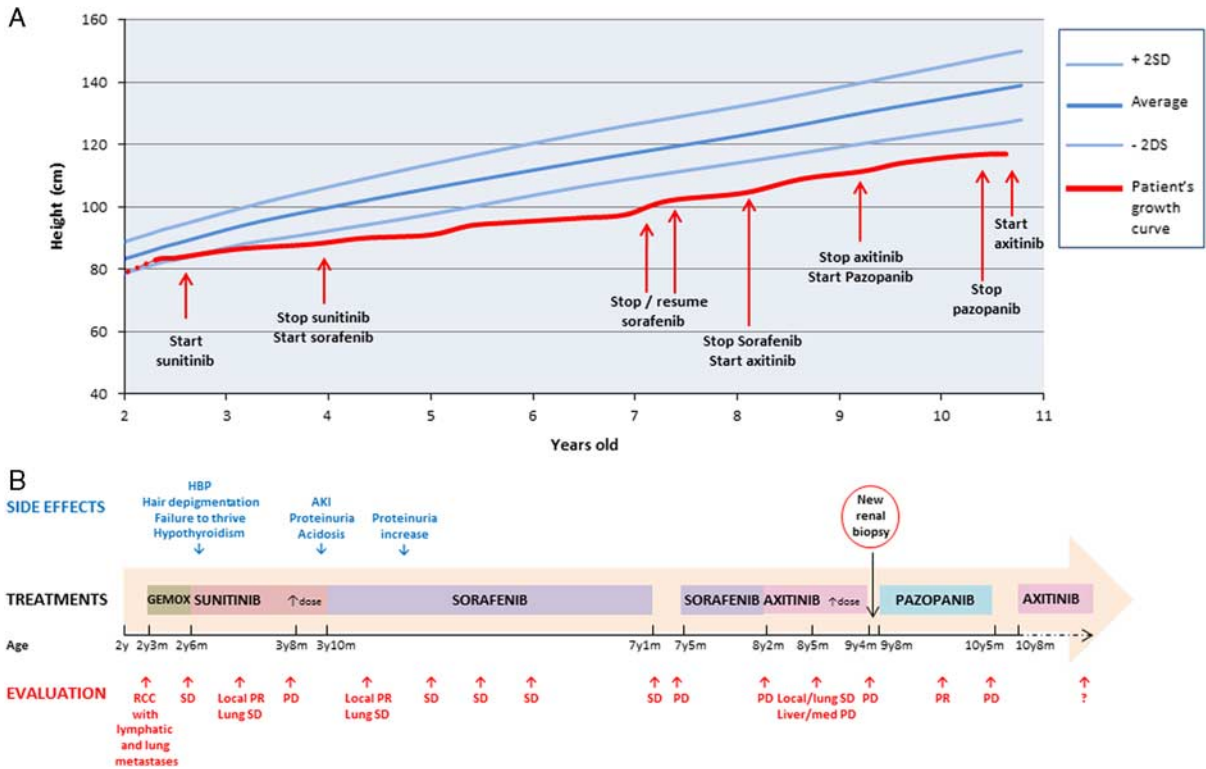


FIGURE 2. Growth curve and chronology of treatments (color legend). A, Growth curve of the patient (red) and treatment details. In blue, female's normal growth curve (average and $\pm 2SD$). B, Chronology of the treatments, tumor response, and side effects. AKI indicates acute kidney injury; HBP, high blood pressure; Med, mediastinum; PD, progressive disease; PR, partial response; RCC, renal cell carcinoma; SD, stable disease. [full color online](#)

The next therapy proposition was a third TKI, axitinib (5 mg/m² bid). The evaluation after 3 months showed a dissociated response, with local and pulmonary SD but hepatic PD and emergence of mediastinal adenopathies. The dose of axitinib was then increased (7 mg/m² bid) and stabilization of the disease could be achieved. No additional toxicity was observed. After 10 months, tumor progression again occurred. It was then decided to discontinue the treatment.

A new core needle biopsy of the primary tumor was then indicated to identify potential other targetable mutations. Using a panel of approximately 50 targetable genes sequenced by next generation sequencing, the molecular analyses showed a *FGFR3* single nucleotide variation located in the tyrosine kinase domain predicted to have functional impact, which could be targeted by pazopanib. On the basis of the doses published in a pediatric phase 1 trial, pazopanib was introduced at 450mg/m² once daily 6 days a week. After 6 months of treatment, all tumor locations showed a PR, notably renal mass that was reduced by 60%. Toxicities remained stable. Subsequent evaluation after 10 months showed an important mediastinal nodal PD, with local, pulmonary and hepatic SD. Pazopanib was therefore stopped.

At this time, a new early clinical trial with atezolizumab was opened in our institution, a fully humanized, engineered monoclonal antibody of IgG1 isotype against the protein programmed cell death ligand 1. Rapid progressive disease in particular at the thoracic and epidural levels, with poor general conditions, hindered the inclusion in that trial. It was then decided to reintroduce the treatment with axitinib at 6.5mg/m² bid, 2 months after stopping pazopanib.

At the present time, patient is 11 years old, and has been treated by 4 successive antiangiogenic drugs during 8 years and a half. She is treated by angiotensin-converting enzyme inhibitor and levothyroxine to equilibrate the adverse events of these drugs. She

measures 119 cm, which corresponds to $-3.5SD$. Figure 2B shows the chronology of the treatments, overall tumor response and side effects. Figures 1C and D show the abdominal and pulmonary imaging evaluation after 9 years of treatment.

DISCUSSION AND REVIEW OF THE LITERATURE OF PEDIATRIC USE OF ANTIANGIOGENIC TREATMENTS

RCC is a rare disease, which seems to have several differences between adults and children as its histologic subtypes, with clear-cell subtype being less frequent in pediatric patients compared with adults. Recent studies have also shown cytogenomic and methylation differences between RCC tumors arising in adult and pediatric/adolescent patients. Thus, translocation RCC tumors from young patients (under 18 y) seems to display fewer genetic alterations and higher levels of global DNA methylation, compared with tumors from adult patients (18 y or above).⁷ Downstream effects of TFE3 fusion proteins are varied and interestingly the alveolar soft-part sarcoma/TFE3 fusion protein enhances the expression of MET tyrosine kinase, which suggested that some translocated RCCs could be treatable with TKIs.⁸ Actually, VEGFR-targeted therapies inhibitors have demonstrated their activity in metastatic Xp11 translocation RCC⁶ and represent the major treatment for mRCC in adults.^{3,9,10}

To date little is known regarding efficacy of antiangiogenic agents in pediatric cancers apart from bevacizumab-based therapy in low-grade gliomas.¹¹ Two

TABLE 1. Main Publications Regarding Pediatric Early Clinical Trials Using Antiangiogenic and Their Main Side Effects

Drug	Main Mechanism of Action	References	Phase Trial	Median Age (Range) (y)	Tumor	Main Adverse Events	Responses
Bevacizumab	Mab anti-VEGF1	Glade Bender ¹²	I	13 (1-21)	Solid tumors	Rash, mucositis, proteinuria, hypertension, hematologic toxicity, nausea, AST/ALT increase, cough	Response not assessed
Semaxanib	TKI anti-VEGFR	Kieran ¹³	I	9.6 (1.5-21)	CNS tumors	AST/ALT increase, headache, hallucinations, hematologic toxicity, allergic reaction, rash	No objective responses
Vandetanib	TKI anti-VEGFR	Broniscer ¹⁴	I	6.4 (2.8-16.4)	DIPG	Rash, mucositis, diarrhea, vomiting, anorexia, AST/ALT increase, proteinuria, hypertension, rash, fatigue, PRES, photosensitivity, prolonged QTc interval, hematologic toxicity, growth plate fusion	Response not assessed
		Fox ¹⁵	II	14 (9-17)	MTC	Diarrhea, hypertension, prolonged QTc, rash, TSH elevation, rash, increased growth plate volume, fatigue, vomiting, hematologic toxicity, electrolyte disorders	PR in 7 of 15 assessable patients with MTC
Cediranib	TKI anti-VEGFR	Fox ¹⁶	I	15 (8-18)	Solid tumors	Vomiting, anorexia, hypertension, decreased left ventricular function, hematologic toxicity, fatigue, prolonged QTc, hypothyroidism, AST/ALT increase, headache, electrolyte disorders	No objective responses
		Kieran ¹⁷	I	13.05 (5.4-21.7)	CNS tumors	AST/ALT increase, diarrhea, hypertension, proteinuria, vomiting, hematologic toxicity, hypo/hyperthyroidism, rash, headache, anorexia, electrolyte disorders, voice alteration	PR in 2 patients* with CPC and pontine glioma
Sunitinib	TKI anti-VEGFR	Dubois ¹⁸	I	13 (3-20)	Solid tumors	AST/ALT increase, diarrhea, anorexia, mucositis, electrolyte disorders, hypothyroidism, hematologic toxicity, left ventricular dysfunction, rash, hypopigmentation, fatigue	No objective responses
Afibercept (VEGF-Trap)	VEGF-A fusion protein (decoy receptor)	Glade Bender ¹⁹	I	12.9 (1.9-21.6)	Solid tumors	Hematologic toxicity, hypertension, proteinuria, fatigue, voice changes, AST/ALT increase, subcutaneous tissue necrosis, tumor bleed	No objective responses
Sorafenib	TKI anti-VEGFR	Widemann ²⁰	I	14 (4-21)	Solid tumors and leukemia	Hematologic toxicity, hypertension, rash, AST/ALT increase, headache, gastrointestinal hemorrhage, anorexia, diarrhea, electrolytic disorders, fatigue, mucositis	OR in 2 of 11 assessable patients with AML and FLT3ITD
		Kim ²¹	I	8 (6-12)	Plexiform neurofibromas	Tumor pain, rash, anorexia, behavior changes, hypertension	No objective responses
		Kim ²²	II	12 (5-21)	Solid tumors	Hematologic toxicity, fatigue, rash, anorexia, AST/ALT increase, electrolyte disorders, pain, proteinuria, dyspnea, pleural effusion	No objective responses
Pazopanib	TKI anti-VEGFR	Glade Bender ²³	I	13.4 (5-21.7)	Solid tumors	AST/ALT increase, proteinuria, hypertension, tumor pain, diarrhea, rash, anorexia, growth plate widening, hematologic toxicity, left ventricular dysfunction, fatigue	PR in 2 patients* with DSRCT and hepatoblastoma
PTC299	Post-transcriptional VEGF expression inhibitor	Packer ²⁴	I	11.2 (5.5-21.1)	CNS tumors	Hyponatremia, fatigue, hematologic toxicity, proteinuria, mood changes, anorexia	No objective responses

*The total number of assessable patients was not available in the publication.

ALT indicates alanine transaminase; AML, acute myeloid leukemia; AST, aspartate transaminase; CNS, central nervous system; CPC, choroid plexus carcinoma; DIPG, diffuse intrinsic pontine glioma; DSRCT, desmoplastic small round cell tumor; FLT3ITD, FLT3 internal tandem duplication; Mab, monoclonal antibody; MTC, medullary thyroid carcinoma; OR, objective response; PR, partial response; QTc, corrected QT interval; TKI, tyrosine-kinase inhibitor; VEGF, vascular endothelial growth factor; VEGFR, VEGF receptor.

TABLE 2. Different Target Spectrum of Sunitinib³¹, Sorafenib³², Pazopanib, and Axitinib⁹

Molecule	VEGFR1	VEGFR2	VEGFR3	PDGFR α	PDGFR β	BRAF/ CRAF	FGFR 1/ 3	EGFR	RET	cMET	c- Kit	FLT3	CSF- 1R
Sunitinib	+	+	+	+	+				+		+	+	+
Sorafenib		+	+			+					+	+	
Pazopanib	+	+	+	+	+		+				+		
Axitinib	+	+	+		+								

EGFR indicates epidermal growth factor receptor; RET, ret proto-oncogene.

pediatric phase II clinical trials with TKI have been published to date with vandetanib and sorafenib (Table 1). Their data concerning efficacy show, respectively: a decrease tumor size in 15 of 15 subjects with medullary thyroid carcinoma with M918T *RET* germline mutation and a confirmed PR in 7 of 15 treated by vandetanib; no objective responses in 20 evaluable patients with solid tumors (Wilms tumor and rhabdomyosarcoma) treated with sorafenib were reported. Among the 11 published phase I clinical trials with antiangiogenics in children, 3 trials reported objective responses in 2 patients treated with sorafenib, 2 after therapy with pazopanib and 2 patients treated with cediranib (Table 1). In addition, several case reports have shown the efficacy of antiangiogenics in pediatric malignancies such as alveolar soft part sarcoma,²⁵ extraneural ependymoma²⁶ and angiosarcoma²⁷ treated by bevacizumab, in alveolar soft part sarcoma treated by sunitinib,²⁸ and hepatoblastoma with combined sorafenib and bevacizumab.²⁹

Although antiangiogenic drugs represent the major treatment for mRCC in adults, in the literature only 1 case report has focused in mRCC in children. Chowdhury et al³⁰ reported a case of an 11-year-old patient with a pulmonary mRCC treated, after initial nephrectomy, by first-line sunitinib for a massive hilar lymph node progression. After 3 months there was no evidence of disease and the treatment was stopped after 6 months because a persistent complete remission. The patient was free of disease after 24 months and showed classic TKIs side effects as bony tenderness, mucositis, and skin and hair depigmentation.

The exceptional characteristic of this case report is that this patient was successively treated by 4 different antiangiogenics for more than 8 years, with the primary tumor still in place. The different kinase spectrum of each TKI (Table 2) justifies the subsequent administration of these 4 drugs to target different molecules. In addition, molecular biology was used as a tool to guide our decision treatment with pazopanib: although the *FGFR3* single nucleotide variation identified in our tumor's patient was not previously reported as a somatic mutation in cancer (no COSMIC ID), it was located in the tyrosine-kinase domain and was predicted to have functional impact using SIFT and Polyphen prediction tools, thus, targetable by pazopanib.

In the case of this patient, the antitumor effect of the subsequent antiangiogenics (sunitinib, sorafenib, axitinib, and pazopanib, respectively) showed the same schema after each introduction: a first phase of tumor response, more or less intense and durable depending on the drug, followed—in all cases—by a tumor progression after several months of treatment and despite the dose increasing. This might reflect the heterogeneity of the tumor and the subsequent mechanisms of drug resistance developed by the tumor cells over time. This phenomenon of tumor resistance to targeted

drugs has already been described in adults with RCC: almost all patients progress at some point due to multiple mechanisms of evasive resistance and may require subsequent therapies.³³ The mechanism underlying this evasive resistance is not fully understood, but several experiments suggest that a hypoxic tumor microenvironment contributes strongly to acquired resistance.³⁴

Hypertension, proteinuria, diarrhea, skin toxicity, thromboembolic events, hemorrhage, and cardiac toxicity are some specific adverse events of these drugs described in adults and posteriorly in children. Toxicities specific to children concern growth abnormalities, secondary to the alteration of growth plate vascularization. For instance, physeal widening with pazopanib,^{23,35} sunitinib³⁵ and vandetanib,^{14,15} and osteonecrosis with bevacizumab³⁶ have been described. These specific adverse events not related to VEGF pathway blockage but related to their other anti-kinases activity (as also skin toxicity, mucositis, and liver toxicity) are called “off-target” effects, and contribute as well to the differential antitumor effects. Table 1 summarizes the publications concerning pediatric phase I/II clinical trials with antiangiogenic drugs and their main side effects. All these adverse events have been brought out at relative short term, and we do not have enough information about the potential long-term effects of these new therapies in the pediatric context. Our patient developed classic acute and subacute side effects previously described for antiangiogenic treatments in adults and children, but also failure to thrive, a long-term side effect that can only appear in children.

To conclude, this last aspect highlights the need to establish systematic methods to register data of children treated by new molecules who are not included in phase I/II clinical trials, to collect more information about antitumor and side effects. This is especially important for long-term effects, which cannot be evaluated in early phase clinical trials as these studies are currently conceived. Another major conclusion of this report is the current crucial role of the molecular biology in the clinical practice to guide, not only the diagnosis, but the treatment of diseases: the finding of a *FGFR3* mutation was the reason to select pazopanib as the fifth-line treatment for our patient. In this sense, we would like to emphasize the role of precision medicine in Pediatric Oncology, which has to be implemented in our current clinical practice to improve the best knowledge and prognostic of high-risk diseases.

ACKNOWLEDGMENTS

The authors thank Nelia et Amadeo Barletta Foundation, Meghanora Association, and Annenberg Foundation for their support.

REFERENCES

- Jain RK. Normalization of tumor vasculature: an emerging concept in antiangiogenic therapy. *Science*. 2005;307:58–62.
- Rini BI, Campbell SC, Escudier B. Renal cell carcinoma. *Lancet*. 2009;373:1119–1132.
- Motzer RJ, Escudier B, Tomczak P, et al. Axitinib versus sorafenib as second-line treatment for advanced renal cell carcinoma: overall survival analysis and updated results from a randomised phase 3 trial. *Lancet Oncol*. 2013;14:552–562.
- Renshaw AA. Pediatric renal cell carcinomas: where do they fit in the new histologic classification of renal cell carcinoma? *Adv Anat Pathol*. 2000;7:135–140.
- Malouf GG, Su X, Yao H, et al. Next-generation sequencing of translocation renal cell carcinoma reveals novel RNA splicing partners and frequent mutations of chromatin-remodeling genes. *Clin Cancer Res*. 2014;20:4129–4140.
- Malouf GG, Camparo P, Oudard S, et al. Targeted agents in metastatic Xp11 translocation/TFE3 gene fusion renal cell carcinoma (RCC): a report from the Juvenile RCC Network. *Ann Oncol*. 2010;21:1834–1838.
- Malouf GG, Monzon FA, Couturier J, et al. Genomic heterogeneity of translocation renal cell carcinoma. *Clin Cancer Res*. 2013;19:4673–4684.
- Tsuda M, Davis IJ, Argani P, et al. TFE3 fusions activate MET signaling by transcriptional up-regulation, defining another class of tumors as candidates for therapeutic MET inhibition. *Cancer Res*. 2007;67:919–929.
- van Geel RM, Beijnen JH, Schellens JH. Concise drug review: pazopanib and axitinib. *Oncologist*. 2012;17:1081–1089.
- Summers J, Cohen MH, Keegan P, et al. FDA drug approval summary: bevacizumab plus interferon for advanced renal cell carcinoma. *Oncologist*. 2010;15:104–111.
- Hwang EI, Jakacki RI, Fisher MJ, et al. Long-term efficacy and toxicity of bevacizumab-based therapy in children with recurrent low-grade gliomas. *Pediatr Blood Cancer*. 2013;60:776–782.
- Glade Bender JL, Adamson PC, Reid JM, et al. Phase I trial and pharmacokinetic study of bevacizumab in pediatric patients with refractory solid tumors: a Children's Oncology Group Study. *J Clin Oncol*. 2008;26:399–405.
- Kieran MW, Supko JG, Wallace D, et al. Phase I study of SU5416, a small molecule inhibitor of the vascular endothelial growth factor receptor (VEGFR) in refractory pediatric central nervous system tumors. *Pediatric Blood & Cancer*. 2009;52:169–176.
- Broniscer A, Baker JN, Tagen M, et al. Phase I study of vandetanib during and after radiotherapy in children with diffuse intrinsic pontine glioma. *J Clin Oncol*. 2010;28:4762–4768.
- Fox E, Widemann BC, Chuk MK, et al. Vandetanib in children and adolescents with multiple endocrine neoplasia type 2B associated medullary thyroid carcinoma. *Clin Cancer Res*. 2013;19:4239–4248.
- Fox E, Aplenc R, Bagatell R, et al. A Phase I Trial and Pharmacokinetic Study of Cediranib, an Orally Bioavailable Pan-Vascular Endothelial Growth Factor Receptor Inhibitor, in Children and Adolescents With Refractory Solid Tumors. *Journal of Clinical Oncology*. 2010;28:5174–5181.
- Kieran MW, Chi S, Goldman S, et al. A phase I trial and PK study of cediranib (AZD2171), an orally bioavailable pan-VEGFR inhibitor, in children with recurrent or refractory primary CNS tumors. *Child's Nervous System*. 2015;31:1433–1445.
- DuBois SG, Shusterman S, Ingle AM, et al. Phase I and Pharmacokinetic Study of Sunitinib in Pediatric Patients with Refractory Solid Tumors: A Children's Oncology Group Study. *Clinical Cancer Research*. 2011;17:5113–5122.
- Glade Bender J, Blaney SM, Borinstein S, et al. A phase I trial and pharmacokinetic study of aflibercept (VEGF Trap) in children with refractory solid tumors: a children's oncology group phase I consortium report. *Clin Cancer Res*. 2012;18:5081–5089.
- Widemann BC, Kim A, Fox E, et al. A Phase I Trial and Pharmacokinetic Study of Sorafenib in Children with Refractory Solid Tumors or Leukemias: A Children's Oncology Group Phase I Consortium Report. *Clinical Cancer Research*. 2012;18:6011–6022.
- Kim A, Dombi E, Tepas K, et al. Phase I trial and pharmacokinetic study of sorafenib in children with neurofibromatosis type I and plexiform neurofibromas. *Pediatric Blood & Cancer*. 2013;60:396–401.
- Kim A, Widemann BC, Krailo M, et al. Phase 2 trial of sorafenib in children and young adults with refractory solid tumors: A report from the Children's Oncology Group. *Pediatric Blood & Cancer*. 2015;62:1562–1566.
- Glade Bender JL, Lee A, Reid JM, et al. Phase I pharmacokinetic and pharmacodynamic study of pazopanib in children with soft tissue sarcoma and other refractory solid tumors: a Children's Oncology Group Phase I Consortium Report. *J Clin Oncol*. 2013;31:3034–3043.
- Packer RJ, Rood BR, Turner DC, et al. Phase I and pharmacokinetic trial of PTC299 in pediatric patients with refractory or recurrent central nervous system tumors: a PBTC study. *Journal of Neuro-Oncology*. 2014;121:217–224.
- Conde N, Cruz O, Albert A, et al. Antiangiogenic treatment as a pre-operative management of alveolar soft-part sarcoma. *Pediatr Blood Cancer*. 2011;57:1071–1073.
- Fischer C, Haque SS, Huse JT, et al. Extraneural ependymoma: distant bone, lung, liver, and lymph node metastases following bevacizumab. *Pediatr Blood Cancer*. 2013;60:143–145.
- Jeng MR, Fuh B, Blatt J, et al. Malignant transformation of infantile hemangioma to angiosarcoma: response to chemotherapy with bevacizumab. *Pediatr Blood Cancer*. 2014;61:2115–2117.
- Hilbert M, Mary P, Larroquet M, et al. Alveolar soft part sarcoma in childhood: is Sunitinib-Sutent® treatment an effective approach? *Pediatr Blood Cancer*. 2012;58:475–476.
- Marsh AM, Lo L, Cohen RA, et al. Sorafenib and bevacizumab for recurrent metastatic hepatoblastoma: stable radiographic disease with decreased AFP. *Pediatr Blood Cancer*. 2012;59:939–940.
- Chowdhury T, Prichard-Jones K, Sebire NJ, et al. Persistent complete response after single-agent sunitinib treatment in a case of TFE translocation positive relapsed metastatic pediatric renal cell carcinoma. *J Pediatr Hematol Oncol*. 2013;35:e1–e3.
- Roskoski R Jr. Sunitinib: a VEGF and PDGF receptor protein kinase and angiogenesis inhibitor. *Biochem Biophys Res Commun*. 2007;356:323–8.
- Desai AA, Stadler WM. Novel kinase inhibitors in renal cell carcinoma: progressive development of static agents. *Curr Oncol Rep*. 2005;7:116–22.
- Schmidinger M. Improving outcomes in metastatic clear cell renal cell carcinoma by sequencing therapy. *Am Soc Clin Oncol Educ Book*. 2014:e228–e238.
- Hammers HJ, Verheul HM, Salumbides B, et al. Reversible epithelial to mesenchymal transition and acquired resistance to sunitinib in patients with renal cell carcinoma: evidence from a xenograft study. *Mol Cancer Ther*. 2010;9:1525–1535.
- Voss SD, Glade-Bender J, Spunt SL, et al. Growth plate abnormalities in pediatric cancer patients undergoing phase I anti-angiogenic therapy: a report from the Children's Oncology Group Phase I Consortium. *Pediatr Blood Cancer*. 2015;62:45–51.
- Fangusaro J, Gururangan S, Jakacki RI, et al. Bevacizumab-associated osteonecrosis of the wrist and knee in three pediatric patients with recurrent CNS tumors. *J Clin Oncol*. 2013;31:e24–e27.

Molecular diagnosis of retinoblastoma by circulating tumor DNA analysis
(*European Journal of Cancer, in press*)

TITLE:

Molecular diagnosis of retinoblastoma by circulating tumor DNA analysis

AUTHOR NAMES AND AFFILIATIONS

Irene Jiménez^{§1,2,3,4}, Éléonore Frouin^{§5}, Mathieu Chicard^{1,2,3,4}, Catherine Dehainault⁶, Jessica Le Gall⁶, Camille Benoist⁵, Arnaud Gauthier⁷, Eve Lapouble⁸, Claude Houdayer⁹, François Radvanyi¹⁰, Virginie Bernard¹¹, Hervé J. Brisse¹², Marion Gauthier-Villars⁶, Dominique Stoppa-Lyonnet⁶, Sylvain Baulande¹³, Nathalie Cassoux^{14,15}, Livia Lumbroso¹⁴, Alexandre Matet^{14,15}, Isabelle Aerts⁴, Victor Renault⁵, François Doz^{4,15}, Lisa Golmard⁶, Olivier Delattre^{2,4}, Gudrun Schleiermacher^{1,2,3,4}

§ These authors contributed equally to this work and are to be considered as joint first co-authors

¹ SiRIC RTOP « Recherche Translationnelle en Oncologie Pédiatrique », Translational Research Department, PSL Research University, Institut Curie Research Center, Paris, France

² INSERM U830, Equipe Labellisée Ligue contre le Cancer, PSL Research University, Institut Curie Research Center, Paris, France

³ Department of Translational Research, Institut Curie Research Center, Paris, France

⁴ SIREDO Center: Care, Innovation and Research for Children, Adolescents and Young Adults with Cancer, Institut Curie, Paris, France

⁵ Clinical Bioinformatics, PSL Research University, Institut Curie, Paris, France

⁶ Department of Genetics, PSL Research University, Institut Curie, Paris, France

⁷ Pathology Department, PSL Research University, Institut Curie, Paris, France

⁸ Somatic Genetics Unit, PSL Research University, Institut Curie, Paris, France

⁹ INSERM U1245, Normandie University, UNIROUEN, Normandy Centre for Genomic and Personalized Medicine and Rouen University Hospital, Department of genetics, Rouen, France

¹⁰ CNRS, UMR144, Equipe Labellisée Ligue Contre le Cancer, Institut Curie, PSL Research University, Paris, France.

¹¹ Centre Hospitalier Universitaire Grenoble-Alpes, Grenoble, France

¹² Imaging Department, PSL Research University, Institut Curie, Paris, France

¹³ Institut Curie Genomics of Excellence (ICGex) Platform, PSL Research University, Research Center, Institut Curie, Paris, France

¹⁴ Ocular Oncology Service, Institut Curie, Paris, France

¹⁵ Université de Paris, Paris, France

CORRESPONDING AUTHOR

Gudrun Schleiermacher

Institut Curie – 26, rue d'Ulm - 75005 Paris (France)

Telephone: +33 144 324 554; Fax: +33 153 102 665

gudrun.schleiermacher@curie.fr

FINANCIAL SUPPORT

This work was supported by grants from the Annenberg Foundation and the Nelia et Amadeo Barletta Foundation. These funding organizations had no role in the design or conduct of this research. High-throughput sequencing was performed by the ICGex NGS platform of the Institut Curie supported by the grants ANR-10-EQPX-03 (Equipex) and ANR-10-INBS-09-08 (France Génomique Consortium) from the Agence Nationale de la Recherche ("Investissements d'Avenir" program), by the ITMO-Cancer Aviesan (Plan Cancer III) and by the SiRIC-Curie program (SiRIC Grant INCa-DGOS- 4654).

ABSTRACT

Purpose: The analysis of circulating tumor DNA (ctDNA), a fraction of total cell-free DNA (cfDNA), might be of special interest in retinoblastoma patients. Since the accessibility to tumor tissue is very limited in these patients, either for histopathological diagnosis of suspicious intraocular masses (biopsies are proscribed) or for somatic *RB1* studies and genetic counseling (due to current successful conservative approaches), we aim to validate the detection of ctDNA in plasma of non-hereditary retinoblastoma patients by molecular analysis of *RB1* gene.

Experimental design: In a cohort of 19 intraocular unilateral nonhereditary retinoblastoma patients for whom a plasma sample was available at diagnosis, we performed high-deep next-generation sequencing (NGS) of *RB1* in cfDNA. Two different bioinformatics/statistics approaches were applied depending on whether the somatic *RB1* status was available or not.

Results: Median plasma sample volume was 600 μ L [100-1000]; median cfDNA plasma concentration was 119 [38-1980] and 27 [11-653] ng/mL at diagnosis and after complete remission, respectively. In the subgroup of patients with known somatic *RB1* alterations (n=11), seven of 9 somatic mutations were detected (median allele fraction: 6.7%). In patients without identified somatic *RB1* alterations (n=8), 6 candidate variants were identified for 7 patients.

Conclusions: Despite small tumor size, blood-ocular barrier, poor ctDNA blood release and limited plasma sample volumes, we confirm that it is possible to detect ctDNA with high-deep NGS in plasma from patients with intraocular nonhereditary retinoblastoma. This may aid in diagnosis of suspicious cases, family genetic counseling or follow-up of residual intraocular disease.

KEY WORDS: Retinoblastoma; circulating tumor DNA; cell-free DNA; *RB1*; molecular diagnosis

INTRODUCTION

Retinoblastoma is the most common pediatric intraocular malignancy. Its diagnosis is based on the clinical examination of the ocular fundus, completed by ocular ultrasound or magnetic resonance imaging (MRI), but histopathological diagnosis is not accessible due to the risk of intraocular or orbital dissemination. Although clinical exam and radiological features are generally sufficient to establish the diagnosis of retinoblastoma, in certain cases it can be difficult to distinguish from other intraocular masses such as Coats' disease, persistent fetal vasculature, vitreous hemorrhage, familial exudative vitreoretinopathy, retinal astrocytomas, toxocariasis granulomas or other infectious retinal lesions, among others (Shields et al., 2013). The diagnosis of intraocular retinoblastoma is therefore always presumptive (Dimaras and Corson, 2019).

Retinoblastoma can occur in both a hereditary and nonhereditary context. The heritable –or germline– form, which represents about 40% of the cases, results in tumors most often developing in children under 1 year and more frequently in both eyes, whereas the nonhereditary –or sporadic– form is always unilateral and appears in slightly older children (Rodriguez-Galindo et al., 2015). Retinoblastoma mostly results from the inactivation of both alleles of the *RB1* tumor suppressor gene, due to point or splicing mutations, large rearrangements or deletions, promoter hypermethylation and, more often, loss of the second allele, giving rise to loss-of-heterozygosity (LOH) (Lohmann and Gallie, 2004). In the hereditary form, one allele carries the *RB1* germline mutation, while the second mutation is somatic. In contrast, in nonhereditary retinoblastoma, both *RB1* alterations are somatic. Interestingly, tumor pathogenic variants have a more severe association with retinoblastoma protein than germline pathogenic variants (Salviat et al., 2020). Distinguishing between these alternative mechanisms is crucial for the management of the patient and family members, as for the genetic counseling. Since globe sparing treatments in the management of retinoblastoma are increasingly successful resulting in fewer enucleations, the access to tumor tissue for somatic *RB1* analysis is limited. When tumor DNA is available for analysis and the two hits of *RB1* inactivation have been identified, their absence in blood proves the absence of retinoblastoma predisposition (except low-level mosaic variant that could be transmitted to the future offspring). In the absence of tumor tissue with blood leukocyte genetic testing only, the absence of detection of *RB1* pathogenic variant can mean that there is no germline *RB1* pathogenic variant, and therefore no retinoblastoma predisposition, but conventional diagnostic genetic testing does not explore the entire *RB1* locus, so an *RB1* germline predisposing pathogenic variant cannot be excluded. Indeed, some germline *RB1* events in regulatory regions such as deep intronic mutations (Dehainault et al., 2007) or epigenetic events (Gelli et al., 2019) have been described. Even if these events are very rare, they justify the follow-up of siblings when no *RB1* pathogenic variant has been detected in blood, without the knowledge of the two hits of *RB1* inactivation that triggered the retinoblastoma development. Thus, the patient and its siblings are subjected to subsequent ophthalmologic follow-up, sometimes under anesthesia.

Cell-free DNA (cfDNA) consists of small 150–200 base pair-long DNA fragments released into the bloodstream by various processes such as tumor cell apoptosis or necrosis (Schwarzenbach et al., 2011b). Both circulating tumor DNA (ctDNA) and normal genomic DNA (gDNA) are fractions of the total cfDNA. The analysis of ctDNA enables the detection of somatic genetic alterations in the plasma originating specifically from tumor cells. Indeed, ctDNA is distinguished from gDNA by the presence of cancer-related mutations. Genetic and epigenetic modifications, such as copy number alterations, mutations, and methylation can be detected (Schwarzenbach et al., 2008b) in the ctDNA, thus providing an extremely specific biomarker for cancer that can be detected and tracked over time. The analysis of ctDNA might be especially useful in retinoblastoma, for which tumor samples –for histopathological or genetic analyses– cannot be obtained. In this work, our aim is to validate the feasibility of the detection of somatic *RB1* alterations in the ctDNA in patients with intraocular nonhereditary retinoblastoma.

METHODS

Patients

This is a retrospective, monocentric study. The Institut Curie is the reference center for retinoblastoma treatment in France. This study was performed in a sub-group of patients which inclusion criteria consisted of the following: (a) pediatric patients diagnosed with nonhereditary unilateral retinoblastoma, (b) treated at the

Ophthalmology and Pediatric departments of the Institut Curie with (c) at least one available plasma sample obtained at diagnosis before any treatment and (d) informed consent from the parents. Patient treatment was performed following standard recommendations and/or specific therapeutic protocols. Plasma samples were collected between April 2013 and May 2015. Clinical characteristics of patients were recorded, including tumor stage according to the Intraocular Retinoblastoma Classification (IRC)(Linn Murphree, 2005). Tumor volume assessment was performed by MRI. In order to determine the percentage of tumor necrosis and the histopathological risk factors according to the Children's Oncology Group Study (Chévez-Barrios et al., 2019), histologic review was performed in tumor samples from enucleated patients. For tumor necrosis assessment, tumors from patients who did not receive any neoadjuvant chemotherapy were reviewed (n=10), since the percentage of necrosis in these enucleation pieces reflected the real degree of necrosis of the tumor. Histopathological risk factors were defined by the presence of the invasion of choroidal vessels, sclera or ciliary body, or a retrolaminar optic nerve extension. The Pearson correlation coefficient was used to study the association between either the cfDNA concentration in plasma or the variant allele fraction (VAF) of a given mutation with the corresponding tumor volume or percentage of necrosis.

Retinoblastoma was considered nonhereditary by the absence of *RB1* germline abnormalities in gDNA from the buffy coat and buccal swab. At the Institut Curie, genetic counseling and constitutional analysis of the *RB1* gene is offered to all retinoblastoma patients. Germline mutational screening was performed as previously described(Chaussade et al., 2019). For somatic *RB1* analysis in enucleated tumors, several techniques were performed: (1) Haloplex enrichment (Agilent) and NextSeq sequencing (Illumina) for point mutations; (2) direct Big Dye Terminator sequencing on ABI 3500 XL genetic analyzer for confirmation of the somatic variants; (3) multiplex ligation-dependent probe amplification on ABI 3130 XL genetic analyzer for large rearrangements; (4) methylation test of *RB1* promoter by enzymatic restriction in quantitative Multiplex polymerase chain reaction (PCR) of Short fluorescent Fragments on ABI 3500 XL genetic analyzer; (5) search for LOH at the *RB1* locus using 8 microsatellite markers comprising 2 intragenic markers (D13S153 and RBi4), 3 centromeric flanking markers and 3 telomeric flanking markers. This study was authorized by the institutional ethics committee of the Institut Curie.

Plasma sample collection and processing. Purification and quantification of cfDNA

Leftover blood samples of patients collected on standard ethylenediamine tetraacetic acid (EDTA) tubes for routine full blood count analyses were retrieved with a maximum delay of 24 hours after venipuncture. Plasma collection and processing, as well as cfDNA purification, quantification and qualification were performed as previously described(Jiménez et al., 2019a).

Targeted sequencing of *RB1* gene on cfDNA

CfDNA sequencing libraries were prepared with Kapa Library Preparation Kit (Kapa Biosystems) with Indexed Adapters included in Roche Nimblegen SeqCap EZ as previously published(Jiménez et al., 2019b). *RB1* has 27 exons, dispersed over about 200 kb of genomic DNA. As introns of this gene consist of large repeated regions(Hong et al., 1989) and the genetic alterations on this gene are distributed throughout the whole gene without punctual recurrent abnormalities, we performed a targeted exon capture of *RB1* with Custom Nimblegen SeqCap. For technical reasons, *KRAS* and *BCOR* genes were added in the design to increase the size of the capture (total length 25 kb) but were not analyzed for this work. Median DNA input for cfDNA library construction was 30 ng [20-200] and 8.5 ng [4-100] in samples obtained at diagnosis and after complete remission, respectively (table 1). After capture, quality control by capillary electrophoresis (2100Bioanalyzer or LabChip) was performed, before *RB1* sequencing by paired-end 150 bp (PE150) MiSeq v3 (Illumina) technology. The same approach was used for *RB1* sequencing in germline DNA (input: 100 ng for all samples), with sequencing system PE150 HiSeq 2500 Rapid Run (Illumina).

The design was performed for depth of coverage of 30,000X. To estimate the sensitivity of the capture design, DNA extracted from the Y79 retinoblastoma cell-line with known splice *RB1* mutation (NM_000321: exon20:c:21061 G>A)(Lee et al., 1988) was serially diluted with DNA from a healthy donor at 50%, 25%, 5%, 2%, 1%, 0.5%, 0.1% and 0.01%. Dilutions were submitted to our deep coverage *RB1* capture sequencing. Application of the bioinformatics pipeline enabled to establish a threshold for SNV detection of 0.5%, below

which SNVs were not distinguishable from the background (Supplementary Figure 1 and Supplementary Figure 2).

The analysis of the depth of coverage showed better coverage in cfDNA samples corresponding to the diagnosis compared to the complete remission timepoint, with a median of 22,100X [17,473-27,865] and 11,517X [676-20,278], respectively (Supplementary Figure 3), which is directly related to the quantity of cfDNA input used for library construction.

Bioinformatics detection of variations

Paired-end reads of 150 bp were first trimmed using Cutadapt v1.18(Martin, 2011) to remove remaining adapters and low-quality bases from the 5' ends (quality less than 20). The reads were then aligned to the human reference genome hg19/GRCh37 using BWA-MEM algorithm v0.7.15 (<http://arxiv.org/abs/1303.3997>).

Since we performed a targeted exon capture of *RB1*, only point mutations or short indels could be highlighted. In order to identify the *RB1* mutations in cfDNA, we used two different bioinformatics approaches depending on whether the information concerning the somatic events was available or not. In the group of patients for whom the somatic analysis of *RB1* was available (n=11), our approach consisted in directly investigating the position of known mutations and counting the number of reads supporting the variation, using DepthOfCoverage function of GATK-3.8 (BaseQuality=28 and MappingQuality=20). The frequency of known mutations observed in each sample (before enucleation and at complete remission) was compared with that detected in control group, constituted by all other sequenced cfDNA samples, to assess statistically relevant differences using one-sided Fisher's exact test. In patients without somatic analysis of *RB1* (n=8), we listed point mutations and sought to differentiate "true" mutations from basal noise on the exonic regions of *RB1*. Mutations were called using two distinct softwares: VarScan2 v2.4.0(Koboldt et al., 2012) and Mutect2 (GATK-3.8). The variants detected with both variant callers were annotated with SnpEff(Cingolani et al., 2012) (v4.3.1) and in-house scripts. Thus, we were able to remove synonymous and recurrent variants, polymorphisms, and variants occurring only at the end of reads. We then focused only on variants with moderate or high impact prediction and ranked them using the p-value of the one-sided Fisher's exact test to determine whether the variant allele fraction was significantly higher in the target sample than in the associated germline sample or all other tumor samples. All candidate variants were reviewed by visual inspection with Integrative Genomic Viewer (IGV)(Robinson et al., 2017).

***RB1* gene analysis with Unique Molecular Identifiers (UMI)**

The results obtained for the 8 cases with unknown variants were compared to a method using enrichment with UMI, also called molecular barcodes, which are indexed to individual DNA fragments and, therefore, are supposed to allow a better distinction of true variants compared to false positives created by PCR or sequencing errors(Salk et al., 2018). *RB1* gene analysis was performed by high throughput sequencing with a SureSelect XT-HS2 (Agilent) enrichment using UMI and a custom gene panel (total length 38 kb), followed by sequencing on MiSeq (Illumina), and bioinformatics analysis with an in-house pipeline that included alignment with BWA-MEM algorithm v0.7.15, variant calling with VarScan2 and annotation with Annovar(Wang et al., 2010). The median coverage of *RB1* was 98.7% at 300X.

RESULTS

Patient characteristics

Nineteen patients (10 males, 9 females) with unilateral nonhereditary intraocular retinoblastoma for whom a plasma sample was available at diagnosis were identified. Eight patients had an additional plasma sample obtained after complete remission, at least 3 months after enucleation. All patients were screened for germline *RB1* status, without any patient harboring a germline defect in this gene. Median age at diagnosis was 25.9 months [3.1– 97.9]. Seven out of 19 patients received a conservative (globe sparing) treatment and

12 of 19 patients were enucleated. The somatic status of *RB1* was available for 11 of 12 enucleated patients (tumor DNA analysis was not contributive in 1 case). The tumor volume assessed by MRI ranged between 130 to 2000 mm³, and the percentage of necrosis in tumor samples for patients without preoperative chemotherapy ranged between 5 to 50%. The histopathological risk factor review did not find any patient with anterior chamber and/or ciliary body seeding, but invasion of choroidal vessels was detected in 4 patients, infiltration of the sclera in 2 patients and 1 patient had a retrolaminar optic nerve extension. Data concerning the somatic *RB1* events was available for 11 enucleated patients: 9 somatic mutations were identified in 11 patients; the remaining *RB1* somatic events included intragenic large deletions, promoter methylations and LOH in *RB1* gene. All clinical information is available in Table 1.

Plasma sample characteristics

Median plasma sample volume was 600 µL, ranging from 100 to 1000 µL. Extraction of cfDNA from plasma showed a median concentration of 119 ng/mL [38-1980] in samples obtained at diagnosis and 27 ng/mL [11-653] in samples obtained after complete remission (Table 1). No statistically significant correlation was found between the cfDNA concentration in plasma and the percentage of necrosis (Pearson's correlation coefficient $r=0.31$), tumor volume ($r=0.04$) or input plasma volume ($r=-0.47$) (Supplementary Figure 4). No correlation could be studied with other factors (such as the IRC stage or the presence of histological risk factors) since subgroups were too small to assess this issue.

Patients with known somatic (tumor) *RB1* alterations

In 11 patients, the somatic status of *RB1* was known. Seven out of 9 *RB1* expected somatic mutations were detected in ctDNA, with VAFs ranging from 0.71% to 16.6%, with a median of 6.68% (Table 2). Two expected single-nucleotide variants (SNVs) were not detected: c.751C>T corresponding to ID_01 and c.1384A>T from ID_09 (in this patient the second hit, a c.2065C>T *RB1* mutation, was detected at very low VAF 0.71%). The tumor volume was significantly and positively correlated with the VAF of these mutations ($r=0.87$), but not the percentage of necrosis ($r=0.21$) (Supplementary Figure 4).

Eight of these 11 patients had an additional plasma sample obtained at complete remission, far from enucleation (median delay between surgery and second plasma sampling: 7.9 months, Table 1). In order to distinguish tumor somatic mutations identified in the pre-enucleation plasma samples from potential germline mosaicism-related events, *RB1* was sequenced in cfDNA from plasma samples obtained after complete remission, more than 3 months after enucleation. If the *RB1* mutations detected in plasma cfDNA before enucleation were due to germline mosaicism DNA contamination, these mutations should still be detected in plasma samples collected after enucleation. In the four patients harboring somatic point mutations for whom a plasma sample was available after complete remission (ID_01, ID_03, ID_07 and ID_11), no variant was detected in cfDNA samples at this timepoint, confirming the absence of ctDNA after removal of the primary tumor, and therefore ruling out the possibility that these particular detected events were germline mosaicism events in these 4 patients (Figure 1 and Supplementary Figure 5).

Patients without identified somatic *RB1* alterations

Somatic *RB1* alterations were not known in 8 patients, consisting in 7 non-enucleated patients and 1 patient for whom the somatic *RB1* analysis was not contributive (ID_12). In this group of patients, we performed an unsupervised bioinformatics/statistics approach that consisted of looking for the events that were significantly higher than the sequencing background noise taking in account the germline DNA. Then, we focused on non-synonymous variants with moderate or high impact prediction and ranked them using the p-value of the one-sided Fisher exact test to determine whether the variant allele fraction was significantly higher in the target sample than in the associated germline sample or other tumor samples. For each patient, the most statistically significant tumor variants with respect to germline were selected and checked with IGV. We identified 7 robust candidate SNVs in 6 of 8 patients. The alternative VAF for the selected candidates ranged between 0.93 and 6.31% (median: 3.41%). Table 3 shows the 7 *RB1* candidate variants selected by our capture approach. No variant was identified as a potential candidate hit in samples ID_13 and ID_17. Figure 2 displays graphically the *RB1* candidate variant selected for patient ID_16.

To validate our approach, we applied this unsupervised bioinformatics/statistics method to the cohort of patients with known somatic alterations. The same 7 SNVs as those detected previously emerged as the most statistically significant with respect to the background noise, hereby validating our analysis approach (Table 2). Secondly, in case ID_12, for which 2 plasma samples were available at diagnosis and at complete remission respectively, the candidate variant identified at diagnosis (c.958C>T; VAF: 3.72%) was no longer detectable at complete remission.

***RB1* gene analysis with UMI**

The results obtained for the 8 samples with unknown *RB1* somatic alterations were compared to a method of high throughput sequencing that uses enrichment with UMI (Table 3). For this purpose, we used the remaining cfDNA available after our capture approach. In 5 cases (ID_13, ID_12, ID_14, ID_16 and ID_18), the analysis was non-contributory due to low DNA input (≤ 6.3 ng). Thus, the comparison with the capture approach could be performed in 3 cases only (ID_15, ID_17 and ID_19): the pathogenic *RB1* c.763C>T candidate variant corresponding to ID_15 was confirmed; one additional pathogenic variant could be identified as a candidate for patient ID_17 (c.1858_1859insTT, VAF 4.6%) which was not identified in our first capture analysis; the splice variant c.2325+1delG corresponding to ID_19 was not confirmed.

DISCUSSION

The study of ctDNA is a noninvasive method for the molecular diagnosis of tumors, which has matured rapidly, and whose clinical utility is currently being evaluated through interventional clinical trials (Cescon et al., 2020) in a wide range of solid and hematological malignancies. It may be of special interest for the diagnosis of tumors for which histopathological evaluation is not performed before starting the treatment, as for retinoblastoma. In addition, in the era of the conservative treatments of retinoblastoma and, thus, limited availability of tumor material, this can be a useful tool for the genetic counseling of nonfamilial unilateral forms with negative germline *RB1* screening in which a mosaicism cannot be excluded since the information concerning the somatic *RB1* status is not accessible. Previous groups have been using the cfDNA from aqueous humor for the molecular profiling of *RB1* (Berry et al., 2018; Gerrish et al., 2019), but obtaining this biological fluid is invasive, not without risks and is not performed routinely (essentially for intravitreal chemotherapy in cases of vitreous seeding relapse) (Munier, 2014).

In this work, we have shown that it is possible to detect ctDNA in patients with intraocular unilateral nonhereditary retinoblastoma. Our capture approach is able to detect 77.8% (7 out of 9) of somatic known mutations even with a very low VAF (median 6.68% [0.71-16.6]), but still significant, with respect to the sequencing background noise. In pediatric cancers, both total cfDNA levels and ctDNA fraction in cfDNA are increased. However, the amounts of cfDNA in retinoblastoma patients are much lower than in other pediatric tumor series, such as neuroblastoma (Chicard et al., 2018b), in which cfDNA concentration in plasma is about 1,000 ng/mL (compared to ≈ 100 ng/mL in our retinoblastoma series). We did not identify any correlation between cfDNA concentration in plasma and tumor volume or percentage of intratumoral necrosis. This could be explained in our cohort by the extremely low proportion of tumoral fraction in the total cfDNA, which subsequently had almost no impact in the final plasma cfDNA concentration. Contamination with gDNA could also contribute to limit these correlations. Since *RB1* mutations are considered as the initiating event in the tumor, which is supposed to be heterozygous, their VAF can be considered as a surrogate of the ctDNA fraction in cfDNA. Interestingly, the tumor volume was significantly correlated with the VAF, meaning that bigger tumors have higher proportions of ctDNA in the total cfDNA.

Since retinoblastoma represents a small volume growing in the limited space of the eyeball, and separated from the systemic circulation by the blood-ocular barriers, one could have presumed that intraocular retinoblastoma may not release ctDNA into the blood. Indeed, studies in uveal melanoma –the most frequent intraocular tumor in adults– have detected ctDNA exclusively in metastatic patients, but not in those with intraocular tumors (Bidard et al., 2014). A previous study on a smaller series of patients has shown that it is possible to detect ctDNA in patients with advanced retinoblastoma (Kothari et al., 2020). Our more extensive

series of enucleated and non-enucleated patients now clearly indicates that intraocular nonhereditary retinoblastoma, even from very small tumors ($\leq 150 \text{ mm}^3$ in our series), releases sufficient amounts of ctDNA into the bloodstream to be detected by deep sequencing, which can be detected from very low plasma volumes obtained in common EDTA tubes of leftover blood from routine exams.

In patients with known *RB1* somatic alterations, we could confirm the presence of 7 out of 9 known mutations (77.8%) in pre-enucleation plasma samples. On the other hand, in the cohort of 8 patients with unknown *RB1* somatic alterations, our capture technique could identify 7 plausible candidates for *RB1* mutations in 6 patients.

Several hypotheses could explain the 4 negative cases. First, an undetectable ctDNA can be primarily attributed to a low tumor burden (Newman et al., 2014) –but variants could be detected for smaller tumors such as ID_07– or to a very low necrosis/apoptosis rate in these tumor masses (this data was not available ID_01). Second, gDNA contamination can reduce the ctDNA fraction in cfDNA, and if this fraction drops below 0.5%, it will not be detectable by our targeted sequencing technique. Third, technical sequencing issues, such as high background noise or low regional coverage rate could contribute to these negative findings. Indeed, in patient ID_09 in whom we expected to detect the second variant at similar VAF than the first one ($\approx 0.7\%$), the depth of coverage of exon 14 (corresponding to the non-detected variant) was 3 times lower than in exon 20 ($\approx 10,000X$ vs. $\approx 30,000X$, respectively). This difference in depth of coverage and the very low allele fraction, at the limit of sensitivity of our sequencing technique, could explain that we did not detect the second variant in this patient (Bellini et al., 2015b). This was not the case either for patient ID_01 (with well covered exon 8, $\approx 30,000X$) or patients ID_01 and ID_17 (with good overall coverage). However, in patient ID_09 the possibility of an *RB1* first-hit mosaic mutation and a second-hit mutation restricted to the tumor cannot be dismissed since for this patient no plasma sample was available at complete remission. Fourth, a stochastic phenomenon could not be excluded: in the context of very low quantities of ctDNA, as in retinoblastoma, and very limited plasma sample volumes, the DNA input for sequencing is extremely low in most cases. Indeed, with 10 ng of cfDNA input (equivalent to approximately 1,000 diploid genomes), and 1% of ctDNA fraction in total cfDNA (corresponding to approximately 10 diploid genomes), for a heterozygous alteration, there would only be 5 haploid genomes with the tumor-related *RB1* alteration in the sample. Therefore, if the ≈ 150 bp-ctDNA fragment containing the mutated allele is not present in the plasma sample, it will not be possible to detect the mutated variant. This is a random ON/OFF phenomenon that cannot be controlled. Finally, regarding tumors with non-determined somatic *RB1* status, we have to consider the possibility that these tumors may not harbor an *RB1* mutation, but other *RB1* molecular abnormalities (or the very rare non-*RB1* genetic abnormalities) not detectable by our capture approach. Indeed, some genetic somatic alterations other than *RB1* have been described in nonhereditary retinoblastoma, such as 13q chromothripsis (McEvoy et al., 2014) or somatic amplifications of the *MYCN* oncogene (Rushlow et al., 2013). Furthermore, retinal cells with biallelic inactivation of *RB1* can form in a first step a benign tumor called retinoma, developing further genomic alterations in the progression to malignancy (Dimaras et al., 2008), and in this disease *BCOR* is the most commonly mutated gene after *RB1* (Zhang et al., 2012).

In this sense, the major limitation of our sequencing targeted approach is its incapacity to detect genetic alterations other than point mutations and short indels. Indeed, large deletions, promoter methylations or LOH cannot be detected. Nevertheless, the main objective of our work was to show that it was possible to detect ctDNA in intraocular nonhereditary retinoblastoma patients despite its small tumor size, blood-ocular barrier protection and very limited pediatric plasma volumes. Now that we have proven that ctDNA can be detected, it should be possible to develop other molecular analysis approaches that allow for the detection of other genetic alterations than point mutations.

Interestingly, we confirmed in 4 enucleated patients that the somatic *RB1* mutations were no more identifiable at complete remission. In the 4 cases (ID_01, ID_03, ID_07 and ID_11), the first *RB1* somatic hit was a point mutation and the second one was an LOH (see Table 1). A mutation identified in cfDNA at diagnosis but disappearing at complete remission is probably restricted to the tumor, so the risk of incidence in the offspring would be nearly zero. Alternatively, a mutation that remains detectable at complete remission could signify mosaicism and therefore a risk of theoretical incidence in the descendants, which is crucial for genetic

counseling.

The importance of determining the genetic origin of retinoblastoma lies in the risk of bilateral disease and other second primary tumors, not only in the patient but in other family members that may be carriers of the same germline mutation. In case of bilateral disease or family history of retinoblastoma, the diagnosis of heritable retinoblastoma can be clinically made. In case of unilateral retinoblastoma (about 15% of unilateral cases are heritable), to assess if a patient is carrier of a germline mutation, *RB1* alterations are first identified in tumor DNA and then investigated in germline DNA. Furthermore, the possibility of detection of somatic *RB1* alterations in cfDNA might be used for surveillance in patients at risk of local relapse, and might be of particular usefulness in situations where fundus examination is difficult and imaging does not enable to distinguish tumor evolution from residual masses.

We tried to take advantage of an alternative UMI enrichment technique to confirm our identified candidates for the cohort of patients for whom the somatic status of *RB1* was not determined. Unfortunately, after the capture approach, the remaining cfDNA material was very limited for the achievement of the UMI technique. Three of eight cases were contributive. Despite this low DNA input, the use of UMI enabled to confirm one case (ID_15) and to detect one additional pathogenic variant (ID_17) that was not detected by the capture approach. Case ID_19 was not confirmed by UMI approach, even if the DNA input (18 ng) was in the range of Agilent kit specifications that recommend a DNA input of 10 to 200 ng. This DNA input might be too low for variants with low allelic ratio, since a minimal DNA input is required to represent the diversity of DNA molecules in the sample, as calculated previously.

Nevertheless, we cannot exclude the possibility of false positive variant candidates in our capture approach as we do not have the somatic information. Despite this, our bioinformatics/statistics capture approach proved its robustness when applying it to the cohort of patients with known somatic mutations, and the detected SNVs emerged as the more statistically significant. The 5 non-contributive cases had a DNA input far below Agilent kit specifications. UMI are increasingly used in high throughput sequencing technologies, and particularly for cfDNA analysis that needs to detect tumor genetic variants present in plasma at low levels, like the variants identified in this study (Volik et al., 2016).

In conclusion, this technique, using low volumes of plasma samples obtained in common EDTA tubes, opens perspectives regarding the molecular diagnosis of retinoblastoma by the analysis of *RB1* in plasma cfDNA of patients with suspicious intraocular masses (or relapses), and may be of special value for the genetic counseling of patients with non-enucleated unilateral retinoblastoma with negative germline *RB1* screening in which a mosaicism cannot be excluded since the information concerning the somatic *RB1* status is not accessible.

DECLARATION OF INTEREST STATEMENT

None declared.

REFERENCES

1. Shields, C. L. et al. Lesions simulating retinoblastoma (pseudoretinoblastoma) in 604 cases: results based on age at presentation. *Ophthalmology* 120, 311–316 (2013).
2. Dimaras, H. & Corson, T. W. Retinoblastoma, the visible CNS tumor: A review. *J. Neurosci. Res.* 97, 29–44 (2019).
3. Rodriguez-Galindo, C., Orbach, D. B. & VanderVeen, D. Retinoblastoma. *Pediatr. Clin. North Am.* 62, 201–223 (2015).
4. Lohmann, D. R. & Gallie, B. L. Retinoblastoma: revisiting the model prototype of inherited cancer. *Am. J. Med. Genet. C Semin. Med. Genet.* 129C, 23–28 (2004).
5. Salviat, F. et al. Association Between Genotype and Phenotype in Consecutive Unrelated Individuals With Retinoblastoma. *JAMA Ophthalmol.* 138, 843–850 (2020).
6. Dehainault, C. et al. A deep intronic mutation in the RB1 gene leads to intronic sequence exonisation. *Eur. J. Hum. Genet. EJHG* 15, 473–477 (2007).
7. Gelli, E. et al. Evidence of predisposing epimutation in retinoblastoma. *Hum. Mutat.* 40, 201–206 (2019).
8. Schwarzenbach, H., Hoon, D. S. B. & Pantel, K. Cell-free nucleic acids as biomarkers in cancer patients. *Nat. Rev. Cancer* 11, 426–437 (2011).
9. Schwarzenbach, H., Stoehlmacher, J., Pantel, K. & Goekkurt, E. Detection and monitoring of cell-free DNA in blood of patients with colorectal cancer. *Ann. N. Y. Acad. Sci.* 1137, 190–196 (2008).
10. Linn Murphree, A. Intraocular retinoblastoma: the case for a new group classification. *Ophthalmol. Clin. N. Am.* 18, 41–53, viii (2005).
11. Chévez-Barrios, P. et al. Study of Unilateral Retinoblastoma With and Without Histopathologic High-Risk Features and the Role of Adjuvant Chemotherapy: A Children’s Oncology Group Study. *J. Clin. Oncol.* 37, 2883–2891 (2019).
12. Chaussade, A. et al. Correlation between RB1 germline mutations and second primary malignancies in hereditary retinoblastoma patients treated with external beam radiotherapy. *Eur. J. Med. Genet.* 62, 217–223 (2019).
13. Jiménez, I. et al. Circulating tumor DNA analysis enables molecular characterization of pediatric renal tumors at diagnosis. *Int. J. Cancer* 144, 68–79 (2019).
14. Jiménez, I. et al. Circulating tumor DNA analysis enables molecular characterization of pediatric renal tumors at diagnosis. *Int. J. Cancer* 144, 68–79 (2019).
15. Hong, F. D. et al. Structure of the human retinoblastoma gene. *Proc. Natl. Acad. Sci. U. S. A.* 86, 5502–5506 (1989).
16. Lee, E. Y. et al. Molecular mechanism of retinoblastoma gene inactivation in retinoblastoma cell line Y79. *Proc. Natl. Acad. Sci. U. S. A.* 85, 6017–6021 (1988).
17. Martin, M. Cutadapt removes adapter sequences from high-throughput sequencing reads. *EMBnet J.* 17, 10 (2011).
18. Koboldt, D. C. et al. VarScan 2: somatic mutation and copy number alteration discovery in cancer by exome sequencing. *Genome Res.* 22, 568–576 (2012).
19. Cingolani, P. et al. A program for annotating and predicting the effects of single nucleotide polymorphisms, SnpEff: SNPs in the genome of *Drosophila melanogaster* strain w1118; iso-2; iso-3. *Fly (Austin)* 6, 80–92 (2012).
20. Robinson, J. T., Thorvaldsdóttir, H., Wenger, A. M., Zehir, A. & Mesirov, J. P. Variant Review with the Integrative Genomics Viewer. *Cancer Res.* 77, e31–e34 (2017).
21. Salk, J. J., Schmitt, M. W. & Loeb, L. A. Enhancing the accuracy of next-generation sequencing for detecting rare and subclonal mutations. *Nat. Rev. Genet.* 19, 269–285 (2018).
22. Wang, K., Li, M. & Hakonarson, H. ANNOVAR: functional annotation of genetic variants from high-throughput sequencing data. *Nucleic Acids Res.* 38, e164–e164 (2010).
23. Cescon, D. W., Bratman, S. V., Chan, S. M. & Siu, L. L. Circulating tumor DNA and liquid biopsy in oncology. *Nat. Cancer* 1, 276–290 (2020).
24. Gerrish, A. et al. Non-invasive diagnosis of retinoblastoma using cell-free DNA from aqueous humour. *Br. J. Ophthalmol.* (2019) doi:10.1136/bjophthalmol-2018-313005.
25. Berry, J. L. et al. Genomic cfDNA Analysis of Aqueous Humor in Retinoblastoma Predicts Eye Salvage: The Surrogate Tumor Biopsy for Retinoblastoma. *Mol. Cancer Res. MCR* 16, 1701–1712 (2018).
26. Munier, F. L. Classification and Management of Seeds in Retinoblastoma Ellsworth Lecture Ghent August 24th 2013. *Ophthalmic Genet.* 35, 193–207 (2014).
27. Chicard, M. et al. Whole-Exome Sequencing of Cell-Free DNA Reveals Temporo-spatial Heterogeneity and Identifies Treatment-Resistant Clones in Neuroblastoma. *Clin. Cancer Res. Off. J. Am. Assoc. Cancer Res.* 24, 939–949 (2018).
28. Bidard, F.-C. et al. Detection rate and prognostic value of circulating tumor cells and circulating tumor DNA in metastatic uveal melanoma. *Int. J. Cancer* 134, 1207–1213 (2014).

29. Kothari, P. et al. Cell-free DNA profiling in retinoblastoma patients with advanced intraocular disease: An MSKCC experience. *Cancer Med.* 9, 6093–6101 (2020).
30. Newman, A. M. et al. An ultrasensitive method for quantitating circulating tumor DNA with broad patient coverage. *Nat. Med.* 20, 548–554 (2014).
31. Bellini, A. et al. Deep Sequencing Reveals Occurrence of Subclonal ALK Mutations in Neuroblastoma at Diagnosis. *Clin. Cancer Res.* 21, 4913–4921 (2015).
32. McEvoy, J. et al. RB1 gene inactivation by chromothripsis in human retinoblastoma. *Oncotarget* 5, 438–450 (2014).
33. Rushlow, D. E. et al. Characterisation of retinoblastomas without RB1 mutations: genomic, gene expression, and clinical studies. *Lancet Oncol.* 14, 327–334 (2013).
34. Dimaras, H. et al. Loss of RB1 induces non-proliferative retinoma: increasing genomic instability correlates with progression to retinoblastoma. *Hum. Mol. Genet.* 17, 1363–1372 (2008).
35. Zhang, J. et al. A novel retinoblastoma therapy from genomic and epigenetic analyses. *Nature* 481, 329–334 (2012).
36. Volik, S., Alcaide, M., Morin, R. D. & Collins, C. Cell-free DNA (cfDNA): Clinical Significance and Utility in Cancer Shaped By Emerging Technologies. *Mol. Cancer Res. MCR* 14, 898–908 (2016).

TABLE 1

Patient	Clinical information								Plasma sample characteristics			
	Age at diagnosis (m)	IRC stage	Tumor vol (mm ³)	Enucleation	Pre-operative chemo	% of tumor necrosis	Histological risk factors	Somatic <i>RB1</i> events from tumor DNA		Plasma timepoint *	Plasma sample volume (μL)	Plasma cfDNA concentration (ng/mL)
								<i>RB1</i> somatic hit #1	<i>RB1</i> somatic hit #2			
ID_01	3,8	E	800	Secondary	Yes [§]	NA	No	c.751C>T ex 8	LOH in <i>RB1</i>	Diagnosis CR (9 m)	450 700	136 11
ID_02	56,4	E	1850	Primary	No	40%	CV	Biallelic promoter methylation	LOH in <i>RB1</i>	Diagnosis CR (13 m)	300 600	119 37
ID_03	13,3	D	2000	Primary	No	15%	RLOH	c.1959del ex 19	LOH in <i>RB1</i>	Diagnosis CR (6 m)	700 940	71 35
ID_04	28,3	E	1150	Primary	No	40%	CV + scl	c.2325+1G>A intr 22	c.2325+1G>T intr 22	Diagnosis	450	49
ID_05	10,1	E	1750	Primary	No	50%	No	Del ex 5 to 27	Del ex 8 and 9	Diagnosis CR (6.8 m)	200 950	1271 653
ID_06	56,9	D	300	Primary [¥]	No	5%	CV	Del promoter to ex 2	Del promoter to ex 17	Diagnosis	600	40
ID_07	35,2	D	350	Primary [¥]	No	30%	No	c.763C>T exon 8	LOH in <i>RB1</i>	Diagnosis CR (3.5 m)	300 850	1980 16
ID_08	34,0	D	350	Primary [¥]	No	35%	No	Del promoter to ex 27	Del promoter to ex 12	Diagnosis CR (9.9 m)	600 900	38 20
ID_09	7,2	D	825	Primary	No	10%	No	c.1384A>T ex 14	c.2065C>T ex 20	Diagnosis	500	523
ID_10	97,9	E	1125	Primary	No	30%	CV + scl	c.1399C>T ex 15	LOH in <i>RB1</i>	Diagnosis	500	240
ID_11	12,5	D	450	Primary [¥]	No	5%	No	c.1450_1451del ex 16	LOH in <i>RB1</i>	Diagnosis CR (3.1 m)	700 1000	92 17
ID_12	60,2	D	400	Secondary	Yes	NA	No	Non-contributory tumor DNA analysis		Diagnosis CR (12 m)	600 900	90 36
ID_13	3,1	D	270	No	NA	NA	NA	NA	NA	Diagnosis	350	72
ID_14	19,8	C	130	No	NA	NA	NA	NA	NA	Diagnosis	650	101
ID_15	23,3	C	600	No	NA	NA	NA	NA	NA	Diagnosis	400	158
ID_16	8,4	B	160	No	NA	NA	NA	NA	NA	Diagnosis	100	623
ID_17	51,9	D	1500	No	NA	NA	NA	NA	NA	Diagnosis	350	981
ID_18	32,8	D	1650	No	NA	NA	NA	NA	NA	Diagnosis	600	60
ID_19	25,9	D	400	No	NA	NA	NA	NA	NA	Diagnosis	600	442

Table 1: Summary of patient and sample characteristics.

* For complete remission (CR) samples, the delay between enucleation and plasma sampling is shown in brackets.

§ Patient ID_01 received pre-operative chemotherapy since he presented with intraocular hypertension.

¥ Patients ID_06, ID_07, ID_08 and ID_11 underwent primary enucleation despite small tumor size because of massive vitreous seeding.

cfDNA: Cell-free DNA; m: months; IRC: Intraocular Retinoblastoma Classification; NA: not applicable (non-enucleated patients); MRI: magnetic resonance imaging; chemo: chemotherapy; Del: deletion; ex: exon; intr: intron; CV: choroidal vessel invasion; scl: sclera invasion; RLOH: retrolaminar optic nerve extension; LOH: loss-of-heterozygosity.

TABLE 2

Patient	RB1 somatic mutations	Plasma cfDNA at diagnosis						Plasma cfDNA at complete remission		
		DNA input (ng)	Detection of the variant	Reads supporting the variant	Total depth at this position	Variant allele fraction	P-value tumoral vs. germline*	Plasma available	DNA input (ng)	Detection of the variant
ID_01	c.751C>T	20	Not detected	NA	NA	NA	NA	Yes	7	Not detected
ID_03	c.1959del	30	Detected	4,801	28,859	16.60%	0 [§]	Yes	30	Not detected
ID_04	c.2325+1G>A	20	Detected	1,139	14,908	7.64%	0 [§]	No	NA	NA
	c.2325+1G>T		Detected	1,055	14,908	7.08%	1.30.10 ⁻³⁰³			NA
ID_07	c.763C>T	200	Detected	1,015	24,829	4.09%	0 [§]	Yes	10	Not detected
ID_09	c.1384A>T	100	Not detected	NA	NA	NA	NA	No	NA	NA
	c.2065C>T		Detected	204	28,693	0.71%	7.61.10 ⁻¹³			NA
ID_10	c.1399C>T	50	Detected	419	6,274	6.68%	5.22.10 ⁻²²¹	No	NA	NA
ID_11	c.1450_1451del	30	Detected	185	13,216	1.40%	1.20.10 ⁻¹⁰³	Yes	4	Not detected

Table 2: Set of 9 somatic *RB1* mutations identified in 7 patients for whom the somatic status of *RB1* was available. Seven out of 9 *RB1* mutations were confirmed in circulating tumor DNA. For confirmed variants, the number of reads supporting the variant, the total depth of coverage at this position, as well as the variant allele fraction (VAF) are detailed. After enucleation, 3 of the previously detected variants were no more identifiable.

* P-value corresponding to the unsupervised analysis approach comparing the target sample with the associated germline sample.

§ Lower than 2.225074.10⁻³⁰⁸ (the smallest accuracy with R software).

NA: not applicable.

TABLE 3

Patient	Genomic position	Ref base	Alt base	Coding DNA reference sequence	Type of mutation	DNA input for library construction (ng)		Detected by	P-value tumor vs. germline*	Reads supporting the variant	Total depth at this position	Variant allele fraction
						Capture	UMI					
ID_12	Chr13:48941648	C	T	c.958C>T	Stop gain	25	6	Capture	1.82.10 ⁻²⁵⁶	877	23,547	3.72%
ID_13	NA	NA	NA	NA	NA	22	0.45	NA	NA	NA	NA	NA
ID_14	Chr13:48916805	A	G	c.335A>G	Missense	30	6.3	Capture	1.30.10 ⁻¹⁰⁰	218	23,411	0.93%
ID_15	Chr13:48936995	C	T	c.763C>T	Stop gain	30	8.25	Capture	1.27.10 ⁻⁹⁷	422	26,353	1.6%
								UMI	NA	365	8,211	4.45%
ID_16	Chr13:48919214	A	G	c.381-2A>G	Splice	50	0.52	Capture	1.10.10 ⁻³¹²	577	12,389	4.66%
ID_17	Chr13:49030383	A	ATT	c.1858_1859insTT	Frameshift	200	43.5	UMI	NA	146	3,183	4.59%
ID_18	Chr13:49050862	AT	A	c.2547delT	Frameshift	20	0.5	Capture	0	1,626	25,774	6.31%
	Chr13:48955550	C	T	c.1666C>T	Stop gain			Capture	0	1,135	33,244	3.41%
ID_19	Chr13:49039245	AG	A	c.2325+1delG	Splice	200	17.7	Capture	1.10.10 ⁻¹⁴⁹	252	12,193	2.07%

Table 3: Candidate variants for *RB1* mutation in 8 non-enucleated patients without known somatic *RB1* events. The analysis of *RB1* by capture method could identify candidate hits for all patients excepting ID_13 and ID_17. The candidate for ID_15 could be confirmed by unique molecular identifier (UMI) technique, which was able to identify an additional candidate variant for ID_17 not detectable by capture approach.

* For capture sequencing approach only.

Ref: reference; Alt: alternative; Nb: number; cfDNA: cell-free DNA; ins: insertion; del: deletion.

FIGURE 1

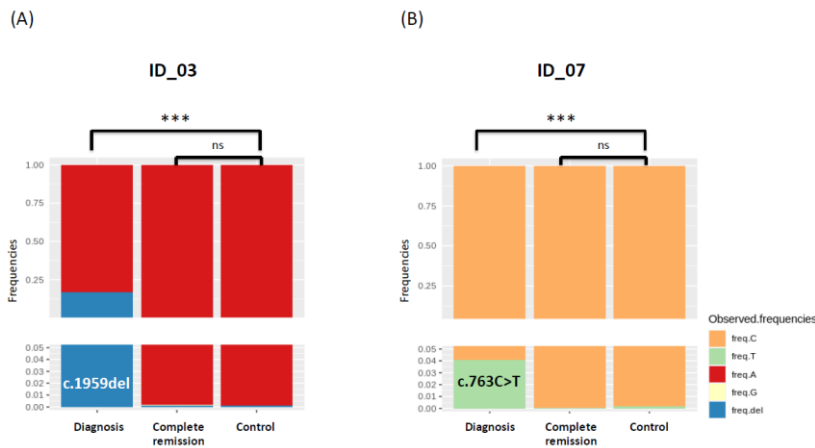


Figure 1: Graphical representation of the observed base frequencies of the mutations identified in cfDNA corresponding to (A) ID_03 and (B) ID_07 patients (c.1959del and c.763C>T, respectively), compared to control group. Both mutations are present at diagnosis (at 16.6% and 4.09% respectively) and disappear after enucleation.

***: p-value ≤ 0.001 ; ns: non-significant p-value > 0.05

FIGURE 2

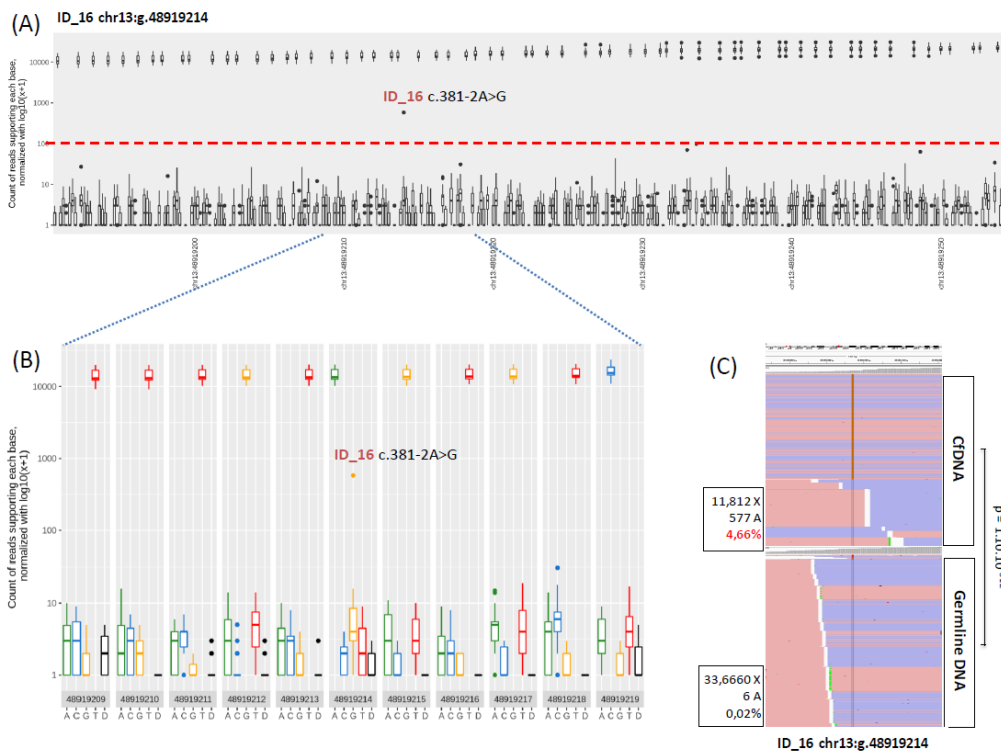
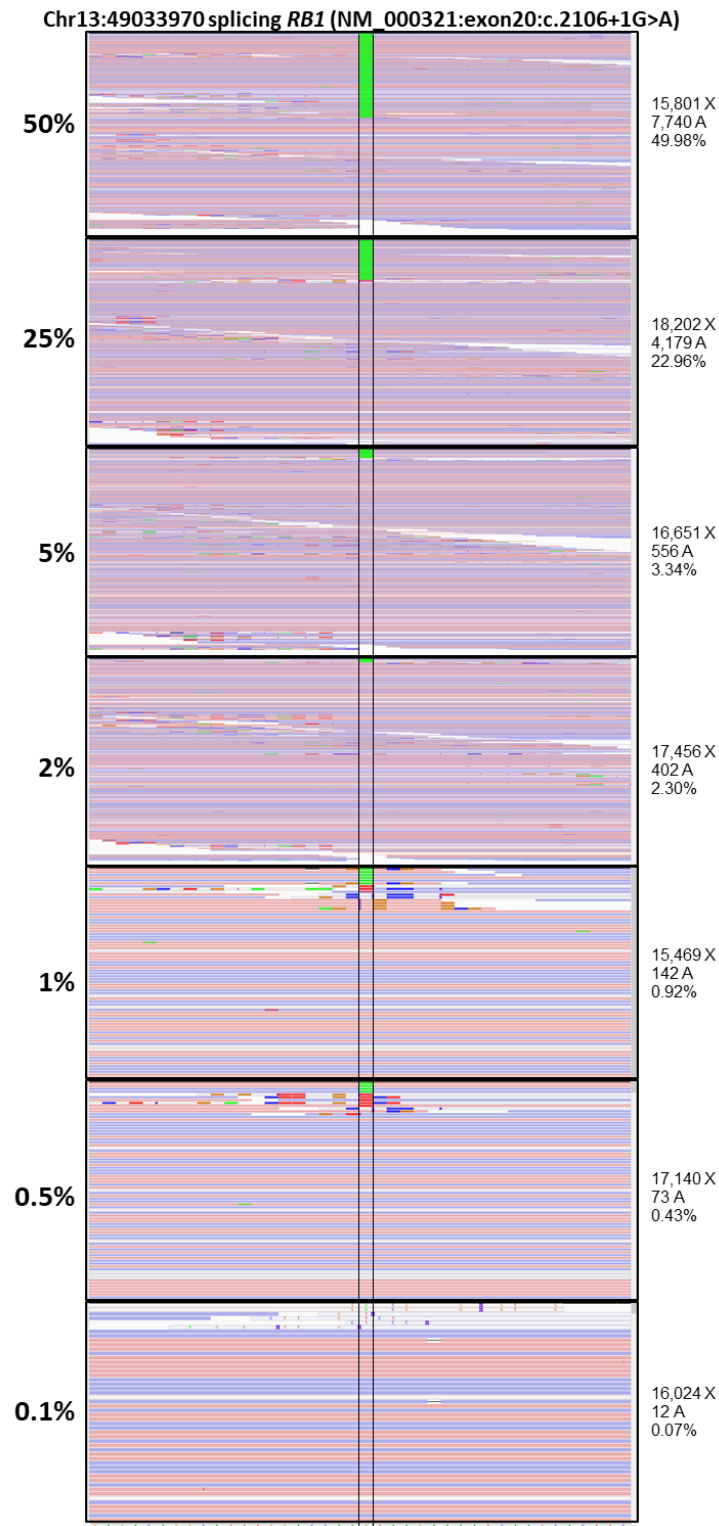


Figure 2: Somatic variant c.381-2A>G selected as candidate for RB1 mutation in patient ID_16, at position Chr13:48919214. The p-value for this somatic variant was $4.69 \cdot 10^{-125}$ with respect to the germline.

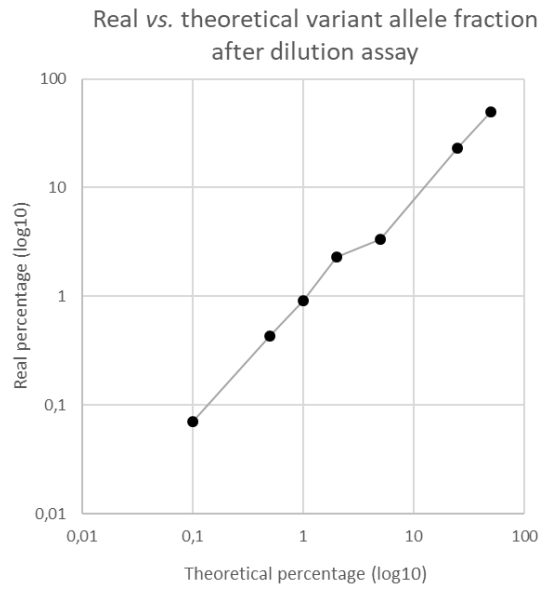
(A) Representation of the selected variant beyond the background noise (virtually represented by the red dot line) and (B) zoom in the position Chr13:48919214 +/- 5 bases. (C) Integrative Genome Viewer representation of the selected variant in cfDNA (top) and the corresponding position in germline DNA. On the left, the number of reads ("X"), the number of alternative reads supporting the mutation ("A"), and the variant allele frequency (%) are noted.

SUPPLEMENTARY FIGURE 1



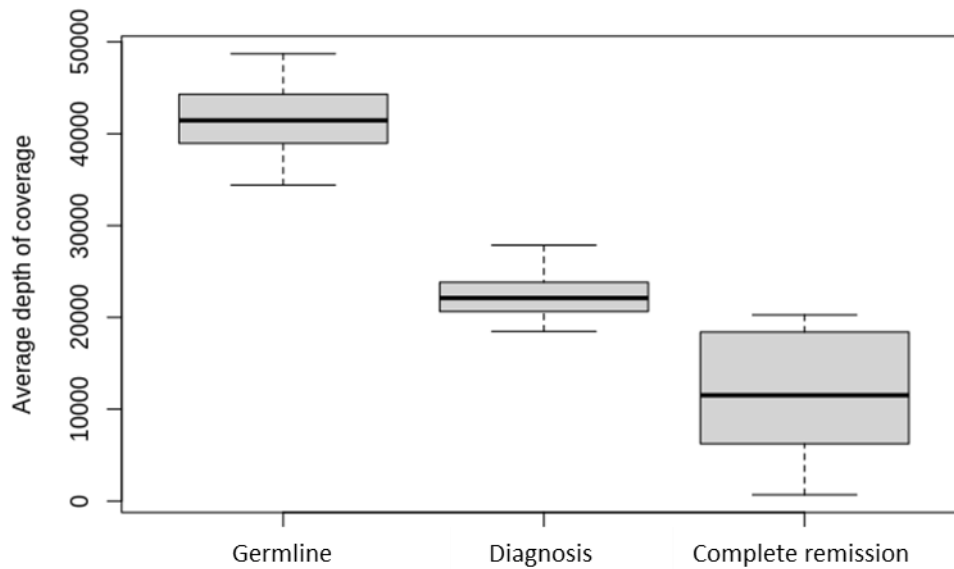
Supplementary Figure 1: Integrative genomics viewer showing the point mutation in the Y79 dilution assay. On the left, theoretical percentages of RB1 dilution. On the right, for each dilution point, the number of reads (“X”), the number of alternative reads supporting the mutation (“A”), and the proportion of alternative reads (%) are noted, corresponding to the variant allele fraction (VAF). For dilution point 0.1%, the mutated position is supported by reads of low quality. Hence, sensibility of the assay was fixed at 0.5%.

SUPPLEMENTARY FIGURE 2



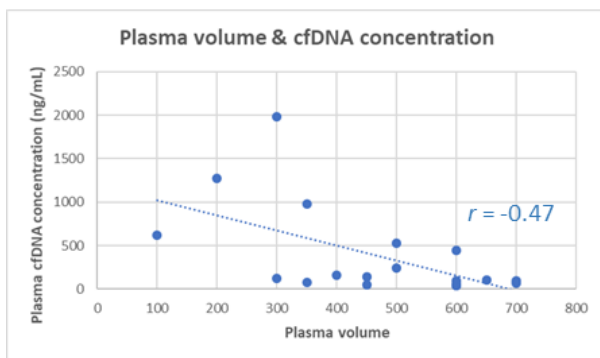
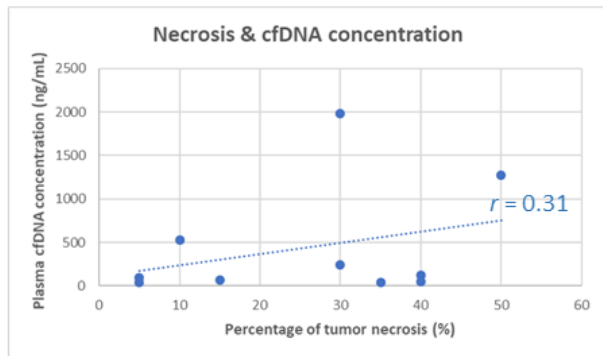
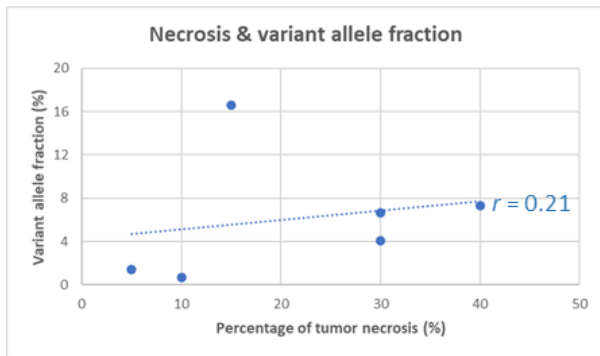
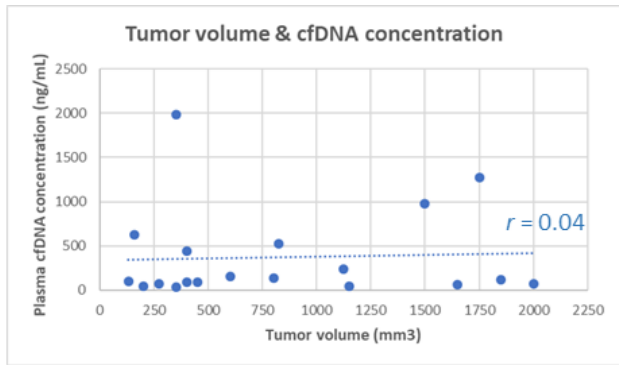
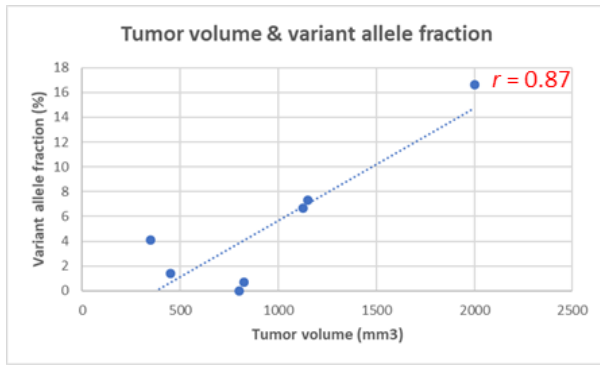
Supplementary Figure 2: Correlation between the theoretical variant allele fraction (VAF) of the *RB1* mutation (c.2106+1G>A) carried by the Y79 cell line (X axis) and the real VAF (Y axis) obtained in the dilution assay.

SUPPLEMENTARY FIGURE 3

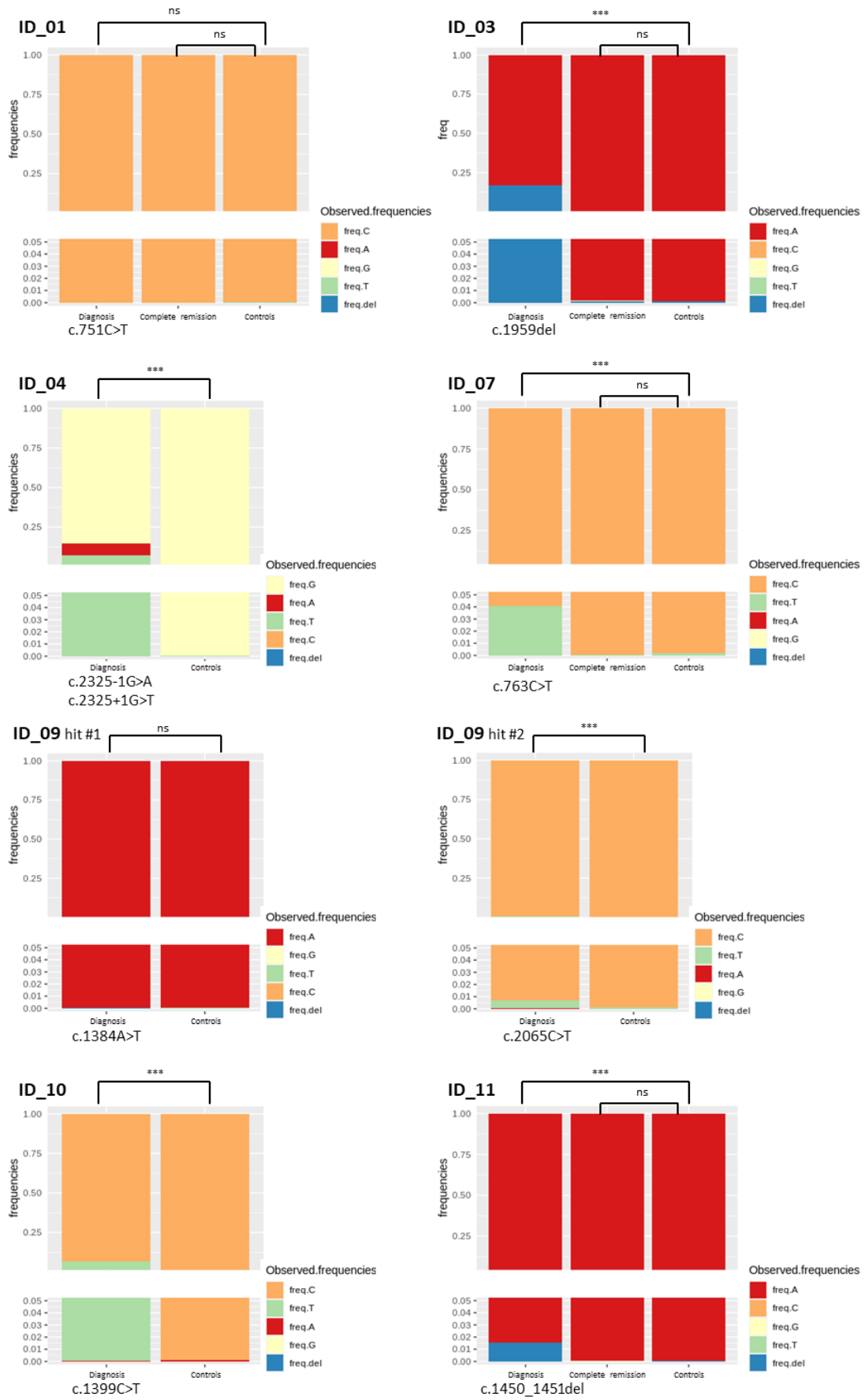


Supplementary Figure 3: Distribution of the coverage depth across the 27 exons samples, corresponding to germline DNA, cfDNA at diagnosis and cfDNA after enucleation.

SUPPLEMENTARY FIGURE 4



SUPPLEMENTARY FIGURE 5





Frequency and Prognostic Impact of *ALK* Amplifications and Mutations in the European Neuroblastoma Study Group (SIOPEN) High-Risk Neuroblastoma Trial (HR-NBL1)

Angela Bellini, PhD^{1,2,3}; Ulrike Pötschger, PhD^{4,5}; Virginie Bernard, PhD⁶; Eve Lapouble, PhD⁷; Sylvain Baulande, PhD⁶; Peter F. Ambros, PhD⁵; Nathalie Auger, PhD⁸; Klaus Beiske, MD, PhD⁹; Marie Bernkopf, PhD⁵; David R. Betts, PhD¹⁰; Jaydutt Bhalshankar, MSc^{1,2,3}; Nick Bown, PhD¹¹; Katleen de Preter, PhD¹²; Nathalie Clément, PhD^{1,2,3}; Valérie Combaret, PhD¹³; Jaime Font de Mora, PhD¹⁴; Sally L. George, MD, PhD¹⁵; Irene Jiménez, MD^{1,2,3}; Marta Jeison, PhD¹⁶; Barbara Marques, PhD¹⁷; Tommy Martinsson, PhD¹⁸; Katia Mazzocco, PhD¹⁹; Martina Morini, PhD²⁰; Annick Mühlethaler-Mottet, PhD²¹; Rosa Noguera, MD²²; Gaelle Pierron, PhD⁷; Maria Rossing, PhD²³; Sabine Taschner-Mandl, PhD⁵; Nadine Van Roy, PhD¹²; Ales Vicha, PhD²⁴; Louis Chesler, MD, PhD²⁵; Walentyna Balwierz, MD²⁶; Victoria Castel, MD, PhD²⁷; Martin Elliott, MD²⁸; Per Kogner, MD, PhD²⁹; Geneviève Laureys, MD, PhD³⁰; Roberto Luksch, MD³¹; Josef Malis, MD²⁴; Maja Popovic-Beck, MD³²; Shifra Ash, MD³³; Olivier Delattre, MD^{2,3,6}; Dominique Valteau-Couanet, MD, PhD³⁴; Deborah A. Tweddle, MD, PhD³⁵; Ruth Ladenstein, MD, PhD^{36,37}; and Gudrun Schleiermacher, MD, PhD^{1,2,3}

PURPOSE In neuroblastoma (NB), the *ALK* receptor tyrosine kinase can be constitutively activated through activating point mutations or genomic amplification. We studied *ALK* genetic alterations in high-risk (HR) patients on the HR-NBL1/SIOPEN trial to determine their frequency, correlation with clinical parameters, and prognostic impact.

MATERIALS AND METHODS Diagnostic tumor samples were available from 1,092 HR-NBL1/SIOPEN patients to determine *ALK* amplification status ($n = 330$), *ALK* mutational profile ($n = 191$), or both ($n = 571$).

RESULTS Genomic *ALK* amplification (*ALKa*) was detected in 4.5% of cases (41 out of 901), all except one with *MYCN* amplification (MNA). *ALKa* was associated with a significantly poorer overall survival (OS) (5-year OS: *ALKa* [$n = 41$] 28% [95% CI, 15 to 42]; no-*ALKa* [$n = 860$] 51% [95% CI, 47 to 54], [$P < .001$]), particularly in cases with metastatic disease. *ALK* mutations (*ALKm*) were detected at a clonal level ($> 20\%$ mutated allele fraction) in 10% of cases (76 out of 762) and at a subclonal level (mutated allele fraction 0.1%-20%) in 3.9% of patients (30 out of 762), with a strong correlation between the presence of *ALKm* and MNA ($P < .001$). Among 571 cases with known *ALKa* and *ALKm* status, a statistically significant difference in OS was observed between cases with *ALKa* or clonal *ALKm* versus subclonal *ALKm* or no *ALK* alterations (5-year OS: *ALKa* [$n = 19$], 26% [95% CI, 10 to 47], clonal *ALKm* [$n = 65$] 33% [95% CI, 21 to 44], subclonal *ALKm* ($n = 22$) 48% [95% CI, 26 to 67], and no alteration [$n = 465$], 51% [95% CI, 46 to 55], respectively, $P = .001$). Importantly, in a multivariate model, involvement of more than one metastatic compartment (hazard ratio [HR], 2.87; $P < .001$), *ALKa* (HR, 2.38; $P = .004$), and clonal *ALKm* (HR, 1.77; $P = .001$) were independent predictors of poor outcome.

CONCLUSION Genetic alterations of *ALK* (clonal mutations and amplifications) in HR-NB are independent predictors of poorer survival. These data provide a rationale for integration of *ALK* inhibitors in upfront treatment of HR-NB with *ALK* alterations.

J Clin Oncol 00. © 2021 by American Society of Clinical Oncology

Licensed under the Creative Commons Attribution 4.0 License

INTRODUCTION

Neuroblastoma (NB), the most frequent solid, extra-cranial malignancy in children, exhibits wide clinical and genetic heterogeneity. High-risk neuroblastoma (HR-NB), defined as metastatic disease over the age of 12 months or *MYCN*-amplified (MNA) disease at any age, remains associated with long-term survival rates of only 50%.¹ Current treatment approaches consist of

intensive induction chemotherapy, surgical resection of the primary tumor, consolidation with high-dose chemotherapy (HDC), and autologous stem-cell rescue, and for minimal residual disease, isotretinoin in combination with human or mouse chimeric anti-GD₂ antibody, ch14.18.²⁻⁸

In NB, several recurrent genetic alterations have been described. MNA is a strong biomarker associated with

ASSOCIATED CONTENT

Appendix
Data Sharing Statement
Protocol

Author affiliations and support information (if applicable) appear at the end of this article.

Accepted on April 21, 2021 and published at ascopubs.org/journal/jco on June 11, 2021; DOI <https://doi.org/10.1200/JCO.21.00086>



Original Research

Phase 1 dose-escalation and pharmacokinetic study of regorafenib in paediatric patients with recurrent or refractory solid malignancies



Birgit Geogerger ^{a,*}, Bruce Morland ^b, Irene Jiménez ^c, Didier Frappaz ^d, Andrew D.J. Pearson ^{e,1}, Gilles Vassal ^a, Patricia Maeda ^f, Jasmine Kincaide ^g, Udo Mueller ^h, Sarah Schlieff ⁱ, Michael Teufel ^{f,2}, Bart A. Ploeger ^j, Adriaan Cleton ^k, Andrea C. Agostinho ^{f,3}, Lynley V. Marshall ^e

^a Department of Pediatric and Adolescent Oncology, Gustave Roussy Cancer Center, Université Paris-Saclay, INSERM U1015, Villejuif, France

^b Department of Oncology, Birmingham Women's and Children's Hospital, Birmingham, UK

^c SIREDO Pediatric Oncology Center, Institut Curie, Paris, France

^d Pediatric Department, Centre Léon Bérard, Lyon, France

^e Children & Young People's Unit, Paediatric and Adolescent Oncology Drug Development Team, The Royal Marsden NHS Foundation Trust and Division of Clinical Studies, Institute of Cancer Research, Sutton, UK

^f Oncology, Bayer HealthCare Pharmaceuticals, Whippany, NJ, USA

^g Oncology, Bayer Oy, Espoo, Finland

^h Department of Statistics, ClinStat GmbH, Cologne, Germany

ⁱ Medical Affairs and Pharmacovigilance, Bayer AG, Berlin, Germany

^j Clinical Pharmacometrics, Bayer AG, Berlin, Germany

^k Translational Medicine, Bayer AG, Berlin, Germany

Received 19 February 2021; received in revised form 27 April 2021; accepted 10 May 2021

* Corresponding author: Department of Pediatric and Adolescent Oncology, Gustave Roussy Cancer Center, Université Paris-Saclay, 114 Rue Edouard Vaillant, Villejuif, 94805, France. Fax: +33 142115275.

E-mail address: birgit.geoerger@gustaveroussy.fr (B. Geogerger).

¹ Retired. ² Current address: Boehringer Ingelheim Pharmaceuticals Inc, Ridgefield, CT, USA. ³ Current address: Global Drug Development Oncology, Novartis Pharmaceutical Corporation, NY, USA.

KEYWORDS

Regorafenib;
Solid tumour;
Paediatric;
Phase 1;
Pharmacokinetics

Abstract Background: This phase 1 study evaluated safety, pharmacokinetics (PK), maximum tolerated dose (MTD), and antitumour activity of regorafenib in paediatric patients with solid tumours.

Patients and methods: Patients (aged 6 months to <18 years) with recurrent/refractory solid tumours received oral regorafenib once daily for 3 weeks on/1 week off. The starting dose (60 mg/m²) was derived from an adult physiology-based PK model and scaled to children; dose escalation was followed by safety expansion of the MTD cohort. Treatment-emergent adverse events (TEAEs) were evaluated using National Cancer Institute Common Terminology Criteria for Adverse Events version 4.0. Regorafenib PK was evaluated using a population PK model.

Results: Forty-one patients (median age 13 years) received regorafenib (four cohorts: 60–93 mg/m²). Five of 23 evaluable patients experienced dose-limiting toxicities (Grade 4 thrombocytopenia, Grade 3 maculopapular rash, pyrexia, hypertension, and exfoliative dermatitis [each n = 1]). The MTD was defined as 82 mg/m². The most common Grade ≥3 drug-related TEAE was thrombocytopenia (10%). The incidence and severity of hypertension, diarrhoea, fatigue, hypothyroidism, and hand–foot skin reaction were lower than reported in adults. Regorafenib exposure increased with dose, with substantial overlap because of moderate-to-high interpatient variability. One patient with rhabdomyosarcoma experienced an unconfirmed partial response; 15 patients had stable disease, five for >16 weeks.

Conclusions: The recommended phase 2 dose of single-agent regorafenib in paediatric patients with solid malignancies is 82 mg/m². Regorafenib demonstrated acceptable tolerability and preliminary antitumour activity, supporting further investigation in paediatric patients.

Clinical trial number: NCT02085148.

© 2021 The Authors. Published by Elsevier Ltd. This is an open access article under the CC BY-NC-ND license (<http://creativecommons.org/licenses/by-nc-nd/4.0/>).

1. Introduction

Angiogenesis plays a critical role in the growth and metastatic spread of paediatric malignancies [1–6]. It is multifactorial and driven by vascular endothelial growth factor (VEGF) and other potentially oncogenic proteins, including platelet-derived growth factor receptor (PDGFR) and/or fibroblast growth factor receptor (FGFR) [7,8]. In addition, *PDGFRA* aberrations have been implicated as oncogenic drivers in paediatric gliomas [9–12] and in the development of resistance [13].

The oral tyrosine kinase inhibitor regorafenib blocks the activity of protein kinases involved in tumour angiogenesis, proliferation, immunity, metastasis, and the micro-environment [14,15] and has shown potent, broad-spectrum antitumour activity in preclinical models [14,15] and in clinical trials in various solid malignancies in adults [16–24]. There is a strong rationale for evaluating regorafenib in selected paediatric solid malignancies because of its antiangiogenic effects and kinase inhibition profile [14,15], which is supported by the antitumour activity demonstrated by regorafenib alone and in combination with standard anticancer treatments in preclinical models of paediatric tumours [25].

We initiated a phase 1 dose-finding study to establish the safety and pharmacokinetics (PK) of regorafenib in paediatric patients with recurrent/refractory solid malignancies. Here, we present the results of the single-agent recommended phase 2 dose (RP2D) part of the study.

2. Methods

2.1. Patients

Eligible paediatric patients (aged 6 months to <18 years) had malignant solid or central nervous system (CNS) tumours recurrent or refractory to standard therapy, with no known effective treatment. Additional inclusion criteria included life expectancy ≥12 weeks; ≥1 measurable or evaluable lesion according to Response Evaluation Criteria in Solid Tumors (RECIST) v1.1; Karnofsky (>12 years of age) or Lansky (≤12 years of age) performance status ≥70%; and adequate organ function. Key exclusion criteria included prior exposure to regorafenib and known hypersensitivity to the study agent or formulation excipients. Other anticancer treatments or radiotherapy were not permitted ≤4 weeks before the start of the study.

2.2. Study design

This was an open-label, non-randomised, phase 1, dose-escalation study of regorafenib conducted across five sites of the European Innovative Therapies for Children with Cancer Consortium (NCT02085148). The study was conducted in accordance with the Declaration of Helsinki and Good Clinical Practice guidelines, and approval was obtained from the appropriate ethics committees or institutional review boards. All patients or their parents or legal

Transition cells between noradrenergic and mesenchymal identities as a source of cell heterogeneity and plasticity in neuroblastoma (in revision)

AUTHORS

Cécile Thirant^{1,2§}, Agathe Peltier^{1,2§}, Simon Durand^{1,2#}, Amira Kramdi^{1,2#}, Caroline Louis-Brennetot^{1,2#}, CécileP-
ierre-Eugène^{1,2#}, AnaCosta^{1,2}, Amandine Grelier^{1,2}, Sakina Zaïdi^{1,2}, Nadège Gruel^{1,4}, **Irene Jiménez**^{2,3,4}, Eve La-
poules, GaëllePierron⁵, HervéJ.Brisset⁶, ArnaudGauthier⁷, Paul Fréneaux⁷, Sandrine Grossetête-Lalami^{1,2},
Laura G. Baudrin⁹, Virginie Raynal^{1,9}, Sylvain Baulande⁹, AngelaBellini^{2,3,4}, JayduttBhalshankar^{2,3,4}, Angel M.
Carcaboso⁸, BirgitGeoerger¹⁰, Hermann Rohrer¹¹, DidierSurdez^{1,2}, Valentina Boeva^{12,13,14}, GudrunSchleierma-
cher^{2,3,4}, OlivierDelattre^{1,2}, IsabelleJanoueix-Lerosey^{1,2*§}

These authors contributed equally to this work.

AFFILIATIONS

1 Institut Curie, PSL Research University Inserm U830, Equipe Labellisée Ligue contre le Cancer, Paris, France.

2 SIREDO: Care, Innovation and Research for Children, Adolescents and Young Adults with Cancer, Institut Curie, Paris, France.

3 Institut Curie, Laboratory Recherche Translationnelle en Oncologie Pédiatrique (RTOP), Laboratoire “Gilles Thomas Paris, France.

4 Institut Curie Department of Translational Research, Paris, France.

5 Institut Curie, Unité de Génétique Somatique, Paris, France. 20 6 Institut Curie, Department of Imaging, PSL Research University, Paris, France. 21 7 Institut Curie, Department of Biopathology, Paris, France. 22

6 Institut Curie, Department of Imaging, PSL Research University, Paris, France.

7 Institut Curie, Department of Biopathology, Paris, France.

8 Institut de Recerca Sant Joan de Déu, Barcelona, Spain.

9 Institut Curie, Genomics of Excellence (Platform, Paris, France.

10 Gustave Roussy Cancer Campus, INSERM U1015, Department of Pediatric and Adolescent 25 Oncology, Univ. Paris Sud, Université Paris Saclay, Villejuif, France.

11 Institute of Clinical Neuroanatomy, Dr. Senckenberg Anatomy, Neuroscience Center, 27 Goethe University, Frankfurt/M, Germany

12 Inserm, U1016, Cochin Institute, CNRS UMR8104, Paris Descartes University, Paris, France.

13 ETH Zürich, Department of Computer Science, Institute for Machine Learning, Zürich, Switzerland.

14 Swiss Institute of Bioinformatics (SIB), Zürich, Switzerland.

Corresponding author: janoueix @curie.fr

ABSTRACT

Two cell identities, noradrenergic and mesenchymal, have been characterized in neuroblastoma cell 35 lines according to their epigenetic landscapes relying on specific circuitries of transcription factors. 36 Here, we demonstrate that the knock-out of GATA3, but not of PHOX2A or PHOX2B, in noradrenergic 37 cells is sufficient to induce a mesenchymal phenotype. Our results show that tumor cell identity of 38 models exhibiting spontaneous plasticity strongly depends on their microenvironment. We 39 characterize a dynamic transition state from the noradrenergic to the mesenchymal state, associated 40 with a specific signature of nine transcription factors. The study of intra-tumor heterogeneity in patient 41 tumors reveals a distinct cell population exhibiting features of transition cells. This work therefore 42 unravels a plasticity cell state in neuroblastoma and highlights the critical role of non-cell autonomous 43 factors in neuroblastoma phenotype.

Titre : Etude de la sensibilité aux drogues et de l'évolution clonale sous thérapies ciblées du neuroblastome de haut risque

Mots clés : Neuroblastome de haut risque ; thérapies ciblées ; évolution clonale ; criblage de drogues ; inhibiteurs de ALK ; ADN tumoral circulant (ctDNA)

Résumé :

Le neuroblastome (NB) est la tumeur solide extra crânienne la plus fréquente de l'enfance. Du point de vue clinique, elle se caractérise par une diversité clinique extrêmement importante, allant de cas de très bon pronostic à des formes dites de haut risque dont la survie à 5 ans ne va pas au-delà de 50% malgré des traitements très intensifs. Le comportement clinique de la maladie est profondément lié à la biologie de la tumeur. Peu d'anomalies génétiques ont été décrites de façon récurrente, les plus fréquentes affectant les gènes *MYCN*, *ALK*, *TERT* ou *ATRX*. Il s'agit d'une des tumeurs les plus hétérogènes du point de vue moléculaire, avec des clones caractérisés par des anomalies génétiques propres, dont le comportement détermine l'évolution de la maladie. Le NB de haut risque (NB-HR) reste un défi pour les cliniciens. Ainsi, il est crucial d'approfondir notre compréhension des principales difficultés auxquelles sont confrontés les cliniciens dans la prise en charge de ces patients : la rechute tumorale et la résistance aux traitements.

Pour y parvenir, il est d'abord impératif d'explorer de nouvelles stratégies de traitement, probablement en combinaison, pour surmonter la résistance au traitement, à la fois primaire et acquise. Sur la base des approches de médecine personnalisée émergentes en oncologie pédiatrique, l'utilisation in vitro de criblages de drogues à haut débit permet l'étude de thérapies ciblées basées sur le profil moléculaire de la tumeur ou la découverte de réponses thérapeutiques non prédites. Nous avons pu valider cette approche dans un groupe de 6 lignées cellulaires (dont 2 lignées de NB) portant des anomalies génétiques ciblables propres : chez toutes les lignées, au moins une classe thérapeutique de drogues prédite comme active a été confirmée. Nous avons exploré cette approche *ex vivo* dans 13 modèles de xénogreffes dérivées de patients (PDXs) de NB-HR en utilisant une librairie de drogues incluant différentes classes thérapeutiques. Cela nous a permis de montrer que l'ensemble des différents

modèles criblés montrent une sensibilité particulière aux inhibiteurs de HDAC.

Deuxièmement, dans une perspective thérapeutique, il est indispensable de mieux comprendre les processus d'hétérogénéité intratumorale qui conduisent à l'évolution clonale afin d'isoler les clones qui seraient susceptibles de déterminer le comportement de la tumeur, notamment la résistance au traitement. En utilisant 6 différents modèles de PDX de NB-HR, l'étude de l'évolution clonale du NB-HR risque sous traitement ciblé nous a permis de montrer que des modifications surviennent dans les cellules tumorales sous traitement, avec évolution des sous-clones et apparition de nouvelles mutations.

Troisièmement, tout cela ouvre une porte aux traitements ciblés, non seulement de deuxième, mais spécialement de première ligne. Seuls quelques biomarqueurs puissants ont été décrits pour prédire la réponse aux traitements, dont les anomalies du gène *ALK*. Nous avons exploré l'efficacité *ex vivo* et *in vivo* des inhibiteurs de ALK, seuls et en combinaison, dans quatre modèles PDX de NB-HR comportant une anomalie de *ALK*. La combinaison spécifique de lorlatinib (inhibiteur de ALK) et idasanutline (inhibiteur de MDM2) a montré une synergie spectaculaire dans un modèle *ALK* amplifié.

En conclusion, ce travail représente une nouvelle approche à l'étude de la résistance ainsi que la sensibilité aux traitements du NB-HR, qui a pour but ultime d'améliorer les stratégies thérapeutiques des enfants atteints de cette maladie. Nous avons pu mettre en évidence *ex vivo* par criblage de drogues à haut débit la cytotoxicité particulière des HDAC inhibiteurs dans le NB-HR. De plus, nous avons pu déchiffrer des événements génétiques sous-jacents à l'évolution clonale du NB-HR après traitement ciblé. Finalement, la combinaison lorlatinib et idasanutline apporte de l'espoir pour l'approche thérapeutique des NB avec des anomalies de *ALK*.

Title: Drug sensitivity and clonal evolution under targeted treatment of high-risk neuroblastoma

Keywords: High-risk neuroblastoma; targeted therapies; clonal evolution; drug screening; ALK inhibitors; circulating tumor DNA (ctDNA)

Abstract:

Neuroblastoma is the most common extracranial solid tumor in childhood. From a clinical point of view, it is characterized by extremely high clinical diversity, ranging from cases with a very good prognosis to high-risk forms with 5-year survival around 50% despite very intensive treatments. The clinical behavior of the disease is deeply linked to the biology of the tumor. Few recurrent genetic abnormalities have been described, the most frequent affecting *MYCN*, *ALK*, *TERT* or *ATRX* genes. From a molecular point of view, neuroblastoma is one of the most heterogeneous tumors, with clones characterized by specific genetic abnormalities. The behavior of these clones determines the course of the disease. High-risk neuroblastoma (HR-NB) remains a challenge for clinicians. It is therefore crucial to improve our knowledge of the main difficulties that physicians face in the management of these patients: tumor relapse and treatment resistance.

To achieve this, first it is imperative to explore new treatment strategies, presumably in combination, to overcome treatment resistance, both primary and acquired. Based on the emergent personalized medicine approaches in pediatric oncology, the use of *in vitro* high-throughput drug screenings enables the study of molecularly-matched targeted drug therapies, or the discovery of non-predicted treatment responses. We were able to validate this approach in a group of 6 cell lines (with 2 neuroblastoma lines) carrying specific genetic targetable abnormalities: in all cell lines, at least one therapeutic class predicted to be active for a given genetic abnormality was confirmed. We explored this approach *ex vivo* using 6 HR-NB patient-derived xenografts (PDXs) models screened with a drug library including drugs from different therapeutic classes. This allowed us to show that all of the different HR-NB PDX models screened showed particular sensitivity to HDAC inhibitors.

Second, from a therapeutic perspective, we need to

better understand the processes of intratumor heterogeneity that lead to clonal evolution in order to isolate the clones that would be able to determine the behavior of the tumor, in particular treatment resistance. Using 6 different HR-NB PDX models, the study of the clonal evolution of HR-NB under targeted treatment allowed us to show that changes occur in tumor cells under treatment, with evolution of subclones and emergence of new mutations.

Third, all of this opens the door to targeted treatments, not only second, but especially first line. As only few strong biomarkers have been described to predict tumor treatment response and *ALK* alterations are among them, we explored the *ex vivo* and *in vivo* efficacy of ALK inhibitors, alone and in combination, in four *ALK*-aberrant HR-NB PDXs. The specific combination of lorlatinib (ALK inhibitor) and idasanutlin (MDM2 inhibitor) showed impressive synergy in an *ALK*-amplified model.

In conclusion, this work represents a new approach for the study treatment resistance mechanisms as well as therapeutic sensitivity of neuroblastoma, which has the ultimate goal of improving the therapeutic strategies of children with this poor prognosis disease. We were able to demonstrate, by *ex vivo* high-throughput drug screening, the particular cytotoxicity of HDAC inhibitors in HR-NB. In addition, we could decipher the genetic events underlying the clonal evolution of HR-NB after targeted therapy. Finally, the combination of lorlatinib and idasanutlin brings hope for the therapeutic approach of *ALK*-aberrant NB.